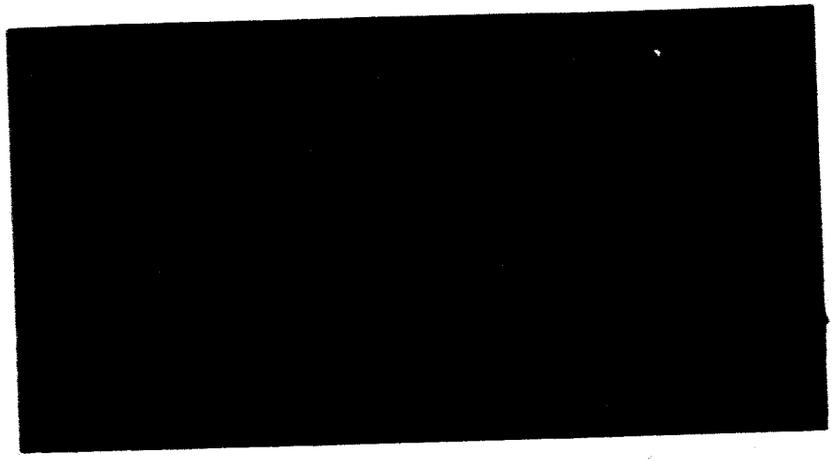

MCDONNELL

DATE 1 September 1965

REVISED _____

CONTROL TECHNIQUES FOR LARGE LAUNCH VEHICLES

REPORT B897 COPY NO. 6

SUBMITTED UNDER _____

PREPARED BY John Zaborszky
Dr. J. Zaborszky
Consultant

AND William J. Luedde
W. J. Luedde
Group Engineer

APPROVED BY J W Twombly
J. W. Twombly
Chief Guidance and Control
Mechanics Engineer

APPROVED BY _____

MCDONNELL AIRCRAFT CORPORATION

LAMBERT-ST. LOUIS MUNICIPAL AIRPORT, BOX 516, ST. LOUIS, MO. 63166

MAC 273B (8 JAN 64)

FOREWORD

This report was prepared by the McDonnell Aircraft Corporation, St. Louis, Missouri, on NASA contract NAS8-11418, "Control Techniques for Large Launch Vehicles." The work was administered under the direction of the Astrodynamics Division of the Aero-Astrodynamics Laboratory of the George C. Marshall Space Flight Center.

The study presented herein began in July 1964 and was concluded in September 1965 and represents the efforts of the Engineering Technology Division of McDonnell. The chief contributors were Dr. John Zaborszky (Consultant), Mr. William J. Luedde (Group Engineer), Mr. David F. Brown (Engineer), Dr. Roger L. Berger, and Mr. Kenneth Kessler. The latter two were with Washington University, participating under a subcontract from McDonnell.

This report is the final report and it concludes the work on Contract NAS8-11418.

TABLE OF CONTENTS

TABLE OF CONTENTS (CONT.)

LIST OF FIGURES

LIST OF FIGURES (CONT.)

LIST OF FIGURES (CONT.)

LIST OF FIGURES (CONT.)

LIST OF FIGURES (CONT.)

LIST OF FIGURES (CONT.)

LIST OF FIGURES (CONT.)

LIST OF TABLES

LIST OF TABLES (CONT.)

LIST OF TABLES (CONT.)

LIST OF TABLES (CONT.)

1. INTRODUCTION

Large boosters for the launching of space vehicles pose major control problems. These problems are largely attributable to the flexibility of such boosters which may result in significant oscillations at as many as four elastic modes in addition to three fuel slosh modes. Control of boosters typified by Study Vehicles I and II is made more difficult by the fact that the first bending mode occurs at a frequency low enough to directly affect the response of the rigid body. Additional difficulties are caused, as in the case of Vehicle II, by the clustering of the frequencies of the first bending mode and the slosh modes in one small region of the s-plane. The fact that these vehicles are also aerodynamically unstable is only a minor difficulty.

In spite of these difficulties, it is possible, as illustrated in Appendix F, to design a linear compensation with very satisfactory performance using only attitude plus attitude-rate feedback for improving transient performance, a second-degree over second-degree compensating network for bending mode stability, and a lead-lag network for improving steady state performance. Such a design nevertheless exhibits certain shortcomings which demand remedial measures and eventually leads to the introduction of digital filtering techniques.

There are two separate and largely independent sets of requirements which lead to two separate and independent digital solutions which may be applied individually or jointly.

(1) When the booster under attitude plus attitude-rate feedback control is passing through extremely severe wind profiles, the vehicle may develop an angle-of-attack which exceeds the structural strength limits. Also, an engine deflection approaching the limits may be required as the vehicle tries to maintain its commanded attitude. These conditions may be alleviated by the use of either acceleration or angle-of-attack feedback to cause the missile to turn into the wind at the expense of an inaccuracy in the vehicle heading angle. This form of control as studied and developed by NASA is based on the "drift minimum control" principle, Reference (1). The use of either acceleration or angle-of-attack feedback, however, has proven to be destabilizing to the control system since these signals usually contain a large bending component. This calls for remedies which fortunately are attained relatively easily, considering that the principal function of the acceleration or angle-of-attack feedback is to pass the gross variations of windshear which are low in frequency compared to the body bending signals present in these signals. Consequently, it is possible to insert filters in the acceleration or angle-or-attack feedback path. A polynomial type digital filter is proposed here; its performance is studied and evaluated, and it is compared to the performance of more conventional linear filters.

(2) Because of the low frequency of the first bending mode, the maximum frequency feasible with linear compensation for the rigid body response is quite low, possibly even inadequate. It may then be necessary to improve the response of the rigid body by artificial means designed to avoid exciting the bending modes. This can be accomplished by the "digital adaptive filter" which is capable of separating from a signal a damped sinusoidal component on the basis of its damping as well as its frequency. Consequently, it can separate an existing rigid body signal even if a poorly damped first bending oscillation of the same frequency is also present. The performance of the digital adaptive filter was previously studied, Reference (2), for a group of space boosters of a more conservative type. This study is hereby extended to Vehicle I.

The studies associated with this program included combinations of analytical work, hybrid simulation and all-digital simulation. The results of these studies are summarized in the body of this report for an easily accessible account of what has been accomplished. Some of the details which the interested reader may want to study have been relegated to the appendices. Appendix A lists the parameters of the two study vehicles and the specifications for the environment of wind and gusts which were used in the study. Appendix B gives details of the hybrid simulator program in which the booster and its linear compensating networks were represented on a PACE analog computer, and the digital operations performed for the "digital polynomial filter", and the "digital adaptive filter" were represented on a Univac 1218 digital computer coupled to the PACE computer through an analog to digital and digital to analog converter. This hybrid operation gave a very flexible representation of the complete control system, permitting the accumulation of considerable amounts of documentation. Appendix C discusses the all-digital program prepared for the IBM 7094 to yield transient responses for the booster under extensive and arbitrary linear control with various feedback combinations and optional digital filters, such as the digital adaptive filter or the digital polynomial filter. This program was designed with considerable flexibility and should prove quite useful in general studies of the elastic booster control problem quite apart from its use in the present projects. Appendices D and E provide more details of the analytical studies of the digital polynomial filter and the digital adaptive filter which were not included in the body of the paper. Appendix F contains some details of the considerations applied in designing linear compensation for these extremely complex systems.

Finally, Appendix G is a preliminary study of the "specification set" type design of linear systems. This is a study which is not tied in directly with the rest of this report. Its aim is to provide a way of designing linear systems to performance specifications, such as used in engineering design, but without the customary cut and try procedures.

2. GENERAL DESCRIPTION OF THE DIGITAL DRIFT MINIMUM CONTROL

To elucidate the aims, possibilities and limitations of the process which uses the digital polynomial filter in a drift minimum control system, it seems best to look at an example and observe the response characteristics of the system with and without such filtering. Let us first consider conventional linear control of the booster with attitude and attitude-rate feedback. For Vehicle I, this type of control is indicated schematically in Figure 1, when switch S is in the open position. Figure 2 shows that quite adequate performance on step attitude commands can be obtained with Vehicle I by the conventional linear compensation of moderate complexity shown in Figure 1. The response shown by Figure 2 was obtained from a complete representation of the Study Vehicle I airframe including the three body bending and three propellant slosh modes. Figure 3 shows the same step response for Vehicle I with all modes except the rigid body modes removed from the airframe. Figures 4 and 5 show the corresponding two responses of the attitude control system to the Marshall Space Flight Center (MSFC) synthetic wind profile which is described in Appendix A and shown in Figure A.3.

These responses, shown in Figures 2 through 5, are stable and may appear to be satisfactory. However, with a maximum equivalent angle-of-attack in the wind profile of $\alpha_w = 12.4°$, there is a maximum actual angle-of-attack of $\alpha = 13.5°$ and an engine deflection angle of $\beta = 4.5°$ for Vehicle I when all modes are considered; corresponding values for the rigid body case are $\alpha = 14°$ and $\beta = 5°$. These values of α and β are high, considering the structural strength and the engine deflection limit angle of 5°. On the other hand, while the commanded attitude angle is $\phi = 0$, there is a final attitude angle at 35 seconds of respectively $\phi = 2.5°$ when all modes are considered, and $\phi = 3.8°$ for the rigid body only. These ϕ values are very acceptable. Considering the limited accuracy requirements of booster guidance, much higher values of drift could be tolerated so a compromise of permitting more drift to reduce the maximum angle-of-attack and the maximum engine deflection angle is apparent. The tool used to implement this compromise could be the addition of an acceleration or angle-of-attack feedback loop with the appropriate gain to produce the proper amount of drift during the crossing of the wind profile to relieve the structure of the missile from excessive stresses. These ideas were developed in Reference (1), which introduces the drift minimum principle.

If the drift minimum loop is added to the system in Figure 1 and switch S is closed to system design I.1, then Figures 6 and 7 show what happens in the wind. The elastic booster becomes unstable as shown in Figure 6. Yet Figure 7, with the rigid body mode only, reveals that if stability can be acquired, very favorable results could be expected. For the rigid body mode only, the maximum angle-of-attack has been reduced from $\alpha = 14°$ to $\alpha = 10°$ and the maximum engine deflection from $\beta = 5°$ to $\beta = 3.8°$ at the expense of increasing the final attitude angle at 35 seconds from $\phi = 3.8°$ to $\phi = 4°$.

It is very difficult to design a staisfactory linear compensation for the high acceleration feedback gain that is required for the drift minimum control of Vehicle I unless some means of filtering is provided in the acceleration

loop. This is because an acceleration feedback with a high gain will emphasize the higher frequencies such as bending and slosh, and drive them unstable. On the other hand, the over-all variation of the wind profile is quite low in frequency. There may be high frequency gusts superimposed on the wind, but it is not expected that the missile will drift appreciably in response to these. The drift control is a slow process then. This realization leads to incorporating a suitable filter in the acceleration feedback path which will pass the low frequency wind profile but suppress the high frequency bending and slosh modes and the high frequency gusts. In fact, the suppression of even the rigid body signal is desirable in the acceleration feedback path since, according to Figure 2, the basic control functions can be quite adequately fulfilled by attitude and attitude-rate feedback. Therefore, the role of the loop filter is to separate the functions of basic control to be established by rate and attitude feedback and the functions of reducing drift while passing through the wind profile. The implication is that some kind of low pass filtering device is required. This could be a conventional linear low-pass filter, and such indeed can be applied, as will be demonstrated later in this report where the performance of such a linear filter will be evaluated.

A study was performed to develop a digital filtering device. This device, the digital polynomial filter, accumulates equally spaced samples of the acceleration (or angle-of-attack) signal over some fixed time interval, T, and fits a low order (zero, first or second) polynomial to these samples in a mean square sense. Then it generates an output computed for the present time from the fitted polynomial. Since the degree of the polynomial is low, its ability to follow signals with wavelengths of a fraction of T is limited. Hence, higher frequencies are attenuated and a low pass filtering effect results.

The characteristics of this device as a filter are discussed in the next section. At this point, only an illustration of its effectiveness is given. Figure 8 shows the passage of the missile through the MSFC synthetic wind profile. Here acceleration feedback (switch S closed upward in Figure 1) with a digital polynomial filter of order zero and a fitting interval of 5 seconds is incorporated. In contrast to Figure 4, which is the corresponding response without acceleration feedback, the maximum angle-of-attack was reduced from $\alpha = 13.5°$ to $\alpha = 11.0°$ and the maximum engine deflection angle from $\beta = 4.5°$ to $\beta = 3.9°$. There is an increased drift from $\phi = 2.5°$ to $\phi = 4.0°$ at 35 seconds.

The stabilizing effect of the filter must, however, be paid off by a slight deterioration of the stress relief. The extent of this can be judged by comparing Figure 7, the response without filtering, and Figure 9, the response with polynomial filtering. Each of these figures show the rigid body response only. With filtering, there is an increase from $\alpha = 10.0°$ to $\alpha = 11.0°$ and from $\beta = 3.8°$ to $\beta = 4.3°$ as well as an only slight change in attitude angle. These changes are moderate. Also, a comparison of the step input response of the control system with the digital polynomial filter in the acceleration feedback, Figures 10 and 11 (rigid body response only) and the step response of the control system without acceleration feedback, Figures 2 and 3 (rigid body only), reveals that the deterioration of the step response effected by the introduction of the filtered acceleration feedback is insignificant, except for the presence of a slow drift in the attitude angle shown in Figures 10 and 11. Figure 10 with

acceleration feedback and the digital polynomial filter actually exhibits better damping at the first bending mode than does Figure 2 with only position and rate feedback. It should be mentioned, however, that the run of Figure 2 is not really optimized in this respect.

It seems then that the filtered acceleration feedback is a highly effective tool in separating the two modes of control, namely:

(1) A conventional linearly compensated attitude and attitude-rate feedback system for stability and response to command signals.

(2) An acceleration, or angle-of-attack, feedback with appropriate filtering for stability to obtain stress relief through controlled drift while passing through the wind profile.

2.1 Characteristics of the Digital Polynomial Filter

The purpose of the digital filter to be used in the acceleration or attitude angle feedback path is to separate the signal representing the low frequency portion of the wind profile from the feedback signal which will contain rigid body, elastic and slosh oscillations, and high frequency gusts in addition to the desired wind profile signal. The separated wind profile signal is used for stress relief.

A filter is then needed which passes quite accurately smooth and slow varying signals and suppresses fast or high frequency components. Of course, a conventional linear low-pass filter possesses many of these characteristics. While such filters will also be investigated, the prime concern here is a digital type filter which is more effective in some ways and which may offer a simpler method of instrumentation depending on the availability of a digital computer on board than the methods used for instrumenting linear filters.

The digital approach depends on fitting polynomials using a least squares criteria to a set of 2M+1 equally spaced present and immediately past samples. Depending on the length of the record used (that is, (2M+1)T if T is the sampling interval) and the degree of the polynomial, such a fitted curve will smooth out fast or high frequency variations and thus it is intuitively apparent that it should possess low-pass filtering characteristics. There are numerous ways of obtaining a polynomial fit.

In this report, the digital filter equations for curve fitting to a polynomial of the form $A + Bt + Ct^2 + \ldots$ will be based on the standard Gram polynomial least-squares fitting equations as discussed in Reference (2). Letting $y(t)$ be the nth degree least-squares Gram polynomial approximation to the digital filter input $f(t)$ over the 2M+1 equally spaced point range

$$N = -M, -M+1, \ldots, -1, 0, 1, \ldots M-1, M \qquad (1)$$

it can be shown that

$$y(t) = \sum_{r=0}^{n} a_r P_r(N,2M) \tag{2}$$

where the P_r are the Gram polynomials

$$P_0(N,2M) = 1 \tag{3a}$$

$$P_1(N,2M) = \frac{N}{M} \tag{3b}$$

$$P_2(N,2M) = \frac{3N^2 - M(M+1)}{M(2M-1)} \tag{3c}$$

and

$$a_r = \frac{1}{\gamma_r} \sum_{N=-M}^{M} f(NT)\, P_r(N,2M) \tag{4}$$

$$\gamma_r = \sum_{N=-M}^{M} P_r{}^2(N,2M) \tag{5}$$

where T is the sample period. P_r and γ_r are independent of the input f(NT) and thus need to be calculated only once for a given value of M. The value of M depends on the filter length.

The polynomial fitting digital filter takes the last 2M+1 samples of f(t), determines the nth order Gram polynomial approximation y(t), and computes an output y(M). Since at time M the Gram polynomials are all unity, the output of the filter at the time of the last measured sample is

$$y(T) = y(M) = \sum_{r=0}^{n} a_r \tag{6}$$

Also, since the sampling rate and filter length are predetermined, the necessary values of γ_r and $P_r(N,2M)$ are calculated in advance. Evaluating a_r by Equation (4) becomes the simple matrix multiplication

$$y(T) = \sum_{r=1}^{n} c_r f(NT) \tag{7}$$

where c_r is a predetermined row matrix and f(NT) is a column matrix composed of the last 2M+1 samples of f(NT).

Equation (7) is then the working equation for the filter. Note its simplicity for digital computer programming. The c_r coefficients are listed for 2M+1 = 25 samples and polynomials of degrees n = 0, 1, 2 are shown in Table I. Note that filtering by n = 0 is especially simple since $c_r = \frac{1}{2M+1}$ for all r and consequently (although not surprisingly), the zero degree fit is simply the average value of the function over the fitting interval. Computing this then requires only the addition of the past 2M+1 samples, a most simple computer program requiring a minimum of time.

For the evaluation of the filtering characteristics of this "digital polynomial filter", two methods present themselves:

(1) Since the filtering by Equation (7) consists of a linear combination of 2M+1 past samples, this is obviously a special case of linear sampled data filtering and can be thought of in terms of z transforms.

(2) Since a relatively large number of samples is to be used in the fitting, the results can be closely approximated by assuming mean square fitting in a continuous sense.

In (1), the filtering represented by Equation (7) can be rephrased in terms of z transforms like:

$$y(z) = \frac{\sum_{r=0}^{2M} c_r z^{2M-r} F(z)}{z^{2M}} \qquad (8)$$

where F(z) and y(z) are respectively z transforms of the filter input and filter output and

$$G(z) = \frac{\sum_{r=0}^{2M} c_r z^{2M-r}}{z^{2M}} \qquad (9)$$

is the z transfer function of the filter.

Now Equation (9) reveals that, regardless of the degree of the polynomial, there will be a pole of multiplicity 2M at the origin of the z plane; in other words, the multiplicity of this pole depends solely on the number of samples used. The number of zeros also depends only on the number of samples used, but the location of the zeros will also be influenced by the degree of the polynomial since the coefficients here are the c_r from Table I.

For the n = 0 degree fit, all 2M zeros are spaced along the unit circle as shown for 2M+1 = 25 in Figure 12. A different arrangement results for n = 1,2 as shown in Figures 13 and 14a. Figure 14b illustrates the location of the 2M zeros outside the unit circle for polynomial fitting of degree greater than n=0.

The presence of zeros on the unit circle which represents the frequency axis indicates that very high attenuation will result at certain select frequencies. This is easy to see for n = 0. The average value of the fitted signal, which is the filter output, will vanish at a frequency where alternate samples or alternate groups of samples are equal and of opposite signs. This will happen when $\omega = \frac{2\pi k}{T}$, k = 1, 2 -- where T is the fitting interval length.

In (2), these matters can be studied more conveniently by approximating the operation by a continuous rather than sampled type of fitting operation. The necessary equations are derived in Appendix D. The frequency response curves are shown in Figures 15, 16 and 17. Each of the gain curves contains a straight line envelope at 6 db/octave slope that is corresponding to the asymptotes of a first order linear low-pass filter. One interesting observation is that the break frequency of this fictitious first order filter is respectively 0.33 at n = 0, 1 at n = 1, and 2 at n = 2. In other words, the equivalent break frequency is increasing with n for a given fitting interval. This, of course, is to be expected since a higher degree polynomial is capable of following higher frequency variations in the input than is a low degree polynomial.

Another interesting feature of Figures 15 through 17 is that such a first degree envelope apparently exists, that is, the attenuation at certain frequencies equals the attenuation of a first order filter while at other frequencies it is lower and it is never higher. The phase angles are quite different from the linear filter, being much larger in the case of the zero degree polynomial.

These features of the digital polynomial filter as compared with conventional linear filters can be expected to manifest themselves in performance characteristics of control systems where such filters are used.

2.2 Fundamental Performance; Comparison with Direct Drift Minimum Control and Drift Minimum Control with Digital Polynomial Filter

In a previous section the basic role of the digital polynomial filter was described as one of producing calculated stress relief by transmitting the low frequency variation of wind profiles in the accelerometer or angle of attack sensing instrument channels, while at the same time suppressing the rigid body, body bending, slosh and gust oscillations, thus permitting the stabilization of these in a standard position plus rate feedback linear control system. The basic features of this operation were previously illustrated for Vehicle I. A systematic documentation for both vehicles follows.

2.2.1 Vehicle II - Compensation Designs and Conventions. - Before one can present the dynamic performance for a vehicle, it is necessary to agree on some fundamental design of the various aspects of the control system. Clearly there is a large amount of freedom associated with the selection of the control system configuration. For the purpose of this study, two fundamental designs were selected to be used for Vehicle II in conjunction with the digital polynomial filter in the acceleration feedback loop. In addition, deviations from these were made for purposes of comparison. These fundamental and comparative designs, which were investigated at the maximum dynamic pressure flight condition, are defined below:

Design II.1 shown in Figure 18 utilizes one second-degree over second-degree linear filter in the forward loop, plus a lead-lag filter for improving steady state operation.

Design II.2 (Figure 19) is similar to Design II.1 except for using two second degree over second-degree filters.

Design II.3 (Figure 20) is identical in structure to Design II.1 except that this design uses a linear low pass filter in the acceleration feedback loop instead of the digital polynomial filter.

Design II.4 (Figure 21) is a design for stable command response with attitude and attitude rate feedback.

Design II.5 (Figure 22) is a design which uses angle-of-attack feedback instead of acceleration feedback to produce stress relief in the presence of wind.

In addition to selecting these standard designs, one must standardize on the types of test runs to be used and on the particulars of evaluating the results of runs.

In this study, two basic types of runs were utilized in evaluating the performance:

(1) A standardized wind profile converted to an equivalent wind angle-of-attack was used in most runs involving tests of wind. This is given in Figure A.3 of Appendix A. In some runs, variations on this profile were used. Specifically, step type windshear, either alone or superimposed on the standard profile was used. In addition, a square wave or sinusoidally varying windshear was sometimes superimposed on the standard wind profile.

(2) To test long range stability and general performance of the control system, command input steps, $\phi_c = 1°$ were used to activate the control system. Except for the time varying nature of the system, this type of test will give an indication of long range stability regardless of the actual presence of steps in the vehicle command signals.

In selecting the quantities used for evaluating the quality of the results, it was attempted to select a set of measurements which summarizes the pertinent performance features. Accordingly,

(1) For evaluating the performance while passing through the wind profile, the quantities selected are:

ϕ_G, attitude at the gyro, at 2 sec. after initiation of wind

ϕ_G, at 15.5 sec., the time of the peak equivalent wind angle of attack

ϕ_{GP}, the largest attitude angle resulting from wind

β, engine deflection at 2 sec.

β_{max}, peak value of engine deflection

β_{mR}, maximum rebound of engine deflection

α_{max}, peak of angle of attack

α_{mR}, maximum angle of attack reached in rebound

η_{1P}, η_{2P}, η_{3P}, and η_{4P} maximum values reached on the respective bending modes including forced oscillations of the bending modes

η_{1PP}, the maximum peak to peak oscillation of the first bending mode at the first bending frequency

The measurement of most of these various quantities is shown in detail in Figure 23. These quantities were selected to give a fast way of comparing the system performance under varying conditions.

(2) For evaluating the response due to a step command input, the following quantities are used:

ϕ_{GP}, the initial peak attitude on a ten step attitude command

T_G, the time of ϕ_{GP} after applying the step

ϕ_{CGM}. the initial peak attitude of the rigid body measured at the center of gravity.

T_{CGM}, the time of ϕ_{CGM}

ϕ_S, the steady state value of attitude ϕ_G

$\dot{\phi}_S$, the steady state attitude rate of ϕ_G

β_{max}, the largest engine deflection resulting for a 1° step attitude command

α_{max}, the largest angle of attack resulting from a 1° step attitude command

$\ddot{\tau}_{max}$, the peak amplitude of the measured normal acceleration $\ddot{\tau}$

z_{1pp}, z_{2pp}, z_{3pp}, maximum peak-to-peak oscillating amplitudes of the three slosh modes

η_{1p}, η_{2p}, η_{3p}, and η_{4p} maximum values reached on the four bending modes including forced motion of these modes

η_{1pp}, η_{2pp}, η_{3pp} and η_{4pp}, peak-to-peak oscillations of the four bending modes at the respective bending frequencies

d, absolute damping of the first bending mode or first slosh mode whichever is predominant

Figure 24 shows in detail an example of measuring most of these quantities. The damping value, d, was measured as follows:

$$d = \frac{1}{T} \ln \frac{b}{a}$$

where a and b are two peak-to-peak amplitudes on the appropriate oscillation T seconds apart, with b coming after a. Since the second, third and fourth modes are well separated, their dampings are readily determined. However, the frequencies of the first bending mode and the slosh modes are almost equal, and usually there are two slightly damped modes; one is associated with the slosh and the other with the first bending mode. Since, in many instances, changes in compensation will improve the damping of one of these modes and spoil that of the other, the best compromise design has both of the modes at about the same damping. This manifests itself in a damped beat oscillation. The ratio b/a is then taken for two amplitudes at the same phase of the beat envelope. If the damping of one mode is higher, then the beat eventually disappears and the lower of the two damping values can be measured on the residual osciallation. In either case, it is not feasible to assign the damping positively to the first body bending mode or one of the slosh modes. Accordingly, the damping, d_1, given in the tables should be interpreted as the lowest damping in the group of modes consisting of the first bending mode and the slosh modes.

2.3 Performance of Vehicle II With the Various Standard Designs

Designs II.1, II.2, II.3 and II.5 represent designs which may be proposed for application as a result of this study. Accordingly, it is important to display and record the fundamental performance achieved in conjunction with these designs. This is done in Figures 25 to 28 for passing through the MSFC standard wind profile and in Figures 29 to 31 for a step attitude command input of $\phi_c = 1°$. The specification numbers for these runs are listed in Table II for the step response and in Table III for the wind response. It may be observed that responses II.1, II.2, and II.3 are rather similar in quality and all are quite suitable from the viewpoint of rise time and peak overshoot, maximum attitude angle, engine deflection and angle-of-attack. About the only unsatisfactory feature is a long persisting oscillation in the first bending and slosh mode frequency area. This unfortunately is an inherent problem with Vehicle II. These modes are very close to each other and so situated that there are always two closed loop modes which get respectively more and less well damped as a result of the application of any compensating poles and zeros which are located at some distance from the first bending and slosh mode complex. The only way to damp these out would be the use of a closely and precisely placed dipole. This technique, however, would have to depend on precise knowledge of the location of the slosh and first bending modes which, of course, is not available. This problem is discussed in more detail in Appendix F.

It should be observed that Designs II.1 and II.2 both represent applications of the digital polynomial filter in the acceleration feedback path while Design II.3 represents the application of a linear lag network in this path; yet the results are quite similar. Design II.5 uses the digital polynomial filter in the angle-of-attack feedback path. Again, the performance is quite similar to the other designs.

It may be said then that acceleration or angle-of-attack feedback with digital polynomial filter or a linear filter can all be optimized to about the same level of performance, although the linear network results in slightly larger angle-of-attack values. There is, however, some difference in the sensitivity of the various designs to parameter variations. These matters will subsequently be discussed in detail.

2.3.1 Vehicle I - Compensation Designs and Conventions - For Vehicle I there is one standard design for acceleration feedback and one for angle-of-attack feedback. Designated Designs I.1 and I.2, these system configurations are shown in Figure 1.

The two standard forms of test runs were also applied for Vehicle I. Transient responses were obtained while passing through the MSFC standard wind profile, and for following an attitude command step of $\phi_c = 1°$. The standardized measurements explained in conjunction to Figures 23 and 24 were also used in the Vehicle I studies with appropriate modifications. The fundamental wind profile and step responses for Vehicle I, Design I.1, are presented in Figures 8 and 10, respectively. For Design I.2, which has angle-of-attack feedback,

the basic wind and step response runs are shown in Figures 32 and 33. Performance data comparing the Design I.1 and I.2 responses to step and wind inputs are given in Tables IV and V.

It may be observed by comparing the tabulated data and the wind response runs of system designs I.1 (Figure 8) and I.2 (Figure 32) or the corresponding step responses (Figures 10 and 33) that the vehicle performance obtained with acceleration feedback is quite similar to that obtained with angle-of-attack feedback for the case of vehicle I. One difference is that the degree of system bending stability of vehicle I with angle-of-attack feedback is greater than that with acceleration feedback. This is illustrated by comparing the system responses with and without (replaced by unity gain) the digital polynomial filter for vehicle designs I.1 (Figure 6 and 8) and I.2 (Figure 33 and 34). The relative degree of system stability can be observed in these figures even though one set of data is for a wind response and the other set is for a step response.

2.4 Documentation of Sensitivity to Variation of Parameters

In the preceding section there are presented some data on the performance of a number of designs which were selected as possible for actual control of Vehicles I and II. These are designs which were experimentally optimized for over-all performance. Such optimized designs do not describe the situation completely since these apply to some exactly described booster, wind profile and compensation. All of these items are subject to variation so it is important to evaluate the deterioration from the optimum performance which results from changes in parameters. A rather detailed study was performed to determine these sensitivities. The study covered the independently variable parameters such as the amount of acceleration feedback, the various gains and the compensating network parameters as well as booster parameters and the booster environment such as the wind profile. Most of this evaluation of parameter variation sensitivity was accomplished with Vehicle II using acceleration feedback.

2.4.1 Sensitivity to Control Parameters: Acceleration Feedback Gain - A principal concern of this study is the achievement of load relief through acceleration or angle-of-attack feedback while the stability is maintained by the use of the digital polynomial filter in the acceleration or angle-of-attack feedback path. The load, which is a function of the angle of attack α, can indeed be reduced by applying acceleration feedback. However, this will usually be accompanied by increased vehicle drift. It is important to investigate the magnitudes of each of these factors in order to make it possible to select the optimum compromise gain values. Accordingly, a detailed study was undertaken on the effects of variations in the acceleration feedback gain, $K_{\ddot{\gamma}}$. These results are presented in Table VI for Vehicle II, using the compensation of Design II.4, while passing through the MSFC wind profile.

The first line of this table records what happens when the rigid body only is controlled by attitude and rate feedback (with no compensation and no acceleration feedback) while passing through the standard wind profile. There

is a significant maximum angle-of-attack of 15.6° (where the maximum equivalent angle-of-attack of the wind profile is only 12.4°); the maximum engine deflection is 2.88° and the maximum vehicle attitude angle is -10.2°. If acceleration feedback is introduced and its gain is gradually raised to $K_{\ddot{\tau}} = 0.21$ as shown in Group 1 of Table VI, then the maximum angle-of-attack is reduced to 7.68°, but the attitude angle increases from -10.2° to 11.0°. The maximum engine deflection is only slightly affected; in fact, it stays between 2.0° and 2.88°. At the "drift minimum gain" of about $K_{\ddot{\tau}} = 0.09$, the numbers are respectively $\alpha = 10°$, $\phi_G = 4.72°$ and $\beta = 2.06°$.

When slosh and bending are added, it becomes necessary to incorporate the digital polynomial filter. This filter in the acceleration feedback produces a certain deterioration in the vehicle performance. The effect of adding the polynomial filter is illustrated by comparing Groups 1 and 2 in Table VI. These two differ only in the presence of the polynomial filter. As may be seen, the presence of the filter causes an increase in the vehicle angle-of-attack from 0.4° to 1.5° and specifically by 0.8° at the drift minimum gain of $K_{\ddot{\tau}} = 0.09$. The maximum attitude angle varied as much as 2.3°. The engine deflection angles variations ranged from a reduction of 0.7° to an increase of 0.2°.

When slosh and bending are considered, there is also need for forward loop compensation such as that of Design II.4 as given in Figure 21. This compensation falls into two groups according to its aim and role. All of the compensation except the lead-lag network is aimed at stabilizing bending and slosh modes. This part will be referred to as "stabilizing compensation." The lead-lag network has the role of reducing steady state errors, deviations in the steady state between booster attitude and the height of the command step. This latter compensation will be referred to as "command compensation." Stabilizing compensation is, of course, absolutely essential. Command compensation might be eliminated if some aspect of it proves objectionable. In view of this, the effects of these two types of compensation are discussed separately.

When the compensating measures are included in the system, some of the advantages of the acceleration feedback in load relief are lost. To see how severe this effect is, first the command compensation is introduced in Group 3 of Table VI without fitting. Comparing Group 3 and 1, it may be seen that the maximum angle-of-attack is actually reduced by as much as 3° at some acceleration gain values although at the drift minimum gain of $K_{\ddot{\tau}} = 0.09$, there is a decrease in α_{max} of 0.2°. The maximum attitude angle is increased at $K_{\ddot{\tau}} = 0.09$ by about 2.3°. Engine deflection is not affected significantly by this compensation. When the digital polynomial filter is added, as in Group 4, then the comparison is between Groups 4 and 2. The comparisons are about the same; in fact, since the command compensation actually improves the load relief effects for low gain values of the acceleration feedback, it should be included.

Stabilizing compensation is also included in Group 5. A comparison of Groups 5 and 4 reveals that this compensation also does not appreciably change the load relief situation produced by acceleration feedback. When slosh and bending are included as in Group 6, there is a slight over-all deterioration in

the maximum attitude angle, angle-of-attack, and engine deflection experienced by the vehicle. Comparing the stripped down system (rigid body, no compensation or filter) in Group 1 with the complete missile (filter, all compensation, slosh and bending) in Group 6 at the drift minimum gain of $K_T' = 0.09$, there is an increase of 0.88° in the angle-of-attack, 3.8° in the attitude angle, and 0.6° in the engine deflection angle.

2.4.2 Sensitivity of Digital Polynomial Filter Parameters: Order of Polynomial, Sampling Rate, Number of Samples - The function of the digital polynomial filter is to separate the low frequency component of windshear from other sensed signals in the acceleration feedback path. This is basically a low pass filtering problem and according to the frequency response curves of Figures 15 thru 17, the zero (A_0), first ($A_0 + A_1$) and second ($A_0 + A_1 + A_2$) degree digital polynomial filters all have a low pass filtering characteristic so each is potentially useful for incorporation in the acceleration feedback path. Because of its simplicity, the zero degree fitting is the most desirable and should be chosen if it can provide satisfactory performance. With the zero order polynomial fit (which is just the average value of the signal over an immediately past interval) there are two parameters to be selected: the sampling rate and the number of past samples to be stored.

Variations in the response to a step command input with zero degree polynomial fitting are shown for Designs II.1 and II.2 in Tables VII and VIII respectively for a variety of sampling rate-sampling interval combinations. The effects on the performance are not very significant except for the effect on system stability. System stability appears to be related more with the over-all interval length (the division of the sampling rate into the number of samples) than with the numbers of samples and sampling rate individually. Roughly speaking, stability is observed for fitting interval lengths of over 8 seconds. The only specification value which is significantly affected by variations of the sampling rate and number of samples seems to be the peak time.

Some investigations were devoted to using first and second degree polynomials in the digital polynomial filter. Since for the same fitting interval a first degree polynomial filter will generally follow the signal closer than a zero degree one, the effective cutoff frequency of a first degree polynomial filter is higher. Consequently, shorter interval lengths are generally required for stability for first order filters. It was found that stabilization is possible for various degree polynomials but that the higher degree fittings were more sensitive to variations in the sample rates and memory lengths than for the zero degree fitting. Accordingly, the selected designs such as Designs II.1, II.2, II.5, I.1 and I.2 all use zero degree fitting.

Since the digital polynomial filters all provide a version of low pass filtering, the logical question is whether comparable performance could be achieved by using a conventional linear low pass filter in the acceleration feedback path. The system configuration is shown in Design II.3, Figure 20. Its performance with varying time constant for the low pass filter is documented in Table IX. Very interestingly, stability is observed for time constants above 8 seconds just as stability with the zero degree polynomial filter is

observed for fitting interval lengths greater than approximately 8 seconds. The performance is quite similar in other respects as well as is evident by comparing Tables VII, VIII (system designs II.1 and II.2) and IX, except a somewhat larger load relief occurs in case of the digital polynomial filter. It seems that the decision whether to use digital polynomial or conventional linear filters may hinge principally on the simplicity of instrumentation.

Digital polynomial filters might be incorporated not only in the acceleration feedback loop but possibly in other parts of the system. One such location might be the rate feedback loop where the digital polynomial filter might be included in association with another digital polynomial filter in the acceleration feedback loop as in Table X where the Design II.1 compensation is used or in Table XI where the Design II.2 compensation is used. As may be observed in Tables X and XI, it is possible to stabilize the booster with digital polynomial filters in the rate feedback loop. Since the rate feedback loop is essentially aimed at stabilizing the rigid body, the filter should pass the rigid body signals but preferably not the bending mode signals. This means that for stability, the fitting interval must be much smaller in the rate loop than in the acceleration feedback loop, about 1 second as against 10 seconds. An exception appears in Table XI, where only the first and second order terms of the fit were used. This latter arrangement raises the cutoff frequency and accordingly intervals of about 10 seconds are needed for stability. A sample run is shown in Figures 35 and 36 where the wind and step responses respectively are shown for a system which incorporates first degree digital polynomial fitting in the attitude rate feedback path. These runs are comparable but not superior to performance without this type of compensation. It must be stated, however, that time limitations did not permit more than a casual examination of this system.

2.4.3 Documentation of Sensitivity to Forward Loop Attitude and Attitude Rate Feedback Gains - To begin the investigation of effects of variations in compensating parameters, first the variations of forward loop gain K and rate feedback gain $K\dot{\phi}$ as defined in Figures 18 through 22 for the various designs were studied. The results are summarized for Designs II.1, II.2, and II.3 in Tables XII through XIV. What is important is that there be a wide range in these gains within which the performance is satisfactory. This indeed is the case according to Tables XII through XIV where a stable range in K of 2.0 to 2.6 can be observed and a stable range of about 4.0 to 5.0 in $K\dot{\phi}$. This 25 percent range for each gain is quite adequate. Very interestingly, the same range applied for Designs II.1, II.2, and II.3, although the latter has a linear network instead of a digital polynomial filter in the acceleration feedback path. This is probably attributable to the fact that the gains K and $K\dot{\phi}$ principally affect the transient response rather than wind-induced drifting. This fact is also apparent from the data in Tables XII through XIV.

2.4.4 Documentation of Sensitivity to Parameters of Command Compensation Network - Of the two compensating methods, the command compensation is intended for influencing the steady state behavior connected with command inputs. It is then somewhat important that it has as little effect as possible on the performance in wind and on the stability. The data in Table XV which was found to be typical for all of the design configurations confirm that indeed there is very little such influence.

2.4.5 Documentation of Sensitivity to Parameters of Stabilizing Compensation Network. - The stabilization compensation networks selected for the Vehicle II control system Designs II.1, II.2, II.3 were determined from experimentation on the hybrid simulation. It was found that variations from 10 to 20 percent in the compensation pole and zero locations generally could be tolerated by the control system. The effect of small variations in the location of the compensation was usually observed as a reduction in the amount of the damping present on the first body bending and/or first slosh mode oscillations. Large excursions of the compensation values usually resulted in a bending mode instability at one or more of the bending modes. The rigid body responses were relatively unaffected by changes in the stability compensation.

2.4.6 Documentation of Sensitivity to Variation of Booster Parameters.- Generally, it is not very difficult to design a linear compensation for a linear system with fixed and known parameters. The real difficulty usually is in designing a system which will control satisfactorily over the range of parameter variations -- or the uncertainty with which the parameters are known -- which normally are sizable even for one given flight condition. Accordingly, an investigation was carried out to document the sensitivity of the control to variations in the aerodynamic coefficients and the parameters of the bending and slosh modes. As is apparent from the data in Table XVI, there is no serious problem with vehicle control coefficients, C_1 and C_2, which are varied by $\pm$ 20%.

The situation, however, is quite different for variations in the frequencies of the body bending modes. Tables XVII, XVIII, and XIX reveal that the tolerance of variations in bending mode frequencies to maintain vehicle stability does not exceed $\pm$ 10% even though the loss of stability is gradual and it probably would be possible to pass through the maximum q condition without harm. These tables show that there is no significant difference in the sensitivity to bending frequency variations between the systems controlled by the digital polynomial filter (Designs II.1, II.2 and Tables XVII, XVIII) and those controlled by linear methods (Design II.3 and Table XIX).

2.4.7 Documentation of Sensitivity to Variation of Wind Profile - The preceding discussions are based on runs obtained in two standardized test situations: the MSFC wind profile shown in Appendix A and attitude command steps of $\phi_c = 1°$. Since the systems and control are linear, superposition applies and gradual variations in the structure of wind and command inputs will tend to produce correspondingly gradual variations in the vehicle response. It is important, however, to show how such environmental variations will affect the performance. Such effects are illustrated in the following figures.

In Figure 37, a step of angle-of-attack $\alpha = 1°$ is applied instead of a wind profile. The system is shown to make a good recovery for this type of input, with a maximum engine deflection of $\beta = 0.37°$, a maximum attitude angle of $\phi_G = -0.9°$, and a maximum angle-of-attack of $\alpha = 1.3°$ that occurs at 2.5 seconds.

In Figures 38 and 39, the response of Vehicle I is shown for a step of wind gust combined with the standard wind profile. Figure 40 shows a similar response for Vehicle II. The effects of the step wind gust can be observed by comparing Figures 38 and 39 to the Figure 8 wind response without gust for Vehicle I and Figure 40 to the Figure 26 wind response without gust for Vehicle II. These figures show that the addition of the relatively severe step wind gusts (3 to 4 degrees) adds directly to the existing angle-of-attack but that the variation in the engine deflection angle remains within the allowed limits.

Another variation of the wind input studied was that of a periodic gust superimposed on the wind profile. The effects of sinusoidal "gusts" of different frequencies superimposed on the standard wind profile are shown for Vehicle II in Table XX and in Figures 41 through 43. Both the illustrations and the table reveal by comparison with corresponding standard cases in Figure 26 and Table III that there is no great deterioration of the control system performance as a result from this type of gust input. The run in Figure 44 shows the comparable response of the system Design II.3 for the sinusoidal-wind profile input.

2.5 Evaluation of Results

The foregoing sections have shown that adequate control performance for Vehicles I and II is obtainable by the use of attitude, attitude rate feedback and acceleration feedback (or angle-of-attack feedback) provided the destabilizing effect of the acceleration feedback at the rigid body and bending modes is suppressed by suitable low pass filtering. The digital polynomial filter was introduced for the purpose of stabilizing the control system with acceleration feedback, and it was compared with conventional means of low pass filtering. It can be concluded from this investigation that comparable control system performance can be obtained by either form of filtering, although the digital polynomial filter shows somewhat better load relief characteristics. On the other hand, the system using the digital polynomial filter is slightly more sensitive to variations in the bending frequencies. The decision of using one or the other should be based on simplicity and reliability of instrumentation. One should not conclude that the zero degree digital polynomial filter is not the simpler one. Indeed, it is extremely simple to mechanize and requires only two operations (addition of the new sample-subtraction of the oldest sample) for each sampling interval, every 0.25 to 0.5 seconds. The continuous linear filter may require demodulations and modulations interspersed by other circuitry.

The results obtained by the combined attitude, attitude rate and filtered acceleration feedback control are fully satisfactory for Vehicle I (Figure 8) where there is a maximum angle-of-attack in the standard wind profile of $\alpha = 11.5°$, a maximum engine deflection $\beta = 3.9°$, and a maximum attitude angle of $\phi_{G_{max}} = 4.4°$. To step inputs (Figure 10), there is a peak value of

ϕ_{GP} = .9°, with the shortest damping elastic or slosh mode having a damping of d = -.038. The corresponding values for Vehicle II (Design II.1) are α = 11.0°, β = 2.6°, $\phi_{G_{max}}$ = 8.6° for the wind input (Figure 25), and for the step input (Figure 29) a ϕ_{GP} = 1.0°, and d = -.023. These are quite desirable results although the rigid body response may be slower than desired, and that there is a lowly damped oscillation present in the vicinity of the first bending mode and slosh mode frequencies.

It is possible to obtain a faster rigid body response by incorporating into the control circuit a digital adaptive filter (in addition to the digital polynomial filter) which is discussed in the following chapter as a means of producing high performance for step command inputs.

The only linear compensation which could eliminate the oscillation in the vicinity of the first bending modes and the slosh mode would be a dipole compensation which would have to be precisely positioned among the slosh modes and first bending mode. It would depend on precise knowledge of the position of these modes which may not be available. This means that a slowly damped mode with a frequency near the first bending mode frequency is inherent in any linear compensation of the Vehicle II. In case it is unacceptable it may be necessary to modify the slosh modes (frequency or damping) to further separate them from the first bending mode.

It was found that the selection of none of the filter parameters is critical whether the filter is digital or a linear network but the corresponding fitting interval or time constant must exceed about eight seconds for Vehicle II. The insensitivity to variations of the several control parameters such as gains and pole-zero locations is quite good. The performance is also sufficiently insensitive to variations in the aerodynamic coefficients.

The one set of parameter variations which have a somewhat unsatisfactory sensitivity are the bending frequencies. About $\pm$ 10% deviation in these frequencies from the nominal values results in a slow system instability, which should be tolerable for a short period of time.

3. DIGITAL ADAPTIVE FILTER

The concern in the preceeding sections of this report was with the stress relief necessary to guide the booster through windshear profiles which may be excessively severe. Such stress relief can be obtained by the use of acceleration or angle of attack feedback utilizing the drift minimum gain values. Bending and slosh control problems result from the destabilizing effects of such feedbacks and it was demonstrated that these problems could be remedied by the use of digital polynomial filtering or other low-pass filtering applied in the acceleration feedback path.

Such design then results in a system which is stable and can pass through expected wind profiles without harm. This does not mean, however, that the system response to command inputs is entirely satisfactory. Specifically it was shown that this response tends to be quite slow especially in the case of Vehicle II where the peak time is on the order of 5 to 10 seconds. The low frequencies of the first body bending mode and the fuel slosh modes make it impractical to speed up the response by the use of linear compensating techniques.

It is possible however to speed up the response to step command inputs by utilizing the digital adaptive filter principle. Arbitrary command inputs may be quantized into a sequence of steps.

The digital adaptive filter is designed to separate a well damped sinusoidal oscillation, such as the rigid body response, from a mixture of other signals which contain lightly damped oscillations near the rigid body frequency. This characteristic permits the use of the digital adaptive filter to produce fast responses to command steps. After the application of a step command the loop is effectively closed for the rigid body signal but is essentially open for the elastic and slosh modes.

The digital adaptive filter will provide firm control of the rigid body as long as a sizable control signal exists. When the control signal attenuates nothing passes through the digital adaptive filter. The loop then opens up completely. Since the rigid body is typically unstable on these vehicles, it then becomes necessary to use another control mode, the secondary filter, which is stable at the rigid and elastic body modes.

3.1 General Description of Digital Adaptive Filter

The digital adaptive filter acts on an immediate past section of length T of the signal $c(t)$ stored in the computer memory in a sampled form. This signal is compared with a damped sinusoidal signal $A\,\epsilon^{-\alpha t}\cos\beta t + B\,\epsilon^{-\alpha t}\sin\beta t$ of fixed frequency β and damping α, and the amplitude parameters A and B (or amplitude and phase) are estimated under the criterion,

$$\underset{A,B}{\text{Min}} \int_0^T \left[c(t) - A\,\epsilon^{-\alpha t}\cos\beta t - B\,\epsilon^{-\alpha t}\sin\beta t\right]^2 dt \qquad (10)$$

That is, A and B are calculated to produce minimum mean square deviation between the measured signal and the damped sinusoidal component.

It is assumed that α and β are known fairly accurately. It can be demonstrated that good estimates result from the computed A and B parameters provided α and β are within 10-20% of their actual values, α is relatively large, and that the remaining signal differs widely from the damped sinusoidal component of interest in damping or in frequency but not necessarily in both.

The working equations for the digital adaptive filters were established earlier (Reference 3). The working equations as used in this study are recorded in Appendices B and C.

3.2 Characteristics of the Digital Adaptive Filter

To evaluate the basic characteristics of the digital adaptive filter, both analytical and simulation studies were carried out. It is quite possible to analyze the characteristics of a digital adaptive filter when it is applied open loop in a linear system, since under these circumstances the signal passing through the filter will be the usual combination of exponential trigonometric and power functions. The filter is a linear one and consequently its effect on these assorted signal components can be studied separately. The output of the filter will not, however, consist of a combination of the same kind of functions as its input, since the filter is a time-varying system, at least until its memory is filled. Consequently, when such a filter is used as a part of a linear lumped constant system this system, even with a step input, will not respond in terms of damped sinusoidal and exponential functions. Consequently, it is very difficult to study a closed loop control system which includes a digital adaptive filter by analytical methods. Accordingly, the analytical studies were largely restricted to open loop systems, and the closed loop studies were carried out using hybrid simulation techniques.

There are basically two modes of operation for the digital adaptive filter. In the fade-in phase the filter memory is not filled. There is an additional sample at the end of every sampling interval and when this is added the record becomes longer by T seconds. The identification of A and B, therefore, is performed over the variable length of the record following the addition of each new sample. So during this mode of operation, the upper limit of the integral in Equation (10) is different at every sampling instant. As a result the digital adaptive filter is a time-varying linear element.

In the steady phase of the filter operation, the variable memory length is filled up, and when the most recent sample is added to the memory the oldest one is dropped. Then the fitting process is performed over a constant memory length and the upper limit of the integral in Equation (10) is fixed. The digital adaptive filter is then a stationary linear element.

To investigate the characteristics of the digital adaptive filter in both situations, it is expedient to study its effect on the various components of

signals found in the free responses of linear systems such as $e^{-at} \cos \gamma t$, $e^{-at} \sin \gamma t$. Equations for this study are established in Appendix E, and some numerical results are presented in Figures 45-49. Each of these figures presents in Part A the time history of the output of the filter and in Part B the time history of the A and B parameters established by the fitting process. In all these curves it was assumed that $\alpha = 1.0$ and $\beta = 1.0$ (which means the desired signal component has a damping factor of $\zeta = 0.707$ and a damped natural frequency of 1 radian per second.) In all these curves the assumption is that the filter starts working with an empty memory at $t = 0$ and the memory is filled as samples are received. When there are only a few samples in the memory there is not enough information for the filter for reliable operation. As a result, values of A and B will be rather erratic for the first one quarter to one half cycle of the desired response and then they settle down to essentially steady values. Correspondingly, the time responses of these outputs will show rather poor filtering characteristics during the initial one quarter to one half cycle, but undesirable signals are attenuated very effectively after this period.

As shown in Figure 45 effective attenuation is even present where the input signal $e^{-at} \sin \gamma t$ is of the same frequency ($\gamma = 1$) as the desired signal but with a different damping ($a = 0$). This illustrates the effectiveness of the digital adaptive filter in separating signals of the same frequency but different damping. When the frequency as well as the damping is different, as in Figures 46-48, the effective attenuation sets in even earlier. The case where the input is $e^{-at} \cos \gamma t$ is shown in Figure 49 with similar results. It should be noted that the A and B responses shown for fitting on a continuous basis were approached quite well when curve fitting of sampled data was done using ten samples per second or more. In Figures 50-53 other types of filter inputs are applied such as steps, ramps, stable and unstable exponentials. Because of the linearity of the digital adaptive filter its output can be obtained by superposition of the A and B parameters if the input signal is broken down into these basic forms. It should be remembered that in these runs the desired signal has a damping value of $\zeta = 0.707$, since the digital adaptive filter output does vary as a function of the α and β values used.

An example with low damping ($\alpha = .003$) for the fitted curve is shown in Figure 54. This figure illustrates the fact that the quality of filtering with the digital adaptive filter depends on the selection of a well damped desired signal. Fortunately the rigid body signal component of elastic missiles generally has this characteristic.

The preceding illustrations reveal that a uniformly good level of attenuation is reached when the memory length exceeds about 1/2 cycle of the desired signal and when this desired signal is well damped. Now after the fade-in phase, when the length of the memory is kept constant and the steady phase sets in, these good attenuation values will persist as far as the output of the system is concerned. Also, these good attenuation values will depend relatively little on the selection of the desired signal. This is illustrated in Figures 55-58.

These curves use the equations for the input signal stored in the memory from Appendix E.

The role of the digital adaptive filter is to separate a damped sinusoidal (rigid body response) with some particular frequency and damping out of a mixture of signals. Such a response will appear in the transient which will follow a discontinuity in the command input or in one of its derivatives. Usually monitoring for the discontinuities in the command input itself and its first derivative will suffice since discontinuities in higher derivative will tend to produce only relatively negligible transients. When a discontinuity is detected the digital adaptive filter is switched into the fade-in phase of operation with stepwise increasing memory length. Since the signal is available only in sampled form discontinuities will have to be monitored by monitoring the size of the first and second back differences. However, the back differences will not be zero even when there is no discontinuity. It is therefore important to select suitable levels of the differences above which a discontinuity is assumed and the fade-in phase is initiated. This limit should be such that no restart is made for even fast varying but continuous control signals, yet the fitting is restarted when a discontinuity is present in sufficient amplitude to initiate a significant transient.

Some aspects of this selection are discussed in the following.

1. The digital adaptive filter will restart if

$$\left| e(t) - e(t-T) \right| \geq L \tag{11}$$

and if

$$\left| e(t) - 2e(t-T) + e(t-2T) \right| \geq \dot{L} \tag{12}$$

where e(t) is the digital filter input signal, T is the sampling interval, and L and $\dot{L}$ are preselected values establishing the restart levels of the system discontinuities.

In order to obtain some insight into the characteristics of the fade-in process exponential ($e^{\alpha t}$) and sinusoidal (sine wt) wave forms were studied by computing the discontinuity levels L and $\dot{L}$ as a function of the sampling interval T.

The position discontinuity level L for the exponential $e^{\alpha t}$ is

$$\left| e^{\alpha t} - e^{\alpha(t-T)} \right| \geq L \tag{13}$$

which can be rewritten as

$$\left| e^{\alpha t} \left(1 - e^{-\alpha T}\right) \right| \geq L \tag{14}$$

Since two samples are required to evaluate equation (14) the discontinuity level of equation (14) will occur at the second sample when t=T. Figure 59a is a plot of this

maximum as a function of αT.

The rate discontinuity level for the exponential $e^{\alpha t}$ as mechanized in equation (12) is

$$\left| e^{\alpha t} - 2e^{\alpha(t-T)} + e^{\alpha(t-2T)} \right| \geq \dot{L} \tag{15}$$

This expression for the rate discontinuity is equivalent to

$$\left| e^{\alpha t} \left[1 - e^{-\alpha T} \right]^2 \right| \geq \dot{L} \tag{16}$$

which is plotted in Figure 59b as a function of αT for the time $t = T$.

For a value of L of .5, Figure 59a indicates that a discontinuity will occur for an αT of 0.4 for positive exponents and 0.66 for negative exponents. For a sampling rate of 20 samples per second, the α values become 8 and 13.2, respectively.

The position discontinuity level for a sine wave is

$$\left| \sin wt - \sin w(t-T) \right| \geq L \tag{17}$$

This expression is a maximum when $wt = \frac{wT}{2}$ or

$$\left| 2 \sin \frac{wT}{2} \right| \geq L \tag{18}$$

The rate discontinuity level for the sine wave is

$$\left| \sin wt - 2 \sin w(t-T) + \sin w(t-2T) \right| \geq \dot{L} \tag{19}$$

This expression is equivalent to

$$\left| 2 \left[1 - \cos w T \right] \sin w(t-T) \right| \geq \dot{L} \tag{20}$$

Equation (20) is a maximum with respect to time when $w(t-T) = \pi/2$ or

$$\left| 2 \left[1 - \cos wT \right] \right| \geq \dot{L} \tag{21}$$

Figure 60 shows the maximized restarting levels of L and $\dot{L}$ for a sine wave input of unity peak amplitude. L is shown to be essentially linear for the wT values shown. A position discontinuity level of .5 is exceeded for wT values greater than .5 or for a frequency of 10 radians/second for a sample rate of 20 samples/second ($T = .05$). The rate discontinuity level of $\dot{L} = .5$ is exceeded when wT is greater than .7 which corresponds to a frequency of 14 radians/second for a sample rate of 20 samples/second.

The use of the digital adaptive filter fade-in routine based on discontinuity levels of the input samples should be sufficient for most applications. If the input signals should include some large amplitude high frequency components which

might unduely trigger the fade-in process some low pass filtering of the input signal may be required. The bandpass of a filter of this type will usually be high enough to avoid affecting the basic rigid body signal components.

3.3 Fundamental Performance of Vehicle I with Digital Adaptive Filter

The digital adaptive filter produces fast and precise response to command inputs, particularly step command inputs. The filter accomplishes this by separating the principal rigid body component from the total error signal while suppressing the body bending and slosh modes. As a result the bending and slosh modes are operating essentially open loop during the control by the digital adaptive filter. If these modes are stable but poorly damped, they will ring with slowly decreasing amplitude during the operation of the digital adaptive filter. Consequently, the gain and compensating parameters associated with the digital adaptive filter can be selected without much regard to elastic and slosh stability. This then permits the selection of gains and compensation to produce a much higher performance rigid body compensation than would be possible when such a compensation is selected for the computer booster in a conventional manner.

The arrangements for the digital adaptive filter compensating circuit are shown for Vehicle I in solid lines in Figure 61 for lift-off and in Figure 62 for maximum q. It is customary to use rate feedback for the stabilization of the rigid body of aerodynamically unstable airframes like Vehicle I. It would be possible to use this kind of compensation in conjunction with the digital adaptive filter but it would not be the most advantageous type of application. The rate feedback would emphasize the amplitude of bending and other higher frequency modes in the error signal on which the digital adaptive filter acts and thereby make its task unnecessarily difficult. For this reason the arrangement shown in solid lines in Figures 61 and 62 is preferable. This incorporates a feed forward network of $\tau s/(\tau s+1)$ and a network inside the loop of $(1+\tau s)/(1+0.025\ s)$. Simple block diagram algebra reveals that this arrangement is equivalent to a control system with a rate feedback. The pole at $s = -1/0.025$ should be considered in this context as part of the basic compensating scheme.

Using the hybrid simulation the response of Vehicle I under the control of the digital adaptive filter was obtained. Results are shown in Figures 63 and 64 for lift-off and maximum q respectively. These show a very good step response with a peak time of 3.2 and 3.0 seconds respectively and a peak overshoot of .2 and .05 degrees. The runs shown in Figures 65 and 66 are identical respectively to Figures 63 and 64 except that the digital adaptive filter is replaced by a unity gain. As may be observed the system at maximum q is quite unstable at the bending and slosh modes; in other words, it could not be used without the digital adaptive filter. However, the runs in Figures 63 and 64 also become unstable in the rigid body at around 20 and 4 seconds respectively. The reason is that at some time previously the fitted curve, the output of the digital adaptive filter fades out. With no input signal to the airframe, the loop then opens up and the basic

aerodynamic instability of the airframe prevails.

It follows then, that some other mode of control must be introduced around this time. This may be a linear control system designed to give over-all stability but not necessarily high performance for step command inputs. One such compensator is shown in dashed lines on Figures 61 and 62. Figure 67 shows the combination run at maximum q where the digital adaptive filter is started at T = 0, the time of initiation of the command input step of one degree. The system then works under the control of the digital filter until 3.2 seconds at which time the secondary filter takes over. This run, shown in Figure 67, combines the fast response and elastic stability of the digital adaptive filter with the long range rigid body stability of the secondary filter.

It is important to emphasize that the secondary filter design shown in Figure 61 is not considered final at this time. Any of the designs proposed for use with the digital polynomial filter in the preceding sections could be used as a secondary filter (incorporating the digital polynomial filter). Then the secondary filter would provide over-all stability and stress relief while passing through the standard wind profile while the digital adaptive filter would be available to provide high performance response to step command inputs when needed.

In summary, the basic mode of operation for the system is as follows:

1) In the quiescent state the system is under the control of the secondary filter which may incorporate an acceleration or angle of attack feedback path with a digital polynomial filter or other low-pass filtering means for stress relief.

2) The command signal is continually monitored for steps or discontinuities using properly selected L and $\dot{L}$ as discussed in the preceding section. When a discontinuity is detected the fade in of the digital adaptive filter (control by the digital adaptive filter with gradually increasing memory length commencing with zero) is initiated.

3) After a fixed time interval elapses, control is returned to the secondary filter.

4) Since digital adaptive filter operation is not desired when the vehicle is subjected to large wind disturbance inputs, the fade-in process may also have to be used on the filtered vehicle acceleration (or angle of attack) signals to prevent the digital adaptive filter operation.

3.4 Conventions for Evaluating Performance with the Digital Filter

In this digest, response curves of the individual runs are presented only as occasional illustrations. The principal information contained in the bulk of the simulation runs has been reduced and is presented in a tabulated form. A total of six quantities have been measured in the response curves and values

for each are presented in the tables. Some of these are conventional definitions, others have been derived for the specific needs of the digital adaptive filter control. A list of the definitions follows with reference to Figure 68, which is the sketch of a typical rigid body response obtained with the digital adaptive filter control loop.

a) Overshoot, m - The ratio of maximum rigid body amplitude over the height of the input step to the amplitude of the input step. A negative value of m implies an undershoot, expressed in percent.

b) Rise time, T_r - The time measured from the application of the step input to the instant where the commanded value is crossed - units of seconds.

c) Peak time, T_p - The time measured from the application of the step input to the instant of reaching the maximum rigid body overshoot - units of seconds.

d) Holding time, T_h - The time interval following the application of the step during which the rigid body response is held within ± 25 percent of the height of the step input. In some cases a ± 50 percent strip was used as indicated in the tables - units of seconds.

e) Leaving slope, S - The slope at which the response curve leaves the ± 25 percent (or ± 50 percent) strip of holding. With reference to Figure 68 S = Tan ψ (length of one degree in inches/length of one second in inches). Positive values of S indicate a divergence away from zero; negative values of S indicate a divergence toward zero - units of degrees per second.

f) Relative engine deflection, δ/θ_c - The maximum engine deflection in degrees required to produce one degree step displacement of the attitude angle-nondimensional.

These six quantities are recorded in the following tabulations of the parametric study in Tables XXI through XXIV under the heading "Reduced Data." In the left-hand section of the table under the heading "Identification" the vehicle and flight condition is identified and the presence or absence of the secondary filter is stated. Any parameters which deviate from the nominal ones shown in Figure 68 are also listed. The actual parameter value is usually expressed in percentages of the nominal, except where the nominal is zero. The parameters which have off nominal values throughout an individual table are listed in the top left portion of the table under "Identification." The parameters which vary from run to run are individually listed in the left-hand side section of the table. Each line of the tables represents an individual run.

3.4.1 Documentation of Sensitivity to Fitting Parameters. - The performance of the digital adaptive filter is reasonably insensitive to variations in the parameters which must be selected for the operation of the digital adaptive filter loop. Most important among these are α and β, the damping and frequency of the desired damped sinusoidal mode which represents the rigid body transient component.

Tables XXI and XXII show at lift-off and at maximum q, respectively, the variation of the sets of performance numbers defined in Figure 68 with variations of the α and β values assumed for the fitting. It is indicated that there is a $\pm$ 10 to $\pm$ 20% range of α and β variation within which the response is satisfactory. This is important, because the damping and frequency of the rigid body will only be known approximately and is subject to variation during the flight. It should be possible, however, to place the α and β values selected for the fitting process within $\pm$ 20% of the actual damping and frequency of the rigid body.

Another group of parameters connected with the digital adaptive filter consists of the sampling rate and the number of samples which together determine the length of the fitting interval after the memory is filled. Table XXIII illustrates, for the lift-off condition, that the performance of the system is quite insensitive to the selection of these parameters provided that there are more than ten samples and the memory is not much shorter than half a predominant rigid body cycle.

3.4.2 Documentation of Sensitivity to Compensating Parameters.- The effect of variation in the compensating network parameters was investigated at lift-off flight condition. The results are summarized in Table XXIV which reveals no sensitivity that could cause a problem.

3.4.3 Documentation of Sensitivity to Airframe Parameters.- One outstanding characteristic of the digital adaptive filter is its insensitivity to variations of airframe parameters, especially frequencies of bending modes. This is illustrated in Figure 69 which reveals that even with variations of -20% at the first bending mode, -50% at the second, and -50% at the third the performance is not seriously deteriorated from the nominal case shown in Figure 63.

3.4.4 Digital Adaptive Filter in Wind.- The digital adaptive filter is a means of improving the performance of highly elastic boosters on step command inputs. It is not a means of improving performance in wind or during the time when the vehicle is passing through windshear profiles. The only thing which can be expected from the digital filter during a passage through the standard windshear profile is that it does not seriously impare the quality of control during this period. The digital adaptive filter can actually fulfill this expectation as is illustrated in Figure 70 where the filter is cut in during the flight through the standard wind profile at 5.2 seconds for a 3.4 second duration. When placed in the circuit, it will make an effort to quickly reduce the existing attitude errors to zero as is evident in Figure 70. Such reduction is fundamentally opposite to the purpose of drift minimum control which attempts stress relief through controlled drift. Consequently, the operation of the digital filter is not desirable during the passage through the wind profile.

3.5 Evaluation of Results

The digital adaptive filter is a means for improving the transient response to step command inputs to a large launch vehicle typified by Study Vehicle I. Results at both lift-off and maximum dynamic pressure flight conditions show response times of less than 3.2 seconds with acceptable overshoot characteristics. The filter was found to be quite insensitive to parameter variations in the filtering routine, in the compensating circuits, or in the airframe itself.

The digital filter is not designed to reduce excessive stress or excessive engine deflections while the missile is passing through a severe wind profile. For these purposes, the remedies are best achieved through the application of filtered acceleration or angle of attack feedback as discussed in the preceding section of this report. The digital adaptive filter is most responsive to step input commands and would thus require resolution of command inputs into a series of steps. Studies required to establish the limits on the step size necessary for discrimination from noise and to evaluate the effect on payload performance were judged by the MSFC sponsors of this study and by McDonnell to have a low probability of demonstrating the applicability of the digital adaptive filter to large launch vehicles. As a consequence, effort was diverted to the study of the digital polynomial filter.

It should be mentioned finally that these studies do not include an investigation of the burnout flight condition for Vehicle I which presents the additional difficulty of having the first bending mode unstable in the open loop due to cross coupling with the slosh modes. (This open loop bending instability was also present in Vehicle II at the maximum q and burnout flight conditions.) The digital adaptive filter effectively opens up the loop for the bending modes, and if they are stable on an open loop basis, they will ring harmlessly even though their damping may be small. If, however, the bending modes are unstable open loop, the amplitude of the oscillation will build up. Even so, the digital adaptive filter curve fitting process can still operate effectively provided that the stability compensation network keeps the bending mode response from diverging to too large an amplitude before control is switched to the secondary filter. The presence of an open loop instability of the body bending modes precludes the use of periodic restarting of the digital adaptive filter suggested in Reference 3 and places a larger burden on the design of the secondary filter. Another approach suggested by these studies is the use of the residual error signal, the difference between the error signal and the digital filter output signal, for damping of the bending modes through an appropriate network. This type of control, however, was not developed because of the shift of interest in the program from the digital adaptive filter to the digital polynomial filter.

4. REFERENCES

1. NASA Technical Note D-555, "Theory of Artificial Stabilization Missiles and Space Vehicles with Exposition of Four Control Principles," Hoelker, R. F., George L. Marshall Space Flight Center, Huntsville, Alabama.

2. Hildebrand, F. B., "Introduction to Numerical Analysis," McGraw Hill, 1956

3. Aeronautical Systems Division TR-63-251, "Development of the Digital Adaptive Filter Technique," Zaborszky, J., Luedde, W. J., and Wendl, M. dated April 1963.

4. "A Model Vehicle for Adaptive Control Studies and Model Vehicle #2 for Advanced Control Studies," Working papers, containing Vehicle Equations of Motion and Aerodynamic Coefficients, prepared by the George L. Marshall Space Flight Center, July 1964

5. AIEE Transactions, Part II, "A Computer Oriented Iterative Design of Linear Control Systems to Open and Closed Loop Specifications," Zaborszky, J., Marsh, R. G., 1962

6. IEEE Transactions Paper 6344, "Multivariable Adaptive Computer Control by Identification Feedback," Zaborszky, J., and Berger, R. L., 1962

7. Masters Thesis, Washington University, "An Iterative Method for the Design of Linear Servo-Mechanisms," Gildenberg, D. I. June 1962

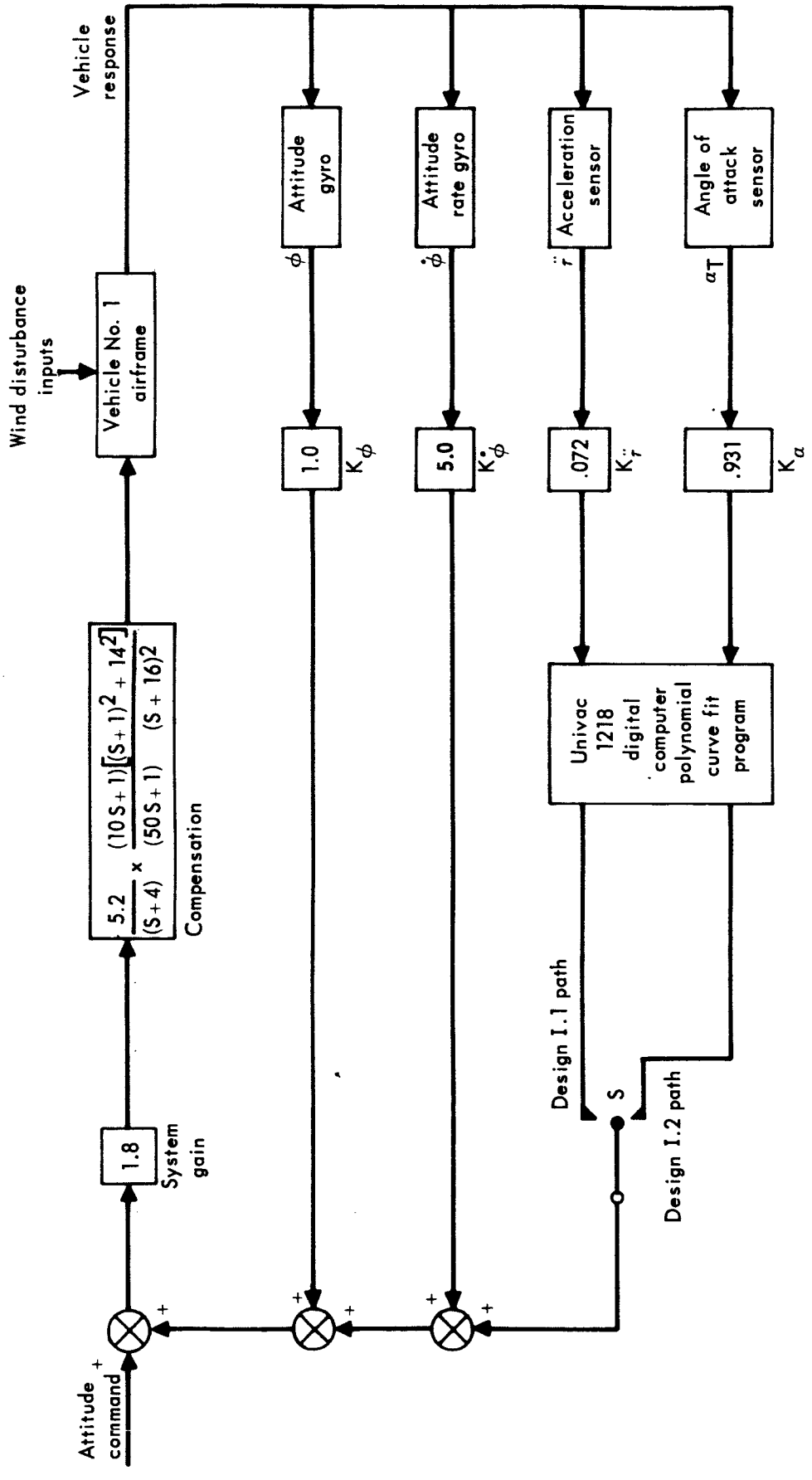

Figure 1 Block Diagram of Study Vehicle No. 1 Control Systems with Polynomial Fitting.

1. Flight condition, maximum q
2. Body bending and fuel slosh, in
3. Control system design, I.1
4. Forward loop gain, K = 1.8
5. Position feedback gain, $K_\phi = 1.0$
6. Rate feedback gain, $K_{\dot{\phi}} = 5.0$
7. Acceleration feedback gain, $K_{\ddot{r}} = 0$

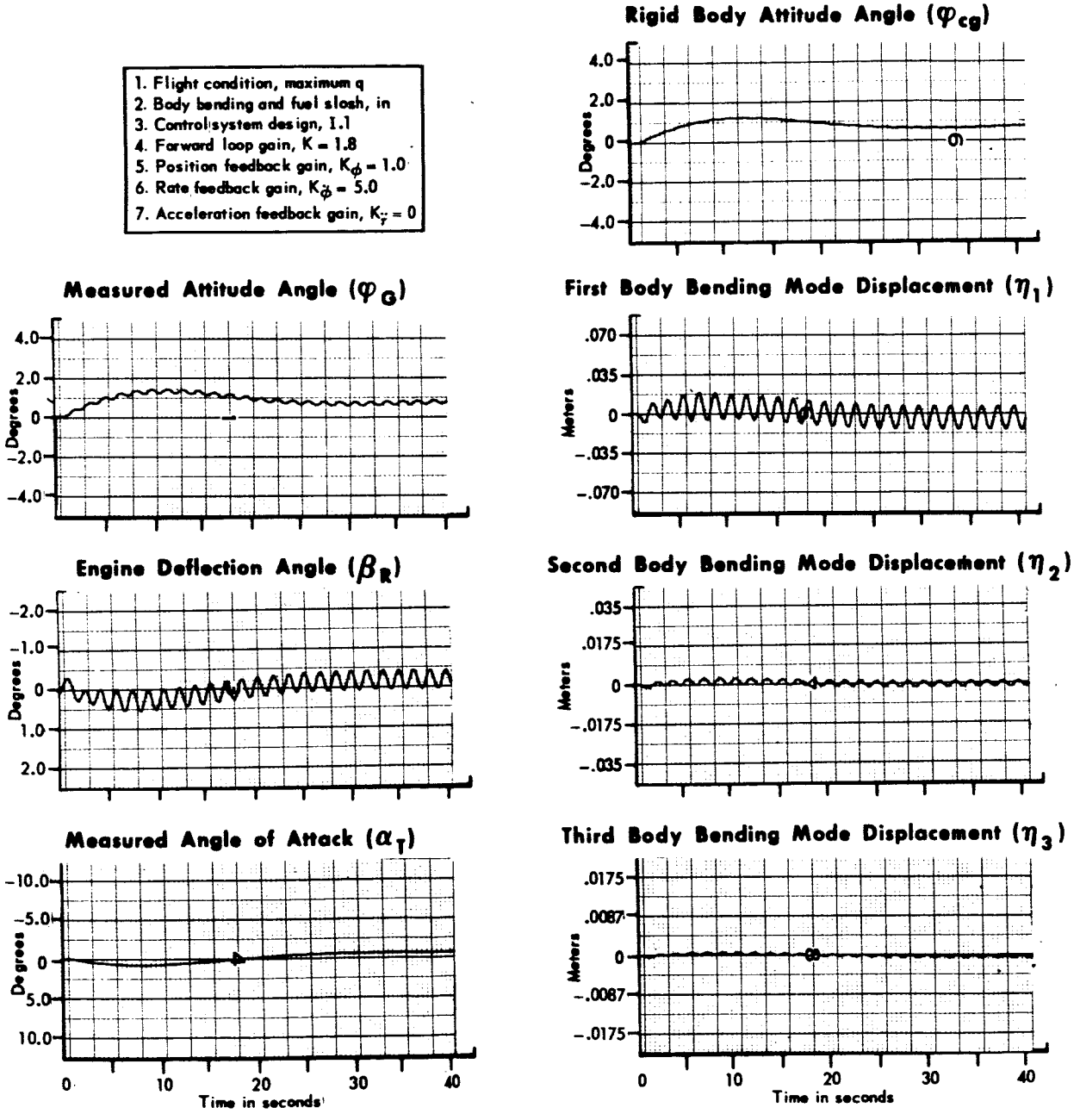

Figure 2 Unit Step Response of Study Vehicle No. 1 With Attitude and Attitude Rate Feedback

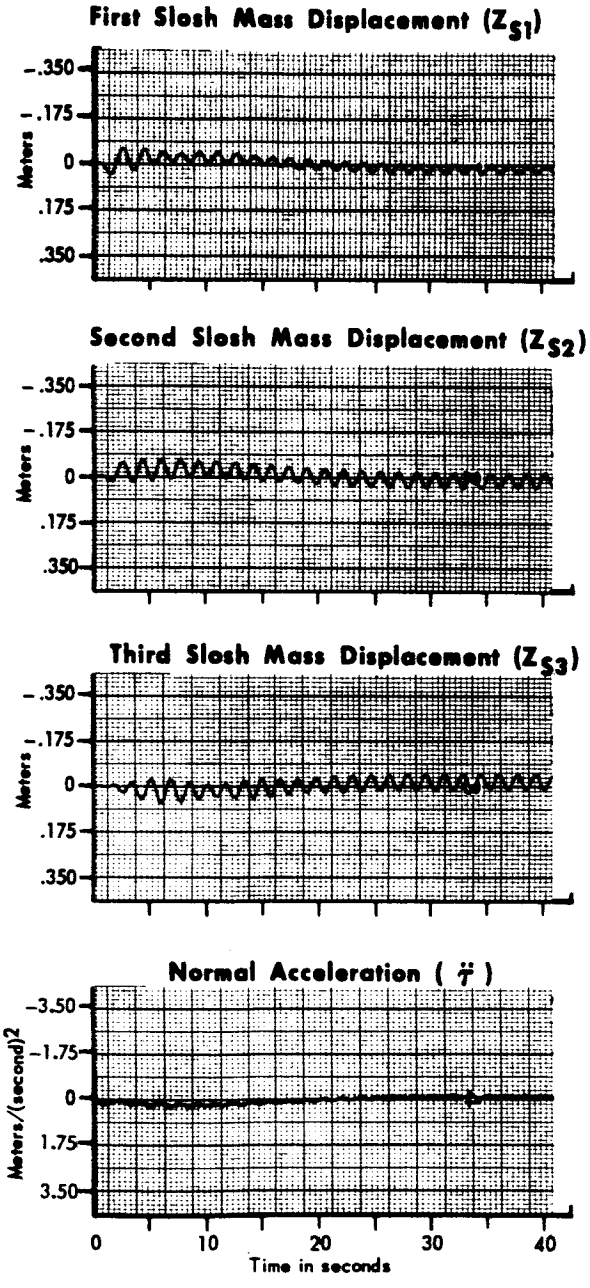

Figure 2 Unit Step Response of Study Vehicle No. 1 With Attitude and Attitude Rate Feedback (Cont.)

1. Flight condition, maximum q 2. Body bending and fuel slosh, out 3. Control system design, I.1 4. Forward loop gain, K = 1.8	5. Position feedback gain, K_{ϕ} = 1.0 6. Rate feedback gain, $K_{\dot{\phi}}$ = 5.0 7. Acceleration feedback gain, $K_{\ddot{r}}$ = 0

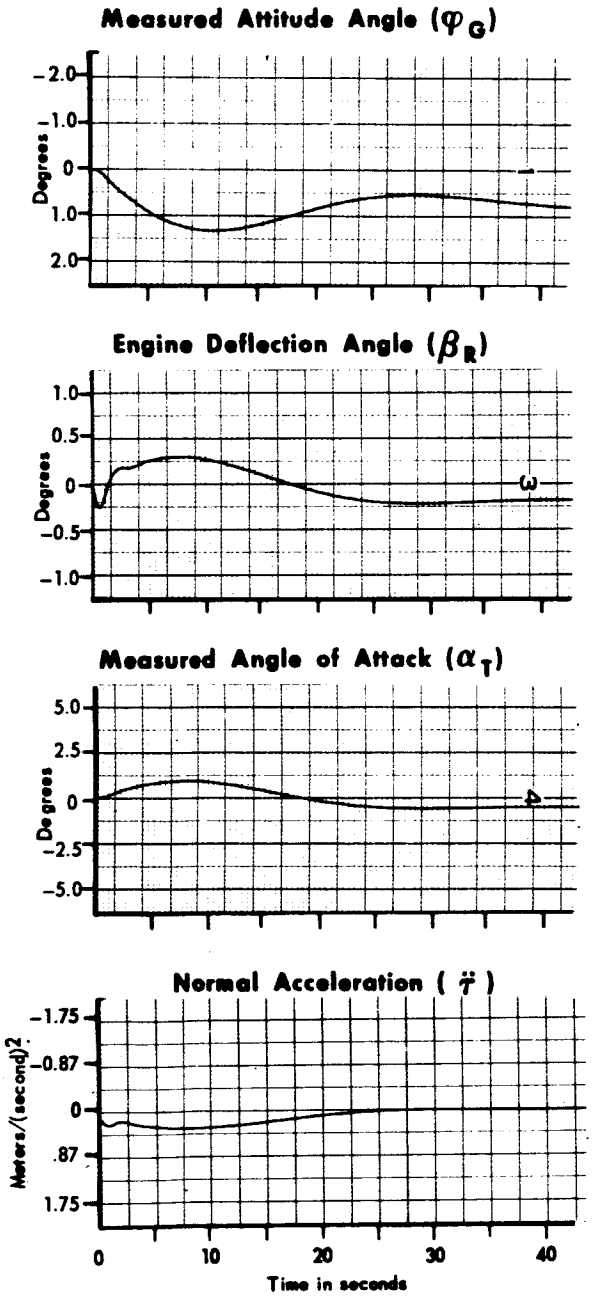

Figure 3 Unit Step Response of Study Vehicle No. I With Attitude and Attitude Rate Feedback

1. Flight condition, maximum q	4. Forward loop gain, K = 1.8
2. Body bending and fuel slosh, in	5. Position feedback gain, K_ϕ = 1.0
3. Control system design, I.1	6. Rate feedback gain, $K_{\dot{\phi}}$ = 5.0
	7. Acceleration feedback gain, K_r = 0

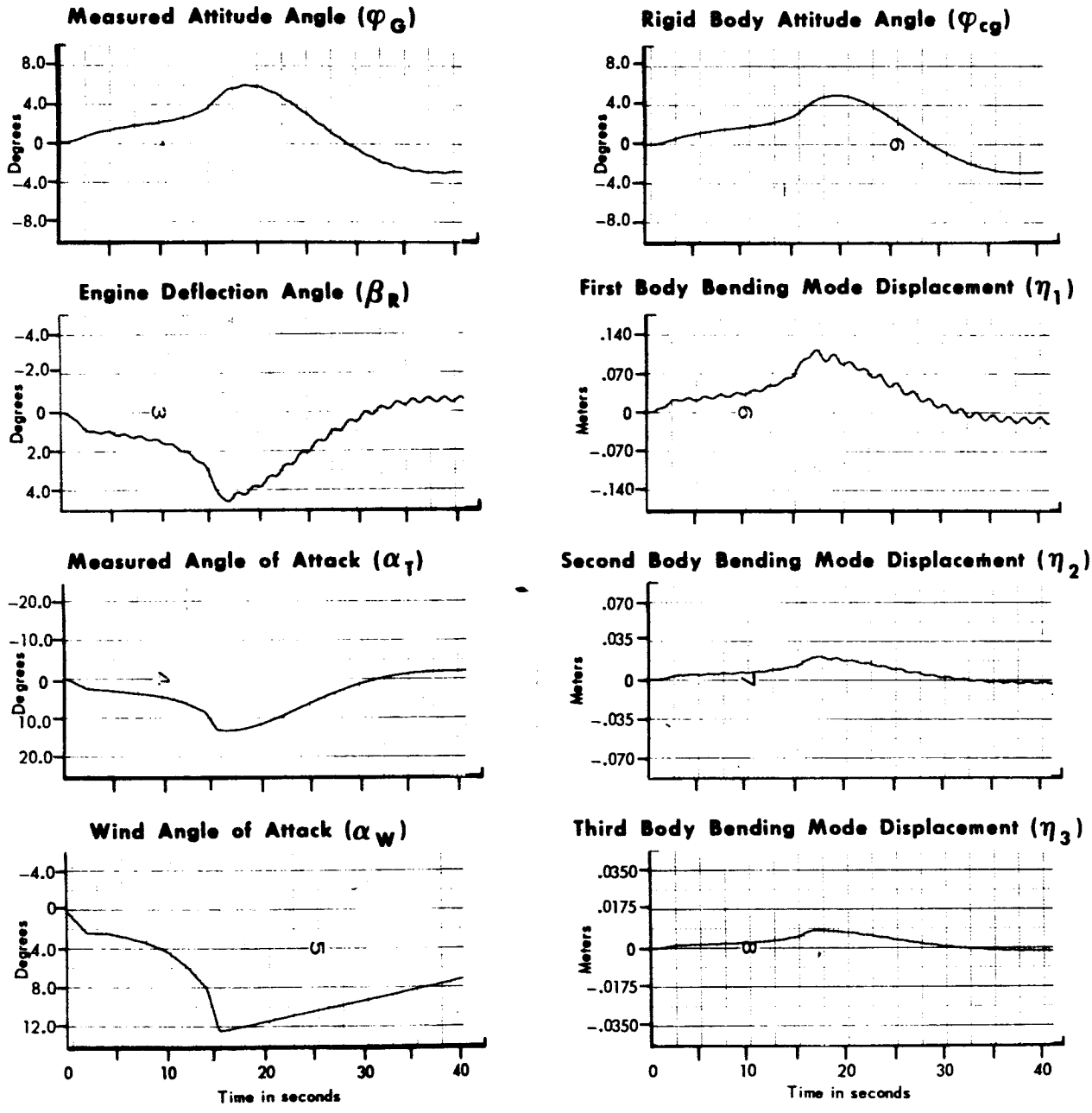

Figure 4 Wind Response of Study Vehicle No. I With Attitude and Attitude Rate Feedback

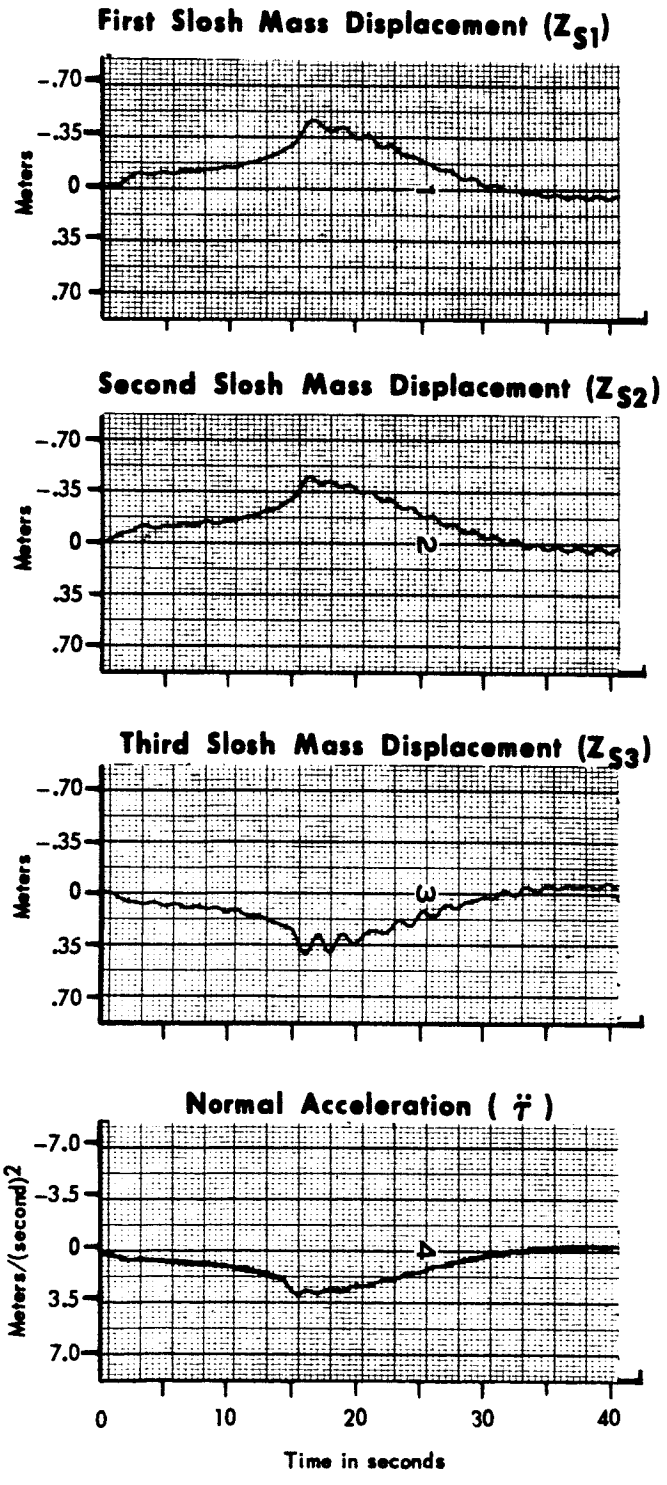

Figure 4 Wind Response of Study Vehicle No. I With Attitude and Attitude Rate Feedback (Cont.)

1. Flight condition, maximum q
2. Body bending and fuel slosh, out
3. Control system design, I.1
4. Forward loop gain, K = 1.8
5. Position feedback gain, K_ϕ = 1.0
6. Rate feedback gain, $K_{\dot{\phi}}$ = 5.0
7. Acceleration feedback gain, $K_{\ddot{\psi}}$ = 0

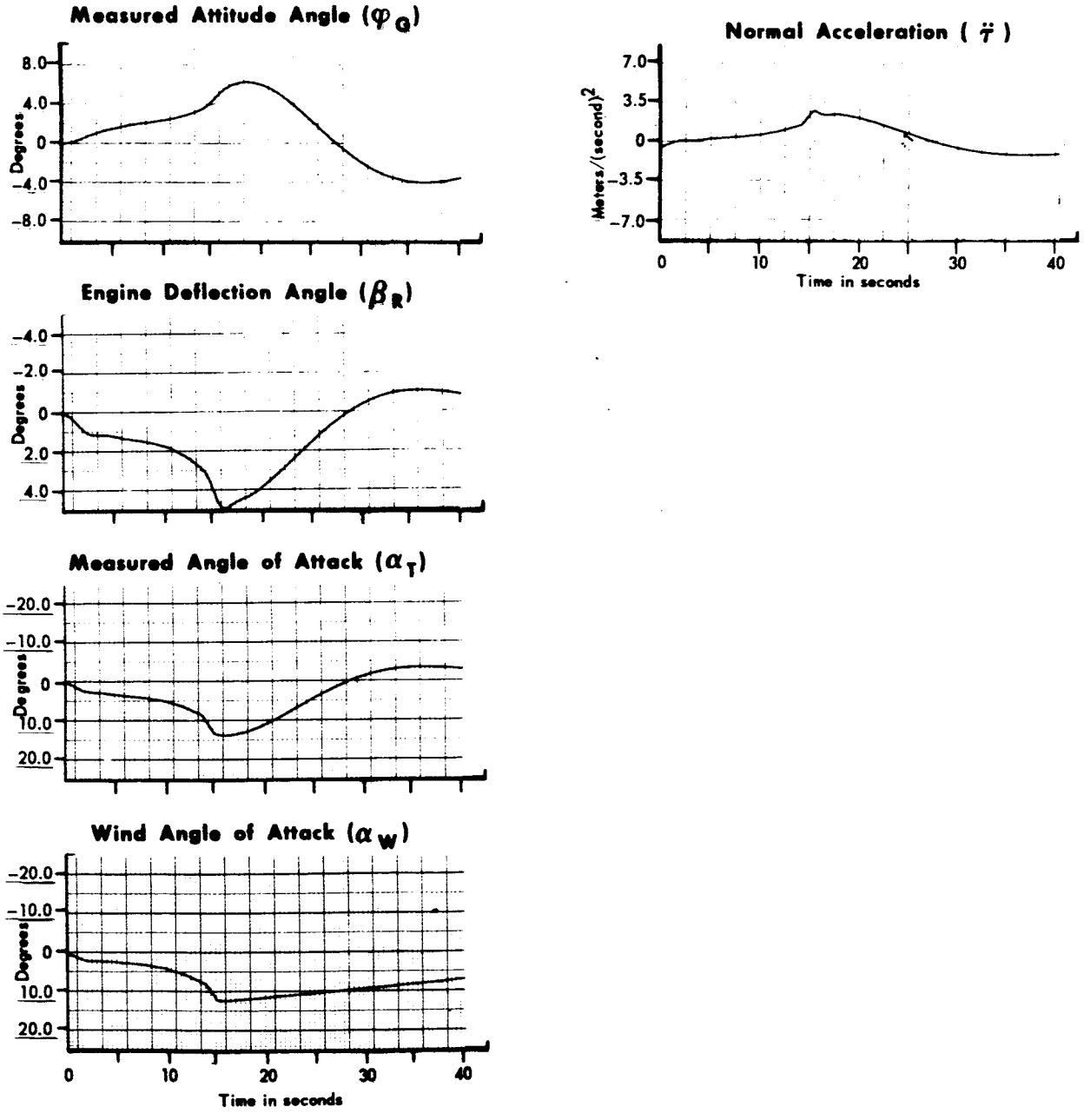

Figure 5 Wind Response of Study Vehicle No. I With Attitude and Attitude Rate Feedback

1. Flight condition, maximum q 2. Body bending and fuel slosh, in 3. Control system design, I.1 4. Forward loop gain, K = 1.8	5. Position feedback gain, $K_{\phi} = 1.0$ 6. Rate feedback gain, $K_{\dot{\phi}} = 5.0$ 7. Acceleration feedback gain, $K_{\ddot{r}} = 0.072$ 8. No polynomial fitting in acceleration feedback

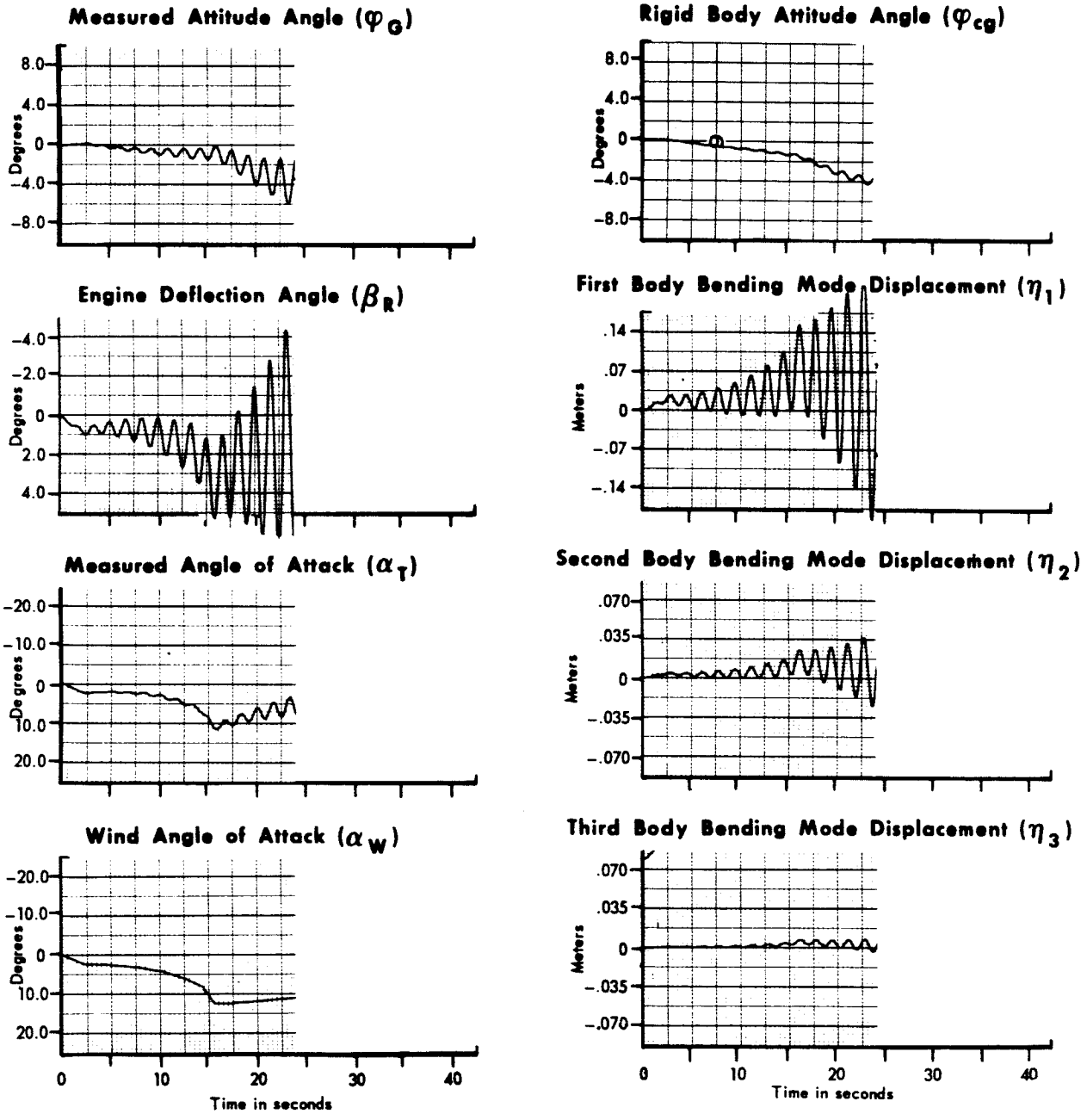

Figure 6 Wind Response of Study Vehicle No. I Without Filtering in the Acceleration Feedback Loop

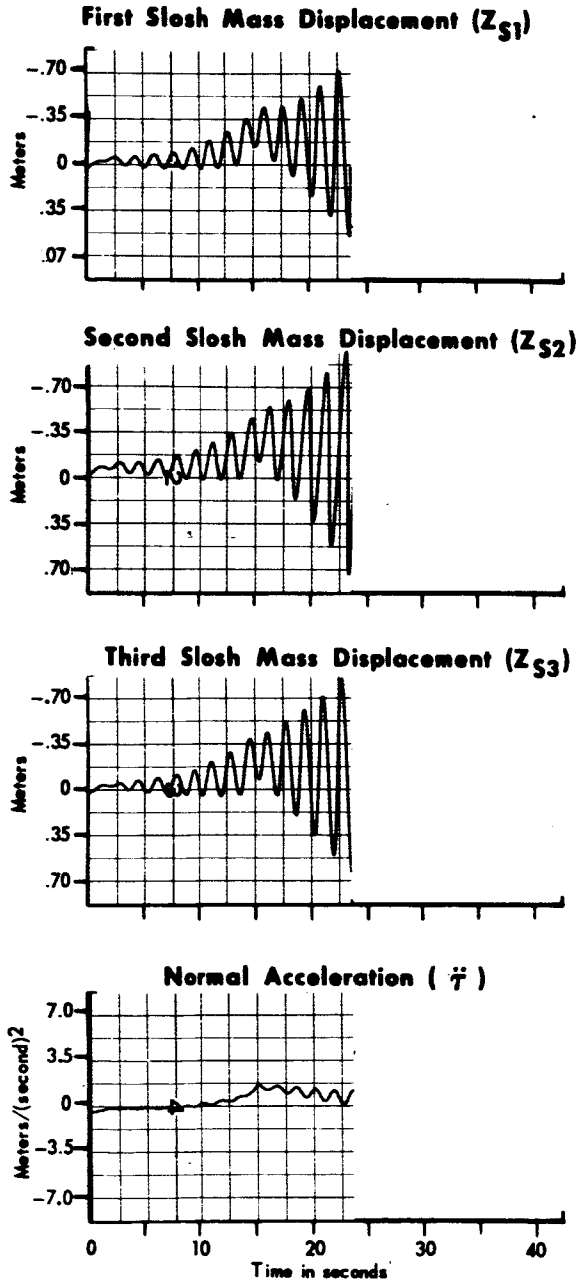

Figure 6 Wind Response of Study Vehicle No. 1 Without Filtering in the Acceleration Feedback Loop (Cont.)

1. Flight condition, maximum q	6. Rate feedback gain, $K_{\dot{\varphi}}$ = 5.0
2. Body bending and fuel slosh, out	7. Acceleration feedback gain $K_{\ddot{r}}$ = 0.072
3. Control system design, I.1	8. No polynomial fitting in acceleration feedback.
4. Forward loop gain, K = 1.8	
5. Position feedback gain, K_{ϕ} = 1.0	

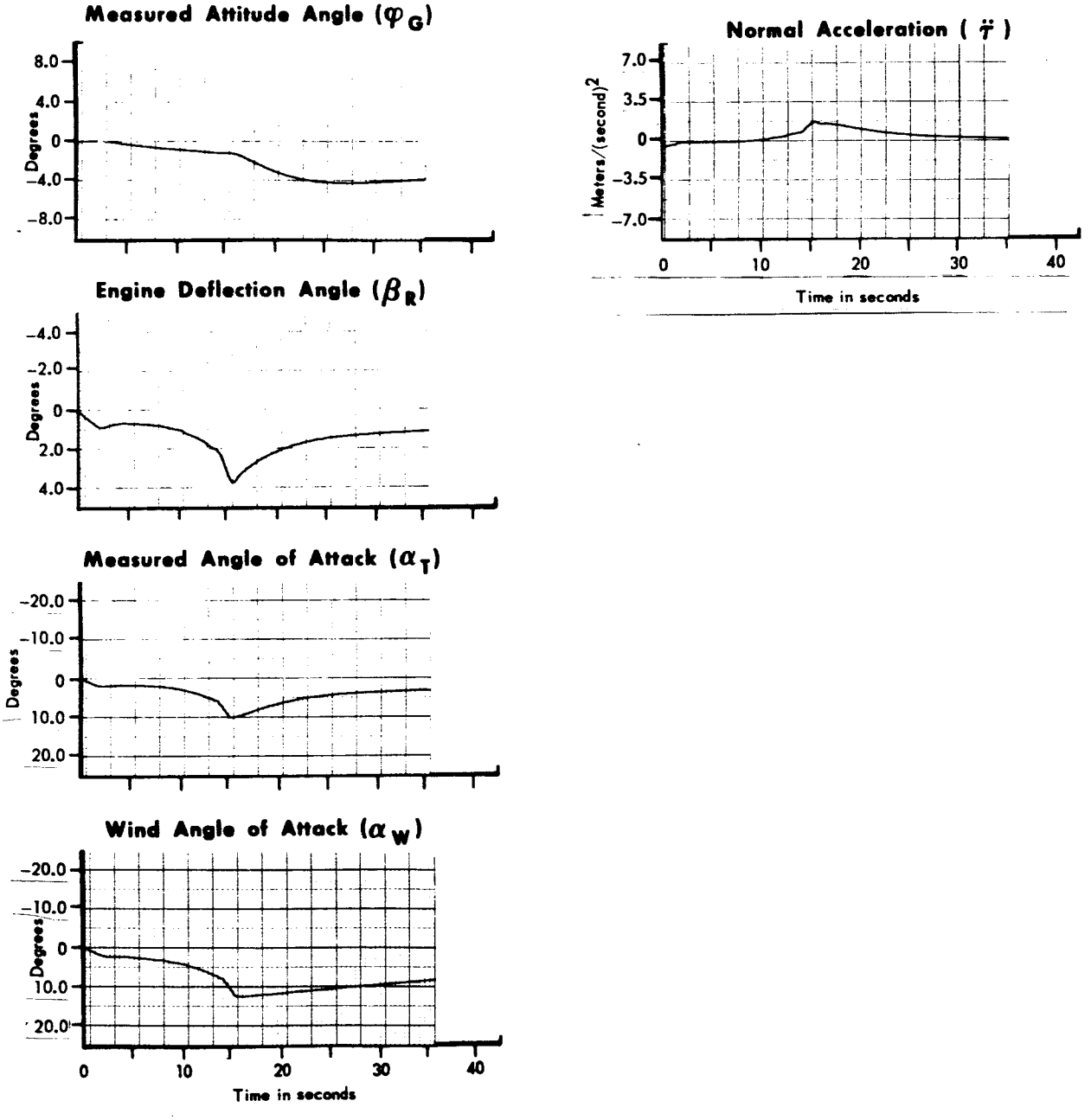

Figure 7 Wind Response of Study Vehicle No. 1 Without Filtering in the Acceleration Feedback Loop

1. Flight condition, maximum q	6. Control system design, I.1
2. Body bending and fuel slosh, in	7. Forward loop gain, K = 1.8
3. Polynomial fitting in acceleration feedback, zero degree (A_0)	8. Position feedback gain, K_ϕ = 1.0
4. Past samples stored, 25	9. Rate feedback gain, $K_{\dot\phi}$ = 5.0
5. Sample rate, 5 per second	10. Acceleration feedback gain, $K_{\ddot\gamma}$ = 0.072

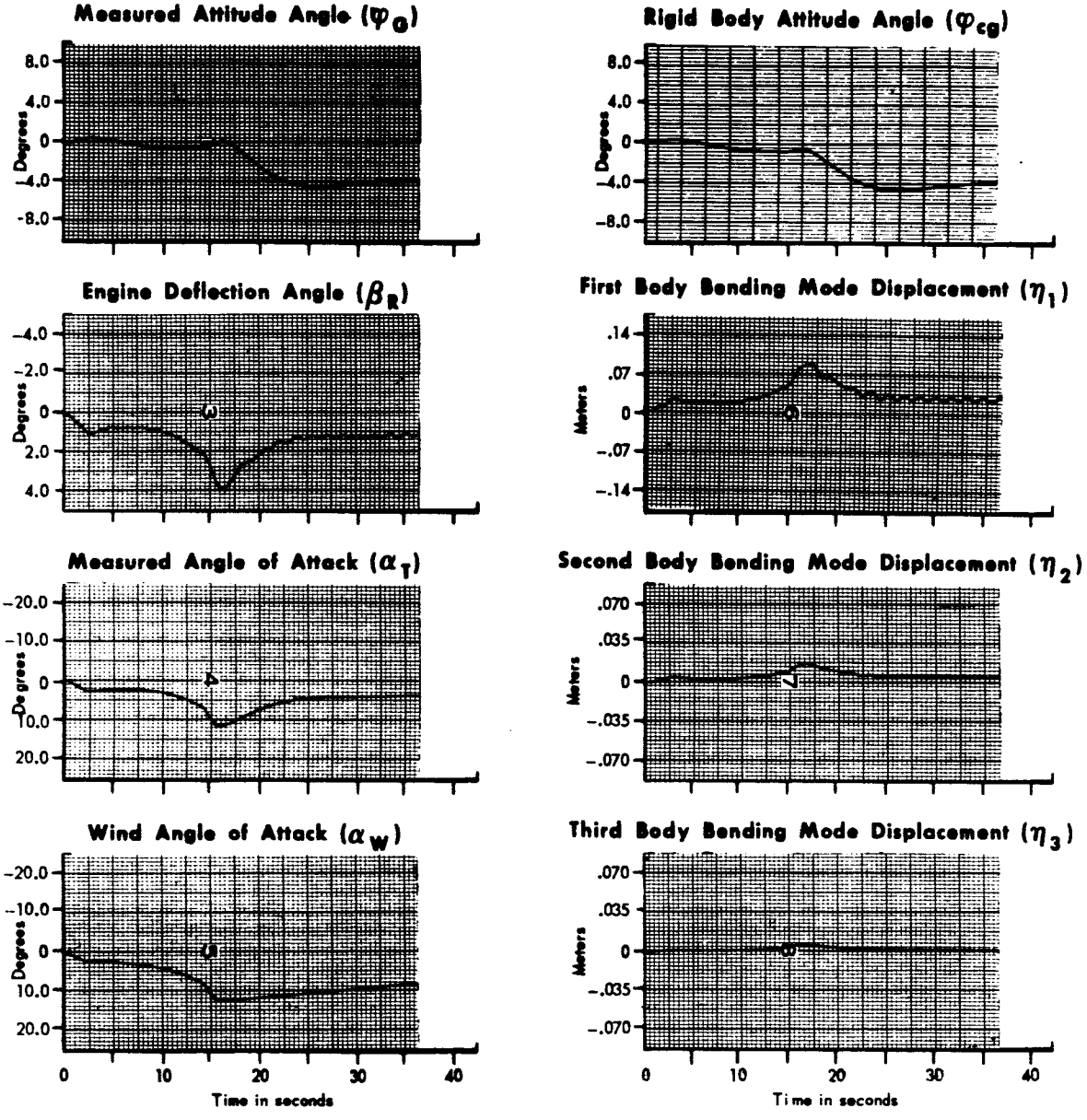

Figure 8 Wind Response of Study Vehicle No. 1 With the Digital Polynomial Filter in the Acceleration Feedback Loop

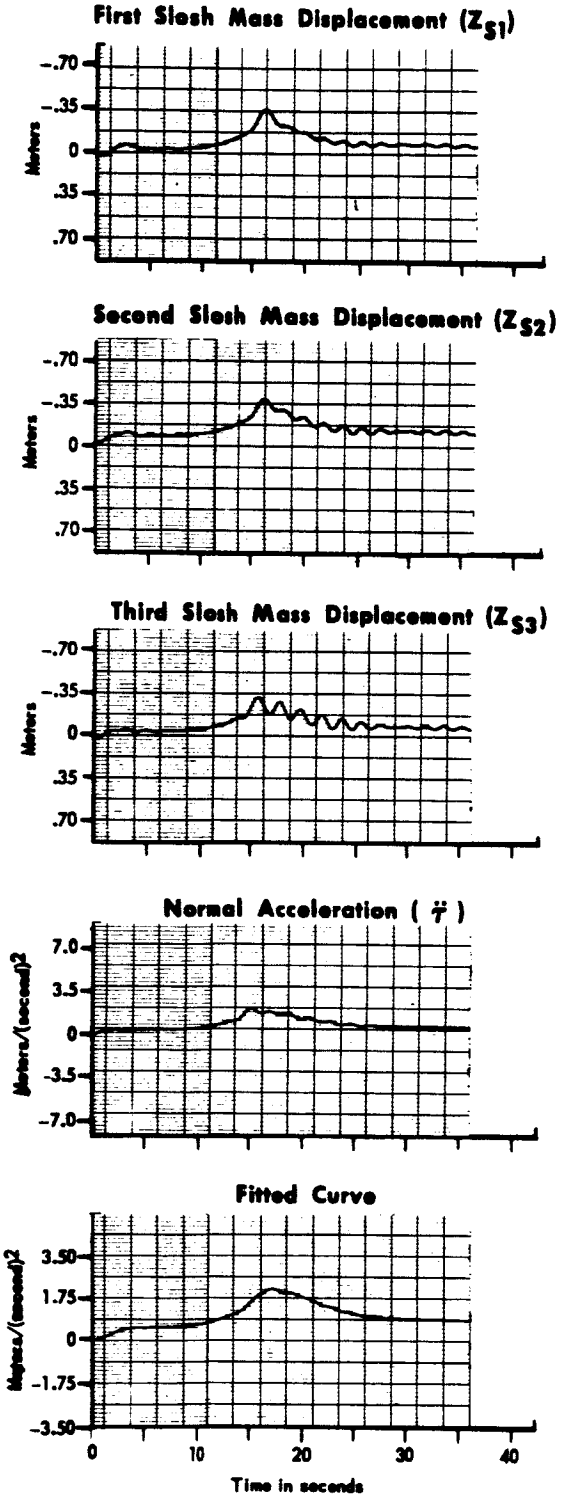

Figure 8 Wind Response of Study Vehicle No. 1 With the Digital Polynomial Filter in the Acceleration Feedback Loop (Cont.)

1. Flight condition, maximum q 2. Body bending and fuel slosh, out 3. Polynomial fitting in acceleration feedback, zero degree (A_0) 4. Past samples stored, 25 5. Sample rate, 5 per second	6. Control system design, I.1 7. Forward loop gain, K = 1.8 8. Position feedback gain, K_ϕ = 1.0 9. Rate feedback gain, $K_{\dot\phi}$ = 5.0 10. Acceleration feedback gain, $K_{\ddot r}$ = 0.072

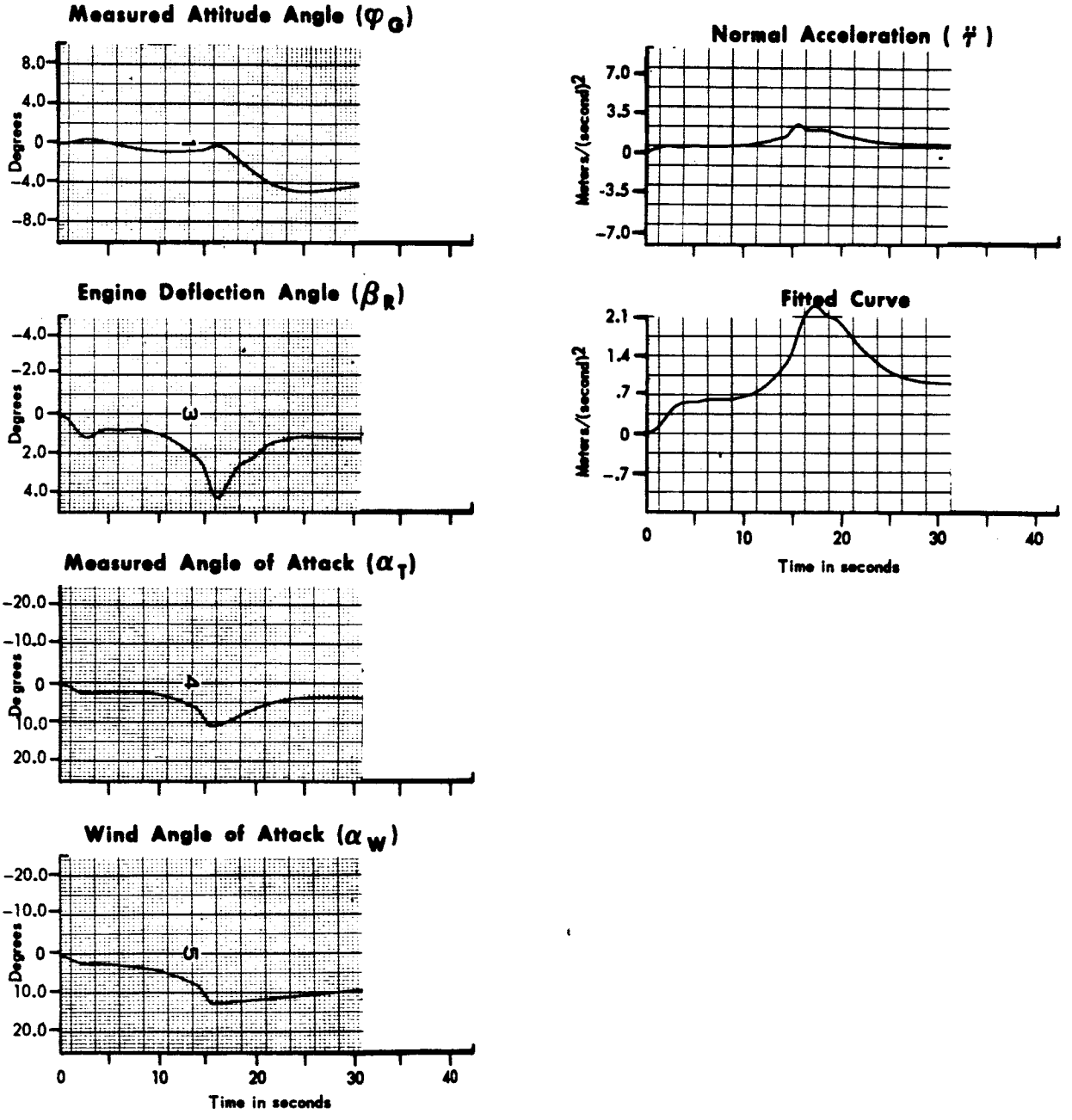

Figure 9 Wind Response of Study Vehicle No. 1 With the Digital Polynomial Filter in the Acceleration Feedback Loop

1. Flight condition, maximum q
2. Body bending and fuel slosh, in
3. Polynomial fitting in acceleration feedback, zero degree (A_0)
4. Past samples stored, 25
5. Sample rate, 5 per second
6. Control system design, I.1
7. Forward loop gain, K = 1.8
8. Position feedback gain, $K_{\dot{\phi}} = 1.0$
9. Rate feedback gain, $K_{\ddot{\phi}} = 5.0$
10. Acceleration feedback gain, $K_{\ddot{r}} = 0.072$

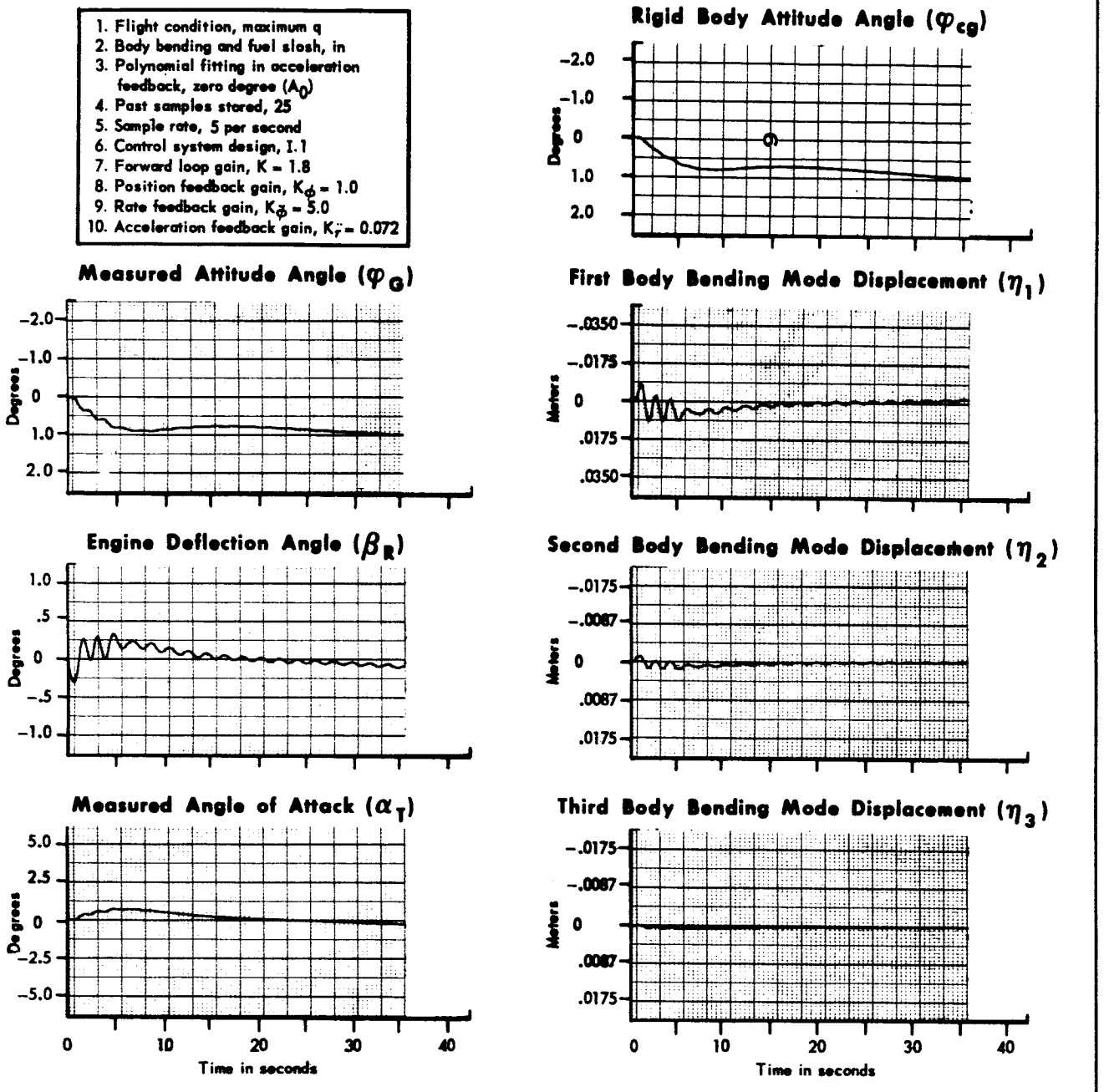

Figure 10 Unit Step Response of Study Vehicle No. 1 With the Digital Polynomial Filter in the Acceleration Feedback Loop

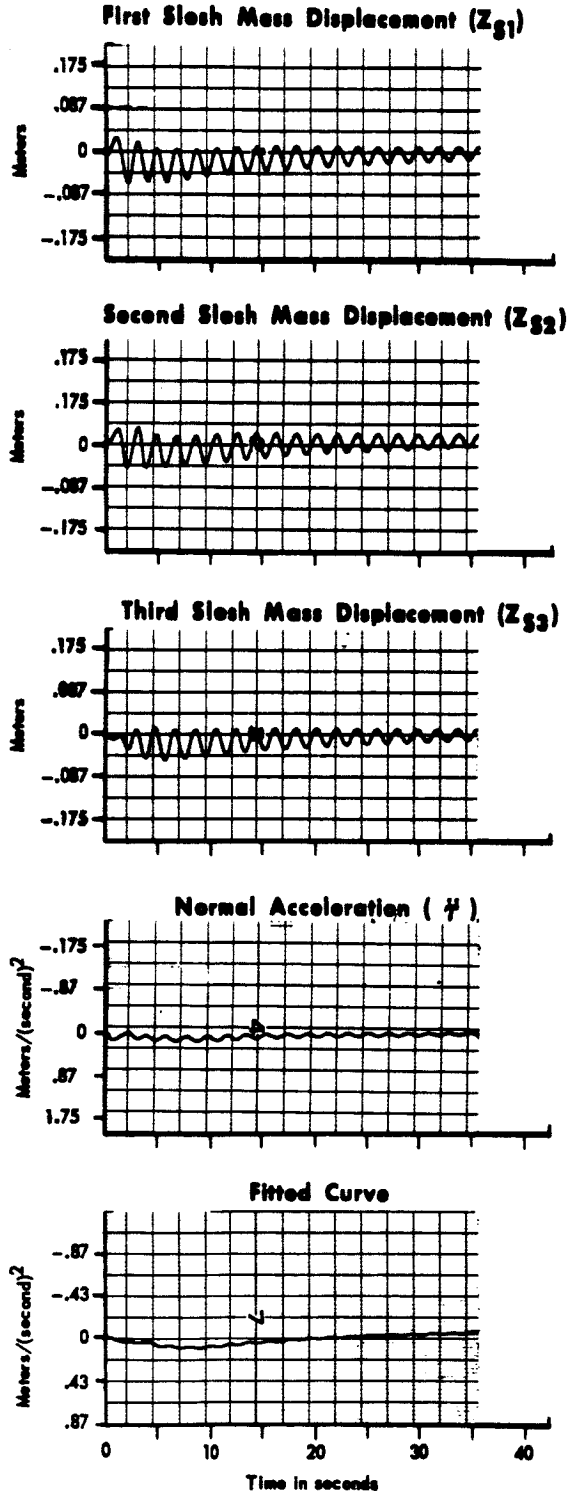

Figure 10 Unit Step Response of Study Vehicle No. 1 With the Digital Polynomial Filter in the Acceleration Feedback Loop (Cont.)

1. Flight condition, maximum q 2. Body bending and fuel slosh out 3. Polynomial fitting in acceleration feedback, zero degree (A_0) 4. Past samples stored, 25 5. Sample rate, 5 per second	6. Control system design, I-1 7. Forward loop gain, K = 1.8 8. Position feedback gain, K_ϕ = 1.0 9. Rate feedback gain, $K_{\dot{\phi}}$ = 3.0 10. Acceleration feedback gain, $K_{\ddot{\gamma}}$ = 0.072

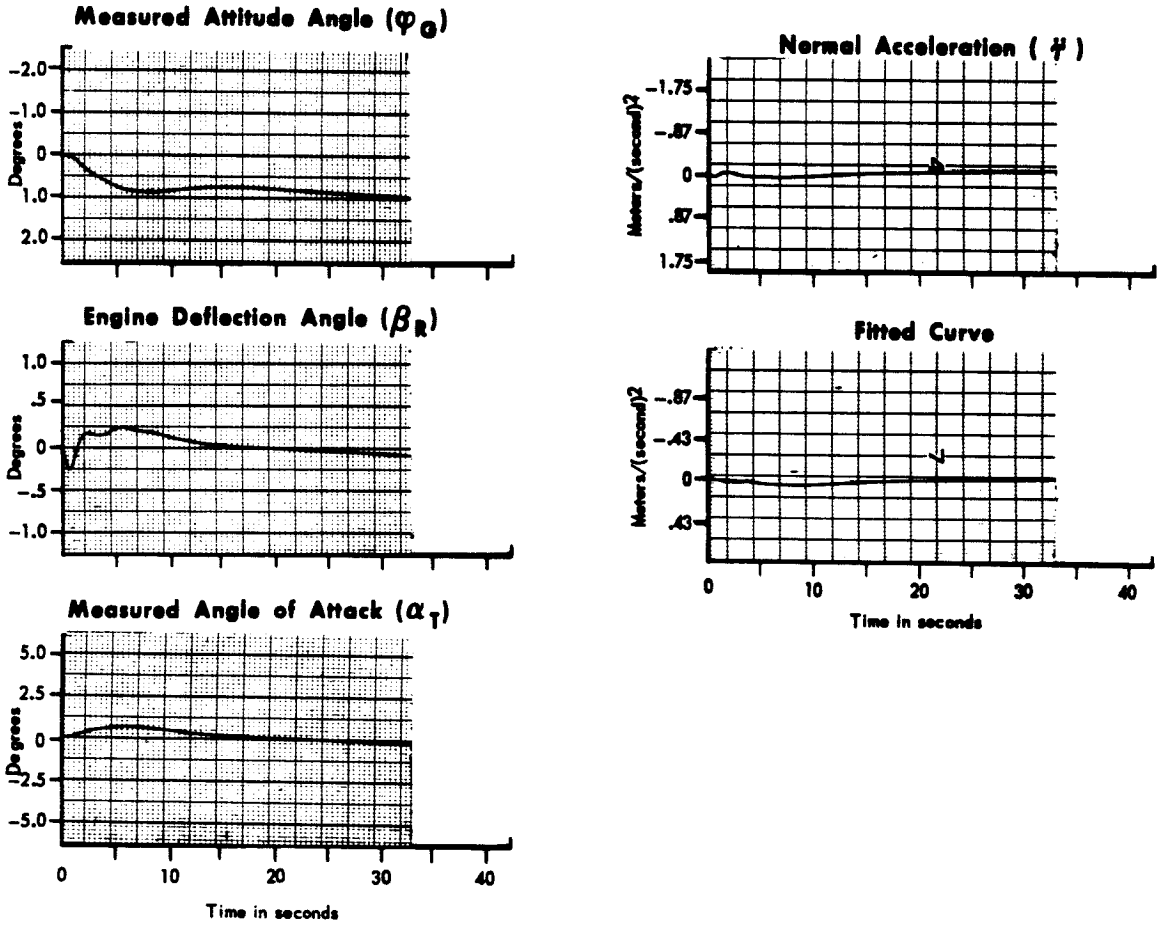

Figure 11 Unit Step Response of Study Vehicle No. 1 With the Digital Polynomial Filter in the Acceleration Feedback Loop

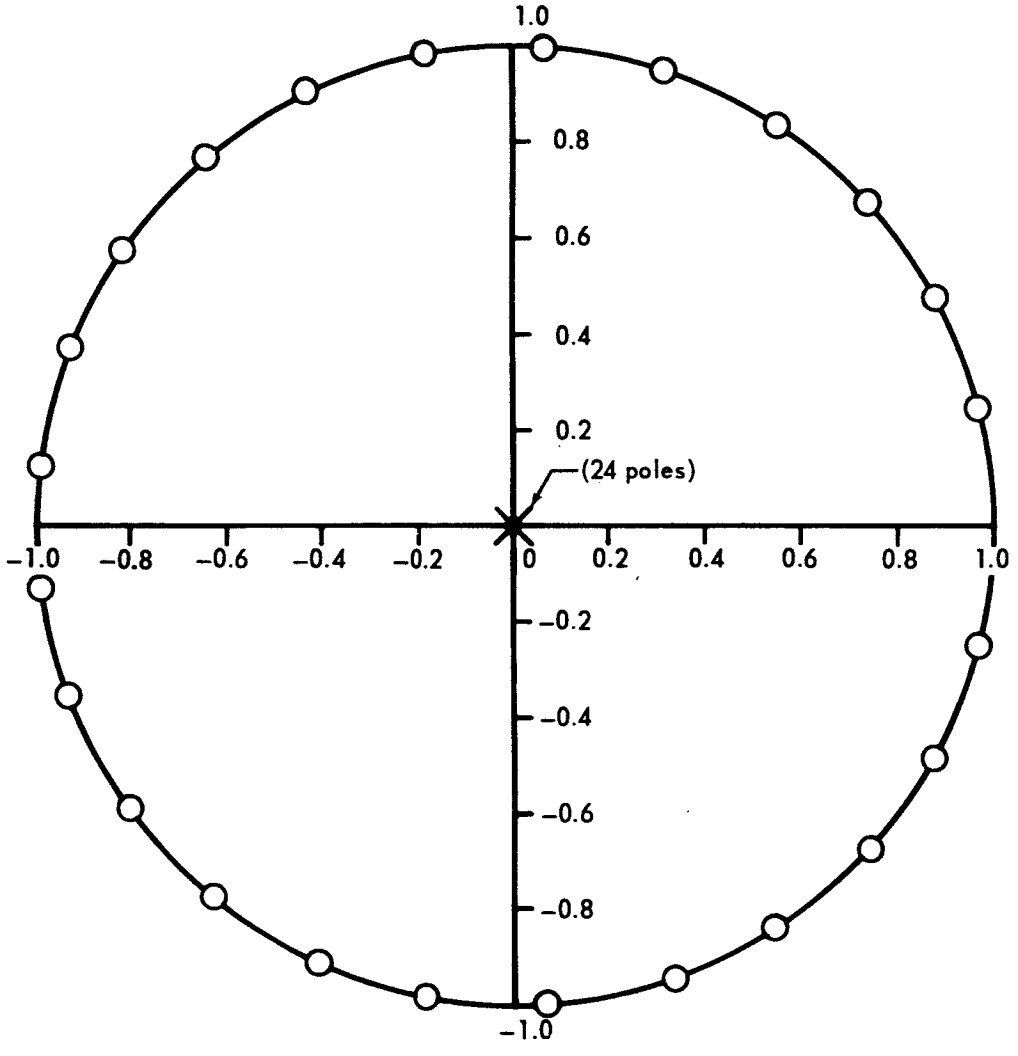

$$\text{Roots of } \frac{[1 + Z + Z^2 + \cdots Z^{2M}]}{Z^{2M}} = \frac{\dfrac{[Z^{2M+1} - 1]}{Z - 1}}{Z^{2M}} = 0$$

Figure 12 Root Location for Zero Degree (A_0) Polynomial Fitting z Transform With M = 12

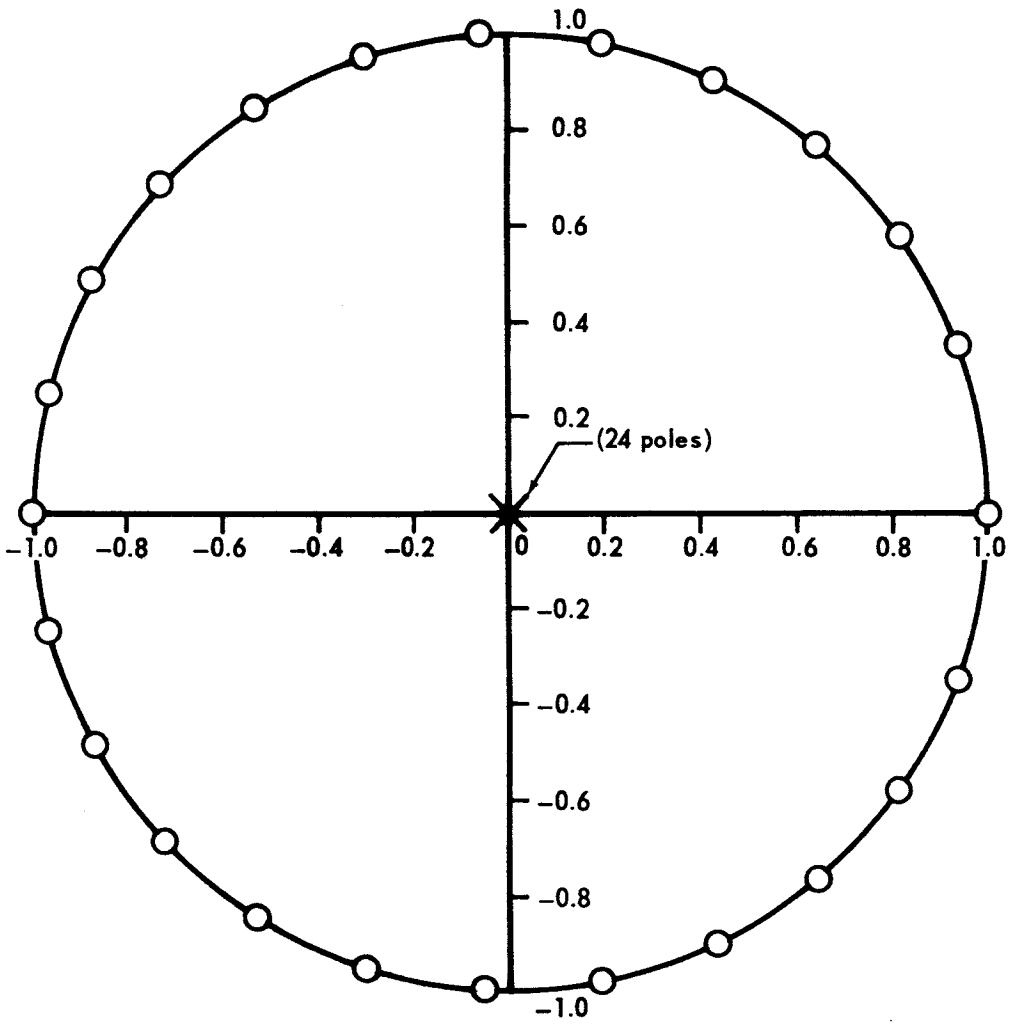

Figure 13 Root Location of First Degree (A_1) Polynomial Fitting z Transform With M = 12

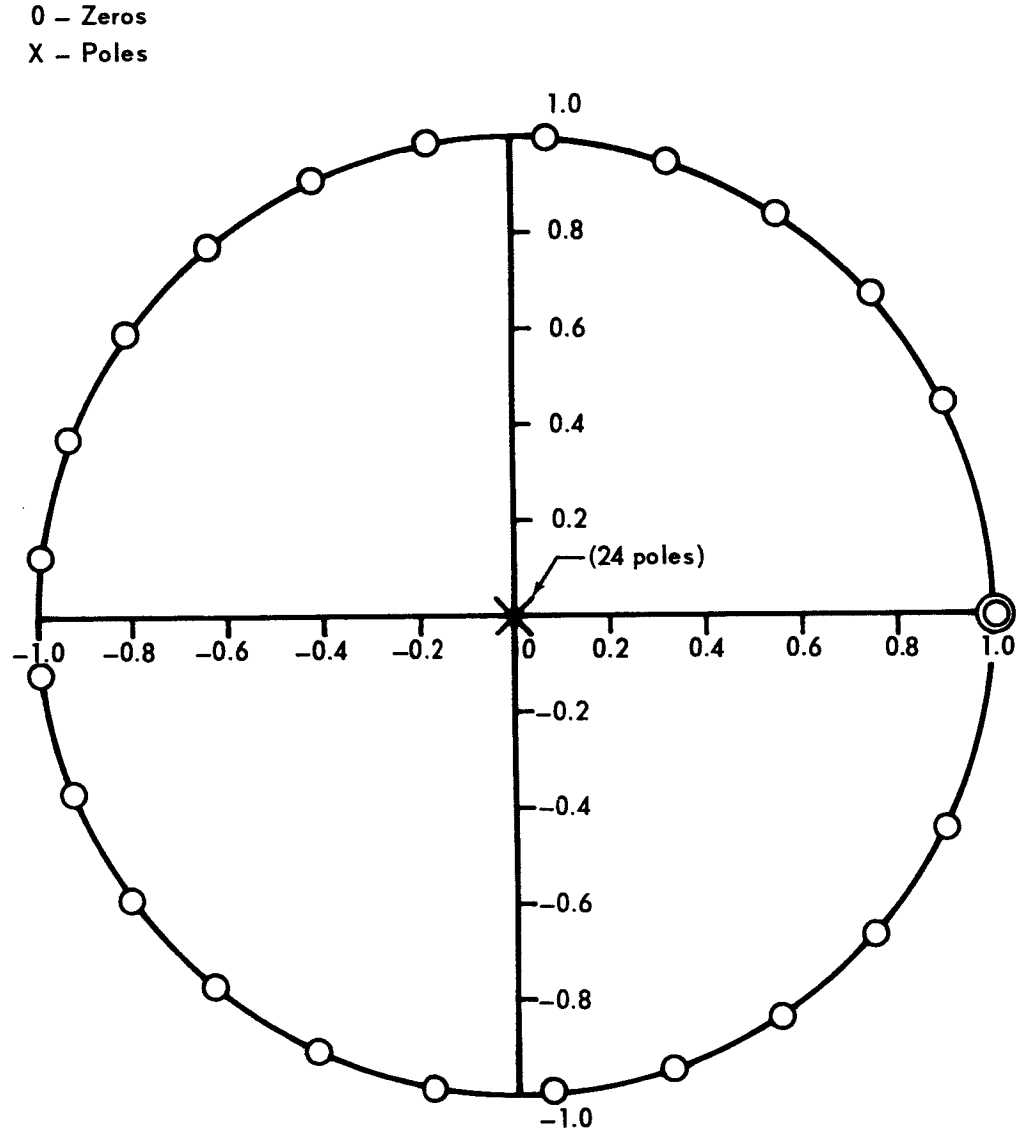

Figure 14a Root Location of Second Degree (A_2) Polynomial Fitting z Transform With M = 12

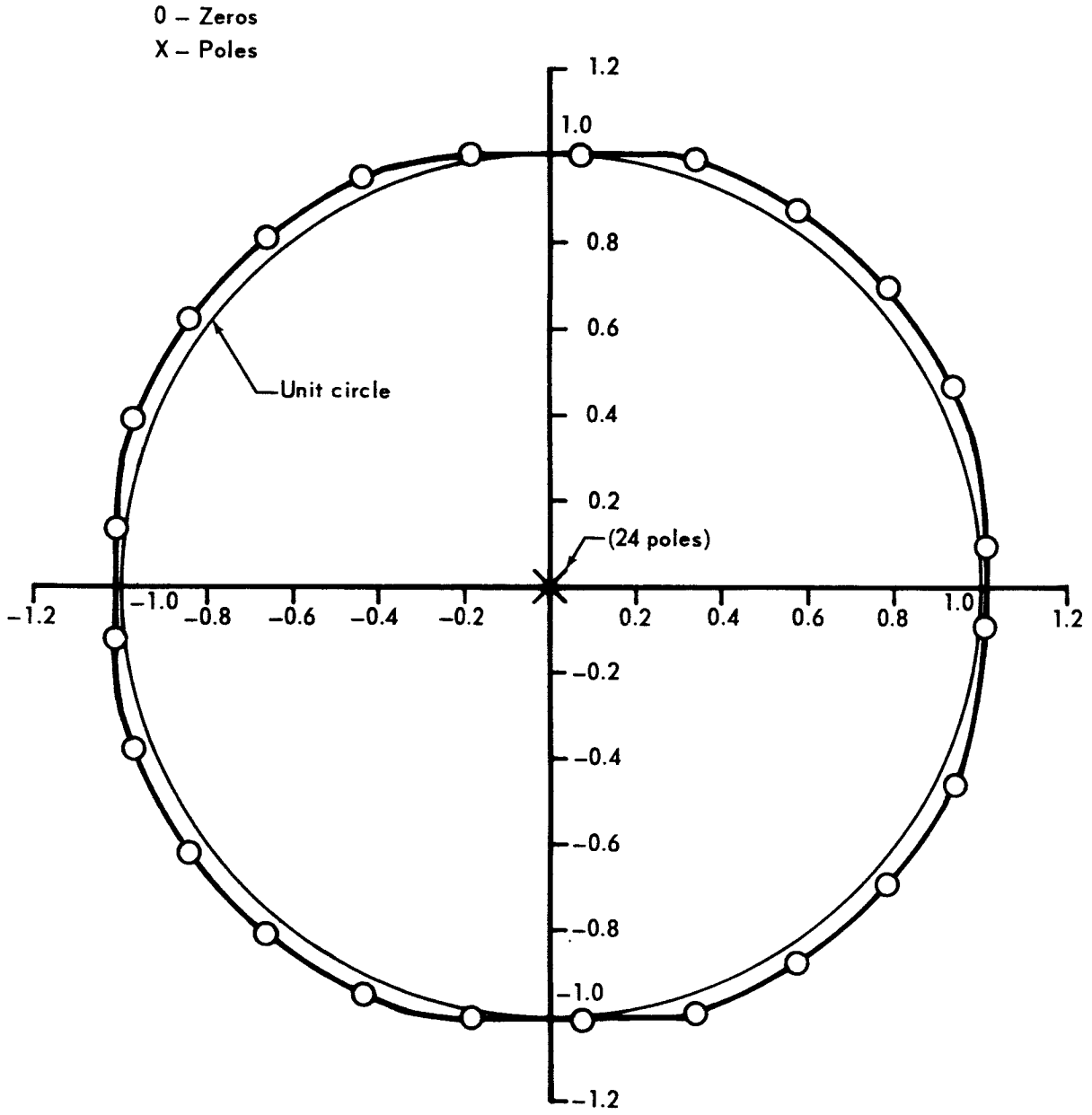

Figure 14b Root Location of Second Degree ($A_0+A_1+A_2$) Polynomial Fitting z Transform With M = 12

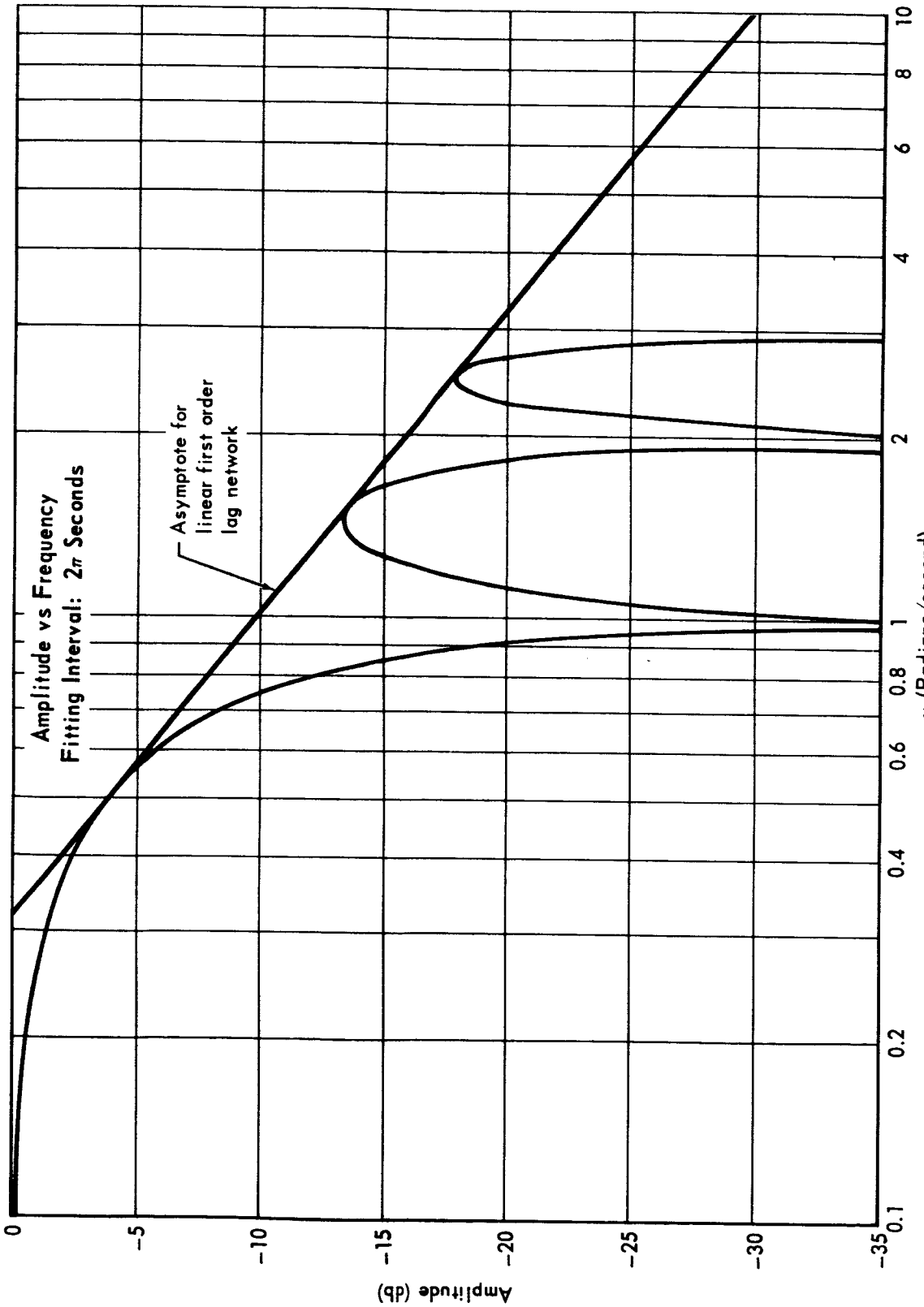

Figure 15 Frequency Response of Zero Degree (A_o) Polynomial Fitting

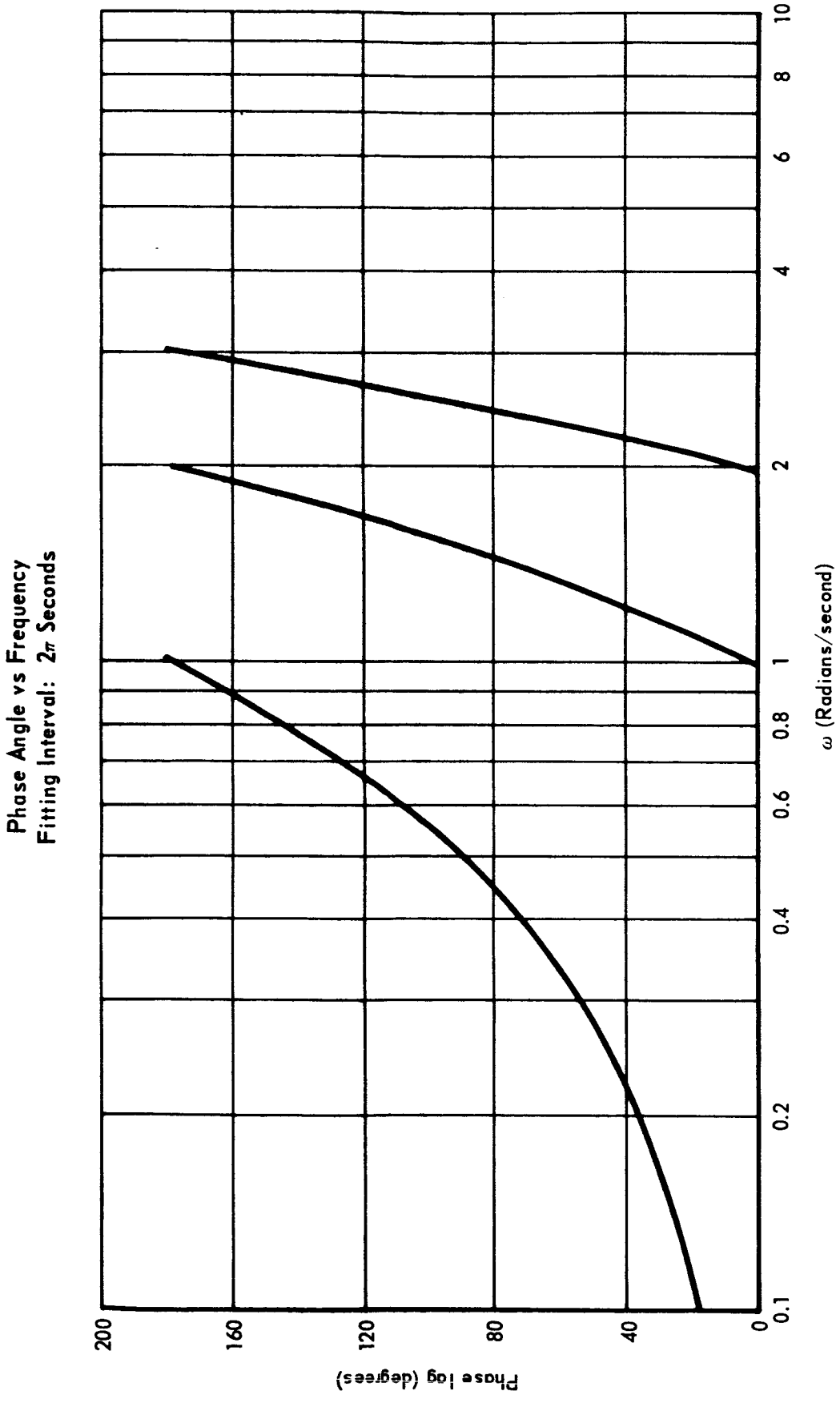

Figure 15 Frequency Response of Zero Degree (A_o) Polynomial Fitting (Cont.)

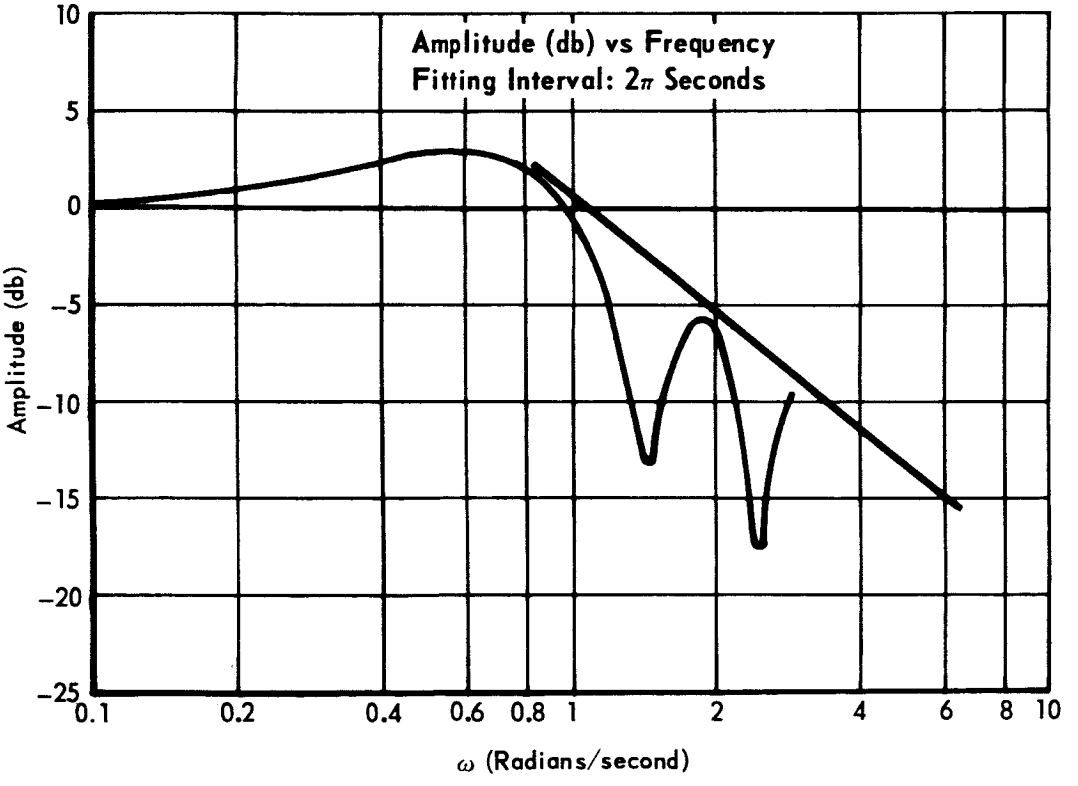

Figure 16 Frequency Response of First Degree ($A_0 + A_1$) Polynomial Fitting

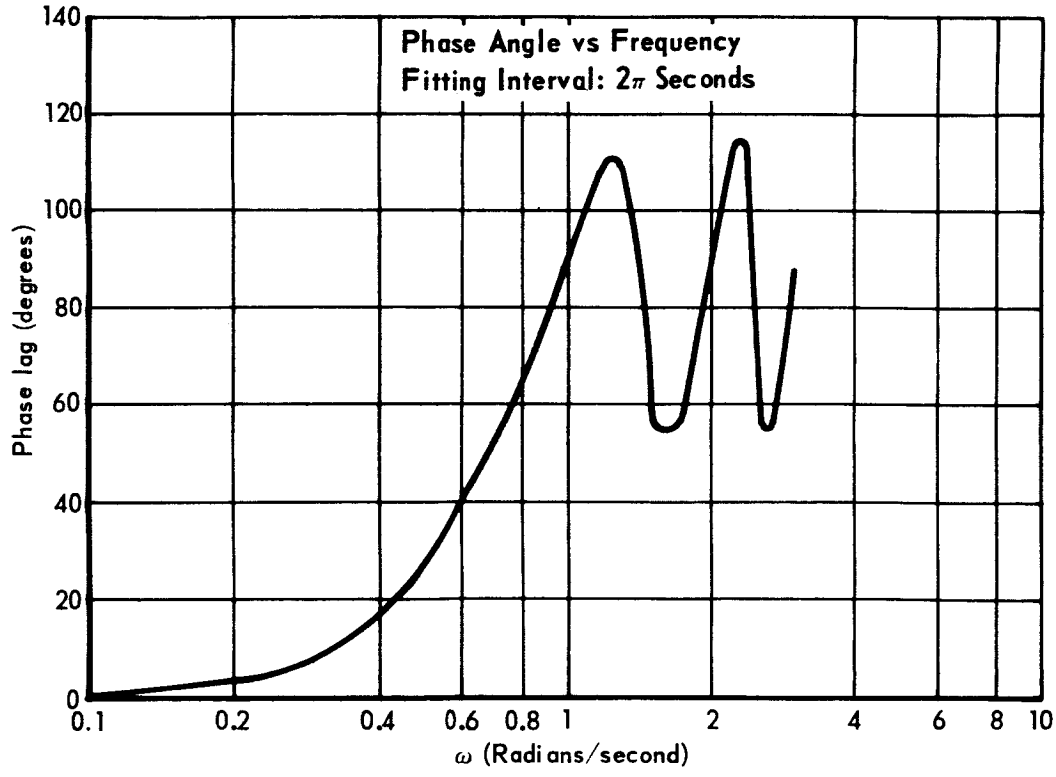

Figure 16 Frequency Response of First Degree $(A_0 + A_1)$ Polynomial Fitting (Cont.)

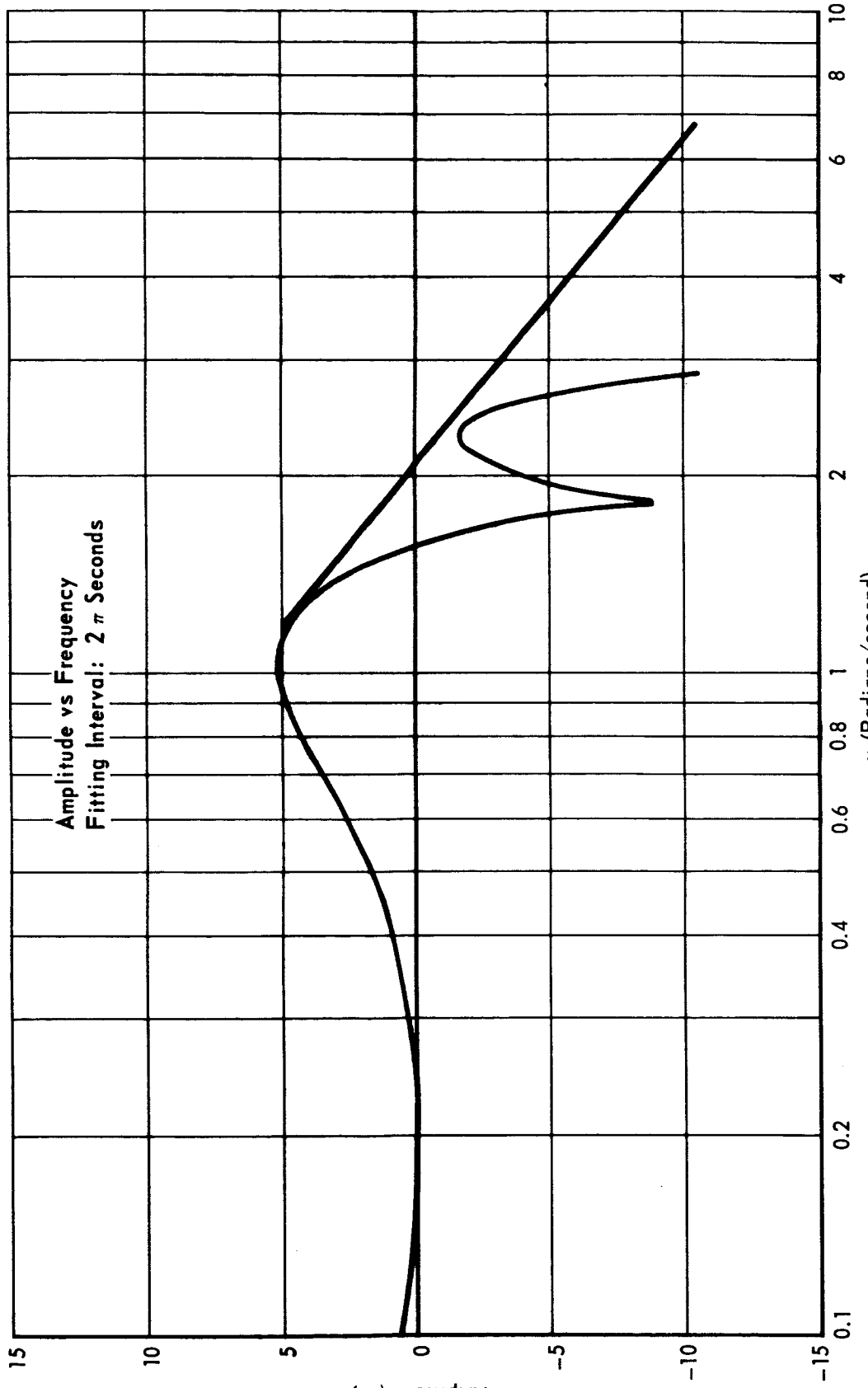

Figure 17 Frequency Response of Second Degree $(A_0 + A_1 + A_2)$ Polynomial Fitting

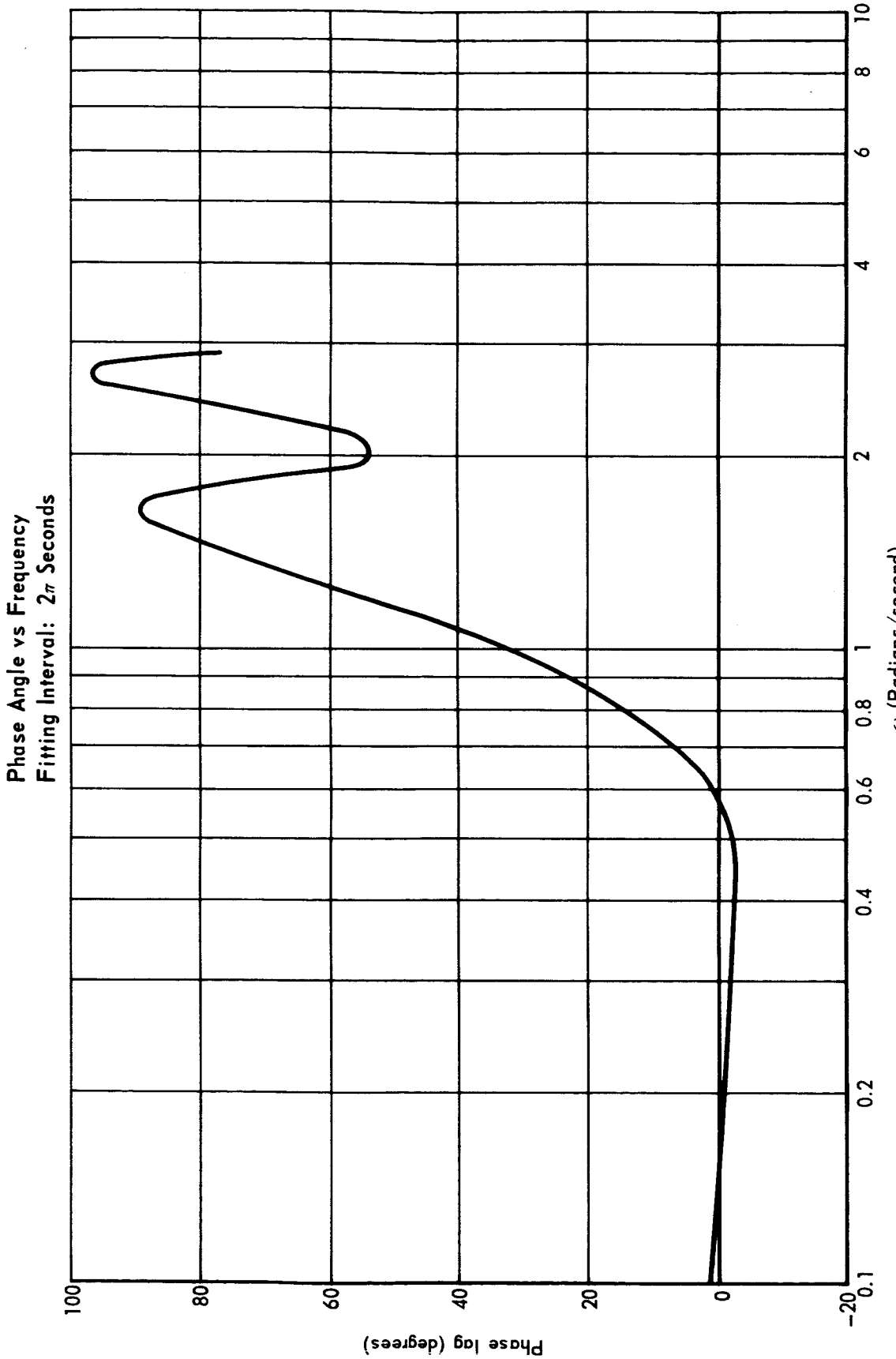

Figure 17 Frequency Response of Second Degree $(A_0 + A_1 + A_2)$ Polynomial Fitting (Cont.)

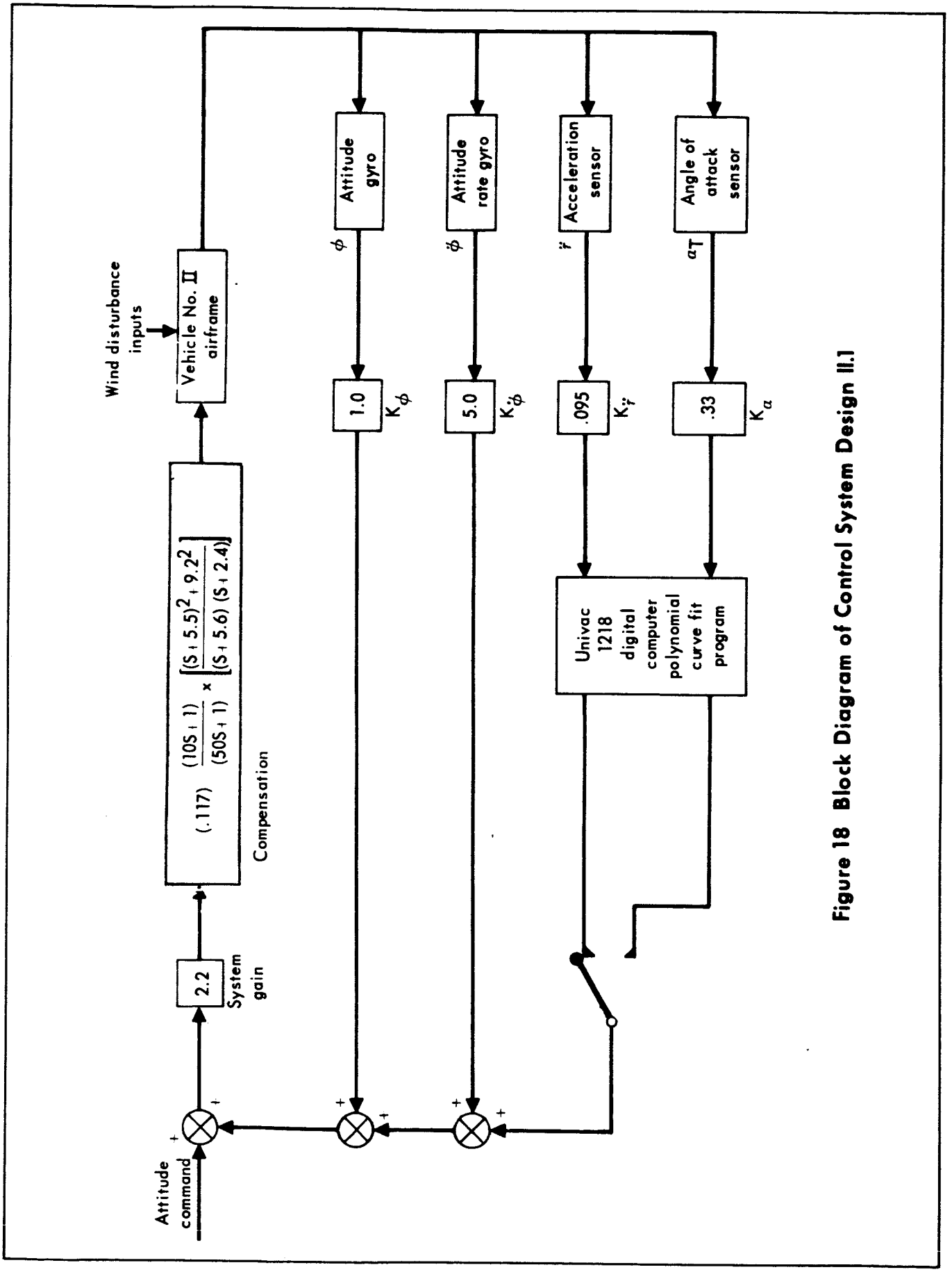

Figure 18 Block Diagram of Control System Design II.1

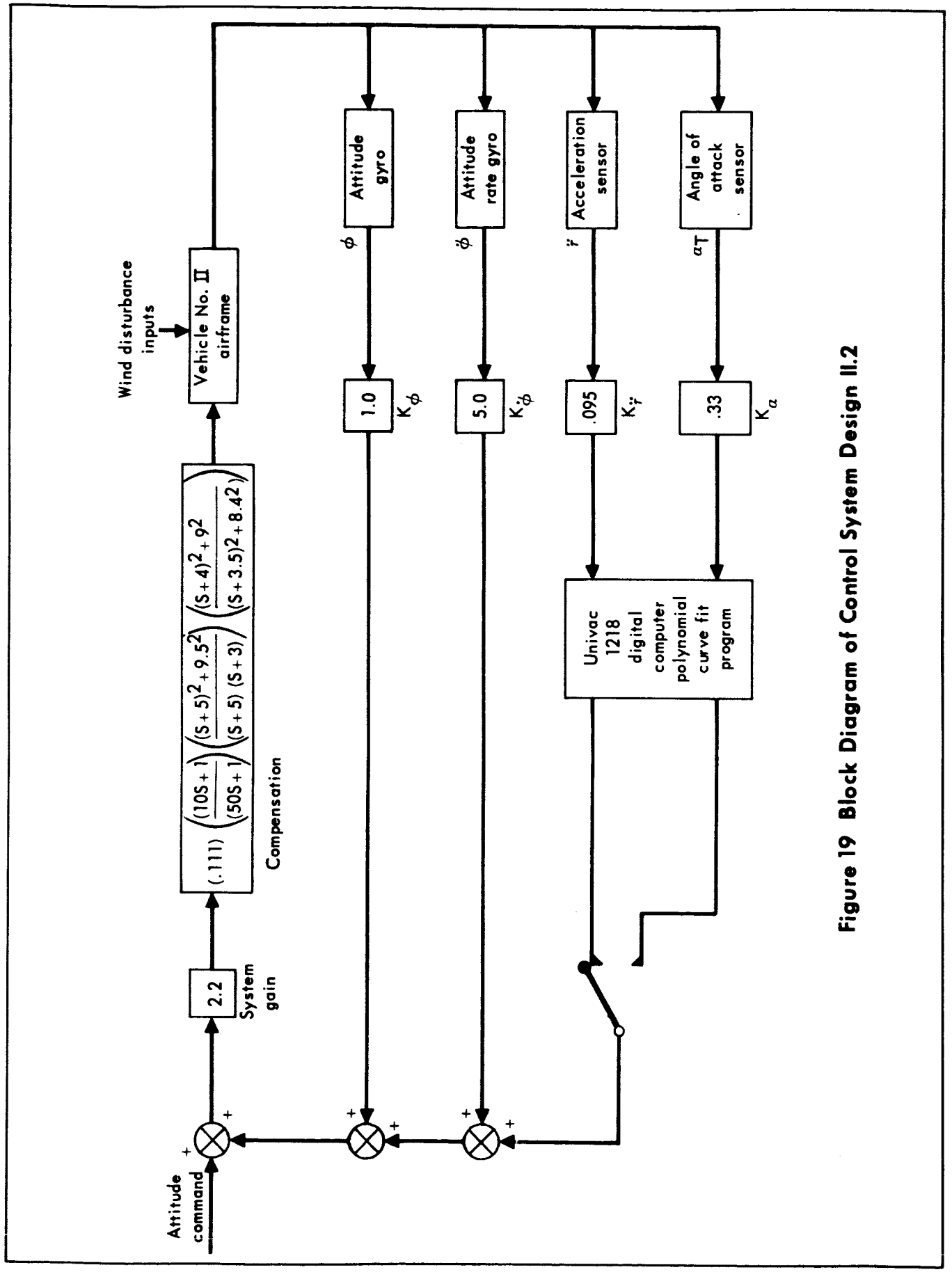

Figure 19 Block Diagram of Control System Design II.2

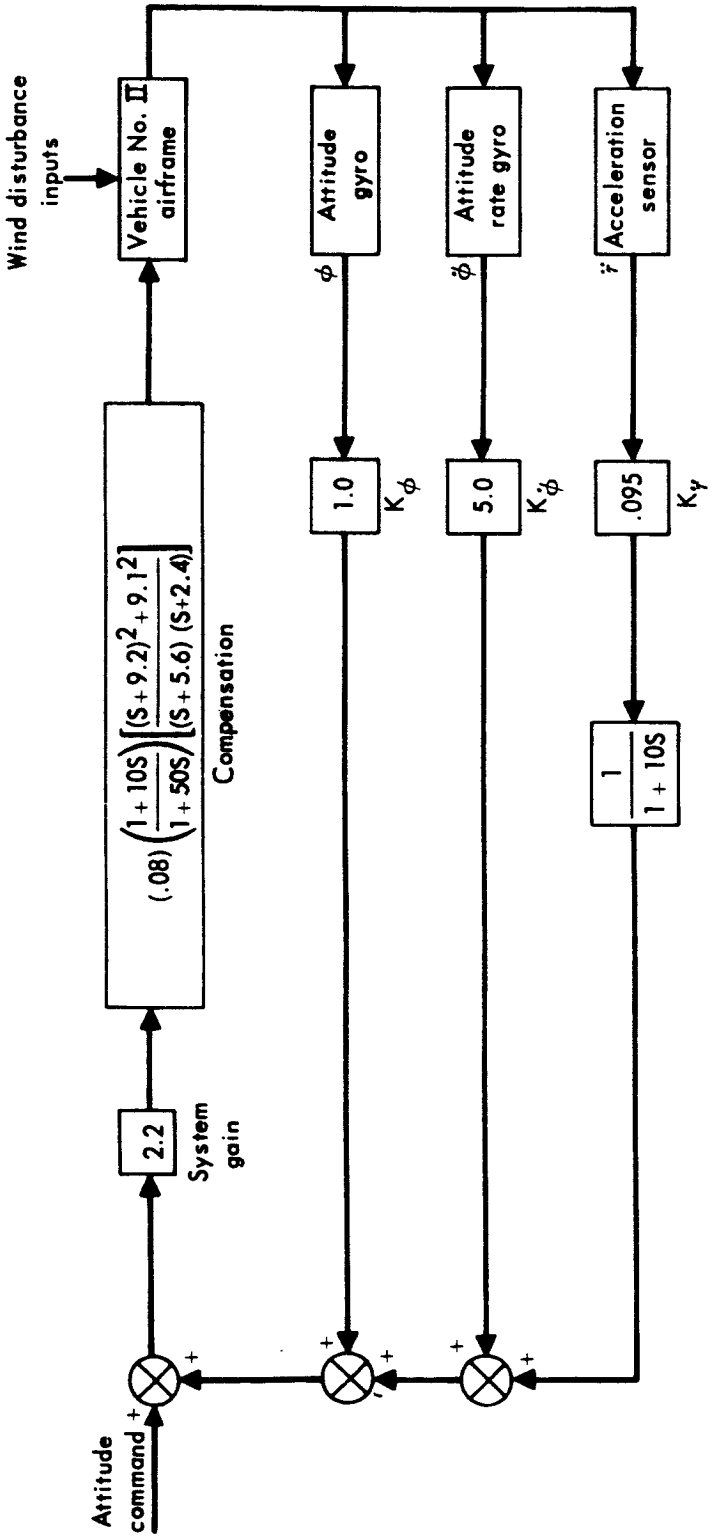

Figure 20 Block Diagram of Control System Design II.3

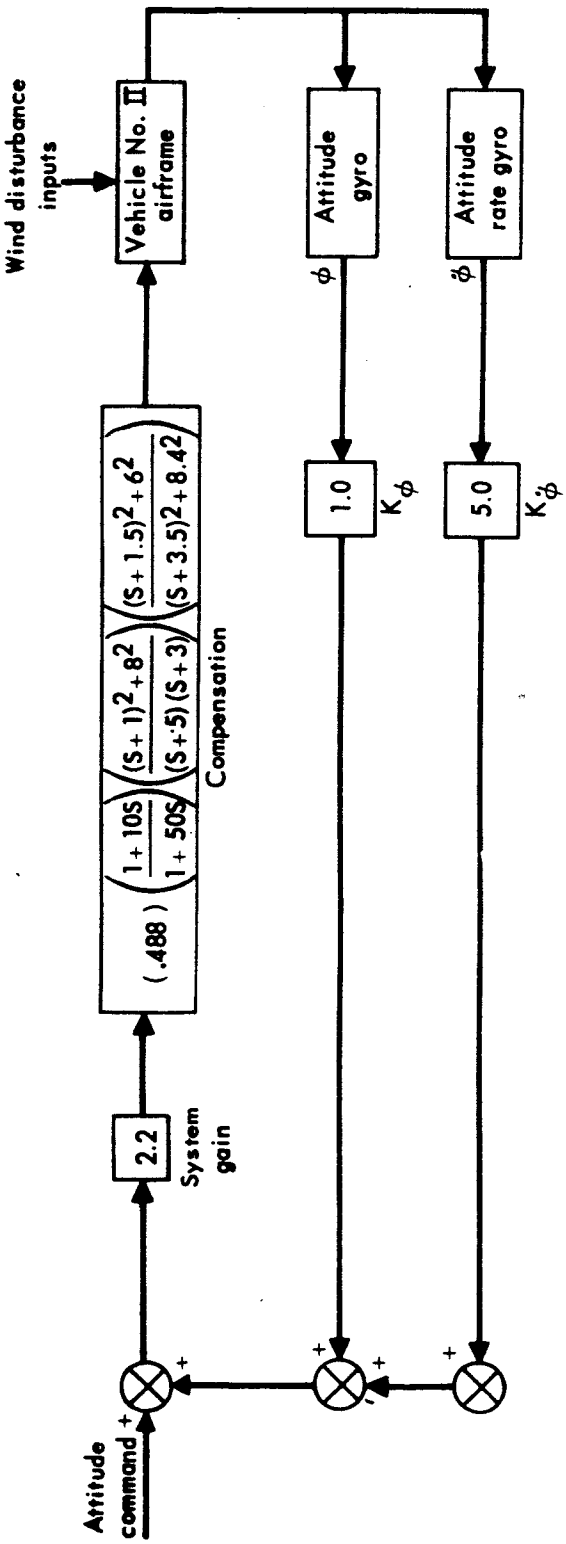

Figure 21 Block Diagram of Control System Design II.4

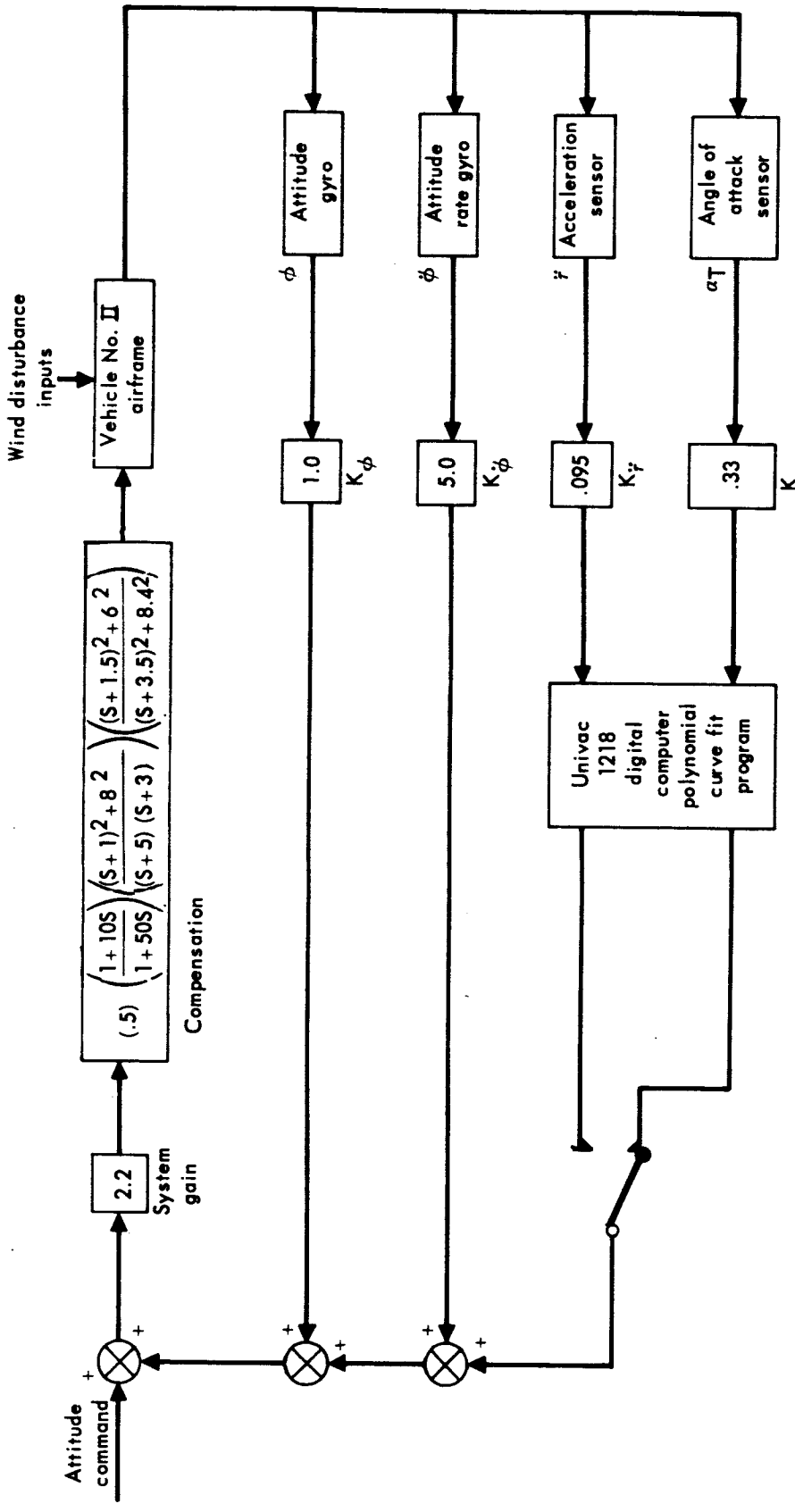

Figure 22 Block Diagram of Control System Design II.5

1. Flight condition, maximum q
2. Body bending and fuel slosh, in
3. Polynomial fitting in acceleration feedback, zero degree (A_0)
4. Past samples, 25
5. Sample rate, 2.5 per second
6. Control system design, II.2
7. Forward loop gain, K = 2.2
8. Position feedback gain, K_ϕ = 1.0
9. Rate feedback gain, $K_{\dot{\phi}}$ = 5.0
10. Acceleration feedback gain, $K_{\ddot{r}}$ = 0.095

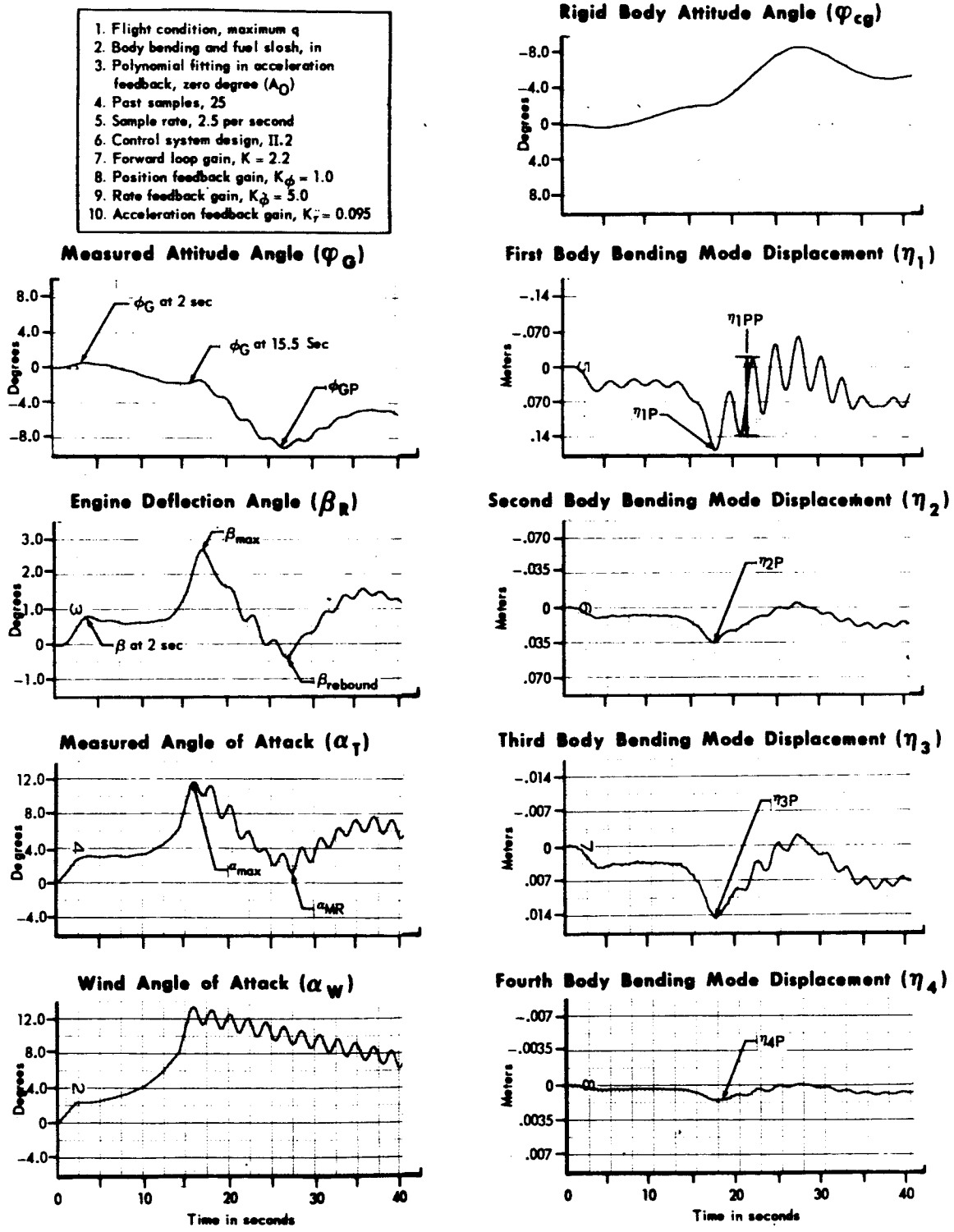

Figure 23 Wind Response of Study Vehicle No. II With the Digital Polynomial Filter in the Acceleration Feedback Loop

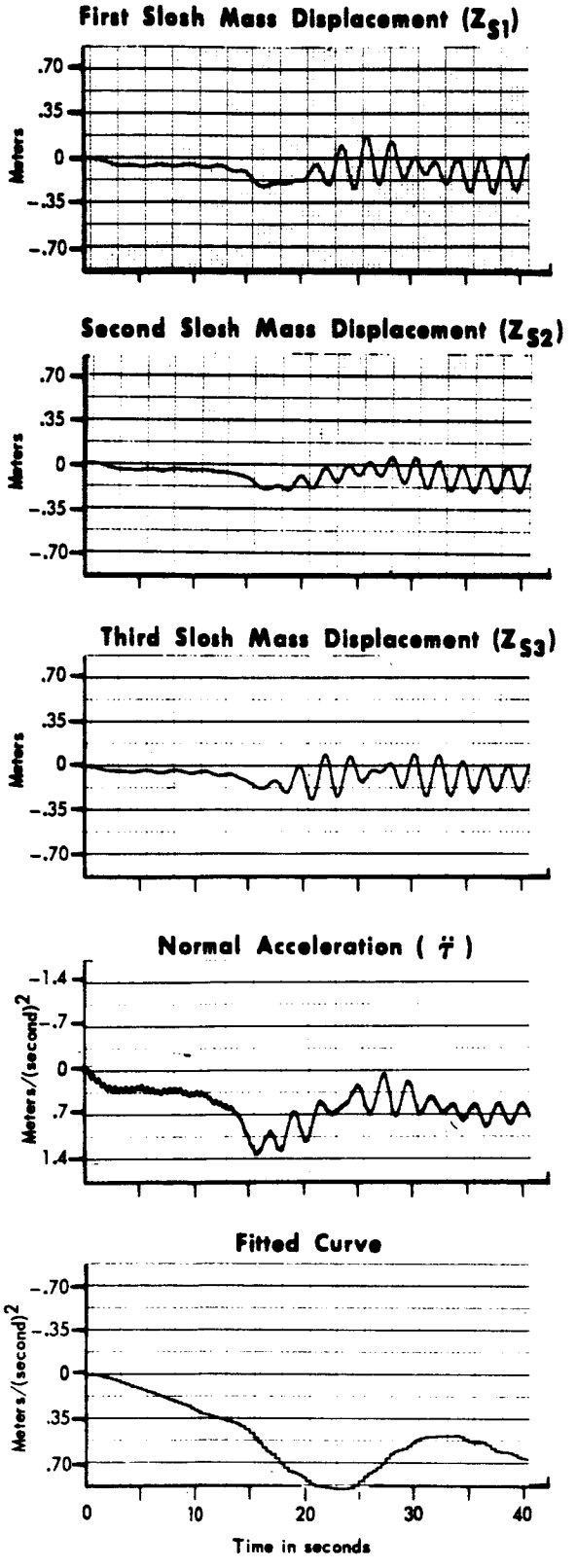

Figure 23 Wind Response of Study Vehicle No. II With the Digital Polynomial Filter in the Acceleration Feedback Loop (Cont.)

1. Flight condition, maximum q	6. Control system design, II.2
2. Body bending and fuel slosh, in	7. Forward loop gain, K = 2.2
3. Polynomial fitting in acceleration feedback – zero degree (A_0)	8. Position feedback gain, K_ϕ = 1.0
4. Past samples stored, 25	9. Rate feedback gain, $K_{\dot\phi}$ = 5.0
5. Sample rate, 2.5 per second	10. Acceleration feedback gain, $K_{\dot\gamma}$ = .095

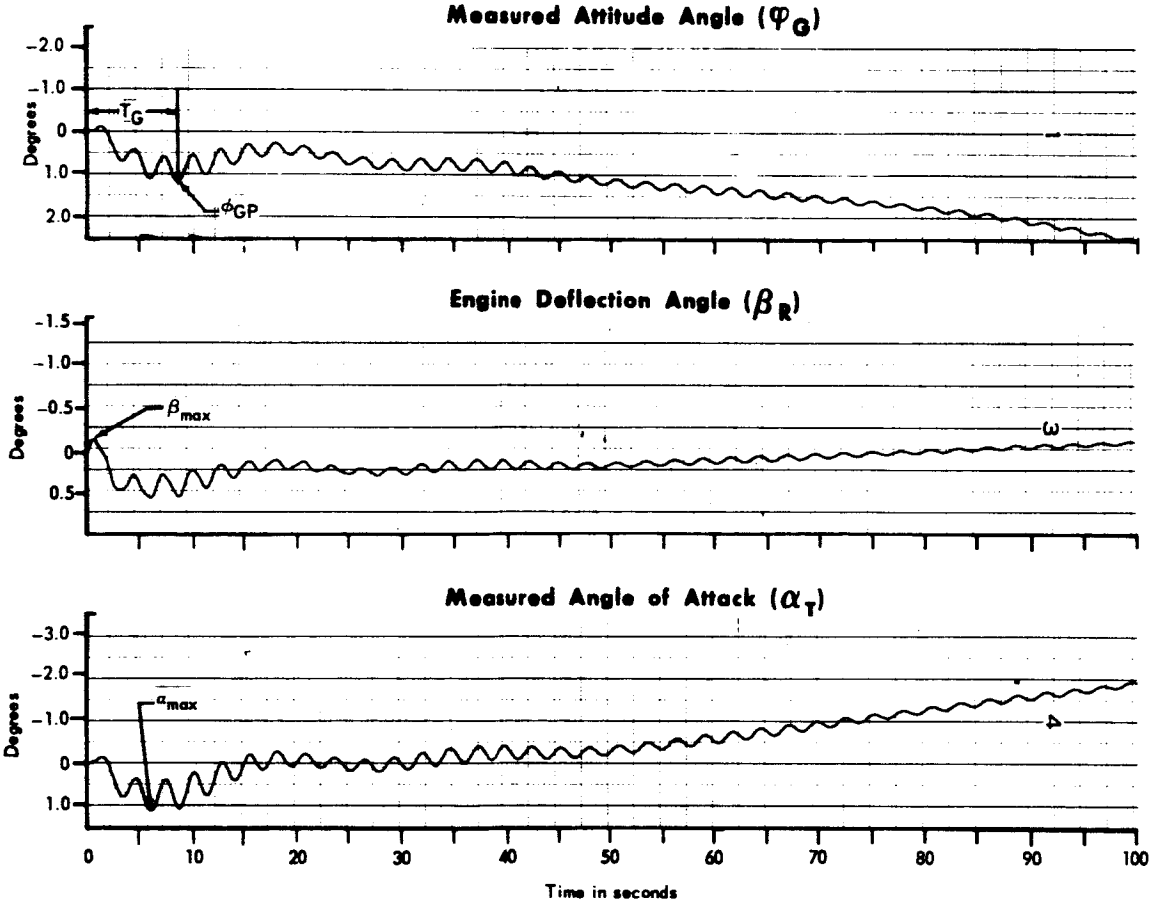

Figure 24 Step Response of Study Vehicle No. II With the Digital Polynomial Filter in the Acceleration Feedback Loop

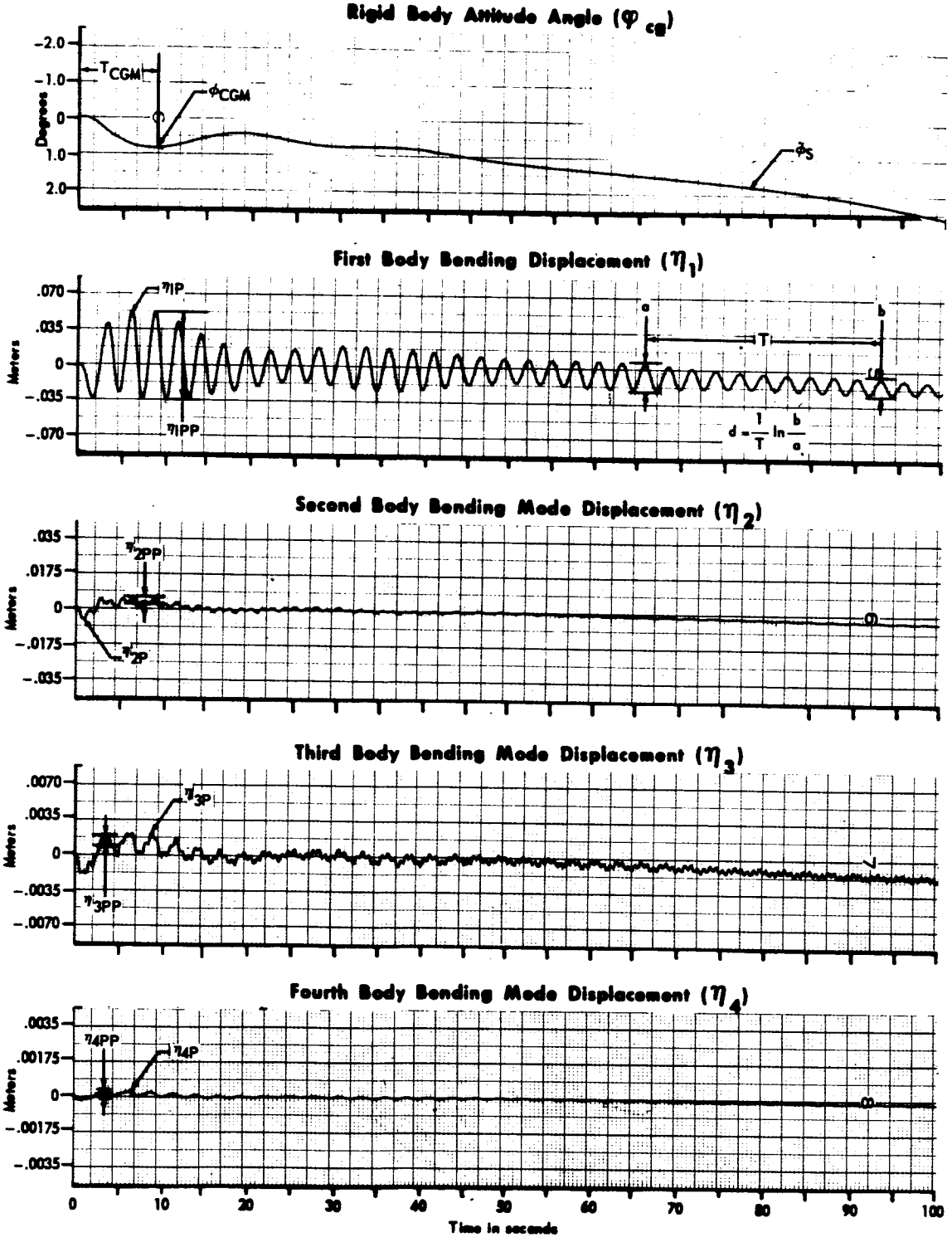

Figure 24 Step Response of Study Vehicle No. II With the Digital Polynomial Filter in the Acceleration Feedback Loop (Cont.)

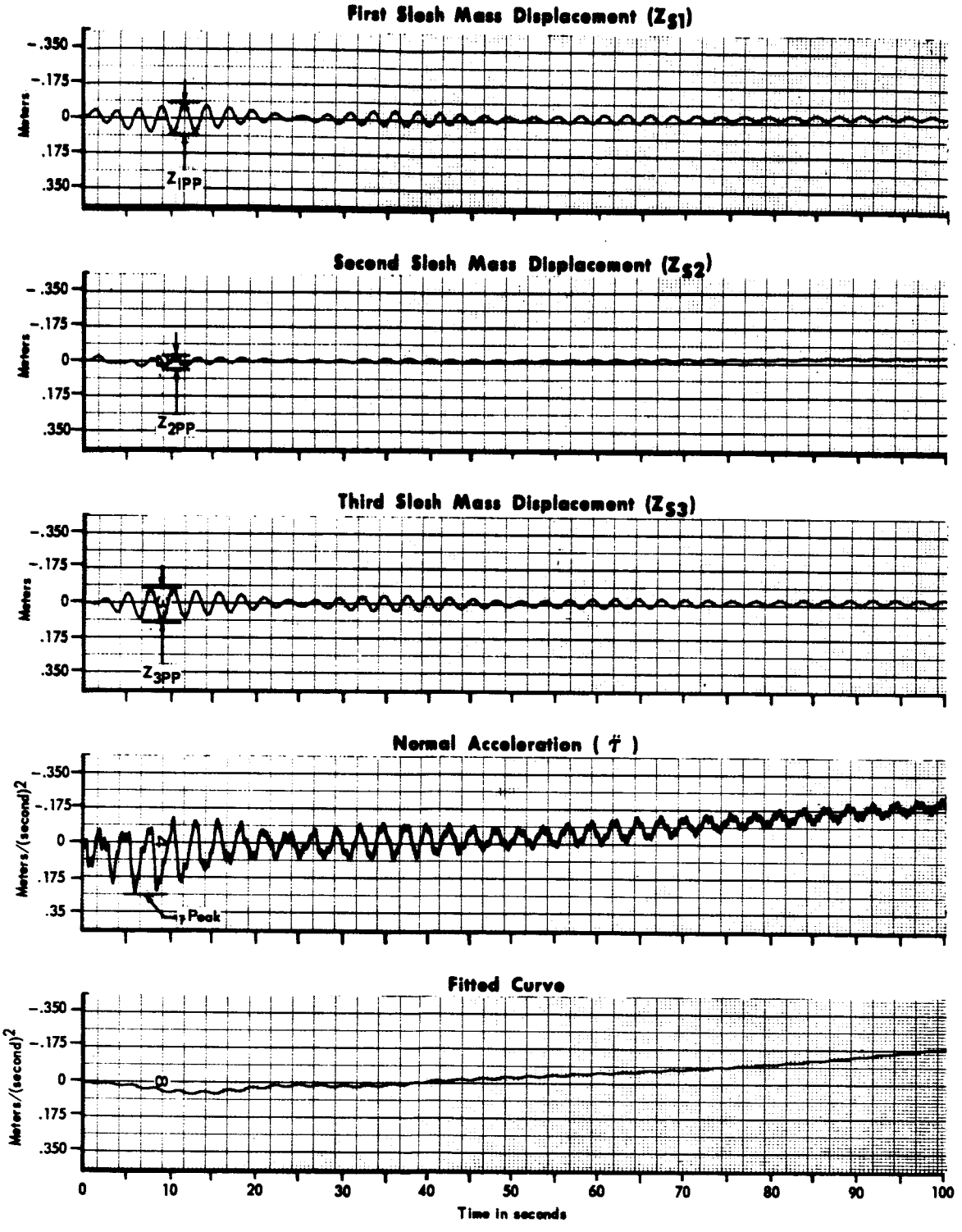

Figure 24 Step Response of Study Vehicle No. II With the Digital Polynomial Filter in the Acceleration Feedback Loop (Cont.)

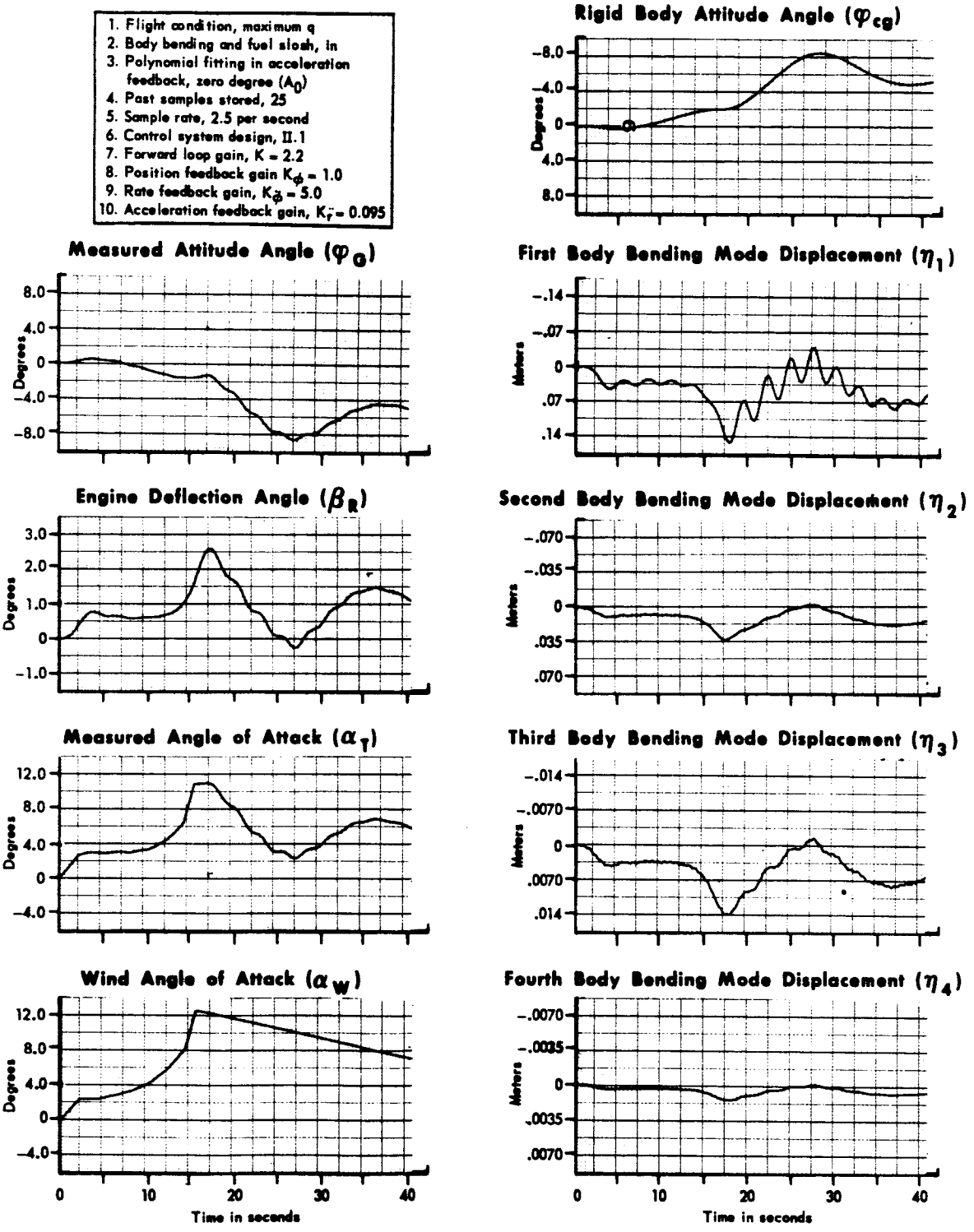

Figure 25 Wind Response of Study Vehicle No. II With the Digital Polynomial Filter in the Acceleration Feedback Loop

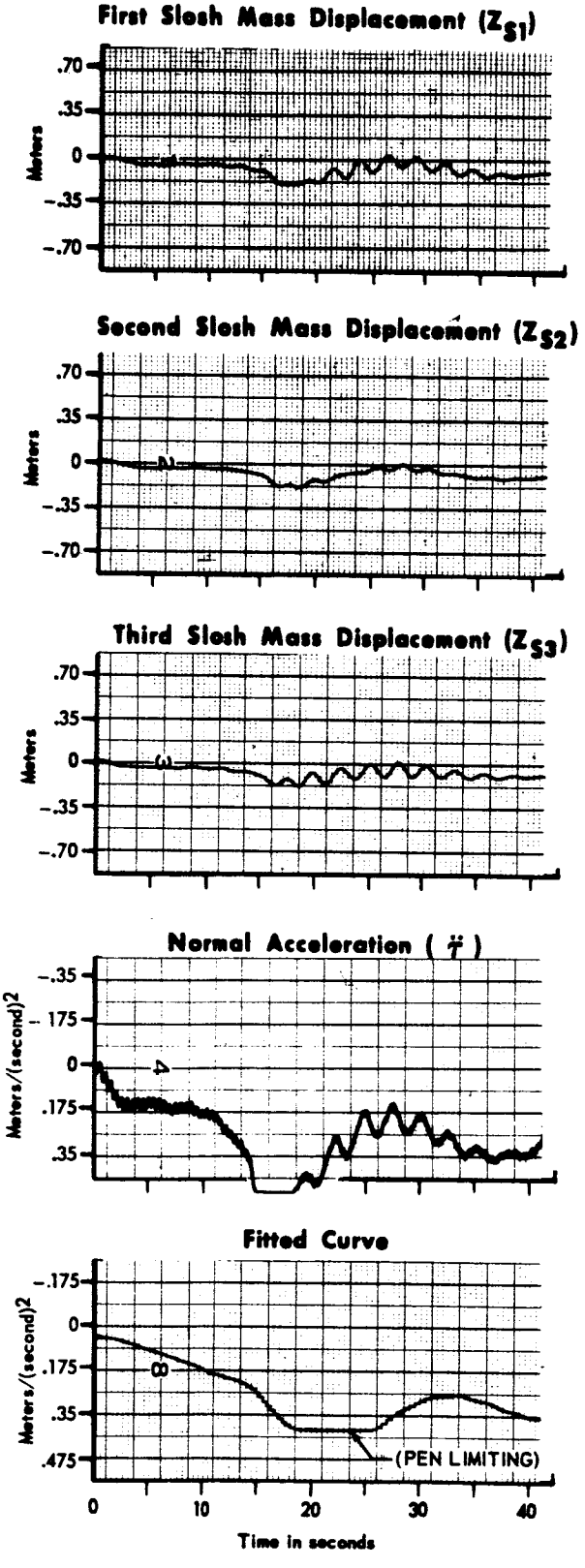

Figure 25 Wind Response of Study Vehicle No. II With the Digital Polynomial Filter in the Acceleration Feedback Loop (Cont.)

1. Flight condition, maximum q
2. Body bending and fuel slosh, in
3. Polynomial fitting in acceleration feedback, zero degree (A_0)
4. Past samples stored, 25
5. Sample rate, 2.5 per second
6. Control system design, II.2
7. Forward loop gain, K = 2.2
8. Position feedback gain, $K_{\dot{\varphi}} = 1.0$
9. Rate feedback gain, $K_{\dot{\beta}} = 5.0$
10. Acceleration feedback gain, $K_{\ddot{r}} = 0.095$

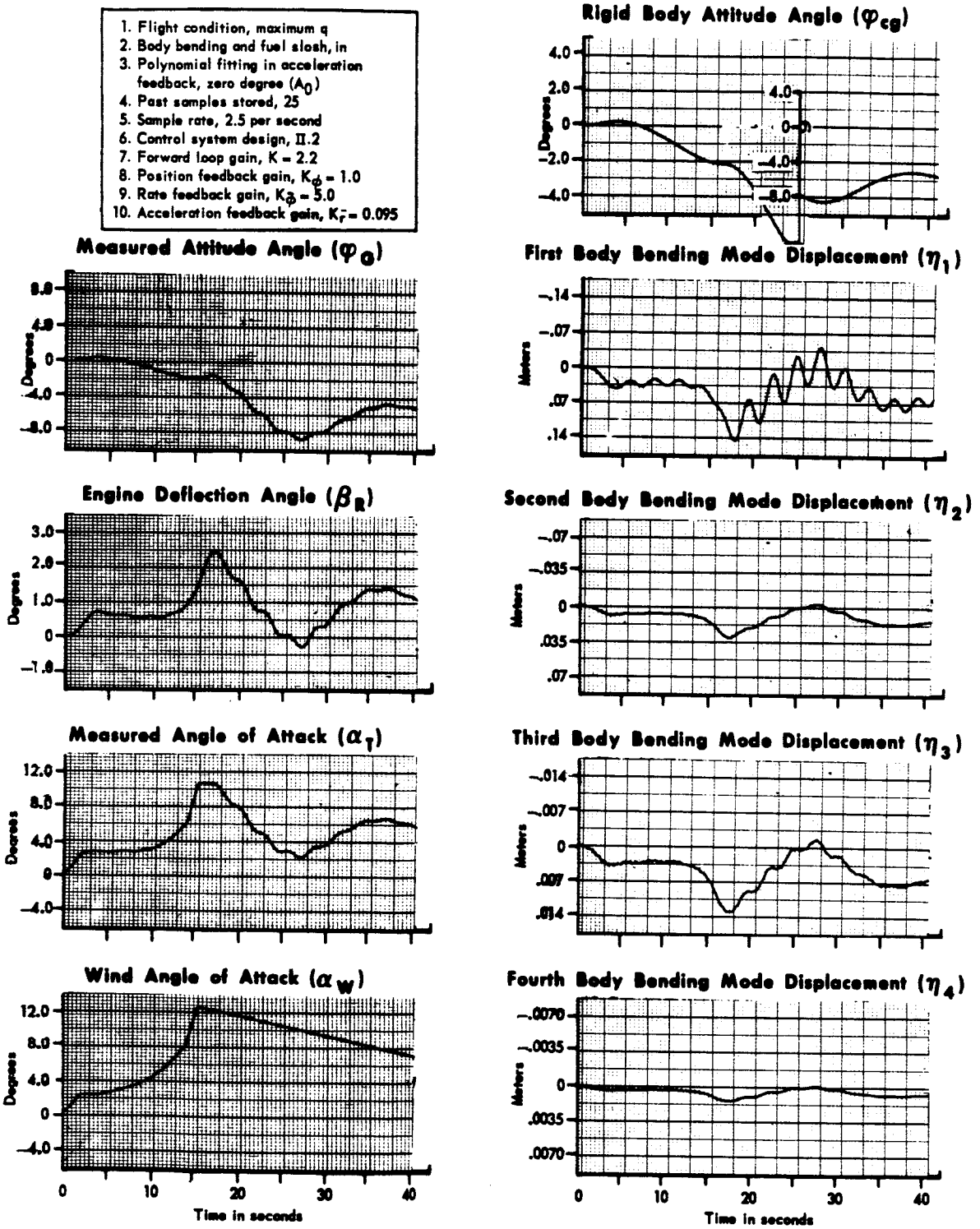

Figure 26 Wind Response of Study Vehicle No. II With the Digital Polynomial Filter in the Acceleration Feedback Loop

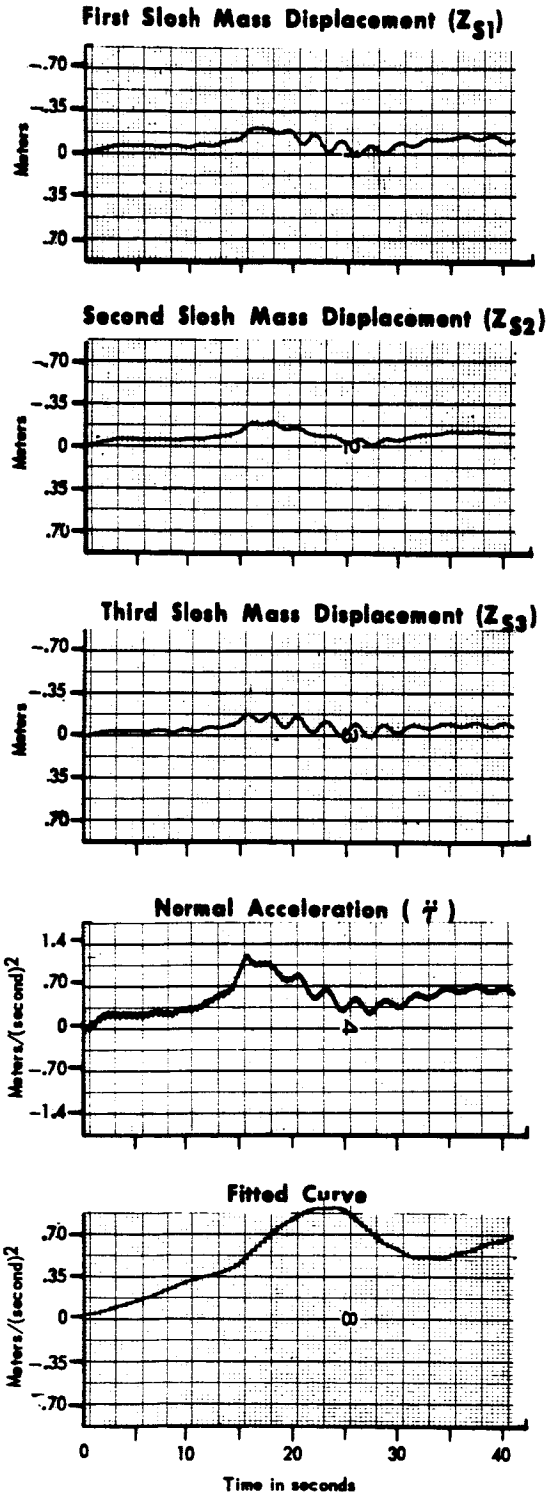

Figure 26 Wind Response of Study Vehicle No. II With the Digital Polynomial Filter in the Acceleration Feedback Loop (Cont.)

1. Flight condition, maximum q
2. Body bending and fuel slosh in
3. Acceleration feedback lag network, $\frac{1}{1+10S}$
4. Control system design, II.3
5. Forward loop gain, K = 2.2
6. Position feedback gain, $K_\phi = 1.0$
7. Rate feedback gain, $K_{\dot{\phi}} = 5.0$
8. Acceleration feedback gain, $K_{\ddot{z}} = 0.095$

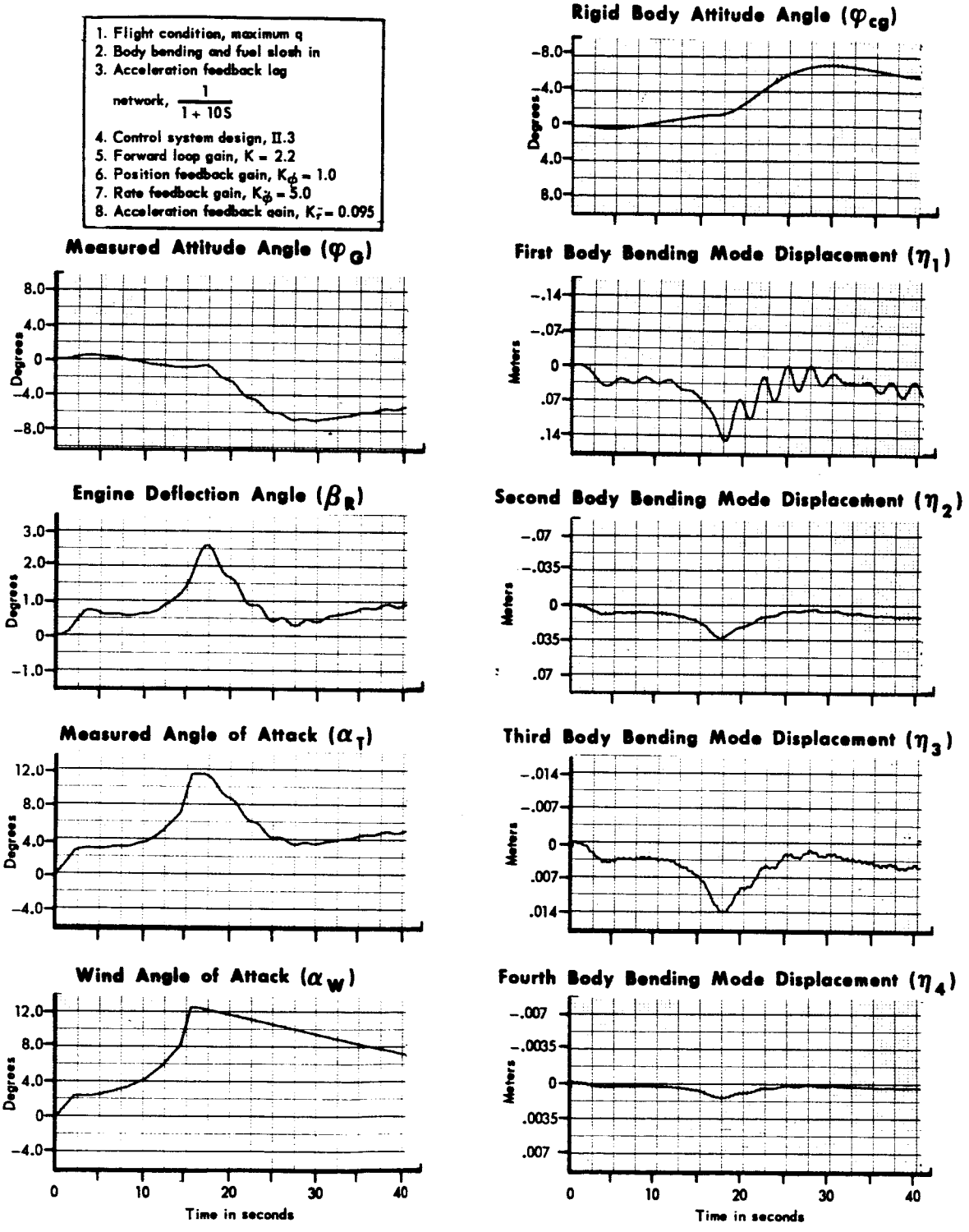

Figure 27 Wind Response of Study Vehicle No. II With a Linear Lag Filter in the Acceleration Feedback Loop

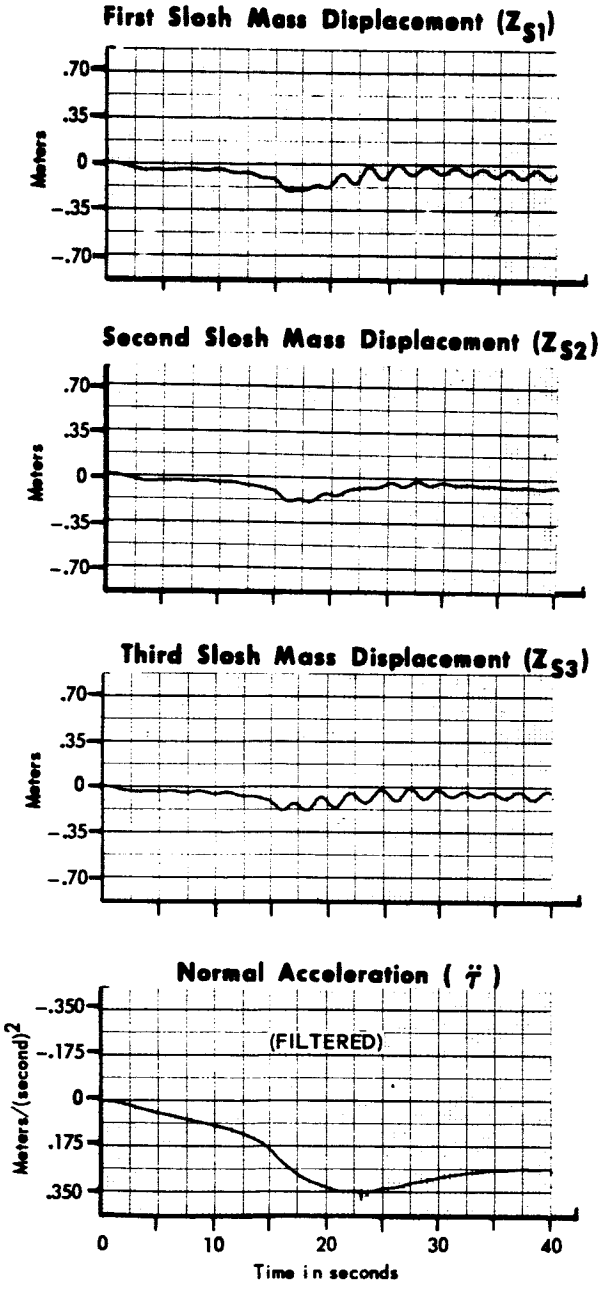

Figure 27 Wind Response of Study Vehicle No. II With a Linear Lag Filter in the Acceleration Feedback Loop (Cont.)

1. Flight condition, maximum q	6. Control system design, II.5
2. Body bending and fuel slosh in	7. Forward loop gain, K = 2.2
3. Polynomial fitting in acceleration feedback, zero degree (A_0)	8. Position feedback gain, K_ϕ = 1.0
4. Past samples stores, 25	9. Rate feedback gain, $K_{\dot\phi}$ = 5.0
5. Sample rate, 2.5 per second	10. Angle-of-attack feedback gain K_α = 0.33

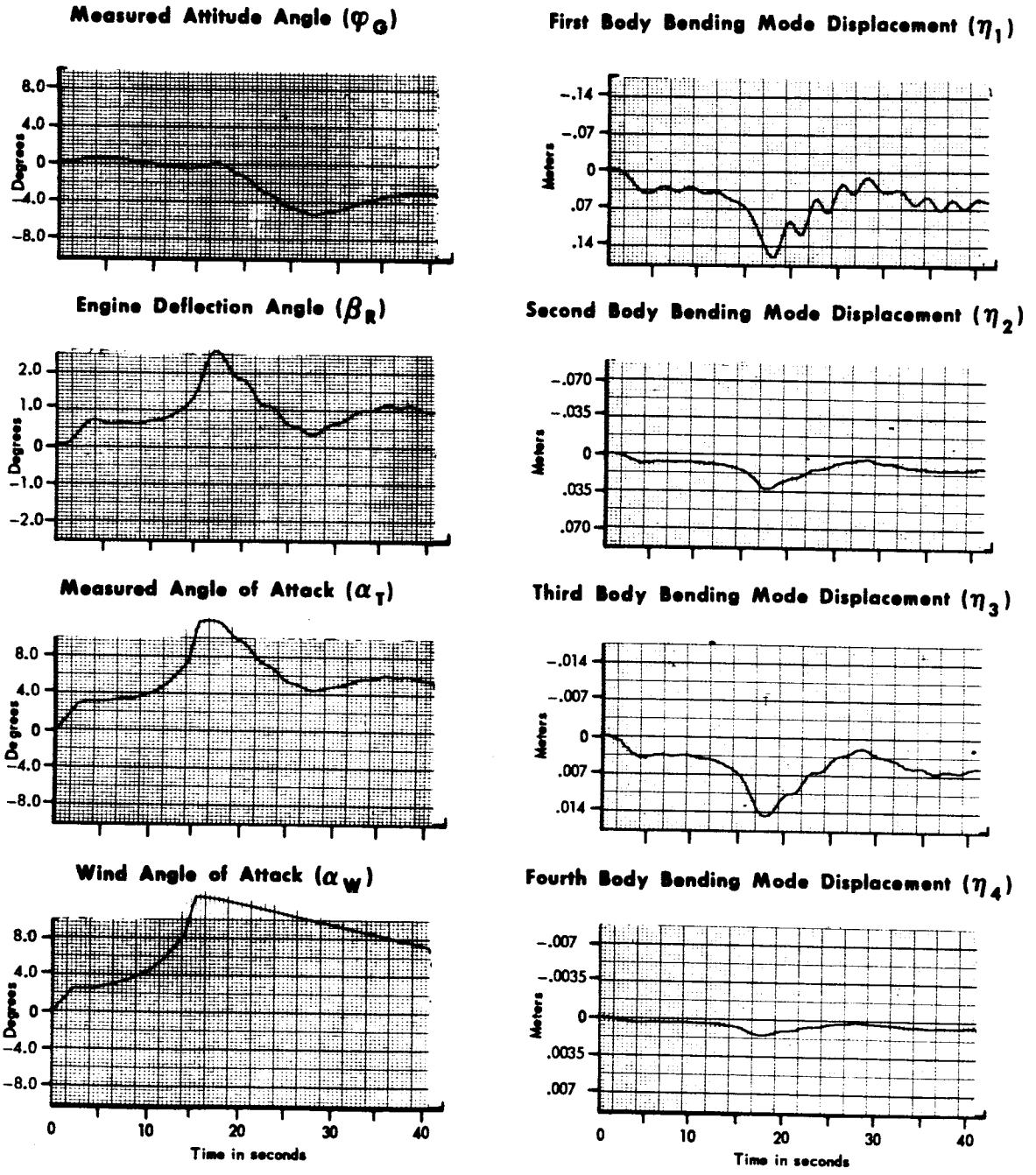

Figure 28 Wind Response of Study Vehicle No. II With the Digital Polynomial Filter in the Angle-of-Attack Feedback Loop

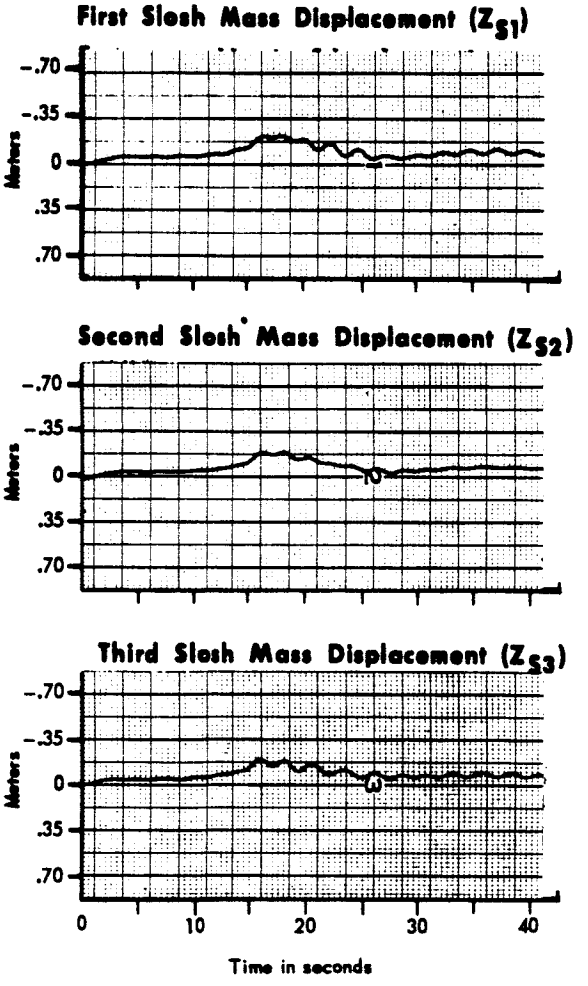

Figure 28 Wind Response of Study Vehicle No. II With the Digital Polynomial Filter in the Angle-of-Attack Feedback Loop (Cont.)

1. Flight condition, maximum q 2. Body bending and fuel slosh in 3. Polynomial fitting in acceleration feedback, zero degree (A_0) 4. Past samples stores, 25 5. Sample rate, 2.5 per second	6. Control system design, II.1 7. Forward loop gain, K = 2.2 8. Position feedback gain, K_ϕ = 1.0 9. Rate feedback gain, $K_{\dot{\phi}}$ = 5.0 10. Acceleration feedback gain, $K_{\ddot{r}}$ = 0.095

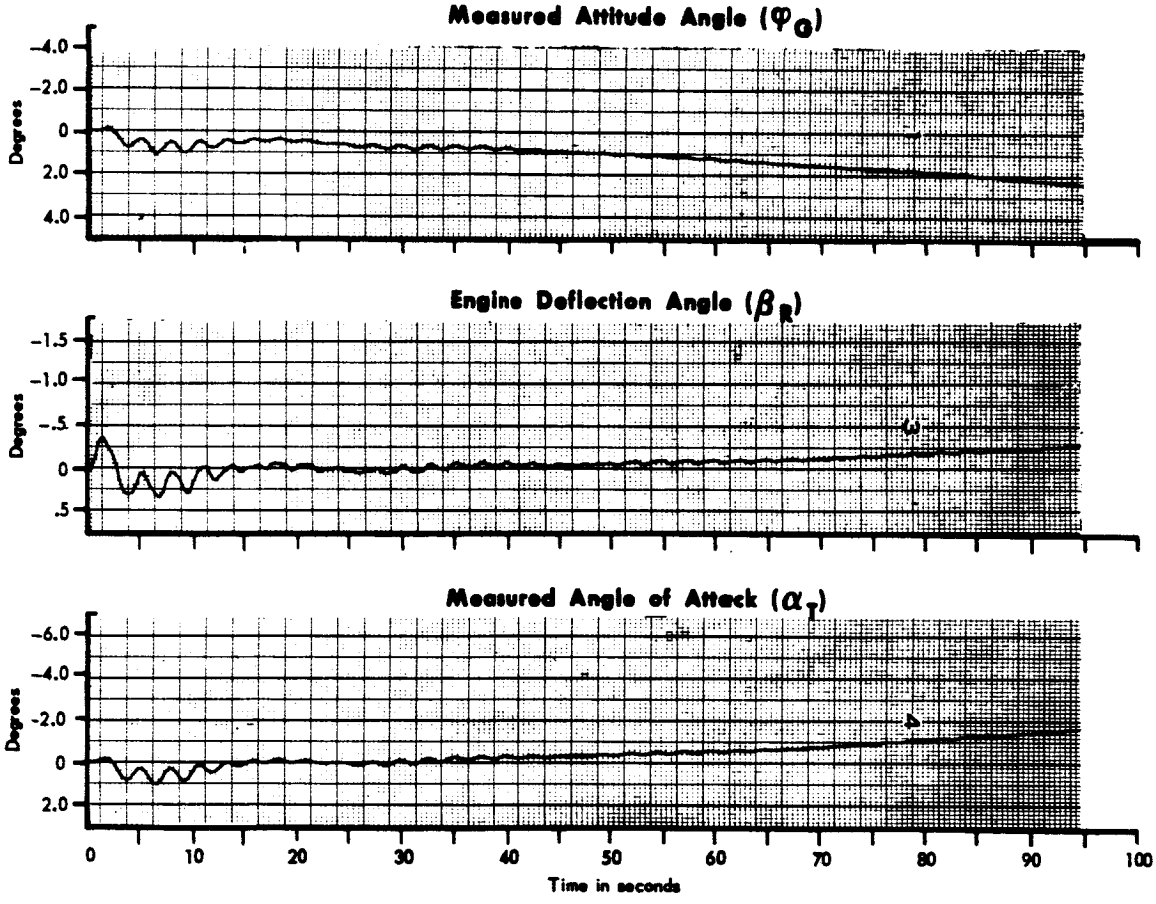

Figure 29 Unit Step Response of Study Vehicle No. II With the Digital Polynomial Filter in the Acceleration Feedback Loop

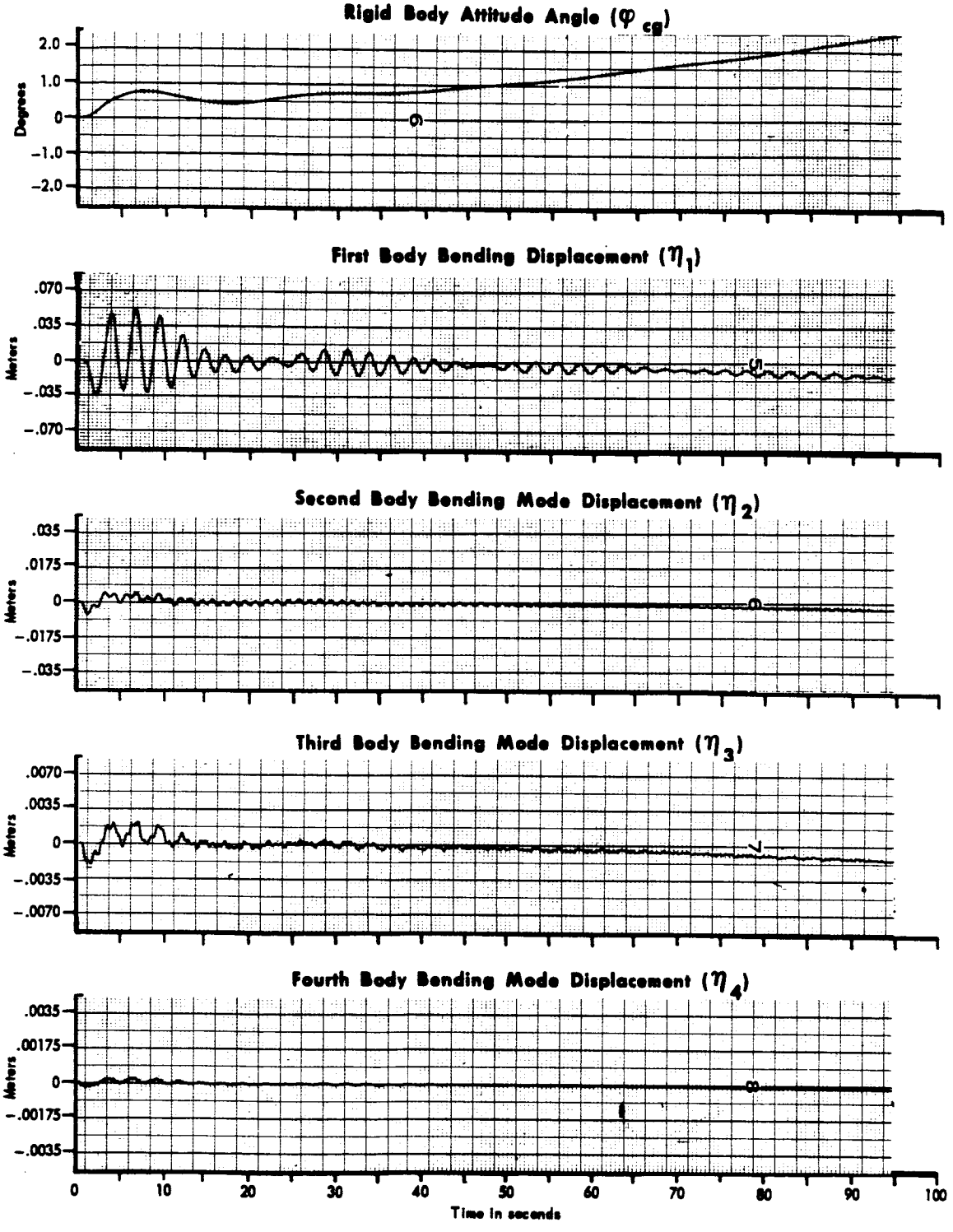

Figure 29 Unit Step Response of Study Vehicle No. II With the Digital Polynomial Filter in the Acceleration Feedback Loop (Cont.)

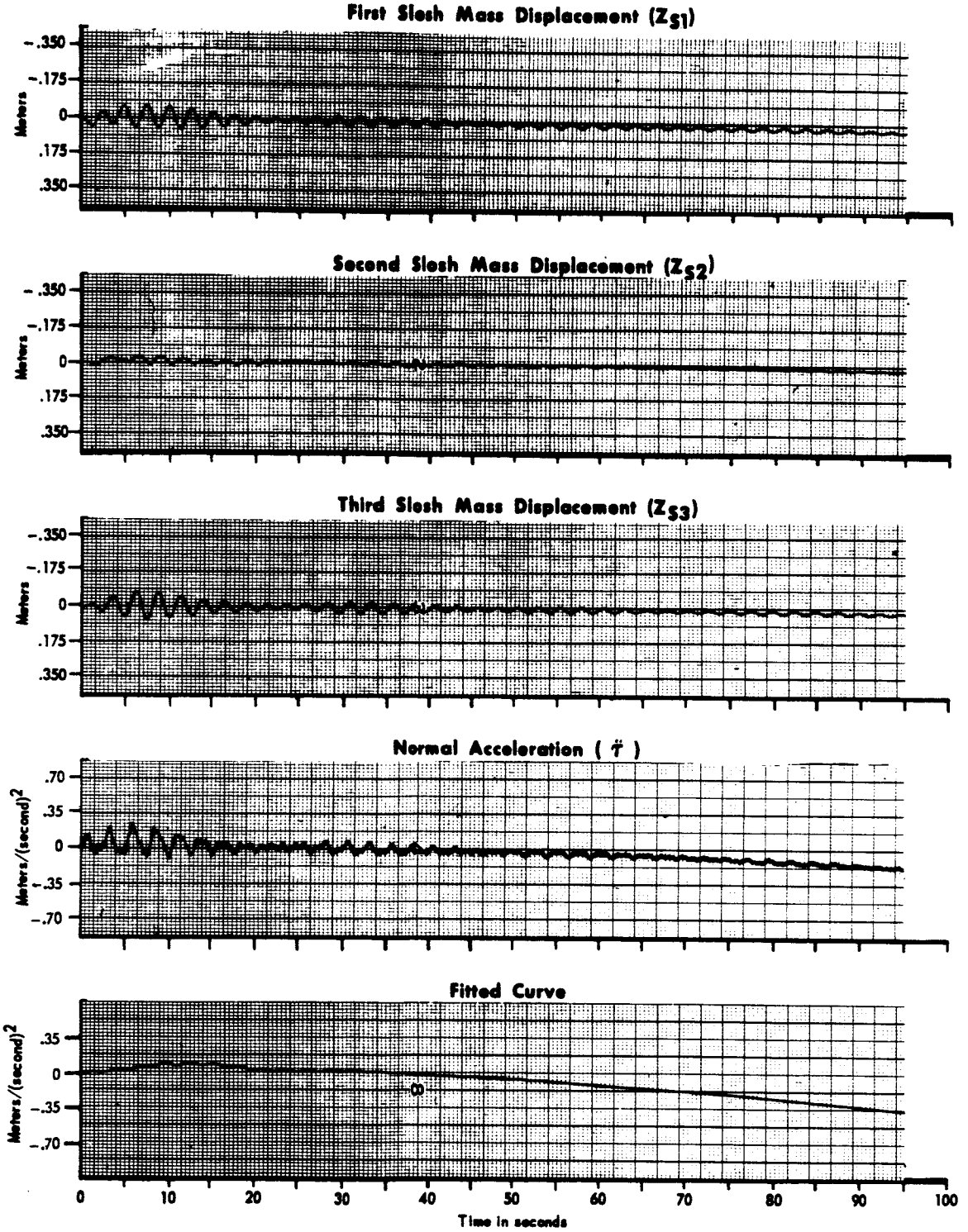

Figure 29 Unit Step Response of Study Vehicle No. II With the Digital Polynomial Filter in the Acceleration Feedback Loop (Cont.)

1. Flight condition, maximum q 2. Body bending and fuel slosh in, 3. Polynomial fitting in acceleration feedback, zero degree (A_0) 4. Past samples stores, 25 5. Sample rate, 2.5 per second	6. Control system design, II.2 7. Forward loop gain, K = 2.2 8. Position feedback gain, K_ϕ = 1.0 9. Rate feedback gain, $K_{\dot\phi}$ = 5.0 10. Acceleration feedback gain, $K_{\ddot\gamma}$ = 0.095

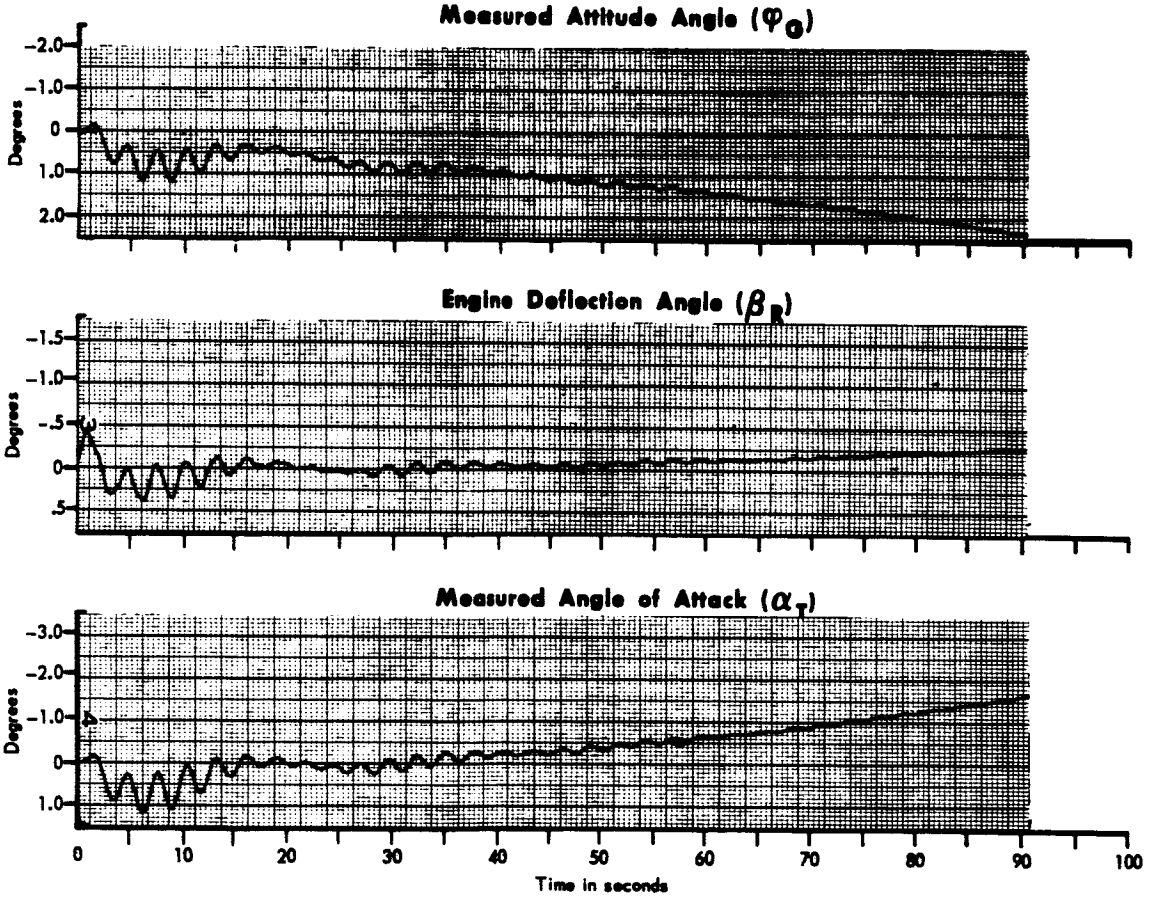

Figure 30 Unit Step Response of Study Vehicle No. II With the Digital Polynomial Filter in the Acceleration Feedback Loop

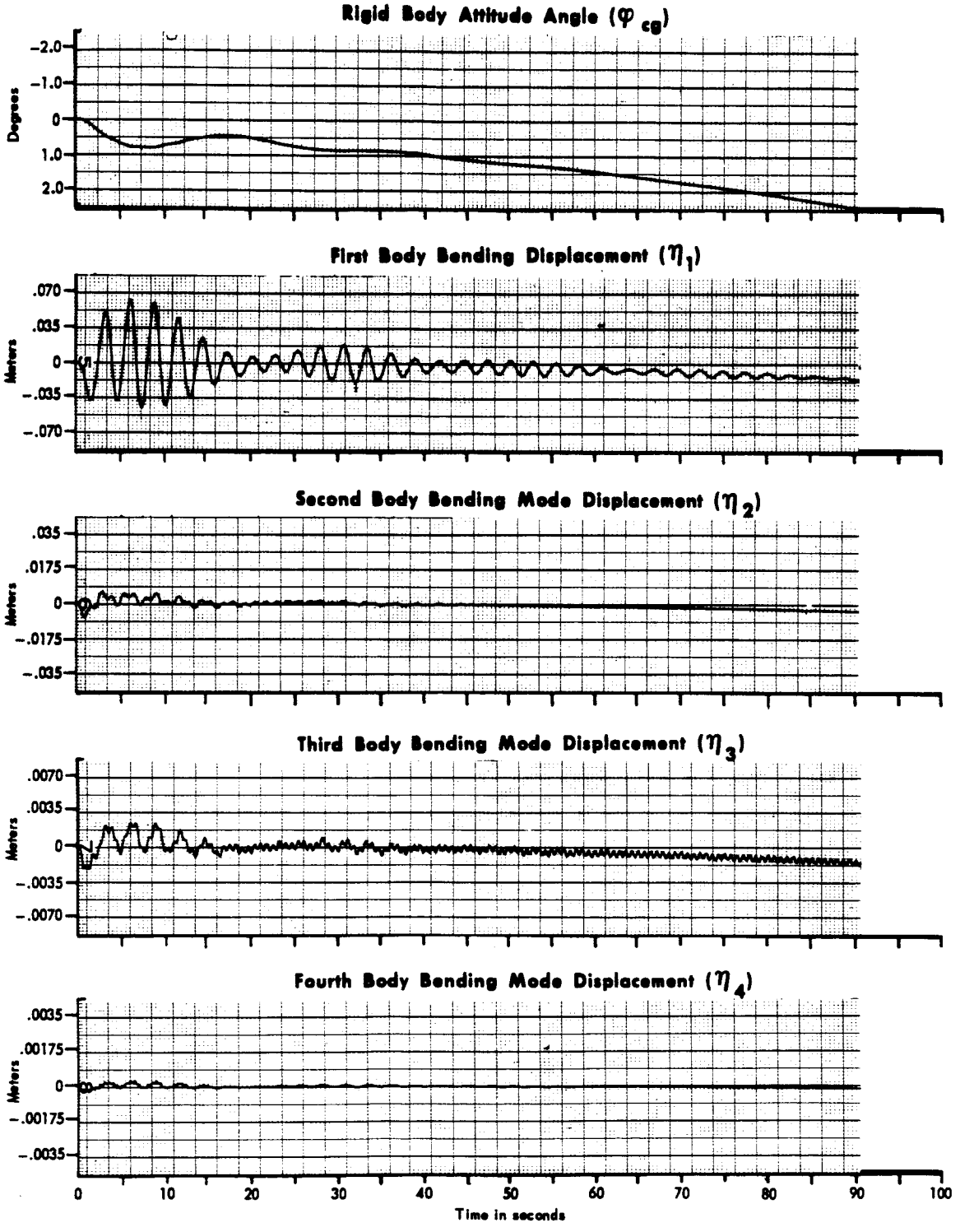

Figure 30 Unit Step Response of Study Vehicle No. II With the Digital Polynomial Filter in the Acceleration Feedback Loop (Cont.)

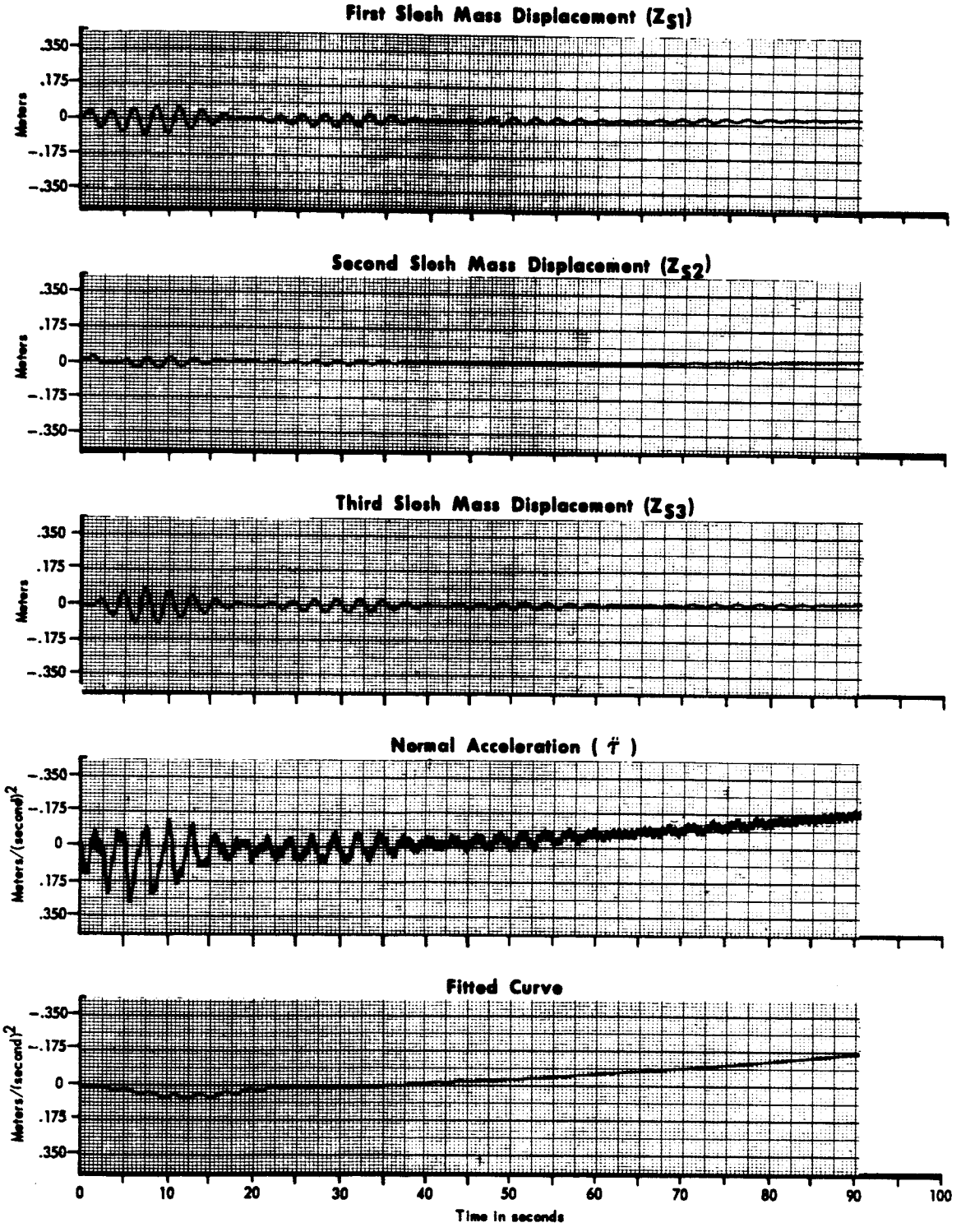

Figure 30 Unit Step Response of Study Vehicle No. II With the Digital Polynomial Filter in the Acceleration Feedback Loop (Cont.)

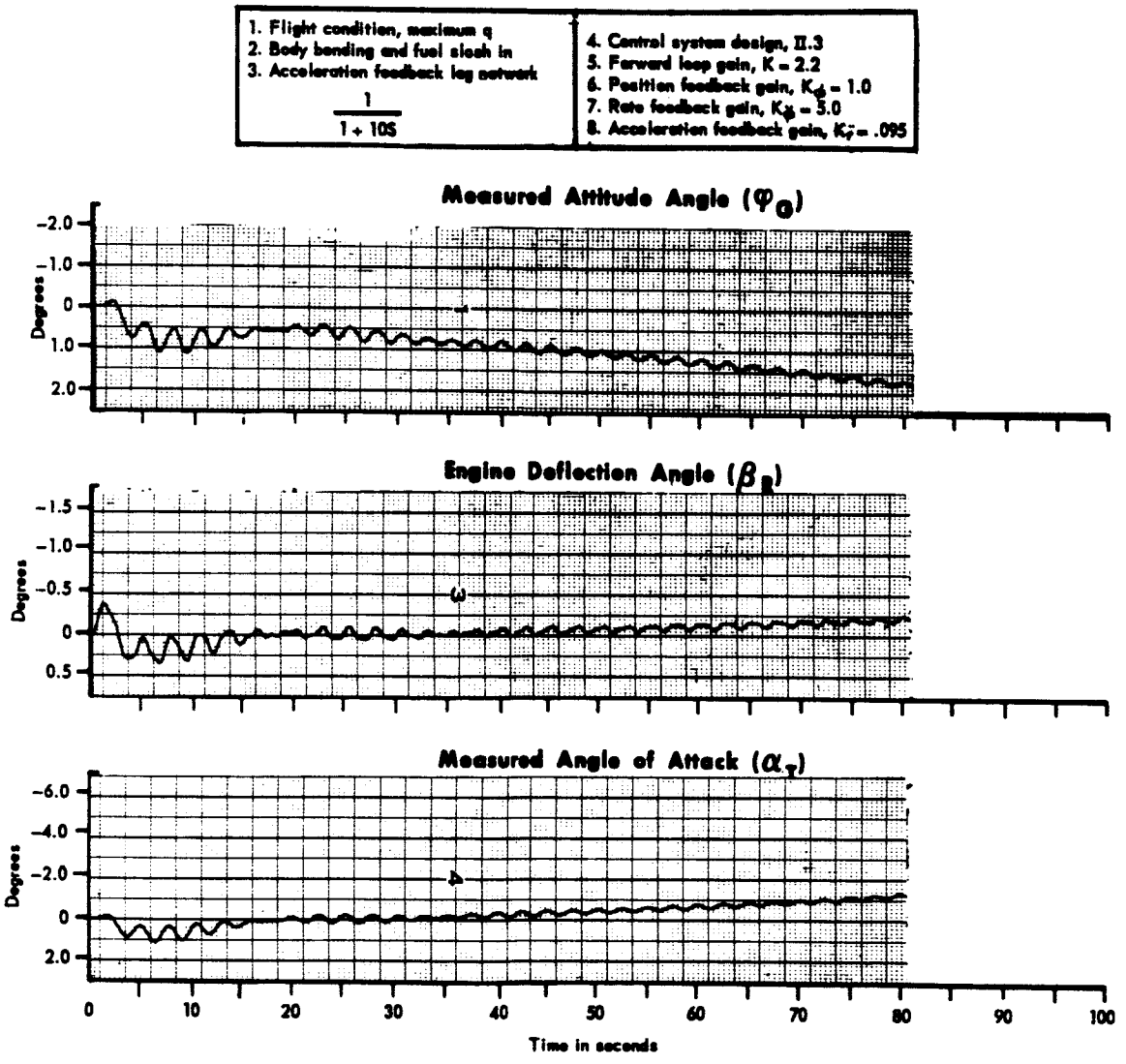

Figure 31 Unit Step Response of Study Vehicle No. II With a Linear Lag Filter in the Acceleration Feedback Loop

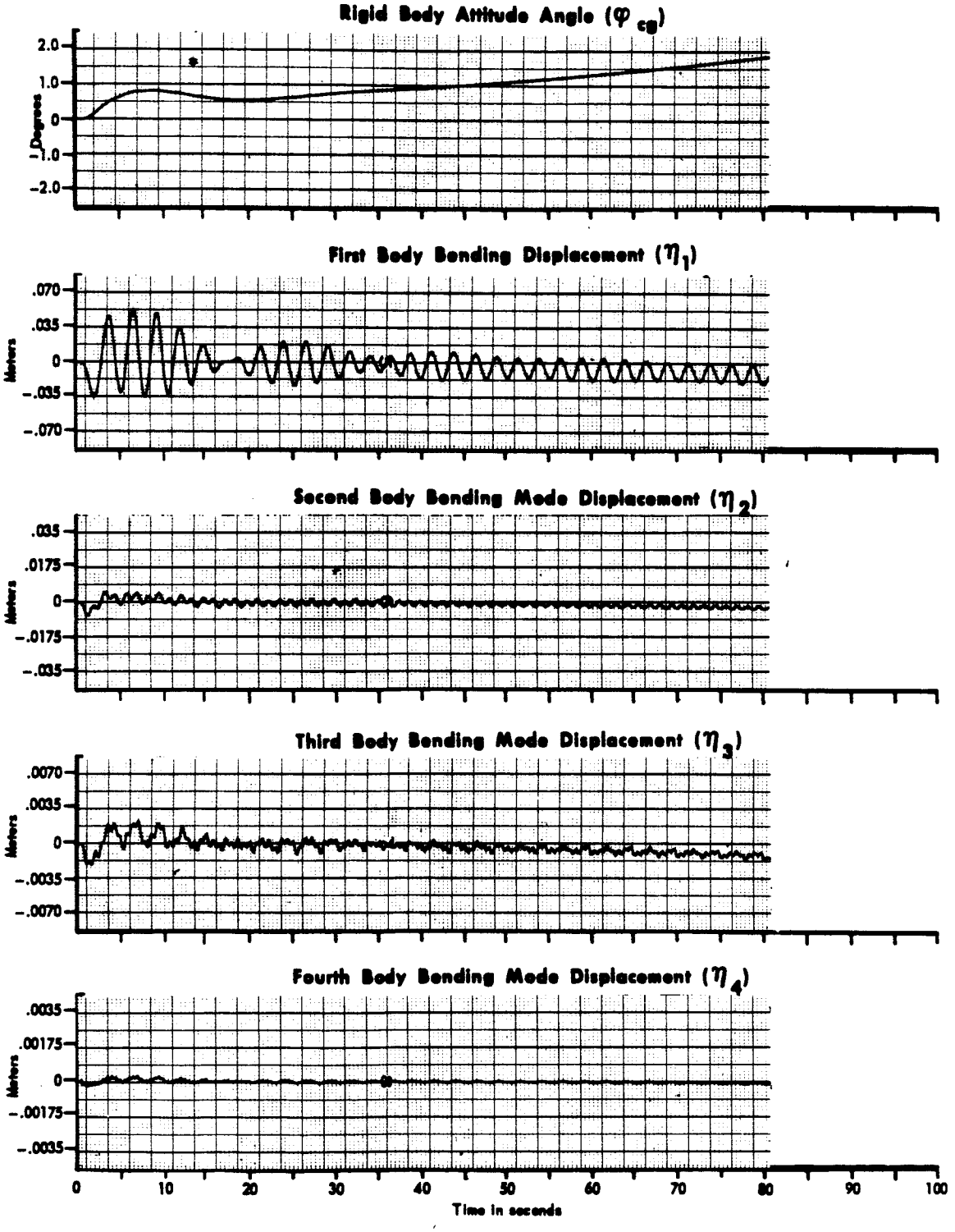

Figure 31 Unit Step Response of Study Vehicle No. II With a Linear Lag Filter in the Acceleration Feedback Loop (Cont.)

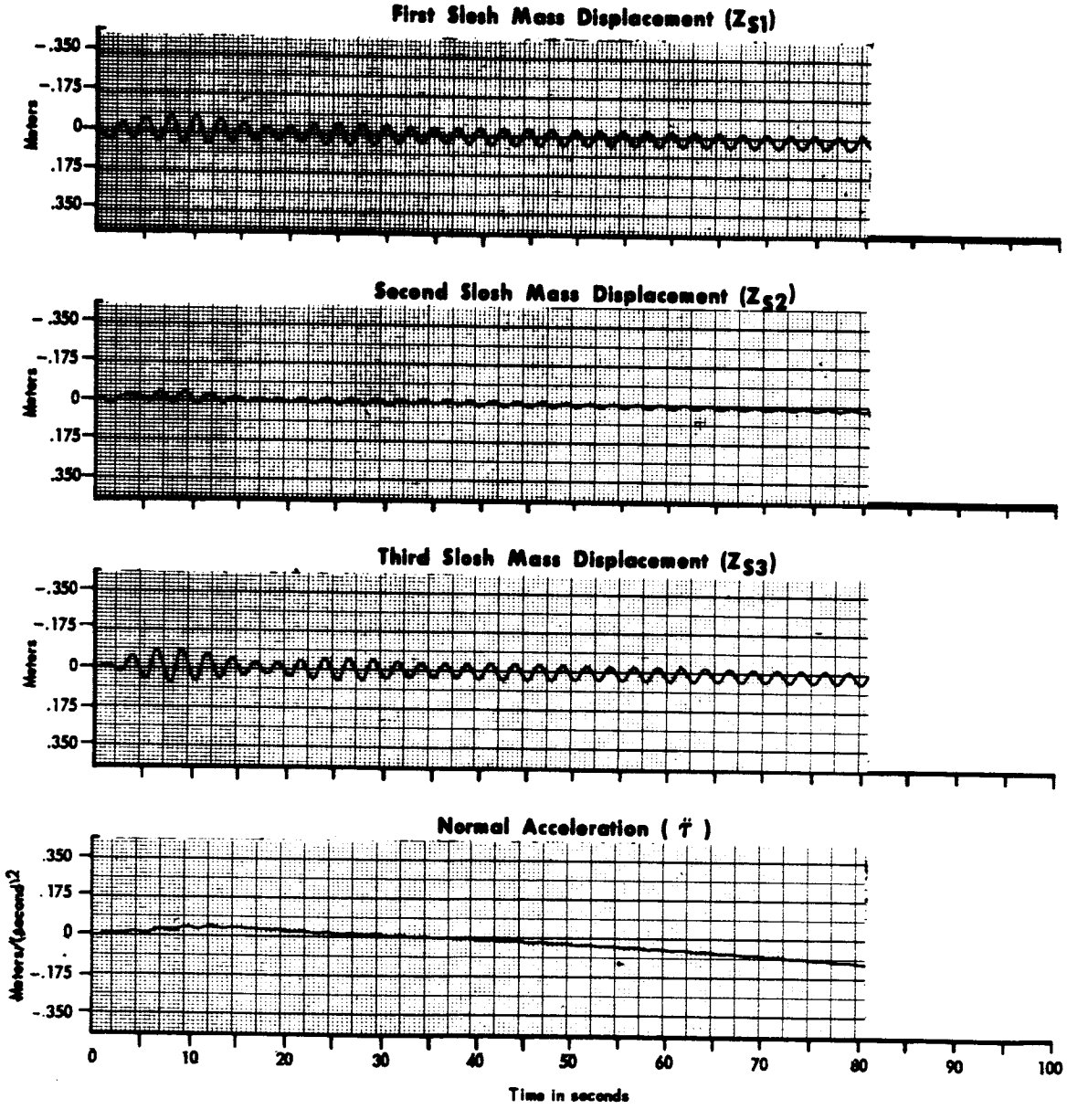

Figure 31 Unit Step Response of Study Vehicle No. II With a Linear Lag Filter in the Acceleration Feedback Loop (Cont.)

1. Flight condition, maximum q
2. Body bending and fuel slosh in
3. Polynomial fitting in angle of attack feedback, zero degree (A_0)
4. Past samples stores, 25
5. Sample rate, 5.0 per second
6. Control system design, I.2
7. Forward loop gain, K = 1.8
8. Position feedback gain, K_ϕ = 1.0
9. Rate feedback gain, $K_{\dot{\phi}}$ = 5.0
10. Angle of attack feedback gain, K_α = .931

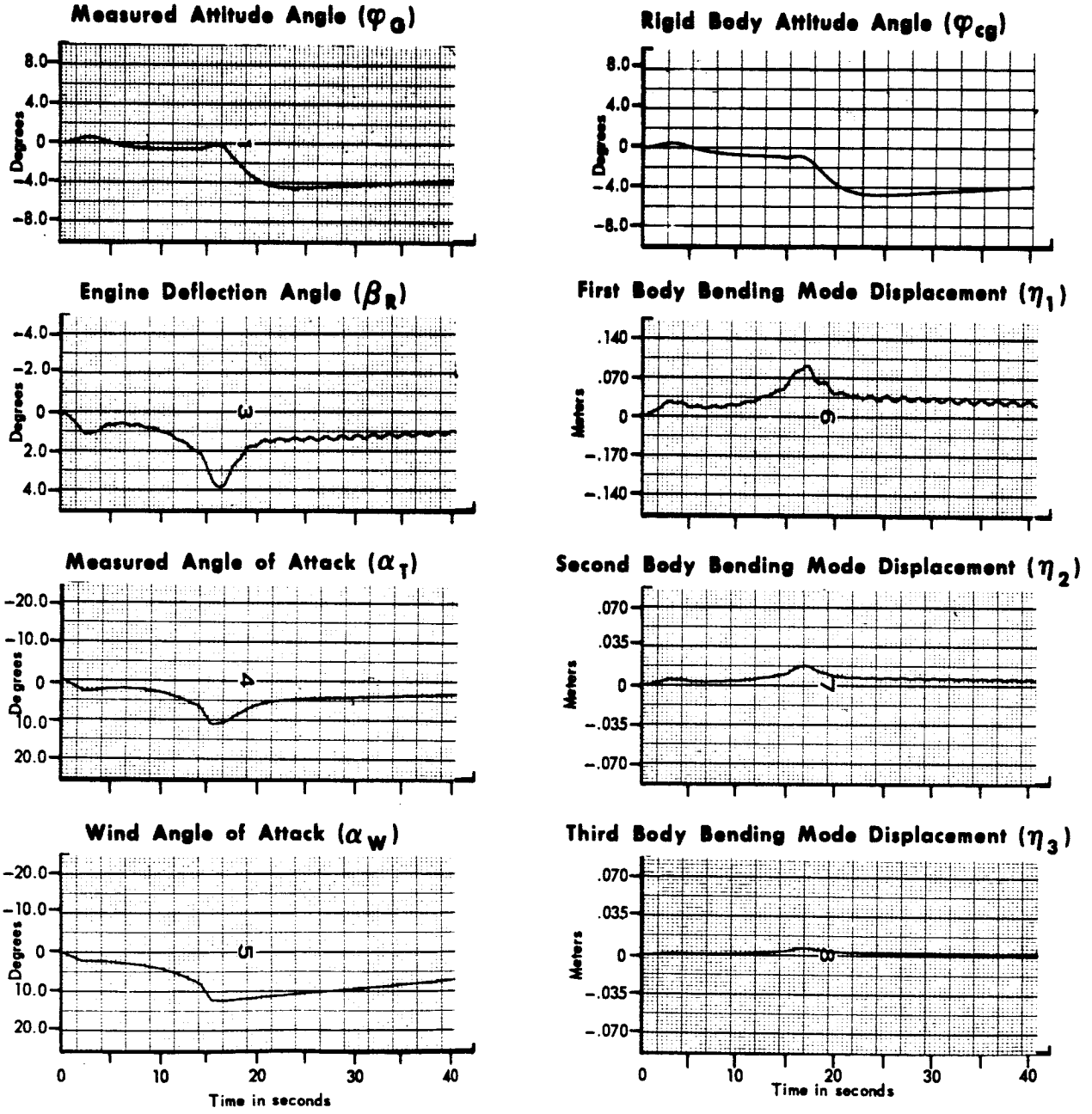

Figure 32 Wind Response of Study Vehicle No. I With the Digital Polynomial Filter in the Angle-of-Attack Feedback Loop

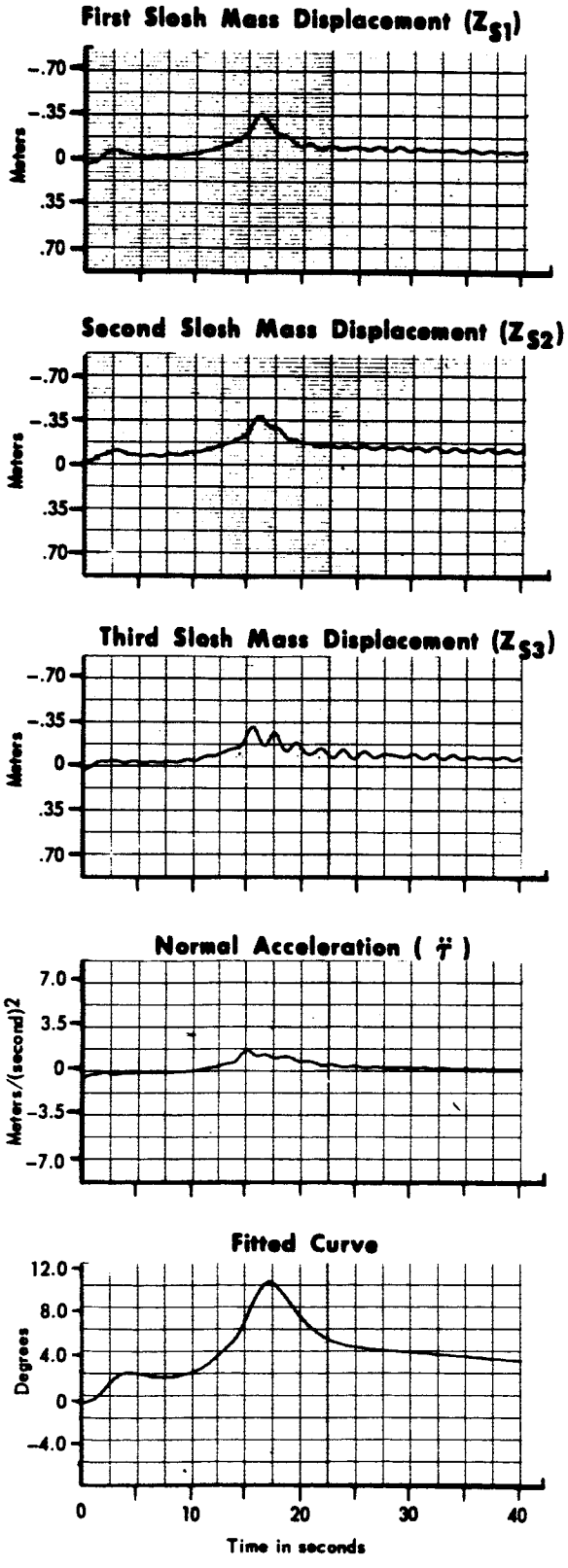

Figure 32 Wind Response of Study Vehicle No. I With the Digital Polynomial Filter in the Angle-of-Attack Feedback Loop (Cont.)

1. Flight condition, maximum q
2. Body bending and fuel slosh in
3. Polynomial fitting in angle of attack feedback, zero degree (A_0)
4. Past samples stored, 25
5. Sample rate, 5.0 per second
6. Control system design, I.2
7. Forward loop gain, K = 1.8
8. Position feedback gain, K_ϕ = 1.0
9. Rate feedback gain, $K_{\dot{\phi}}$ = 5.0
10. Angle of attack feedback gain, K_α = .931

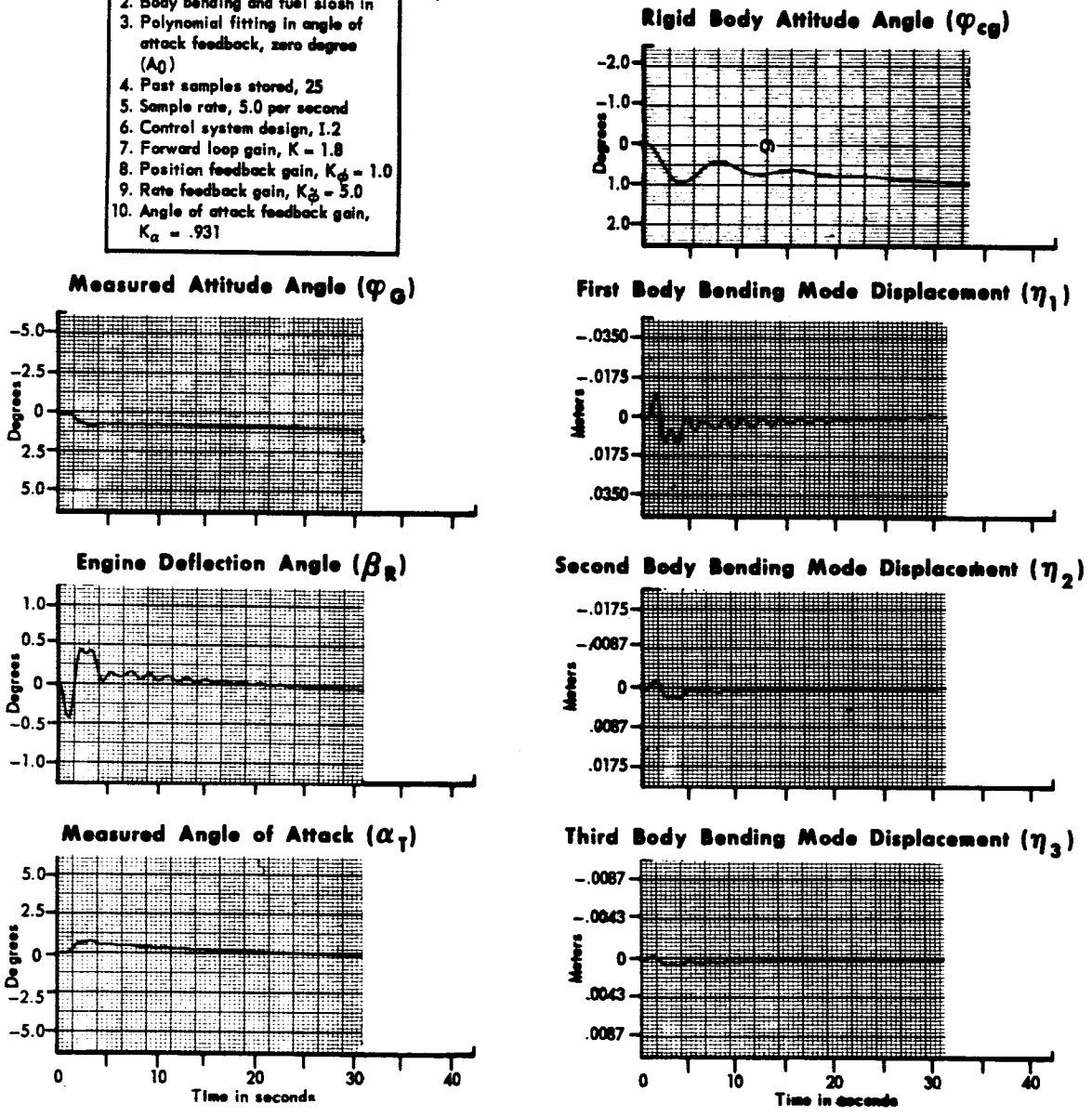

Figure 33 Unit Step Response of Study Vehicle No. I With the Digital Polynomial Filter in the Angle-of-Attack Feedback Loop

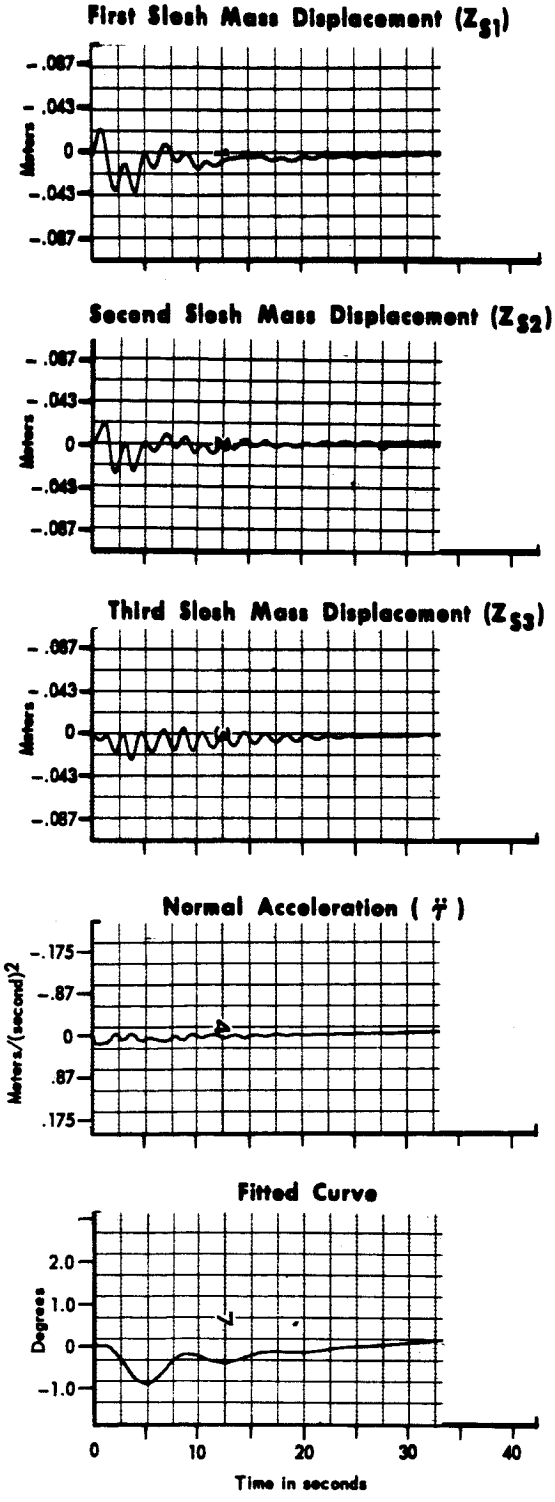

Figure 33 Unit Step Response of Study Vehicle No. I With the Digital Polynomial Filter in the Angle-of-Attack Feedback Loop (Cont.)

1. Flight condition, maximum q
2. Body bending and fuel slosh in
3. Control system design, I.2
4. Forward loop gain, K = 1.8
5. Position feedback gain, K_ϕ = 1.0
6. Rate feedback gain, $K_{\dot{\phi}}$ = 5.0
7. Angle of attack feedback gain, K_α = .931
8. No polynomial fitting in acceleration feedback

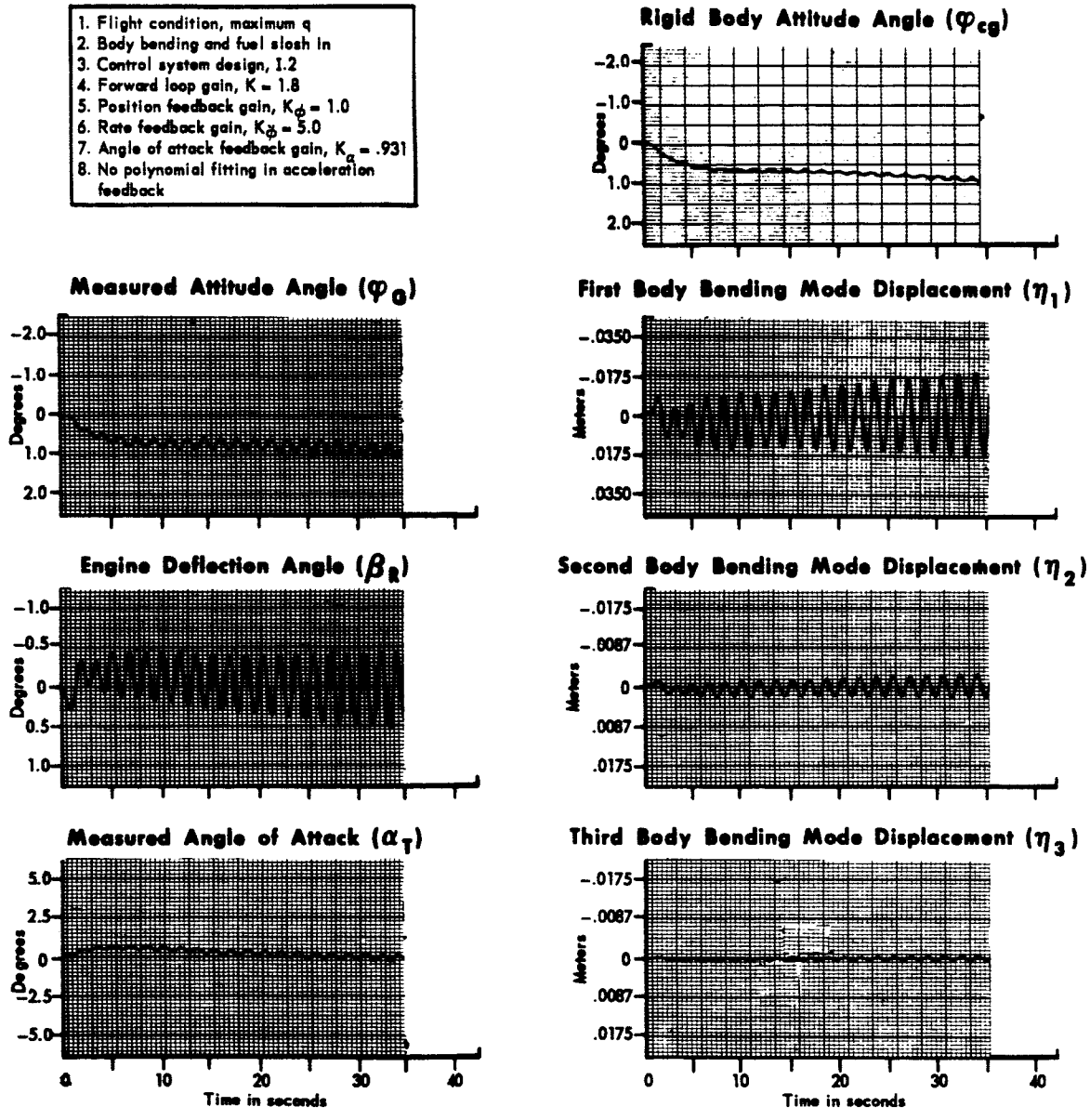

Figure 34 Unit Step Response of Study Vehicle No. I Without Filtering in the Angle-of-Attack Feedback Loop

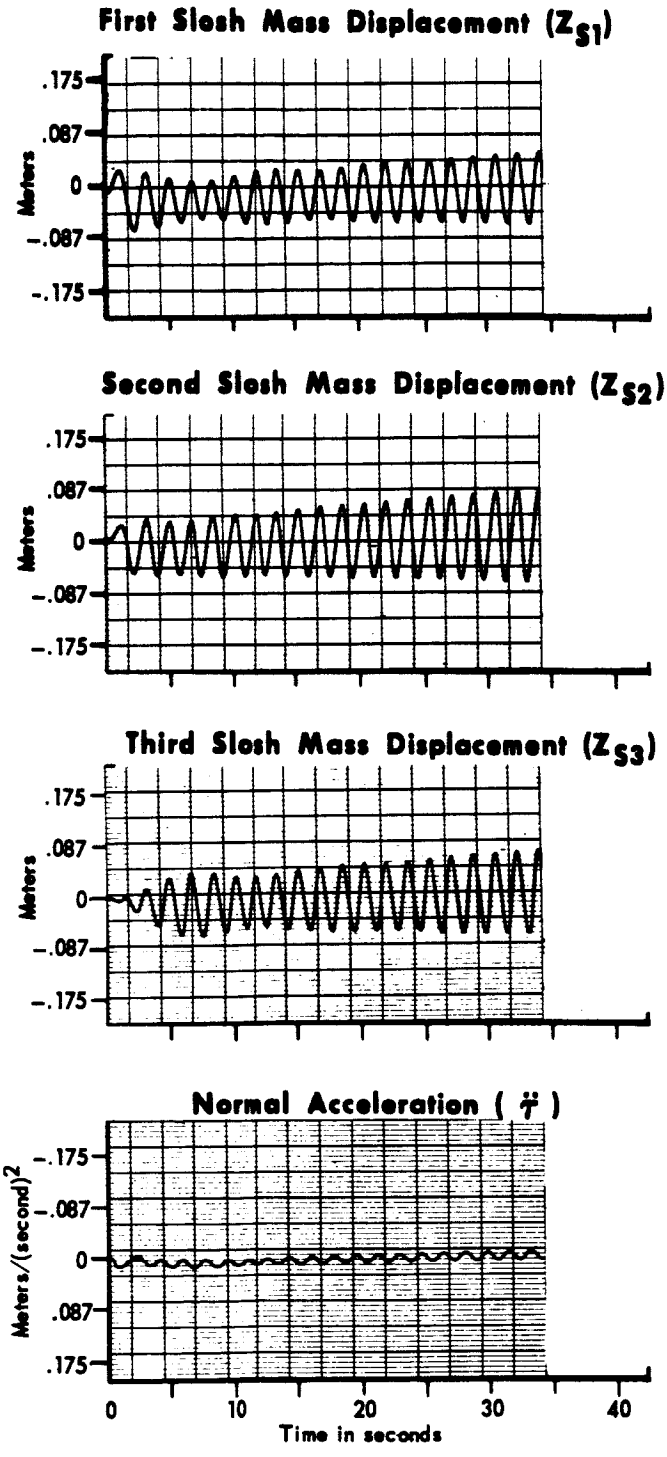

Figure 34 Unit Step Response of Study Vehicle No. I Without Filtering in the Angle-of-Attack Feedback Loop (Cont.)

1. Flight condition, maximum q
2. Body bending and fuel slosh in
3. Polynomial fitting in acceleration feedback, zero degree (A_0)
4. Past samples stores, 25
5. Sample rate, 5 per second
6. Polynomial fitting in rate feedback, zero plus first degree ($A_0 + A_1$)
7. Past samples stored, 5
8. Sample rate, 5 per second
9. Control system stability compensation $\frac{(S+8.6)^2+6.3^2}{(S+5)(S+3)}$
10. Forward loop gain, K = 2.2
11. Position feedback gain, $K_\phi = 1.0$
12. Rate feedback gain, $K_{\dot\phi} = 5.0$
13. Acceleration feedback gain, $K_{\dot\gamma} = 0.095$

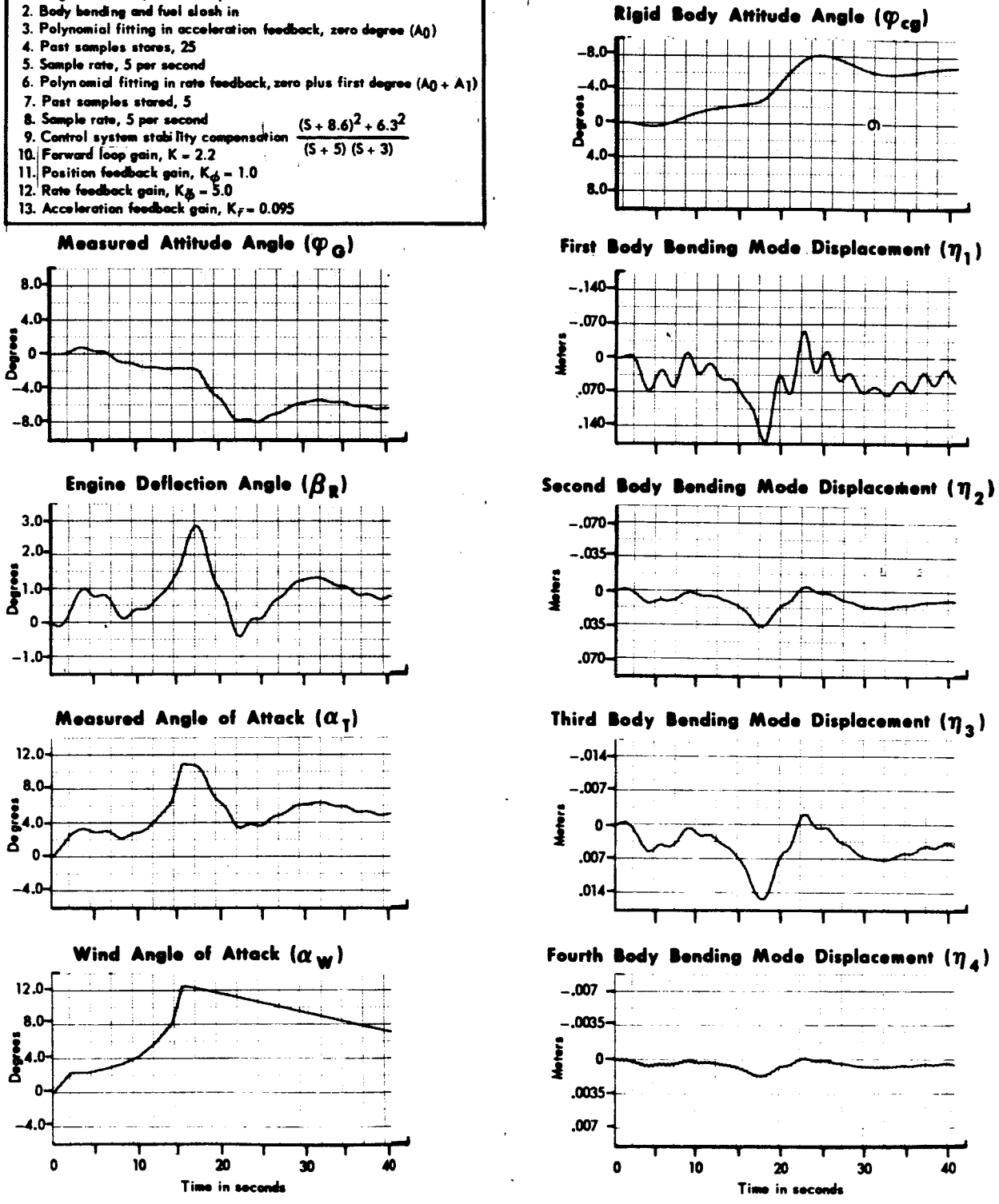

Figure 35 Wind Response of Study Vehicle No. II With the Digital Polynomial Filter in the Acceleration and Attitude Rate Feedback Loop

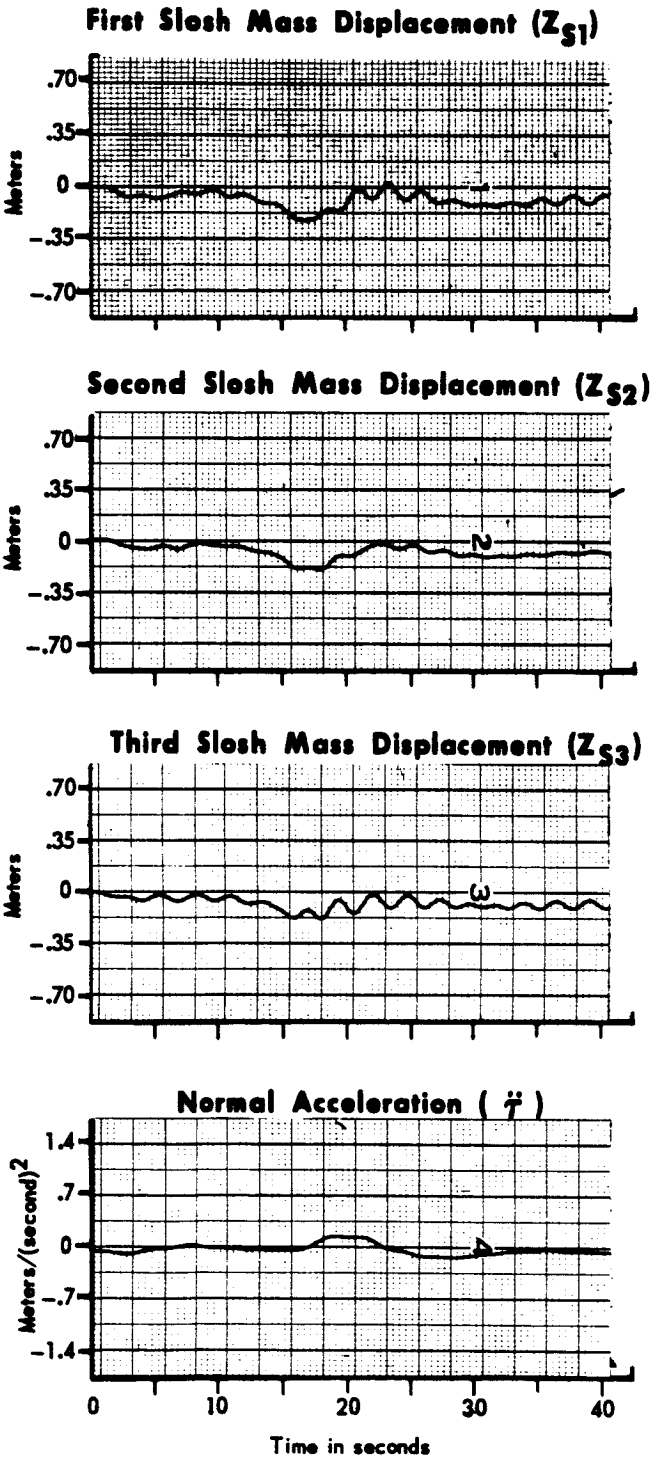

Figure 35 Wind Response of Study Vehicle No. II With the Digital Polynomial Filter in the Acceleration and Attitude Rate Feedback Loop (Cont.)

1. Flight condition, maximum q 2. Body bending and fuel slosh, in 3. Polynomial fitting in acceleration feedback, zero degree (A_0) 4. Past samples stored, 25 5. Sample rate, 5 per second 6. Polynomial fitting in rate feedback, zero plus first degree ($A_0 + A_1$) 7. Past samples stored, 5 8. Sample rate, 5 per second	9. Control system stability compensation, $\frac{(S+8.6)^2+6.3^2}{(S+5)(S+3)}$ 10. Forward loop gain, K = 2.2 11. Position feedback gain, $K_\phi = 1.0$ 12. Rate feedback gain, $K_{\dot{\phi}} = 5.0$ 13. Acceleration feedback gain, $K_{\ddot{r}} = 0.095$

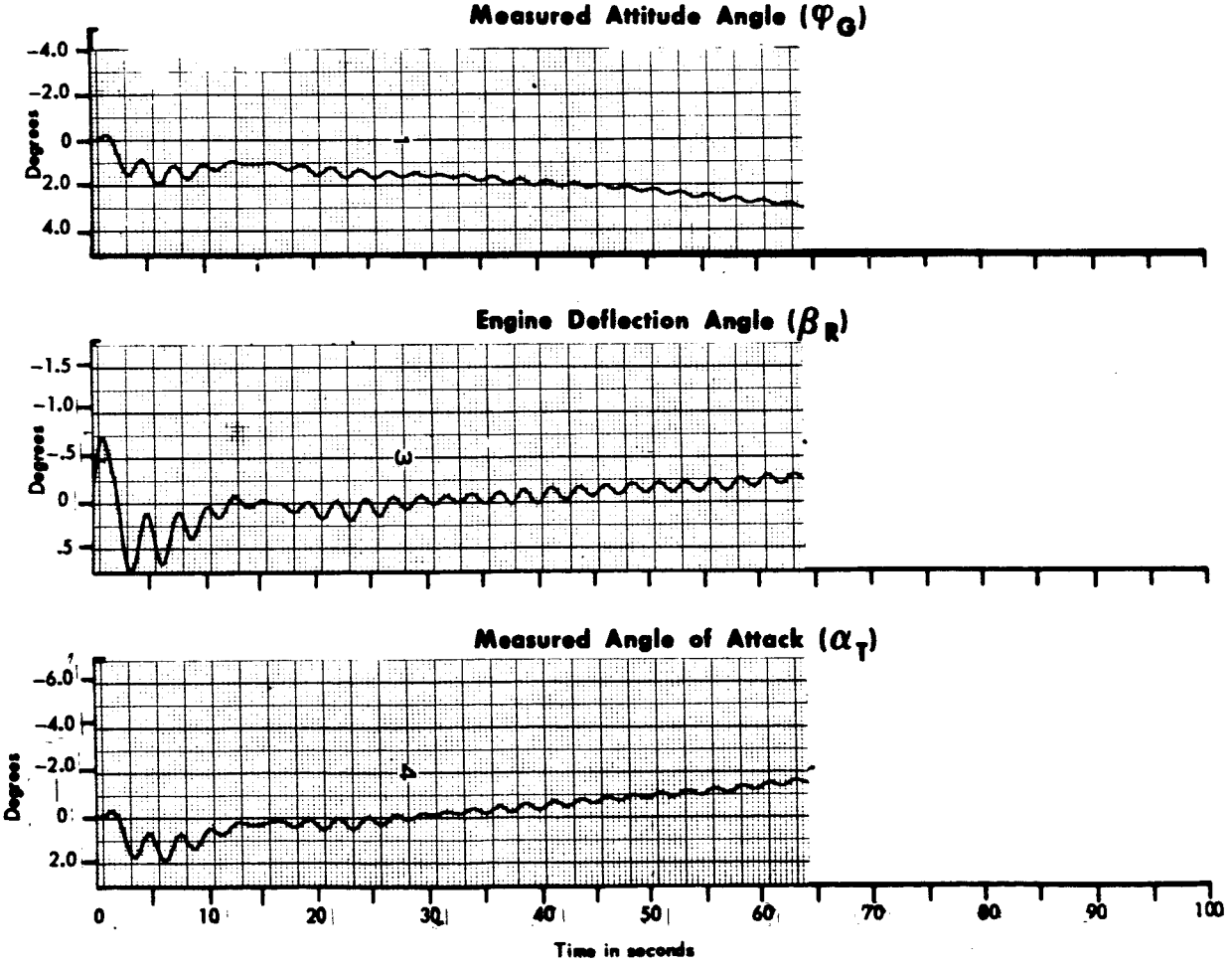

Figure 36 Unit Step Response of Study Vehicle No. II With the Digital Polynomial Filter in the Acceleration and Attitude Rate Feedback Loop

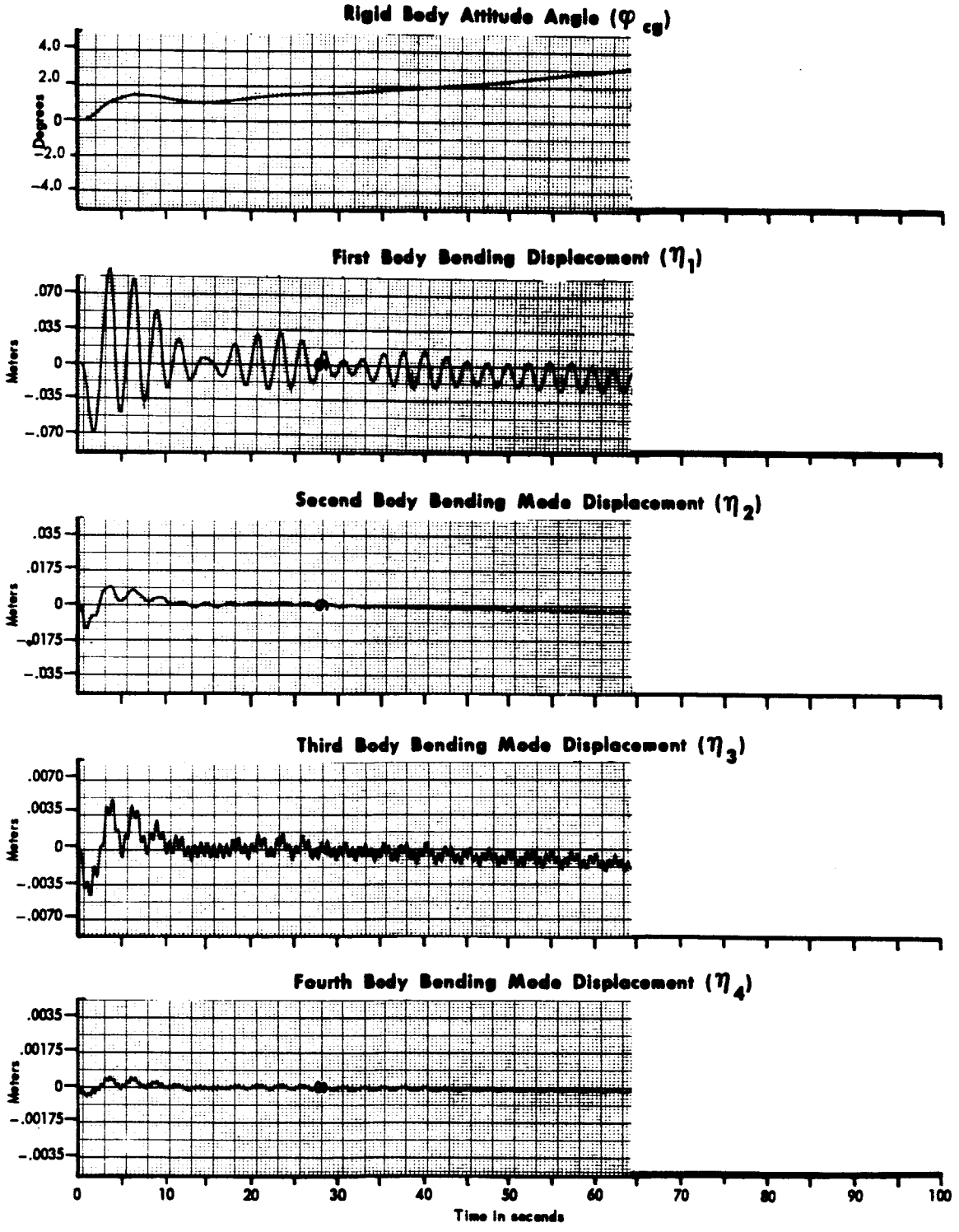

Figure 36 Unit Step Response of Study Vehicle No. II With the Digital Polynomial Filter in the Acceleration and Attitude Rate Feedback Loop (Cont.)

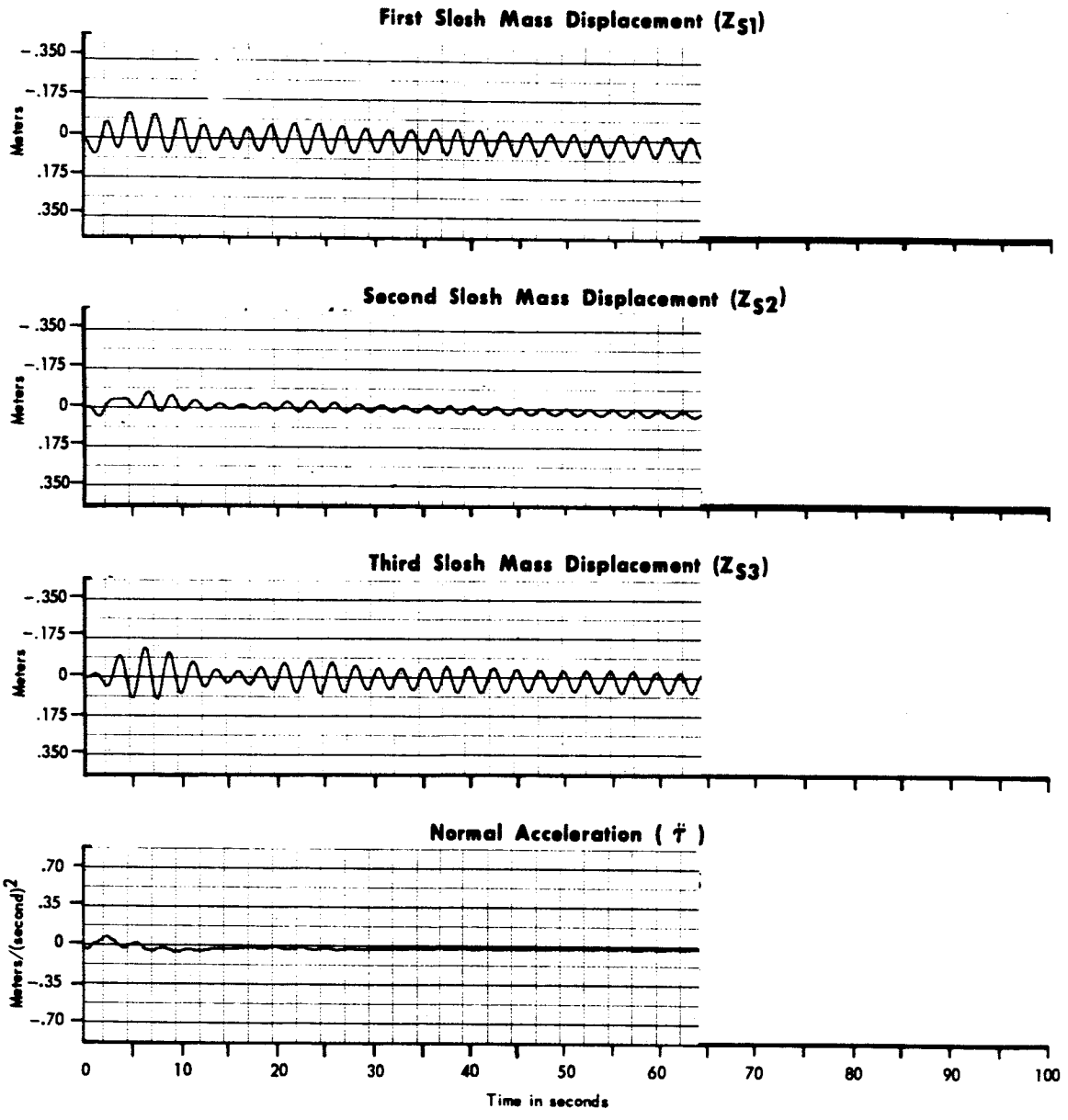

Figure 36 Unit Step Response of Study Vehicle No. II With the Digital Polynomial Filter in the Acceleration and Attitude Rate Feedback Loop (Cont.)

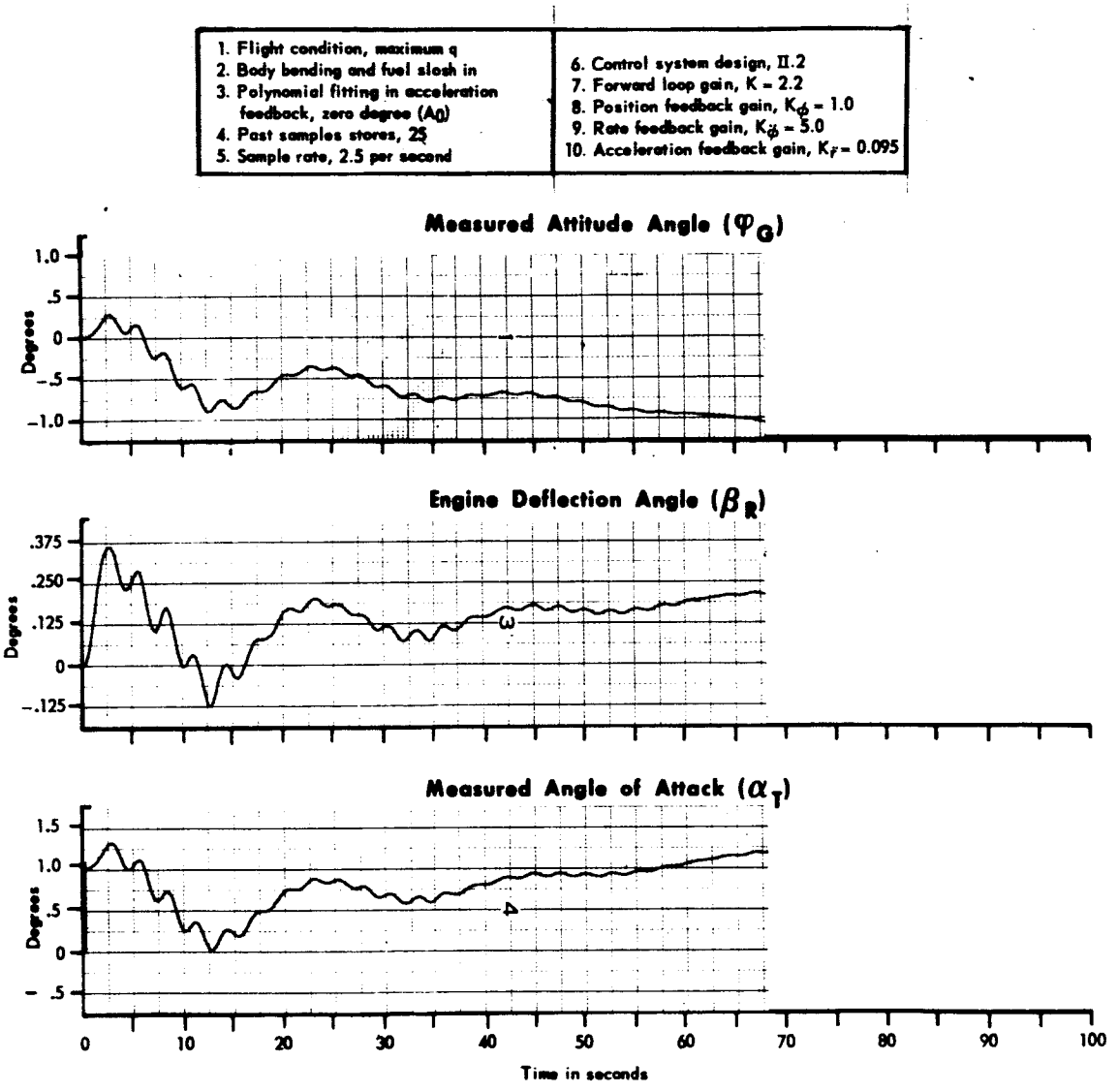

Figure 37 Wind Step Response of Study Vehicle No. II With the Digital Polynomial Filter in the Acceleration Feedback Loop

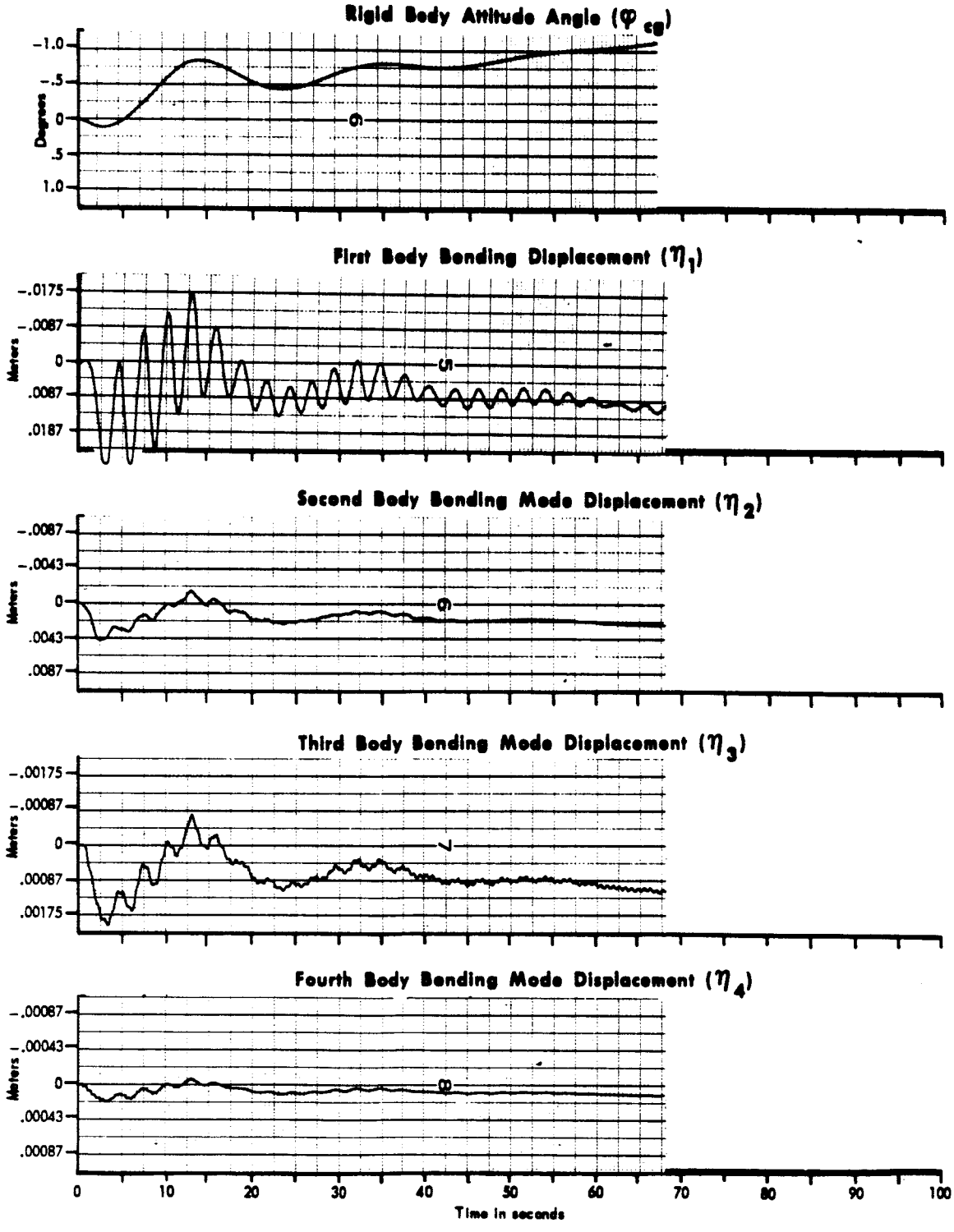

Figure 37 Wind Step Response of Study Vehicle No. II With the Digital Polynomial Filter in the Acceleration Feedback Loop (Cont.)

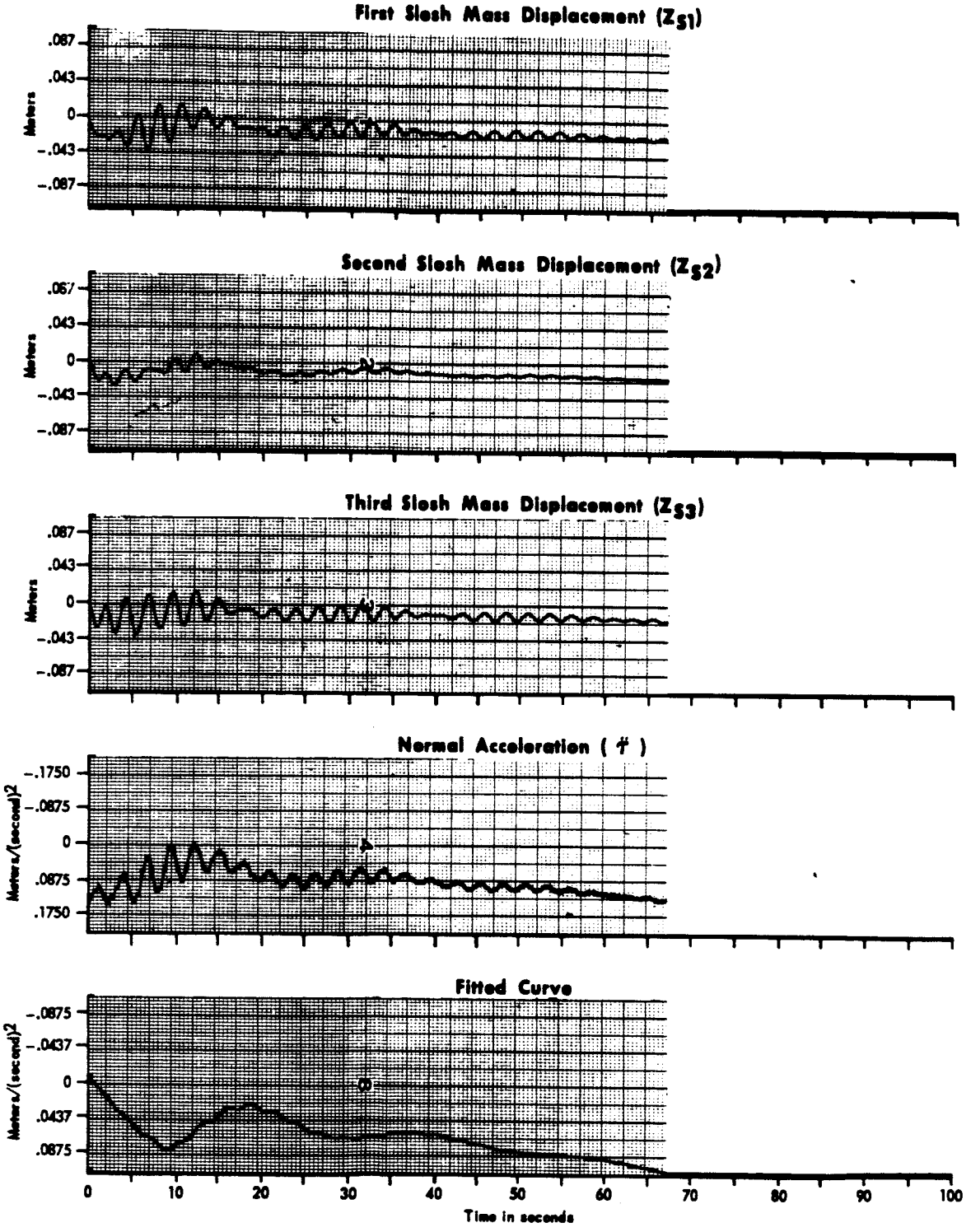

Figure 37 Wind Step Response of Study Vehicle No. II With the Digital Polynomial Filter in the Acceleration Feedback Loop (Cont.)

1. Flight condition, maximum q	6. Control system design, I.1
2. Body bending and fuel slosh in	7. Forward loop gain, K = 1.8
3. Polynomial fitting in acceleration feedback, zero degree (A_0)	8. Position feedback gain, K_ϕ = 1.0
4. Past samples stores, 25	9. Rate feedback gain, $K_{\dot\phi}$ = 5.0
5. Sample rate, 5 per second	10. Acceleration feedback gain, $K_{\ddot\gamma}$ = 0.072

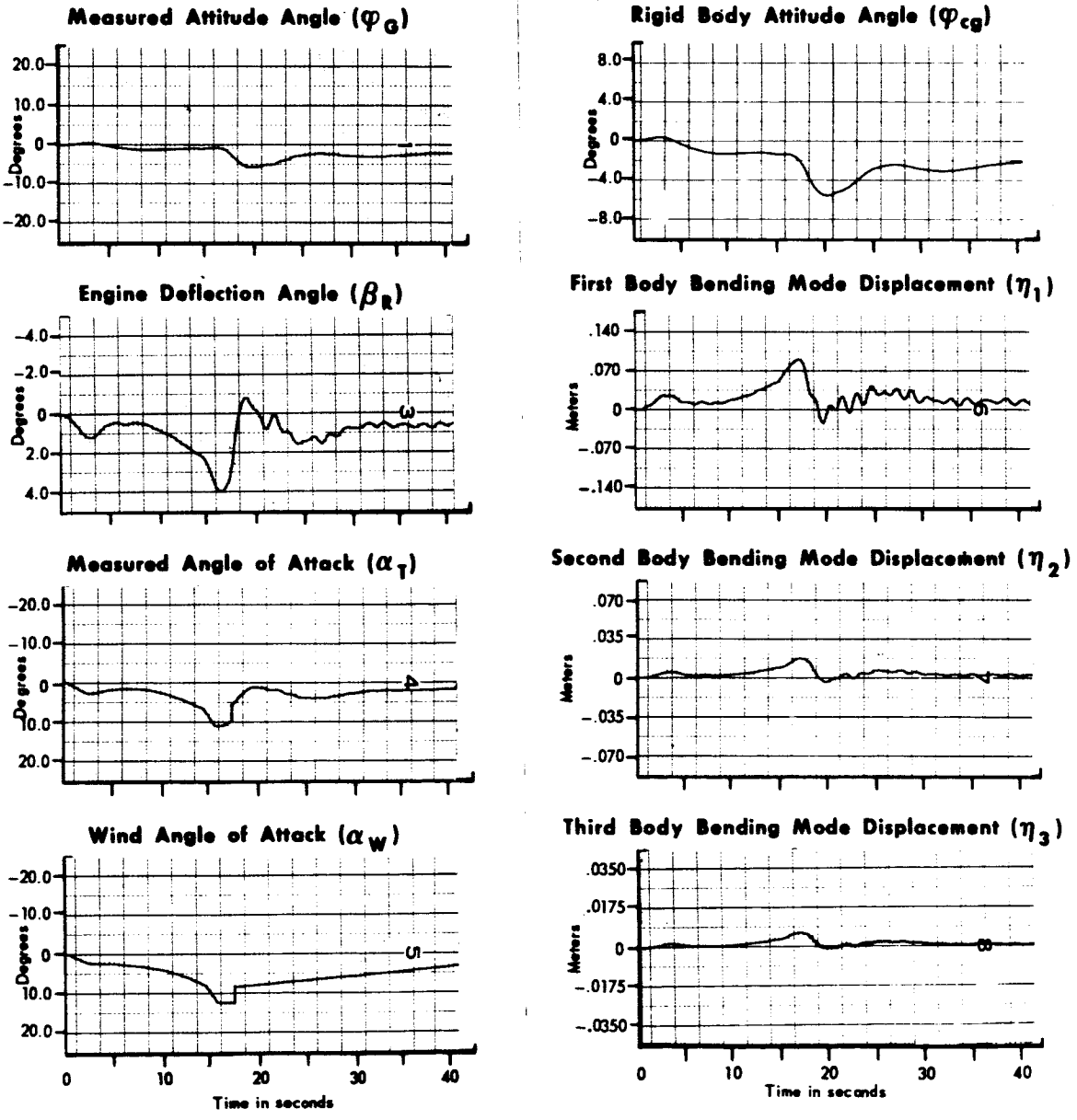

Figure 38 Wind With Step Response of Study Vehicle No.1 With the Digital Polynomial Filter in the Acceleration Feedback Loop

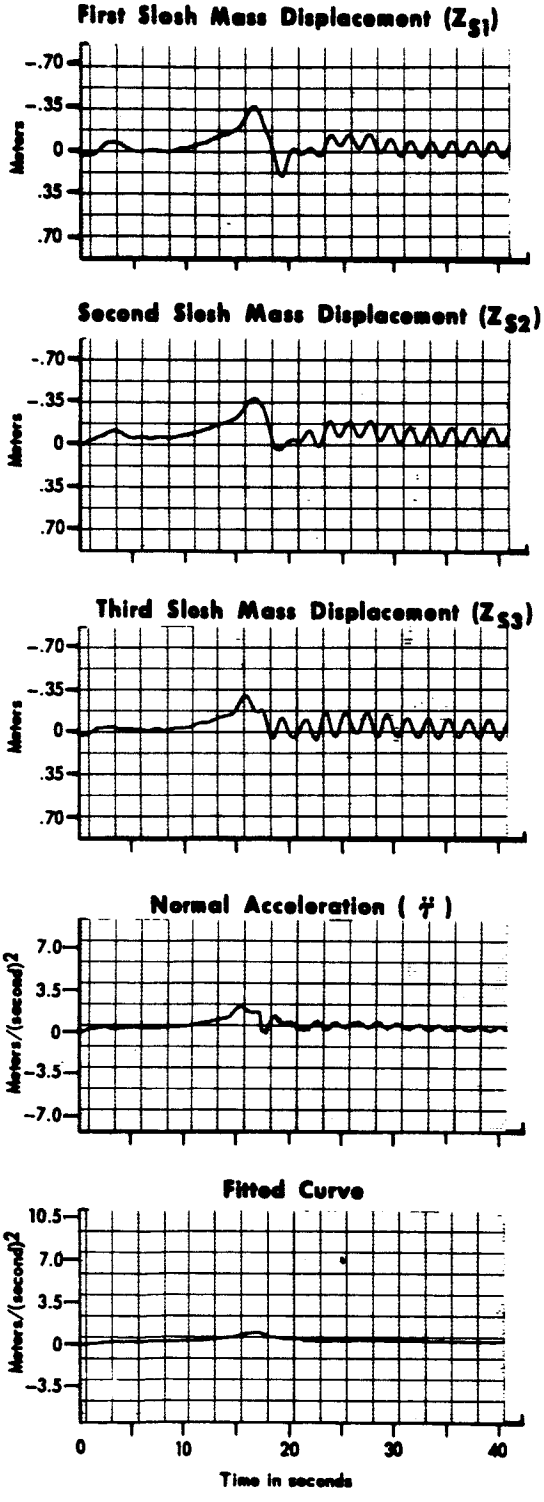

Figure 38 Wind With Step Response of Study Vehicle No. I With the Digital Polynomial Filter in the Acceleration Feedback Loop (Cont.)

1. Flight condition, maximum q	6. Control system design I.1
2. Body bending and fuel slosh, in	7. Forward loop gain, K = 1.8
3. Polynomial fitting in acceleration feedback, zero degree (A_0)	8. Position feedback gain, K_ϕ = 1.0
4. Past samples stored, 25	9. Rate feedback gain, $K_{\dot\phi}$ = 5.0
5. Sample rate, 5 per second	10. Acceleration feedback gain, $K_{\ddot\gamma}$ = 0.072

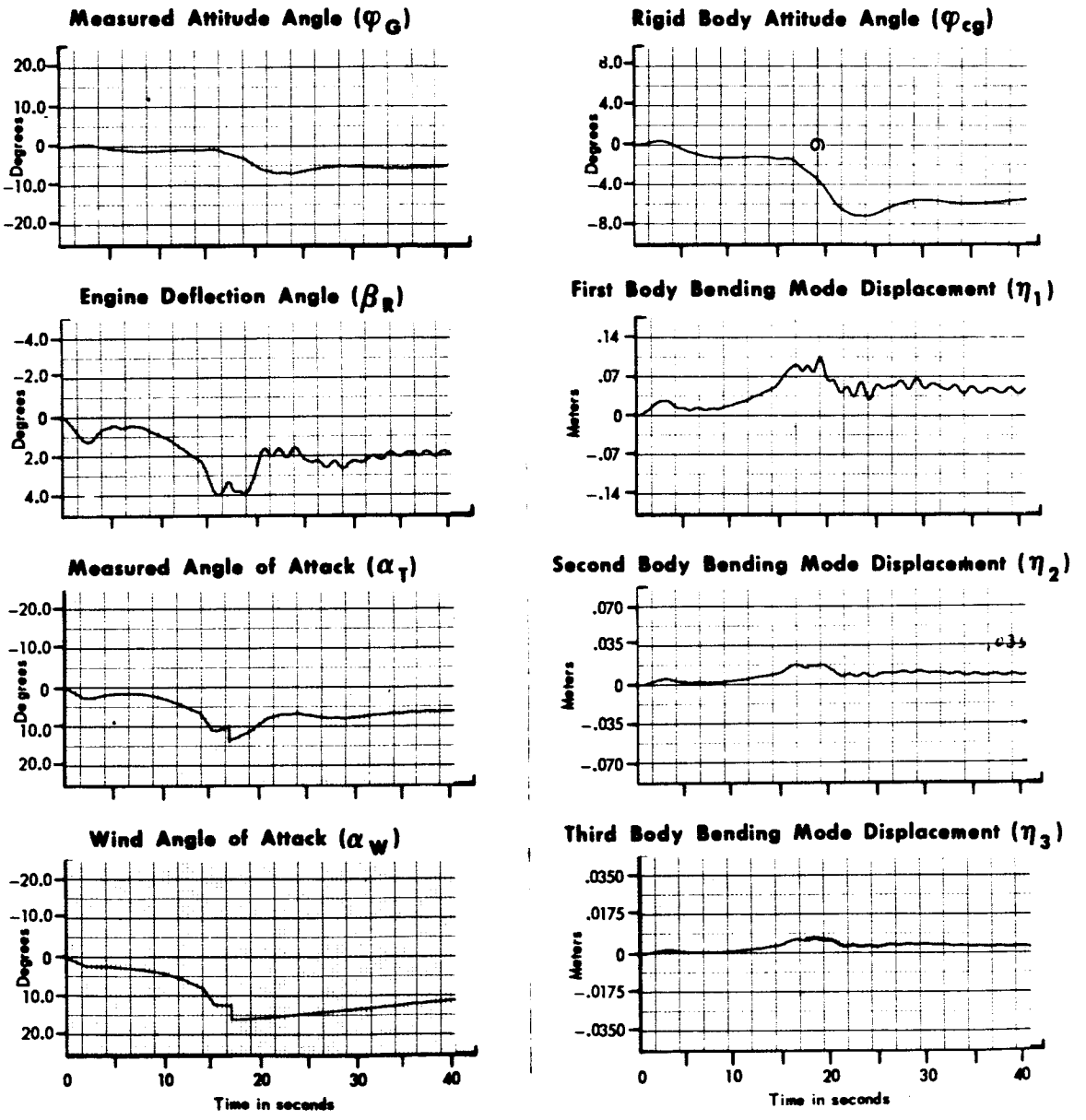

Figure 39 Wind With Step Response of Study Vehicle No. I With the Digital Polynomial Filter in the Acceleration Feedback Loop

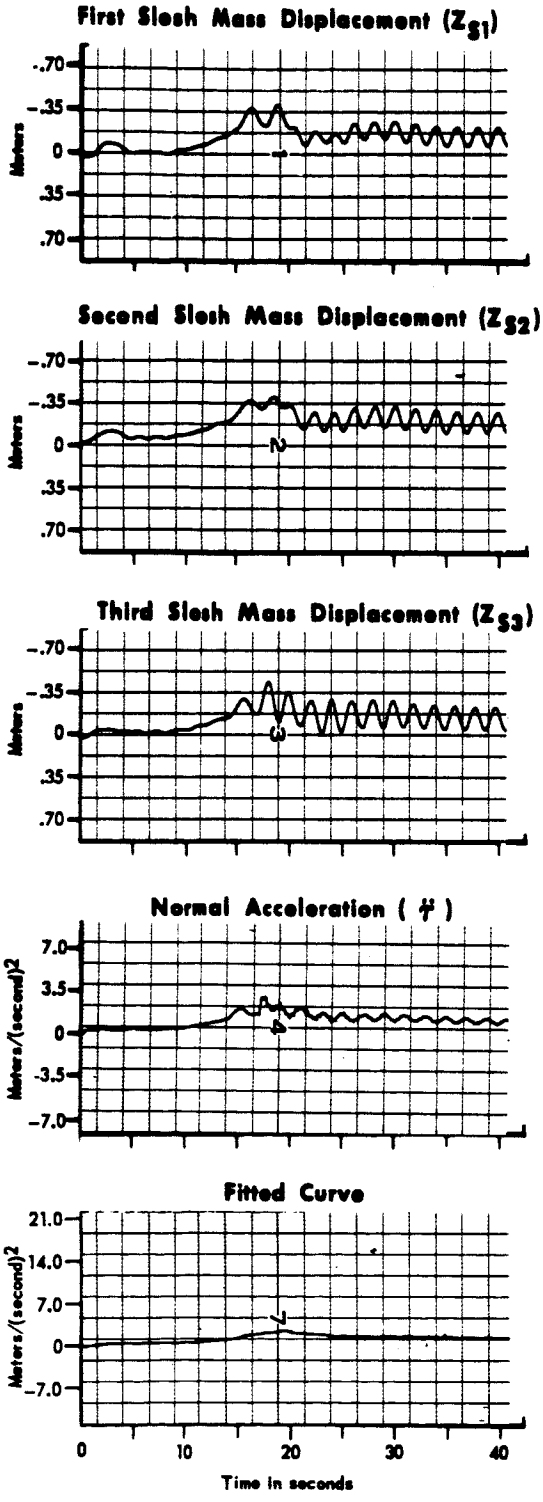

Figure 39 Wind With Step Response of Study Vehicle No. 1 With the Digital Polynomial Filter in the Acceleration Feedback Loop (Cont.)

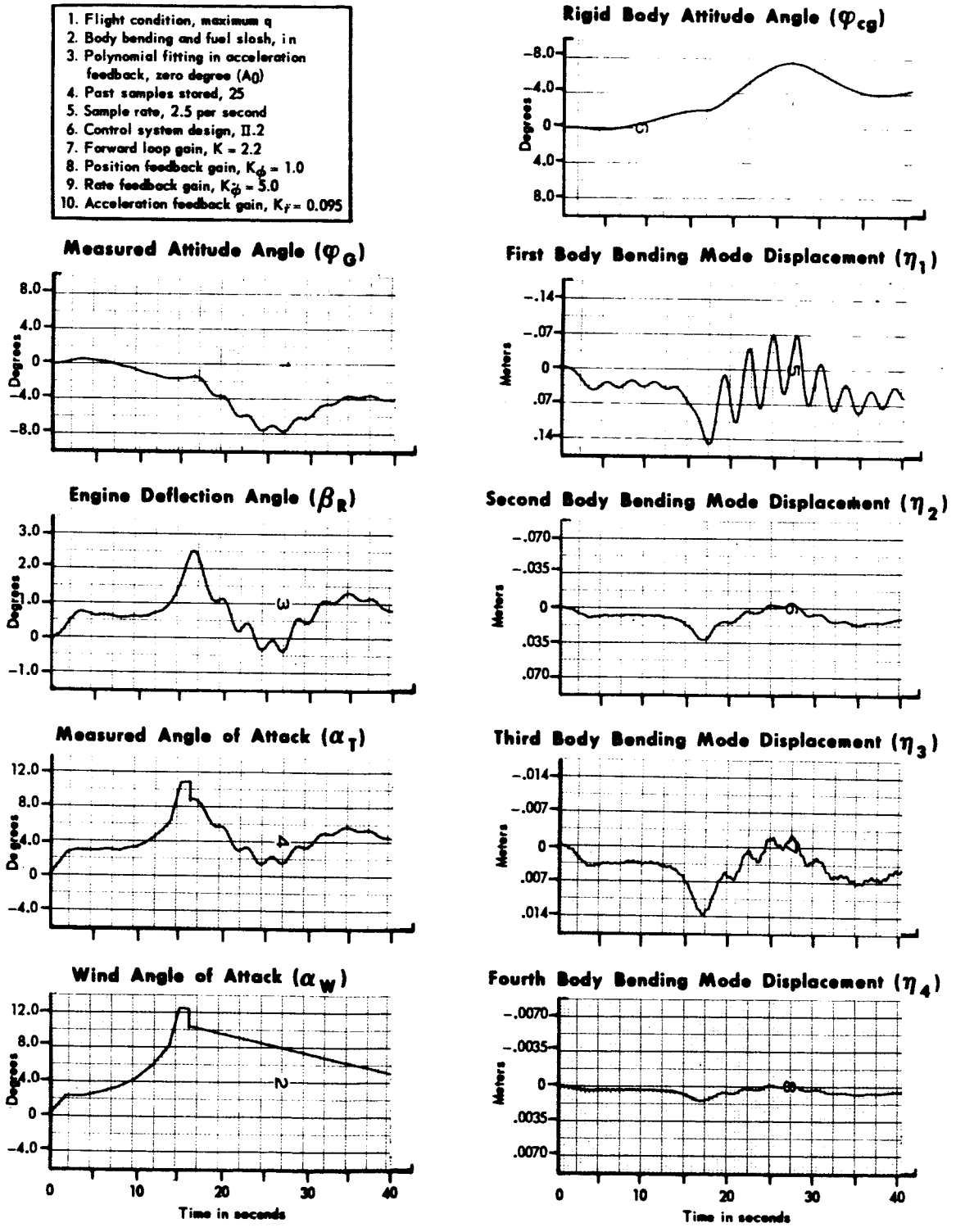

Figure 40 Wind With Step Response of Study Vehicle No. II With the Digital Polynomial Filter in the Acceleration Feedback Loop

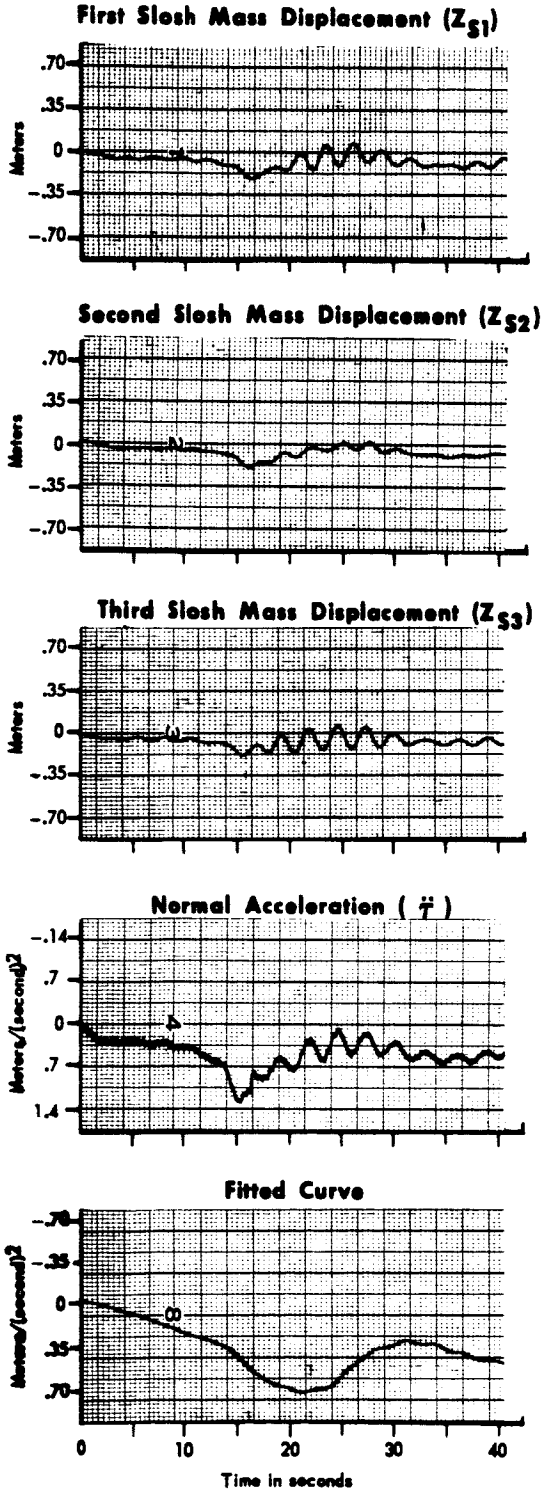

Figure 40 Wind With Step Response of Study Vehicle No.II With the Digital Polynomial Filter in the Acceleration Feedback Loop (Cont.)

1. Flight condition, maximum q
2. Body bending and fuel slosh in
3. Polynomial fitting in acceleration feedback, zero degree (A_0)
4. Past samples stored, 25
5. Sample rate, 2.5 per second
6. Wind frequency, 1 rad/sec
7. Control system design, II.2
8. Forward loop gain, K = 2.2
9. Position feedback gain, K_ϕ = 1.0
10. Rate feedback gain, $K_{\dot\phi}$ = 5.0
11. Acceleration feedback gain, $K_{\ddot r}$ = .095

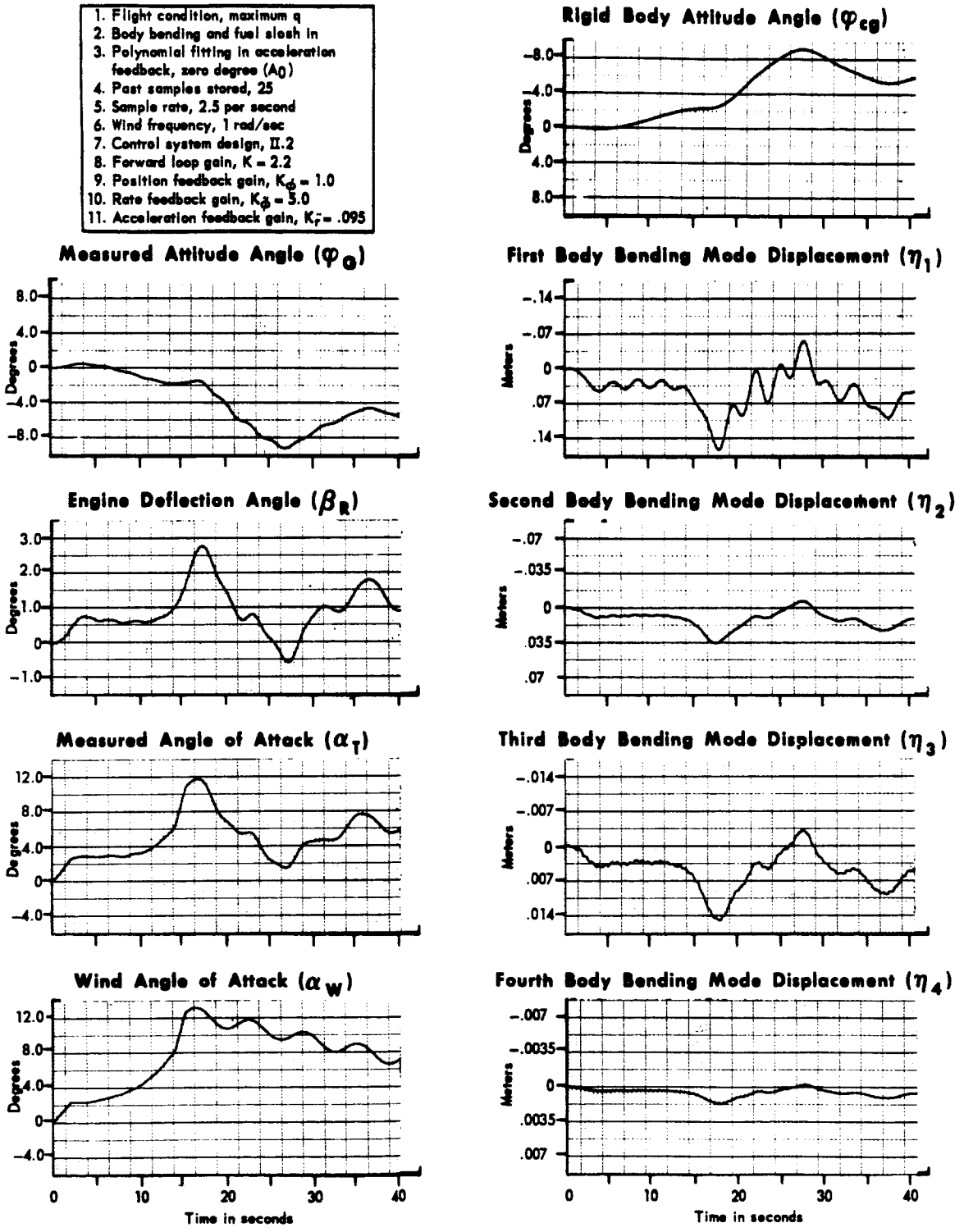

Figure 41 Wind With Sine Wave Response of Study Vehicle No. II With the Digital Polynomial Filter in the Acceleration Feedback Loop

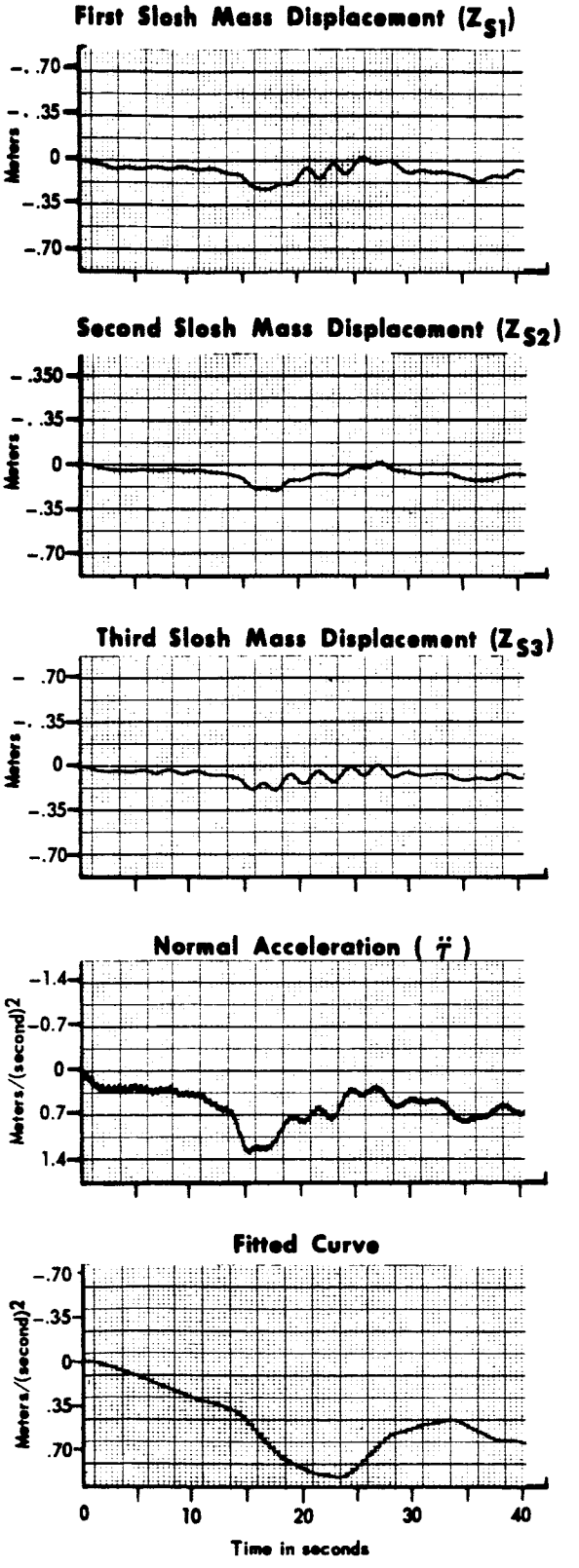

Figure 41 Wind With Sine Wave Response of Study Vehicle No. II With the Digital Polynomial Filter in the Acceleration Feedback Loop (Cont.)

1. Flight condition, maximum q
2. Body bending and fuel slosh, in
3. Polynomial fitting in acceleration feedback, zero degree (A_0)
4. Wind frequency, 2 rad/sec
5. Control system design, II.2
6. Forward loop gain, K = 2.2
7. Position feedback gain, K_ϕ = 1.0
8. Rate feedback gain, $K_{\dot\phi}$ = 5.0
9. Acceleration feedback gain, $K_{\ddot\gamma}$ = 0.095

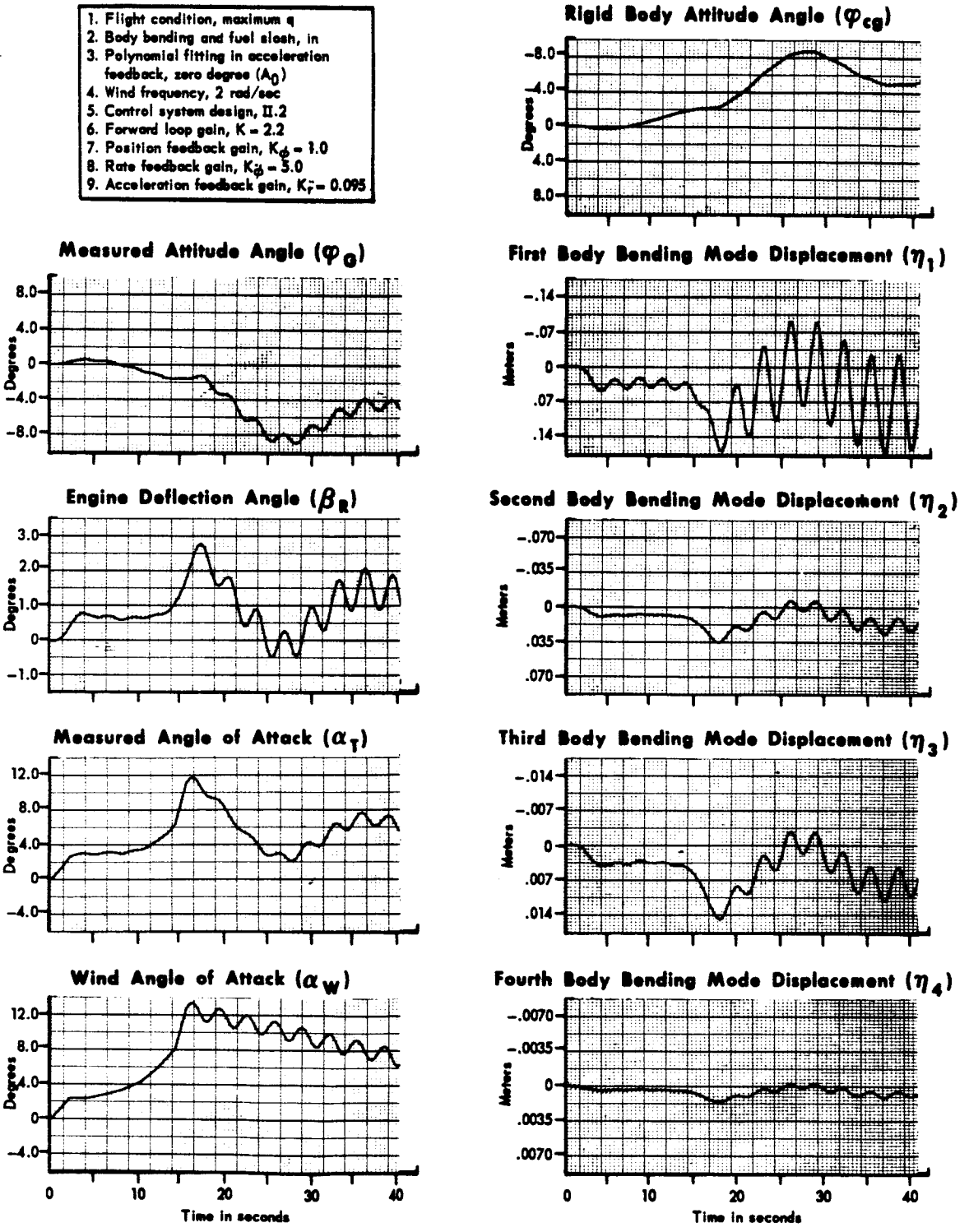

Figure 42 Wind With Sine Wave Response of Study Vehicle No. II With the Digital Polynomial Filter in the Acceleration Feedback Loop

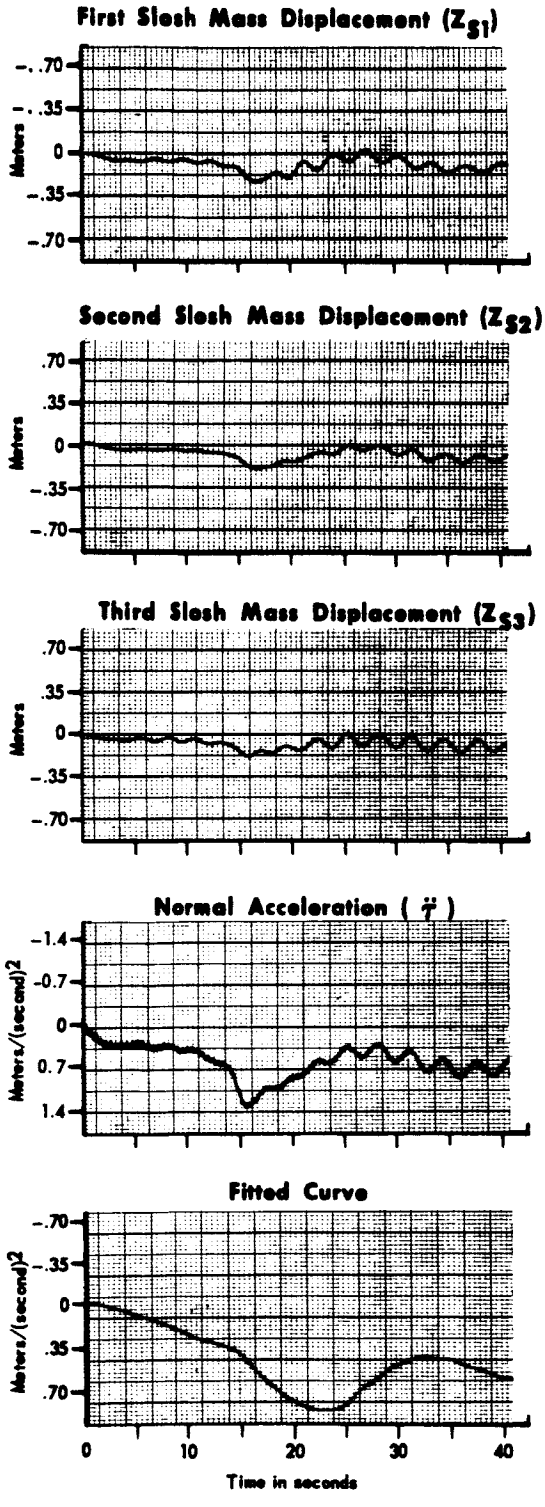

Figure 42 Wind With Sine Wave Response of Study Vehicle No. II With the Digital Polynomial Filter in the Acceleration Feedback Loop (Cont.)

1. Flight condition, maximum q
2. Body bending and fuel slosh, in
3. Polynomial fitting in acceleration feedback, zero degree (A_0)
4. Past samples stored, 25
5. Sample rate, 2.5 per second
6. Wind frequency, 3 rad/sec
7. Control system design, II.2
8. Forward loop gain, K= 2.2
9. Position feedback gain, K_ϕ = 1.0
10. Rate feedback gain, $K_{\dot\phi}$ = 5.0
11. Acceleration feedback gain, $K_{\dot r}$ = 0.095

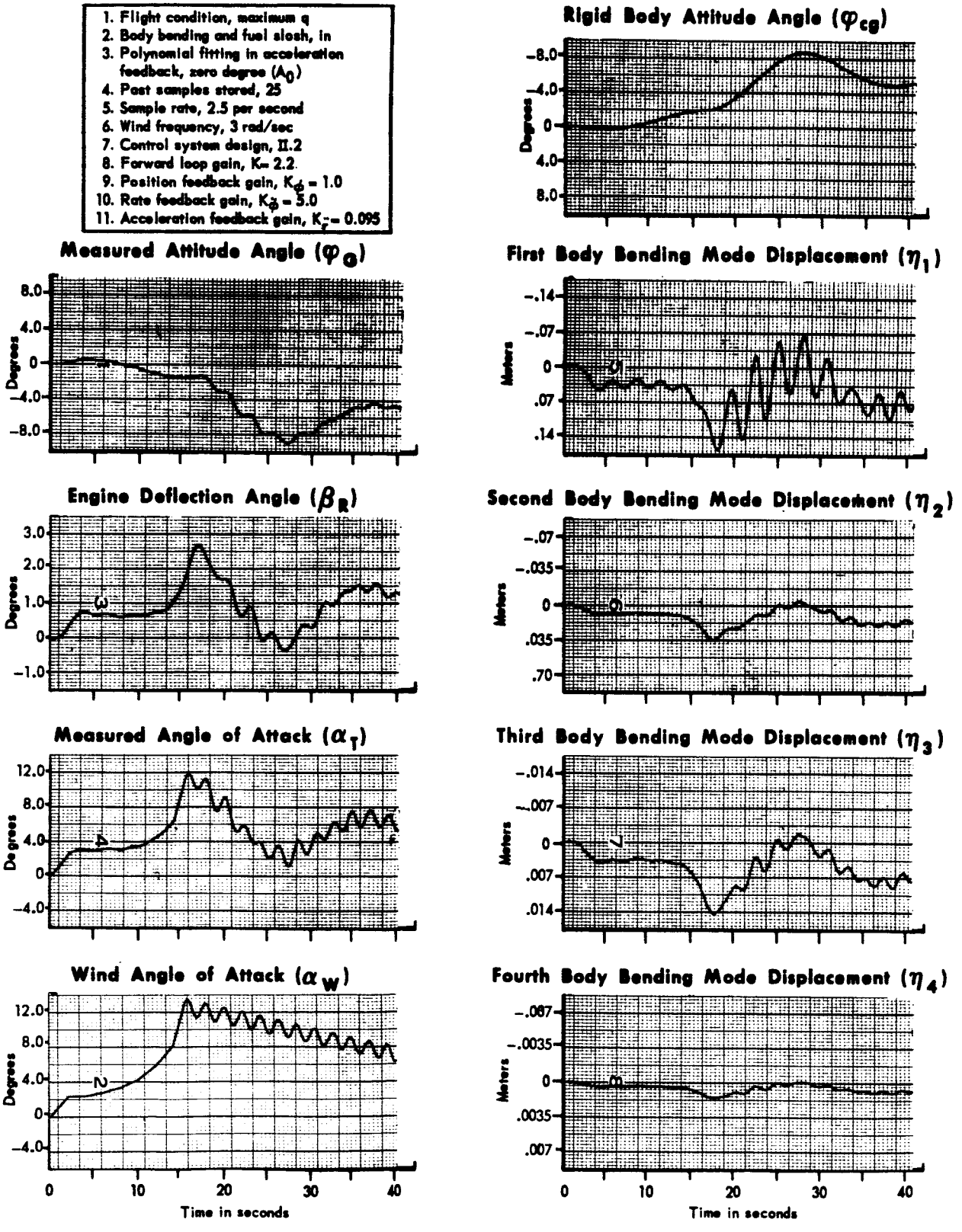

Figure 43 Wind With Sine Wave Response of Study Vehicle No. II With the Digital Polynomial Filter in the Acceleration Feedback Loop

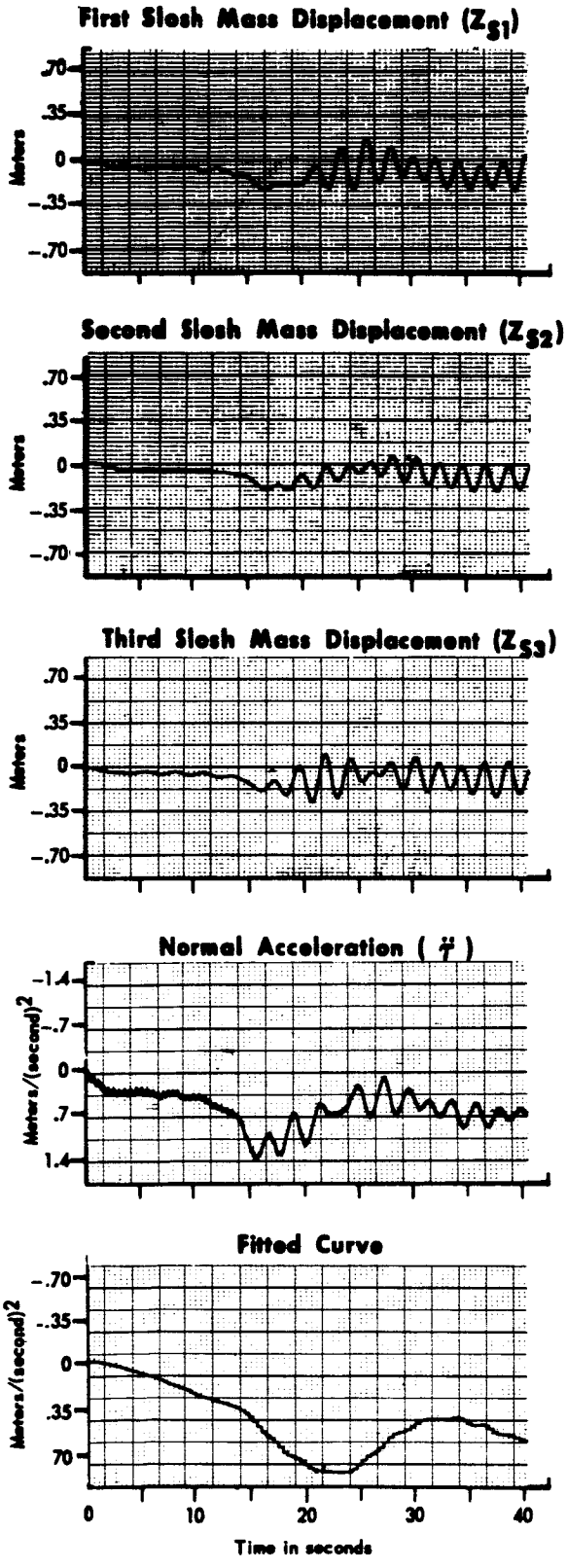

Figure 43 Wind With Sine Wave Response of Study Vehicle No. II With the Digital Polynomial Filter in the Acceleration Feedback Loop (Cont.)

1. Flight condition, maximum q
2. Body bending and fuel slosh, in
3. Acceleration feedback lag network, $\left(\frac{1}{1+10S}\right)$
4. Wind frequency, 2 rad/sec
5. Control system design, II.3
6. Forward loop gain, K = 2.2
7. Position feedback gain, $K_\phi = 1.0$
8. Rate feedback gain, $K_{\dot\phi} = 3.0$
9. Acceleration feedback gain, $K_{\dot\gamma} = 0.095$

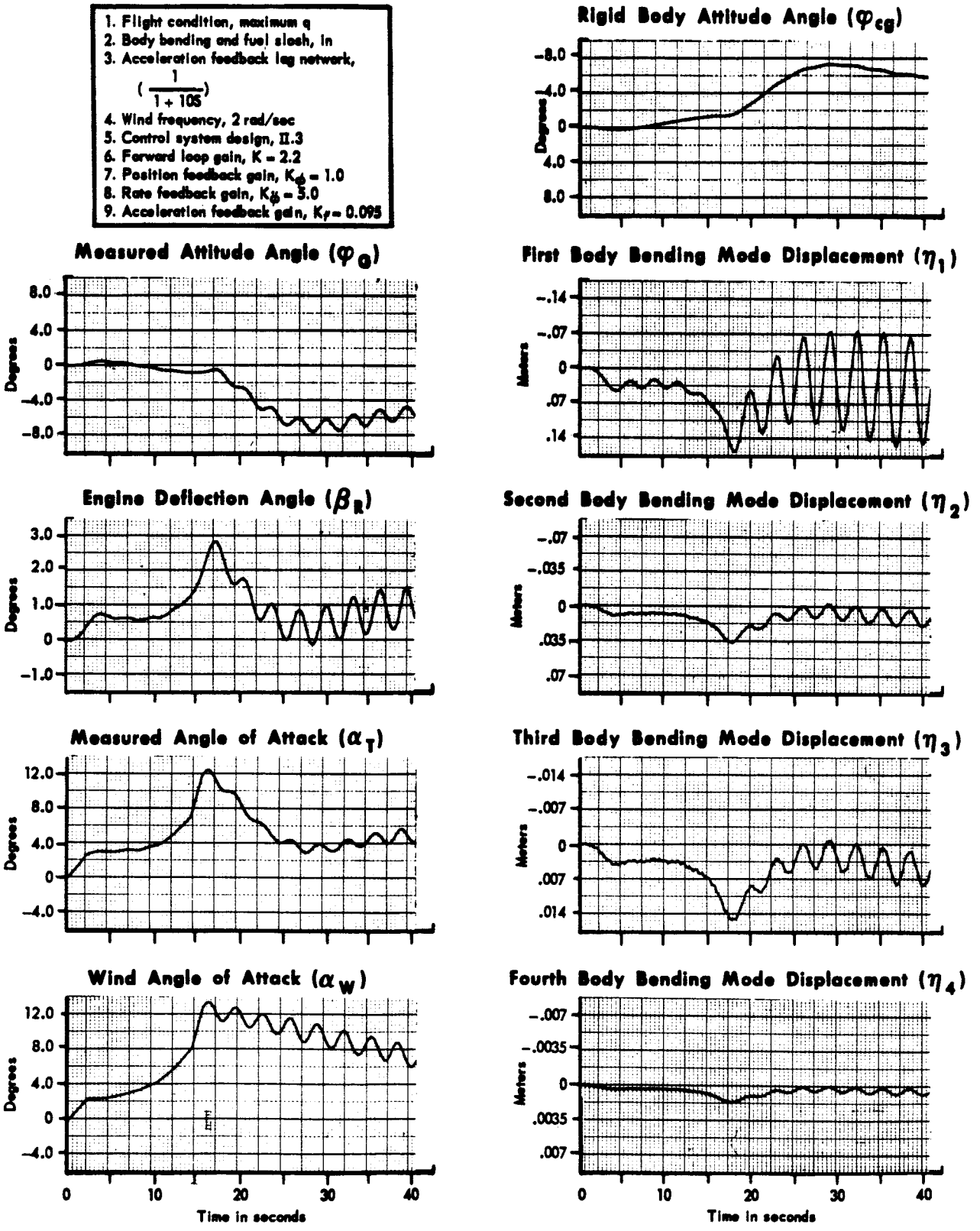

Figure 44 Wind With Sine Wave Response of Study Vehicle No. II With a Linear Lag Filter in the Acceleration Feedback Loop

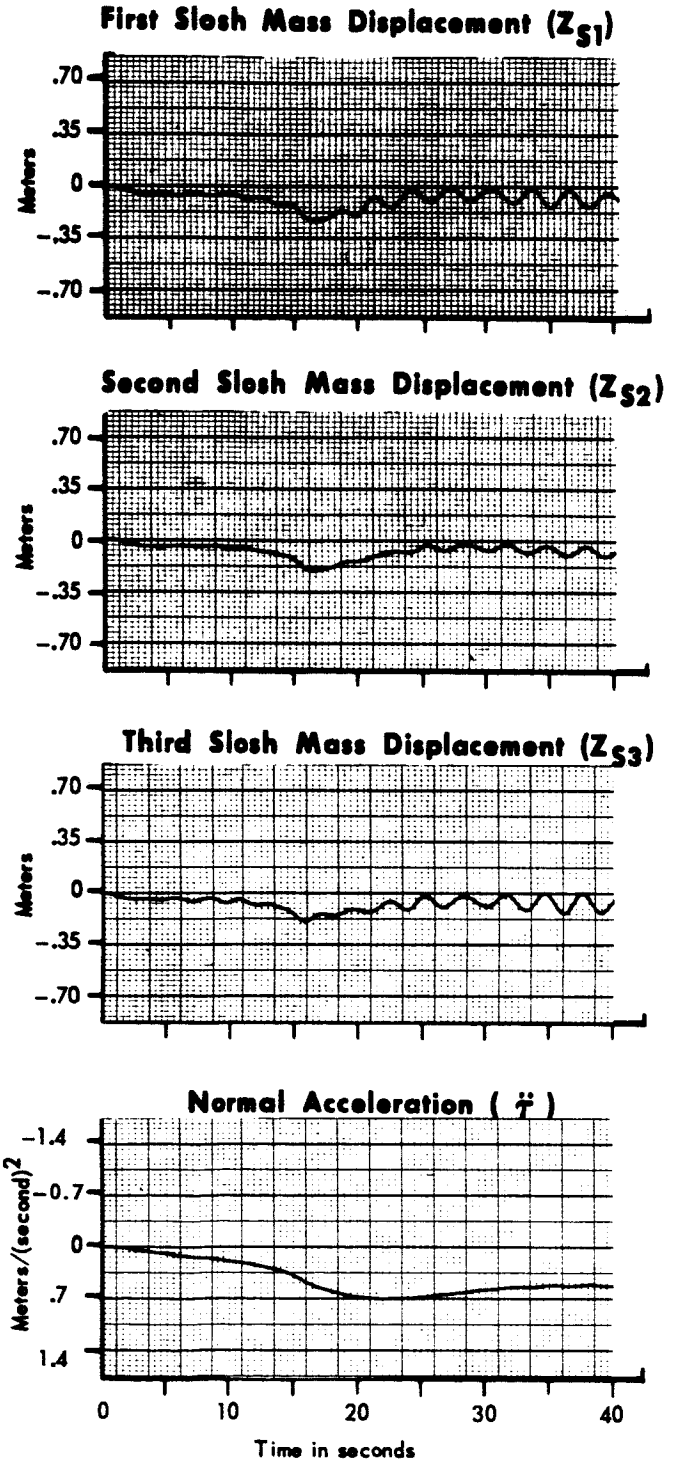

Figure 44 Wind With Sine Wave Response of Study Vehicle No. II With a Linear Lag Filter in the Acceleration Feedback Loop (Cont.)

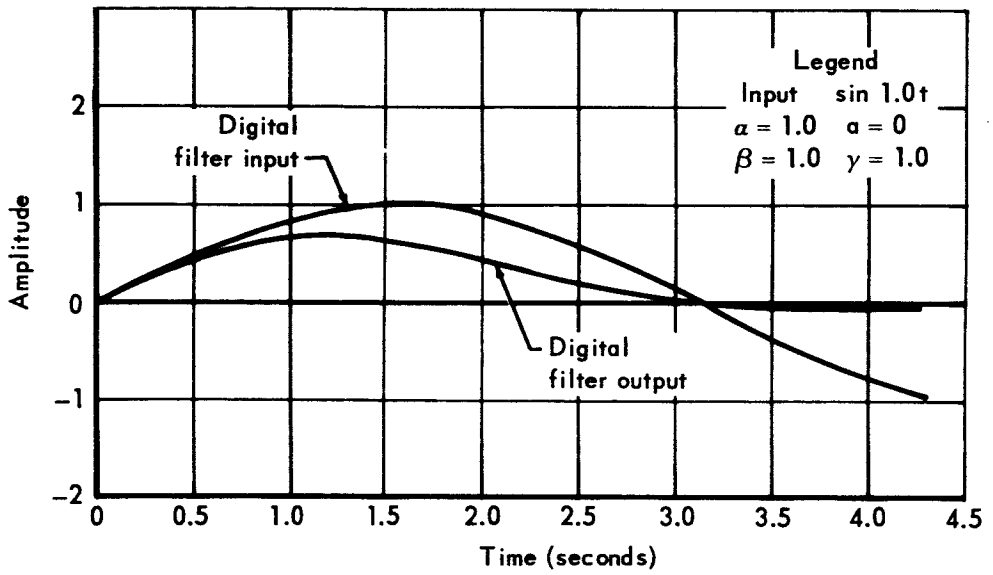

Figure 45a Digital Filter Output Response to Undamped Sine Wave Input

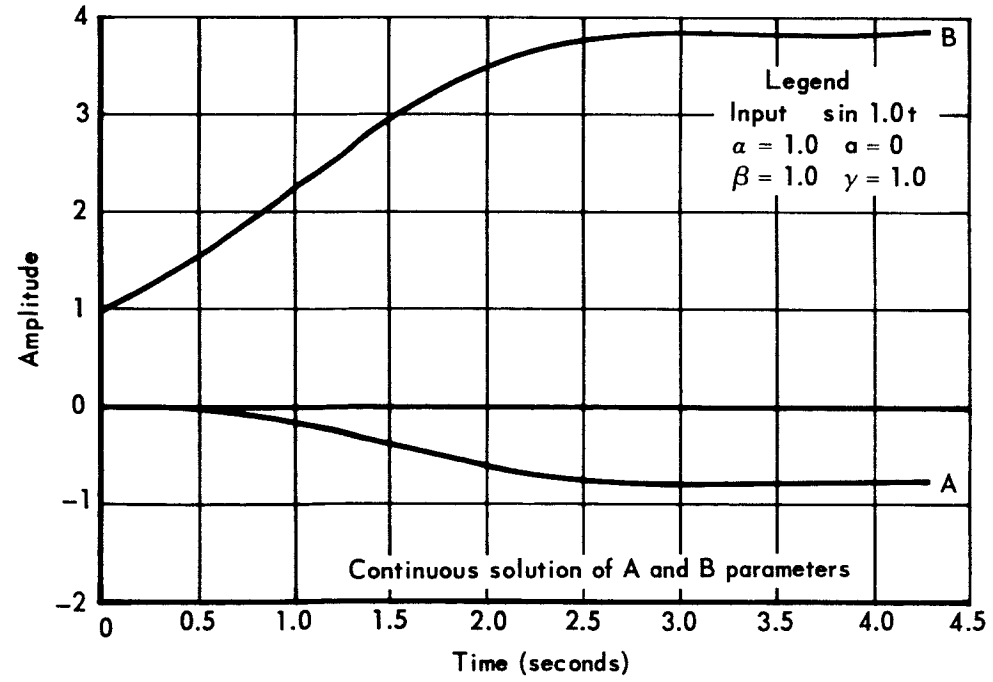

Figure 45b A and B Time Histories to Undamped Sine Wave Input

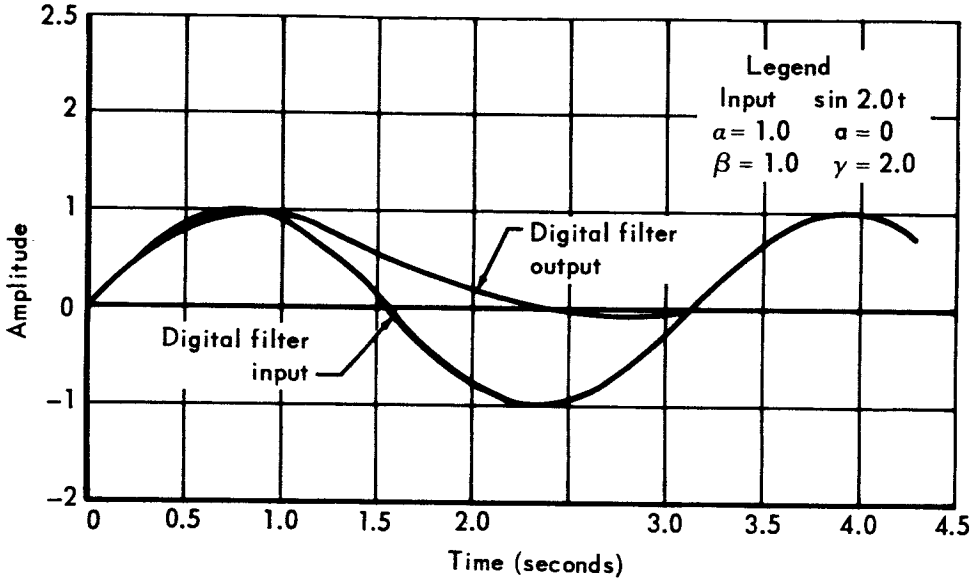

Figure 46a Digital Filter Output Response to Undamped Sine Wave Input

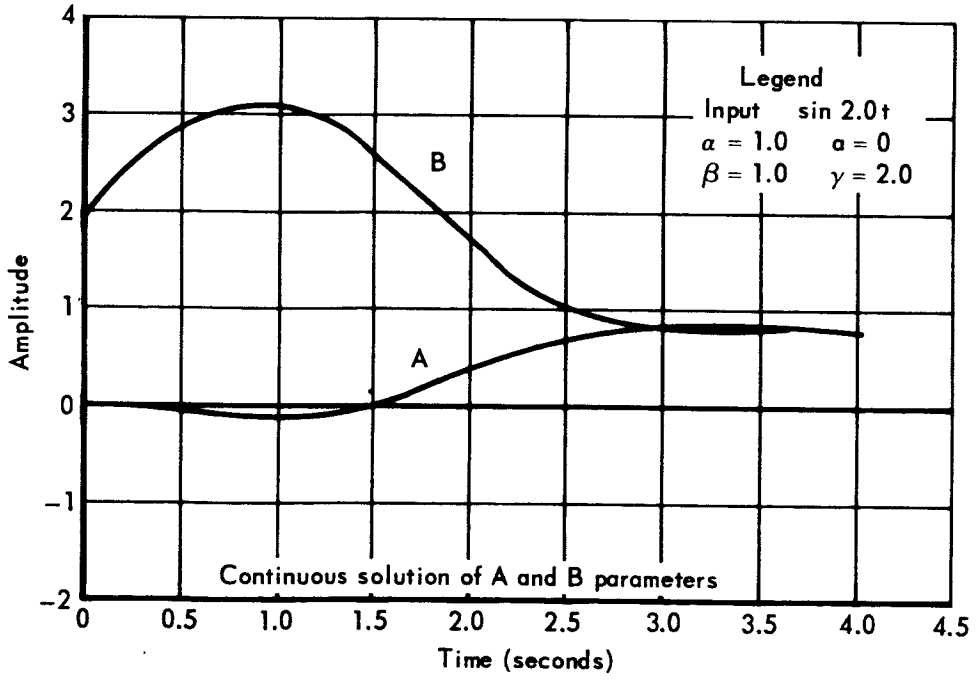

Figure 46b A and B Time Histories to Undamped Sine Wave Input

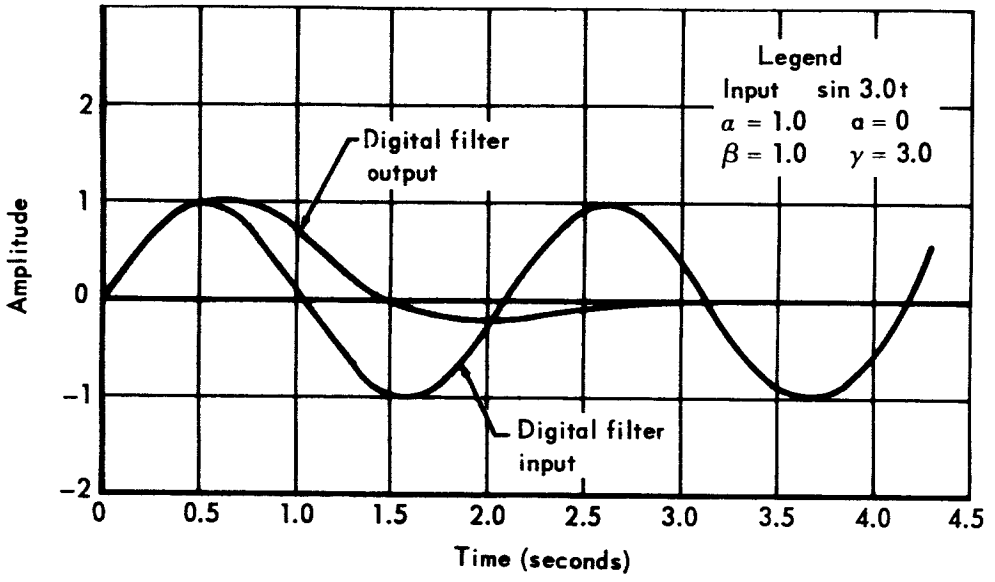

Figure 47a Digital Filter Output Response to Undamped Sine Wave Input

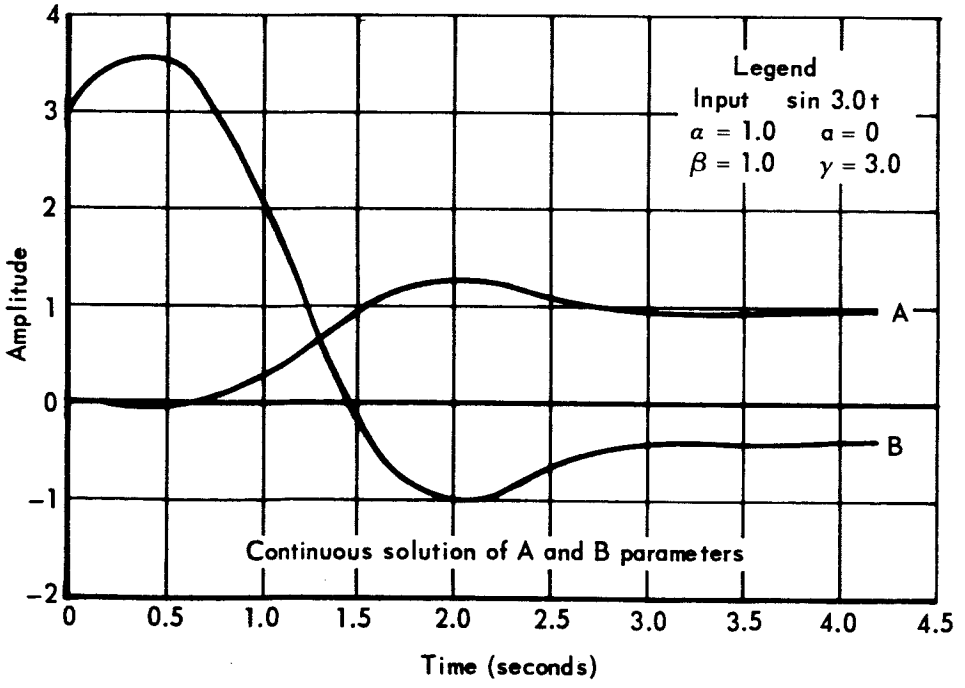

Figure 47b A and B Time Histories to Undamped Sine Wave Input

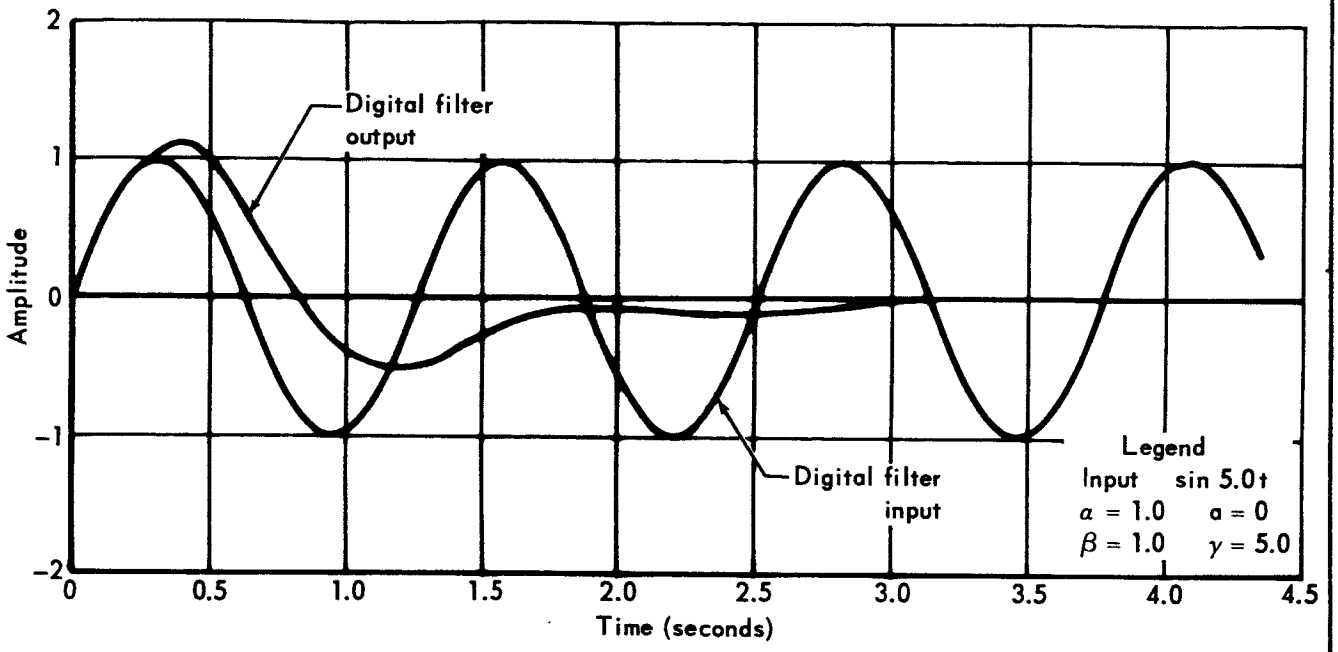

Figure 48a Digital Filter Output to Undamped Sine Wave Input

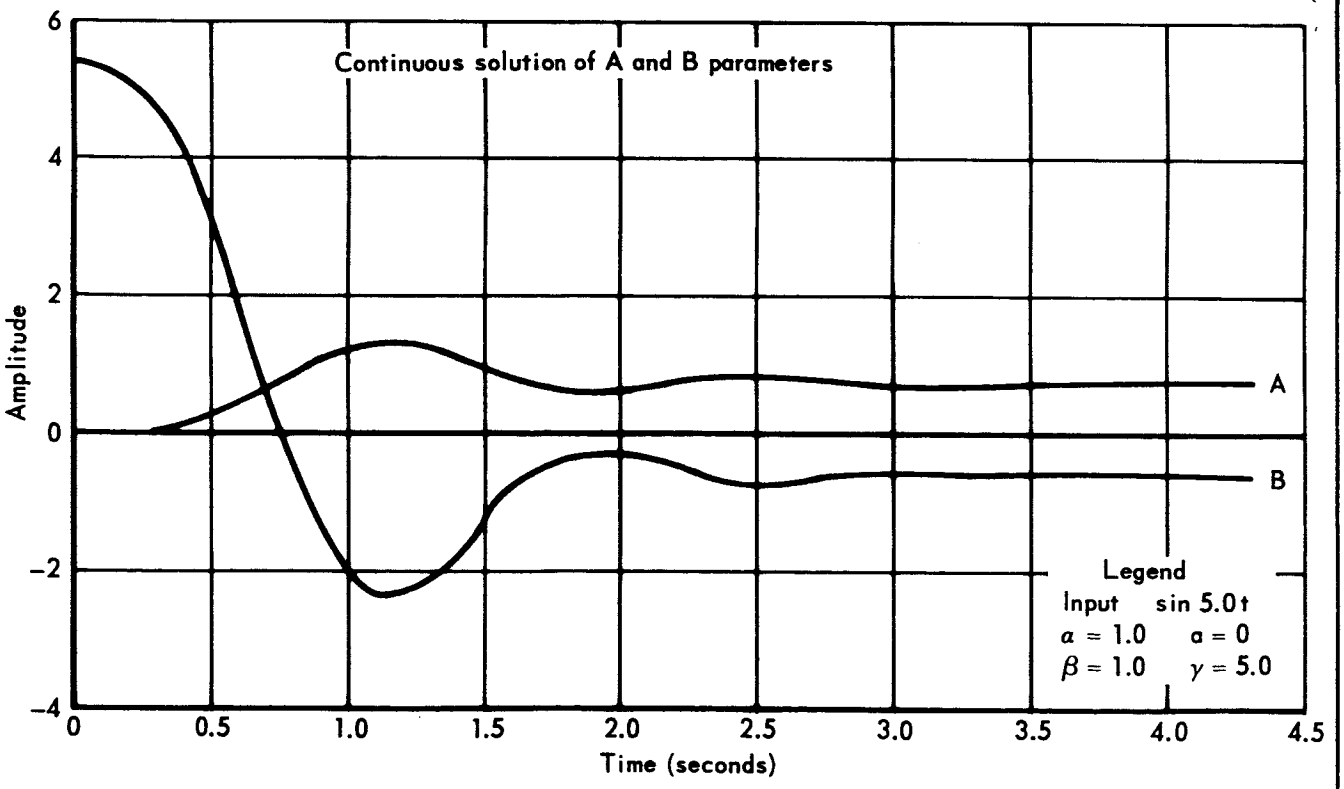

Figure 48b A and B Time Histories to Undamped Sine Wave Input

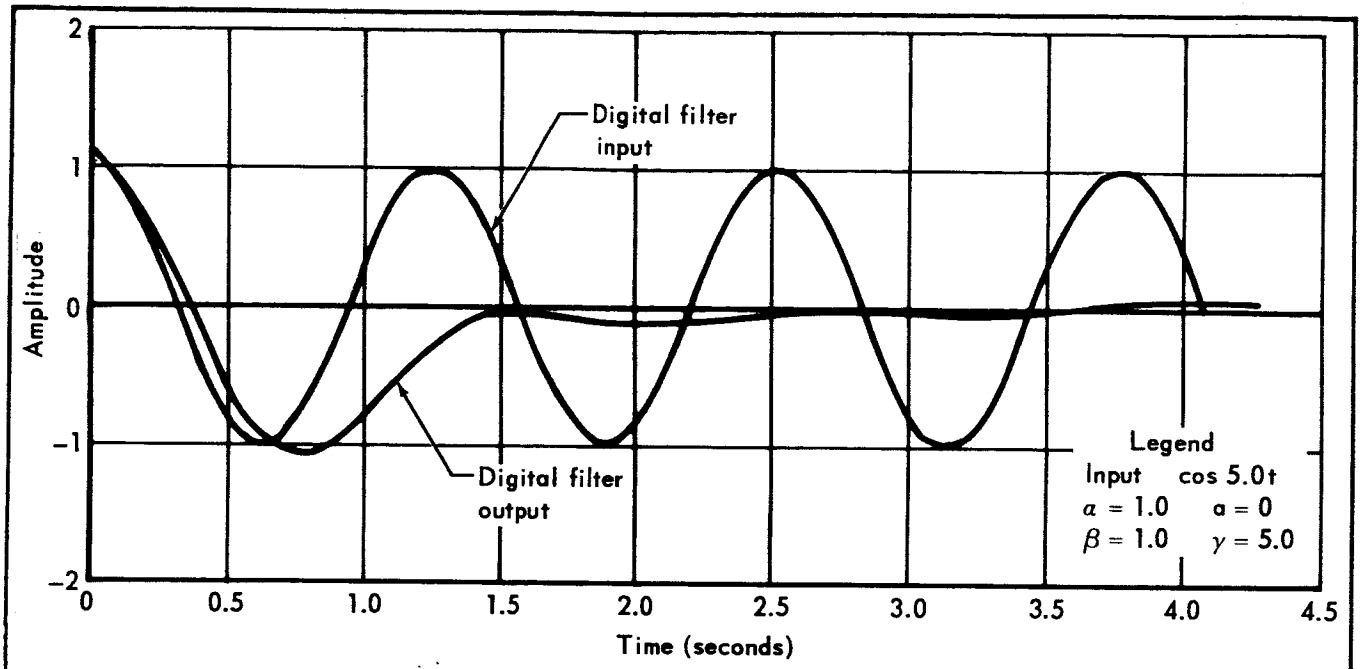

Figure 49a Digital Filter Output Response to Undamped Cosine Wave Input

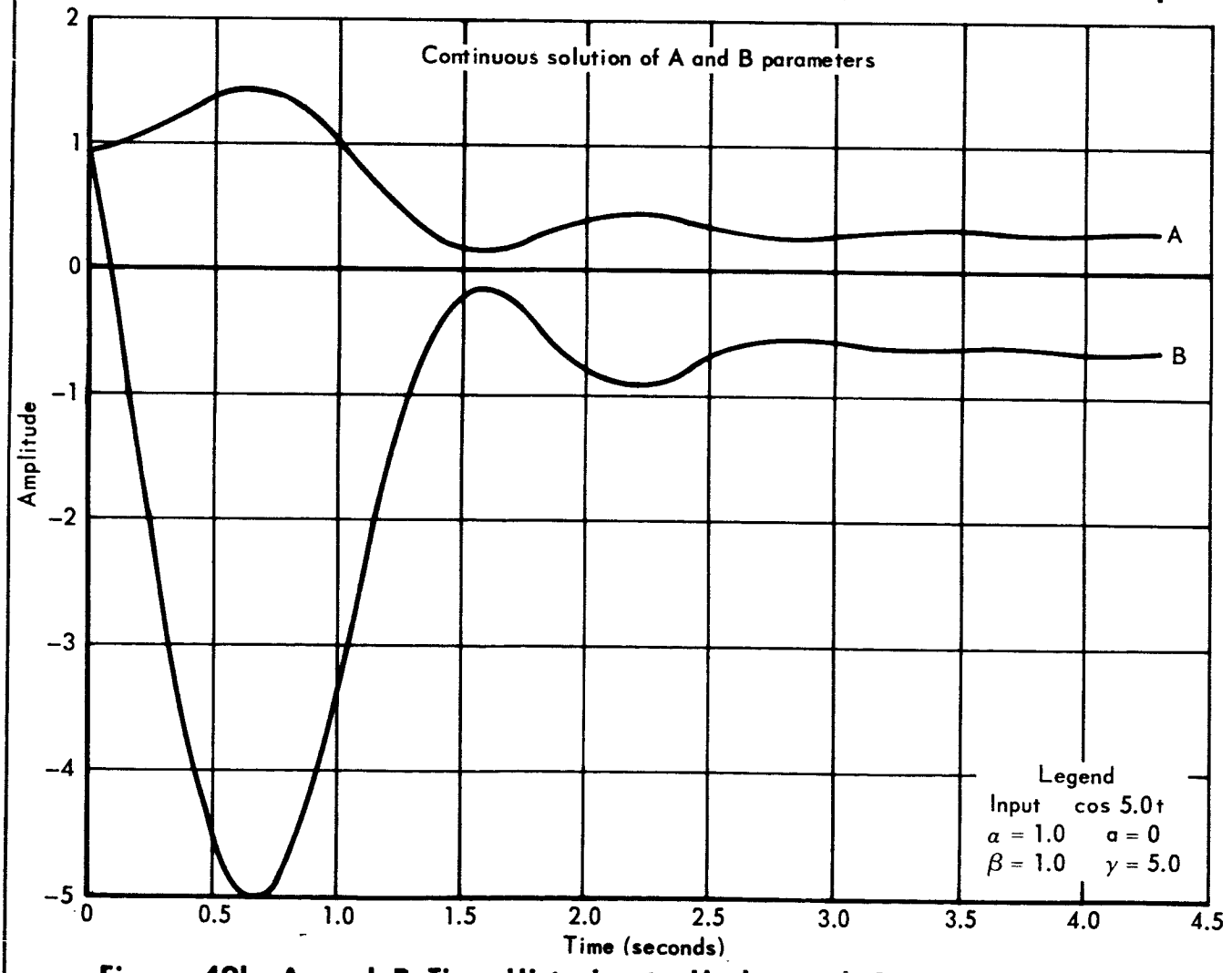

Figure 49b A and B Time Histories to Undamped Cosine Wave Input

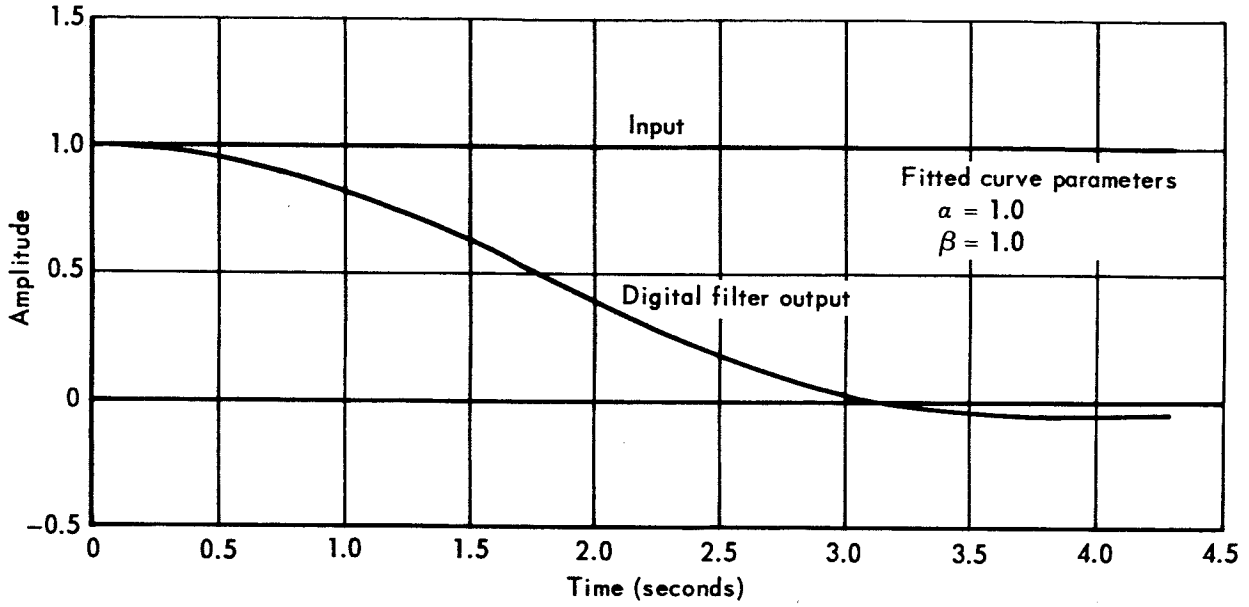

Figure 50a Digital Filter Response to a Step Input

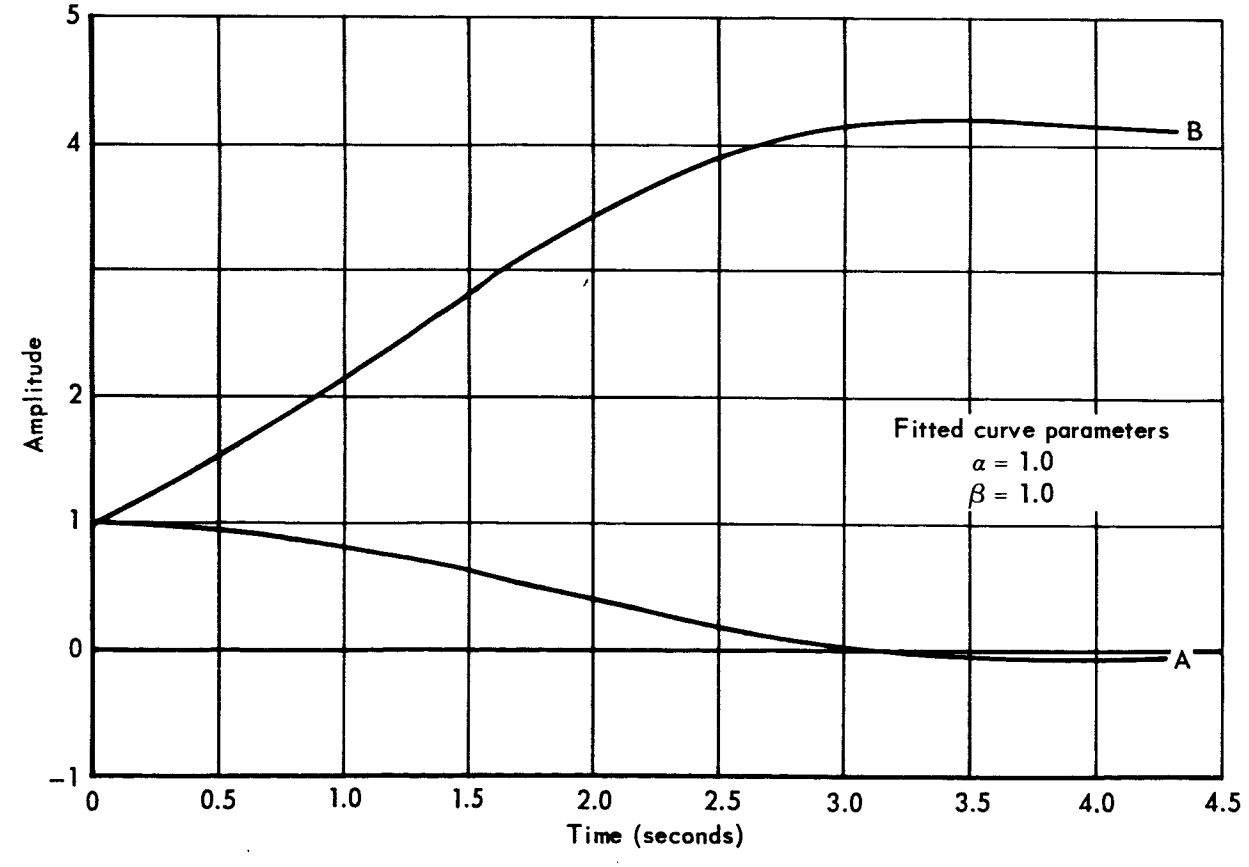

Figure 50b Computed A and B Values to a Step Input

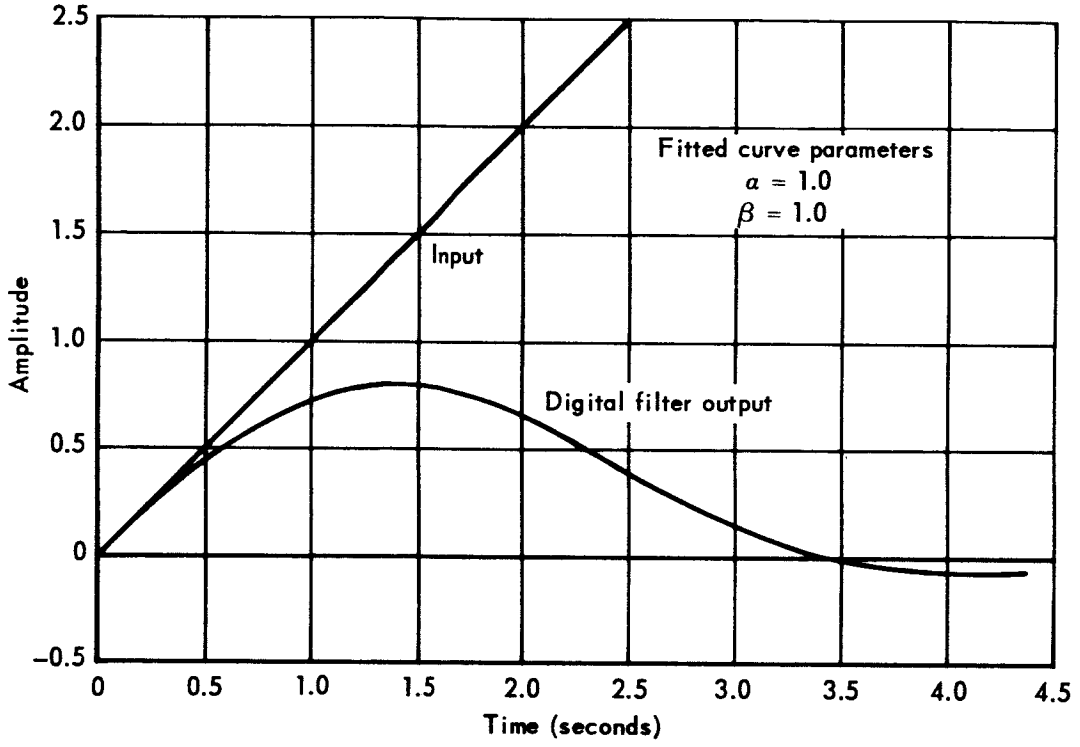

Figure 51a Digital Filter Response to a Ramp Input

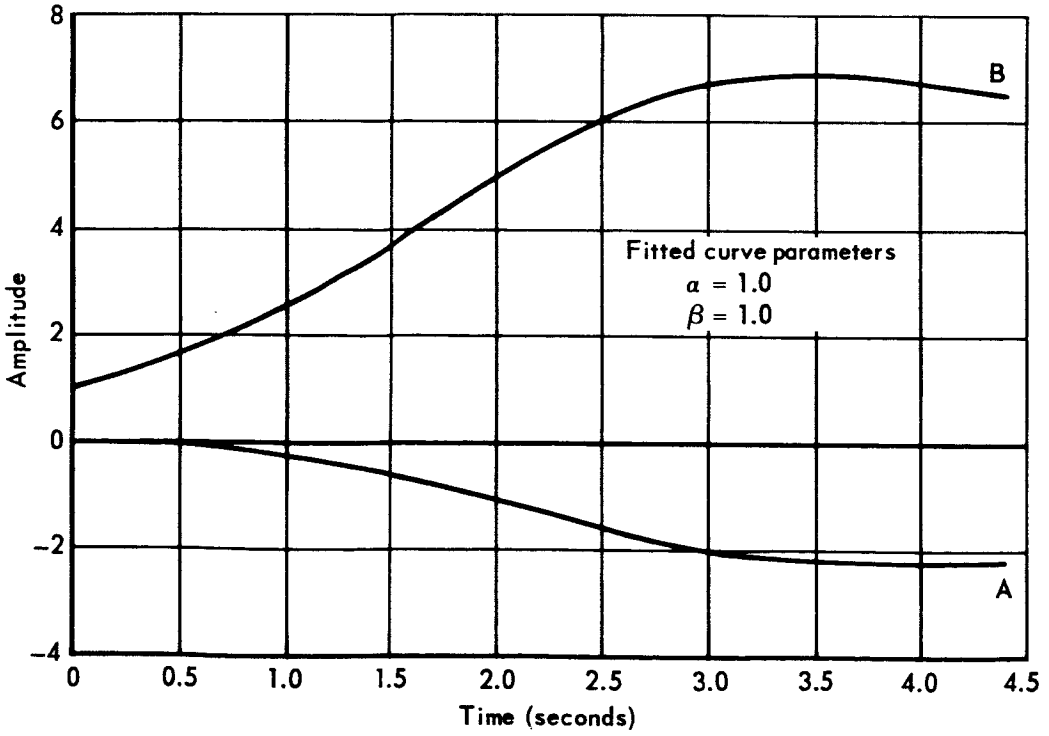

Figure 51b Computed A and B Values to a Ramp Input

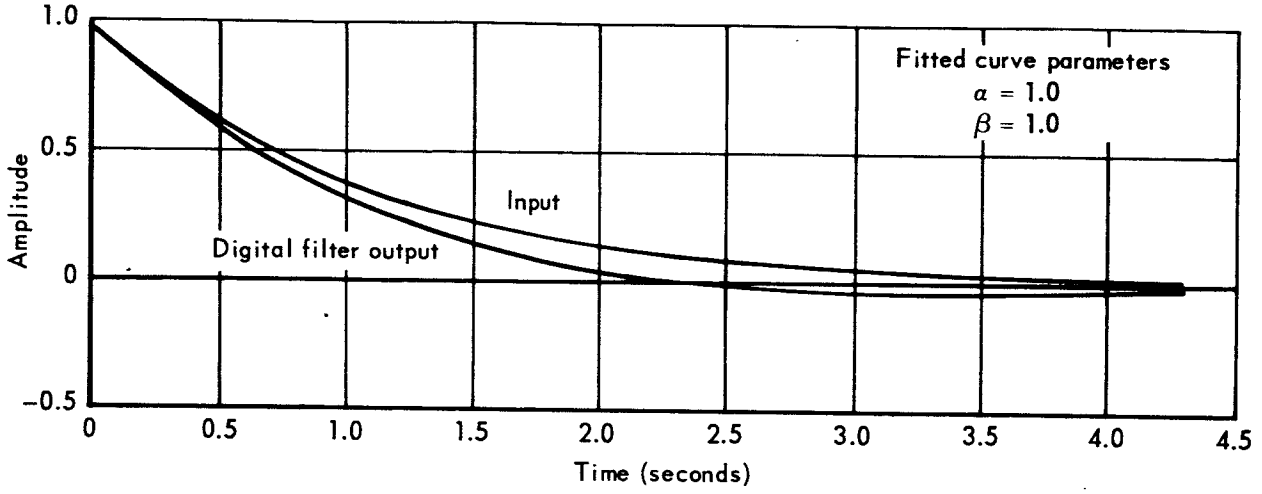

Figure 52a Digital Filter Response to a Decaying Exponential (ε^{-t})

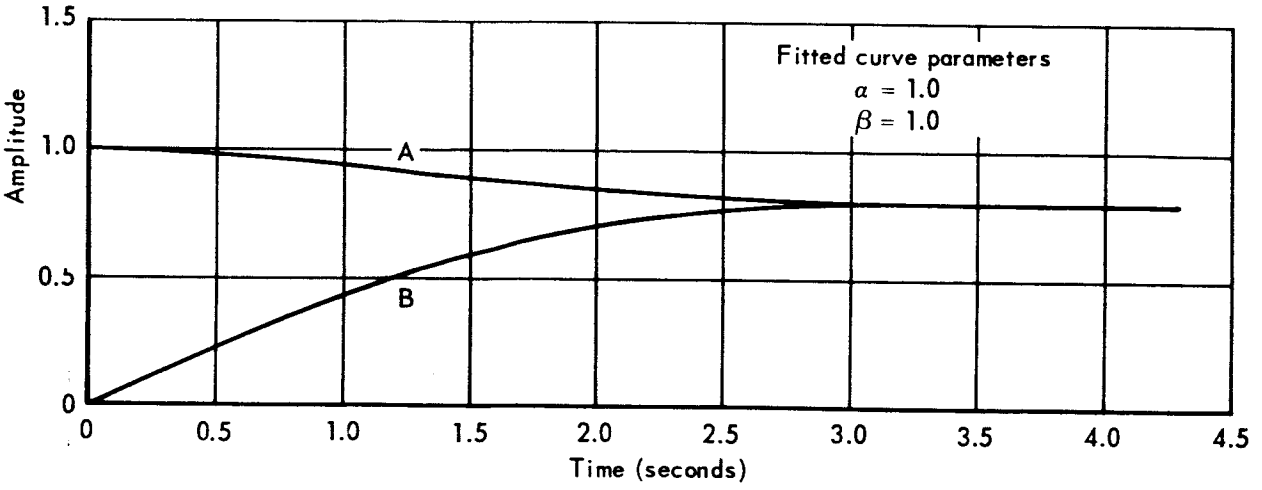

Figure 52b Computed A and B Values to a Decaying Exponential (ε^{-t})

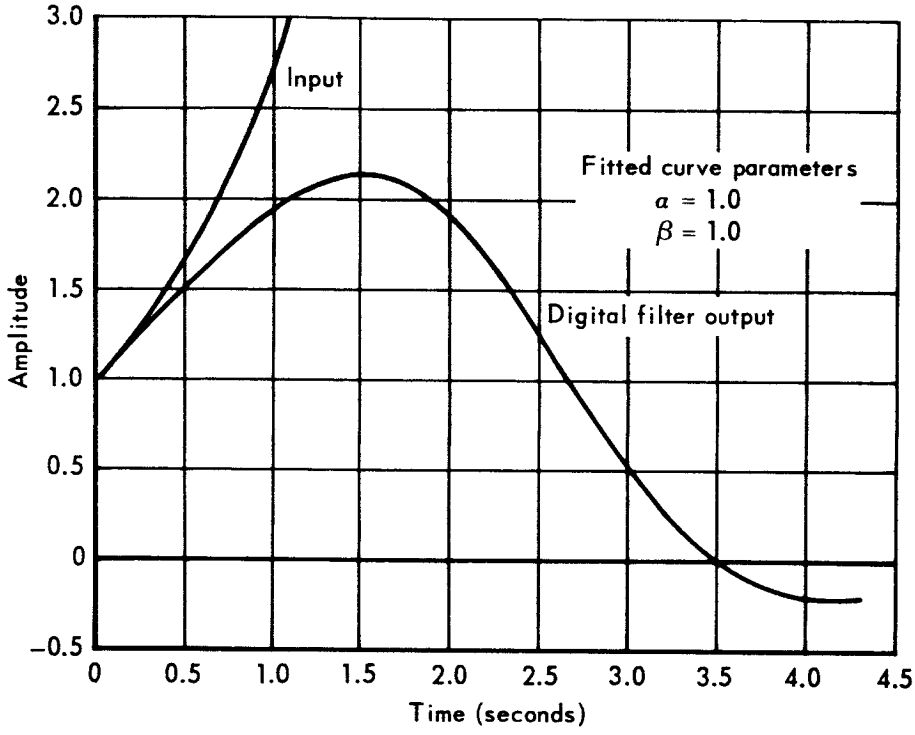

Figure 53a Digital Filter Response to a Rising Exponential (ε^t)

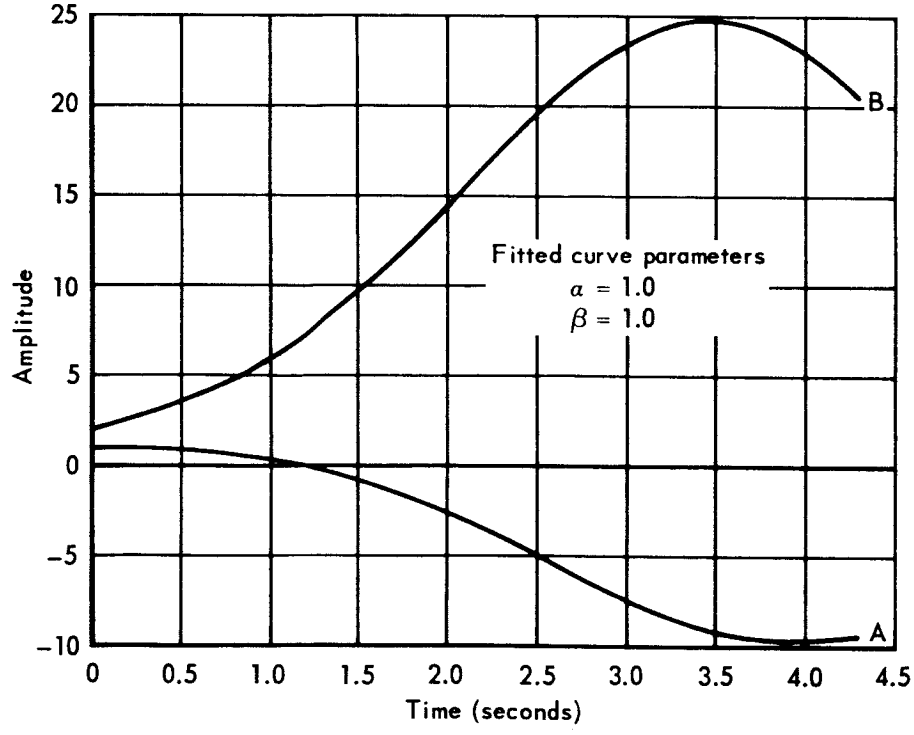

Figure 53b Computed A and B Values to a Rising Exponential (ε^t)

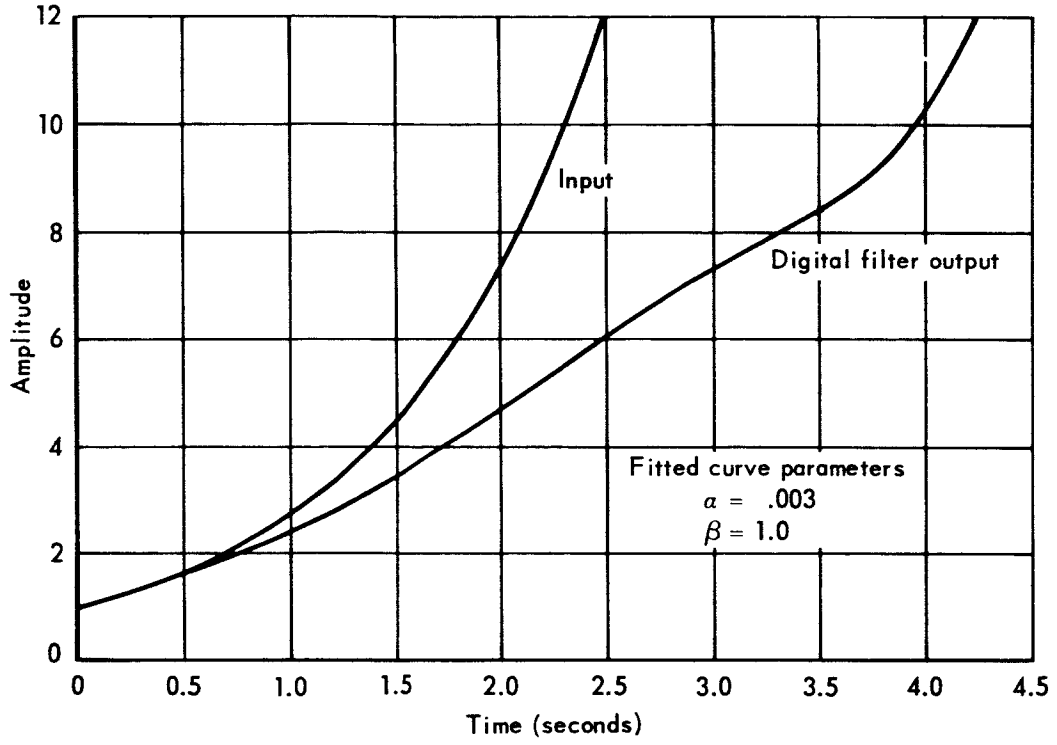

Figure 54a Digital Filter Response to a Rising Exponential (ε^t)

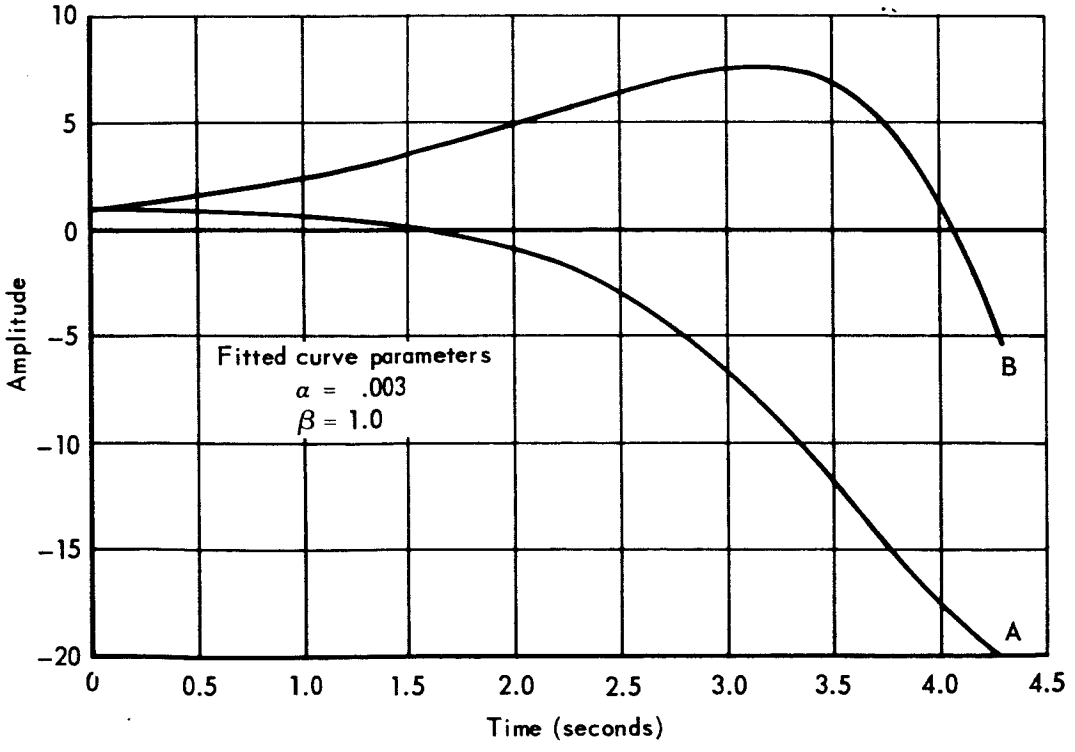

Figure 54b Computed A and B Values to a Rising Exponential (ε^t)

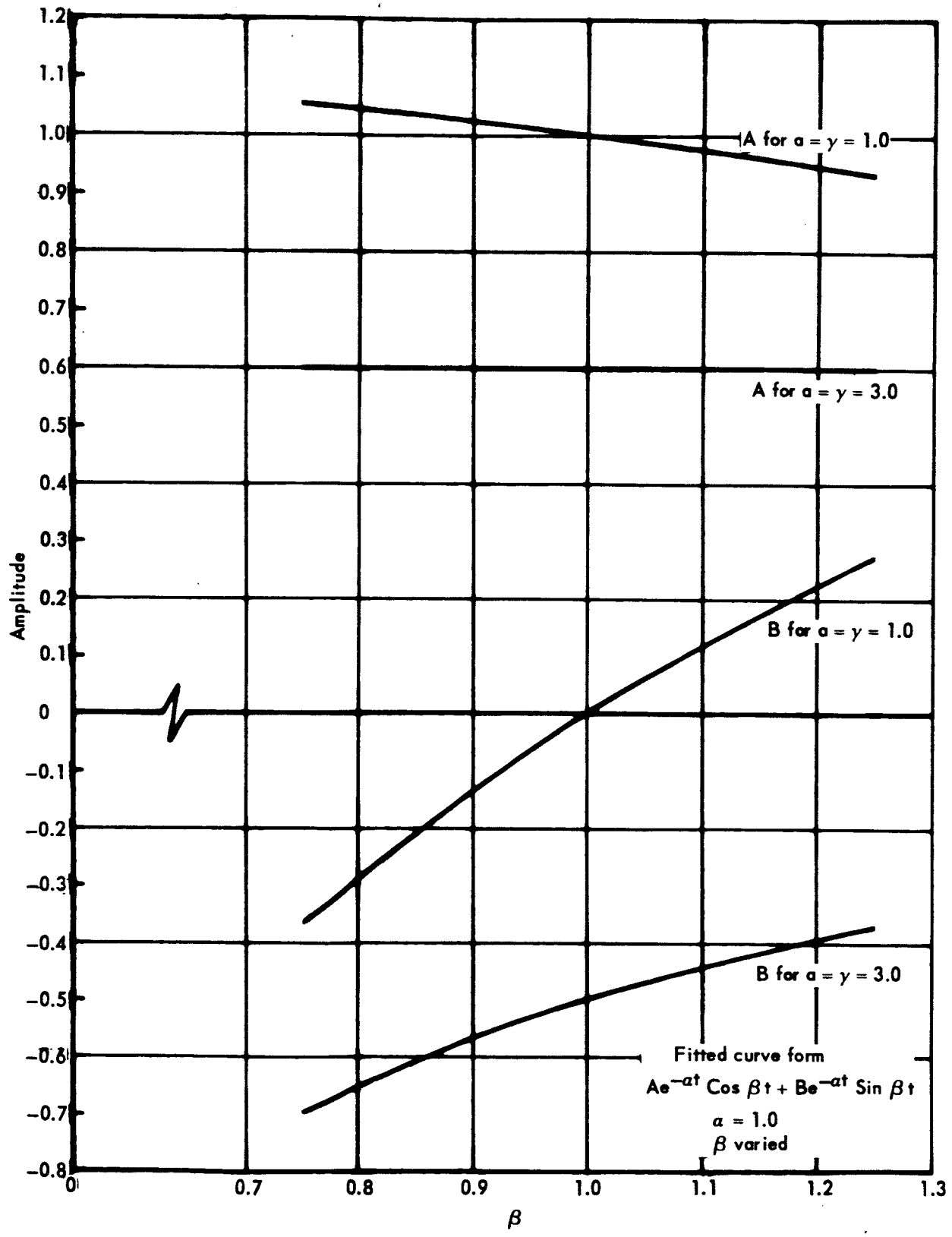

Figure 55 Steady State Amplitude Parameters for Two Parameter Fitting for an input of $e^{-at}\cos\gamma t$

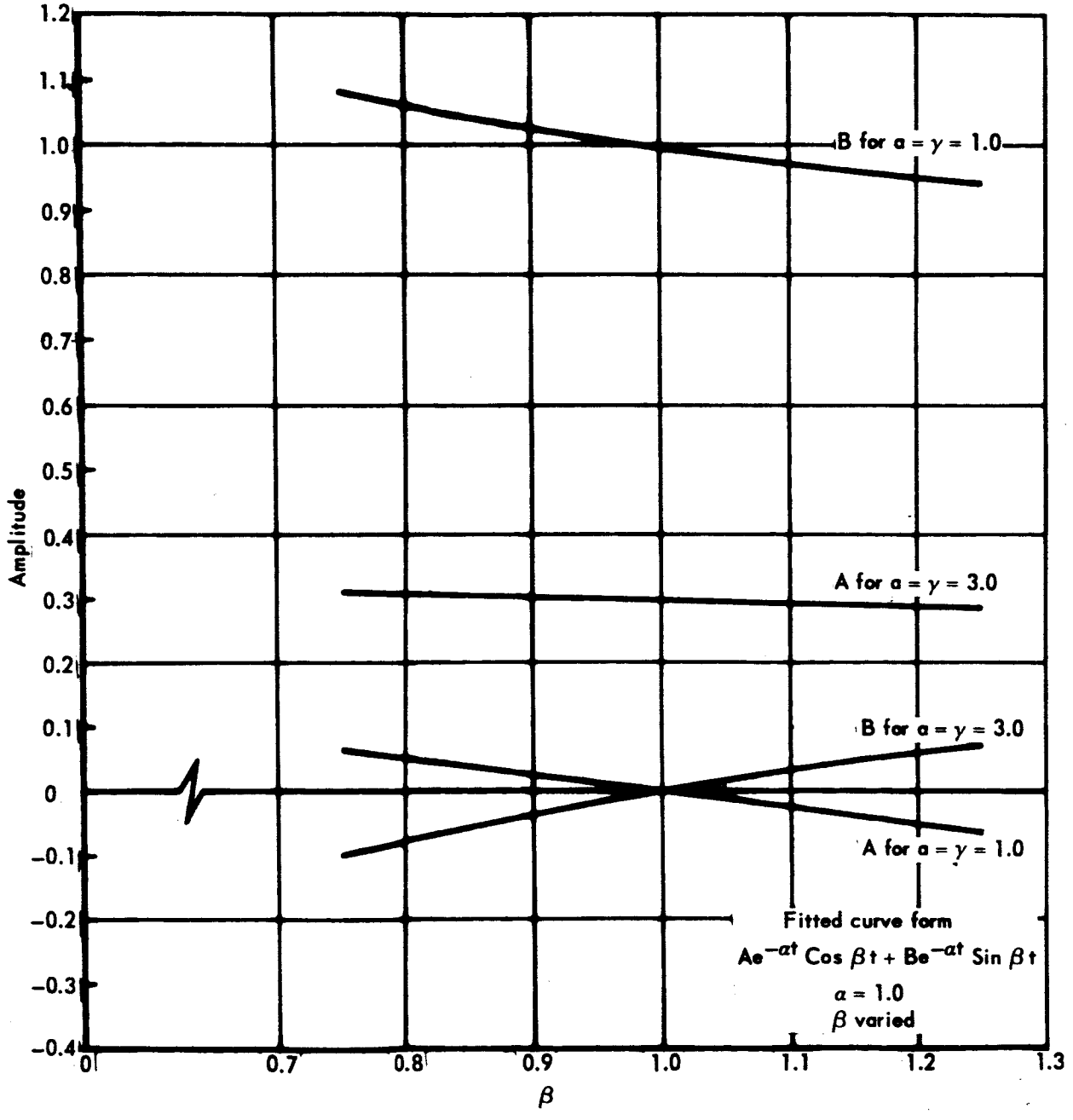

Figure 56 Steady State Amplitude Parameters for Two Parameter Fitting for an Input of e^{-at} Sin γ t

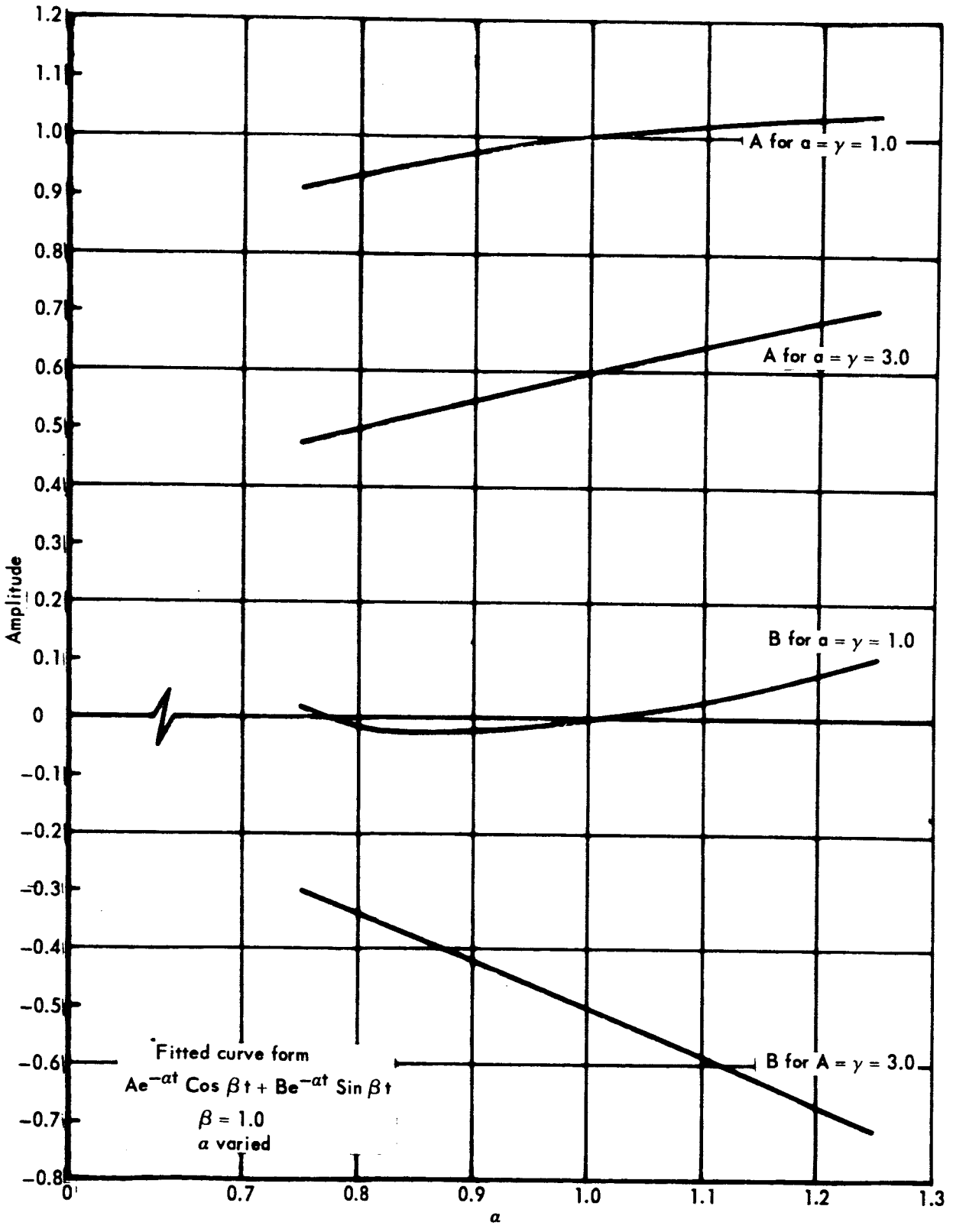

Figure 57 Steady State Amplitude Parameters for Two Parameter Fitting for an Input of $e^{-\alpha t} \cos \gamma t$

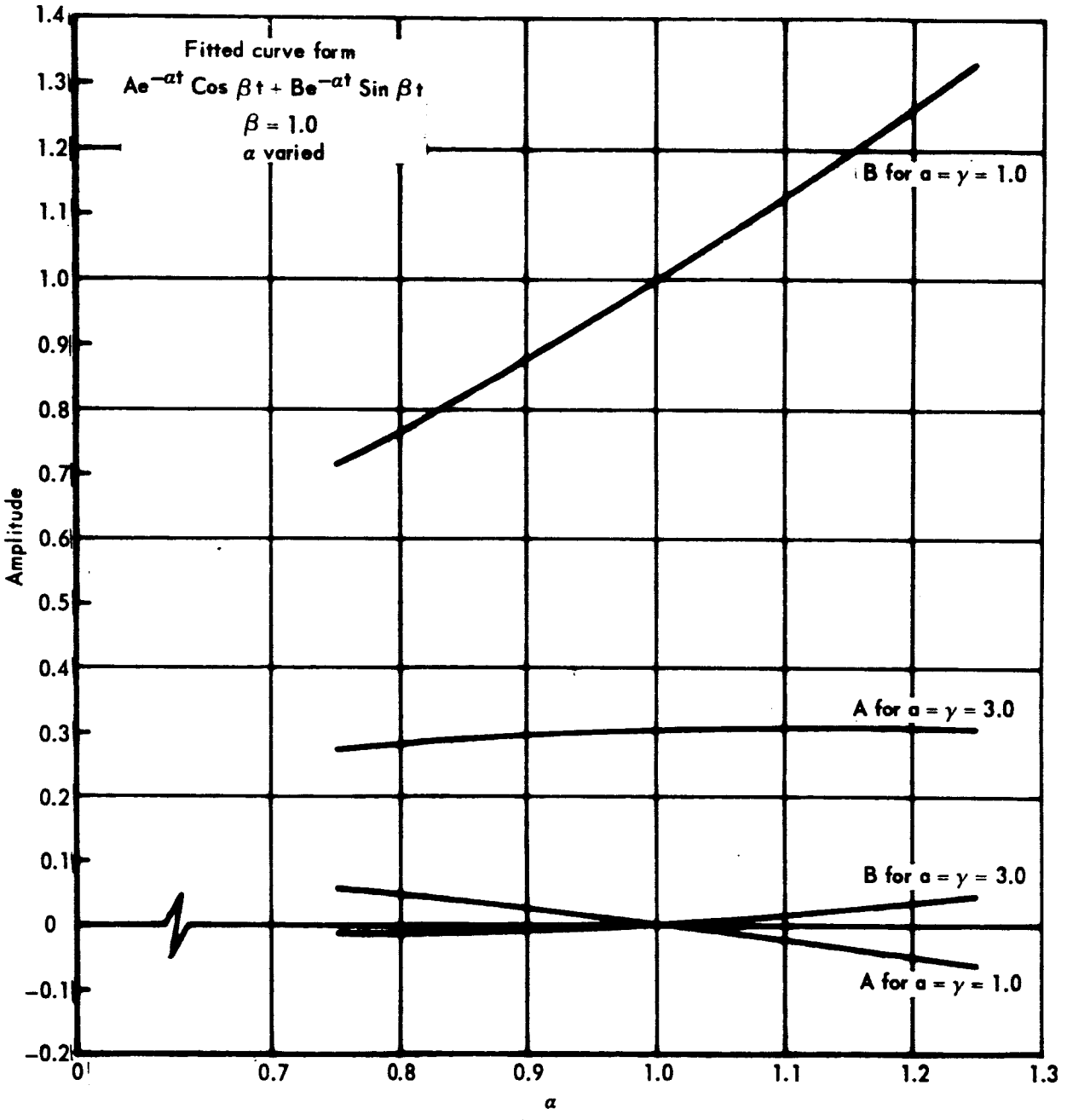

Figure 58 Steady State Amplitude Parameters for Two Parameter Fitting for an Input of $e^{-at} \sin \gamma t$

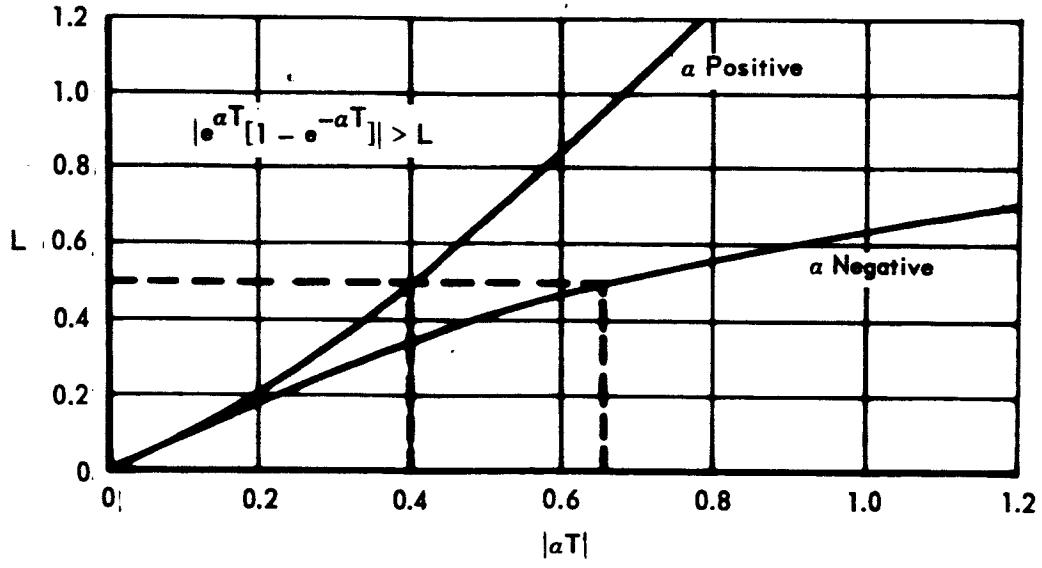

Figure 59a Maximum Discontinuity Levels for Exponential Inputs

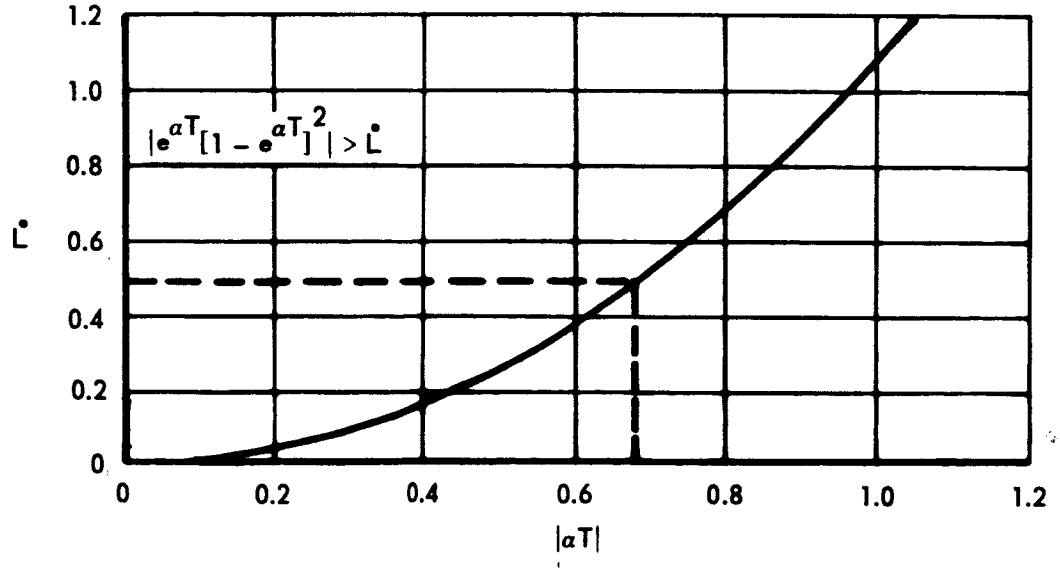

Figure 59b Maximum Discontinuity Levels for Exponential Inputs

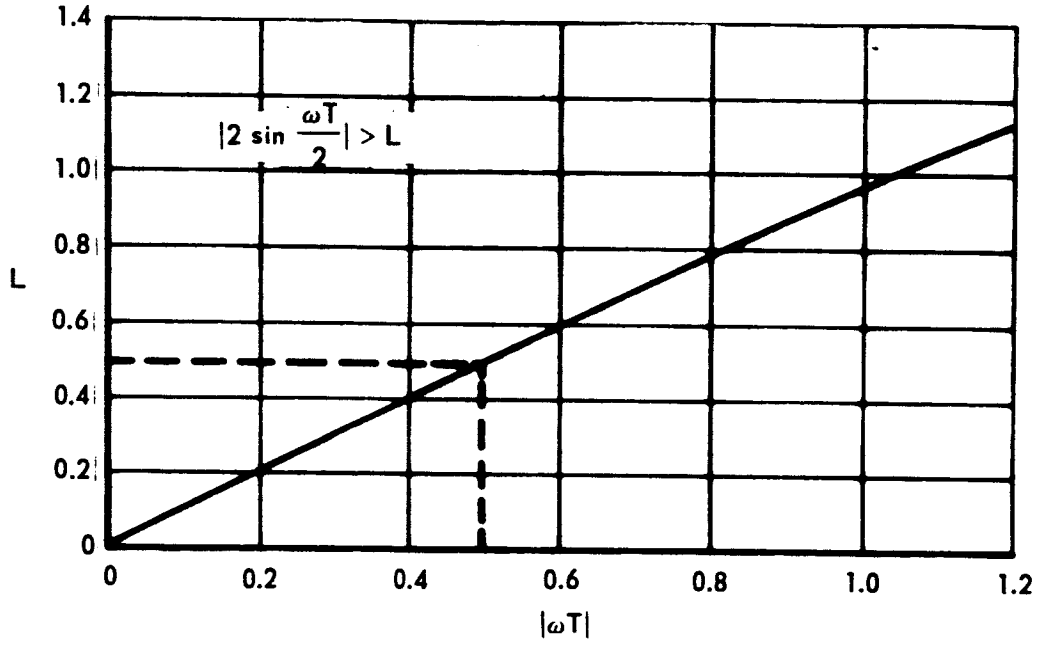

Figure 60a Maximum Discontinuity Levels for Sinusoidal Input

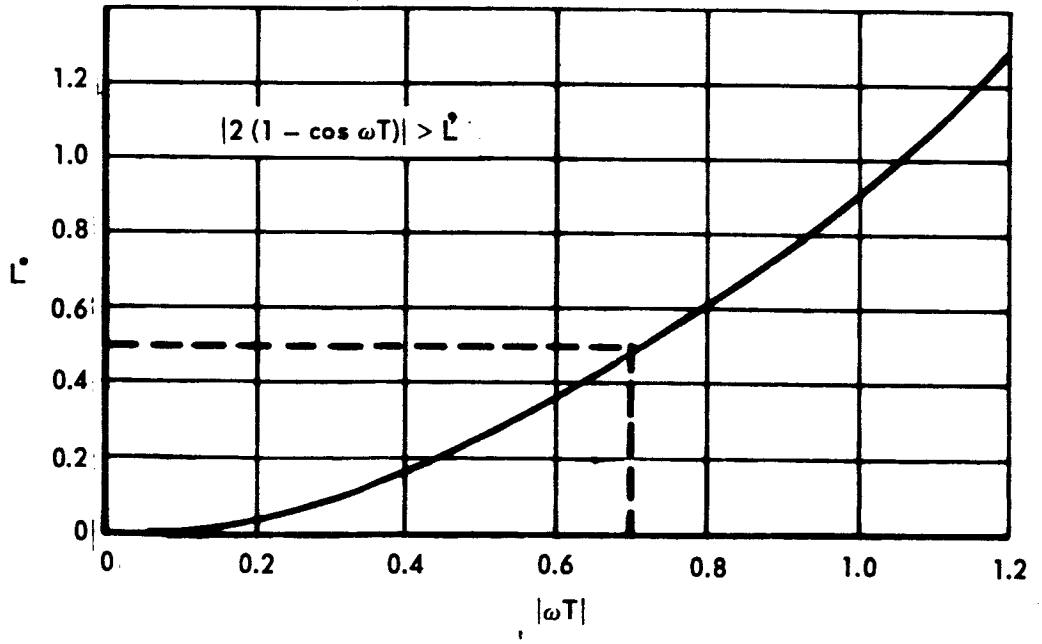

Figure 60b Maximum Discontinuity Levels for Sinusoidal Input

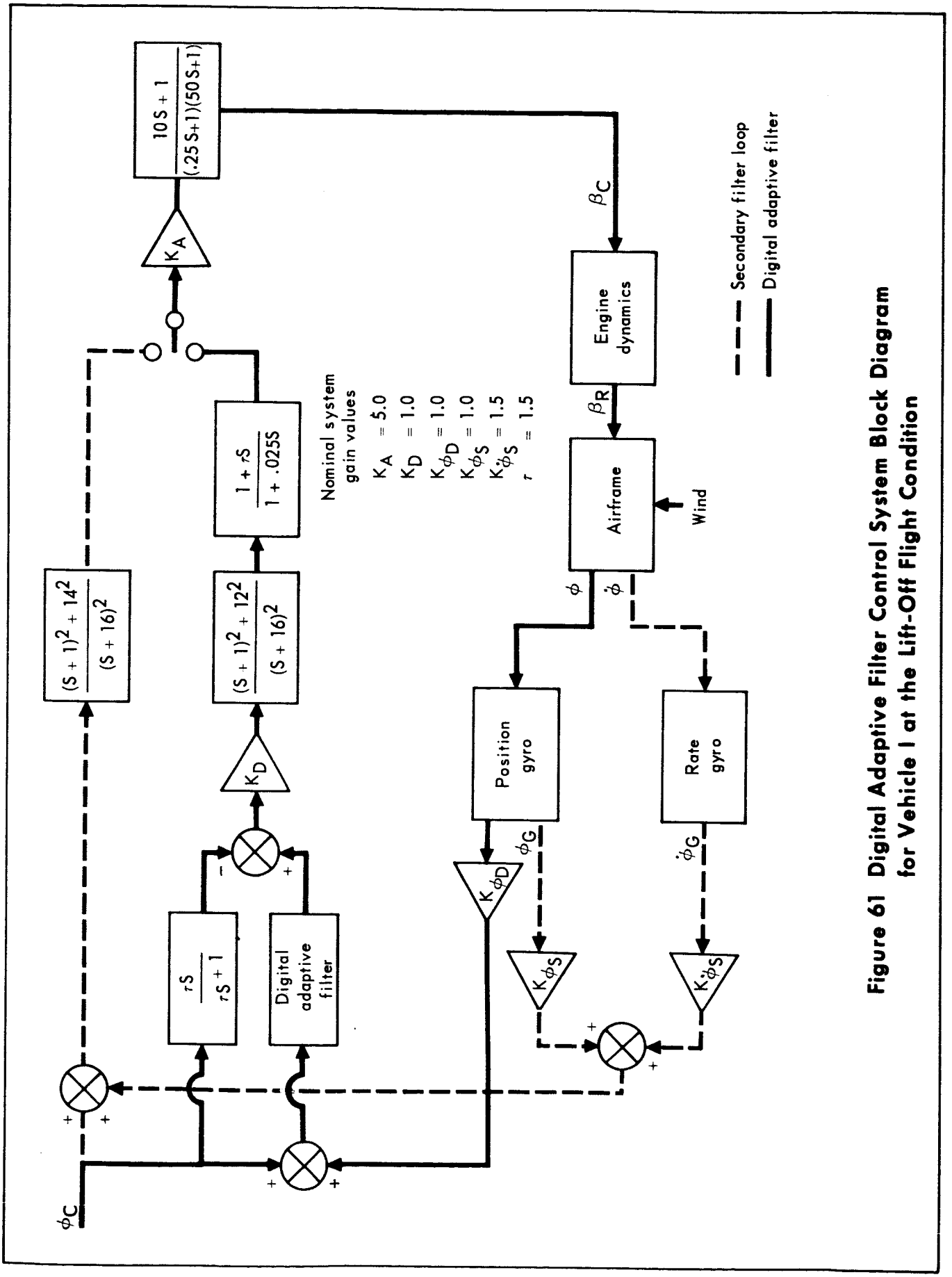

Figure 61 Digital Adaptive Filter Control System Block Diagram for Vehicle I at the Lift-Off Flight Condition

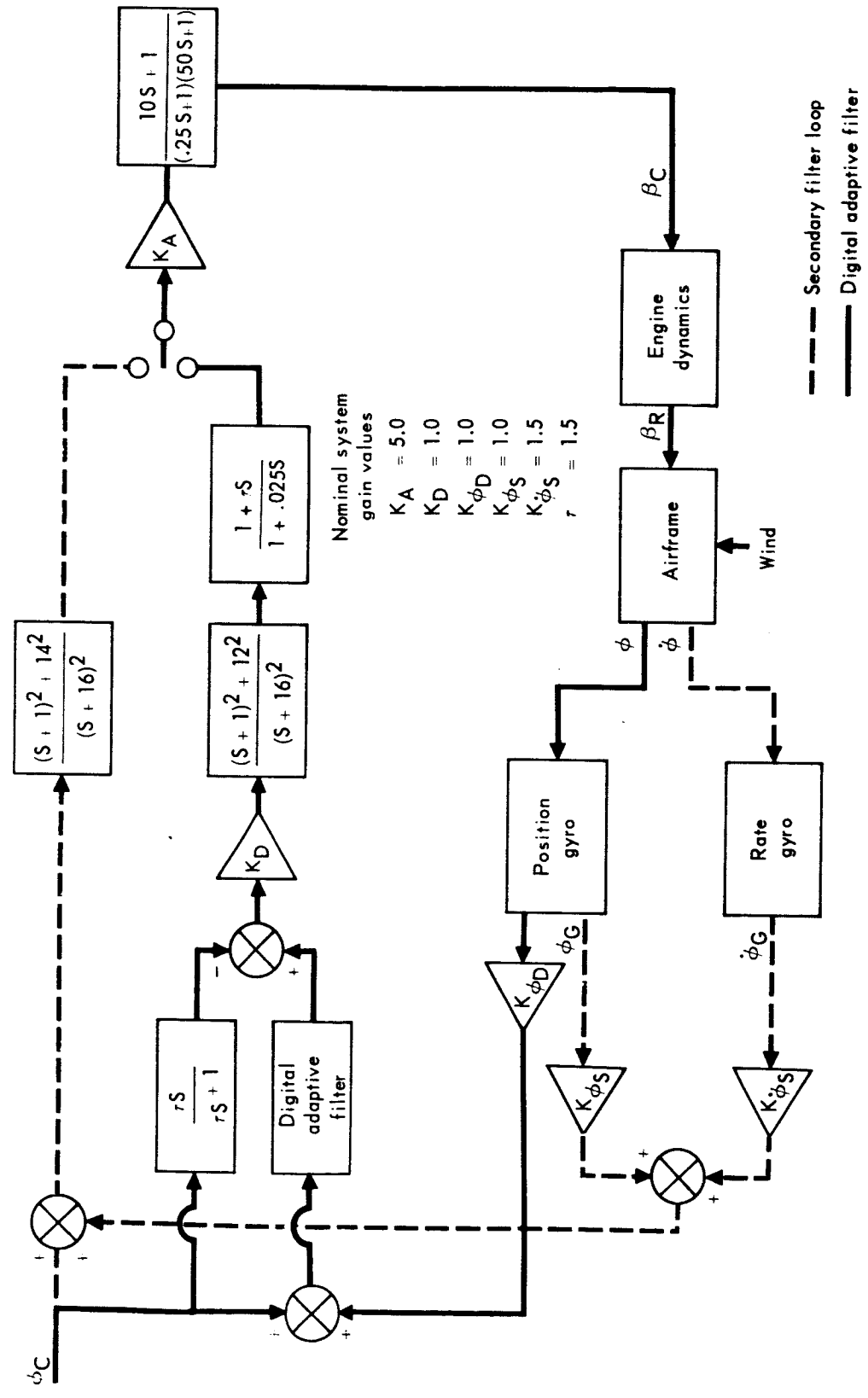

Figure 62 Digital Adaptive Filter Control System Block Diagram for Vehicle I at the Maximum Q Flight Condition

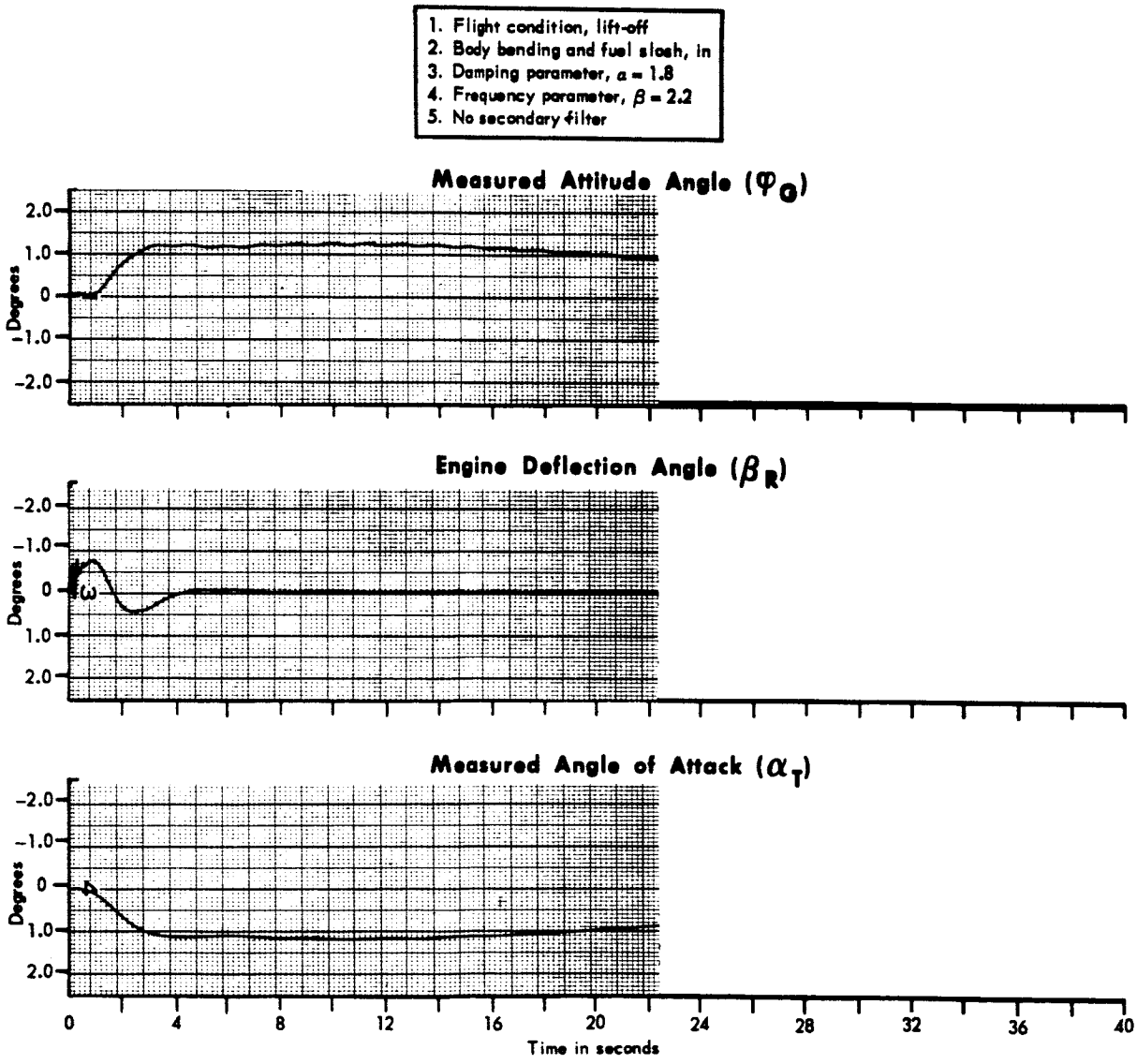

Figure 63 Unit Step Response of Study Vehicle No. I With the Digital Adaptive Filter

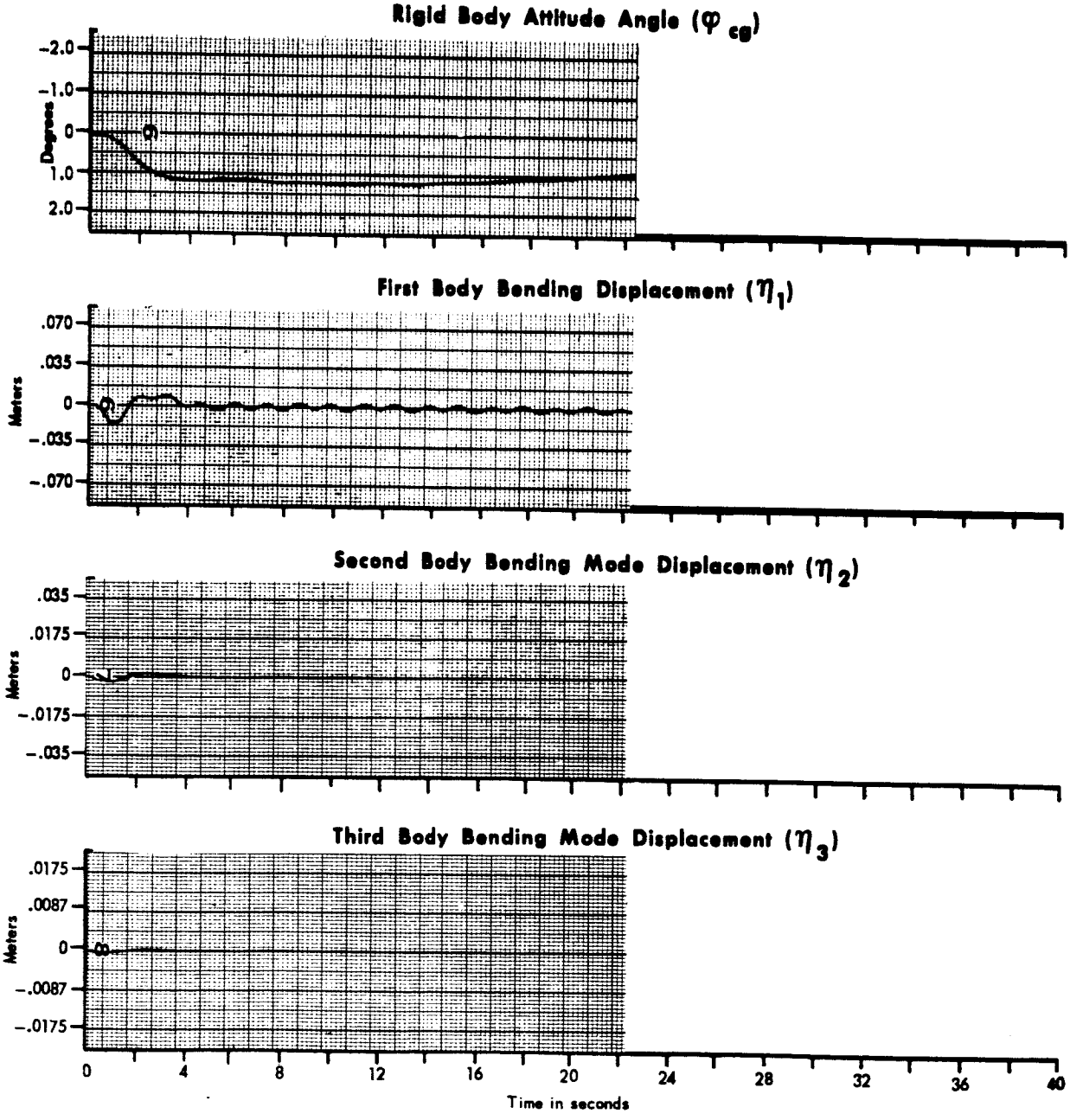

Figure 63 Unit Step Response of Study Vehicle No. I With the Digital Adaptive Filter (Cont.)

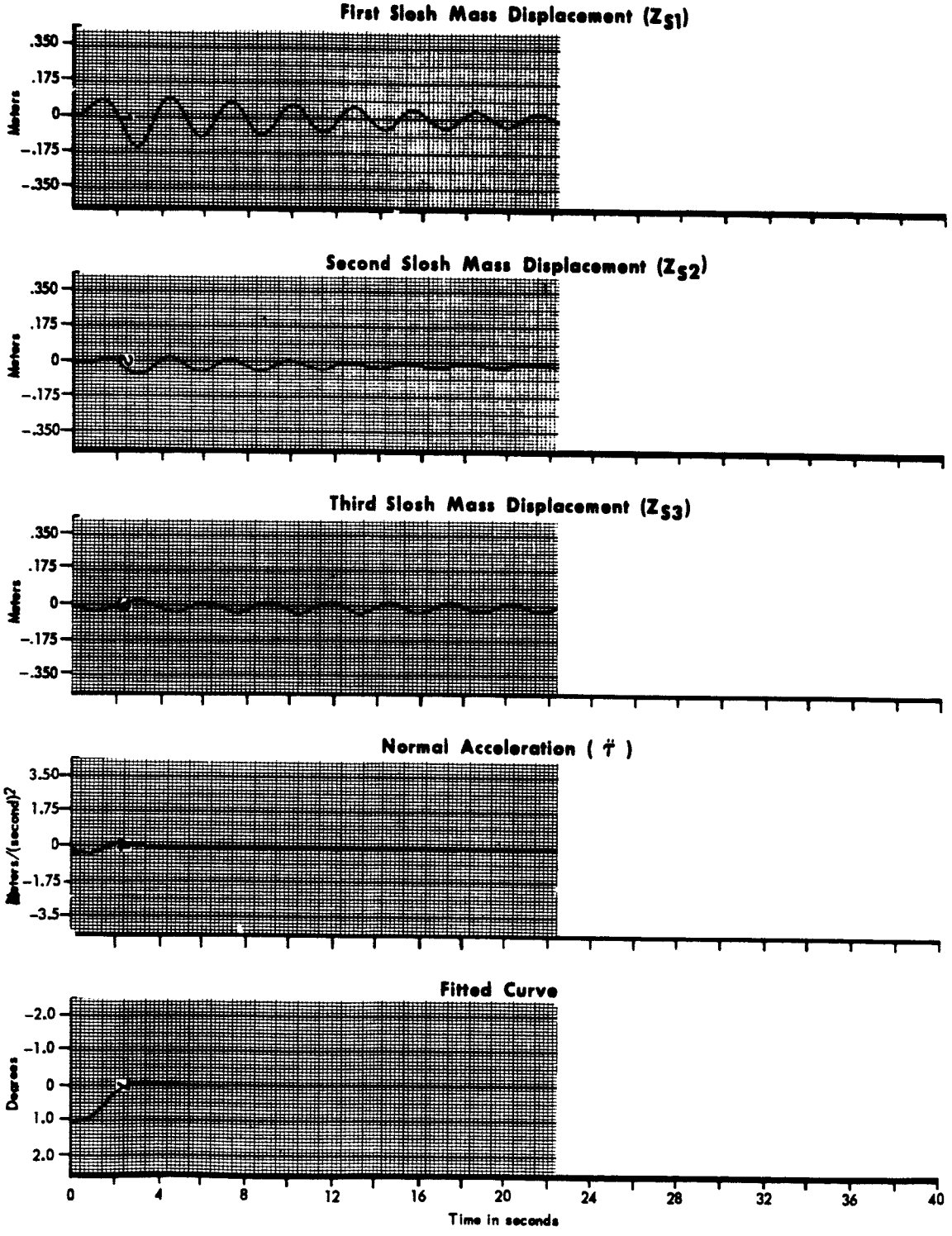

Figure 63 Unit Step Response of Study Vehicle No. I With the Digital Adaptive Filter (Cont.)

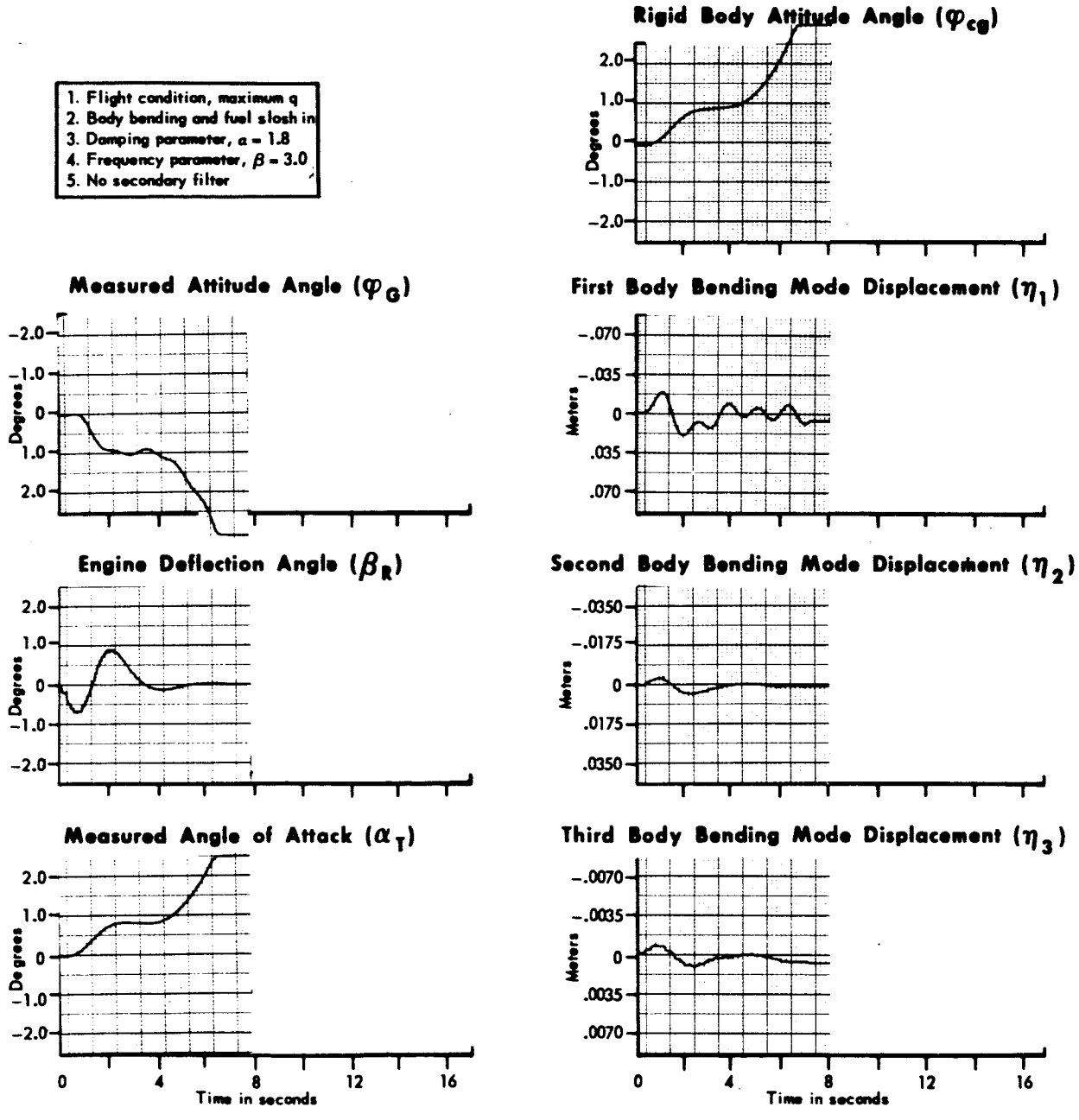

Figure 64 Unit Step Response of Study Vehicle No. I With the Digit Adaptive Filter

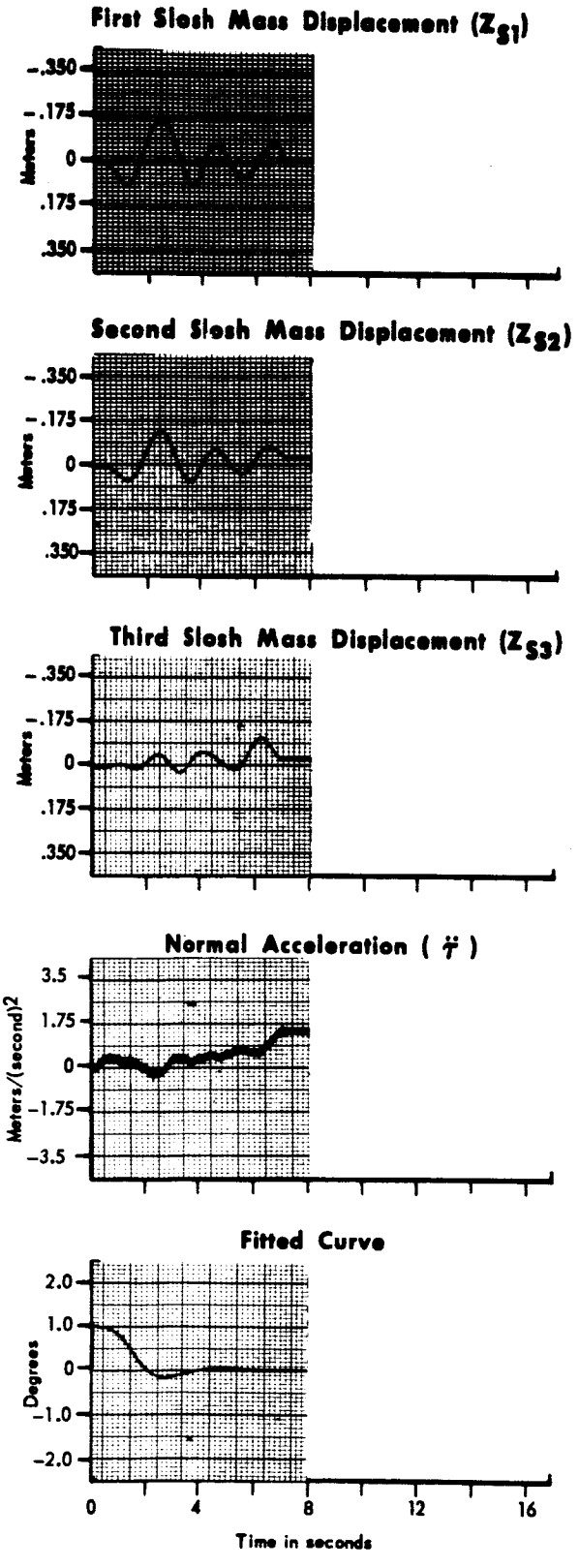

Figure 64 Unit Step Response of Study Vehicle No. 1 With the Digital Adaptive Filter (Cont.)

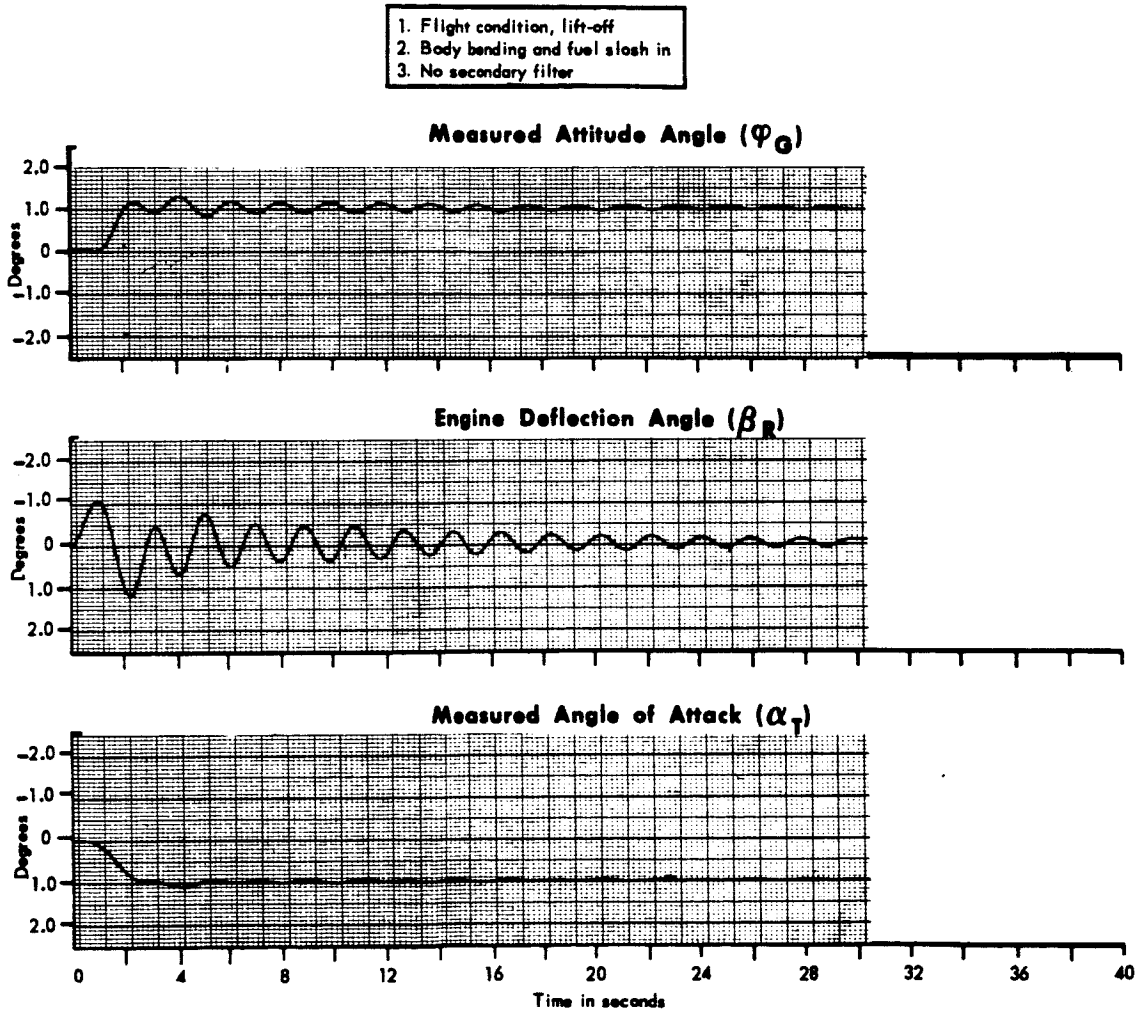

Figure 65 Unit Step Response of Study Vehicle No. I Without the Digital Adaptive Filter

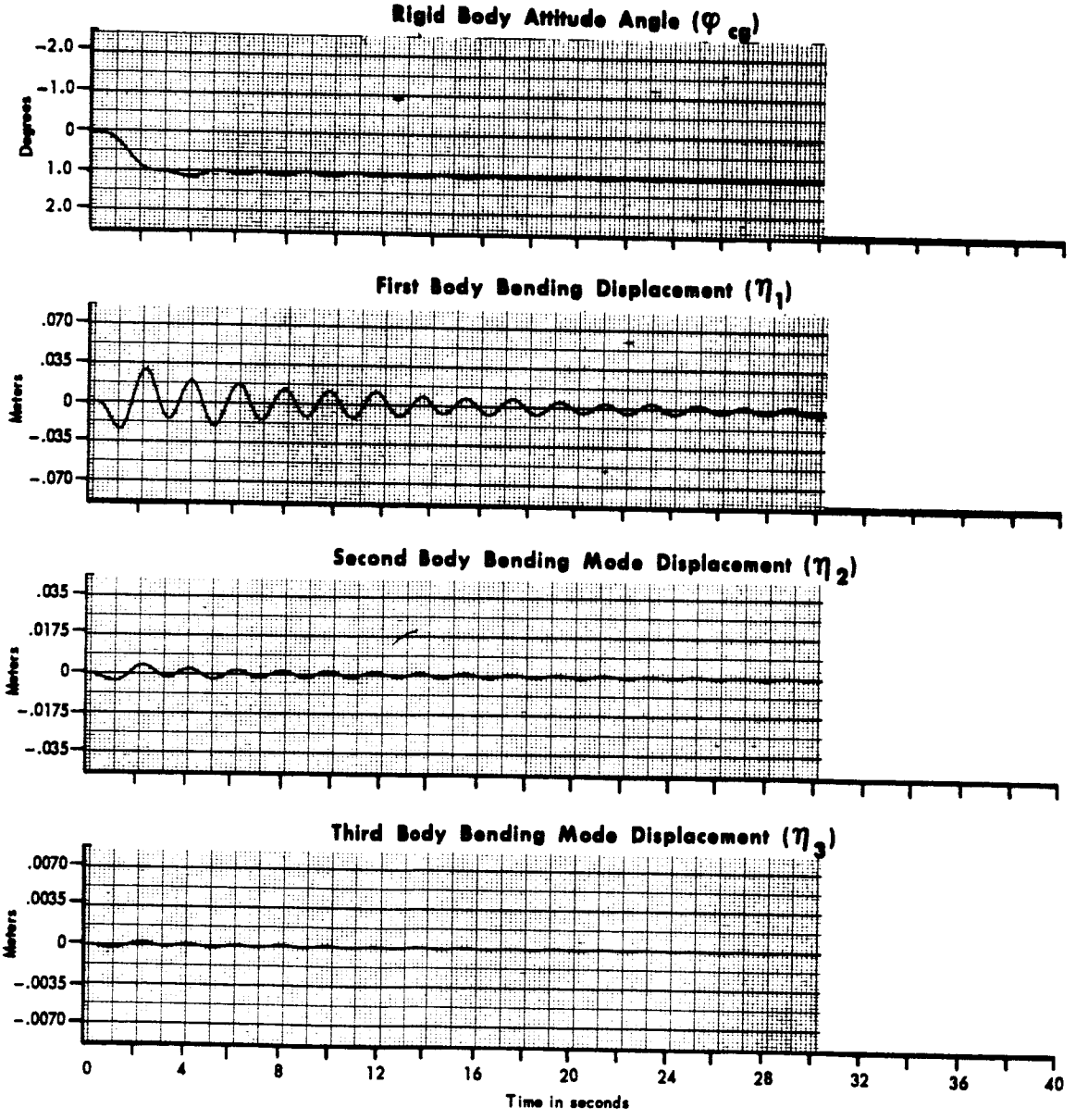

Figure 65 Unit Step Response of Study Vehicle No. I Without the Digital Adaptive Filter (Cont.)

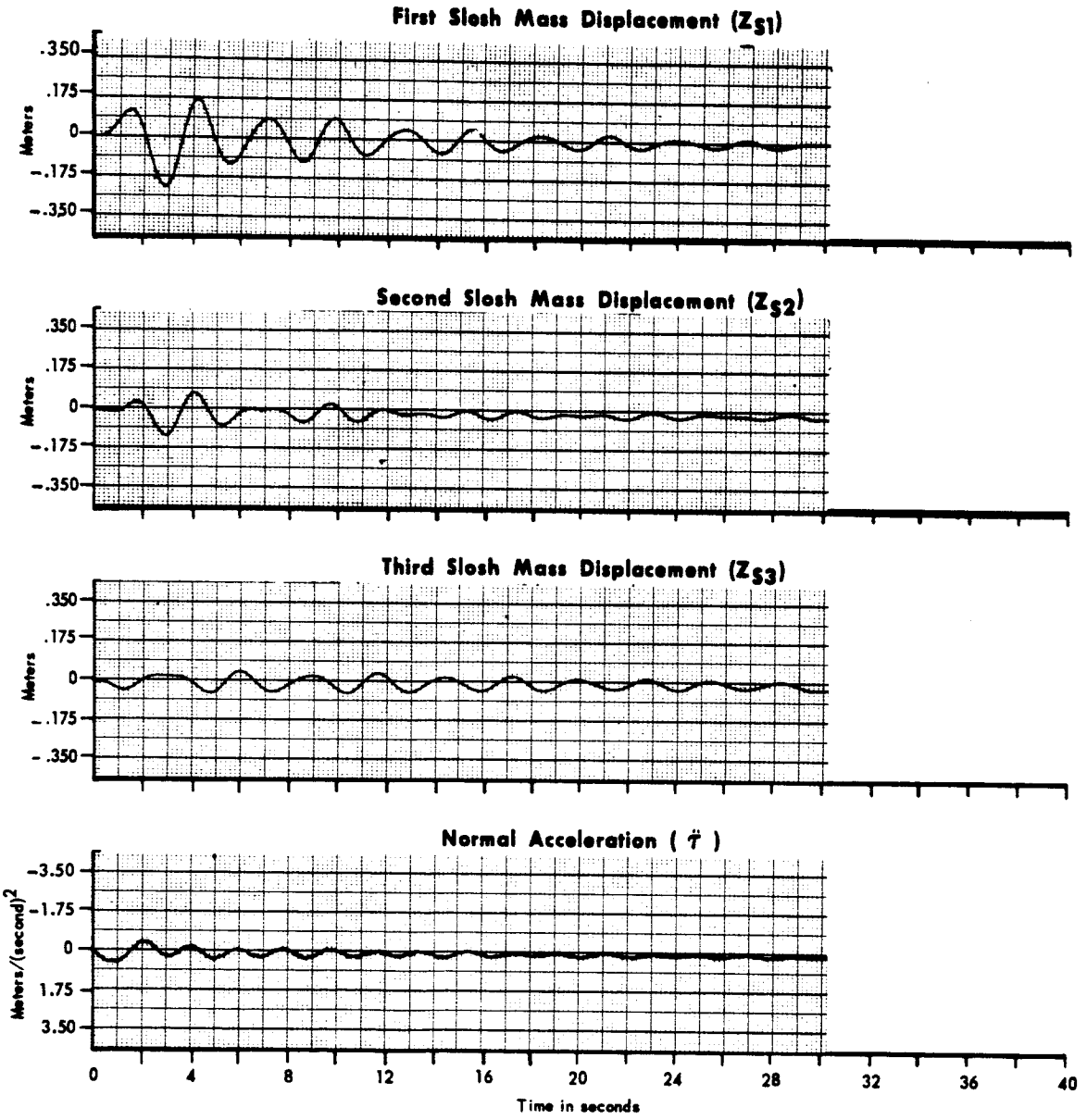

Figure 65 Unit Step Response of Study Vehicle No. I Without the Digital Adaptive Filter (Cont.)

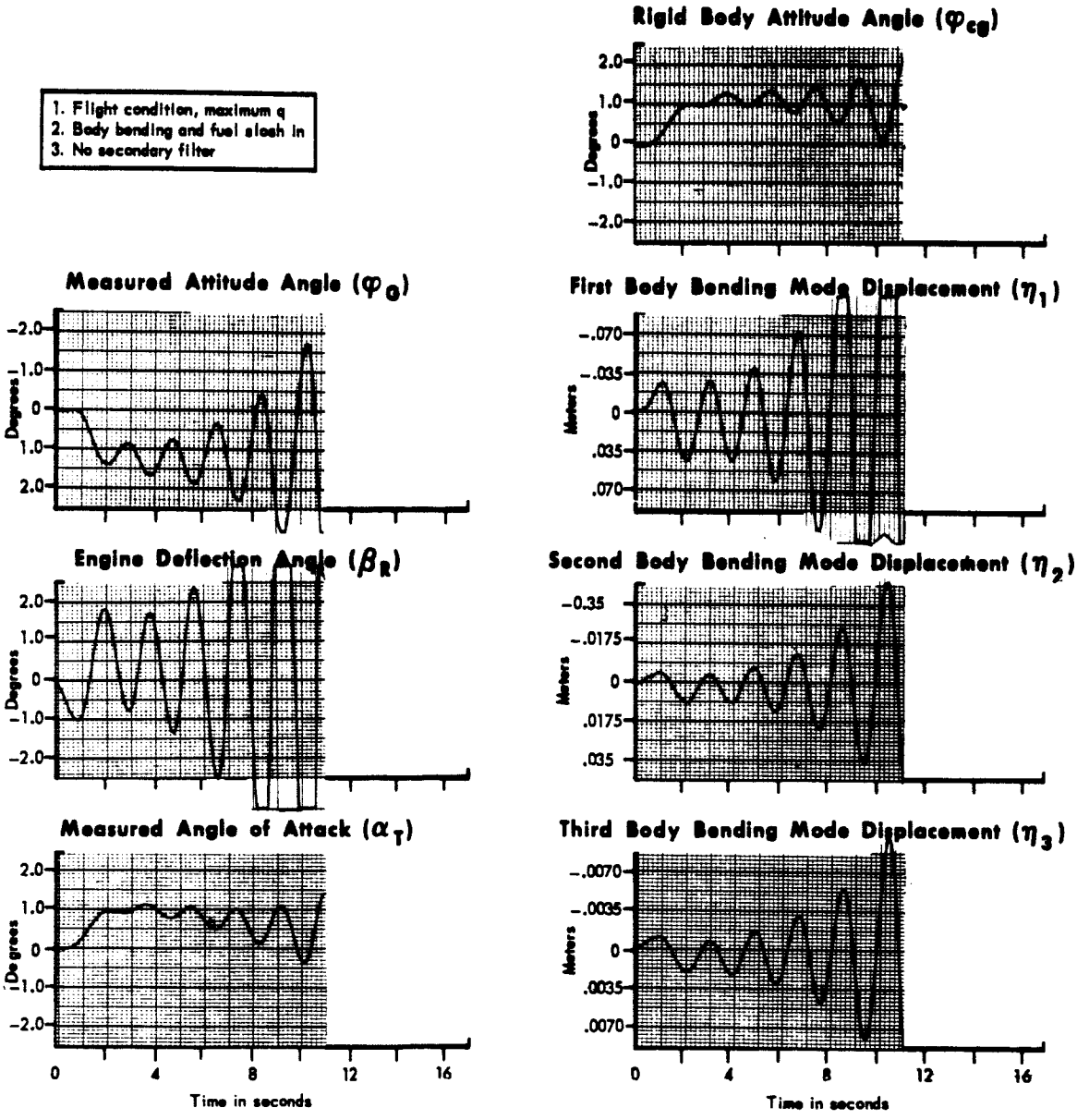

Figure 66 Unit Step Response of Study Vehicle No. I Without the Digital Adaptive Filter

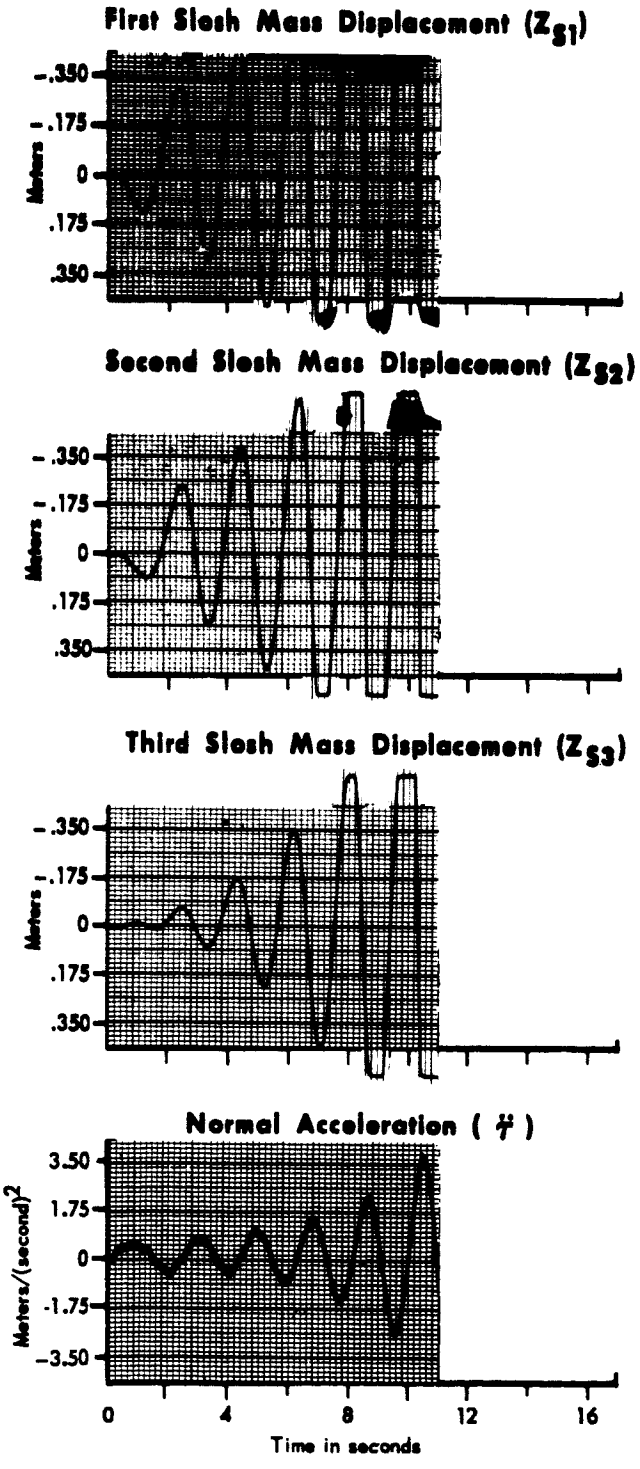

Figure 66 Unit Step Response of Study Vehicle No. I Without the Digital Adaptive Filter (Cont.)

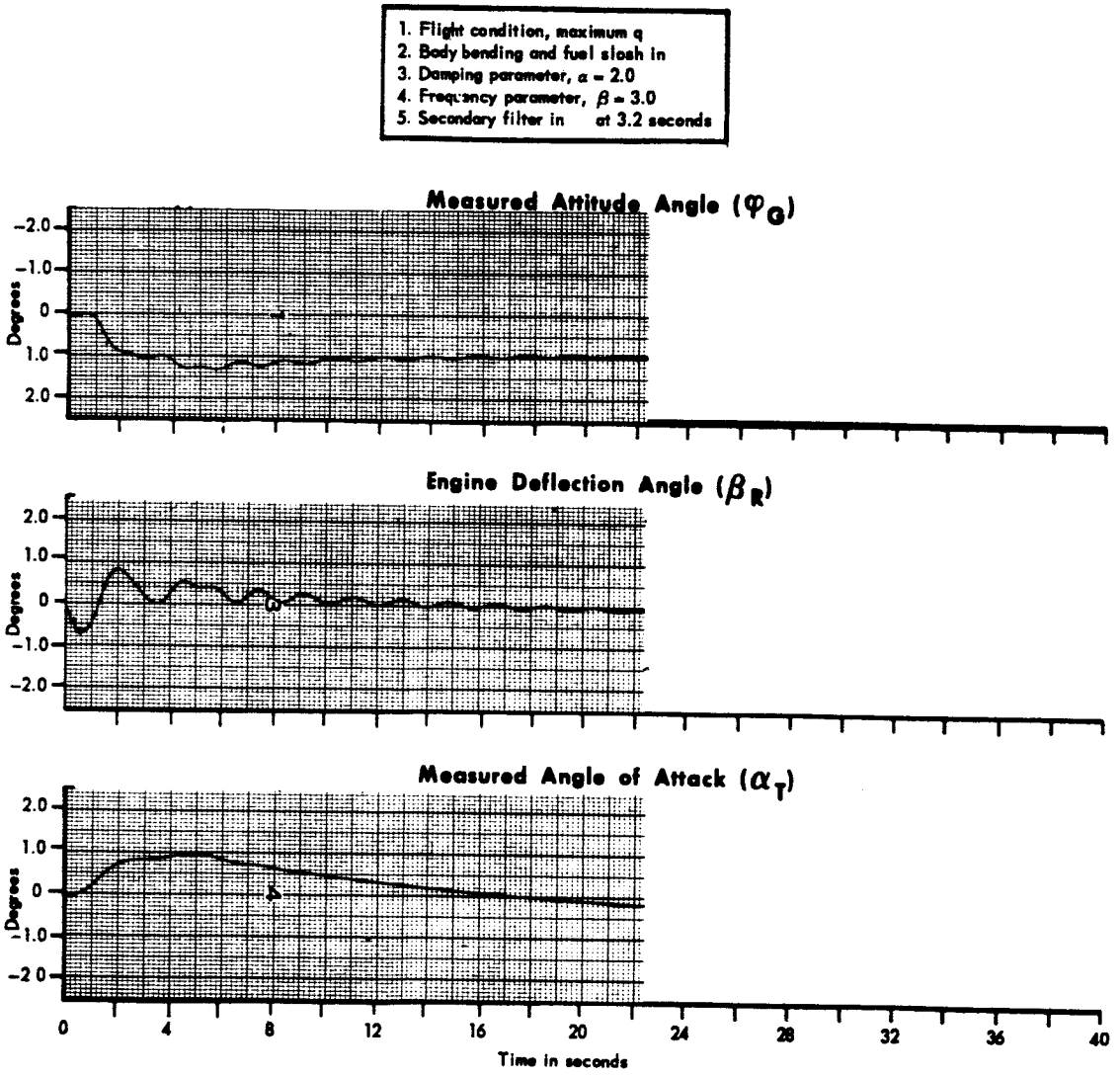

Figure 67 Unit Step Response of Study Vehicle No. I With the Digital Adaptive Filter

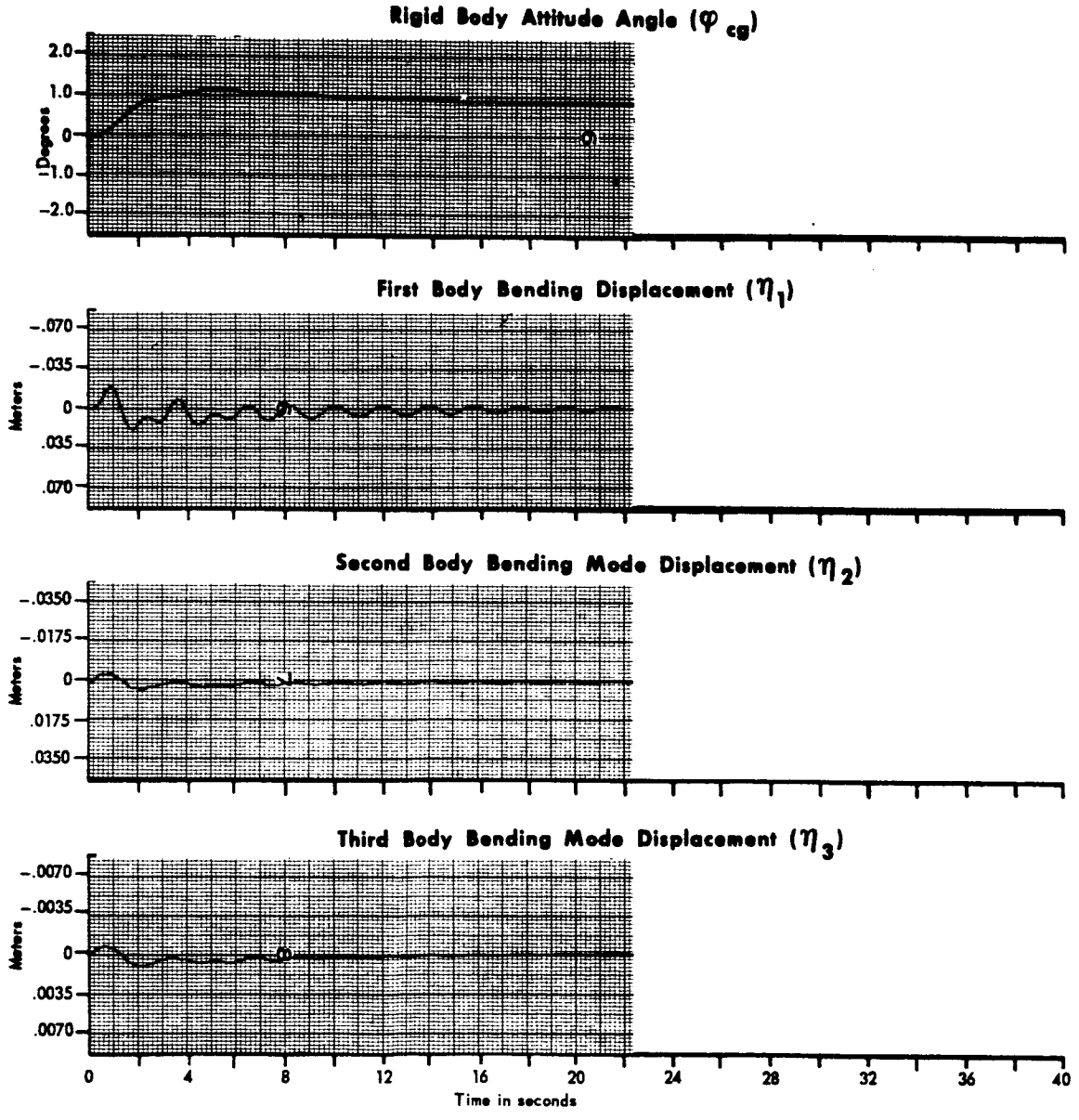

Figure 67 Unit Step Response of Study Vehicle No. I With the Digital Adaptive Filter (Cont.)

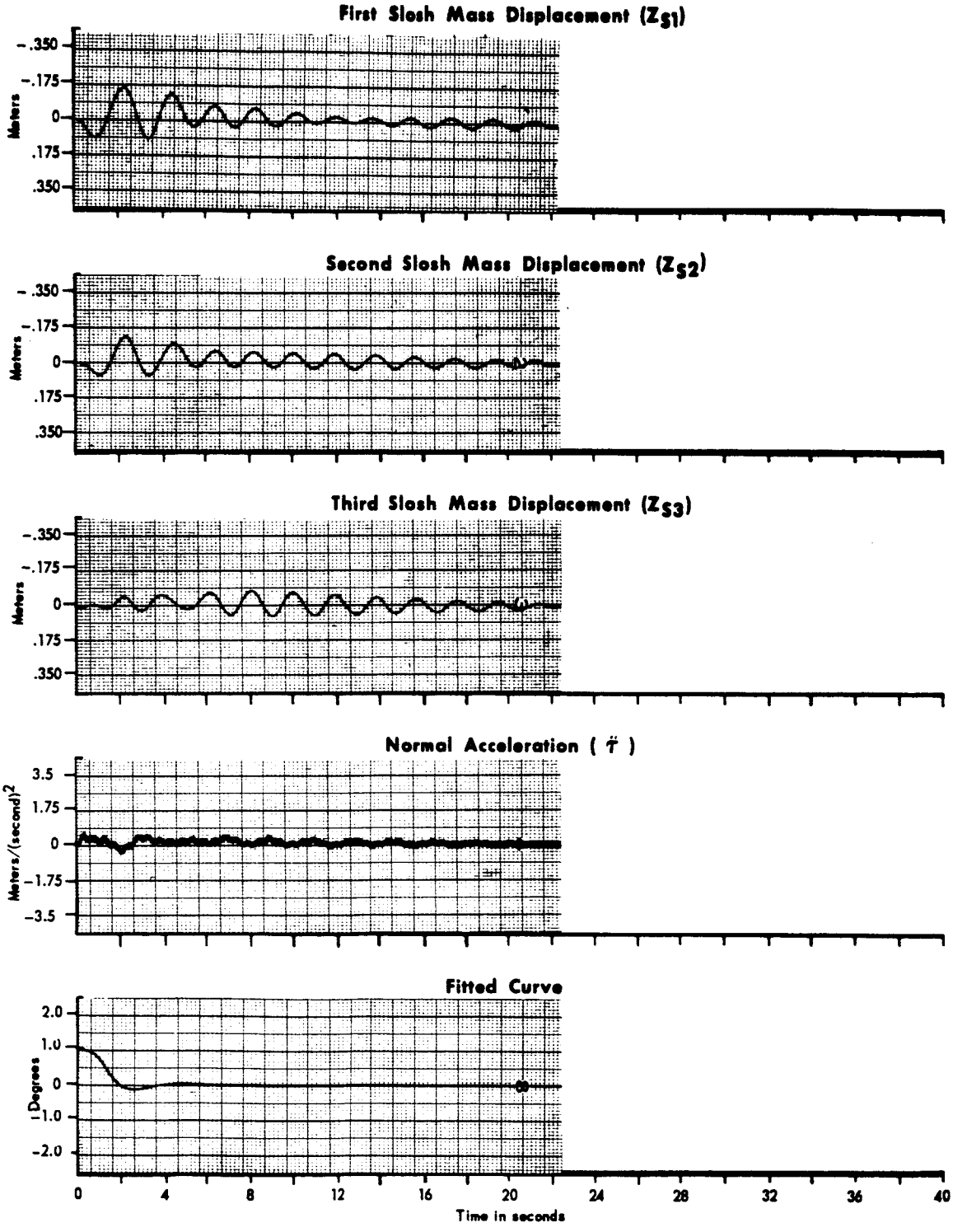

Figure 67 Unit Step Response of Study Vehicle No. I With the Digital Adaptive Filter (Cont.)

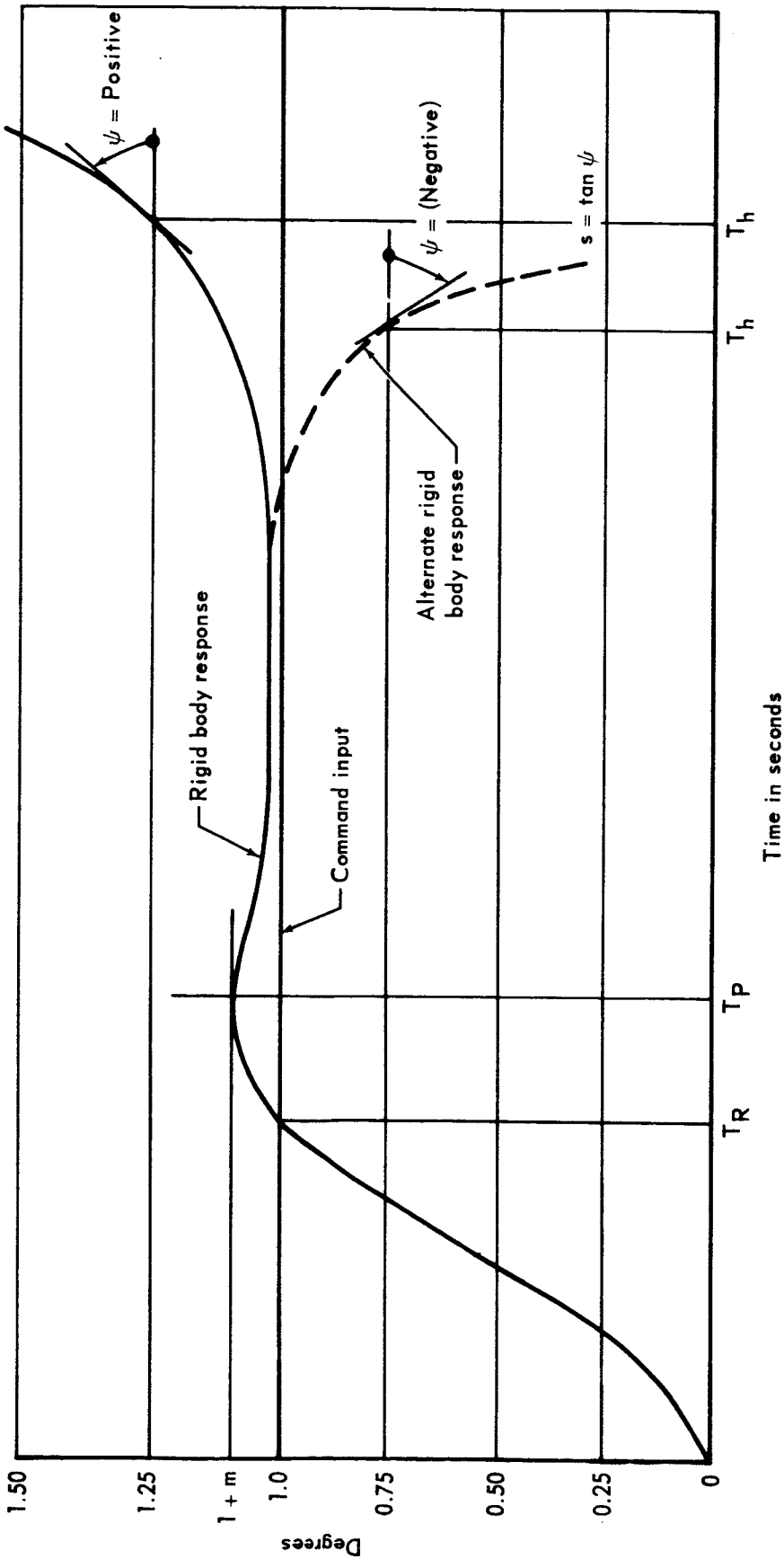

Figure 68 Performance Parameters Used for Evaluating Rigid Body Response to a Unit Step Command Input

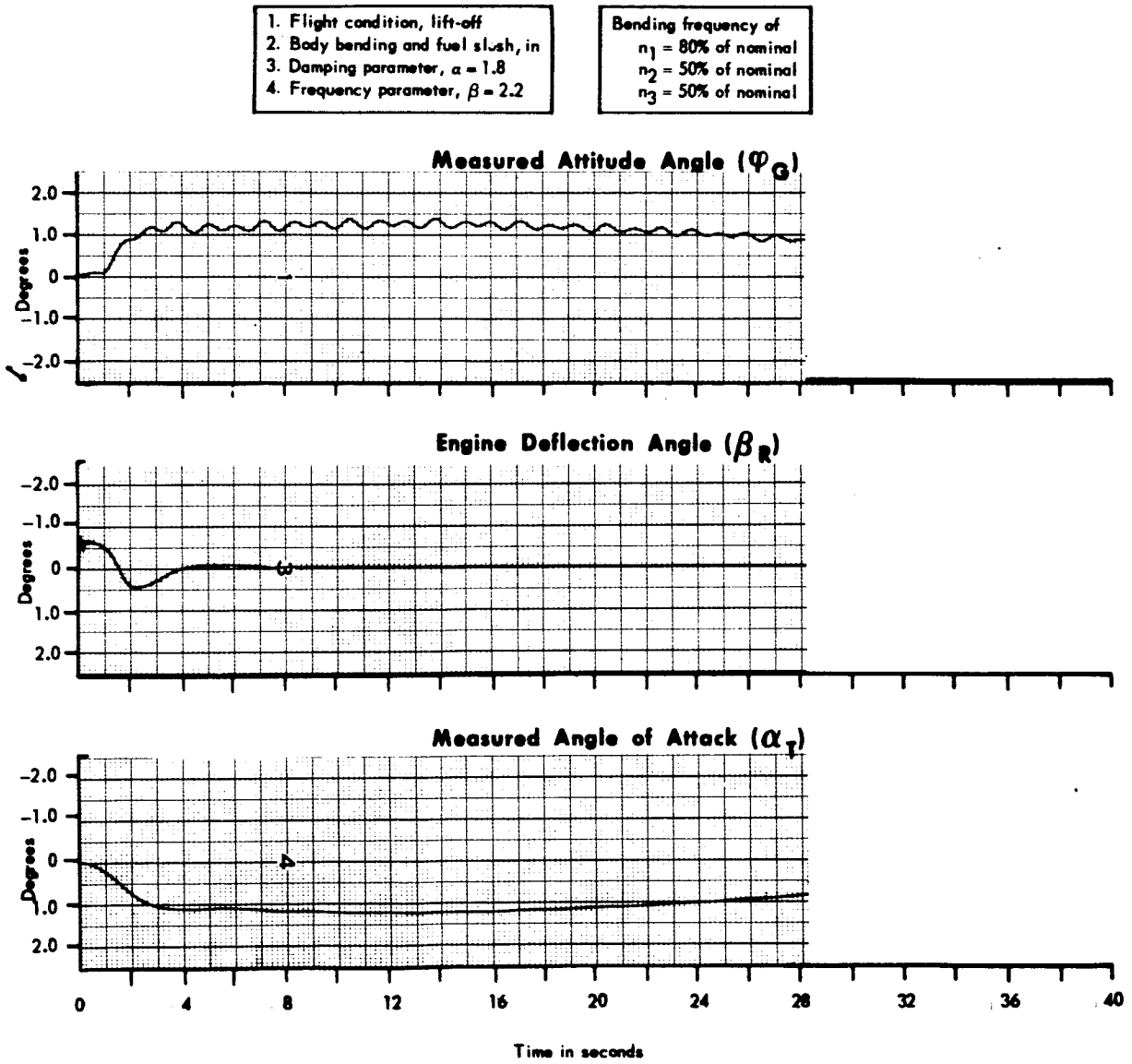

Figure 69 Unit Step Response of Study Vehicle No. I With the Digital Adaptive Filter

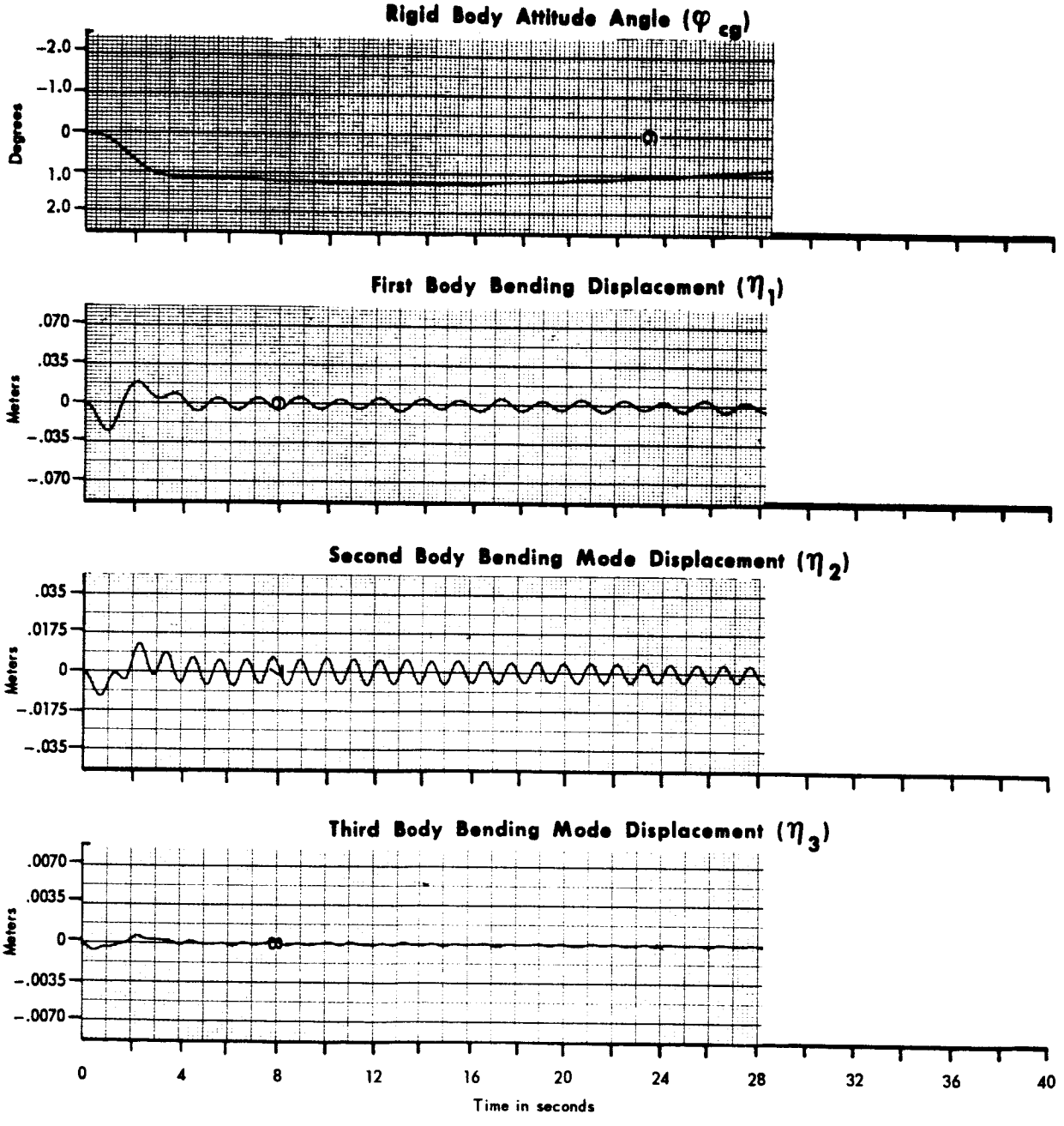

Figure 69 Unit Step Response of Study Vehicle No. I With the Digital Adaptive Filter (Cont.)

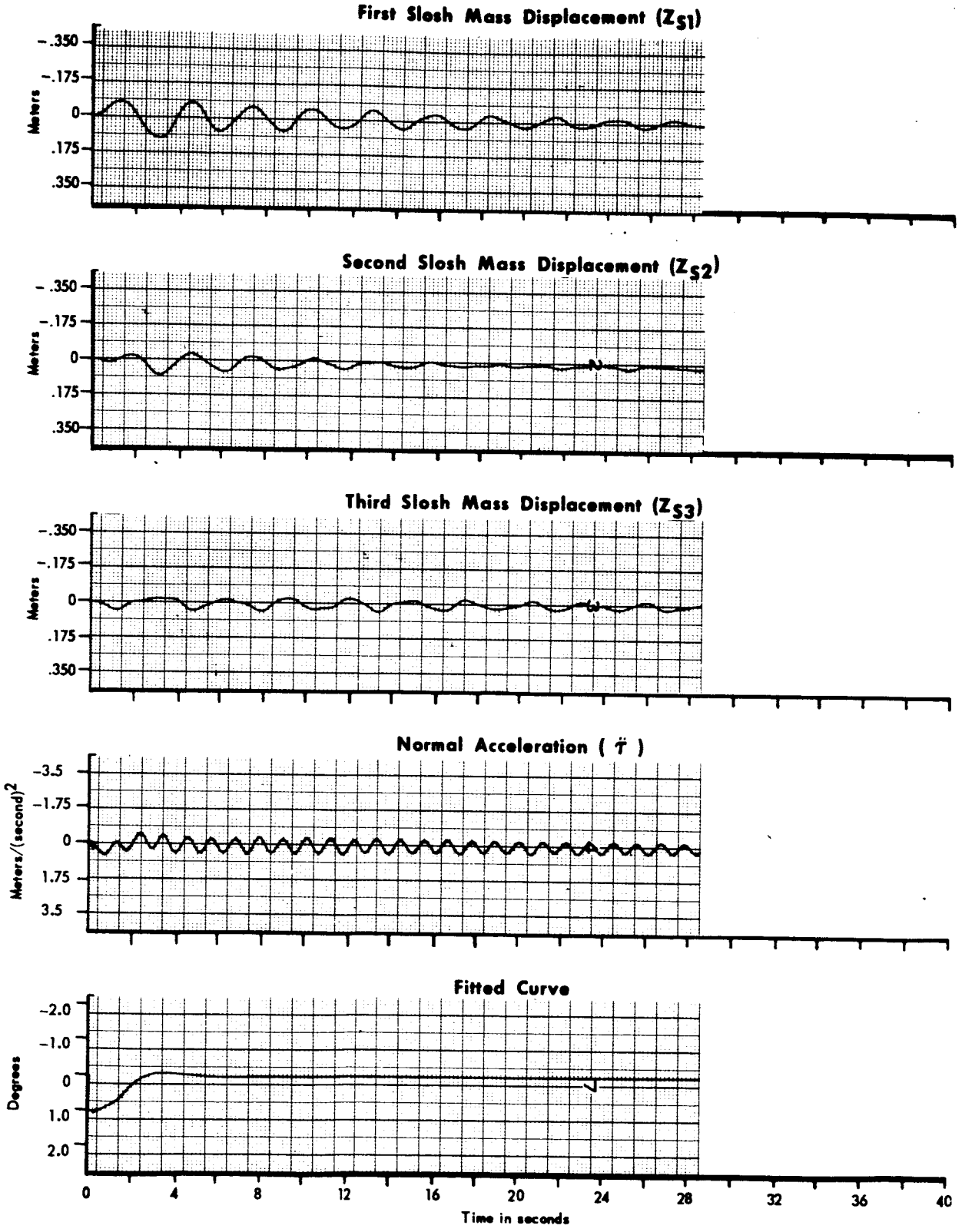

Figure 69 Unit Step Response of Study Vehicle No. I With the Digital Adaptive Filter (Cont.)

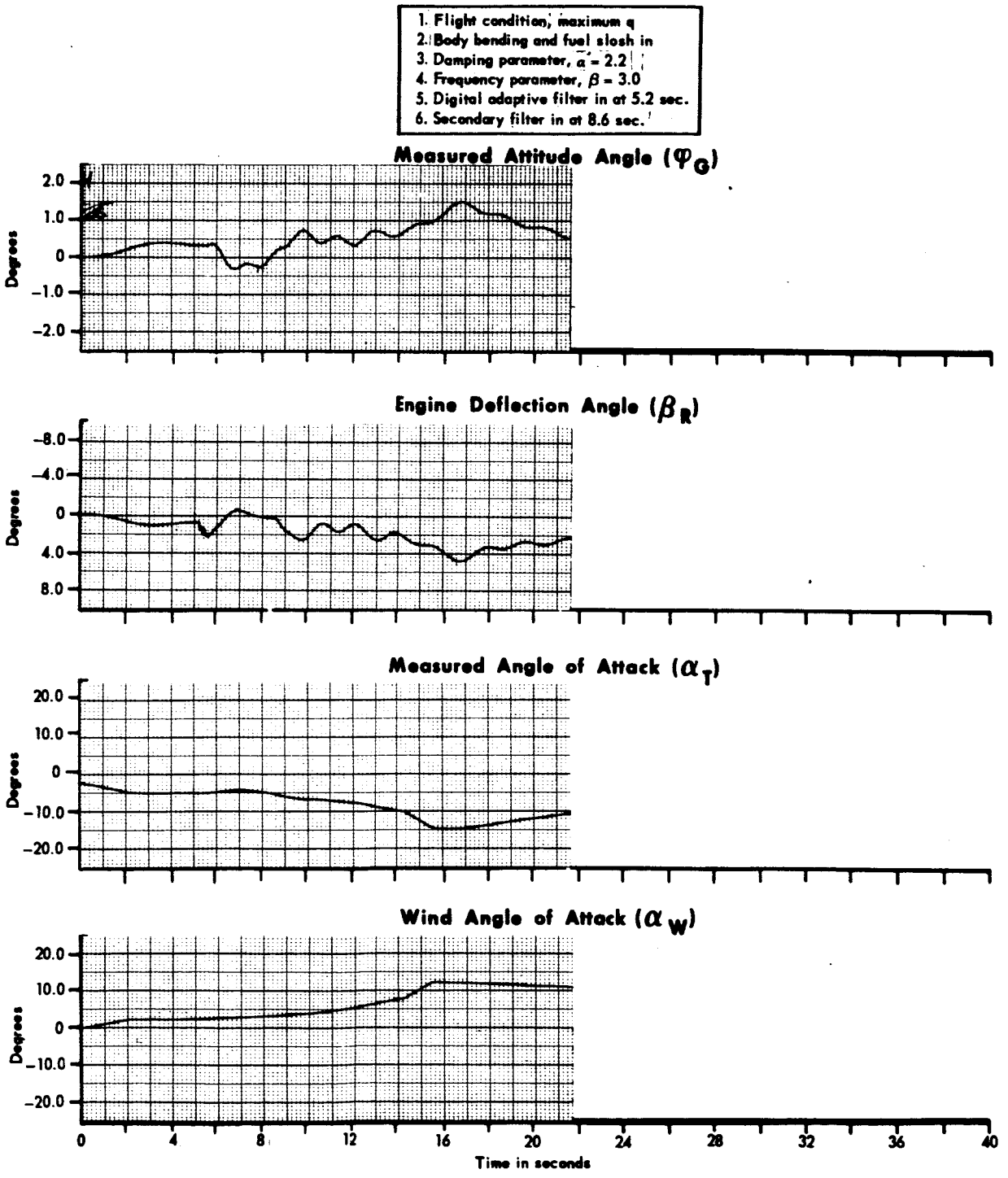

Figure 70 Wind Response of Study Vehicle No. 1 With the Digital Adaptive Filter

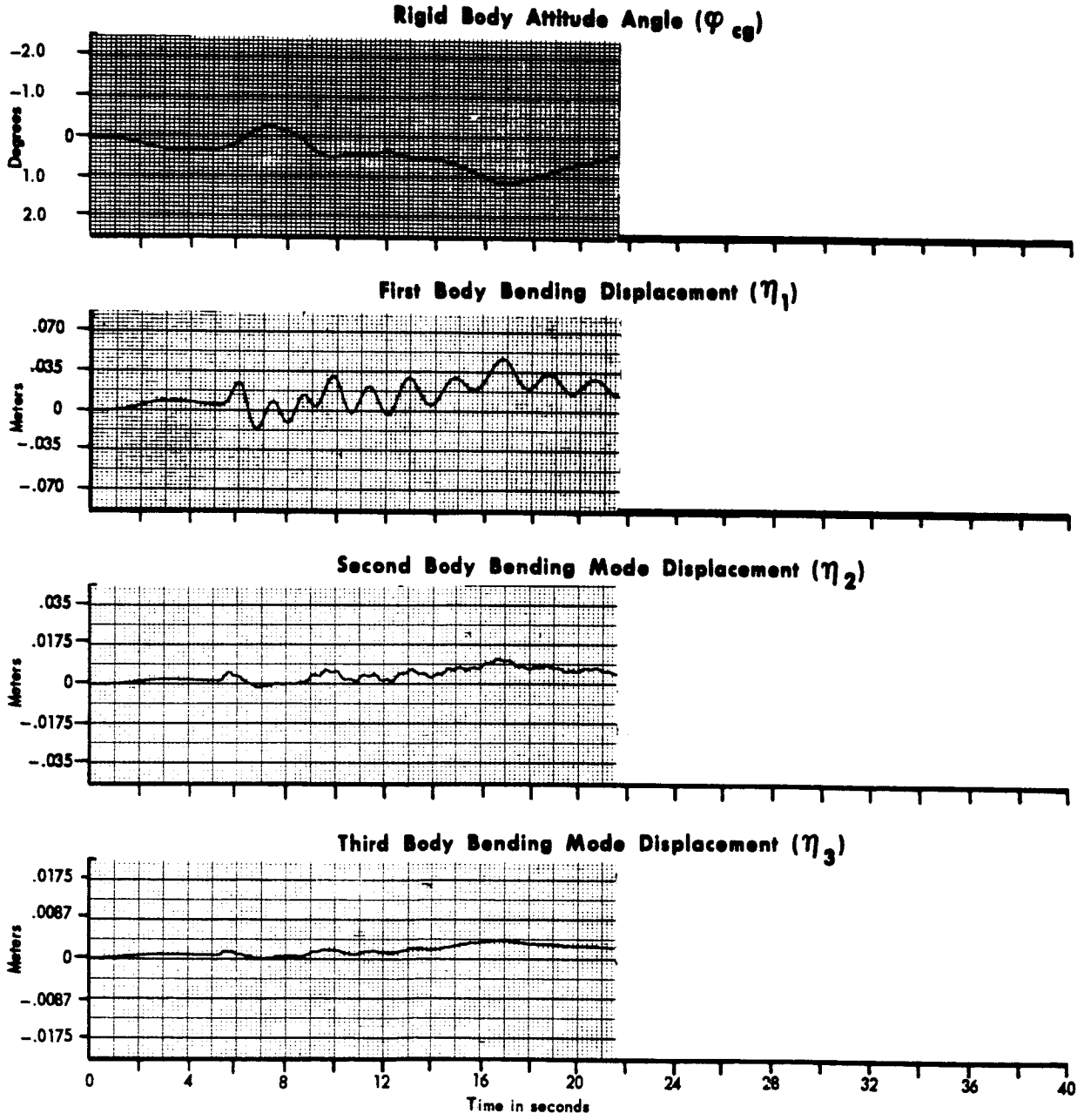

Figure 70 Wind Response of Study Vehicle No. 1 With the Digital Adaptive Filter (Cont.)

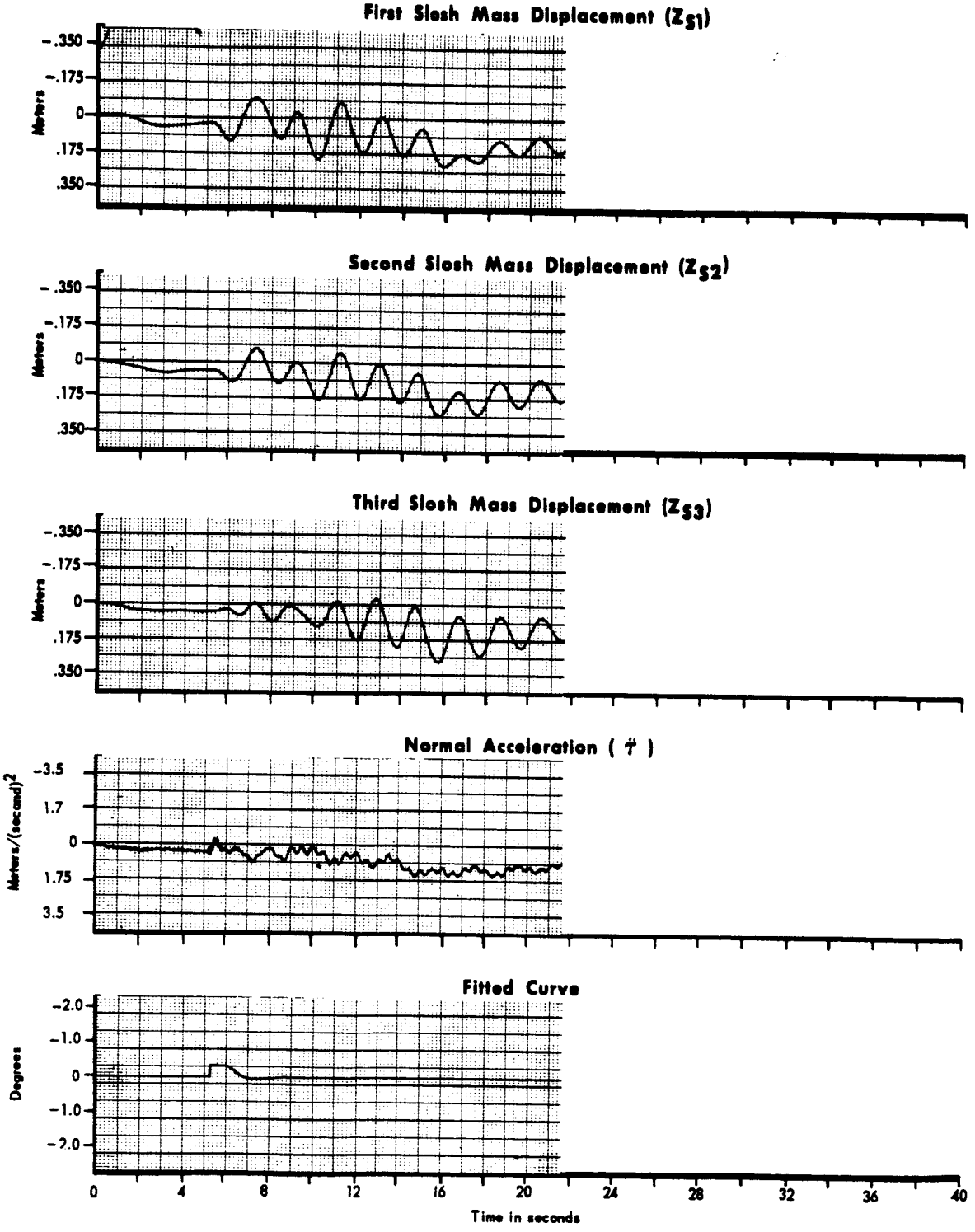

Figure 70 Wind Response of Study Vehicle No. 1 With the Digital Adaptive Filter (Cont.)

TABLE I

POLYNOMIAL CURVE FIT COEFFICIENTS FOR M = 12

c_r Coefficients	n = 0	n = 1	n = 2
c_{-12}	.04	-.1107692	.1572650
c_{-11}	.04	-.1015384	.1179487
c_{-10}	.04	-.0923077	.0820513
c_{-9}	.04	-.0830769	.0495726
c_{-8}	.04	-.0738461	.0205128
c_{-7}	.04	-.0646154	-.0051282
c_{-6}	.04	-.0553846	-.0273504
c_{-5}	.04	-.0461538	-.0461538
c_{-4}	.04	-.0369231	-.0615385
c_{-3}	.04	-.0276923	-.0735043
c_{-2}	.04	-.0184615	-.0820513
c_{-1}	.04	-.0092308	-.0871795
c_0	.04	0	-.0888889
c_1	.04	.0092308	-.0871795
c_2	.04	.0184615	-.0820513
c_3	.04	.0276923	-.0735043
c_4	.04	.0369231	-.0615385
c_5	.04	.0461538	-.0461538
c_6	.04	.0553846	-.0273504
c_7	.04	.0646154	-.0051282
c_8	.04	.0738461	.0205128
c_9	.04	.0830769	.0495726
c_{10}	.04	.0923077	.0820513
c_{11}	.04	.1015384	.1179487
c_{12}	.04	.1107692	.1572650

TABLE II

STEP RESPONSE CHARACTERISTICS OF VEHICLE II CONTROL SYSTEM

MEASURED PARAMETERS	SYSTEM DESIGN II.1	SYSTEM DESIGN II.2	SYSTEM DESIGN II.3
MEASURED ALTTITUDE ANGLE, ϕ_g			
FIRST PEAK AMPLITUDE	.76 deg.	.79 deg.	.76 deg.
FIRST PEAK TIME	3.5 sec.	3.3 sec.	3.3 sec.
SECOND PEAK AMPLITUDE	1.04 deg.	1.15 deg.	1.10 deg.
SECOND PEAK TIME	6.25 sec.	6.0 sec.	6.0 sec.
ATTITUDE RATE	.032 deg./sec.	.031 deg./sec.	.023 deg./sec.
PEAK TO PEAK BENDING OSCILLATION ON ϕ_g	.46 deg.	.7 deg.	.6 deg.
MAXIMUM ENGINE DEFLECTION	.35 deg.	.4 deg.	.4 deg.
MAXIMUM PEAK TO PEAK OSCILLATION ON FIRST BENDING MODE	.084 meters	.108 meters	.091 meters

TABLE III

WIND RESPONSE CHARACTERISTICS OF VEHICLE II CONTROL SYSTEM

MEASURED PARAMETERS	DESIGN II.1 VALUE	DESIGN II.2 VALUE	DESIGN II.3 VALUE
MAXIMUM WIND ANGLE OF ATTACK (DEGREES)	12.5	12.5	12.5
MAXIMUM VEHICLE ANGLE OF ATTACK (DEGREES)	11.0	10.8	11.6
MAXIMUM ENGINE DEFLECTION (DEGREES)	+2.6	+2.5	+2.6
ENGINE REBOUND (DEGREES)	-.25	-.27	+.3
MAXIMUM EXCURSION OF ϕ_g (DEGREES)	-8.6	-8.8	-6.8
MAXIMUM FIRST BODY BENDING MODE (METERS)	.154	.154	.154
MAXIMUM SECOND BODY BENDING MODE (METERS)	.0314	.0314	.0314
MAXIMUM THIRD BODY BENDING MODE (METERS)	.133	.133	.0715
MAXIMUM FOURTH BODY BENDING MODE (METERS)	.014	.014	.014
MAXIMUM BODY BENDING OSCILLATION ON ENGINE (DEGREES)	.15	.25	.2

TABLE IV

STEP RESPONSE CHARACTERISTICS OF VEHICLE I CONTROL SYSTEM

MEASURED PARAMETERS	SYSTEM DESIGN I.1	SYSTEM DESIGN I.2
MEASURED ATTITUDE ANGLE, ϕ_g		
FIRST PEAK AMPLITUDE	.9 deg.	1.4 deg.
ATTITUDE RATE OF ϕ_g	.014 deg./sec.	.0083 deg./sec.
PEAK TO PEAK BENDING OSCILLATION ON ϕ_g	.1 deg.	.1 deg.
MAXIMUM ENGINE DEFLECTION	.3 deg.	.45 deg.
MAXIMUM PEAK TO PEAK OSCILLATION ON FIRST BENDING MODE	.105 meters	.007 meters
PEAK ANGLE OF ATTACK	.75 deg.	.75 deg.

TABLE V

WIND RESPONSE CHARACTERISTICS OF VEHICLE I CONTROL SYSTEMS

MEASURED PARAMETERS	DESIGN I.1 VALUE	DESIGN I.2 VALUE
MAXIMUM WIND ANGLE OF ATTACK (DEGREES)	12.4 deg.	12.4 deg.
MAXIMUM VEHICLE ANGLE OF ATTACK (DEGREES)	11.5 deg.	11.0 deg.
MAXIMUM ENGINE DEFLECTION	3.95 deg.	3.9 deg.
ENGINE REBOUND (DEGREES)	1.2 deg.	1.4 deg.
MAXIMUM EXCURSION OF ϕ_g (DEGREES)	-4.4 deg.	-4.4 deg.
MAXIMUM FIRST BODY BENDING MODE (METERS)	.091 meters	.091 meters
MAXIMUM SECOND BODY BENDING MODE (METERS)	.0175 meters	.0175 meters
MAXIMUM THIRD BODY BENDING MODE (METERS	.006 meters	.007 meters
MAXIMUM BODY BENDING OSCILLATION ON ENGINE (DEGREES)	.2 degree (peak to peak)	.2 degree (peak to peak)

DATE 1 September 1965

REVISED

REVISED

MCDONNELL
ST. LOUIS, MISSOURI

VEHICLE II
DESIGN II.4 Compensation
2.5 SPS, 25 Stored Samples
Number of Samples = 25
System Gain, $K_{\dot{}}$ = 2.4
$K\emptyset$ = 5.0

RESPONSE CHARACTERIST

FOR VARIATIONS IN

Run No.	Group	A_o Polynominal Fitting in $\ddot{\tau}$ Feedback	Stability Compensation	Command Compensation
1 2 3 4 5 6 7 8	1	out	out	out
9 10 11 12 13 14	2	in	out	out
15 16 17 18	3	out	out	in
19 20 21 22 23 24	4	in	out	in
25 26 27 28 29 30	5	in	in	in
31 32 33 34 35 36	6	in	in	in

TABLE VI

ICS OF VEHICLE II, DESIGN II.4

ACCELERATION FEEDBACK GAIN

Slosh Modes	Bending Modes	Acceleration Feedback Gain, K''_{τ}	Measured Attitude: ϕ_G at 2 sec. (deg)	Measured Attitude: ϕ_G at 15.5 sec. (deg)	Measured Attitude: ϕ_{GP} peak amp. (deg)	Engine Deflection: β at 2 sec. (deg)	Engine Deflection: β max. peak amp. (deg)	Engine Deflection: β_{MR} Rebound amp. (deg)	α_m pe am (d
out	out	0	+.16	+4	+10.2	+.4	+2.88	-	+
		.03	+.08	+1.6	+3.0	+.3	+2.1	+.26	+
		.06	0	-.8	-1.6	+.44	+2.0	+.70	+
		.09	0	-3.2	-4.72	+.56	+2.06	+.84	+
		.12	0	-3.2	-6.8	+.64	+2.18	+.48	
		.15	-.4	-4.0	-8.6	+.72	+2.16	+.12	
		.18	-.4	-5.2	-10.0	+.8	+2.34	-.2	
		.21	-.08	-5.2	-11.0	+.9	+2.44	-.48	
out	out	0	+.4	+10.0	+10.4	+.30	+2.9	-.9	+
		.03	+.4	+2.4	+4.8	+.3	+1.4	-.12	+
		.06	+.8	+.8	-4.2	+.5	+2.2	+.01	+
		.09	+.6	-.8	-7.04	+.3	+2.3	-.2	+
		.12	+.64	-1.28	-8.8	+.3	+2.0	-.46	+
		.15	+.4	-3.2	-11.6	+.5	+1.8	-.70	
out	out	0	+.4	+.8	+2.4	+.4	+2.2	-.24	+
		.03	0	-.8	-2.4	+.44	+1.98	+.70	+
		.06	-.08	-2.4	-4.9	+.58	+2.06	+.88	
		.09	-.08	-3.6	-7.0	+.70	+2.26	+.4	
out	out	0	+.4	+1.2	+2.2	+.4	+2.11	-.24	+
		.03	+.4	-.04	-3.2	+.5	+2.1	+.56	+
		.06	+.32	-.96	-5.8	+.52	+2.1	+.22	+
		.09	+.24	-2.24	-8.4	+.6	+2.0	-.12	+
		.12	+.2	-3.2	-10.4	+.62	+2.0	-.42	
		.15	+.08	-3.6	-11.2	+.62	+2.1	-.7	
out	out	0	+.4	+1.2	+2.4	+.58	+2.48	+.30	+
		.03	+.44	0	-3.2	+.6	+2.36	+.58	+
		.06	+.4	-1.36	-6.4	+.64	+2.30	+.16	+
		.09	+.4	-1.76	-8.0	+.70	+2.30	-.2	+
		.12	+.32	-3.12	-10.48	+.74	+2.28	-.50	
		.15	+.24	-3.6	-11.92	+.76	+2.30	-.8	
in	in	0	+.72	+2.0	+3.0	+.66	+2.92	+.44	+
		.03	+.56	+.04	-3.2	+.70	+2.98	+.72	+
		.06	+.56	-.8	-6.08	+.74	+2.72	+2.6	+
		.09	+.56	-1.88	-8.48	+.82	+2.64	-.12	+
		.12	+.6	-2.48	-10.4	+.86	+2.70	-.44	+
		.15	+.52	-3.44	-12	+.92	+2.76	-.74	+

Measured Angle of Attack		Normalized Bending Mode Deflections				
ax. ak p. eg)	α_{MR} Rebound amp. (deg)	η_{1P} peak amp. (meters)	η_{2P} peak amp. (meters)	η_{3P} peak amp. (meters)	η_{4P} peak amp. (meters)	η_{1PP} peak amp. (meters)
5.6	-					
2.8	+1.6					
1.1	+4.2					
0.0	+6.1					
9.3	+4.1					
8.6	+4.1					
8.1	+3.3					
7.6	+2.8					
6.0	-5.2					
3.44	-.4					
2.	-2.					
0.8	+1.68					
0.4	+1.2					
9.1	+.56					
2.6	+1.6					
0.8	+4.0					
9.8	+4.8					
8.8	+5.2					
2.5	+1.6					
1.5	+4.0					
0.8	+3.5					
0.	+2.7					
9.3	+1.9					
9.2	+1.3					
12.72	+1.6					
11.6	+4.0					
10.6	+3.52					
10.24	+2.56					
9.4	+1.6					
9.0	+.84					
14	+2.4	+.188	+.037	+.0154	+.0017	.066
12.8	+4.8	+.177	+.036	+.0148	.0016	.072
11.84	+3.8	+.1745	+.035	+.0145	.0015	.085
10.88	+2.72	+.172	+.035	+.014	.0015	.098
10.52	+1.62	+.173	+.034	+.0142	.0015	.108
10	+1.0	+.1745	+.035	+.0142	.0084	.114

DATE 1 September 1965

REVISED

REVISED

MCDONNELL
ST. LOUIS, MISSOURI

VEHICLE II, UNIT STEP INPUT
DESIGN II.1
$K\ddot{\tau} = .095$ With Zero Degree (AO) Polynomial Fitting in $\ddot{\tau}$

RESPONSE OF STU

FOR DIFFERENT SAM

			Measured Attitude		Rigid Body Attitude			
Run No.	Sample Rate (1/sec)	No. of Stored Samples 'M'	ϕ_{GP} Peak Amp. (deg)	T_G Peak Time (sec)	$\phi_{C.G.M.}$ Peak Amp. (deg)	$\phi_{C.G.M.}$ Peak Time (sec)	Att. Rate $\dot{\phi}_s$ $(\frac{deg}{sec})$	Steady State Att. ϕ_s (deg)
1	1.0	9*	1.02	6.2	.70	7.0	.0225	
2	1.0	25	1.22	9.0	.90	9.3		1.00
3	1.5	9*	1.00	8.7	.70	9.0		.70
4	1.5	15	1.01	6.2	.75	7.5	.0215	
5	2.5	9*	.92	6.2	.65	8.0	.0253	.60
6	2.5	13*	1.10	6.0	.80	6.8	.0253	
7	2.5	17*	1.00	6.0	.70	6.75	.0116	
8	2.5	21*	1.12	6.2	.80	7.0	.0145	
9	2.5	23*	1.17	9.0	.82	8.5	.025	
10	2.5	23*	1.00	6.5	.68	6.5	.00765	
11	2.5	25	1.04	6.5	.74	6.5	.00769	
12	2.5	25	1.07	6.1	.76	7.5	.038	
13	2.5	27*	1.17	8.8	.88	9.0	.018	
14	4.0	35*	1.10	6.0	.80	7.0	.015	
15	4.0	37*	1.10	6.3	.80	7.5	.016	
16	4.0	39	1.04	6.5	.76	7.5	.00833	
17	4.0	41	1.04	6.5	.80	7.5	.0074	
18	4.0	43*	1.04	6.5	.78	7.5	.01111	

*unstable run - values given apply to first

156-1

TABLE VII

DY VEHICLE II, DESIGN II.1,

PLE RATES AND MEMORY LENGTHS

Engine Angle β_{max}, (deg)	Angle of Attack α_{max}, (deg)	Slosh-Peak to Peak Amplitude Z_{1PP} (meters)	Z_{2PP} (meters)	Z_{3PP} (meters)	Normal Acceler. $\ddot{\tau}$ Peak Amp. (meters /sec^2)	Damping Factor d (1/sec)	T Peak Amp. (meters)
-.36	1.00	.122	.04	.134	+.135	+.0179	
-.39	1.16	.108	.04	.136	+.144	-.0252	+.054
-.35	.88	.176	.038	.143	+.143	+.0258	
-.36	1.00	.122	.04	.138	+.142	-.021	-.050
-.35	.90	.497	.061	.394	+.220	+.109	
-.38	1.04	.154	.052	.164	+.155	+.01185	
-.36	1.00	.218	.038	.218	+.148	+.0514	
-.40	1.16	.147	.049	.1605	+.158	+.0201	
-.35	1.20	.148	.044	.157	+.153	+.0937	
-.36	1.02	.138	.044	.157	.1380	+.01975	
-.37	1.02	.131	.04	.147	-.1400	-.0202	+.051
-.39	1.04	.133	.04	.154	+150	-.0227	+.053
+.38	1.14	.147	.04	.145	+150	+.0084	
-.38	1.14	.15	.044	.157	+150	+.0107	
-.37	1.16	.14	.047	.154	+.148	+.00537	
-.37	1.06	.136	.04	.147	-.1400	-.0382	+.051
-.38	1.04	.131	.04	.148	-.1400	-.00893	+.052
-.37	1.06	.122	.04	.166	-.1400	+.01025	

20 seconds

Body Bending Modes

η_1	η_2		η_3		η_4	
Peak to Peak Osc. (meters)	Peak Amp. (meters)	Peak to Peak Osc. (meters)	Peak Amp. (meters)	Peak to Peak Osc. (meters)	Peak Amp. (meters)	Peak to Peak Osc. (meters)
		.003		.00075		5.2×10^{-5}
.088	-.007	.003	+.0024	.00073	+.0003	3.5×10^{-5}
		.003		.00073		7.0×10^{-5}
.080	-.0066	.0031	+.0022	.00077	-.00021	5.2×10^{-5}
		.003		.00075		3.5×10^{-5}
		.0033		.00084		3.5×10^{-5}
		.0033		.00087		3.5×10^{-5}
		.0031		.00080		3.5×10^{-5}
		.0028		.00075		3.5×10^{-5}
		.0047		.00122		1.7×10^{-4}
.084	-.0068	.0049	+.0023	.00122	-.0003	1.7×10^{-4}
.087	-.007	.0035	+.0023	.00075	-.00028	3.5×10^{-5}
		.0028		.00077		5.2×10^{-5}
		.0031		.000785		5.2×10^{-5}
		.0031		.00084		5.2×10^{-5}
.084	-.0068	.0047	+.0021	.0012	-.00028	.00017
.087	-.0068	.0051	+.0022	.0012	-.00033	.00017
		.0051		.0012		.00017

DATE 1 September 1965

REVISED

REVISED

MCDONNELL
ST. LOUIS, MISSOURI

VEHICLE II, UNIT STEP INPUT
DESIGN II.2
$K\ddot{\tau} = .095$
A_0 Fitting in $\ddot{\tau}$

TABLE VII

RESPONSE OF VEHICLE II,

DIFFERENT SAMPLE RATES A

			Measured Attitude		Rigid Body Attitude			
Run No.	Sample Rate (1/sec)	No. of Stored Samples M'	ϕ_{GP} Peak Amp. (deg)	T_G Peak Time (sec)	$\phi_{C.G.M.}$ Peak Amp. (deg)	$\phi_{C.G.M.}$ Peak Time (sec)	Att. Rate $\dot{\phi}_s$ ($\frac{deg}{sec}$)	Steady State Att. ϕ_s (deg)
1	2.5	25	1.21	8.75	.80	8.25	.0526	
2*	4	35	1.50	9.0	1.12	12.		.70
3	4	37	1.21	8.7	.85	8.5	.0308	
4	4	41	1.13	6.2	.75	6.5	.0308	
5*	4	43	1.23	8.3	.86	8.6	.0201	
6	5	49	1.11	9.00	.75	8.0	.0267	

* Unstable run-values given apply to first 20 seconds.

I

DESIGN II.2, FOR

ND MEMORY LENGTHS.

Engine Angle $\beta_{max.}$ (deg)	Angle of Attack $\alpha_{max.}$ (deg)	Slosh-Peak to Peak Amplitude			Normal Acceler. $\ddot{\tau}_{max.}$ Peak Amp. (meters /sec^2)	Damping Factor d (1/sec)	η Peak Amp. (meters)
		Z_{1PP} (meters)	Z_{2PP} (meters)	Z_{3PP} (meters)			
-.40	1.19	.129	.054	.162	+.1600	-.0431	-.063
.200	1.40	.106	.068	.157	+.170	+.0129	
.162	1.20	.138	.052	.162	+.169	-.00412	-.0632
.160	1.16	.136	.058	.161	+.166	-.0162	-.0632
.162	1.20	.136	.056	.161	+.166	+.0129	
-.4	1.14	.134	.056	.162	+.1590	-.0458	-.059

Body Bending Modes

	η_2		η_3		η_4	
Peak to Peak Osc. (meters)	Peak Amp. (meters)	Peak to Peak Osc. (meters)	Peak Amp. (meters)	Peak to Peak Osc. (meters)	Peak Amp. (meters)	Peak to Peak Osc. (meters)
.108	+.0066	.0059	-.0024	.0016	-.0003	.00017
		.00035		.00089		3.5×10^{-5}
.105	.00715	.00035	-.0024	.00092	-.0003	3.5×10^{-5}
.1075	.00715	.00035	-.0024	.00092	.00031	3.5×10^{-5}
		.00035		.00094		3.5×10^{-5}
.104	+.0063	.0059	-.0024	.00141	-.00033	.00017

DATE 1 September 1965

REVISED

REVISED

MCDONNELL
ST. LOUIS, MISSOURI

VEHICLE II, UNIT STEP INPUT
DESIGN II.3
$K = .095$
$\frac{1}{1 + \tau aS}$ Lag Network in $\ddot{\tau}$ Feedback RESPONSE FOR DIFFERENT TIM

Run No.	Time Constant of $\ddot{\tau}$ Feedback γ_a	Measured Attitude ϕ_{GP} Peak Amp. (deg)	Measured Attitude T_G Peak Time (sec)	Rigid Body Attitude ϕ_{CGM} Peak Amp. (deg)	Rigid Body Attitude T_{CGM} Peak Time (sec)	Rigid Body Attitude Att Rate $\dot{\phi}_s$ $(\frac{deg}{sec})$	Rigid Body Attitude Steady State Attitude ϕ_s (deg)	Engine Angle β_{max} (deg)
1	7*	+1.1	8.75	+.78	8.5	.0200	- -	-.39
2	8	+1.13	8.5	+.81	8.5	.0200	- -	-.4
3	9	+1.63	6.0	+1.1	6.0	.0222	- -	-.6
4	10	+1.13	9.0	+.82	8.5	.0200	- -	-.38
5	11	+1.18	8.75	+.84	8.5	.0213	- -	-.39
6	12	+1.19	8.75	+.84	8.5	.0213	- -	-.39
7	15	+1.22	8.75	+.88	8.5	.0192	- -	-.39
8	20	+1.25	9.0	+.92	9.0	.0182	- -	-.4
9	30	+1.28	9.0	+.94	9.0	.0185	- -	-.4

***Unstable run - values given apply to first 20 seconds**

TABLE IX

OF VEHICLE II, DESIGN II.3,

E CONSTANT VALUES OF THE LAG NETWORK

Angle of Attack α_{max} (deg)	Slosh Modes-Peak to Peak Amplitude			Normal Acceleration $\ddot{\zeta}_{max}$ Peak Amp. (meters/sec^2)	Damping Factor d (1/sec)	η_1	
	Z_{1PP} (meters)	Z_{2PP} (meters)	Z_{3PP} (meters)			Peak Amp. (meters)	Peak to Peak Osc. (meters)
+1.1	.143	.049	.157	+.028	+.009	Unstable	
+1.1	.122	.047	.157	+.028	-.0041	+.053	.088
+1.64	.208	.075	.239	+.055	-.0005	+.084	.140
+1.12	.129	.045	.152	+.025	-.003	+.053	.089
+1.16	.131	.049	.155	+.024	-.0206	+.056	.094
+1.16	.126	.049	.155	+.023	-.0115	+.055	.093
+1.2	.122	.049	.154	+.021	-.033	+.056	.091
+1.2	.122	.049	.152	+.019	-.029	+.057	.092
+1.2	.113	.052	.148	+.013	-.026	+.057	.097

Body Bending Modes

η_2		η_3		η_4	
Peak Amp. (meters)	Peak to Peak Osc. (meters)	Peak Amp. (meters)	Peak to Peak Osc. (meters)	Peak Amp. (meters)	Peak to Peak Osc. (meters)
- - -	.0028	- - -	.00150	- - -	.00017
-.0072	.0026	+.0023	.00154	+.00035	.00017
-.0106	.0042	+.0035	.00227	+.00045	.00017
-.0070	.0026	+.0023	.00230	+.00035	.00017
-.0073	.0028	+.0023	.00150	+.00035	.00017
-.0072	.0028	+.0023	.00150	+.00035	.00017
-.0073	.0028	+.0023	.00150	+.00035	.00017
-.0073	.0028	+.0024	.00140	+.00035	.00017
-.0070	.0028	+.0024	.00140	+.00035	.00017

DATE 1 September 1965

REVISED

REVISED

MCDONNELL
ST. LOUIS, MISSOURI

VEHICLE II, UNIT STEP INPUT

TABLE X

RESPONSE CHARACTERISTICS OF VI

WITH POLYNOMIAL FITTING IN THE ATTITUDE RA

Run No.	Computation Network Zero Variation		Polynomial Fitting of $\ddot{\tau}$ Feedback	
	Real σ	Imag. ω	Type Fitting	No. of Stored Samples M'
1*	5.5	9.2	A_o	25
2*	5.5	9.2	A_o	25
3*	4.8	8.8	A_o	25
4	6.0	8.0	A_o	25
5*	8.6	8.3	A_o	25
6*	6.9	8.2	A_o	25
7	8.6	6.4	A_o	25

Run No.	Slosh - Peak to Peak Amplitude			Normal Accelerat $\ddot{\tau}_m$ Peak Amp. (meters/s
	Z_{1PP} (meters)	Z_{2PP} (meters)	Z_{3PP} (meters)	
1*	.230	.0628	.246	+.064
2*	.180	.0768	.216	.066
3*	.178	.0663	.201	.066
4	.227	.127	.293	.092
5*	.1745	.0733	.216	-.066
6*	.181	.0785	.209	-.064
7	.183	.0942	.244	-.066

*Unstable run, values given apply to first 20 seconds

HICLE II, DESIGN II.1

TE AND THE ACCELERATION FEEDBACK

	Polynomial Fitting of $\dot{\phi}$ Feedback			Measured Attitude		Rigid Attitu
Gain $K_{\ddot{\tau}}$	Type Fitting	No. of Stored Samples M'	Gain $K\dot{\phi}$	$\dot{\phi}_{GP}$ Peak Amp. (deg)	T_G Peak Time (sec)	$\dot{\phi}_{CGM}$ Peak Amp. (deg)
.095	$A_o + A_1$	3	5.0	+1.7	6.0	+1.36
.095	$A_o + A_1$	5	5.0	+1.7	6.0	+1.4
.095	$A_o + A_1$	5	5.0	+1.8	6.25	+1.44
.095	$A_o + A_1$	5	5.0	+2.6	6.0	+1.94
.095	$A_o + A_1$	5	5.0	+1.8	6.0	+1.44
.095	$A_o + A_1$	5	5.0	+1.7	6.0	+1.28
.095	$A_o + A_1$	5	5.0	+1.9	6.0	+1.4

ion x. c^2)	Damping Factor d (1/sec)	Body Bending Modes η_1 Peak Amp. (meters)	η_1 Peak to Peak Osc. (meters)	η_2 Peak Amp. (meters)	η_2 Peak to Peak Osc. (meters)	Peak Amp. (meters)
	+.0747		.152		.00611	
	+.0251				.00558	
	+.0256				.00524	
	-.0192	+.14	.236	-.0157	.00698	+.00733
	+.0196				.00524	
	+.0171				.00611	
	-.0183	+.101	.171	+.0122	.00698	+.00524

Body e T_{CGM} Peak Time (sec)	Attitude Rate $\dot{\phi}_s$ $(\frac{deg}{sec})$	Engine Angle β_{max} (deg)	Angle of Attack α_{max} (deg)	
6.5	.0385	-.72	+1.66	
6.5	.04	+.81	+1.76	
7.5	.04	+.8	+1.74	
6.25	.0345	+1.06	+2.52	
7.0	.0303	+.8	+1.76	
6.25	.0417	+.79	+1.64	
6.5	.0435	+.8	+1.84	

η_3		η_4	
	Peak to Peak Osc. (meters)	Peak Amp. (meters)	Peak to Peak Osc. (meters)
			.000174
	.00227		.000174
	.00209		.000174
	.0030	+.000733	.000174
	.00244		.00035
	.00262		.000174
	.0030	+.000541	.000174

DATE 1 September 1965

REVISED

REVISED

MCDONNELL
ST. LOUIS, MISSOURI

VEHICLE II, UNIT STEP INPUT

TAI

RESPONSE CHARACTERISTICS

WITH POLYNOMIAL FITTING IN THE ATTIT

Run No.	Computation Network Zero Variation		K	Polynomial Fitting of $\ddot{\tau}$ Feedback	
	Real σ	Imag. ω		Type Fitting	No. of Stored Samples M′
1*	7.0	8.0	2.3	A_o	49
2	7.0	8.0	2.3	A_o	49
3	7.0	8.0	2.2	A_o	49
4	7.0	8.0	2.4	A_o	49
5*	7.0	7.7	2.4	A_o	49
6*	7.0	7.7	2.4	A_o	49
7*	7.0	7.7	2.4	A_o	49
8*	7.0	7.7	2.4	A_o	49
9*	7.0	7.7	2.4	A_o	49
10*	7.0	7.7	2.4	A_o	49
11*	7.0	7.7	2.4	A_o	49

Run No.	Slosh - Peak to Peak Amplitude			No Accel P A (mete
	Z_{1PP} (meters)	Z_{2PP} (meters)	Z_{3PP} (meters)	
1*	.0733	.0785	.127	+.
2	.089	.0471	.113	+.
3	.0907	.0436	.112	+.
4	.082	.0524	.120	+.
5*	.148	.0576	.173	+.
6*	.157	.0593	.180	+.
7*	.113	.0436	.127	+.
8*	.105	.0558	.143	+.
9*	.110	.0593	.126	+.
10*	.131	.0646	.126	+.
11*	.178	.0611	.143	+.

* unstable run, values given apply to first 20 seconds

LE XI

OF VEHICLE II, DESIGN II.2

UDE RATE AND THE ACCELERATION FEEDBACK.

	Polynomial Fitting of $\dot{\phi}$ Feedback			Measured Attitude		Rigid Attit
Gain $K_{\dot{T}}$	Type Fitting	No. of Stored Samples M'	Gain $K_{\dot{\phi}}$	ϕ_{GP} Peak Amp. (deg)	T_G Peak Time (sec)	ϕ_{CGM} Peak Amp. (deg)
.095	$A_o + A_1$	5	5.0	1.15	6.50	.76
.095	$A_o + A_1$	5	4.0	1.13	6.25	.89
.095	$A_o + A_1$	5	4.0	1.11	6.50	.89
.095	$A_o + A_1$	5	4.0	1.10	6.30	.85
.095	$A_o + A_1$	5	4.0	1.29	6.00	.89
.095	$A_o + A_1$	5	4.0	1.30	6.00	.88
.095	A_o	5	4.0	1.10	4.00	.80
.095	$A_o + A_1$	3	4.0	1.23	6.00	.90
.095	$A_o + A_1$	7	4.0	1.09	6.75	.83
.095	$A_o + A_1$	9	4.0	1.08	7.75	.89
.095	$A_o + A_1$	11	4.0	1.34	8.20	.97

rmal eration . max. eak mp. s/sec^2)	Damping Factor d (1/sec)	Body η_1 Peak Amp. (meters)	η_1 Peak to Peak Osc. (meters)	η_2 Peak Amp. (meters)	η_2 Peak to Peak Osc. (meters
.130	+.0408				.00349
.110	-.00418	-.0541	.096	-.00681	.00349
.150	-.00512	-.0489	.089	+.00611	.00297
.090	-.00740	.0576	.101	+.00698	.00366
.920	+.0278		.103		
.940	+.0263		.106		
.140	+.0779				.00436
.350	+.0766		.106		.00436
.010	+.0452		.105		.00401
.000	+.0617				.00349
.120	+.0246				.00366

Body ıde T_{CGM} Peak Time (sec)	Attitude Rate, $\dot{\phi}_s$ $(\frac{deg}{sec})$	State Attitude ϕ_s (deg)	Engine Angle β_{max} (deg)	Angle of Attack α_{max} (deg)
7.00	.03334		+.58	1.21
7.00	.050		+.46	1.11
7.25	.03334		+.41	1.10
7.00	.0570		+.50	1.10
7.00	.0250		-.45	1.29
6.75	.017		-.46	1.30
5.00		.80	+.75	1.19
7.00		.75	±.50	1.22
7.50	.017392		∓.49	1.13
7.50	.03334		+.62	1.14
8.00		.90	+.80	1.28

Bending Modes

)	η_3		η_4	
	Peak Amp. (meters)	Peak to Peak Osc. (meters)	Peak Amp. (meters)	Peak to Peak Osc. (meters)
)		.00192		.00017
)	-.00332	.00157	-.000349	.00017
	-.00297	.00157	-.000332	.00017
	-.00349	.00174	-.000366	.00017
		.00174		.00017
	-.00262	.00174	-.000332	.00017
		.00122		.00017
				.00017
				.00017
		.00140		.00017
		.00140		.00017

DATE 1 September 1965

REVISED

REVISED

MCDONNELL
ST. LOUIS, MISSOURI

VEHICLE II, UNIT STEP INPUT

TABLE XII

RESPONSE CHARACTERISTICS OF VEHICLE

FOR VARIATIONS IN THE SYSTEM GAINS

Run No.	Forward Loop System Gain K	Rate Feedback Gain $K\dot{\phi}$	Measured Attitude		Rigid Body Attitude		Att. rate $\dot{\phi}_S$ deg/sec	Engine angle β_{MAX} (deg)
			ϕ_{GP} peak amp. (deg)	T_G peak time (sec)	ϕ_{CGM} peak amp. (deg)	T_{CGM} peak time (sec)		
1*	1.8	5.0	+1.04	8.6	+.80	7.3	.029	±.120
2	2.0	5.0	+1.00	6.0	+.75	7.5	.025	.140
3	2.2	5.0	+1.02	6.3	+.75	7.5	.029	-.144
4	2.4	5.0	+1.11	6.0	+.82	7.5	.041	-.164
5	2.6	5.0	+1.20	6.2	+.80	7.5	.029	±.180
6*	2.6	3.5	+1.27	6.0	+1.05	7.3	.026	+.166
7	2.6	4.0	+1.20	6.0	+1.00	7.5	.029	-.156
8	2.6	6.0	+1.20	9.0	+.81	7.5	.033	+.166
9	2.6	7.5						

*Unstable run, values given apply to first 20 seconds.

II, DESIGN II.1,

K AND K $\dot{\phi}$

ngle of ttack MAX deg)	Slosh Peak to Peak Amplitude			Normal Acceleration $\ddot{r}_{max.}$ peak amp. (meters/sec^2)	Damping Factor d (1/sec)	η_1	
	Z_{1PP} (meters)	Z_{2PP} (meters)	Z_{3PP} (meters)			peak amp. (meters)	peak to peak osc. (meters)
-1.00	.181	.038	.181	-.1300	+.00605		
-1.01	.145	.042	.164	.1210	-.0176	-.0454	.0736
-1.03	.134	.049	.152	.1430	-.0272	-.0502	.0841
-1.12	.122	.052	.157	.1640	-.0453	-.0600	.102
-1.23	.122	.063	.174	.1550	-.0234	-.0698	.122
-1.27					-.0159		
-1.20	.162	.037	.174	.1230	-.0143	-.0457	.0663
-1.16	.124	.056	.164	.1420	+.0443	-.0698	.126
				Unstable	+.214		

Body Bending Modes

η_2		η_3		η_4	
peak amp. (meters)	peak to peak osc. (meters)	peak amp. (meters)	peak to peak osc. (meters)	peak amp. (meters)	peak to peak osc. (meters)
	.00021		.00077		.000052
.00524	.00021	-.0018	.00070	-.00023	.000052
.00541	.00021	-.0021	.00087	-.00024	.000035
-.00681	.0003	-.00239	.00091	.00035	.00007
-.00786	.00035	-.00279	.00105	-.00035	.000035
	.00028		.00077		.000035
.00541	.00026	-.00237	.00082	-.00031	.000035
-.00611	.0003	-.00244	.00087	-.00028	.000035

VEHICLE II, UNIT STEP INPUT

TABLE XIII

RESPONSE CHARACTERISTICS OF VEHICLE I

FOR VARIATIONS IN THE SYSTEM GAIN

Run No.	Forward Loop Gain K	Rate Feedback Gain $K_{\dot{\phi}}$	Measured Attitude		Rigid Body Attitude		Att. Rate $\dot{\phi}_s$ $(\frac{deg}{sec})$	Engine Angle β_{max} (deg)	Angle of Attack α_{max} (deg)
			ϕ_{GP} Peak Amp. (deg)	T_G Peak Time (sec)	ϕ_{CGM} Peak Amp. (deg)	T_{CGM} Peak Time (sec)			
1*	1.7	5.0	1.20	8.5	.90	9.0	.0098	-.30	1.08
2*	1.8	5.0	1.21	9.0	.88	8.5	.0444	-.32	1.10
3	2.0	5.0	1.19	9.0	.84	9.0	.05	-.36	1.12
4	2.2	5.0	1.19	9.0	.80	7.5	.04	-.4	1.2
5	2.4	5.0	1.21	6.5	.74	6.5	.0267	$\pm$.43	1.24
6*	2.5	5.0	1.21	6.5	.70	6.5	.0222	+.49	1.28
7*	2.6	5.0	1.24	6.5	.69	6.0		+.56	1.31
8*	2.2	3.0	1.39	6.5	1.11	7.0		-.47	1.39
9*	2.2	3.5	1.25	6.5	.98	7.0	.0588	+.41	1.24
10*	2.2	4.0	1.14	6.0	.84	7.5	.0476	-.38	1.14
11*	2.2	5.5	1.16	9.5	.70	8.5	.0444	+.40	1.16
12*	2.2	6.0	1.29	9.5	.65	9.0		-.52	1.30

*Unstable run, values given apply to first 20 seconds.

, DESIGN II.2,

K AND K $\dot{\phi}$

Slosh Modes - Peak to Peak Amplitude			Normal Acceler. $\ddot{\tau}$ Peak Amp. (meters /sec^2)	Damping Factor d (1/sec)	η_1	
Z_{1PP} (meters)	Z_{2PP} (meters)	Z_{3PP} (meters)			Peak Amp. (meters)	Peak to Peak Osc. (meters)
.166	.035	.174	+.1420	+.0130		
.157	.037	.154	+.1420	+.0029		
.143	.047	.134	+.1470	-.0157	-.052	.087
.131	.056	.164	+.1650	-.0288	-.063	.108
.126	.066	.183	+.1700	-.0222	-.073	.131
.122	.072	.190	+.1750	+.00499		
.122	.980	.192	+.1800	+.086		
.169	.052	.174	+.1420	+.0186		
.178	.044	.174	+.1450	+.0017	-.049	.077
.157	.044	.154	+.1410	-.00787	-.051	.0785
.126	.065	.17	+.1650	+.0182	-.0715	.131
.192	.089	.195	+.1770	+.109	UNSTAB	

Body Bending Modes

η_2		η_3		η_4	
Peak Amp. (meters)	Peak to Peak Osc. (meters)	Peak Amp. (meters)	Peak to Peak Osc. (meters)	Peak Amp. (meters)	Peak to Peak Osc. (meters)
	.0037		.00105		.00017
	.0040		.00105		.00017
+.0058	.0045	-.0023	.00122	-.00030	.00017
+.0066	.0056	-.0024	.00157	-.00035	.00017
-.0075	.0063	-.0026	.00174	-.00033	.00017
	.0070		.00188		.00017
	.0073		.00205		.00017
	.0035		.00087		.00017
$\pm$.0059	.0044	-.0024	.00113	-.00031	.00017
.0063	.0049	-.0024	.00105	-.0003	.00017
$\pm$.0065	.0063	-.0025	.00174	-.00031	.00017
LE			UNSTABLE		

DATE 1 September 1965

REVISED

REVISED

MCDONNELL
ST. LOUIS, MISSOURI

VEHICLE II, UNIT STEP INPUT

TABLE XIV

RESPONSE CHARACGERISTICS OF VI

FOR VARIATIONS IN THE SYSTE

Run No.	Forward Loop Gain K	Rate Feedback Gain $K_{\dot{\phi}}$	Measured Attitude		Rigid Body Attitude		Att. rate $\dot{\phi}_S$ deg/sec	Engine angle β_{MAX}, (deg)
			ϕ_{GP} peak amp. (deg)	T_G peak time (sec)	CGM peak amp. (deg)	T_{CGM} peak time (sec)		
1	1.8	5	1.20*	8.5	.94	8.5	.019	-.315
2	2.0	5	1.15	9.5	.86	8.0	.026	-.35
3	2.2	5	1.13	8.6	.80	8.75	.027	-.40
4	2.4	5	1.16	6.2	.84	8.5	.027	-.415
5	2.6	5	1.21	6.1	.80	9.0	.028	-.45
6	2.7	5*	1.28	6.1	.80	8.75	.017	+.51
7	2.8	5			U N S T A B L E			
8*	2.2	4.0	1.20	6.0	1.00	7.0	.019	-.3975
9*	2.2	4.5	1.13	8.6	.85	7.0	.021	-.395
10	2.2	5.5	1.17	8.9	.82	8.5	.019	-.3975
11*	2.2	6.0	1.25	9.0	.76	8.5	.0133	+.45

*Unstable run, values given apply to first 20 seconds.

EHICLE II, DESIGN II-3

I GAINS K AND K $\dot{\varphi}$

Angle of attack α_{MAX} (deg)	Slosh Peak to Peak Amplitude			Normal Acceleration $\ddot{r}$ peak amp. (meters /sec^2)	Damping Factor d (1/sec)	η_1	
	Z_{1PP} (meters)	Z_{2PP} (meters)	Z_{3PP} (meters)			peak amp. (meters)	peak to peak osc. (meters)
+1.06	.157	.0366	.150	.030	+.00915	-.0454	.0375
+1.10	.141	.042	.141	.030	-.00464	-.0482	.038
+1.10	.124	.052	.157	.010	-.01065	-.0548	.045
+1.20	.122	.054	.159	.011	-.0192	-.0628	.054
+1.27	.122	.070	.174	.030	-.00324	-.0736	.065
-1.32	.122	.077	.187	.030	+.0159		
	.122	.089	.195	.030	-.0664		
+1.20	.157	.0419	.154	.030	+.0292		
+1.12	.14	.038	.147	.030	-.00794	-.0607	.053
+1.11	.126	.054	.157	.029	-.014		
-1.21	.127	.066	.174	.030	+.0226		

Body Bending Modes					
η_2		η_3		η_4	
peak amp. meters)	peak to peak osc. (meters)	peak amp. (meters)	peak to peak osc. (meters)	peak amp. (meters)	peak to peak osc. (meters)
.0052	.0026	-.0021	.00087	-.00019	.000035
.0054	.0024	-.0021	.00087	-.00033	.00007
-.0059	.0028	-.0024	.00104	-.0003	.000052
-.0070	.003	-.0027	.00094	-.00035	.00007
-.0084	.0037	-.0029	.00112	-.00035	.00007
	.0073		.00206		.00007
	.0028		.00087		.00007
	.003		.00080		.000035
-.061	.0035	-.0024	.00092	-.0003	.000052

TABLE XV

VEHICLE II, WIND INPUT
DESIGN II.2
$K\dot{\tau} = .095$
System Gain K = 2.4

RESPONSE CHARACTERISTICS OF VE

FOR VARIATIONS IN THE COMMAND

Run No.	Command Compensation Network	Measured Attitude ϕ_G at 2 sec. (deg)	Measured Attitude ϕ_G at 15.5 sec. (deg)	
1	$\frac{1 + 10s}{1 + 50s}$	+.20	- 2.00	
2	$\frac{1 + 20s}{1 + 100s}$	+.20	-1.60	
3	$\frac{1 + 40s}{1 + 200s}$	+.30	-1.00	
4	$\frac{1 + 2s}{1 + 10s}$	+.10	- 2.00	

HICLE II, DESIGN II.2

COMPENSATION NETWORK

	Engine Deflection			Measured Angle of Attack		
ϕ_{GP} peak amp. (deg)	β at 2 sec. (deg)	$\beta_{max.}$ peak amp. (deg)	β_{MR} Rebound amp. (deg)	$\alpha_{max.}$ peak amp. (deg)	α_{MR} Rebound amp. (deg)	η_{1P} peak amp. (mete
9.02	+.36	+1.28	-.12	+10.6	+2.04	.16
8.80	+.32	+1.26	-.10	+11.0	+2.24	.16
8.00	+.32	+1.30	-.10	+11.0	+2.60	.16
8.30	+.42	+1.40	0	+10.8	+3.00	.18

Normalized Bending Mode Deflections

t rs)	η_{2P} peak amp. (meters)	η_{3P} peak amp. (meters)	η_{4P} peak amp. (meters)	η_{1PP} peak amp. (meters)
3	.098	.034	.0141	.00171
3	.094	.034	.0140	.00171
8	.088	.033	.0142	.00171
6	.131	.036	.0159	.00178

DATE 1 September 1965

REVISED

REVISED

MCDONNELL
ST. LOUIS, MISSOURI

VEHICLE II, UNIT STEP INPUT

TABLE XVI

RESPONSE CHARACTERISTICS OF VEHICLE II, I

FOR VARIATIONS OF THE AERODYNAMIC AND ENGINE MO

Run No.	C_1 Aero. Moment Coeff.	C_2 Engine Moment Coeff.	Measured Attitude		Rigid Body Attitude		Att. Rate $\dot{\phi}_s$ ($\frac{deg}{sec}$)	Engine Angle β_{max} (deg)
			ϕ_{GP} Peak Amp. (deg)	T_G Peak Time (sec)	ϕ_{CGM} Peak Amp. (deg)	T_{CGM} Peak Time (sec)		
1	Nom.	Nom.	1.04	6.25	.75	7.5	.0385	-.36
2	Nom.	-20%	1.1	6.00	.80	7.5	.0198	+.44
3	Nom.	+20%	1.55	6.20	.97	6.5	.0147	+.54
4	-20%	Nom.	1.10	6.15	.80	8.0	.0323	-.38
5	+20%	Nom.	1.08	6.20	.78	7.4	.0328	+.38

165-1

ESIGN II.1,

MENT COEFFICIENTS

Angle of Attack α_{max} (deg)	Slosh Modes - Peak Peak Amplitude			Normal Acceler. $\ddot{\tau}$ Peak Amp. (meters /sec^2)	Damping Factor d (1/sec)	η_h	
	Z_{1PP} (meters)	Z_{2PP} (meters)	Z_{2PP} (meters)			Peak Amp. (meters)	Peak to Peak Osc. (meters)
1.00	.1134	.0419	.1414	+.2548	-.029	-.0506	.0838
1.08	.1291	.0401	.1309	+.2618	-.039	-.0524	.0803
1.56	.1745	.0803	.2426	+.3979	-.039	-.0925	.1640
1.06	.1222	.0436	.1431	+.3438	-.031	-.0541	.0897
1.04	.1204	.0401	.1414	+.3386	-.036	-.0551	.0873

Body Bending Modes					
η_2		η_3		η_4	
Peak Amp. (meters)	Peak to Peak Osc. (meters)	Peak Amp. (meters)	Peak to Peak Osc. (meters)	Peak Amp. (meters)	Peak to Peak Osc. (meters)
.0061	.0052	-.0022	.0014	.00026	.00017
.0070	.0052	-.0027	.0010	.00026	.00017
.0092	.0079	-.0034	.0023	.00037	.00017
.0061	.0049	-.0022	.0012	-.00031	.00017
.0061	.0047	-.0025	.0013	-.00031	.00017

DATE 1 September 1965

REVISED

REVISED

MCDONNELL
ST. LOUIS, MISSOURI

VEHICLE II, UNIT STEP INPUT
DESIGN II.1
System Gain, K = 2.2
2.5 SPS, 25 Stored Samples

TAI

STEP RESPONSE CHARACTERIST

FOR VARIATION OF THE

Run No.	No. of Stored Samples M	Percent Change in Bending Frequency ω_1	ω_2	ω_3	Measured Attitude ϕ_{GP} Peak Amp. (deg)	Measured Attitude T_{GP} Peak Time (sec)	Rigid Body Attitude ϕ_{CGM} Peak Amp. (deg)	Rigid Body Attitude T_{CGM} Peak Time (sec)	Att Rate $\dot{\phi}_s$ ($\frac{deg}{sec}$)	Engi Ang β_{ma} Pe Am (de
1	25	+5%	+5%	+5%						
2	25	-5%	-5%	-5%	1.14	6.50	.80	7.0	.025	-.
3*	23				1.05	1.20	.70	6.8	.02	-.
4	27				1.16	6.5	.83	8.0	.0123	-.
5	29				1.12	6.7	.79	7.0	.0385	-.
6*	25	-10%	0	0	-1.2	7	+.83	7.2	.018	-.
7	25	+10%	0	0						
8	29	+10%	0	0						
9	33	+10%	0	0						
10	41	+10%	0	0						
11*	25	-10%	0	0	-1.15	7	+.8	8.5	.017	+.
12	29	-10%	0	0	-1.14	7	+.76	7.5	.016	+.
13	25	0	+10%	0	-1.12	9	+.81	9	.020	+.
14	25	0	-10%	0	-1.18	9	-.82	9	.020	-.
15	25	0	-10%	+10%	-1.1	6.25	+.75	6.5	.021	+.
16	25	0	-10%	-10%	-1.18	8.25	+.84	9	.018	-.
17*	25	-10%	-10%	-10%	-1.22	7	+.82	7.5		+.
18*	27	-10%	-10%	-10%	-1.24	6.75	+.85	7.5	.020	+.
19*	29	-10%	-10%	-10%	-1.18	6.75	+.78	7.5	.017	+.
20*	25	-10%	10%	-10%	-1.08	3.75	+.75	7.5	.017	-.
21*	27	-10%	10%	-10%	-1.08	6.75	+.78	7.5	.024	-.
22*	31	-10%	10%	-10%	-1.16	7	+.84	7.5	.017	-.

*Unstable run, values given apply to first 20 seco

160-1

LE XVII

ICS FOR VEHICLE II, DESIGN II.1

BENDING MODE FREQUENCIES

ne le x. ak). g)	Angle of Attack $\alpha_{max.}$ (deg)	Slosh Modes - Peak to Peak Amplitude Z_{1PP} (meters)	Z_{2PP} (meters)	Z_{3PP} (meters)	Normal Acceler. $\ddot{\tau}_{max.}$ Peak Amp. (meters /sec^2)	Damping Factor d (1/sec)	η_1 Peak Amp. (meters)	η_1 Peak to Peak Osc (mete
						+.094		
39	1.08	.087	.041	.118	-.18	-.011	-.057	.0988
39	.97	.0873	.0414	.1187	-.18	+.005		
38	1.10	.0785	.0414	.1169	-.18	-.0166	-.056	.096
39	1.06	.0838	.0419	.1169	-.18	-.006	-.058	.0987
41	+1.1	.0838	.0419	.0960	-.12	+.0217	UNSTABLE	
					-.28	+.0183	UNSTABLE	
					-.27	+.018	UNSTABLE	
					-.28	+.018	UNSTABLE	
					-.27	+.0178	UNSTABLE	
39	-1.1	.0768	.0384	.0908	-.11	+.0141	UNSTABLE	
4	+1.04	.0768	.0384	.0908	-.11	-.0179	-.062	.104
37	-1.06	.1396	.0384	.1449	+.12	-.0301	-.048	.080
41	+1.16	.1571	.0524	.1745	-.13	-.0116	- - -	.0994
39	+1.04	.1431	.0436	.1571	-.15	-.0228	-.053	.090
39	+1.16	.1396	.0436	.1571	-.15	-.0228	-.052	.087
4	+1.2	.0750	.0436	.0942	-.12	+.0276	UNSTABLE	
41	+1.24	.0838	.0471	.0942	-.12	-.013	UNSTABLE	
4	+1.14	.0838	.0471	.0942	-.12	-.0691	- - -	.109
38	+1.04	.0733	.0384	.0908	-.11	+.00284	UNSTABLE	
4	+1.04	.0768	.0366	.0873	-.10	-.0196	-.061	.104
41	+1.1	.0785	.0366	.090	-.11	-.00893	-.061	.104

nds.

Body Bending Modes						
	η_2		η_3		η_4	
k k . rs)	Peak Amp. (meters)	Peak to Peak Osc. (meters)	Peak Amp. (meters)	Peak to Peak Osc. (meters)	Peak Amp. (meters)	Peak to Peak Osc. (meters)
		.0045		.0012		.00017
	.0073	.0059	-.0026	.0015	-.00026	.00017
		.0062		.0015		.00017
	.0073	.0057	-.0025	.0016	-.00026	.00017
	.00750	.0059	-.0027	.0015	-.00030	.00017
	- - -	.0047	- - -	.0012	- - -	.00017
	- - -	.0052	- - -	.0014	- - -	.00017
	- - -	.0048	- - -	.0013	- - -	.00019
	- - -	.0050	- - -	.0014	- - -	.00017
	- - -	.0052	- - -	.0013	- - -	.00017
	- - -	.0048	- - -	.0012	- - -	.00017
	.0067	.0048	-.0026	.0013	-.00035	.00017
	.0055	.0031	+.0022	.0010	-.00031	.00017
	UNSTABLE		- - -	.0016	- - -	.00017
	.0069	.0052	+.0019	.0010	-.00031	.00017
	.0069	.0045	-.0028	.0014	-.0003	.00017
	- - -	.0078	- - -	.00202	- - -	.00017
	- - -	.0076	- - -	.0019	- - -	.00017
	UNSTABLE		- - -	.0019	- - -	.00017
	- - -	.0029	- - -	.00094	- - -	.00017
	.0052	.0027	-.0030	.00087	-.00035	.00017
	.0055	.0027	-.0030	.00087	-.00035	.00017

DATE 1 September 1965

REVISED

REVISED

MCDONNELL
ST. LOUIS, MISSOURI

VEHICLE II, UNIT STEP INPUT

TABLE XVIII

STEP RESPONSE CHARACTERISTICS FOR VEHICLE II

FOR VARIATIONS OF THE BODY BENDING MODE

Run No.	No. of Stored Samples M	Percent Change in Bending Frequency			Measured Attitude		Rigid Body Attitude		Att Rate	Engi Ang
		ω_1	ω_2	ω_3	ϕ_{GP} Peak Amp. (deg)	T_{GP} Peak Time (sec)	ϕ_{CGM} Peak Amp. (deg)	T_{CGM} Peak Time (sec)	$\dot{\phi}_s$ ($\frac{deg}{sec}$)	β_{ma} Pea Amp (deg
1*	25	-5%	-5%	-5%	1.17	6.5	.74	7.0	.0220	-.
2*	29	-5%	-5%	-5%	1.24	6.5	.80	6.5	.02857	+.
3	25	-5%	-5%	-5%						
4	29	-5%	-5%	-5%						
5	25	+5%	0	0						
6*	25	-5%	0	0	1.18	6.5	.80	7.0	.0263	+.
7	27	-5%	0	0	1.17	6.5	.78	7.0	.0323	+.
8*	29	-5%	0	0	1.10	7.0	.74	6.5		+.

*Unstable run, values given apply to first 20 sec

, DESIGN II.2

'REQUENCIES

ne le x. k .)	Angle of Attack $\alpha_{max.}$ (deg)	Slosh Modes - Peak to Peak Amplitude			Normal Acceler. $\ddot{\tau}_{max.}$ Peak Amp. (meters/sec^2)	Damping Factor d (1/sec)	η_1	
		Z_{1PP} (meters)	Z_{2PP} (meters)	Z_{3PP} (meters)			Peak Amp. (meters)	Pea to Pea Osc (mete
1	1.10	.091	.052	.127	.1500	+.0188	UNSTABLE	
2	1.22	.110	.054	.131	.1600	+.037	UNSTABLE	
						+.1025	UNSTABLE	
						+.0985	UNSTABLE	
						+.0827	UNSTABLE	
3	1.18	.089	.045	.124	.1400	+.0213	UNSTABLE	
4	1.18	.089	.049	.127	.1420	-.04	-.066	.1
2	1.08	.087	.044	.124	.1400	+.016	UNSTABLE	

nds.

Body Bending Modes						
	η_2		η_3		η_4	
k k . rs)	Peak Amp. (meters)	Peak to Peak Osc. (meters)	Peak Amp. (meters)	Peak to Peak Osc. (meters)	Peak Amp. (meters)	Peak to Peak Osc. (meters)
	- - -	.0073	- - -	.0019	- - -	.00017
	- - -	.0077	- - -	.0019	- - -	.00017
	- - -	.0049	- - -	.0014	- - -	.00017
	- - -	.0044	- - -	.0012	- - -	.00017
	- - -	.0058	- - -	.0016	- - -	.00017
	- - -	.0056	- - -	.0016	- - -	.00017
8	+.0070	.0061	-.0030	.0016	-.00031	.00017
	- - -	.0065	- - -	.0015	- - -	.00017

DATE 1 September 1965

REVISED

REVISED

MCDONNELL
ST. LOUIS, MISSOURI

VEHICLE II, UNIT STEP INPUT

TABLE XIX

STEP RESPONSE CHARACTERISTICS FOR VEHICLE

FOR VARIATIONS OF THE BODY BENDING MO

Run No.	Percent Change in Bending Frequency ω_1 ω_2 ω_3	Measured Attitude		Rigid Body Attitude		Att Rate	Engi Ang
		ϕ_{GP} Peak Amp. (deg)	T_{GP} Peak Time (sec)	ϕ_{CGM} Peak Amp. (deg)	T_{CGM} Peak Time (sec)	$\dot{\phi}_s$ $(\frac{deg}{sec})$	β_{ma} Pea Amp (deg
1	-5% 0 0	1.05	6.5	.78	9.0		.3
2	-5% 0 0	1.02	6.5	.79	9.0	.025	±.3
3	-10% 0 0	1.14	6.8	.82	7.5	.0256	.4
4*	-10% -10% -10%	1.20	6.8	.80	7.5	.02	±.4
5	-5% -5% -5%	1.12	6.5	.80	7.5	.037	-.3
6*	+5% +5% +5%						
7*	-5% -5% -5%	1.17	6.2	.80	6.9	.04	-4.1
8	-5% Nominal	1.50	16.0	1.10	10.0		4.6
9	Nominal	1.16	8.8	.83	11.0	.0244	3.7

*Unstable run, values given apply to first 20 secon

II, DESIGN II.3,

E FREQUENCY

ne le x. k .)	Angle of Attack $\alpha_{max.}$ (deg)	Slosh Modes - Peak to Peak Amplitude Z_{1PP} (meters)	Z_{2PP} (meters)	Z_{3PP} (meters)	Normal Acceler. $\ddot{\tau}_{max.}$ Peak Amp. (meters /sec^2)	Damping Factor d (1/sec)	η_1 Peak Amp. (meters)	Peak to Peak Osc. (mete
	1.04	.079	.035	.106	+.024	-.0311	-.052	.089
	1.00	.080	.037	.112	+.021	-.0274	-.052	.089
)	1.00	.061	.035	.096	+.03	-.00507	-.068	.110
)	1.14	.079	.040	.091	+.029	+.00739	UNSTABLE	
)	1.08	.084	.040	.117	+.022	-.0111	- - -	.094
						+.0868	UNSTABLE	
	1.12	.092	.049	.127	+.028	-.0186	- - -	.095
	1.30	.079	.044	.119	+.028	-.0285	-.058	.090
	1.10	.122	.044	.157	+.05	-.0147	-.058	.094

ds.

	Body Bending Modes					
	η_2		η_3		η_4	
s)	Peak Amp. (meters)	Peak to Peak Osc. (meters)	Peak Amp. (meters)	Peak to Peak Osc. (meters)	Peak Amp. (meters)	Peak to Peak Osc. (meters)
9	+.0061	.0052	-.0026	.0013	-.00031	.00017
9	-.0061	.0049	-.0026	.0014	-.00033	.00017
0	-.0073	.0052	-.0028	.0014	-.00033	.00017
	- - -	.0087	- - -	.0021	- - -	.00017
+	UNSTABLE		- - -	.0017	- - -	.00017
	- - -	.0045	- - -	.0012	- - -	.00017
9	UNSTABLE		- - -	.0017	- - -	.00017
6	+.0066	.0054	+.0031	.0014	-.00031	.00017
+	-.0066	.0056	-.0024	.0014	+.00044	.00017

DATE 1 September 1965

REVISED

REVISED

MCDONNELL
ST. LOUIS, MISSOURI

VEHICLE II, WIND INPUT
DESIGN II.2
2.5 SPS K = 2.2
Number os Samples stored 25

TABLE

RESPONSE CHARACTERISTICS

FOR VARIATIONS IN THE

Run No.	Frequency of Wind Oscillation W_α (2° amplitude)	2 Deg. Step of Wind on Profile	Body Bending	Slosh
1	0	out	in	in
2	1.0	out	in	in
3	2.0	out	in	in
4	3.0	out	in	in
5	5.0	out	in	in
6	9.0	out	in	in
7	0	in	in	in
8	0	in	out	out
9	0	out	out	out
10	1.0	out	out	out
11	.5	out	out	out
12	2.0	out	out	out

169-1

XX

OF VEHICLE II, DESIGN II.2,

WIND DISTURBANCE INPUT

Measured Attitude			Engine Deflection			Meas Angl At
ϕ_G at 2 sec. (deg)	ϕ_G at 15.5 sec. (deg)	ϕ_{GP} peak amp. (deg)	β at 2 sec. (deg)	$\beta_{max.}$ peak amp. (deg)	β_{MR} Rebound amp. (deg)	$\alpha_{max.}$ peak amp. (deg)
+0.4	-1.8	-9.2	+.7	+2.66	-3.6	+11.6
+0.3	-1.8	-9.2	+.74	+2.78	-5.8	+11.7
+0.4	-1.6	-8.96	+.78	+2.78	-4.8	+11.7
+0.3	-1.48	-8.92	+.76	+2.70	-3.7	+11.8
+0.4	-1.8	-9.08	+.77	+2.62	-3.0	+11.8
+0.2	-1.48	-8.84	+.74	+2.6	-3.4	+12.0
+0.3	-1.6	-7.72	+.76	+2.5	-3.8	+10.8
+0.2	-2.2	-7.2	+.7	+2.12	-3.0	+9.6
+0.16	-2.0	-8.8	+.67	+2.24	-2.8	+10.1
+0.14	-2.2	-9.16	+.65	+2.4	-5.4	+10.6
+0.2	-2.2	-9.16	+.70	+2.30	-5.8	+10.2
+0.2	-2.0	-8.6	+.70	+2.34	-2.2	+10.8

ured e of ack	Normalized Bending Mode Deflections				
α_{MR} Rebound amp. (deg)	η_{1P} peak amp. (meters)	η_{2P} peak amp. (meters)	η_{3P} peak amp. (meters)	η_{4P} peak amp. (meters)	η_{1PP} peak amp. (meters)
+2.2	.073	.033	.0140	.0140	.0384
+1.48	.081	.035	.0150	.0168	.0454
+2.0	.086	.035	.0147	.0157	.1065
+1.12	.082	.035	.0143	.0157	.0838
+1.56	.079	.034	.0140	.0140	.0977
+1.2	.077	.034	.0143	.0154	.0558
+1.4	.075	.031	.0136	.0140	.0733
+1.8					
+2.36					
+1.4					
+1.28					
+1.6					

TABLE XXI

RESPONSE CHARACTERISTICS OF THE DIGITAL ADAPTIVE FILTER WITH VEHICLE I AT THE LIFT-OFF FLIGHT CONDITION, α AND β PARAMETER VARIATIONS

IDENTIFICATION			REDUCED DATA						
RUN NO.	α	β	m %	T_R SEC.	T_P SEC.	$T_h(\pm 25\%)$ SEC.	$T_h(50\%)$ SEC.	S DEG/SEC.	β_R DEG.
1	1.2	2.0	+41	2.1	3.3	5.1	22.6	-. 20	+ .83
2	1.2	2.2	+27	2.3	3.2	3.4	8.3	-.143	+ .84
3	1.5	2.0	-	2.3	4.6	-	5.9	+.111	+ .83
4	1.5	2.2	+24	2.4	3.3	14.1	1.7	-.179	+ .80
5	1.8	2.4	+ 4	2.8	3.2	5.4	8.5	-.111	+ .74
6	2.0	2.2	+16	2.7	4.6	25% > 19 SEC.	-	0	+ .73

TABLE XXII

RESPONSE CHARACTERISTICS WITH VEHICLE I AT THE MAXIMUM q FLIGHT CONDITION, α AND β PARAMETER VARIATIONS

IDENTIFICATION			REDUCED DATA						
RUN NO.	α	β	m %	T_R SEC.	T_P SEC.	$T_h(\pm 25\%)$ SEC.	$T_h(50\%)$ SEC.	S DEG/SEC.	β_R DEG.
1	1.5	3.2	-10	-	2.0	3.0	3.4	-.417	+1.06
2	1.5	3.5	-21	-	1.9	2.2	2.7	-.333	+1.2
3	1.8	2.4	-	1.9	-	2.3	2.6	+.476	- .8
4	1.8	2.8	+33	2.0	3.32	-	4.0	+.435	+ .79
5	1.8	3.2	-16	-	1.95	3.0	3.6	-.370	+ .99
6	2.0	2.4	-	2.0	-	2.4	2.8	+.476	- .8
7	2.0	2.8	+23	2.3	3.0	3.6	4.1	+.435	- .76
8	2.0	3.0	+ 2	2.8	3.0	6.8	7.1	+.333	+ .83
9	2.0	3.2	-19	-	1.9	3.0	3.8	-.333	+ .90
10	2.2	2.8	+19	2.4	3.2	3.7	4.1	+.417	- .77
11	2.2	3.0	- 3	-	2.9	4.8	5.6	+.192	+ .8
12	2.2	3.2	-22	-	2.0	2.2	3.8	-.104	- .85
13	2.5	3.5	-37	-	1.9	-	2.2	-.400	+ .9

TABLE XXIII

RESPONSE CHARACTERISTICS OF THE DIGITAL ADAPTIVE FILTER WITH VEHICLE I AT THE LIFT-OFF FLIGHT CONDITION, SAMPLE RATE AND MEMORY SIZE VARIATION, $\alpha = 1.8$, $\beta = 2.2$

IDENTIFICATION			REDUCED DATA						
RUN NO.	MEMORY CORE SIZE	SAMPLE RATE m	m %	T_R SEC.	T_P SEC.	$T_h(\pm 25\%)$ SEC.	$T_h(50\%)$ SEC.	S DEG/SEC	β_R DEG.
1	20	10	+29	2.4	3.4	3.7	50% > 23.2 SEC.	-.133	+ .78
2	30	5	+25	2.4	4.7	6.9	50% > 19.4 SEC.	+.0526	+ .90
3	30	10	+22	2.5	4.4	25% > 1.99 SEC.		0	+ .79
4	50	10	+21	2.5	3.3	9.6	16	+.0476	+ .80
5	60	10	+ 9	2.9	4.4	12.4	50% > 22.8 SEC.	+.0217	+ .62
6	70	10	+19	2.5	4.5	25% > 22.2 SEC.		0	+ .75

TABLE XXIV

RESPONSE CHARACTERISTICS OF THE DIGITAL ADAPTIVE FILTER AT THE LIFT-OFF FLIGHT CONDITION, COMPENSATION NETWORK VARIATION, $\alpha = 1.8$, $\beta = 2.2$

IDENTIFICATION		REDUCED DATA						
RUN NO.	COMPENSATION NETWORK	m %	T_R SEC.	T_P SEC.	$T_h(\pm 25\%)$ SEC.	$T_h(50\%)$ SEC.	S DEG/SEC.	θ_R DEG.
1	$\frac{(S+1)^2 + 10^2}{(S+16)^2}$	+20	2.5	4.6	12.5	50% > 25.8	-.025	+ .79
2	$\frac{(S+1)^2 + 16^2}{(S+16)^2}$	+25	2.3	4.4	6.8	15.2	+.0426	+ .80
3	$\frac{(S+1)^2 + 12^2}{(S+16)^2}$	21	2.5	3.3	9.6	16.	.0476	+ . 8

APPENDIX A

VEHICLE REPRESENTATION AND DATA

This appendix summarizes the data used in the digital filter simulation studies. Included are the rigid body, elastic airframe, and sloshing propellant data for the two study vehicles. Also included are the equations of motion used in the analysis together with a matrix representation of the equations and the numerical values of the vehicle coefficients. Additional data defines the engine transfer function and three wind profiles used in the analog computer analysis.

The data is tabulated for both study vehicles for each of the three flight times investigated. The times studied correspond to three distinct flight regimes along the booster vehicle trajectory; they are lift-off (t = 0), maximum dynamic pressure (t = 80 sec.), and the first stage burn-out (t = 156 sec. for vehicle I and t = 157 sec. for vehicle II).

A.1 Basic Data

The data used for calculation of the study vehicle coefficients were obtained from Reference 4 and are tabulated in Tables (A.1) and (A.10) for vehicles I and II respectively for the three flight times investigated, lift-off, maximum dynamic pressure (max q), and stage 1 burn-out. The normalized bending deflections and slopes as a function of body station, also obtained from Reference 4 , are tabulated in Tables (A.2) through (A.4) and (A.11) through (A.13) for vehicles I and II respectively. In these tables $Y_i(x)$ is defined as the bending deflection of the i^{th} mode at station x and $Y_i'(x)$ is the i^{th} mode bending slope at station x. The same source provided bending mode mass and frequency data as a function of flight time. These data are tabulated in Tables (A.5) and (A.14) for vehicles I and II. Sloshing propellant data from Reference 4 are tabulated in Tables (A.6) and (A.15) for vehicles 1 and 2 respectively.

A.2 Computed Bending Data

The bending deflection and slope values used in this study are tabulated in Tables (A.7) through (A.9) and (A.16) through (A.18) for vehicles I and II respectively. In addition the tables show the station location of the feedback sensors used in the study.

A.3 Equations of Motion

The pitch axis response of the study vehicles using the body fixed coordinate system of Figures (A.1) and (A.2) can be described by the following equations of motion:

Moment Equation

$$\ddot{\varphi}_{cg} = -C_1\alpha - C_2\beta_R + \ddot{\varphi}_B + \ddot{\varphi}_S + \ddot{\varphi}_E \tag{A.1}$$

where

$$\ddot{\varphi}_B = \frac{F\ell_{cg}}{I_{xx}} \sum_i^4 Y_i'(x_\beta)\,\eta_i - \frac{F}{I_{xx}} \sum_i^4 Y_i(x_\beta)\,\eta_i \tag{A.1a}$$

$$\ddot{\varphi}_S = \frac{1}{I_{xx}} \sum_j^3 \left[\ell_{sj}\ddot{Z}_{sj} + \left(\frac{F-X}{m}\right) Z_{sj}\right] m_{sj} \tag{A.1b}$$

$$\ddot{\varphi}_E = -\left[\frac{\ell_{cg}}{I_{xx}} S_E + \frac{I_E}{I_{xx}}\right]\ddot{\beta}_R - \left(\frac{F-X}{m}\right)\frac{S_E}{I_{xx}}\beta_R \tag{A.1c}$$

Normal Force Equation

$$\ddot{Z} = \ddot{Z}_R + \ddot{Z}_B + \ddot{Z}_S \tag{A.2}$$

where

$$\ddot{Z}_R = \left(\frac{F-X}{m}\right)\varphi_{cg} + \frac{R'}{m}\beta_R + \frac{N'}{m}\alpha \tag{A.2a}$$

$$\ddot{Z}_B = -\sum_i^4 \frac{F}{m} Y_i'(x_\beta)\,\eta_i \tag{A.2b}$$

$$\ddot{Z}_S = -\sum_j^3 \frac{m_{sj}\ddot{Z}_{sj}}{m} \tag{A.2c}$$

Angular Equation

$$\alpha = \alpha_w + \varphi_{cg} - \theta \tag{A.3}$$

where

$$\Theta = \frac{\ddot{Z}_m}{F-X} \qquad \text{(Lift-off)} \qquad \text{(A.3a)}$$

$$\Theta = \frac{\dot{Z}}{V} \qquad \text{(Max-Q and Burn-out)} \qquad \text{(A.3b)}$$

Bending Equation

$$\ddot{\eta}_i + 2\zeta_i\omega_i\dot{\eta}_i + \omega_i^2\eta_i = \frac{R'}{M_i} Y_i(x_\beta)\beta_R \qquad \text{(A.4 - A.7)}$$

$$+ \frac{S_E Y_i(x_\beta) + I_E Y_i'(x_\beta)}{M_i} \ddot{\beta}_R + \frac{1}{M_i} \sum_j^3 m_{sj}\left[\ddot{Z}_{sj}Y_i(x_{sj}) + \frac{(F-X)}{m} Y_i'(x_{sj})Z_{sj}\right]$$

$$+ \frac{Q\alpha}{M_i}\alpha \qquad i = 1,2,3,4$$

Slosh Equation

$$\ddot{Z}_{sj} + 2\xi_{sj}\omega_{sj}\dot{Z}_{sj} + \omega_{sj}^2 Z_{sj} = \ell_{sj}\ddot{\varphi}_{cg} - \ddot{Z} \qquad \text{(A.8 - A.10)}$$

$$+ \left(\frac{F-X}{m}\right)\varphi_{cg} - \sum_i^4 \left[Y_i(x_{sj})\ddot{\eta}_i + \left(\frac{F-X}{m}\right) Y_i'(x_{sj})\eta_i\right]$$

$$j = 1,2,3$$

Control Sensor Equations

$$\varphi_G = \varphi_{cg} - \sum_i^4 Y_i'(x_\varphi)\eta_i \qquad \text{(A.11)}$$

$$\dot{\varphi}_G = \dot{\varphi}_{cg} - \sum_i^4 Y_i'(x_\varphi)\dot{\eta}_i \qquad \text{(A.12)}$$

$$\ddot{\tau} = \frac{R'}{m}\beta_R + \frac{N'}{m}\alpha - \ell_A\ddot{\varphi}_{cg} + \sum_i^4 Y_i(x_{\ddot{\tau}})\ddot{\eta}_i \qquad \text{(A.13)}$$

$$- \sum_i^4 \frac{F}{m} Y_i'(x_\beta)\eta_i - \sum_j^3 \frac{m_{sj}\ddot{Z}_{sj}}{m}$$

$$\alpha_T = \alpha - \sum_i^4 Y_i'(x_\alpha)\eta_i - \frac{1}{V}\sum_i^4 Y_i(x_\alpha)\dot{\eta}_i + \frac{\dot{\varphi}_{cg}\ell_\alpha}{V} \qquad \text{(A.14)}$$

(Equations A.13 and A.14 are written for ℓ_A and ℓ_α negative at the maximum q flight condition.)

Miscellaneous Equations

$$C_1 = \frac{N'}{I_{xx}} \ell_{cp} \quad (A.15)$$

$$C_2 = \frac{R'}{I_{xx}} \ell_{cg} \quad (A.16)$$

$$\ell_\alpha = x_{cg} - x_\alpha \quad (A.17)$$

$$\ell_A = x_{cg} - x_A \quad (A.18)$$

$$\ell_{cp} = x_{cg} - x_{cp} \quad (A.19)$$

$$\ell_{cg} = x_{cg} - x_\beta \quad (A.20)$$

$$\ell_{sj} = x_{cg} - x_{sj} \quad (A.21)$$

$$\beta = \beta_R - \sum_i^4 Y_i' (x_\beta) \eta_i \quad (A.22)$$

A.4 Matrix Representation

To facilitate control system analysis the vehicle equations defined in A.3 were written in matrix form and the coefficients were evaluated for each vehicle and flight time. The vehicle I equations are illustrated in Table A.19 and the coefficient values are presented in Tables A.20 through A.22 for the three flight times.

Notice that the coefficient matrix at liftoff (Table A.20) contains one less row and column than is illustrated in (Table A.19). This simplication is possible since the angle of attack α is zero at this time allowing the removal of the third row and seventh column.

Tables A.23 through A.26 illustrate the corresponding data for vehicle II. Here the third row and eighth column are removed from the coefficient matrix at liftoff (Table A.24).

A.5 Engine Dynamics

The study vehicle I configuration contains five similar engines, four of which are controllable. Only four of the eight engines present on vehicle II

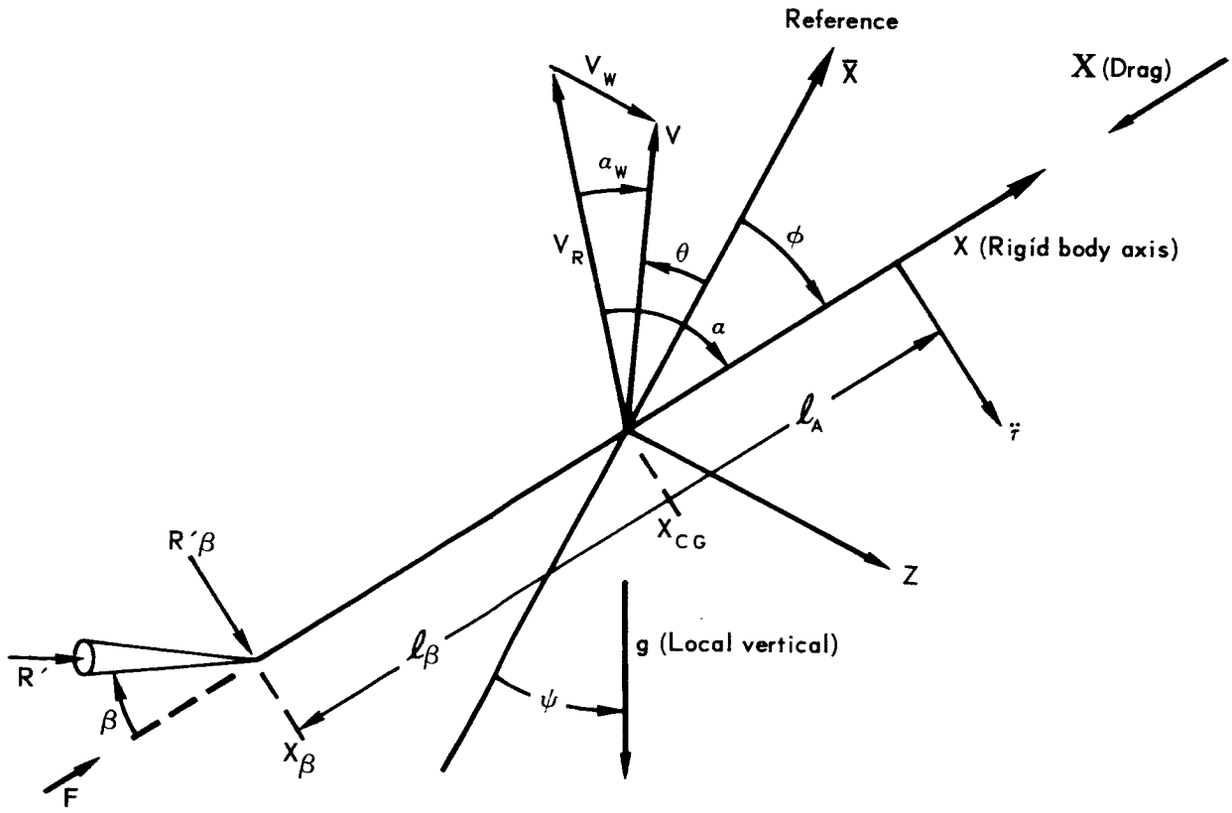

Figure A.1 Rigid Body Coordinate System

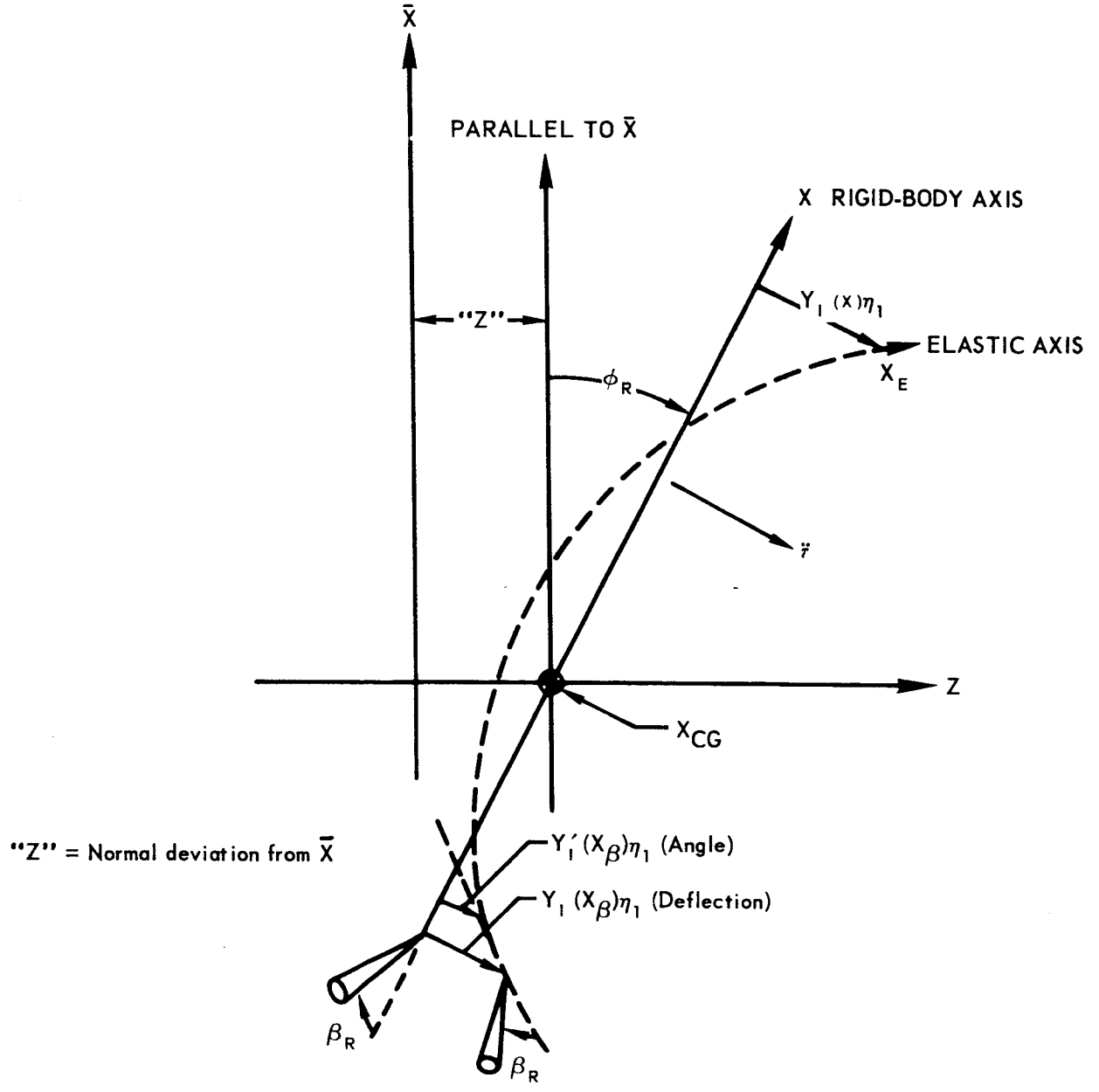

Figure A.2 First Bending Mode Geometry

can be gimballed. The engine actuator dynamics used for both vehicles had the following operational limits on the gimballed engines:

$$\beta_R \text{max} = 5 \text{ degrees}$$

$$\dot{\beta}_R \text{max} = \pm 10 \text{ degrees/second}$$

$$\ddot{\beta}_R \text{max} \pm 700 \text{ degrees/second}^2$$

where β_R is the engine angle referenced to the rigid body axis at the gimbal point. The following transfer function, obtained from Reference 4, relates the engine gimbal angle (β_R) to the engine command angle (β_c).

$$\frac{\beta_R}{B_c} = \frac{31129.6}{(s + 14.64)(s + 4.538 \pm j\, 45.88)}$$

A.6 Wind Data

The wind data used in the Digital Adaptive Filter study of the two study vehicles is based on the George C. Marshall Space Flight Center "Synthetic Wind Profile" contained in Reference 4. The wind angle of attack (α_w) value as a function of time for the max-q flight condition is shown in Figure (A.3a). This is defined as wind profile 1 for this study. Two variations of this profile were used in the analog computer study. Figure (A.3b) illustrates wind profile 2 which includes a 2° step reduction in wind angle of attack at time 17.5 seconds. Wind profile 3, shown in Figure (A.3c) consists of wind profile 1 with a sine wave superimposed beginning at time 15.5 seconds. The frequency of the sine wave and the size of the step were varied in the studies.

TABLE A.1

STUDY VEHICLE I DATA

Symbol	Definition	Units	Lift-off	Max-q	Burn-out
F	Total booster engine thrust	kg	3.403×10^6	3.837×10^6	3.134×10^6
R'	Control engine thrust	kg	2.72×10^6	3.07×10^6	2.51×10^6
m	Vehicle mass	$kg\text{-}sec^2/m$	277621.	172335.	76541.
I_{xx}	Pitch moment of inertia	$kg\text{-}m\text{-}sec^2$	8.43×10^7	7.62×10^7	4.35×10^7
V	Vehicle velocity	m/sec	0	519.3	2520.5
C_1	Aerodynamic moment coefficient	$1/sec^2$	0	-.3421	-.00436
C_2	Control moment coefficient	$1/sec^2$	.8115	1.0741	2.3213
N'	Aerodynamic force	kg	0	1.252×10^6	22177.
X	Aerodynamic drag	kg	1500.	198350.	921.
A	Cross sectional reference area	m^2	79.49	79.49	79.49
cp	Center of pressure	m	44.28	50.02	54.32
cg	Center of gravity	m	25.15	26.66	40.23
$C_{z\alpha}$	Lift coefficient	1/rad	3.85	4.1	3.0
q	Dynamic pressure	kg/m^2	0	3841.	93.
S_E	Control engine first moment of swivel	$kg\text{-}sec^2$	4445.6	4445.6	4445.6
I_E	Control engine moment of inertia	$kg\text{-}m\text{-}sec^2$	13825.5	13825.5	13825.5
M_1	Generalized first mode bending mass	$kg\text{-}sec^2/m$	117218.	102829.	22405.
M_2	Generalized second mode bending mass	$kg\text{-}sec^2/m$	107821.	66610.	93194.
M_3	Generalized third mode bending mass	$kg\text{-}sec^2/m$	249941.	149595.	150447.

TABLE A.1 (Continued)

STUDY VEHICLE I DATA

Symbol	Definition	Units	Lift-off	Max-q	Burn-out
ξ_1	First bending mode damping	Unitless	.005	.005	.005
ξ_2	Second bending mode damping	Unitless	.005	.005	.005
ξ_3	Third bending mode damping	Unitless	.005	.005	.005
ω_1	First bending mode frequency	rad/sec	5.037	5.504	6.377
ω_2	Second bending mode frequency	rad/sec	11.99	13.35	15.68
ω_3	Third bending mode frequency	rad/sec	18.13	18.43	29.34
m_{s1}	First slosh mode mass	kg-sec^2/m	11158.	11612.	338.
m_{s2}	Second slosh mode mass	kg-sec^2/m	17048.	18399.	772.
m_{s3}	Third slosh mode mass	kg-sec^2/m	11173.	11173.	11173.
ξ_{s1}	First slosh mode damping	Unitless	.03	.03	.03
ξ_{s2}	Second slosh mode damping	Unitless	.03	.03	.03
ξ_{s3}	Third slosh mode damping	Unitless	.03	.03	.03
ω_{s1}	First slosh mode frequency	rad/sec	2.136	2.765	3.5814
ω_{s2}	Second slosh mode frequency	rad/sec	2.136	2.765	3.77
ω_{s3}	Third slosh mode frequency	rad/sec	2.136	2.828	4.712
ℓ_{s1}	Distance from cg to first slosh mass	m	16.076	20.825	36.574
ℓ_{s2}	Distance from cg to second slosh mass	m	-3.85	5.085	22.42
ℓ_{s3}	Distance from cg to third slosh mass	m	-20.04	-18.54	-4.956
ℓ_α	Distance from cg to angle of attack sensor	m	-75.614	-74.105	-60.526
ℓ_A	Distance from cg to acceleration sensor	m	-42.01	-40.51	-26.93
ℓ_{cg}	Distance from cg to engine gimbal point	m	22.65	24.15	37.73

TABLE A.1 (Continued)

STUDY VEHICLE I DATA

Symbol	Definition	Units	Lift-off	Max-q	Burn-out
ℓ_{cp}	Distance from cg to center of pressure	m	-16.6	-20.82	-8.55
x_{β}	Engine gimbal point	m	2.54	2.54	2.54

m - meter

Kg - Kilogram

sec - second

TABLE A.2

NORMALIZED BENDING DEFLECTIONS AND SLOPES vs. STATION - VEHICLE 1 LIFT-OFF

X (m)	Y_1	Y_1' (1/meter)	Y_2	Y_2' (1/meter)	Y_3	Y_3' (1/meter)
0	1.0000	.040027	1.0000	.06075	1.0000	.07359
2.5	.8844	.04824	.8525	.06192	.8196	.07622
4.9	.7686	.04849	.7036	.06319	.6361	.07879
7.3	.6508	.04962	.5448	.06874	.4328	.08950
9.7	.5308	.05034	.3758	.07163	.2122	.09320
12.1	.4095	.050612	.2033	.07161	-.008496	.08944
14.5	.2846	.052817	.01884	.07925	-.2364	.09565
16.9	.1601	.050838	-.16032	.06962	-.4447	.07728
19.3	.04105	.0483515	-.3125	.05536	-.6004	.04535
21.7	-.06435	.042856	-.3968	.02849	-.6267	-.004573
24.1	-.1649	.040828	-.4504	.01595	-.5817	-.03265
26.5	-.2600	.038347	-.4727	.002538	-.4723	-.05784
28.9	-.3486	.035458	-.4625	-.01098	-.3085	-.07757
31.3	-.4299	.03222	-.4205	-.02385	-.1060	-.08986
33.7	-.5031	.02926	-.3469	-.05045	.1224	-.13685
36.1	-.5655	.02312	-.2053	-.06552	.4481	-.13532
38.5	-.6145	.01794	-.04099	-.071175	.7547	-.12068
40.9	-.6518	.01313	.1383	-.07790	1.0333	-.11055
43.3	-.6773	.008238	.3312	-.08244	1.2801	-.09411
45.7	-.6894	.0013809	.5256	-.7762	1.4316	-.02172
48.1	-.6845	-.004859	.7024	-.072199	1.3941	+.03724
50.5	-.6670	-.009664	.8749	-.07133	1.2752	+.06134
52.9	-.6383	-.01422	1.0439	-.06938	1.1018	.08267
55.3	-.5990	-.01851	1.2071	-.06646	.8809	.10094
57.7	-.5470	-.029097	1.3671	-.07282	.5940	.17539
60.1	-.4655	-.03857	1.5290	-.06299	.1375	.20287
62.5	-.3623	-.04717	1.6700	-.05406	-.3732	.22243
64.9	-.2368	-.05721	1.7861	-.04217	-.9260	.23697
67.3	-.08696	-.06772	1.8689	-.02572	-1.5025	.24028
69.7	.08747	-.07744	1.9071	-.005928	-2.0654	.22676
72.1	.2838	-.08597	1.8957	.01594	-2.5781	.19733
74.5	.4992	-.09331	1.8303	.03847	-3.0029	.15503
76.9	.7307	-.09947	1.7116	.06028	-3.3153	.10420
79.3	.9757	-.10448	1.5421	.08064	-3.4987	.04801
81.7	1.2855	-.13646	1.2123	.16603	-3.4595	-.09819
84.1	1.6259	-.14702	.7601	.20828	-3.0530	-.23066
86.5	1.9891	-.15518	.2196	.24090	-2.3707	-.3369
88.9	2.3547	-.15008	-.3892	.26462	-1.2787	-.5548
91.3	2.7182	-.15249	-1.0453	.28070	.1497	-.6300
93.7	3.0904	-.15878	-1.7503	.31081	1.7865	-.7465
96.1	3.4780	-.15784	-2.5297	.31299	3.7149	-.7756
98.5	3.8524	-.15411	-3.2635	.29755	5.5209	-.7227
100.9	4.2162	-.14920	-3.9483	.27344	7.1404	-.6271

TABLE A.3

NORMALIZED BENDING DEFLECTIONS AND SLOPES vs. STATION VEHICLE I MAX-q

X (m)	Y_1	Y_1' (1/meter)	Y_2	Y_2' (1/meter)	Y_3	Y_3' (1/meter)
0	1.0000	.05097	1.0000	.06693	1.0000	.07659
2.5	.8773	.05122	.8373	.06837	.8123	.07930
4.9	.7543	.05151	.6728	.06985	.6214	.08186
7.3	.6290	.05283	.4969	.07623	.4109	.09240
9.7	.5012	.05346	.3099	.07843	.1841	.09467
12.1	.3736	.05284	.1254	.07510	-.03632	.08861
14.5	.2449	.05386	-.06336	.07976	-.2627	.09586
16.9	.1179	.05192	-.2431	.06968	-.4722	.07808
19.3	-.003921	.04955	-.3947	.05402	-.6304	.04611
21.7	-.1141	.04493	-.4790	.02767	-.6617	-.002788
24.1	-.2197	.04294	-.5284	.01334	-.6201	-.03155
26.5	-.3199	.04058	-.5429	-.000884	-.5130	-.05623
28.9	-.4151	.03867	-.5324	-.007722	-.3675	-.06465
31.3	-.5054	.03662	-.5063	-.01393	-.2046	-.07063
33.7	-.5909	.03604	-.4647	-.02850	-.02549	-.1070
36.1	-.6718	.03127	-.3838	-.03867	+.2349	-.1092
38.5	-.7406	.02625	-.2836	-.04463	.4841	-.09881
40.9	-.7982	.02171	-.1686	-.05102	.7139	-.09192
43.3	-.8446	.01690	-.3958	-.05626	.9212	-.08009
45.7	-.8763	.008959	+.09996	-.05935	1.0578	-.02574
48.1	-.8881	.001829	.2429	-.06033	1.0515	+.01905
50.5	-.8864	-.003258	.3897	-.06186	.9834	.03729
52.9	-.8727	-.008119	.5389	-.06227	.8740	.05360
55.3	-.8476	-.01274	.6878	-.06163	.7279	.06775
57.7	-.8090	-.02364	.8399	-.07291	.5317	.1233
60.1	-.7397	-.03391	1.0081	-.06786	.2073	.1452
62.5	-.6468	-.04356	1.1656	-.06302	-.1603	.1609
64.9	-.5299	-.05408	1.3085	-.05554	-.5623	.1732
67.3	-.3864	-.06559	1.5290	-.04374	-.9858	.1744
69.7	-.2158	-.07636	1.5155	-.02809	-1.4037	.1693
72.1	-.02079	-.08593	1.5615	-.009608	-1.7886	.1492
74.5	.1957	-.09425	1.5607	.01032	-2.1125	.1194
76.9	.4306	-.1013	1.5119	.03027	-2.3565	.08302
79.3	.6809	-.1071	1.4160	.04946	-2.5075	.04229
81.7	1.0037	-.1430	1.1845	.1235	-2.5064	-.06005
84.1	1.3616	-.1551	.8365	.1638	-2.2371	-.1567
86.5	1.7457	-.1645	.4044	.1952	-1.7654	-.2353
88.9	2.1338	-.1595	-.1044	.226368	-.9853	-.4009
91.3	2.5204	-.1624	-.6694	.2431	+.04937	-.4571
93.7	2.9174	-.1697	-1.2341	.2730	1.2393	-.5436
96.1	3.3323	-.1687	-1.9730	.2763	2.6457	-.5659
98.5	3.7321	-.1644	-2.6196	.2614	3.9632	-.5269
100.9	4.1197	-.1487	-3.2176	.2373	5.1424	-.4559

TABLE A.4

NORMALIZED BENDING DEFLECTIONS AND SLOPES vs. STATION - VEHICLE I BURN-OUT

X (m)	Y_1	Y_1' (1/meter)	Y_2	Y_2' (1/meter)	Y_3	Y_3' (1/meter)
0	1.0000	.03500	1.0000	.06345	1.0000	.1252
2.5	.9155	.03535	.8449	.06545	.6903	.1314
4.9	.8306	.03536	.6878	.06537	.3764	.1299
7.3	.7448	.03528	.5316	.06463	.06913	.1257
9.7	.6614	.03505	.3782	.06309	-.2251	.1192
12.1	.5777	.03473	.2292	.06100	-.5013	.1107
14.5	.4939	.03489	.08093	.06150	-.7690	.1089
16.9	.4112	.03404	-.06050	.05621	-1.0072	.08927
19.3	.3305	.03332	-.1877	.04923	-1.1831	.04687
21.7	.2538	.03156	-.2899	.04054	-1.2715	.03070
24.1	.1789	.03090	-.3827	.03672	-1.3309	.01881
26.5	.1056	.03015	-.4659	.03252	-1.3616	.006775
28.9	.03420	.02931	-.5385	.02795	-1.3634	-.005261
31.3	-.03506	.09838	-.5998	.02303	-1.3365	-.01711
33.7	-.1021	.02848	-.6494	.02172	-1.2808	-.03348
36.1	-.1678	.0620	-.6879	.01025	-1.1730	-.05623
38.5	-.2275	.02365	-.6975	-.001728	-1.0152	-.07424
40.9	-.2816	.02138	-.6804	-.01267	-.8154	-.09217
43.3	-.3300	.01892	-.6360	-.02443	-.5725	-.1100
45.7	-.3707	.01472	-.5467	-.05262	-.2479	-.1631
48.1	-.4008	.01087	-.3901	-.07336	+.1738	-.1821
50.5	-.4236	.008154	-.2017	-.08330	+.6147	-.1840
52.9	-.4400	.004428	+.007960	-.09104	1.0502	-.1777
55.3	-.4502	.003004	.2335	-.09656	1.4620	-.1642
57.7	-.4532	-.002636	.4847	-.1335	1.8537	-.1865
60.1	-.4399	-.008332	.8101	-.1377	2.2334	-.1377
62.5	-.4136	-.01366	1.1437	-.1398	2.5236	-.1013
64.9	-.3738	-.01953	1.4777	-.1376	2.7086	-.05101
67.3	-.3192	-.02603	1.7982	-.1273	2.7554	+.01735
69.7	-.2492	-.03221	2.0812	-.1076	2.6182	.09645
72.1	-.1651	-.03779	2.3081	-.07981	2.2887	.1796
74.5	-.06837	-.04272	2.4603	-.04649	1.7667	.2523
76.9	.03938	-.04695	2.5291	-.01057	1.0960	.3024
79.3	.1564	-.05047	2.5104	+.02613	.3374	.3250
81.7	.3156	-.07145	2.2861	.1456	-1.1540	.6149
84.1	.4961	-.07880	1.8333	.2258	-2.5062	.5125
86.5	.6924	-.08446	1.2136	.2890	-3.5805	.3748
88.9	.8921	-.08221	.3975	.3831	-2.4441	-.4266
91.3	1.0919	-.08406	-.5723	.4219	-2.1751	-.6208
93.7	1.2981	-.08857	-1.6529	.4862	-.4226	-.8526
96.1	1.5154	-.08808	-2.8936	.4977	+1.9288	-.9976
98.5	1.7238	-.08548	-4.0549	.4670	4.2607	-.9198
100.9	1.9245	-.08194	-5.1126	.4148	6.2292	-.7167

TABLE A.5

BENDING MODE MASS AND FREQUENCY vs.
FLIGHT TIME - STUDY VEHICLE I

t (sec)	f_{B1} (cps)	M_{B1} (kg_m - sec^2/m)	f_{B2} (cps)	M_{B2} (kg_m - sec^2/m)	f_{B3} (cps)	M_{B3} (kg_m - sec^2/m)	f_{B4} (cps)	M_{B4} (kg_m - sec^2/m)
0	.802	117218	1.908	107621	2.885	249941	4.701	114222
10	.811	114365	1.916	102790	2.886	263374	4.786	201064
20	.820	111803	1.928	97252	2.887	272561	4.835	394941
30	.832	110008	1.949	90349	2.887	273216	4.864	841215
40	.841	108065	1.969	84762	2.888	265268	4.875	1299802
50	.852	107165	2.002	78974	2.892	237765	4.882	2036912
60	.861	105492	2.033	74174	2.898	214441	4.884	3147951
70	.869	103665	2.069	69858	2.910	186875	4.885	3624899
80	.876	102829	2.124	66610	2.934	149595	4.885	3892932
90	.887	100073	2.172	64994	2.966	117642	4.885	3719120
100	.895	96308	2.226	65630	3.015	91156	4.886	3368989
110	.904	92159	2.295	70214	3.121	65306	4.888	2610864
120	.913	84561	2.348	77518	3.354	49190	4.894	1888277
130	.924	74139	2.396	89309	3.461	37856	4.906	1060140
140	.939	59394	2.442	114694	3.915	32090	4.964	329046
150	.964	40795	2.471	123248	4.444	46478	5.247	60717
156	1.015	22405	2.496	193194	4.669	150447	6.198	38869

$\zeta_{B_1} = .005$

$\zeta_{B_2} = .005$ $\qquad .0005 < \zeta_{B_i} \leq .025$

$\zeta_{B_3} = .005$

Subscripts

B_1 = 1st bending mode

B_2 = 2nd bending mode

B_3 = 3rd bending mode

B_4 = 4th bending mode

TABLE A.6

SLOSHING PROPELLANT DATA - VEHICLE I

t(sec)	X_{s_1}(m)	M_{s_1}(kg-sec^2/m)	f_{s_1}(cps)	ℓ_{s_1}(m)
0	11.620	11158	.34	18.771
80	8.370	11612	.44	23.959
157	6.200	338	.57	44.126
t(sec)	X_{s_2}(m)	M_{s_2}(kg-sec^2/m)	f_{s_2}(cps)	ℓ_{s_2}(m)
0	31.546	17048	.34	-1.180
80	24.110	18399	.44	8.220
157	20.350	772	.60	29.980
t(sec)	X_{s_3}(m)	M_{s_3}(kg-sec^2/m)	f_{s_3}(cps)	ℓ_{s_3}(m)
0	47.730	11173	.34	-17.310
80	47.730	11173	.45	-15.400
157	47.730	11173	.75	2.600

ξ_{s_j} = .005 without baffles; .03 with baffles $\qquad .055 \leq \xi_{s_j} \leq .03$

$\ell_{s_j} = X_{CG} - X_{s_j}$: Distance from the slosh mass CG to the vehicle CG.

Subscripts: 1 - 1st stage RP - 1
2 - 1st stage LOX
3 - 2nd stage LOX

TABLE A.7

NORMALIZED BENDING DEFLECTIONS AND SLOPES
FOR STATIONS OF INTEREST - VEHICLE I LIFT-OFF

Symbol	Definition	Location	$Y_1(x)$	$Y_1'(x)$	$Y_2(x)$	$Y_2'(x)$	$Y_3(x)$	$Y_3'(x)$
x_β	Engine gimbal station	2.54	.9981	.04016	.9975	.06077	.997	.07363
x_{s1}	First slosh mass cg station	11.62	.5548	.0502	.4096	.07105	.2563	.09246
x_{s2}	Second slosh mass cg station	31.55	-.3571	.03512	-.4581	-.01232	-.2874	-.07885
x_{s3}	Third slosh mass cg station	47.73	-.6875	.002438	.4956	-.07836	1.4082	-.03288
x_{cg}	Vehicle cg station	25.15	-.1083	.04197	-.4203	.023	-.607	-.01686
x_φ	Attitude gyro station	93.7	2.7182	-.15249	-1.0453	.2807	.1497	-.63
$x_{\dot\varphi}$	Attitude rate gyro station	69.7	-.08696	-.06772	1.8689	-.02572	-1.5025	.24028
x_α	Angle of attack sensor station	103.3	4.2162	-.1492	-3.9483	.27344	7.1404	-.6271
$x_{\ddot\tau}$	Acceleration sensor station	69.7	-.08696	-.06772	1.8689	-.02572	-1.5025	.24028

TABLE A.8

NORMALIZED BENDING DEFLECTIONS
AND SLOPES - VEHICLE I MAX q

Symbol	Definition	Location	$Y_1(x)$	$Y_1'(x)$	$Y_2(x)$	$Y_2'(x)$	$Y_3(x)$	$Y_3'(x)$
x_β	Engine gimbal station	2.54	.9980	.050974	.99729	.06695	.9969	.07664
x_{s1}	First slosh mass cg station	8.37	.6984	.052098	.59438	.07269	.5276	.08656
x_{s2}	Second slosh mass cg station	24.11	-.11454	.044938	-.4792	.02761	-.6615	-.002908
x_{s3}	Third slosh mass cg station	47.73	-.8714	.010183	.07845	-.05887	1.0367	-.03412
x_{cg}	Vehicle cg station	26.65	-.22596	.042793	-.5293	.01245	-.6134	-.03309
x_φ	Attitude gyro station	93.7	2.5204	-.1624	-.6694	.2431	.04937	-.4571
$x_{\dot\varphi}$	Attitude rate gyro station	69.7	-.3864	-.06559	1.529	-.04374	-.9858	.1744
x_α	Angle of attack sensor station	103.3	4.1197	-.1487	-3.2176	.2373	5.1424	-.4559
$x_{\ddot\tau}$	Acceleration sensor station	69.7	-.3864	-.06559	1.529	-.04374	-.9858	.1744

TABLE A.9

NORMALIZED BENDING DEFLECTIONS
AND SLOPES - VEHICLE I BURN-OUT

Symbol	Definition	Location	$Y_1(x)$	$Y_1'(x)$	$Y_2(x)$	$Y_2'(x)$	$Y_3(x)$	$Y_3'(x)$
x_β	Engine gimbal station	2.54	.9986	.03501	.9974	.06348	.9948	.1253
x_{s1}	First slosh mass cg station	6.20	.8695	.03536	.7598	.06541	.5203	.1306
x_{s2}	Second slosh mass cg station	20.35	.3759	.03372	-.1162	.05316	-1.0842	.0707
x_{s3}	Third slosh mass cg station	47.73	-.3644	.01537	-.5605	-.04827	-.2979	-.1549
x_{cg}	Vehicle cg station	40.23	-.2108	.03436	-.6948	.00161	-1.0593	-.06921
x_ω	Attitude gyro station	93.7	1.0919	-.08406	-.5723	.4219	-2.1751	-.6208
$x_{\dot\varphi}$	Attitude rate gyro station	69.7	-.3192	-.02603	1.7982	-.1273	2.7554	.01735
x_α	Angle of attack sensor station	103.3	1.9245	-.08194	-5.1126	.4148	6.2292	-.7167
$x_{\ddot r}$	Acceleration sensor station	69.7	-.3192	-.02603	1.7982	-.1273	2.7554	.01735

TABLE A.10

STUDY VEHICLE II DATA

Symbol	Definition	Units	Lift-off	Max-q	Burn-out
F	Total booster engine thrust	kg	5.1932×10^6	5.8198×10^6	6.1504×10^6
R'	Control engine thrust	kg	2.5966×10^6	2.9099×10^6	3.0752×10^6
m	Vehicle mass	$kg\text{-}sec^2/m$	423565.	266051.	116412.
I_{xx}	Pitch moment of inertia	$kg\text{-}m\text{-}sec^2$	2.83×10^8	2.52×10^8	9.2×10^7
V	Vehicle velocity	m/sec	0	519.3	2520.5
C_1	Aerodynamic moment coefficient	$1/sec^2$	0	-.0726	.00124
C_2	Control moment coefficient	$1/sec^2$	.3208	.4461	2.1616
N'	Aerodynamic force	kg	0	1.488×10^6	24370.
X	Aerodynamic drag	kg	0	227178.	1735.
A	Cross sectional reference area	m^2	79.414	79.414	79.414
cp	Center of pressure	m	46.5	53.5	62.5
cg	Center of gravity	m	37.5	41.2	67.2
$C_{z\alpha}$	Lift coefficient	1/rad	4.55	4.88	3.30
q	Dynamic pressure	kg/m^2	0	3841.	93.
S_E	Control engine first moment of swivel	$kg\text{-}sec^2$	4445.6	4445.6	4445.6
I_E	Control engine moment of inertia	$kg\text{-}m\text{-}sec^2$	13825.5	13825.5	13825.5
M_1	Generalized first mode bending mass	$kg\text{-}sec^2/m$	193188.	170748.	17866.5
M_2	Generalized second mode bending mass	$kg\text{-}sec^2/m$	165516.	115674.	29067.6
M_3	Generalized third mode bending mass	$kg\text{-}sec^2/m$	112155.	98114.7	119961.

TABLE A.10 (Continued)

STUDY VEHICLE II DATA

Symbol	Definition	Units	Lift-off	Max-q	Burn-out
M_4	Generalized fourth mode bending mass	kg-sec^2/m	350111.	565744.	203336.
ξ_1	First bending mode damping	Unitless	.005	.005	.005
ξ_2	Second bending mode damping	Unitless	.005	.005	.005
ξ_3	Third bending mode damping	Unitless	.005	.005	.005
ξ_4	Fourth bending mode damping	Unitless	.005	.005	.005
ω_1	First bending mode frequency	rad/sec	2.155	2.317	2.913
ω_2	Second bending mode frequency	rad/sec	5.059	5.642	6.589
ω_3	Third bending mode frequency	rad/sec	8.778	9.179	11.705
ω_4	Fourth bending mode frequency	rad/sec	12.35	12.497	24.849
m_{s1}	First slosh mode mass	kg-sec^2/m	11158.	11612.	338.
m_{s2}	Second slosh mode mass	kg-sec^2/m	17048.	18399.	772.
m_{s3}	Third slosh mode mass	kg-sec^2/m	11173.	11173.	11173.
ξ_{s1}	First slosh mode damping	Unitless	.03	.03	.03
ξ_{s2}	Second slosh mode damping	Unitless	.03	.03	.03
ξ_{s3}	Third slosh mode damping	Unitless	.03	.03	.03
ω_{s1}	First slosh mode frequency	rad/sec	2.135	2.763	3.579
ω_{s2}	Second slosh mode frequency	rad/sec	2.135	2.763	3.768
ω_{s3}	Third slosh mode frequency	rad/sec	2.135	2.826	4.71
ℓ_{s1}	Distance from cg to first slosh mass	m	21.71	31.04	60.96
ℓ_{s2}	Distance from cg to second slosh mass	m	-5.35	10.12	42.36
ℓ_{s3}	Distance from cg to third slosh mass	m	-23.55	-20.15	5.85

TABLE A.10 (Continued)

STUDY VEHICLE II DATA

Symbol	Definition	Units	Lift-off	Max-q	Burn-out
ℓ_α	Distance from cg to angle of attack sensor	m	-102.51	-98.81	-72.81
ℓ_A	Distance from cg to acceleration sensor	m	-42.97	-39.27	-13.27
ℓ_{cg}	Distance from cg to engine gimbal point	m	34.96	38.66	64.66
ℓ_{cp}	Distance from cg to center of pressure	m	-9.0	-12.3	4.7
x_β	Engine gimbal point	m	2.54	2.54	2.54

TABLE A.11

NORMALIZED BENDING DEFLECTIONS AND SLOPES
VS. STATION - VEHICLE II LIFT-OFF

Location	Y_1	Y'_1	Y_2	Y'_2	Y_3	Y'_3	Y_4	Y'_4
0	1.0	.03472	1.0	.04399	1.0	.05192	1.0	.06227
2	.93051	.03477	.91173	.04429	.89073	.05509	.87366	.06407
4	.86092	.03481	.82290	.04448	.77883	.05565	.74412	.06516
6	.79122	.03495	.73350	.04523	.66734	.05771	.61158	.06897
8	.72105	.03521	.64171	.04651	.54838	.06110	.46728	.07495
10	.65041	.03541	.54769	.04746	.42376	.06332	.31358	.07830
12	.57944	.03554	.45218	.04797	.29607	.06414	.15614	.07864
14	.50830	.03559	.35611	.04802	.16822	.06347	.00115	.07586
16	.43715	.03555	.26045	.04756	.04323	.06128	-.14521	.07003
18	.36618	.03540	.16623	.04657	-.07582	.05754	-.27699	.06133
20	.29483	.03614	.07114	.04934	-.19279	.06103	-.39669	.06010
22	.22330	.03537	-.02399	.04569	-.30628	.05226	-.50347	.04644
24	.15345	.03446	-.11118	.04139	-.40088	.04201	-.58132	.03080
26	.08770	.03245	-.17975	.03212	-.45397	.02081	-.60239	.00098
28	.02332	.03191	-.24103	.02910	-.48693	.01205	-.58865	-.01469
30	-.03986	.03126	-.29589	.02570	-.50188	.00286	-.54399	-.02982
32	-.10167	.03053	-.34361	.02197	-.49826	-.00648	-.47032	-.04359
34	-.16190	.02969	-.38357	.01796	-.47609	-.01565	-.37107	-.05529
36	-.22037	.02877	-.41529	.01373	-.43598	-.02436	-.25102	-.06431
38	-.27692	.02776	-.43837	.00934	-.37914	-.03235	-.11598	-.07021
40	-.33136	.02667	-.45259	.00487	-.30727	-.03935	.02749	-.07271
42	-.38355	.02551	-.45784	.00038	-.22255	-.04517	.17247	-.07172
44	-.43336	.02428	-.45417	-.00404	-.12754	-.04962	.31204	-.06734
46	-.48065	.02300	-.44177	-.00833	-.02508	-.05260	.43970	-.05987
48	-.52537	.02135	-.41433	-.01865	.10569	-.07371	.57304	-.06833
50	-.56559	.01887	-.37055	-.02506	.25506	-.07536	.70013	-.05846

TABLE A.11 (Continued

NORMALIZED BENDING DEFLECTIONS AND SLOPES
VS. STATION - VEHICLE II LIFT-OFF

Location	Y_1	Y'_1	Y_2	Y'_2	Y_3	Y'_3	Y_4	Y'_4
52	-.60080	.01627	-.31479	-.02748	.40433	-.06909	.80405	-.04079
54	-.63124	.01416	-.25121	-.03405	.54101	-.06734	.87451	-.02940
56	-.65740	.01200	-.17882	-.03828	.67253	-.06394	.92036	-.01618
58	-.67889	.00943	-.09796	-.04255	.78961	-.05186	.92287	.01613
60	-.69508	.00676	-.00909	-.04620	.87801	-.03626	.85505	.05139
62	-.70594	.00411	.08634	-.04911	.93381	-.01939	.71961	.08338
64	-.71179	.00181	.18751	-.05191	.96248	-.01045	.53351	.10009
66	-.71324	-.00035	.29367	-.05419	.97626	-.00335	.32174	.11133
68	-.71044	-.00245	.40397	-.05604	.97599	.00358	.08975	.12030
70	-.70348	-.00450	.51757	-.05749	.96210	.01027	-.15788	.12696
72	-.69247	-.00649	.63366	-.05854	.93511	.01667	-.41652	.13131
74	-.67754	-.00843	.75145	-.05919	.89567	.02271	-.68154	.13335
76	-.65879	-.01031	.87015	-.05945	.84451	.02838	-.94837	.13313
78	-.63636	-.01212	.98897	-.05934	.78245	.03361	-1.21255	.13071
80	-.60681	-.01756	1.11928	-.06823	.69091	.05617	-1.52925	.17145
82	-.56725	-.02196	1.25431	-.06670	.56819	.06630	-1.86068	.15952
84	-.51992	-.02546	1.38111	-.06029	.43273	.06959	-2.14251	.12315
86	-.46488	-.02968	1.49590	-.05440	.28820	.07506	-2.35507	.08886
88	-.40073	-.03461	1.59804	-.04745	.13195	.08133	-2.49430	.04837
90	-.32584	-.04033	1.68320	-.03762	-.03808	.08869	-2.52788	-.01563
92	-.23961	-.04585	1.74792	-.02701	-.22105	.09384	-2.43080	-.08123
94	-.14266	-.05103	1.79169	-.01732	-.41202	.09729	-2.21126	-.13297
96	-.03571	-.05587	1.81788	-.00888	-.60851	.09913	-1.90795	-.16955
98	.08062	-.06041	1.82721	-.00046	-.80735	.09944	-1.53668	-.20087
100	.20571	-.06464	1.81977	.00789	-1.0051	.09804	-1.10831	-.22661
102	.33896	-.06856	1.79574	.01612	-1.19841	.09502	-.63423	-.24655

TABLE A.11 (Continued)

NORMALIZED BENDING DEFLECTIONS AND SLOPES
VS. STATION - VEHICLE II LIFT-OFF

Location	Y_1	Y'_1	Y_2	Y'_2	Y_3	Y'_3	Y_4	Y'_4
104	.47974	-.07217	1.75540	.02419	-1.38413	.09046	-.12622	-.26052
106	.62745	-.07549	1.69912	.03205	-1.55925	.08445	.40369	-.26844
108	.78237	-.08207	1.62626	.04407	-1.72346	.08693	.95708	-.32508
110	.95410	-.08954	1.51795	.06401	-1.87461	.06404	1.59895	-.31474
112	1.13999	-.09623	1.37096	.08284	-1.97808	.03898	2.20616	-.29011
114	1.33844	-.10210	1.18720	.10078	-2.02858	.01110	2.74907	-.25049
116	1.54764	-.10671	.96766	.11953	-2.01575	-.02990	3.18324	-.16437
118	1.76455	-.11036	.70960	.13746	-1.90451	-.07571	3.38495	-.05427
120	1.98908	-.11408	.42023	.15163	-1.72251	-.10592	3.42703	.01202
122	2.22062	-.11742	.10385	.16462	-1.48193	-.13450	3.33742	.07755
124	2.45882	-.12087	-.23871	.17831	-1.18288	-.16551	3.11088	.15175
126	2.70495	-.12546	-.61273	.19675	- .81216	-.20830	2.71077	.25798
128	2.96020	-.12960	-1.02558	.21535	- .34495	-.25742	2.05303	.39694
130	3.22250	-.13253	-1.47094	.22931	.21072	-.29666	1.13749	.51488
132	3.48961	-.13444	-1.93990	.23902	.83467	-.32570	.01130	.60702
134	3.75978	-.13571	-2.42475	.24565	1.50719	-.34595	-1.2719	.67263
136	4.03209	-.13652	-2.92065	.24982	2.21314	-.35880	-2.6627	.71452
138	4.30549	-.13681	-3.42235	.25153	2.93744	-.36447	-4.11461	.73413
140	4.57904	-.13665	-3.92527	.25096	3.66657	-.36335	-5.58489	.73201
142	4.85209	-.13643	-4.42601	.24995	4.39006	-.36060	-7.03953	.72392
144	5.12473	-.13619	-4.92478	.24870	5.10789	-.35682	-8.47666	.71176

TABLE A.12

NORMALIZED BENDING DEFLECTIONS AND SLOPES
VS. STATION - VEHICLE II MAX-q

Location	Y_1	Y_1'	Y_2	Y_2'	Y_3	Y_3'	Y_4	Y_4'
0	1.0	.03563	1.0	.04727	1.0	.05660	1.0	.06362
2	.92869	.03569	.90509	.04764	.88583	.05758	.87095	.06544
4	.85725	.03573	.80950	.04788	.76990	.05818	.73864	.06654
6	.78569	.03590	.71321	.04878	.65226	.06038	.60333	.07037
8	.71359	.03619	.61403	.05033	.52773	.06397	.45623	.07634
10	.64096	.03642	.51220	.051428	.39729	.06625	.29982	.07961
12	.56795	.03657	.40870	.05197	.26381	.06695	.13990	.07977
14	.49493	.03643	.30541	.05118	.13163	.06498	-.01645	.07625
16	.42230	.03619	.20423	.04995	.00446	.06207	-.16423	.07133
18	.35020	.03590	.10583	.04839	-.11612	.05840	-.30095	.06519
20	.27818	.03626	.00796	.05016	-.23514	.06215	-.43455	.07078
22	.20636	.03554	-.08870	.04641	-.35094	.05346	-.56208	.05644
24	.13608	.03472	-.17730	.04208	-.44804	.04330	-.65878	.03952
26	.06905	.03317	-.24862	.03349	-.50418	.02215	-.68654	.00267
28	.00317	.03270	-.31244	.03026	-.53929	.01288	-.67400	-.01522
30	-.06168	.03214	-.36944	.02669	-.55543	.00324	-.62599	-.03265
32	-.12534	.03150	-.41899	.02283	-.55221	-.00643	-.54436	-.04869
34	-.18764	.03079	-.46063	.01878	-.52993	-.01577	-.43279	-.06248
36	-.24844	.03002	-.49416	.01495	-.48992	-.02353	-.29691	-.07223
38	-.30776	.02929	-.52120	.01210	-.43829	-.02800	-.14774	-.07670
40	-.36556	.02851	-.54258	.00929	-.37832	-.37832	-.00882	-.07962
42	-.42176	.02768	-.55838	.00652	-.31121	-.03513	.16969	-.08101
44	-.47627	.02682	-.56867	.00379	-.23820	-.03779	.33177	-.08084
46	-.52900	.02591	-.57356	.00111	-.16048	-.03983	.49199	-.07914

TABLE A.12 (Continued)

NORMALIZED BENDING DEFLECTIONS AND SLOPES
VS. STATION - VEHICLE II MAXIMUM q

Location	Y_1	Y'_1	Y_2	Y'_2	Y_3	Y'_3	Y_4	Y'_4
48	-.58057	.02518	-.57065	-.00443	-.06234	-.05526	.68639	-.10592
50	-.62880	.02303	-.55620	-.01001	.05015	-.05702	.88844	-.09562
52	-.67258	.02055	-.53078	-.01504	.16377	-.05317	1.06395	-.07167
54	-.71176	.01863	-.49622	-.01950	.26953	-.05242	1.19367	-.05759
56	-.74704	.01662	-.45282	-.02389	.37264	-.05051	1.29210	-.04040
58	-.77778	.01403	-.39924	-.02985	.46701	-.04300	1.33109	.00517
60	-.80310	.01128	-.33364	-.03566	.54309	-.03284	1.26940	.05629
62	-.82290	.00852	-.25705	-.04082	.59754	-.02146	1.10849	.10381
64	-.83757	.00623	-.17121	-.04471	.63371	-.01549	.87274	.12800
66	-.84787	.00409	-.07861	-.04783	.65986	-.01067	.59997	.14430
68	-.85393	.00198	.01983	-.05054	.67642	-.00590	.29760	.15759
70	-.85583	-.00008	.12327	-.05283	.68350	-.00120	-.02828	.16779
72	-.85363	-.00210	.23087	-.05471	.68132	.00336	-.37143	.17487
74	-.84744	-.00408	.34181	-.05617	.67018	.00775	-.72561	.17882
76	-.83736	-.00600	.45525	-.05721	.65045	.01194	-1.08458	.17968
78	-.82348	-.00787	.57039	-.05786	.62257	.01590	-1.44224	.17752
80	-.80264	-.01319	.70000	-.06906	.57488	.03104	-1.87573	.23626
82	-.77166	-.01776	.83839	-.06921	.50475	.03892	-2.33486	.22220
84	-.73244	-.02155	.97139	-.06402	.42347	.04265	-2.73004	.17419
86	-.68494	-.02606	1.09510	-.05962	.33302	.04791	-3.03430	.12935
88	-.62770	-.03133	1.20939	-.05441	.23130	.05398	-3.24263	.07633
90	-.55890	-.03751	1.31055	-.04666	.11574	.06161	-3.31212	-.00799
92	-.47783	-.04351	1.39530	-.03796	-.01385	.06767	-3.20899	-.09493
94	-.38513	-.04911	1.46270	-.02997	-.15363	.07192	-2.94327	-.16361

TABLE A.12 (Continued)

NORMALIZED BENDING DEFLECTIONS AND SLOPES
VS. STATION - VEHICLE II MAXIMUM q

Location	Y_1	Y'_1	Y_2	Y'_2	Y_3	Y'_3	Y_4	Y'_4
96	-.28164	-.05433	1.51575	-.02306	-.30064	.07486	-2.56652	-.21212
98	-.16803	.05923	1.55482	-.01599	-.45211	.07638	-2.09945	-.25385
100	-.04495	-.06380	1.57966	-.00884	-.60522	.07651	-1.55606	-.28839
102	.08697	-.06806	1.59013	-.00163	-.75723	.07529	-.95108	-.31539
104	.22707	-.07199	1.58619	.00557	-.90550	.07278	-.29982	-.33464
106	.37471	-.07560	1.56788	.01272	-1.04751	.06905	.38205	-.34600
108	.53020	-.08271	1.53464	.02269	-1.18311	.07299	1.09672	-.42140
110	.73093	-.09089	1.47034	.04143	-1.31345	.05716	1.93131	-.41047
112	.89320	-.09823	1.36944	.05939	-1.41034	.03933	2.72556	-.38067
114	1.09628	-.10472	1.23315	.07681	-1.46905	.01901	3.44045	-.33117
116	1.31126	-.10988	1.06147	.09601	-1.48083	-.01204	4.01787	-.22122
118	1.53502	-.11403	.84921	.11487	-1.41705	-.04725	4.29693	-.07974
120	1.76733	-.11818	.60480	.12927	-1.29939	-.07015	4.37131	.00520
122	2.00746	-.12191	.33288	.14253	-1.13723	-.09189	4.27669	.08937
124	2.25505	-.12577	.03420	.15654	-.93050	-.11559	4.00599	.18490
126	2.51150	-.13091	-.29672	.17549	-.66896	-.14838	3.51170	.32192
128	2.77820	-.13557	-.66796	.19499	-.33290	-.18655	2.68403	.50219
130	3.05285	-.13888	-1.07344	.20977	.07211	-.21725	1.52149	.65557
132	3.33294	-.14106	-1.50403	.22016	.53069	-.24010	.08470	.77567
134	3.61652	-.14251	-1.95169	.22728	1.02756	-.25607	-1.55685	.86125
136	3.90255	-.14342	-2.41118	.23177	1.55078	-.26621	-3.33877	.81591
138	4.18980	-.14376	-2.87695	.23363	2.08852	-.27072	-5.20052	.94156
140	4.47723	-.14358	-3.34409	.23305	2.63014	-.26988	-7.08634	.93886
142	4.76411	-.14333	-3.80895	.23199	3.16740	-.26773	-8.95187	.92835
144	5.05052	-.14306	-4.27173	.23065	3.70022	-.26476	-10.79460	.91249

TABLE A.13

NORMALIZED BENDING DEFLECTIONS AND SLOPES
VS. STATION - VEHICLE II BURN-OUT

Location	Y_1	Y'_1	Y_2	Y'_2	Y_3	Y'_3	Y_4	Y'_4
0	1.0	.02090	1.0	.03091	1.0	.04932	1.0	.10303
2	.95810	.02100	.93768	.03143	.89977	.05093	.78675	.11012
4	.91601	.02107	.87438	.03178	.79662	.05195	.56162	.11380
6	.87386	.02108	.81076	.03183	.69260	.05204	.33419	.11342
8	.83169	.02108	.74710	.03181	.58863	.05189	.10887	.11169
10	.78954	.02107	.68356	.03172	.48521	.05149	-.11163	.10859
12	.74744	.02103	.62031	.03150	.38292	.05074	-.32470	.10436
14	.70544	.02097	.55760	.03118	.28246	.04968	-.52844	.09922
16	.66358	.02089	.49563	.03078	.18436	.04836	-.72095	.09314
18	.62190	.02079	.43455	.03029	.08911	.04683	-.90040	.08617
20	.58028	.02087	.37381	.03061	-.00474	.04742	-1.06985	.08389
22	.53877	.02064	.31370	.02948	-.09620	.04397	-1.22398	.07005
24	.49774	.02039	.25600	.02820	-.18034	.04011	-1.34929	.05503
26	.45766	.01993	.20293	.02601	-.25154	.03409	-1.43712	.03908
28	.41795	.01978	.15162	.02528	-.31758	.03192	-1.50749	.03123
30	.37854	.01962	.10185	.02448	-.37910	.02958	-1.56187	.02310
32	.33948	.01944	.05374	.02361	-.43576	.02705	-1.59974	.01475
34	.30078	.01925	.00745	.02267	-.48719	.02436	-1.62077	.00626
36	.26249	.01904	-.03688	.02166	-.53306	.02149	-1.62476	-.00228
38	.22463	.01882	-.07912	.02057	-.57304	.01846	-1.61169	-.01079
40	.18723	.01858	-.11913	.01942	-.60681	.01528	-1.58168	-.01919
42	.15034	.01832	-.15676	.01820	-.63407	.01196	-1.53513	-.02733
44	.11396	.01805	-.19187	.01690	-.65453	.00849	-.147253	-.03523
46	.07815	.01776	-.22433	.01554	-.66793	.00489	-1.39445	-.04280

TABLE A.13 (Continued)

NORMALIZED BENDING DEFLECTIONS AND SLOPES
VS. STATION - VEHICLE II BURN-OUT

Location	Y_1	Y'_1	Y_2	Y'_2	Y_3	Y'_3	Y_4	Y'_4
48	.04266	.01757	-.25511	.01450	-.67565	.00118	-1.28929	-.06224
50	.00820	.01688	-.28092	.01128	-.66974	-.00712	-1.15026	-.07663
52	-.02482	.01606	-.30002	.00752	-.64677	-.01635	- .98400	-.08690
54	-.05631	.01543	-.31216	.00460	-.60679	-.02368	- .79970	-.09733
56	-.08651	.01477	-.31833	.00155	-.55178	-.03136	- .59471	-.10748
58	-.11527	.01397	-.31678	-.00334	-.47353	-.04786	- .33768	-.15142
60	-.14235	.01309	-.30491	-.00851	-.36145	-.06374	- .00838	-.17231
62	-.16762	.01218	-.28291	-.01344	-.22105	-.07605	.32648	-.15699
64	-.19117	.01139	-.25236	-.01681	-.06123	-.08269	.62850	-.14658
66	-.21320	.01064	-.21597	-.01955	.10838	-.08669	.91093	-.13515
68	-.23372	.00988	-.17436	-.02203	.28455	-.08925	1.16617	-.11945
70	-.25273	.00913	-.12804	-.02425	.46438	-.09035	1.38620	-.10006
72	-.27023	.00838	-.07754	-.02620	.64501	-.09006	1.56447	-.07787
74	-.28624	.00763	-.02341	-.02788	.82368	-.08840	1.69625	-.05364
76	-.30075	.00689	.03381	-.02929	.99772	-.08544	1.77815	-.02813
78	-.31379	.00615	.09356	-.03042	1.16460	-.08125	1.80850	-.00224
80	-.32451	.00438	.16521	-.03959	1.35141	-.09689	1.73897	.07291
82	-.33143	.00255	.24622	-.04131	1.53273	-.08426	1.55266	.11177
84	-.33486	.00085	.32664	-.03930	1.67567	-.05902	1.31181	.13062
86	-.33463	-.00112	.40397	-.03803	1.76924	-.03412	1.02646	.15483
88	-.33017	-.00341	.47861	-.03650	1.80955	-.00483	.69163	.18123
90	-.32061	-.00617	.54891	-.03376	1.77486	.04004	.28505	.22417
92	-.30555	-.00888	.61305	-.03026	1.64964	.08483	- .18733	.24372
94	-.28522	-.01140	.66998	-.02696	1.44148	.11995	- .67512	.24446

TABLE A.13 (Continued)

NORMALIZED BENDING DEFLECTIONS AND SLOPES
VS. STATION - VEHICLE II BURN-OUT

Location	Y_1	Y'_1	Y_2	Y'_2	Y_3	Y'_3	Y_4	Y'_4
96	-.26008	-.01372	.72111	-.02412	1.17593	.14497	-1.16119	.23999
98	-.23043	-.01592	.76629	-.02102	.86442	.16589	-1.62815	.22545
100	-.19651	-.01798	.80501	-.01767	.51531	.18254	-2.0567	.20177
102	-.15859	-.01992	.83682	-.01411	.13728	.19480	-2.42979	.17018
104	-.11693	-.02172	.86135	-.01039	-.26084	.20262	-2.73304	.13221
106	-.07180	-.02339	.87828	-.00653	-.67015	.20599	-2.95548	.08965
108	-.02306	-.02657	.88733	-.00232	-1.09156	.24404	-3.08855	.03932
110	.03398	-.03041	.88103	.00855	-1.56725	.23028	-3.04568	-.07765
112	.09833	-.03388	.85322	.01928	-2.00580	.20657	-2.78684	-.18053
114	.16926	-.03698	.80389	.03006	-2.38621	.17219	-2.32724	-.27808
116	.24596	-.03958	.73195	.04304	-2.67609	.10309	-1.64366	-.44312
118	.32727	-.04175	.63132	.05636	-2.78319	.01691	- .57074	.59148
120	.41289	-.04382	.50880	.06600	-2.76438	-.03549	.64991	-.62230
122	.50240	-.04567	.36778	.07494	-2.64198	-.08681	1.89667	-.62053
124	.59563	-.04760	.20865	.08446	-2.41283	-.14440	3.10335	-.57681
126	.69329	-.05018	.02758	.09741	-2.04934	-.22620	4.16101	-.44971
128	.79614	-.05256	-.18151	.11119	-1.49018	-.33065	4.72448	-.10309
130	.90308	-.05428	-.41499	.12181	-.73832	-.41831	4.54584	.28345
132	1.01285	-.05542	-.66665	.12939	.16941	-.48616	3.60289	.65240
134	1.12447	-.05618	-.93084	.13462	1.19234	-.53428	1.99085	.93754
136	1.23736	-.05666	-1.20371	.13792	2.29430	-.56497	-.08568	1.12589
138	1.35090	-.05684	-1.48122	.13932	3.44087	-.57919	-2.45320	1.22801
140	1.46455	-.05676	-1.75983	.13894	4.60056	-.57745	-4.93591	1.23725
142	1.57791	-.05663	-2.03683	.13819	5.74846	-.57142	-7.38051	1.21098
144	1.69104	-.05648	-2.31232	.13721	6.88342	-.56249	-9.75684	1.15772

TABLE A.14

BENDING MODE MASS AND FREQUENCY
VS. FLIGHT TIME - STUDY VEHICLE II

t (sec)	f_{B_1} (cps)	M_{B_1} ($kg - sec^2/m$)	f_{B_2} (cps)	M_{B_2} ($kg - sec^2/m$)	f_{B_3} (cps)	M_{B_3} ($kg - sec^2/m$)	f_{B_4} (cps)	M_{B_4} ($kg - sec^2/m$)
0	.3432	193188	.8056	165516.2	1.3978	162154.5	1.9665	350110.7
10	.3468	190179.6	.8124	156252.3	1.3983	165879.3	1.9764	423460.6
20	.3503	187663.4	.8206	147492.4	1.3989	165517.7	1.9824	498270.4
30	.3537	185474.8	.8302	139430.6	1.4006	160882.0	1.9856	582366.3
40	.3570	183447.2	.8413	132266.6	1.4041	152473.5	1.9870	643847.6
50	.3602	181332.2	.8537	126158.6	1.4105	141015.6	1.9873	690353.0
60	.3632	178807.2	.8676	121270.6	1.4212	127235.5	1.9873	700359.1
70	.3661	175455.7	.8825	117722.5	1.4375	112894.8	1.9880	640126.6
80	.3690	170748.1	.8984	115674.3	1.4616	98114.7	1.9900	565743.8
90	.3719	164030.3	.9148	115194.1	1.4958	84381.6	1.9947	460784.2
100	.3750	154477.3	.9312	116055.5	1.5432	72794.8	2.0050	323332.1
110	.3784	141217.7	.9472	117700.5	1.6063	64581.8	2.0268	198745.3
120	.3828	123324.7	.9625	118416.8	1.6839	63649.8	2.0763	102021.2
130	.3889	100064.3	.9772	114087.9	1.7621	81053.7	2.1963	50113.5
140	.3990	71417.6	.9924	99897.4	1.8180	131216.5	2.4798	28619.2
150	.4280	34467.2	1.0223	55256.9	1.8534	169695.1	3.2215	16001.4
157	.4639	17866.5	1.0492	29067.6	1.8639	169960.9	3.9569	203335.9

$\zeta_{B_1} = .005$ $\zeta_{B_4} = .005$

$\zeta_{B_2} = .005$ $.0005 = \zeta_{B_i} \leq .025$

$\zeta_{B_3} = .005$

Subscripts

B_1 = 1st bending mode
B_2 = 2nd bending mode
B_3 = 3rd bending mode
B_4 = 4th bending mode

TABLE A.15

SLOSHING PROPELLANT DATA -
VEHICLE II

t (sec)	X_{s_1}(m)	M_{s_1}(kg-sec^2/m)	f_{s_1}(cps)	l_{s_1}(m)
0	16.09	11158	.34	21.71
80	10.16	11612	.44	31.04
157	6.24	338	.57	60.96
t (sec)	X_{s_2}(m)	M_{s_2}(kg-sec^2/m)	f_{s_2}(cps)	l_{s_2}(m)
0	43.15	17048	.34	-5.35
80	31.08	18399	.44	10.12
157	24.84	772	.60	42.36
t (sec)	X_{s_3}(m)	M_{s_3}(kg-sec^2/m)	f_{s_3}(cps)	l_{s_3}(m)
0	61.35	11173	.34	-23.55
80	61.35	11173	.45	-20.15
157	61.35	11173	.75	5.85

$$\xi_{s_j} = \begin{cases} .005 \text{ without baffles} \\ .03 \text{ with baffles} \end{cases} \qquad .055 \leq \xi_{s_j} \leq .03$$

$\xi_{s_j} = X_{CG} - X_{s_j}$: Distance from the slosh mass CG to the vehicle CG.

Subscripts:

1 - 1st stage RP - 1
2 - 1st stage LOX
3 - 2nd stage LOX

MAC 231UM (REV 14 JUN 62)

TABLE A.16

NORMALIZED BENDING DEFLECTIONS
AND SLOPES - VEHICLE II LIFT-OFF

Symbol	Definition	Location	$Y_1(x)$	$Y_1'(x)$	$Y_2(x)$	$Y_2'(x)$	$Y_3(x)$	$Y_3'(x)$	$Y_4(x)$	$Y_4'(x)$
x_β	Engine gimbal station	2.54	.93051	.03477	.91173	.04429	.89073	.05509	.87366	.06407
x_{s1}	First slosh mass cg station	16.09	.45316	.03556	.28197	.04766	.07135	.06177	- .11228	.07134
x_{s2}	Second slosh mass cg station	43.15	-.39855	.02514	-.45674	-.00094	- .19405	-.04651	.21434	-.07041
x_{s3}	Third slosh mass cg station	61.35	-.69942	.0057	.02908	-.04736	.90233	-.02951	.80087	.06419
x_{cg}	Vehicle cg station	37.8	-.256	.02813	-.42983	.01096	- .40017	-.02939	- .16594	-.06803
x_φ	Attitude gyro station	120.7	2.0076	-.11435	.39493	.15267	-1.70326	-.10821	3.41986	.01726
$x_{\dot\varphi}$	Attitude rate gyro station	80.47	-.6077	-.0174	1.11537	-.06796	.69366	.05549	-1.51975	.17023
x_α	Angle of attack sensor station	140.82	4.61727	-.13662	-3.99537	.25082	3.76786	-.36296	-5.78854	.73088
$x_{\ddot r}$	Acceleration sensor station	80.47	-.6077	-.0174	1.11537	-.06796	.69366	.05549	-1.51975	.17023

TABLE A.17

NORMALIZED BENDING DEFLECTIONS
AND SLOPES - VEHICLE II MAXIMUM q

Symbol	Definition	Location	$Y_1(x)$	$Y_1'(x)$	$Y_2(x)$	$Y_2'(x)$	$Y_3(x)$	$Y_3'(x)$	$Y_4(x)$	$Y_4'(x)$
x_β	Engine gimbal station	2.54	.92869	.03569	.90509	.04764	.88583	.05758	.87095	.06544
x_{s_1}	First slosh mass cg station	10.16	.65476	.03638	.53155	.05122	.42207	.06582	.32954	.07899
x_{s_2}	Second slosh mass cg station	31.08	-.07887	.03197	- .38282	.02565	- .55456	.00063	- .60395	-.03698
x_{s_3}	Third slosh mass cg station	61.35	-.81102	.01018	- .303	-.03772	.56487	-.02829	1.20504	.0753
x_{cg}	Vehicle cg station	41.3	-.38692	.02819	- .54858	.00824	- .35282	-.03292	.05901	-.08012
x_φ	Attitude gyro station	120.7	1.78654	-.11848	.58305	.13033	-1.28642	-.07189	4.36374	.01193
x_φ^*	Attitude rate gyro station	80.47	-.80327	-.01303	.69611	-.06872	.57631	.03059	-1.86273	.2345
x_α	Angle of attack sensor station	140.82	4.51739	-.14354	-3.40917	.2329	2.70536	-.26958	-7.34751	.93739
$x_{\ddot{r}}$	Acceleration sensor station	80.47	-.80327	-.01303	.69611	-.06872	.57631	.03059	-1.86273	.2345

MAC 231UM (REV 14 JUN 62)

TABLE A.18

NORMALIZED BENDING DEFLECTIONS
AND SLOPES - VEHICLE II BURN-OUT

Symbol	Definition	Location	$Y_1(x)$	$Y_1'(x)$	$Y_2(x)$	$Y_2'(x)$	$Y_3(x)$	$Y_3'(x)$	$Y_4(x)$	$Y_4'(x)$
x_β	Engine gimbal station	2.54	.9581	.021	.93768	.03143	.89977	.05093	.78675	.11012
x_{s_1}	First slosh mass cg station	6.24	.88018	.02108	.8203	.03182	.70820	.05203	.3683	.11348
x_{s_2}	Second slosh mass cg station	24.84	.49173	.02032	.24804	.02787	- .19102	.03921	-1.36246	.05264
x_{s_3}	Third slosh mass cg station	61.35	-.15246	.01273	- .29611	-.01048	- .30529	-.06866	.12556	-.16618
x_{cg}	Vehicle cg station	67.8	-.22613	.01016	- .18976	-.02111	.21934	-.0883	1.07173	-.12526
x_φ	Attitude gyro station	120.7	.42005	-.04397	.49752	.06672	-2.75459	-.0396	.74965	-.62216
$x_{\dot\varphi}$	Attitude rate gyro station	80.47	-.32419	.00443	.16306	-.03931	1.34581	-.09642	1.74106	.07066
x_α	Angle of attack sensor station	140.82	1.48042	-.05674	-1.79861	.13883	4.76127	-.57661	-5.27815	1.23357
$x_{\ddot\tau}$	Acceleration sensor station	80.47	-.32419	.00443	.16306	-.03931	1.34581	-.09642	1.74106	.07066

TA

STUDY VEHICLE I EQUATI

$\frac{F}{I_{xx}} Y_1(X_\beta) - \frac{F\ell_{cg}}{I_{xx}} Y'_1(X_\beta)$	$\frac{F}{I_{xx}} Y_2(X_\beta) - \frac{F\ell_{cg}}{I_{xx}} Y'_2(X_\beta)$	$\frac{F}{I_{xx}} Y_3(X_\beta) - \frac{F\ell_{cg}}{I_{xx}} Y'_3(X_\beta)$	$\frac{-\ell_{s1}}{I_{xx}} m_{s1} S^2 - \left(\frac{F-X}{m}\right)\frac{m_{s1}}{I_{xx}}$	$\frac{-\ell_{s2}}{I_{xx}} m_{s2} S^2 - \left(\frac{F-X}{m}\right)\frac{m_s}{I_x}$
$\frac{F}{m} Y'_1(X_\beta)$	$\frac{F}{m} Y'_2(X_\beta)$	$\frac{F}{m} Y'_3(X_\beta)$	$\frac{m_{s1}}{m} S^2$	$\frac{m_{s2}}{m} S^2$
0	0	0	0	0
$S^2 + 2\zeta_1\omega_1 S + \omega_1^2$	0	0	$\frac{-m_{s1}}{M_1}\left[Y_1(X_{s1})S^2 + \left(\frac{F-X}{m}\right)Y'_1(X_{s1})\right]$	$\frac{-m_{s2}}{M_1}\left[Y_1(X_{s2})S^2 + \left(\frac{F-X}{m}\right)Y'_2\right.$
0	$S^2 + 2\zeta_2\omega_2 S + \omega_2^2$	0	$\frac{-m_{s1}}{M_2}\left[Y_2(X_{s1})S^2 + \left(\frac{F-X}{m}\right)Y'_2(X_{s1})\right]$	$\frac{-m_{s2}}{M_2}\left[Y_2(X_{s2})S^2 + \left(\frac{F-X}{m}\right)Y'_2\right.$
0	0	$S^2 + 2\zeta_3\omega_3 S + \omega_3^2$	$\frac{-m_{s1}}{M_3}\left[Y_3(X_{s1})S^2 + \left(\frac{F-X}{m}\right)Y'_3(X_{s1})\right]$	$\frac{-m_{s2}}{M_3}\left[Y_3(X_{s2})S^2 + \left(\frac{F-X}{m}\right)Y'_3\right.$
$Y_1(X_{s1})S^2 + \left(\frac{F-X}{m}\right)Y'_1(X_{s1})$	$Y_2(X_{s1})S^2 + \left(\frac{F-X}{m}\right)Y'_2(X_{s1})$	$Y_3(X_{s1})S^2 + \left(\frac{F-X}{m}\right)Y'_3(X_{s1})$	$S^2 + 2\zeta_{s1}\omega_{s1} S + \omega_{s1}^2$	0
$Y_1(X_{s2})S^2 + \left(\frac{F-X}{m}\right)Y'_1(X_{s2})$	$Y_2(X_{s2})S^2 + \left(\frac{F-X}{m}\right)Y'_2(X_{s2})$	$Y_3(X_{s2})S^2 + \left(\frac{F-X}{m}\right)Y'_3(X_{s2})$	0	$S^2 + 2\zeta_{s2}\omega_{s2} S + \omega'^2_s$
$Y_1(X_{s3})S^2 + \left(\frac{F-X}{m}\right)Y'_1(X_{s3})$	$Y_2(X_{s3})S^2 + \left(\frac{F-X}{m}\right)Y'_2(X_{s3})$	$Y_3(X_{s3})S^2 + \left(\frac{F-X}{m}\right)Y'_3(X_{s3})$	0	0

BLE A.19

ONS - MATRIX REPRESENTATION

	$\frac{-\ell_{s3}}{I_{xx}} m_{s3} S^2 - \left(\frac{F-X}{m}\right)\frac{m_{s3}}{I_{xx}}$	C_1	S^2	0	$\left[\frac{\ell_{cg}}{I_{xx}} S^2 + \frac{I_E}{I_{xx}}\right] S^2 + \left[C_2 + \left(\frac{F-X}{m}\right)\frac{S_E}{I_{xx}}\right]$	η_1
	$\frac{m_{s3}}{m} S^2$	$-\frac{N'}{m}$	$-\left(\frac{F-X}{m}\right)$	$VS + \left(\frac{F-X}{m}\right)$	$-\frac{R'}{m}$	η_2
	0	1	-1	1	0	η_3
$X_{s2})\Big]$	$\frac{-m_{s3}}{M_1}\left[Y_1(X_{s3})S^2 + \left(\frac{F-X}{m}\right)Y_1'(X_{s3})\right]$	$\frac{-\sum_n (qA)\frac{\alpha C_{z\alpha}}{\alpha X_n}\Delta X_n Y_1(X_n)}{M_1}$	0	0	$\frac{\left[S_E Y_1(X_\beta) + I_E Y_1'(X_\beta)\right]S^2}{-M_1} - \frac{R' Y_1(X_\beta)}{M_1}$	Z_{s1}
$(X_{s2})\Big]$	$\frac{-m_{s3}}{M_2}\left[Y_2(X_{s3})S^2 + \left(\frac{F-X}{m}\right)Y_2'(X_{s3})\right]$	$\frac{-\sum_n (qA)\frac{\alpha C_{z\alpha}}{\alpha X_n}\Delta X_n Y_2(X_n)}{M_2}$	0	0	$\frac{\left[S_E Y_2(X_\beta) + I_E Y_2'(X_\beta)\right]S^2}{-M_2} - \frac{R' Y_2(X_\beta)}{M_2}$	Z_{s2}
$(X_{s2})\Big]$	$\frac{-m_{s3}}{M_3}\left[Y_3(X_{s3})S^2 + \left(\frac{F-X}{m}\right)Y_3'(X_{s3})\right]$	$\frac{-\sum_n (qA)\frac{\alpha C_{z\alpha}}{\alpha X_n}\Delta X_n Y_3(X_n)}{M_3}$	0	0	$\frac{\left[S_E Y_3(X_\beta) + I_E Y_3'(X_\beta)\right]S^2}{-M_3} - \frac{R' Y_3(X_\beta)}{M_3}$	Z_{s3}
	0	0	$-\ell_{s1}S^2 - \left(\frac{F-X}{m}\right)$	$VS + \left(\frac{F-X}{m}\right)$	0	α
	0	0	$-\ell_{s2}S^2 - \left(\frac{F-X}{m}\right)$	$VS + \left(\frac{F-X}{m}\right)$	0	ϕ_{cg}
	$S^2 + 2\zeta_{s3}\omega_{s3}S + \omega_{s3}^2$	0	$-\ell_{s3}S^2 - \left(\frac{F-X}{m}\right)$	$VS + \left(\frac{F-X}{m}\right)$	0	θ
						β_R

TABLE A.20

MATRIX COEFFICIENTS - STUDY VEHICLE I LIFT-OFF

(η_1)	(η_2)	(η_3)	(Z_{s1})
.0035547	-.015224	-.026947	$-.0021177s^2$ -.0016140
.492266	.74487	.90251	$.040191s^2$
$1.0s^2$ + .050370s +25.371	0	0	$-.052811s^2$ -.058548
0	$1.0s^2$ + .11990s +143.76	0	$-.042388s^2$ -.090087
0	0	$1.0s^2$ +.18130s +328.69	$-.011441s^2$ -.050573
$.55480s^2$ +.61506	$.40960s^2$ +.87052	$.25630s^2$ +1.1328	$1.0s^2$ +.12816s +4.5624
$-.35710s^2$ +.43030	$-.45810s^2$ -.15094	$-.28740s^2$ -.96609	0
$-.68750s^2$ +.029871	$.49560s^2$ -.96009	$1.4082s^2$ -.40285	0

(Z_{s2})	(Z_{s3})	(ϕ_{CG})	(B_R)
$.00077490s^2$ $-.0024660$	$.0026435s^2$ $-.0016162$	$1.0s^2$	$.0013520s^2$ $+.81214$
$.061407s^2$	$.040245s^2$	-12.252	-9.7975
$.051936s^2$ $-.062582$	$.065531s^2$ $-.0028472$	0	$-.042590s^2$ -23.160
$.072431s^2$ $+.023867$	$-.051356s^2$ $+.099489$	0	$-.048920s^2$ -25.163
$.019603s^2$ $+.065895$	$-.062950s^2$ $+.018008$	0	$-.021806s^2$ -10.849
0	0	$-16.076s^2$ -12.252	0
$1.0s^2$ $+.12816s$ 4.5624	0	$3.8500s^2$ -12.252	0
0	$1.0s^2$ $+.12816s$ $+4.5624$	$20.040s^2$ -12.252	0

TABLE A.21

MATRIX COEFFICIENTS - STUDY VEHICLE I MAXIMUM q

(η_1)	(η_2)	(η_3)	(Z_{s1})	$(Z_{s}$
-.011733	-.031197	-.043000	$-.0031734s^2$ -.0032175	-.0012 -.0050
1.13430	1.48980	1.70545	$+.067380s^2$	.1067
0	0	0	0	0
$1.0s^2$ $+.055040s$ +30.294	0	0	$-.078867s^2$ -.12421	.0204 -.1697
0	$1.0s^2$ $+.13350s$ +178.22	0	$-.10361s^2$ -.26755	.1323 -.1610
0	0	$1.0s^2$ $+.18430s$ +339.66	$-.040953s^2$ -.14186	.0813 +.0075
$.69840s^2$ +1.0999	$.59438s^2$ +1.5347	$.52760s^2$ +1.8276	$1.0s^2$ $+.16590s$ +7.6452	0
$-.11454s^2$ +.94881	$-.47920s^2$ +.58295	$-.66150s^2$ -.061398	0	$1.0s^2$ +.1659 +7.6452
$-.87140s^2$ +.21500	$.078450s^2$ -1.2429	$1.0367s^2$ -.72040	0	0

)	(Z_{s3})	(α)	(ϕ_{CG})	(θ)	(B_R)
$78s^2$ 80	$.0027184s^2$ $-.0030958$	$-.34210$	$1.0s^2$	0	$.0015903s^2$ $+1.0753$
s^2	$.064833s^2$	-7.2649	-21.113	$519.30s$ $+21.113$	-17.814
	0	1.0	-1.0	1.0	0
$4s^2$	$.094682s^2$ $-.023361$	0	0	0	$-.049999s^2$ -29.795
s^2	$-.013159s^2$ $+.20849$	0	0	0	$-.080455s^2$ -45.964
$9s^2$ 15	$-.077429s^2$ $+.053805$	0	0	0	$-.036708s^2$ -20.458
	0	0	$-20.825s^2$ -21.113	$519.30s$ $+21.113$	0
s	0	0	$-5.0850s^2$ -21.113	$519.30s$ $+21.113$	0
	$1.0s^2$ $+.16968s$ $+7.9975$	0	$18.540s^2$ -21.113	$519.30s$ $+21.113$	0

TABLE A.22

MATRIX COEFFICIENTS - STUDY VEHICLE I BURN-OUT

(η_1)	(η_2)	(η_3)	(Z_{s1})	(Z_{s2})
-.023222	-.10069	-.26893	$-.00028418s^2$ -.00031805	-.000397 -.000726
1.43344	2.59919	5.1304	$.0044159s^2$	.010086
0	0	0	0	0
$1.0s^2$ $.063770s$ 40.666	0	0	$-.013117s^2$ -.021835	-.012952 -.047559
0	$1.0s^2$ $.15680s$ 245.86	0	$-.0027556s^2$ -.0097106	.000962 -.018025
0	0	$1.0s^2$ $.29340s$ 860.83	$-.0011689s^2$ -.012010	.005563 -.014850
$.86950s^2$ 1.4474	$.75980s^2$ 2.6774	$.52030s^2$ 5.3458	$1.0s^2$ $.21488s$ 12.826	0
$.37590s^2$ 1.38020	$-.11620s^2$ 2.1760	$-1.0842s^2$ 2.8939	0	$1.0s^2$ $.22620s$ 14.212
$-.36440s^2$ .62914	$-.56050s^2$ -1.9758	$-.29790s^2$ -6.3405	0	0

	(Z_{s3})	(α)	(ϕ_{CG})	(θ)	(B_R)
$895s^2$ 44	$.0012729s^2$ -.010513	-.0043600	$1.0s^2$	0	$.0041737s^2$ 2.3254
s^2	$.14597s^2$	-.28974	-40.933	2520.0s 40.933	-32.792
	0	1.0	-1.0	1.0	0
s^2	$.18172s^2$ -.31374	0	0	0	$-.21974s^2$ -111.87
$57s^2$	$.067198s^2$ .23688	0	0	0	$-.056995s^2$ -26.863
$4s^2$	$.022123s^2$ .47088	0	0	0	$-.040910s^2$ -16.596
	0	0	$-36.574s^2$ -40.933	2520.0s 40.933	0
	0	0	$-22.420s^2$ -40.933	2520.0s 40.933	0
	$1.0s^2$ .28272s 22.202	0	$4.9560s^2$ -40.933	2520.0s 40.933	0

$\frac{F}{I_{xx}} Y_1(X_\beta) - \frac{F\ell_{cg}}{I_{xx}} Y_1'(X_\beta)$	$\frac{F}{I_{xx}} Y_2(X_\beta) - \frac{F\ell_{cg}}{I_{xx}} Y_2'(X_\beta)$	$\frac{F}{I_{xx}} Y_3(X_\beta) - \frac{F\ell_{cg}}{I_{xx}} Y_3'(X_\beta)$	$\frac{F}{I_{xx}} Y_4(X_\beta) - \frac{F\ell_{cg}}{I_{xx}} Y_4'(X_\beta)$
$\frac{F}{M} Y_1'(X_\beta)$	$\frac{F}{m} Y_2'(X_\beta)$	$\frac{F}{m} Y_3'(X_\beta)$	$\frac{F}{m} Y_4'(X_\beta)$
0	0	0	0
$S^2 + 2\zeta_1\omega_1 S + \omega_1^2$	0	0	0
0	$S^2 + 2\zeta_2\omega_2 S + \omega_2^2$	0	0
0	0	$S^2 + 2\zeta_3\omega_3 S + \omega_3^2$	0
0	0	0	$S^2 + 2\zeta_4\omega_4 S + \omega_4^2$
$Y_1(X_{S1})S^2 + \left(\frac{F-X}{m}\right)Y_1'(X_{S1})$	$Y_2(X_{S1})S^2 + \left(\frac{F-X}{m}\right)Y_2'(X_{S1})$	$Y_3(X_{S1})S^2 + \left(\frac{F-X}{m}\right)Y_3'(X_{S1})$	$Y_4(X_{S1})S^2 + \left(\frac{F-X}{m}\right)Y_4'(X_{S1})$
$Y_1(X_{S2})S^2 + \left(\frac{F-X}{m}\right)Y_1'(X_{S2})$	$Y_2(X_{S2})S^2 + \left(\frac{F-X}{m}\right)Y_2'(X_{S2})$	$Y_3(X_{S2})S^2 + \left(\frac{F-X}{m}\right)Y_3'(X_{S2})$	$Y_4(X_{S2})S^2 + \left(\frac{F-X}{m}\right)Y_4'(X_{S2})$
$Y_1(X_{S3})S^2 + \left(\frac{F-X}{m}\right)Y_1'(X_{S3})$	$Y_2(X_{S3})S^2 + \left(\frac{F-X}{m}\right)Y_2'(X_{S3})$	$Y_3(X_{S3})S^2 + \left(\frac{F-X}{m}\right)Y_3'(X_{S3})$	$Y_4(X_{S3})S^2 + \left(\frac{F-X}{m}\right)Y_4'(X_{S3})$

TABLE A.23

STUDY VEHICLE II EQUATIONS - MATRIX REPRESENTATION

$\frac{-\ell_{S1}}{I_{XX}} m_{S1} S^2 - \left(\frac{F-X}{m}\right)\frac{m_{S1}}{I_{XX}}$	$\frac{-\ell_{S2}}{I_{XX}} m_{S2} S^2 - \left(\frac{F-X}{m}\right)\frac{m_{S2}}{I_{XX}}$	$\frac{-\ell_{S3}}{I_{XX}} m_{S3} S^2 - \left(\frac{F-X}{m}\right)\frac{m_{S3}}{I_{XX}}$	C_1
$\frac{m_{S1}}{m} S^2$	$\frac{m_{S2}}{m} S^2$	$\frac{m_{S3}}{m} S^2$	$-\left(\frac{N'}{m}\right)$
0	0	0	1
$\frac{-m_{S1}}{M_1}\left[Y_1(X_{S1})S^2 + \left(\frac{F-X}{m}\right)Y_1'(X_{S1})\right]$	$\frac{-m_{S2}}{M_1}\left[Y_1(X_{S2})S^2 + \left(\frac{F-X}{m}\right)Y_1'(X_{S2})\right]$	$\frac{-m_{S3}}{M_1}\left[Y_1(X_{S3})S^2 + \left(\frac{F-X}{m}\right)Y_1'(X_{S3})\right]$	$\frac{-\sum_n (qA)\frac{\alpha C_{Z\alpha}}{\alpha X_n}\Delta X_n Y_1(}{M_1}$
$\frac{-m_{S1}}{M_2}\left[Y_2(X_{S1})S^2 + \left(\frac{F-X}{m}\right)Y_2'(X_{S1})\right]$	$\frac{-m_{S2}}{M_2}\left[Y_2(X_{S2})S^2 + \left(\frac{F-X}{m}\right)Y_2'(X_{S2})\right]$	$\frac{-m_{S3}}{M_2}\left[Y_2(X_{S3})S^2 + \left(\frac{F-X}{m}\right)Y_2'(X_{S3})\right]$	$\frac{-\sum_n (qA)\frac{\alpha C_{Z\alpha}}{\alpha X_n}\Delta X_n Y_2(}{M_2}$
$\frac{-m_{S1}}{M_3}\left[Y_3(X_{S1})S^2 + \left(\frac{F-X}{m}\right)Y_3'(X_{S1})\right]$	$\frac{-m_{S2}}{M_3}\left[Y_3(X_{S2})S^2 + \left(\frac{F-X}{m}\right)Y_3'(X_{S2})\right]$	$\frac{-m_{S3}}{M_3}\left[Y_3(X_{S3})S^2 + \left(\frac{F-X}{m}\right)Y_3'(X_{S3})\right]$	$\frac{-\sum_n (qA)\frac{\alpha C_{Z\alpha}}{\alpha X_n}\Delta X_n Y_3(}{M_3}$
$\frac{-m_{S1}}{M_4}\left[Y_4(X_{S1})S^2 + \left(\frac{F-X}{m}\right)Y_4'(X_{S1})\right]$	$\frac{-m_{S2}}{M_4}\left[Y_4(X_{S2})S^2 + \left(\frac{F-X}{m}\right)Y_4'(X_{S2})\right]$	$\frac{-m_{S3}}{M_4}\left[Y_4(X_{S3})S^2 + \left(\frac{F-X}{m}\right)Y_4'(X_{S3})\right]$	$\frac{-\sum_n (qA)\frac{\alpha C_{Z\alpha}}{\alpha X_n}\Delta X_n Y_4(}{M_4}$
$S^2 + 2\zeta_{S1}\omega_{S1} S + \omega_{S1}^2$	0	0	0
0	$S^2 + 2\zeta_{S2}\omega_{S2} S + \omega_{S2}^2$	0	0
0	0	$S^2 + 2\zeta_{S3}\omega_{S3} S + \omega_{S3}^2$	0

	S^2	0	$\left[\frac{\ell_{cg}}{I_{XX}}\right]S_E + \left[C_2 + \left(\frac{F-X}{m}\right)\frac{S_E}{I_{XX}}\right]$	η_1
	$-\left(\frac{F-X}{m}\right)$	$VS + \left(\frac{F-X}{m}\right)$	$-\frac{R'}{m}$	η_2
	-1	1	0	η_3
$(_n)$	0	0	$\frac{\left[S_E Y_1(X_\beta) + I_E Y'_1(X_\beta)\right]S^2}{-M_1} - \frac{R' Y_1(X_\beta)}{M_1}$	η_4
$X_n)$	0	0	$\frac{\left[S_E Y_2(X_\beta) + I_E Y'_2(X_\beta)\right]S^2}{-M_2} - \frac{R' Y_2(X_\beta)}{M_2}$	Z_{S1}
$X_n)$	0	0	$\frac{\left[S_E Y_3(X_\beta) + I_E Y'_3(X_\beta)\right]S^2}{-M_3} - \frac{R' Y_3(X_\beta)}{M_3}$	Z_{S2}
$_n)$	0	0	$\frac{\left[S_E Y_4(X_\beta) + I_E Y'_4(X_\beta)\right]S^2}{-M_4} - \frac{R' Y_4(X_\beta)}{M_4}$	Z_{S3}
	$-\ell_{S1} S^2 - \left(\frac{F-X}{m}\right)$	$VS + \left(\frac{F-X}{m}\right)$	0	α
	$-\ell_{S2} S^2 - \left(\frac{F-X}{m}\right)$	$VS + \left(\frac{F-X}{m}\right)$	0	ϕ_{cg}
	$-\ell_{S3} S^2 - \left(\frac{F-X}{m}\right)$	$VS + \left(\frac{F-X}{m}\right)$	0	θ
				β_R

$= 0$

TABLE A.24

MATRIX COEFFICIENTS - STUDY VEHICLE II LIFT-OFF

(η_1)	(η_2)	(η_3)	(η_4)	(Z_{s1})
-.0052308	-.011682	-.018996	- .02507	-.00085597 -.0004834
.4263	.54302	.67544	.78554	$.026343s^2$
$1.0s^2$ +.021550s +4.6440	0	0	0	$-.026173s^2$ -.025181
0	$1.0s^2$ +.050590s +25.593	0	0	$-.019008s^2$ -.039392
0	0	$1.0s^2$ +.087780s +77.053	0	$-.0049096s^2$ -.052113
0	0	0	$1.0s^2$ +.12350s +152.52	$.0035783s^2$ -.027875
$.45316s^2$ +.43599	$.28197s^2$ +.58434	$.071350s^2$ +.75734	$-.11228s^2$ +.87467	$1.0s^2$ +.12810s +4.5582
$-.39855s^2$ +.30823	$-.45674s^2$ -.011525	$-.19405s^2$ -.57024	$.21434s^2$ -.86327	0
$-.69942s^2$ +.069885	$.029080s^2$ -.58066	$.90233s^2$ -.36181	$.80087s^2$ +.78701	0

	(Z_{s2})	(Z_{s3})	(ϕ_{CG})	(B_R)
^{2}	$.00032228s^2$ $-.00073858$	$.00092976s^2$ $-.00048405$	$1.0s^2$	$.00059803s^2$ $+.32099$
	$.040248s^2$	$.026378s^2$	-12.260	-6.1303
	$.035170s^2$ $-.027200$	$.040450s^2$ $-.0040418$	0	$-.023901s^2$ -12.506
	$.047043s^2$ $+.0011870$	$-.0019630s^2$ $.039197$	0	$-.028187s^2$ -14.303
	$.020401s^2$ $+.059952$	$-.062173s^2$ $.024930$	0	$-.029117s^2$ -14.263
	$-.010436s^2$ $+.042035$	$-.025557s^2$ $-.025115$	0	$-.013623s^2$ -6.4795
	0	0	$-21.710s^2$ -12.260	0
	$1.0s^2$ $+.12810s$ $+4.5582$	0	$5.3500s^2$ -12.260	0
	0	$1.0s^2$ $+.12810s$ $+4.5582$	$23.550s^2$ -12.260	0

TABLE A.25

MATRIX COEFFICIENTS - STUDY VEHICLE II MAXIMUM q

(η_1)	(η_2)	(η_3)	(η_4)	(Z_{s1})	
-.010417	-.021631	-.030951	-.038312	$-.0014303s^2$ -.00096862	-.
.78070	1.04210	1.25954	1.43148	$.043645s^2$	.
0	0	0	0	0	
$1.0s^2$ +.023170s +5.3684	0	0	0	$-.044528s^2$ -.052007	. -.
0	$1.0s^2$ +.056420s +31.832	0	0	$-.053359s^2$ -.10808	. -.
0	0	$1.0s^2$ +.091740s +84.162	0	$-.049952s^2$ -.16375	. -.
0	0	0	$1.0s^2$ +.12497s +156.17	$-.0067638s^2$ -.034080	. +.
$.65476s^2$ +.76473	$.53155s^2$ +1.0766	$.42207s^2$ +1.3835	$.32954s^2$ +1.6604	$1.0s^2$ +.16578s +7.6341	
$-.078870s^2$ +.67203	$-.38282s^2$ +.53918	$-.55456s^2$ +.013243	$-.60395s^2$ -.77735	0	1. +. +7.
$-.81102s^2$ +.21399	$-.30300s^2$ -.79290	$.56487s^2$ -.59468	$1.2050s^2$ +1.5828	0	

(Z_{s2})	(Z_{s3})	(α)	(ϕ_{CG})	(θ)	(B_R)
$)0073888s^2$ $)015347$	$.00089339s^2$ $-.00093200$	$-.072600$	$1.0s^2$	0	$.00073687s^2$ $+.44647$
$)69155s^2$	$.041995s^2$	-5.5929	-21.020	519.30s $+21.02$	-10.937
0	0	1.0	-1.0	1.0	0
$)084986s^2$ $)72415$	$.053069s^2$ $-.014002$	0	0	0	$-.027069s^2$ -15.826
$)60890s^2$ $)85762$	$.029266s^2$ $+.076587$	0	0	0	$-.040478s^2$ -22.768
$L0399s^2$ $)024834$	$-.064325s^2$ $+.067720$	0	0	0	$-.048250s^2$ -26.272
$)19641s^2$ $)25280$	$-.023798s^2$ $-.031260$	0	0	0	$-.0084431s^2$ -4.4797
0	0	0	$-31.040s^2$ -21.020	519.30s $+21.02$	0
$)s^2$ $L6578s$ 5341	0	0	$-10.120s^2$ -21.020	519.30s $+21.02$	0
0	$1.0s^2$ $+.16956s$ $+7.9862$	0	$20.150s^2$ -21.020	519.30s $+21.02$	0

TABLE A.26

MATRIX COEFFICIENTS - STUDY VEHICLE II BURN-OUT

(η_1)	(η_2)	(η_3)	(η_4)	(Z_{s1})	
-.026724	-.073175	-.16000	-.42341	$-.00022396s^2$ -.00019404	-
1.10948	1.66054	2.6906	5.8178	$.0029034s^2$	
0	0	0	0	0	
$1.0s^2$ $+.029130s$ $+8.4855$	0	0	0	$-.016651s^2$ -.021063	-
0	$1.0s^2$ $+.065890s$ $+43.414$	0	0	$-.0095385s^2$ -.019542	-
0	0	$1.0s^2$ $+.11705s$ $+137.00$	0	$-.0014083s^2$ -.0054651	-
0	0	0	$1.0s^2$ $+.24849s$ $+617.47$	$-.00061221s^2$ -.0099633	-
$.88018s^2$ $+1.1134$	$.82030s^2$ $+1.6806$	$.7082s^2$ $+2.7481$	$.36830s^2$ $+5.9938$	$1.0s^2$ $+.21474s$ $+12.809$	
$.49173s^2$ $+1.0732$	$.24804s^2$ $+1.4720$	$-.19102s^2$ $+2.0709$	$-1.3624s^2$ $+2.7803$	0	1. + +14.
$-.15246s^2$ $+.67237$	$-.29611s^2$ -.55353	$-.30529s^2$ -3.6264	$.12556s^2$ -8.7773	0	

(Z_{s2})	(Z_{s3})	(α)	(θ_{CG})	(ϕ)	(B_R)
$.00035545s^2$ $.00044321$	$-.00071045s^2$ $-.0064145$	$.0012400$	$1.0s^2$	0	$.0032747s^2$ $+2.1641$
$.0066316s^2$	$.095978s^2$	$-.20934$	-52.818	$2520.5s$ $+52.818$	-26.416
0	0	1.0	-1.0	1.0	0
$.021247s^2$ $.046375$	$.095342s^2$ $-.42047$	0	0	0	$-.25464s^2$ -164.90
$.0065876s^2$ $.039095$	$.11381s^2$ $+.21276$	0	0	0	$-.15835s^2$ -99.201
$.00086765s^2$ $.0094069$	$.020069s^2$ $+.23840$	0	0	0	$-.027677s^2$ -16.280
$.0051728s^2$ $.010556$	$-.0068993s^2$ $+.48230$	0	0	0	$-.024688s^2$ -11.898
0	0	0	$-60.960s^2$ -52.818	$2520.5s$ $+52.818$	0
$.0s^2$ $.22608s$ $.197$	0	0	$-42.360s^2$ -52.818	$2520.5s$ $+52.818$	0
0	$1.0s^2$ $+.28260s$ $+22.184$	0	$-5.8500s^2$ -52.818	$2520.5s$ $+52.818$	0

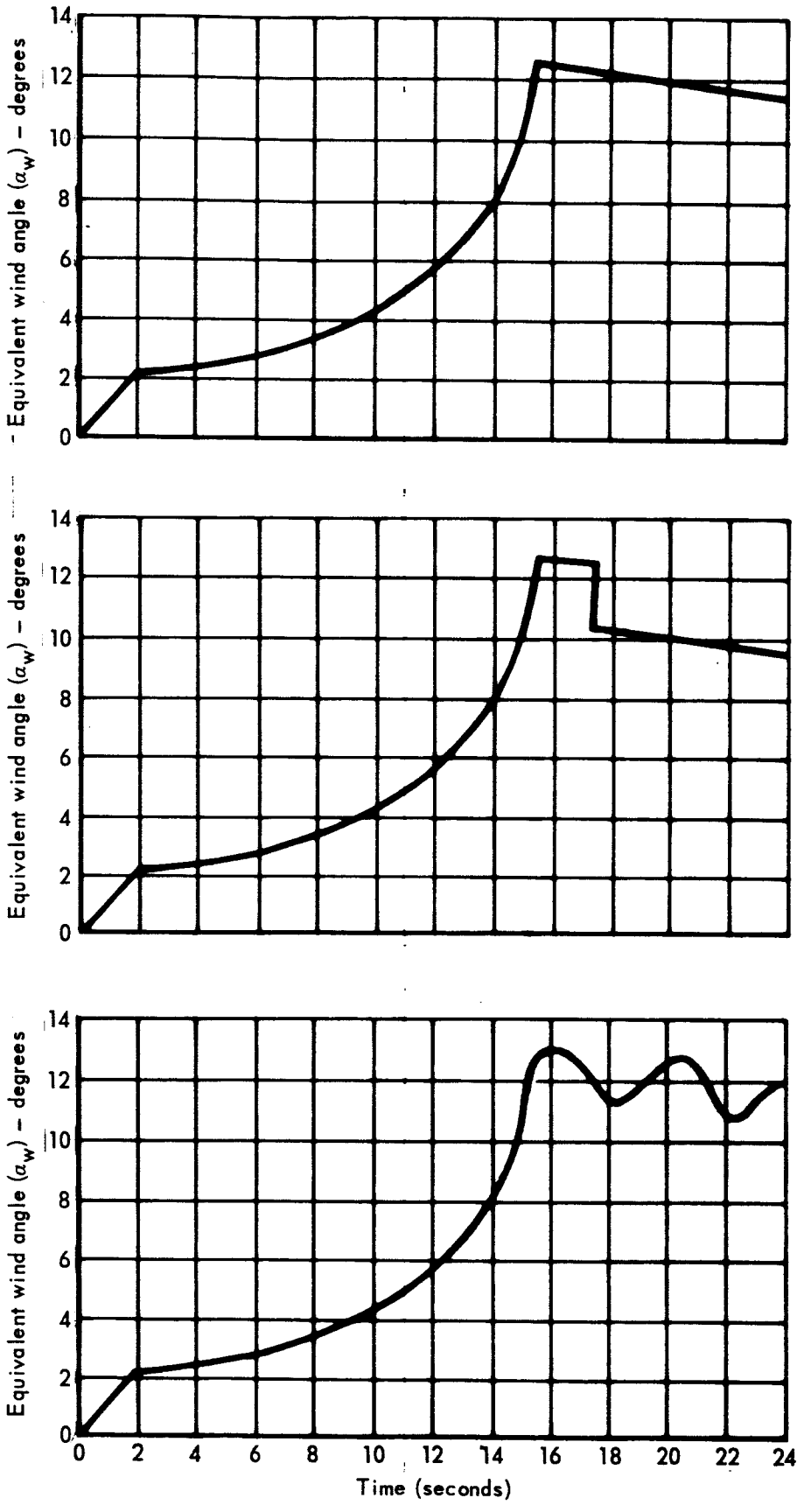

Figure A.3 Synthetic Wind Profiles

APPENDIX B

ANALOG-DIGITAL COMPUTER SIMULATION

This appendix presents the mechanization details of the Digital Filter hybrid simulation studies which used the PACE 231R analog computer and the UNIVAC 1218 digital computer. The analog computer simulated the study vehicle equations of motion, the engine dynamics and the control loop compensating networks. Control signals generated by the analog computer were applied to the UNIVAC 1218 digital computer through A-D conversion equipment. Individual programs were written for the UNIVAC 1218 digital computer for the Digital Adaptive Filter and for the polynomial filter.

The UNIVAC 1218 digital computer input and output signals were processed by the ADAGE A-D and D-A conversion equipment. The computational speed (memory access time (read and write) of 4 micro seconds), the core memory (16 thousand) and the fixed point (fixed word 18 bits) features of the UNIVAC 1218 digital computer were sufficient to provide real time operation for the studied range of sampling rates and digital computer program lengths.

B.1 Digital Filter Polynomial Curve Fit Program

The polynomial curve fit is a least-squares polynomial approximation to a given number of dependent variable values (samples), all of which are assumed to be equally reliable. In general the approximation can be performed to any desired degree polynomial; however, the fitted polynomial in the digital simulation was limited to the second degree. The following specific equations which are based on a derivation given in Reference (2), were mechanized on the UNIVAC 1218:

$$A_i = \frac{1}{R_i} \sum_{N=-M}^{+M} f\,(NT)\; P_i\,(N,2M) \qquad (B.1)$$

where A_i is the polynomial approximation and

$$R_i = \sum_{N=-M}^{+M} P_i^{\,2}\,(N,2M) \qquad (B.2)$$

$f\,(NT)$ = filter input samples

$$M = \frac{M'(\text{number of samples considered}) - 1}{2}$$

(M' is an integer)

T = sample period

i = 0, 1, or 2

and

$$P_0 (N,2M) = 1 \tag{B.3}$$

$$P_1 (N,2M) = \frac{N}{M} \tag{B.4}$$

$$P_2 (N,2M) = \frac{3N^2 - M(M+1)}{M(2M-1)} \tag{B.5}$$

The least-squares fit polynomial approximation for t = M T (output corresponding to the most recent sample) is defined as:

$$y(t = M\,T) = \sum_{i=0}^{n} A_i \tag{B.6}$$

where n = 0, 1, or 2

The value of n corresponds to zero, first, and second degree polynomial curve fitting. Since equations (B.2) through (B.5) are not functions of the sample values, they were evaluated only once prior to the hybrid simulation run for selected value of M'. Prior to a run the computer sample storage block of 2M +1 samples was filled with zeros. As the samples were received from the A-D converter, each value in the storage block was shifted one location, the oldest value being shifted out of the block.

B.2 Digital Adaptive Filter Simulation

The hybrid simulation of the Digital Adaptive Filter had the following equations mechanized on the UNIVAC 1218. The fitted curve forms (also the digital filter output) programmed were

(1) Two parameter fitting

$$e_F (t) = A\epsilon^{-\alpha t} \cos \beta t + B\epsilon^{-\alpha t} \sin \beta t \tag{B.7}$$

(2) Three parameter fitting

$$e_F (t) = A\epsilon^{-\alpha t} \cos \beta t + B\epsilon^{-\alpha t} \sin \beta t + C\epsilon^{-\delta t} \tag{B.8}$$

where α and β for two parameter fitting and α, β and δ for three parameter fittings were preselected program inputs for each hybrid run. The digital filter program solved for the amplitude coefficients A, B, and C from the following expressions.

Two Parameter Fitting

$$\begin{bmatrix} A \\ B \end{bmatrix} = \begin{bmatrix} \bar{u}_A \cdot \bar{u}_A & \bar{u}_A \cdot \bar{u}_B \\ \bar{u}_B \cdot \bar{u}_A & \bar{u}_B \cdot \bar{u}_B \end{bmatrix}^{-1} \begin{bmatrix} \bar{u}_A \cdot \bar{E} \\ \bar{u}_B \cdot \bar{E} \end{bmatrix} \tag{B.9}$$

Three Parameter Fitting

$$\begin{bmatrix} A \\ B \\ C \end{bmatrix} = \begin{bmatrix} \bar{u}_A \cdot \bar{u}_A & \bar{u}_A \cdot \bar{u}_B & \bar{u}_A \cdot \bar{u}_C \\ \bar{u}_B \cdot \bar{u}_A & \bar{u}_B \cdot \bar{u}_B & \bar{u}_B \cdot \bar{u}_C \\ \bar{u}_C \cdot \bar{u}_A & \bar{u}_C \cdot \bar{u}_B & \bar{u}_C \cdot \bar{u}_C \end{bmatrix}^{-1} \begin{bmatrix} \bar{u}_A \cdot \bar{E} \\ \bar{u}_B \cdot \bar{E} \\ \bar{u}_C \cdot \bar{E} \end{bmatrix} \tag{B.10}$$

where

$u_{Ai} = e^{-\alpha t_i} \cos \beta t_i \qquad u_{Ci} = e^{-\delta t_i}$

$u_{Bi} = e^{-\alpha t_i} \sin \beta t_i \qquad i = 0,1,---M_{max}-1$

and, as an example

$$\bar{u}_A \cdot \bar{u}_B = \sum_{i=1}^{M} u_{A_i} u_{B_i}$$

also

$$\bar{u}_A \cdot \bar{E} = \sum_{i=1}^{M} u_{A_i} E_i$$

where E_i is the value of the i^{th} sample of the stored input signal. The value of M was increased by 1 as each input sample was received, starting with M = 1, until M = M_{max} (the maximum number of samples to be stored) was reached. After the memory is filled the oldest stored sample is dropped as each new sample is received.

The program also included the fade-in logic which provided for the comparison of the two most recent samples. If a discontinuity exceeding a predetermined value was detected in the sampled signal or its first derivative, the curve fitting process was restarted.

B.4 Analog Computer Simulation

The analog computer diagram of the study vehicle equations of motion for the rigid body, elastic body, and sloshing propellants, together with the feedback sensor equations is illustrated in Figures (B.1) and (B.2). The .

computer mechanization of the two control methods studied are illustrated individually on Figures B.3 and B.4 for the Polynomial Curve Fit and the Digital Adaptive Filter loops, respectively. The diode function generator circuits used to generate the wind profiles are omitted from the diagrams. For simplicity, the analog computer is shown tied directly to the UNIVAC 1218 digital computer. The A-D and D-A conversion blocks are omitted.

The Polynomial Curve Fit Control Loop, Figure B.3, accepted inputs from all four feedback sensors. Each of these signals was available directly or as an output of the Polynomial Curve Fit program. The Polynomial Curve Fit Program outputs were each available as a zero, one, or two degree polynomial curve fit. The computer parameters varied were the sample rate at which the UNIVAC 1218 input signals were processed and the number of stored samples as determined by M (Equation B.2).

The Digital Adaptive Filter Control Loop, Figure B.4, contained two separate error summation and filter channels, one for the digital filter control and one for the secondary filter control. Control was alternated between the two loops manually as a function of time. The error signal sample rate and the number of samples stored in the UNIVAC 1218 were both capable of being varied between runs.

As is the case with most analog computer simulations, numerous changes were made in the individual components and the system scaling and switching to satisfy the specific study requirements.

The nominal potentiometer settings used for study vehicles I and II are tabulated in Table B.1. Toggle switches provided on the PACE analog console were connected to provide for necessary sign inversions when the simulation was changed from one flight time or study vehicle to another. Additional switches were utilized to connect or remove the bending and slosh modes from the simulation. The switch positions as a function of study vehicle and flight time are defined in Table B.2

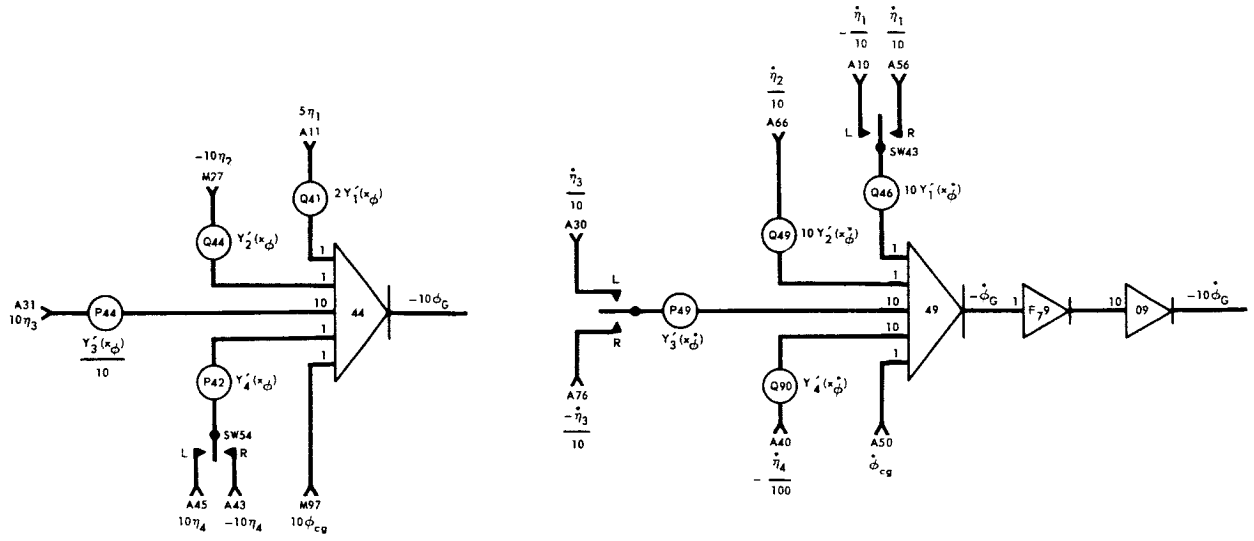

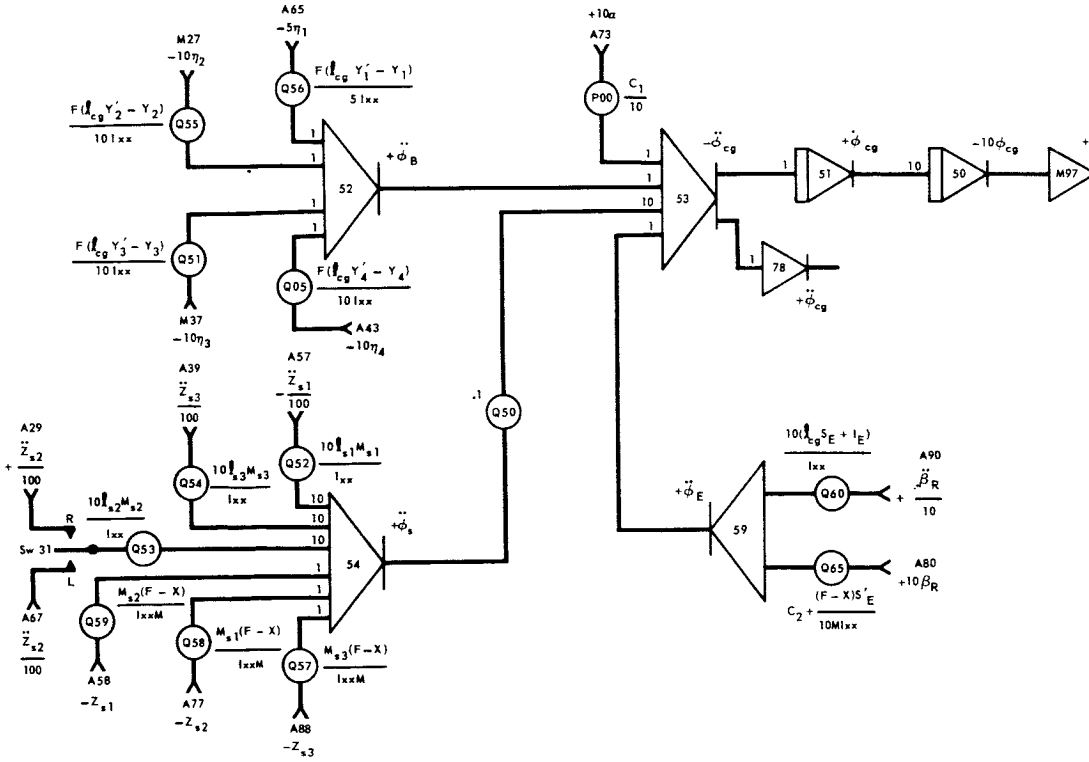

222-1

Figure B.1 Analog Computer Rigid Body and Sensor Simulation

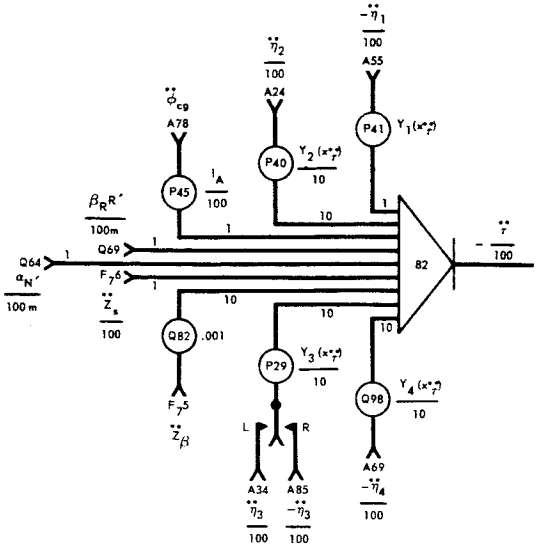

ACCELERATION SENSOR

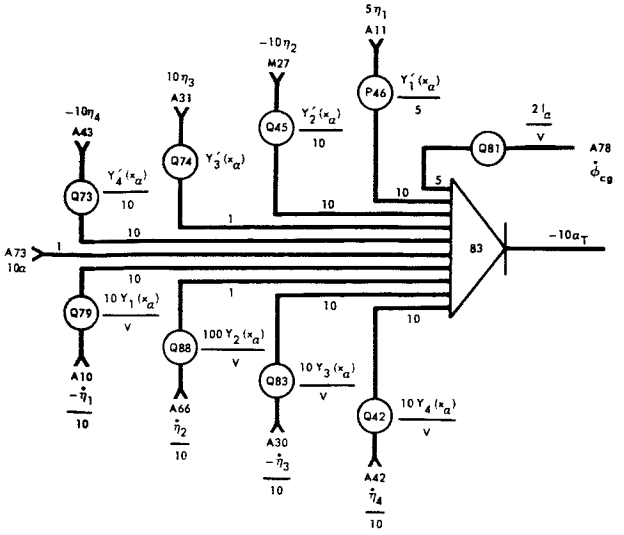

ANGLE OF ATTACK SENSOR

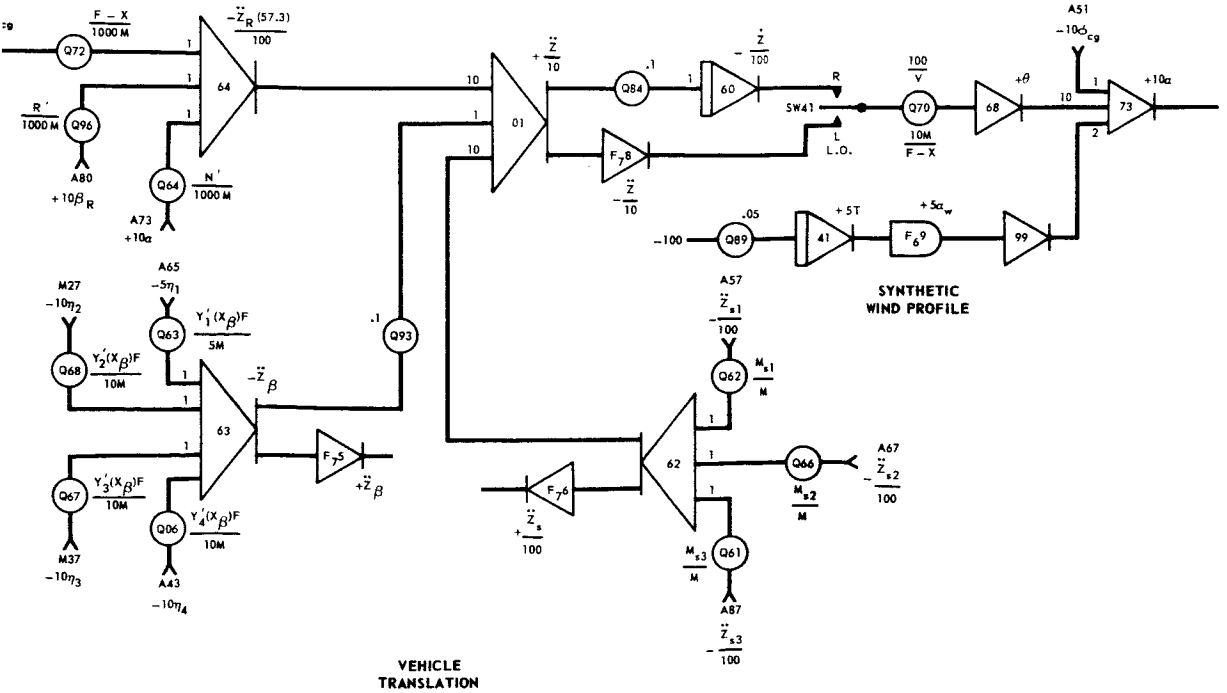

SYNTHETIC WIND PROFILE

VEHICLE TRANSLATION

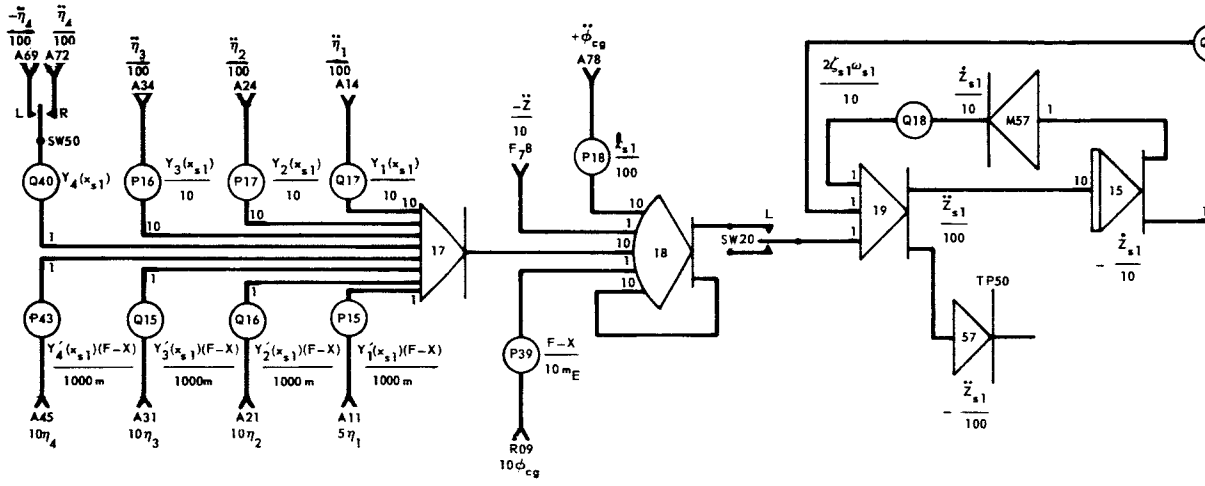

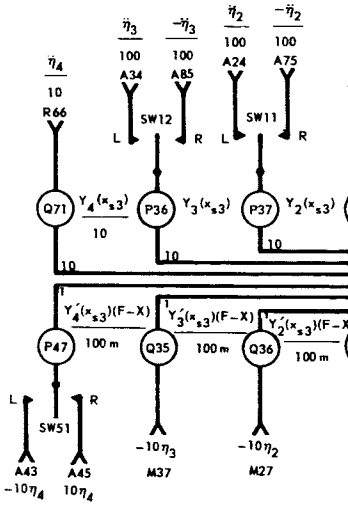

223-1

Figure B.2 - Analog Computer Vehicle Bending and Propellant Slosh Simulation

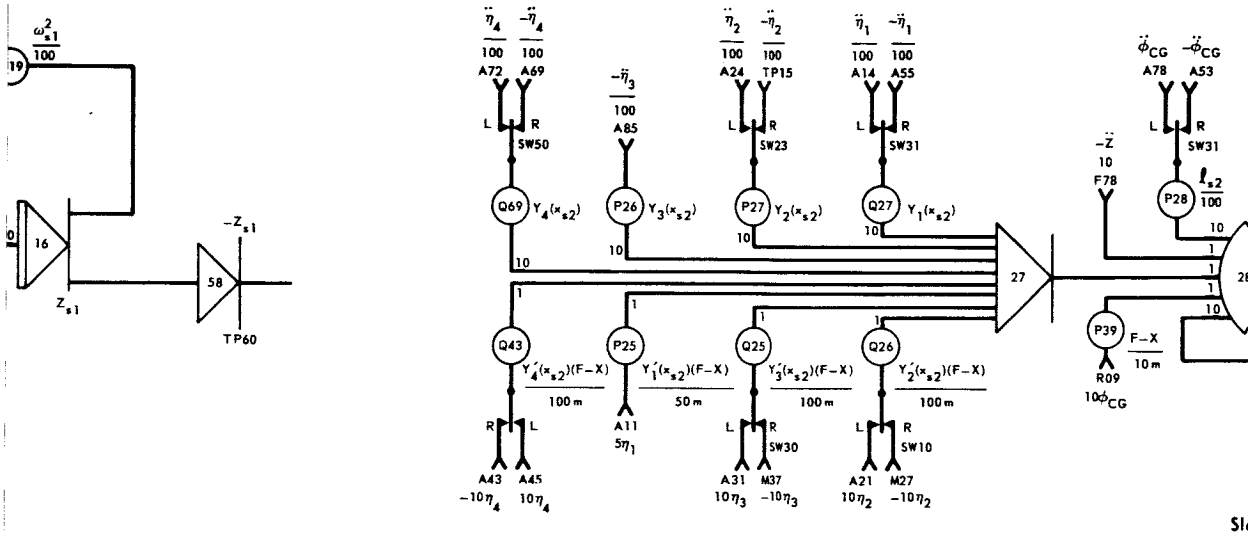

Sl

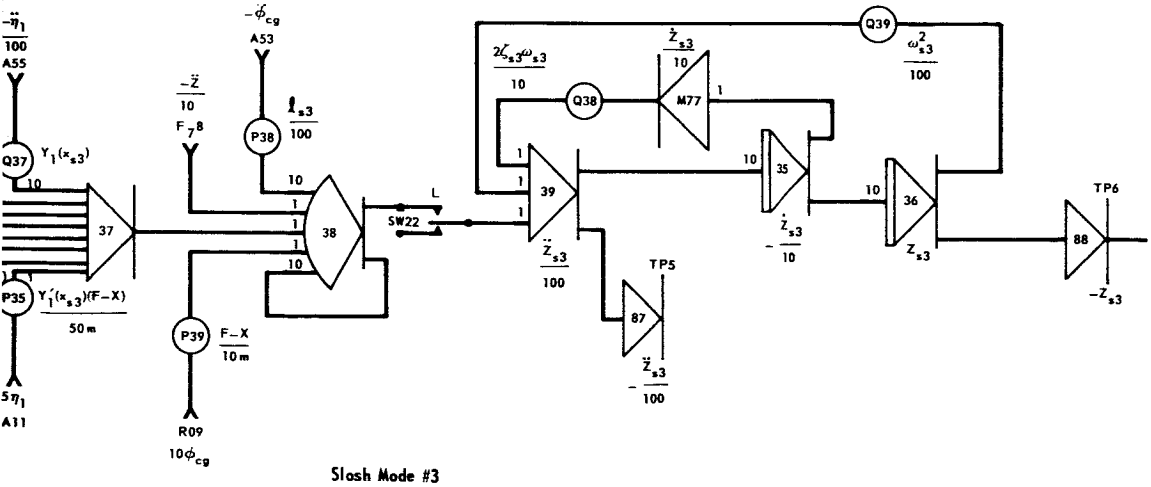

Slash Mode #3

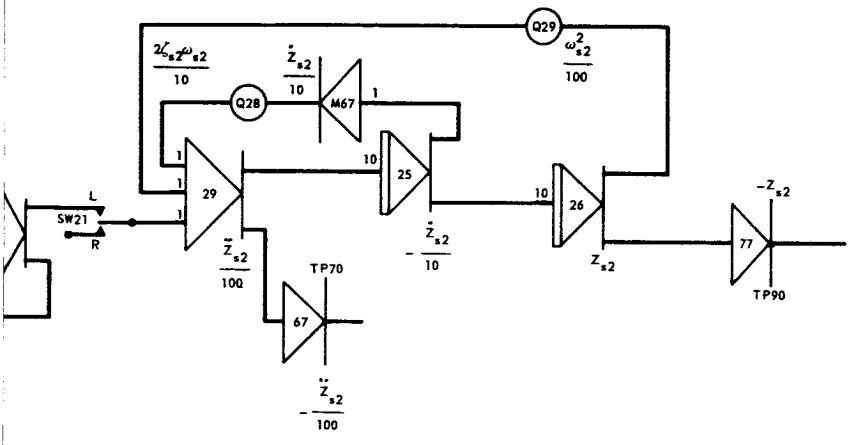
Q29
$\frac{2\zeta_{s2}\omega_{s2}}{10}$
$\frac{\dot{Z}_{s2}}{10}$
$\frac{\omega_{s2}^2}{100}$
Q28
M67
1
10
25
29
L
SW21
R
$\frac{\ddot{Z}_{s2}}{100}$
$-\frac{\dot{Z}_{s2}}{10}$
10
26
Z_{s2}
$-Z_{s2}$
77
TP90
TP70
67
$-\frac{\ddot{Z}_{s2}}{100}$

sh Mode #2

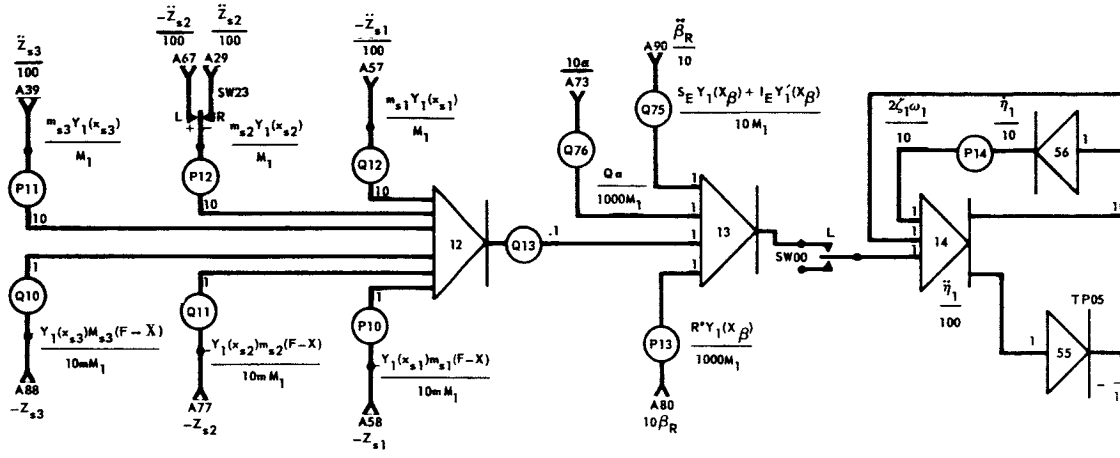

Bending Mode #1

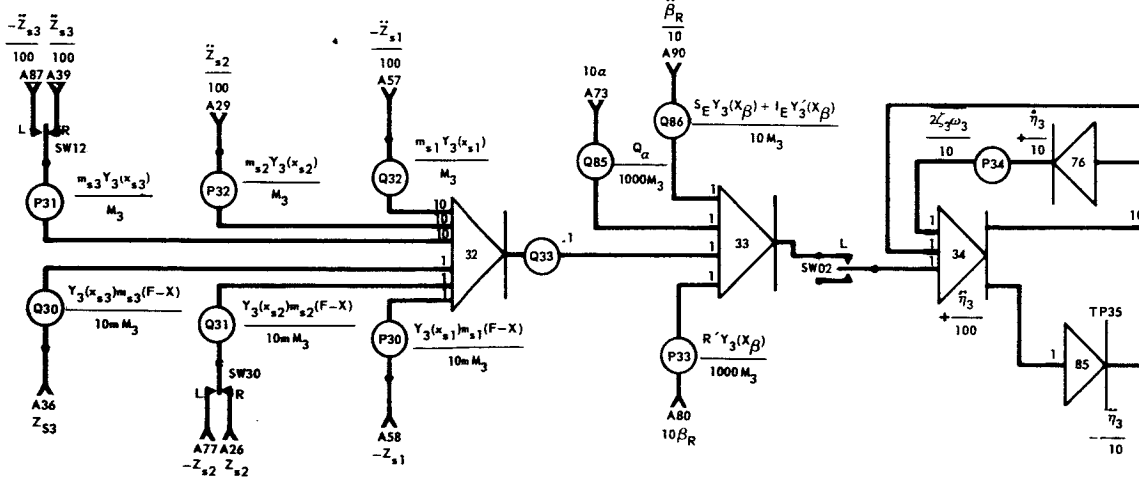

Bending Mode #3

224-1

Figure B.2 Analog Computer Vehicle Bending and Propellant Slosh Simulation

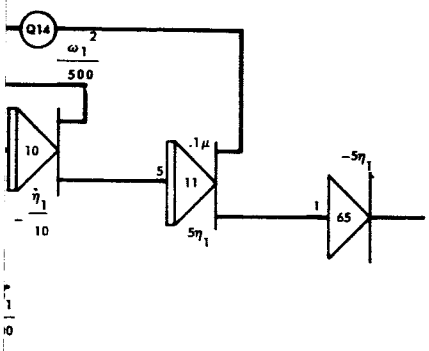
Q14
$\frac{\omega_1^2}{500}$
10
$\frac{\dot{\eta}_1}{10}$
.1μ
11
$5\eta_1$
$-5\eta_1$
65

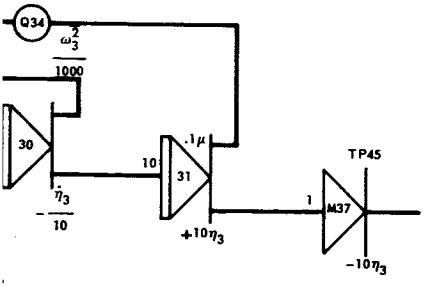
Q34
$\frac{\omega_3^2}{1000}$
30
$\frac{\dot{\eta}_3}{10}$
.1μ
31
$+10\eta_3$
TP45
M37
$-10\eta_3$

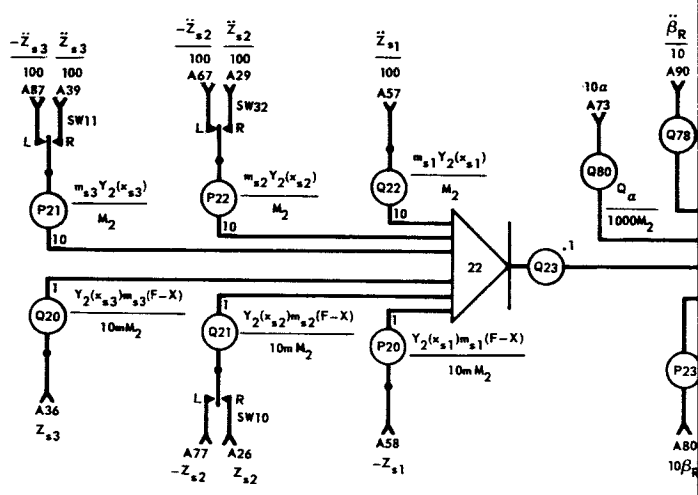
$\frac{-\ddot{z}_{s3}}{100}$ A87
$\frac{\ddot{z}_{s3}}{100}$ A39
SW11
$\frac{m_{s3}Y_2(x_{s3})}{M_2}$
P21
$\frac{-\ddot{z}_{s2}}{100}$ A67
$\frac{\ddot{z}_{s2}}{100}$ A29
SW32
$\frac{m_{s2}Y_2(x_{s2})}{M_2}$
P22
$\frac{\ddot{z}_{s1}}{100}$ A57
$\frac{m_{s1}Y_2(x_{s1})}{M_2}$
Q22
$\frac{\ddot{\beta}_R}{10}$ A90
Q78
10α A73
Q80
$\frac{Q_\alpha}{1000M_2}$
22
Q23
.1
$\frac{Y_2(x_{s3})m_{s3}(F-X)}{10mM_2}$
Q20
$\frac{Y_2(x_{s2})m_{s2}(F-X)}{10mM_2}$
Q21
$\frac{Y_2(x_{s1})m_{s1}(F-X)}{10mM_2}$
P20
P23
A36 Z_{s3}
SW10
A77 $-Z_{s2}$
A26 Z_{s2}
A58 $-Z_{s1}$
A80 $10\beta_R$

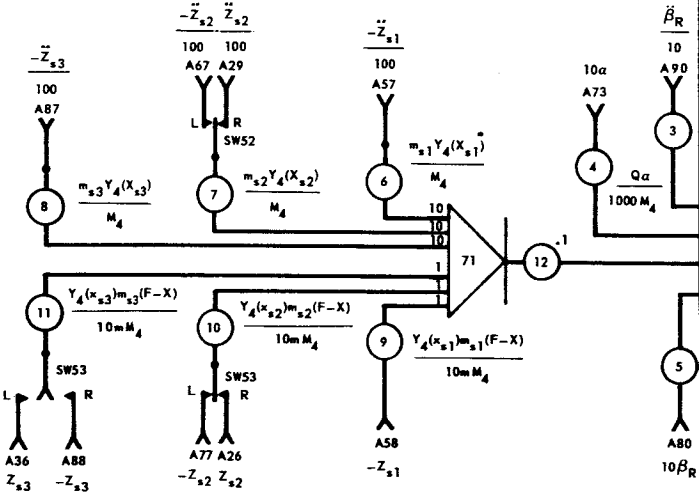
$\frac{-\ddot{z}_{s3}}{100}$ A87
$\frac{-\ddot{z}_{s2}}{100}$ A67
$\frac{\ddot{z}_{s2}}{100}$ A29
SW52
$\frac{-\ddot{z}_{s1}}{100}$ A57
$\frac{\ddot{\beta}_R}{10}$ A90
10α A73
8
$\frac{m_{s3}Y_4(X_{s3})}{M_4}$
7
$\frac{m_{s2}Y_4(X_{s2})}{M_4}$
6
$\frac{m_{s1}Y_4(X_{s1})}{M_4}$
3
4
$\frac{Q_\alpha}{1000M_4}$
71
12
.1
11
$\frac{Y_4(x_{s3})m_{s3}(F-X)}{10mM_4}$
10
$\frac{Y_4(x_{s2})m_{s2}(F-X)}{10mM_4}$
9
$\frac{Y_4(x_{s1})m_{s1}(F-X)}{10mM_4}$
5
SW53
A36 Z_{s3}
A88 $-Z_{s3}$
A77 $-Z_{s2}$
A26 Z_{s2}
A58 $-Z_{s1}$
A80 $10\beta_R$

224-2

(Cont.)

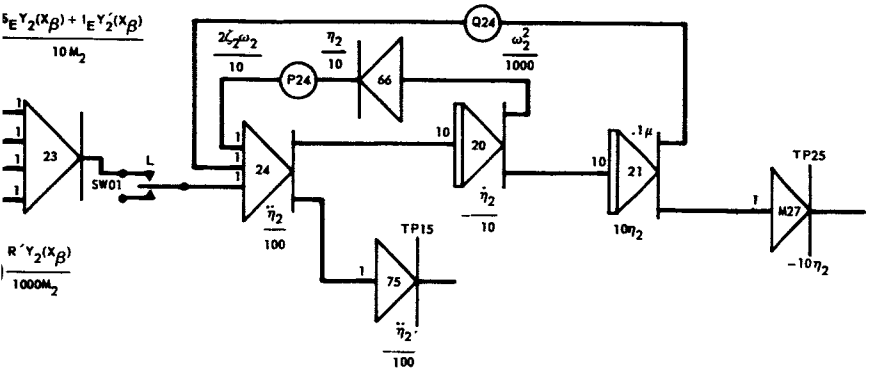

Bending Mode #2

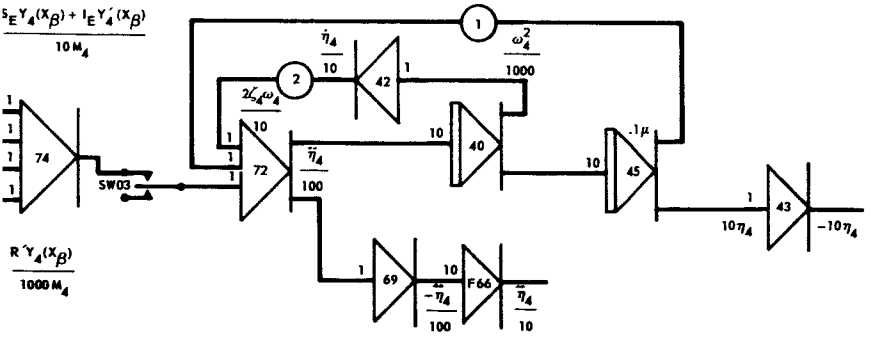

Bending Mode #4

224-3

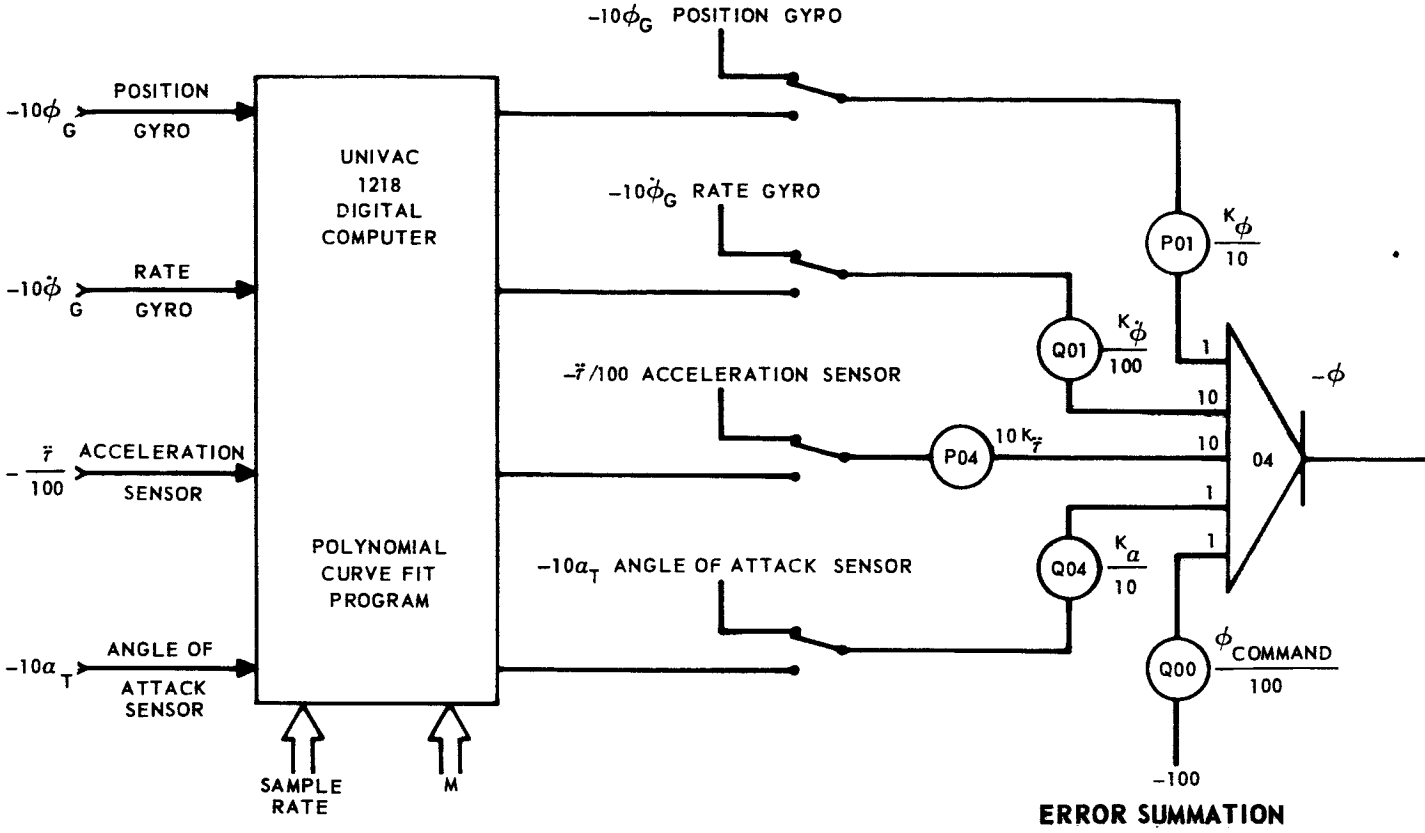

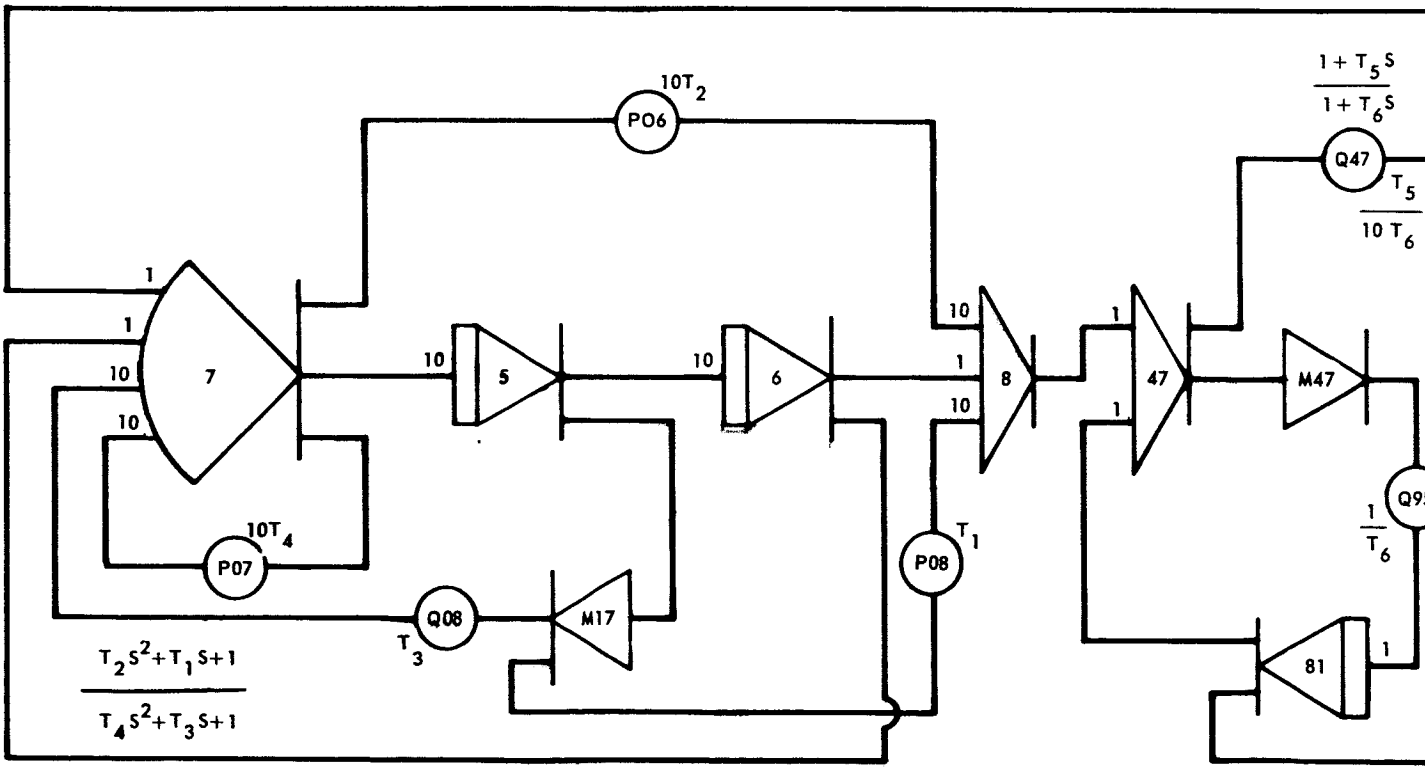

Figure B.3 Analog Computer Polynomial Curve Fit Control Loop Simulation

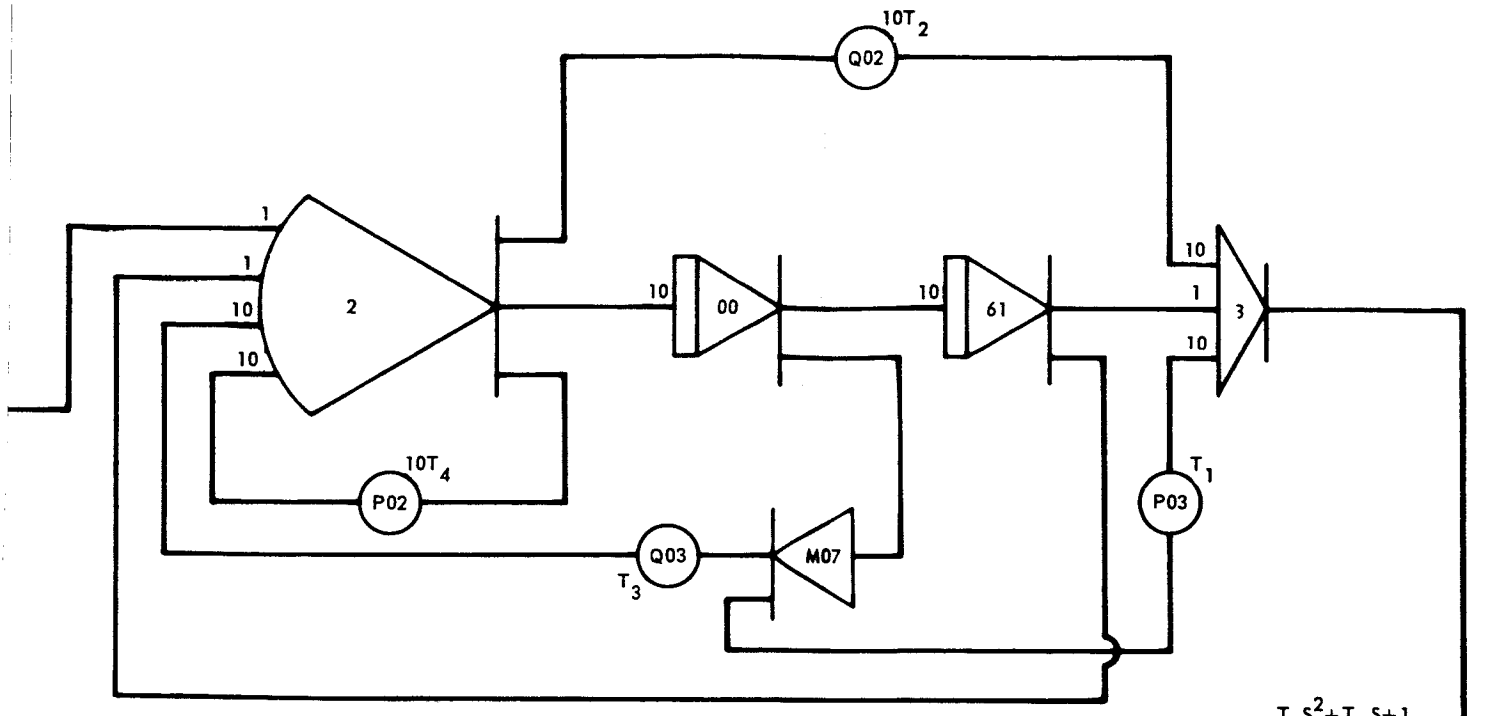

NOTCH FILTER #1

$$\frac{T_2S^2+T_1S+1}{T_4S^2+T_3S+1}$$

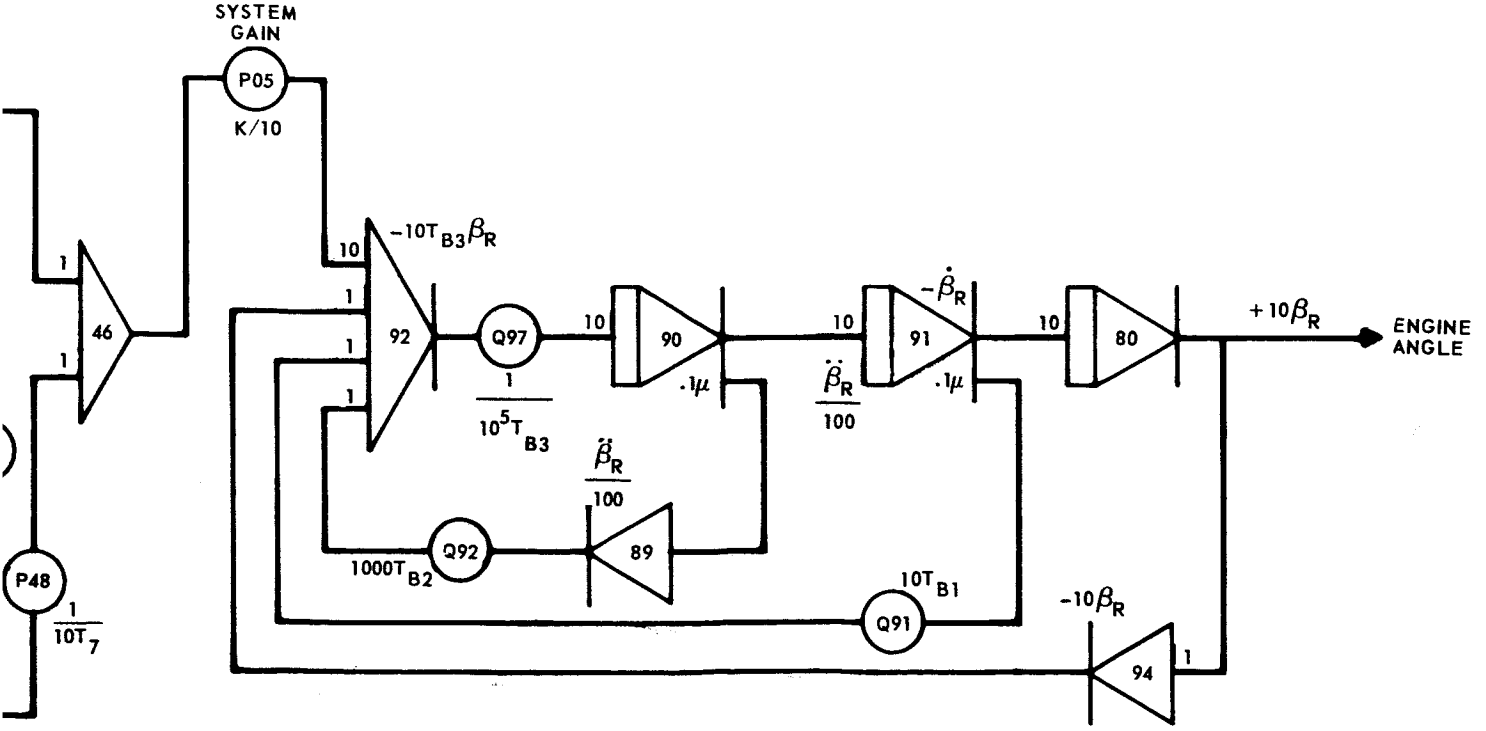

ENGINE DYNAMICS

225-2

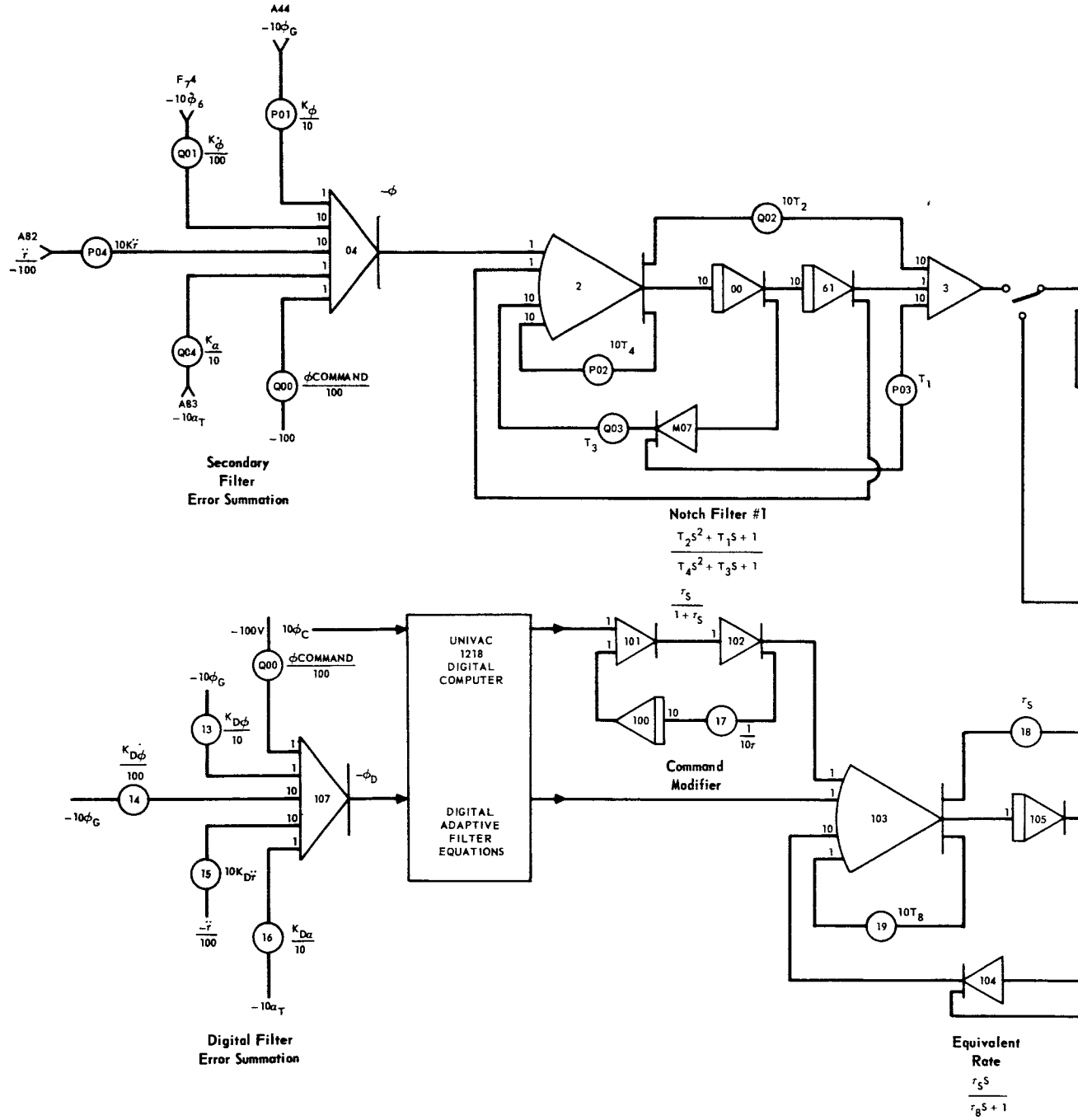

226-1

Figure B.4 Analog Computer Digital Adaptive Filter Control Loop Simulation

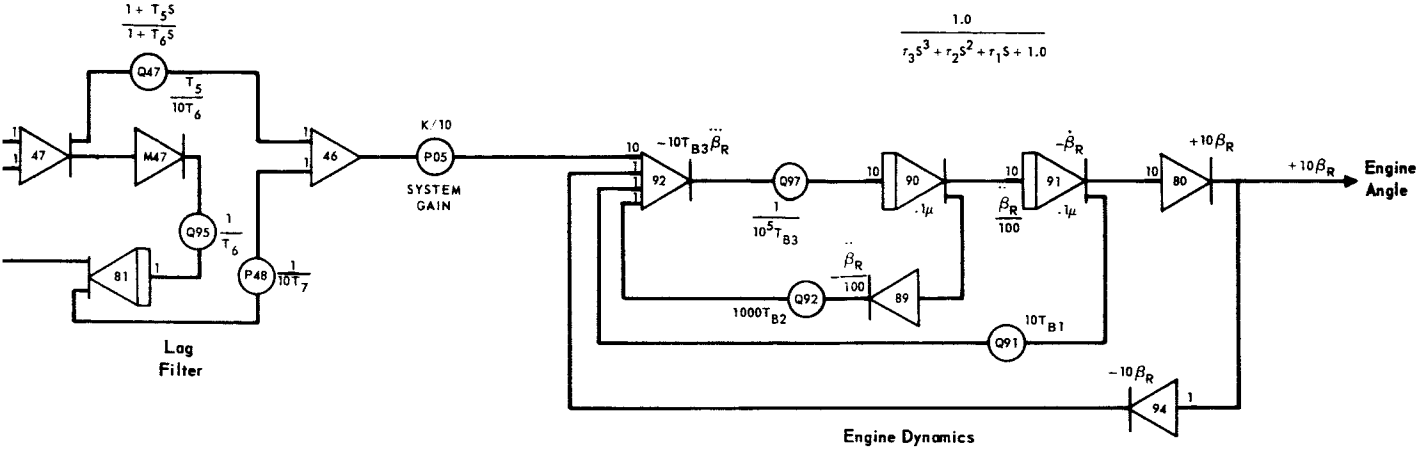
$\frac{1+T_5S}{1+T_6S}$
Q47
$\frac{T_5}{10T_6}$
47
M47
46
K/10
P05
SYSTEM GAIN
Q95
$\frac{1}{T_6}$
81
P48
$\frac{1}{10T_7}$
Lag Filter
$\frac{1.0}{r_3S^3+r_2S^2+r_1S+1.0}$
$-10T_{B3}\ddot{\beta}_R$
92
Q97
$\frac{1}{10^5T_{B3}}$
90
.1μ
$-\dot{\beta}_R$
91
$\frac{\ddot{\beta}_R}{100}$
.1μ
80
$+10\beta_R$
$+10\beta_R$
Engine Angle
$\frac{\ddot{\beta}_R}{100}$
Q92
89
$1000T_{B2}$
$10T_{B1}$
Q91
$-10\beta_R$
94
Engine Dynamics

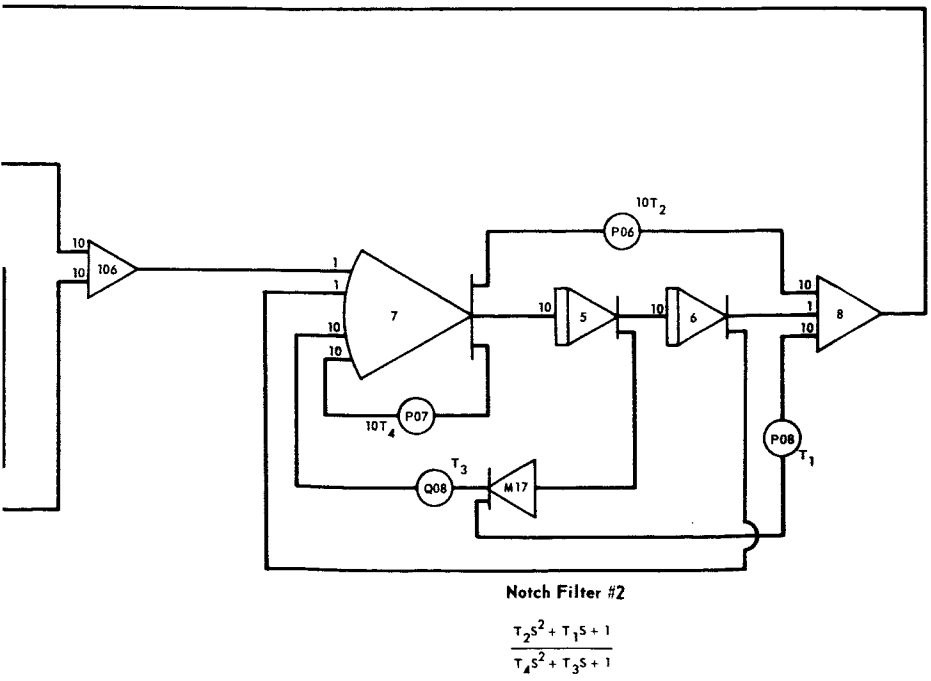
106
7
$10T_2$
P06
5
6
8
P07
$10T_4$
T_3
Q08
M17
P08
T_1
Notch Filter #2
$\frac{T_2S^2+T_1S+1}{T_4S^2+T_3S+1}$

226-2

TABLE B.1

NOMINAL POTENTIOMETER SETTINGS

POTENTIOMETER	VARIABLE	VEHICLE 1			VEHICLE 2		
		LIFT-OFF	MAX q	BURN-OUT	LIFT-OFF	MAX q	BURN-OUT
P00	$C_1/10$	0	.0342	.0004	0	.0073	.0001
P01	$K_Q/10$	-	-	-	-	-	-
P02	$10T_4$	-	-	-	-	-	-
P03	T_1	-	-	-	-	-	-
P04	K	-	-	-	-	-	-
P05	K/10	-	-	-	-	-	-
P06	$10T_2$	-	-	-	-	-	-
P07	$10T_4$	-	-	-	-	-	-
P08	T_1	-	-	-	-	-	-
P09		OPEN	OPEN	OPEN	OPEN	OPEN	OPEN
P10	$Y_1'(x_{s1})m_{s1}(F-X)/mM_1$	.0059	.0124	.0022	.0025	.0052	.0021
P11	$m_{s3}Y_1(x_{s3})/M_1$	.0655	.0947	.1817	.0405	.0531	.0953
P12	$m_{s2}Y_1(x_{s2})/M_1$	.0519	.0205	.0129	.0352	.0085	.0212
P13	$R'Y_1(x\beta)/1000M_1$	.0232	.0298	.1119	.0125	.0158	.1649
P14	$2\zeta_1 W_1/10$	.0050	.0055	.0064	.0022	.0023	.0029
P15	$Y_1'(x_{s1})(F-X)/500m$	.0012	.0022	.0029	.0009	.0015	.0022

TABLE B.1 (Continued)

NOMINAL POTENTIOMETER SETTINGS

POTENTIOMETER	VARIABLE	VEHICLE 1			VEHICLE 2		
		LIFT-OFF	MAX q	BURN-OUT	LIFT-OFF	MAX q	BURN-OUT
P16	$Y_3(x_{s1})/10$	.0256	.0528	.0520	.0071	.0422	.0708
P17	$Y_2(x_{s1})/10$	.0410	.0594	.0760	.0282	.0532	.0820
P18	$\ell_{s1}/100$	.1608	.2083	.3657	.2171	.3104	.6096
P19	m/f	.0816	.0449	.0244	.0816	.0457	.0189
P20	$Y_2'(x_{s1})m_{s1}(F-X)/10mM_2$	.0090	.0268	.0010	.0039	.0108	.1954
P21	$m_{s3}Y_2(x_{s3})/M_2$	.0514	.0132	.0672	.0020	.0293	.1138
P22	$m_{s2}Y_2(x_{s2})/M_2$	.0724	.1324	.0010	.0470	.0609	.0066
P23	$R'Y_2(x\beta)/1000M_2$	.0252	.0460	.0269	.0143	.0228	.0992
P24	$2\zeta_2\omega_2/10$	.0120	.0134	.0157	.0051	.0056	.0066
P25	$Y'(x_{s2})(F-X)/50m$	.0086	.0190	.0276	.0062	.0134	.0215
P26	$Y_3(x_{s2})$	.2874	.6615	1.0842	.1941	.5546	.1910
P27	$Y_2(x_{s2})$	.4581	.4792	.1162	.4567	.3828	.2480
P28	$\ell_{s2}/100$	.0385	.0509	.2242	.0535	.1012	.4236
P29	$Y_3(x_T^{\cdot\cdot})/10$	.1503	.0986	.2755	.0694	.0576	.1346
P30	$Y_3'(x_{s1})m_{s1}(F-X)/10mM_3$	.0051	.0142	.0012	.0052	.0164	.0005
P31	$m_{s3}Y_3(x_{s3})/M_3$	.0629	.0774	.0221	.0622	.0643	.0201

TABLE B.1 (Continued)

NOMINAL POTENTIOMETER SETTINGS

POTENTIOMETER	VARIABLE	VEHICLE 1			VEHICLE 2		
		LIFT-OFF	MAX q	BURN-OUT	LIFT-OFF	MAX q	BURN-OUT
P32	$m_{s2}Y_3(x_{s2})/M_3$	.0196	.0814	.0056	.0204	.1040	.0009
P33	$R'Y_3(x\beta)/1000M_3$	.0108	.0205	.0166	.0143	.0263	.0163
P34	$2\zeta_3\omega_3/10$	.0181	.0184	.0293	.0088	.0092	.0117
P35	$Y_1'(x_{s3})(F-X)/50m$	.0006	.0043	.0126	.0014	.0042	.0134
P36	$Y_3(x_{s3})$	1.4082	1.037	.2979	.9023	.5649	.3053
P37	$Y_2(x_{s3})$	.4956	.0785	.5605	.0291	.3030	.2961
P38	$\ell_{s3}/100$	.2004	.1854	.0496	.2355	.2015	.0585
P39	$F-X/100m$	.1225	.2111	.4093	.1226	.2102	.5282
P40	$Y_2(x_T'')/10$	.1869	.1529	.1798	.1115	.0696	.0163
P41	$Y_1(x_T'')$	.0870	.3864	.3192	.6077	.8033	.3242
P42	$Y_4'(x_\varphi)$	-	-	-	.173	.0119	.6222
P43	$Y_4(x_{s1})(F-X)/1000m$	-	-	-	.0009	.0017	.0060
P44	$Y_3'(x_\varphi)/10$	.0630	.0457	.0621	.0108	.0072	.0040
P45	$\ell_A/100$	.4201	.4051	.2693	.4297	.3927	.1327
P46	$Y_1'(x_\alpha)/5$	.0298	.0297	.0164	.0273	.0287	.0113
P47	$Y_4'(x_{s3})(F-X)/100m$	-	-	-	.0008	.0016	.0088

TABLE B.1 (Continued)

NOMINAL POTENTIOMETER SETTINGS

POTENTIOMETER	VARIABLE	VEHICLE 1			VEHICLE 2		
		LIFT-OFF	MAX q	BURN-OUT	LIFT-OFF	MAX q	BURN-OUT
P48	$1/10T_7$	-	-	-	-	-	-
P49	$Y_3(x_{\dot{\varphi}})$	.2403	.1744	.0174	.0555	.0306	.0964
Q00	φ Command/100	.01	.01	.01	.01	.01	.01
Q01	$K_{\dot{\varphi}}/100$	-	-	-	-	-	-
Q02	$10T_2$	-	-	-	-	-	-
Q03	T_3	-	-	-	-	-	-
Q04	$K_\alpha/10$	-	-	-	-	-	-
Q05	$F(\ell_{cq}Y_4'(x_\beta) - Y_4(x_\beta))/10I_{xx}$	-	-	-	.0025	.0038	.0423
Q06	$Y_4'(x_\beta)F/10m$	-	-	-	.0786	.1431	.3818
Q07		OPEN	OPEN	OPEN	OPEN	OPEN	OPEN
Q08	T_3	-	-	-	-	-	-
Q09		OPEN	OPEN	OPEN	OPEN	OPEN	OPEN
Q10	$Y_1'(x_{s3})m_{s3}(F-X)/10mM_1$	.0003	.0023	.0314	.0004	.0014	.0420
Q11	$Y_1'(x_{s2})m_{s2}(F-X)/10mM_1$	.0063	.0170	.0048	.0027	.0072	.0046
Q12	$m_{s1}Y_1(x_{s1})/M_1$	.0528	.0789	.0131	.0262	.0445	.0167
Q13	Scale Factor .1	.1	.1	.1	.1	.1	.1

TABLE B.1 (Continued)

NOMINAL POTENTIOMETER SETTINGS

POTENTIOMETER	VARIABLE	VEHICLE 1			VEHICLE 2		
		LIFT-OFF	MAX q	BURN-OUT	LIFT-OFF	MAX q	BURN-OUT
Q14	$\omega_1^2/500$	.0507	.0606	.0813	.0093	.0107	.0170
Q15	$Y_3'(x_{s1})(F-X)/1000m$	.0011	.0018	.0053	.0008	.0014	.0027
Q16	$Y_2'(x_{s1})(F-X)/1000m$	.0009	.0015	.0027	.0006	.0011	.0017
Q17	$Y_1(x_{s1})10$	.0555	.0698	.0869	.0453	.0655	.0880
Q18	$2\zeta_{s1}\omega_{s1}/10$	.0128	.0166	.0215	.0128	.0166	.0215
Q19	$\omega_{s1}^2/100$	.0456	.0765	.1283	.0456	.0763	.1281
Q20	$Y_2'(x_{s3})m_{s3}(F-X)/10mM_2$	.0099	.0208	.0237	.0039	.0077	.0213
Q21	$Y_2'(x_{s2})m_{s2}(F-X)/10mM_2$	.0024	.0161	.0018	.0001	.0086	.0039
Q22	$m_{s1}Y_2(x_{s1})/M_2$	.0424	.1036	.0028	.0190	.0534	.0095
Q23	Scale Factor .1	.1	.1	.1	.1	.1	.1
Q24	$\omega_2^2/1000$	.1438	.1782	.2459	.0256	.0318	.0434
Q25	$Y_3'(x_{s2})(F-X)/100m$	.0097	.0006	.0289	.0057	.0001	.0207
Q26	$Y_2'(x_{s2})(F-X)/100m$	.0015	.0058	.0218	.0002	.0054	.0147
Q27	$Y_1(x_{s2})$	.3571	.1145	.3759	.3986	.0789	.4917
Q28	$2\zeta_{s2}\omega_{s2}/10$	.0128	.0166	.0226	.0128	.0166	.0226

TABLE B.1 (Continued)

NOMINAL POTENTIOMETER SETTINGS

POTENTIOMETER	VARIABLE	VEHICLE 1			VEHICLE 2		
		LIFT-OFF	MAX q	BURN-OUT	LIFT-OFF	MAX q	BURN-OUT
Q29	$\omega_{s2}^2/100$	.0456	.0765	.1421	.0456	.0763	.1420
Q30	$Y_3'(x_{s3})m_{s3}(F-X)/10mM_3$	.0018	.0054	.0471	.0025	.0068	.0238
Q31	$Y_3'(x_{s2})m_{s2}(F-X)/10mM_3$	.0066	.0008	.0015	.0060	.0002	.0009
Q32	$m_{s1}Y_3(x_{s1})/M_3$	.0114	.0409	.0012	.0049	.0499	.0014
Q33	Scale Factor .1	.1	.1	.1	.1	.1	.1
Q34	$\omega_3^2/1000$	.3287	.3397	.8608	.0770	.0841	.1370
Q35	$Y_3'(x_{s3})(F-X)/100m$	.0040	.0072	.0634	.0036	.0059	.0362
Q36	$Y_2'(x_{s3})(F-X)/100m$	.0096	.0124	.0198	.0058	.0079	.0055
Q37	$Y_1(x_{s3})$	.6875	.8714	.3644	.6994	.8110	.1525
Q38	$2\zeta_{s3}\omega_{s3}/10$	.0128	.0169	.0283	.0128	.0169	.0283
Q39	$\omega_{s3}/100$	.0456	.0799	.2220	.0456	.0799	.2218
Q40	$Y_4(x_{s1})$	-	-	-	.1123	.3295	.3683
Q41	$2Y_1'(x_\varphi)$	.3050	.3248	.1681	.2287	.2370	.0879
Q42	$10Y_4(x_\alpha)/V$	-	-	-	∞	.1415	.0208
Q43	$Y_4'(x_{s2})(F-X)/100m$	-	-	-	.0009	.0078	.0028
Q44	$Y_2'(x_\varphi)/10$	.2807	.2431	.4219	.1527	.1303	.0667

TABLE B.1 (Continued)

NOMINAL POTENTIOMETER SETTINGS

POTENTIOMETER	VARIABLE	VEHICLE 1			VEHICLE 2		
		LIFT-OFF	MAX q	BURN-OUT	LIFT-OFF	MAX q	BURN-OUT
Q45	$Y_2'(x_\alpha)/10$	.0273	.0237	.0415	.2508	.0232	.1388
Q46	$10Y_1'(x_\varphi)$	.6772	.6559	.2603	.1740	.1303	.0443
Q47	$T_5/10T_6$	-	-	-	-	-	-
Q48		OPEN	OPEN	OPEN	OPEN	OPEN	OPEN
Q49	$10Y_2'(x_\varphi)$	.2572	.4374	.1273	.6796	.6872	.3931
Q50	Scale Factor .1	.1	.1	.1	.1	.1	.1
Q51	$F(\ell_{cg}Y_3'(x_\beta) - Y_3(x_\beta))/10I_{xx}$	.0027	.0043	.0269	.0019	.0031	.0160
Q52	$10\ell_{s1}m_{s1}/I_{xx}$	.0212	.0317	.0028	.0086	.0143	.0022
Q53	$10\ell_{s2}m_{s2}/I_{xx}$	.0077	.0123	.0040	.0032	.0074	.0036
Q54	$10\ell_{s3}m_{s3}/I_{xx}$	.0264	.0272	.0127	.0093	.0089	.0071
Q55	$F(\ell_{cg}Y_2'(x_\beta) - Y_2(x_\beta))/10I_{xx}$	.0015	.0031	.0101	.0012	.0022	.0073
Q56	$F(\ell_{cg}Y_1'(x_\beta) Y_1(x_\beta))/5I_{xx}$	.0007	.0023	.0046	.0010	.0021	.0053
Q57	$m_{s3}(F-X)/I_{xx}m$	.0016	.0031	.0105	.0005	.0009	.0064
Q58	$m_{s2}(F-X)/I_{xx}m$	.0025	.0051	.0007	.0007	.0015	.0004
Q59	$m_{s1}(F-X)/I_{xx}m$	.0016	.0032	.0003	.0005	.0010	.0002
Q60	$10(\ell_{cg}S_E + I_E)/I_{xx}$	.0135	.0159	.0417	.0060	.0074	.0327

TABLE B.1 (Continued)

NOMINAL POTENTIOMETER SETTINGS

POTENIOMETER	VARIABLE	VEHICLE 1			VEHICLE 2		
		LIFT-OFF	MAX q	BURN-OUT	LIFT-OFF	MAX q	BURN-OUT
Q61	m_{s3}/m	.0402	.0648	.1460	.0264	.0420	.0960
Q62	m_{s3}/m	.0402	.0674	.0044	.0263	.0436	.0029
Q63	$Y_1'(x_\beta)F/5m$	.0985	.2269	.2867	.0853	.1561	.2219
Q64	$N'/1000m$	0	.0073	.0003	0	.0056	.0002
Q65	$C_2 + (F-X)S_E/10mI_{xx}$	.0812	.1075	.2325	.0321	.0446	.2164
Q66	M_{s2}/m	.0614	.1068	.0101	.0402	.0692	.0066
Q67	$Y_3'(x_\beta)F/10m$	.0903	.1705	.5130	.0675	.1259	.2691
Q68	$Y_2'(x_\beta)F/10m$	.0745	.1490	.2599	.0543	.0502	.1661
Q69	$Y_4(x_{s2})$	-	-	-	.0214	.6039	.1362
Q70	$100/V$	.8160	.1927	.0396	.8156	.1926	.0397
Q71	$Y_4(x_{s3})$	-	-	-	.0801	.1205	.0126
Q72	$(F-X)/1000m$	.0122	.0211	.0409	.0123	.0210	.0528
Q73	$Y_4'(x_\alpha)/10$	-	-	-	.0731	.0937	.1234
Q74	$Y_3'(x_\alpha)$	.6271	.4559	.7167	.3630	.2696	.5766
Q75	$S_E Y_1(x_\beta) + I_E Y_1'(x_\beta) /10M_1$	.0042	.0050	.0220	.0024	.0027	.0255
Q76	$Q_\alpha/1000M_1$	0	.0042	0	0	.0027	0

TABLE B.1 (Continued)

NOMINAL POTENTIOMETER SETTINGS

POTENTIOMETER	VARIABLE	VEHICLE 1			VEHICLE 2		
		LIFT-OFF	MAX q	BURN-OUT	LIFT-OFF	MAX q	BURN-OUT
Q77		OPEN	OPEN	OPEN	OPEN	OPEN	OPEN
Q78	$S_E Y_2(x_\beta) + I_E Y_2'(x_\beta)/10M_2$	.0049	.0080	.0060	.0028	.0040	.0158
Q79	$10Y_1(x_\alpha)/V$	0	.0079	.0008	0	.0087	.0006
Q80	$Q_\alpha/1000M_2$	0	.0003	0	0	.0001	0
Q81	$2\ell_\alpha/V$	0	.2854	.0480	0	.3056	.0578
Q82	Scale Factor .001	.001	.001	.001	.001	.001	.001
Q83	$10Y_3(x_\alpha)/V$	0	.0990	.0247	0	.0521	.0189
Q84	Scale Factor .1	.1	.1	.1	.1	.1	.1
Q85	$Q_\alpha/1000M_3$	0	.0051	0	0	.0066	0
Q86	$S_E Y_3(x_\beta) + I_E Y_3'(x_\beta)/10M_3$	.0022	.0037	.0041	.0029	.0048	.0028
Q87	Scale Factor .1	.1	.1	.1	.1	.1	.1
Q88	$10Y_2(x_\alpha)/V$	0	.6196	.2029	0	.6565	.0714
Q89	Time Rate .05	.05	.05	.05	.05	.05	.05
Q90	$Y_4(x_\varphi^\cdot)$	-	-	-	.1702	.2345	.0707
Q91	$10T_{B1}$	.7257	.7257	.7257	.7257	.7257	.7257
Q92	$1000T_{B2}$	.7620	.7620	.7620	.7620	.7620	.7620

TABLE B.1 (Continued)

NOMINAL POTENTIOMETER SETTINGS

POTENTIOMETER	VARIABLE	VEHICLE 1			VEHICLE 2		
		LIFT-OFF	MAX q	BURN-OUT	LIFT-OFF	MAX q	BURN-OUT
Q93	Scale Factor .1	.1	.1	.1	.1	.1	.1
Q94	Scale Factor .15	.15	.15	.15	.15	.15	.15
Q95	$1/T_6$	-	-	-	-	-	-
Q96	$R'/1000m$	.0098	.0178	.0328	.0061	.0109	.0264
Q97	$1/10^5 T_{B3}$	.3160	.3160	.3160	.3160	.3160	.3160
Q98	$Y_4(x_\tau)/10$	-	-	-	.1520	.1863	.1741
Q99	Scale Factor .3	.3	.3	.3	.3	.3	.3
1	$\omega_4^2/1000$	-	-	-	.1525	.1560	.6175
2	$2\zeta_4\omega_4/10$	-	-	-	.0124	.0125	.0248
3	$S_E Y_4(x_\beta) + I_E Y_4'(x_\beta)/10M_4$	-	-	-	.0014	.0008	.0025
4	$Q/1000M_4$	-	-	-	0	.0002	0
5	$R' Y_4(x_\beta)/1000M_4$	-	-	-	.0065	.0045	.0119
6	$m_{s1} Y_4(x_{s1})/M_4$	-	-	-	-.0036	.0068	.0006
7	$m_{s2} Y_4(x_{s2})/M_4$	-	-	-	-.0104	.0196	.0052
8	$m_{s3} Y_4(x_{s3})/M_4$	-	-	-	.0255	.0238	.0069

TABLE B.1 (Continued)

NOMINAL POTENTIOMETER SETTINGS

POTENTIOMETER	VARIABLE	VEHICLE 1			VEHICLE 2		
		LIFT-OFF	MAX q	BURN-OUT	LIFT-OFF	MAX q	BURN-OUT
9	$Y_4'(x_{s1})m_{s1}(F-X)/10mM_4$	-	-	-	.0279	.0034	.0099
10	$Y_4'(x_{s2})m_{s2}(F-X)/10mM_4$	-	-	-	.0420	.0025	-.0106
11	$Y_4'(x_{s3})m_{s3}(F-X)/10mM_4$	-	-	-	.0251	.0031	-.4823
12	Scale Factor .1	-	-	-	.1	.1	.1
13	$K_{D\varphi}/10$ DIGITAL FILTER LOOP	-	-	-	-	-	-
14	$K_{D\dot{\varphi}}/100$ DIGITAL FILTER LOOP	-	-	-	-	-	-
15	$10K_{D\tau}$ DIGITAL FILTER LOOP	-	-	-	-	-	-
16	$K_{D\alpha}/10$ DIGITAL FILTER LOOP	-	-	-	-	-	-
17	$1/10\tau$ DIGITAL FILTER LOOP	-	-	-	-	-	-
18	τ	-	-	-	-	-	-
19	$10T_8$	-	-	-	-	-	-

TABLE B.2

ANALOG COMPUTER SWITCH POSITIONS

SWITCH	VEHICLE 1			VEHICLE 2		
	LIFT-OFF	MAX q	BURN-OUT	LIFT-OFF	MAX q	BURN-OUT
00	Right - Bending Mode #1 Out Left - Bending Mode #1 In					
01	Right - Bending Mode #2 Out Left - Bending Mode #2 In					
02	Right - Bending Mode #3 Out Left - Bending Mode #3 In					
03	Right - Bending Mode #4 Out Left - Bending Mode #4 In					
10	Right	Left	Left	Right	Left	Left
11	Left	Left	Right	Left	Right	Right
12	Left	Left	Right	Left	Left	Right
20	Right - Slosh Mode #1 Out Left - Slosh Mode #1 In					
21	Right - Slosh Mode #2 Out Left - Slosh Mode #2 In					
22	Right - Slosh Mode #3 Out Left - Slosh Mode #3 In					
23	Right	Right	Left	Right	Right	Left
30	Right	Right	Left	Right	Left	Left
31	Right	Left	Left	Right	Left	Left
32	Right	Right	Right	Right	Right	Left
40	Right	Right	Left	Left	Left	Left
41	Left	Right	Right	Left	Right	Right
42	Open	Open	Open	Open	Open	Open

TABLE B.2 (Continued)

ANALOG COMPUTER SWITCH POSITIONS

SWITCH	VEHICLE 1			VEHICLE 2		
	LIFT-OFF	MAX q	BURN-OUT	LIFT-OFF	MAX q	BURN-OUT
43	Right	Right	Right	Right	Right	Left
50	Center	Center	Center	Left	Right	Right
51	Center	Center	Center	Right	Right	Left
52	Center	Center	Center	Left	Right	Right
53	Center	Center	Center	Right	Right	Left
54	Center	Center	Center	Right	Right	Left

APPENDIX C

DIGITAL COMPUTER SIMULATION OF THE DIGITAL FILTER CONTROL SYSTEM

A digital simulation of the digital adaptive filter control system was performed on the IBM 7094. This program consisted of eight different subroutines to simulate the various elements of the control system as shown in Figure C.1. These subroutines performed the following functions.

Subroutine A - Input function generation

Subroutine B - Digital adaptive filter and secondary filter computation

Subroutine C - Linear compensation of digital filter and secondary filter paths

Subroutine D - Engine actuator dynamics

Subroutine E - Simulation of the vehicle equations of motion including the body bending and fuel slosh equations

Subroutine F - Control system feedback paths for the digital filter and the secondary filter

Subroutine G - Feedback summation of the digital filter and secondary filter

Subroutine H - Generation of the control system wind inputs

A description of the elements and functions of each subroutine follows.

C.1 Subroutine A

This subroutine generates the system input signal $r(t)$ where

$$r(t) = r_1(t) + r_2(t)$$

where $r_1(t)$ is a table look of function with a linear interpolation between selected amplitudes and their corresponding times and $r_2(t)$ determines the time history response of the transfer function

$$\theta(s) = \frac{\sum_{r=0}^{M} a_r S^r}{(S^N + \sum_{r=0}^{N-1} b_r S^r) S^g} \sum_{r=0}^{H} \frac{r!\, R_r}{S^{r+1}}$$

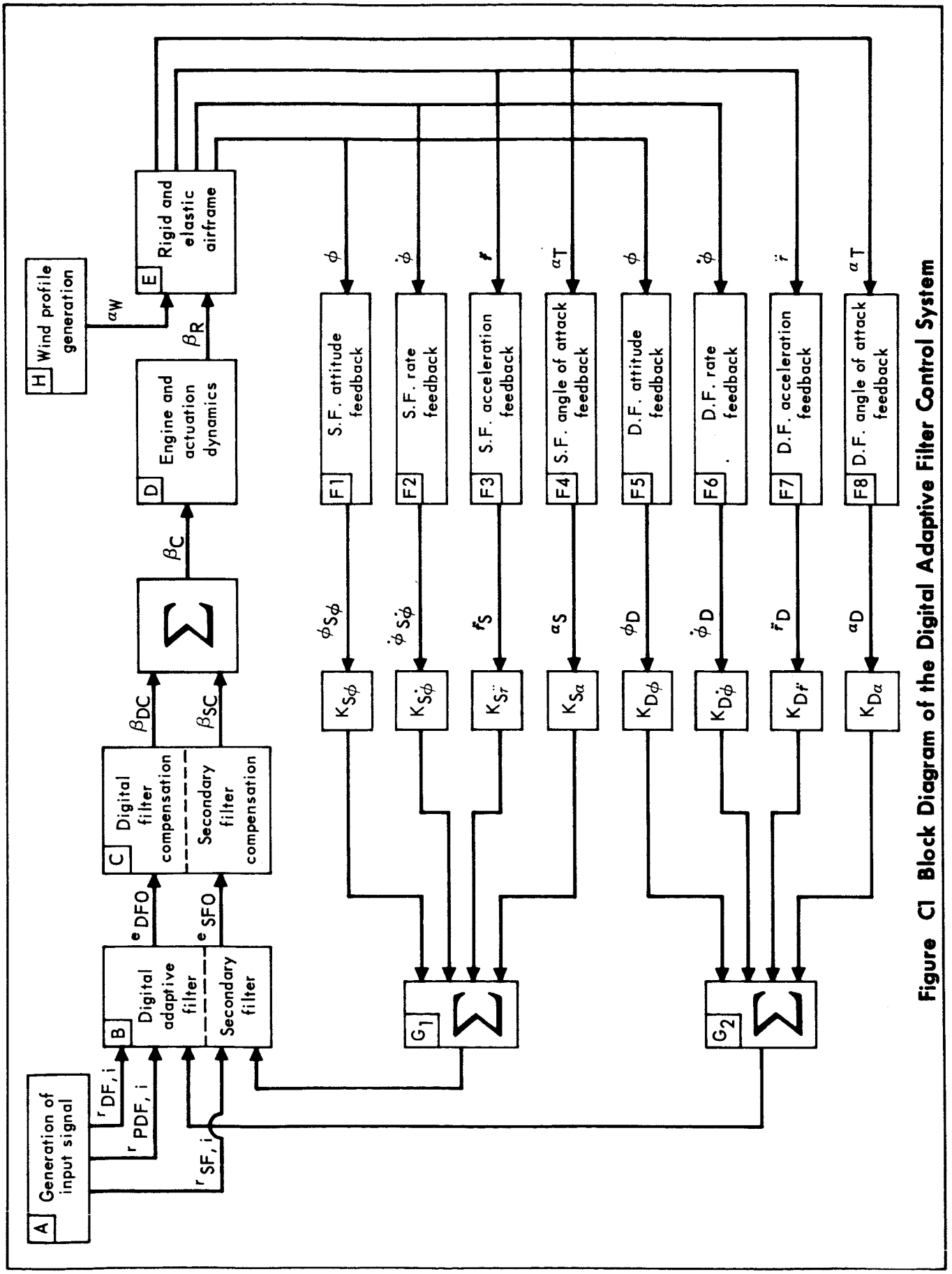

Figure C1 Block Diagram of the Digital Adaptive Filter Control System

The r(t) is used as an input to both the digital adaptive filter and the secondary filter after being processed by two linear prefilters. Thus,

$$r_{PDF}(t) = \mathcal{L}^{-1}\left[\frac{K_{DR1} + \tau_{DR1}S}{1 + \tau_{DR2}S}\right] r(S)$$

$$r_{PSF}(t) = \mathcal{L}^{-1}\left[\frac{K_{SR1} + \tau_{SR1}S}{1 + \tau_{SR2}S}\right] r(S)$$

C.2 Subroutine B

The block diagram (Figure C.2) shows the paths and the functions of the equations programmed in Subroutine B. The basic digital filter path contains the fade-in function, the curve fitting process with options for one, two, and three parameter amplitude fitting, Z transform compensation, and signal updating. Two other functions contained in the simulation are the generation of the residual curve (error signal with the rigid body component subtracted out) and the secondary filter forward loop compensation. With reference to the numbered blocks in Figure C.2 the simulated equations are:

1. Input Signals, r(t)

The inputs are generated in Subroutine A.

2. Sampler

2a. The Digital Filter input and feedback signals are sampled at a rate of m per second.

2b. The Secondary Filter input and feedback signals are sampled at a rate of ms samples per second.

3. Prefilter

3a. The Digital Filter command input is prefiltered.

Filter form:

$$r_{DFF,i} = \sum_j R_{jR1}\, r_{DF,i-j} - \sum_s C_{sR1}\, r_{DFF,i-s}$$

$i = 1,2,\text{---}M \qquad M \le M_{max}$

$j = 1,2,\text{---}J$

$s = 1,2,\text{---}S \qquad (J_{max} = S_{max} = 50)$

3b. The Secondary Filter command input is prefiltered.

$$r_{SFF,i} = \sum_j R_{jR2}\, r_{SF,i-j} - \sum_s C_{sR2}\, r_{SFF,i-s}$$

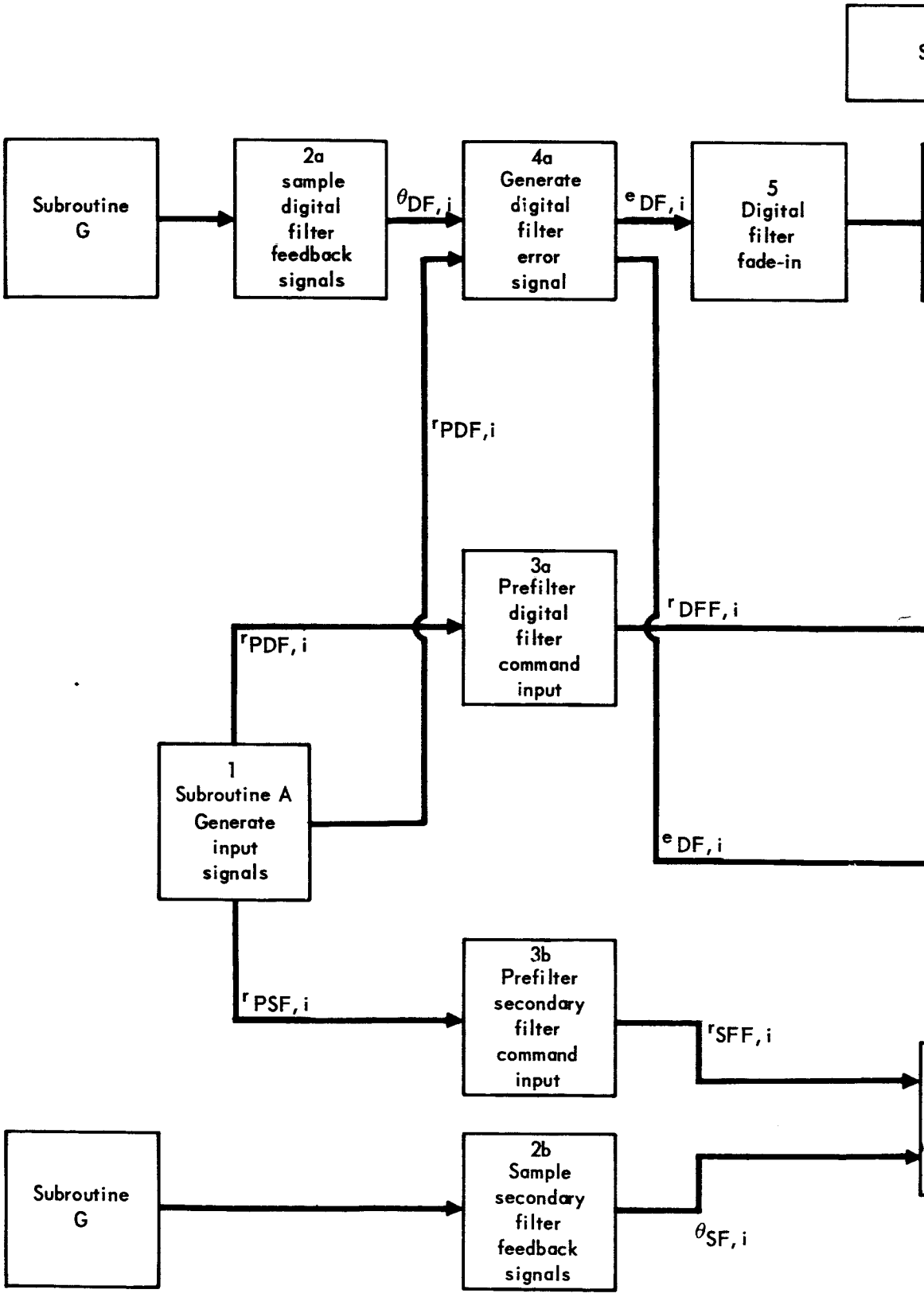

Figure C2 Block Diagram of Subroutine B

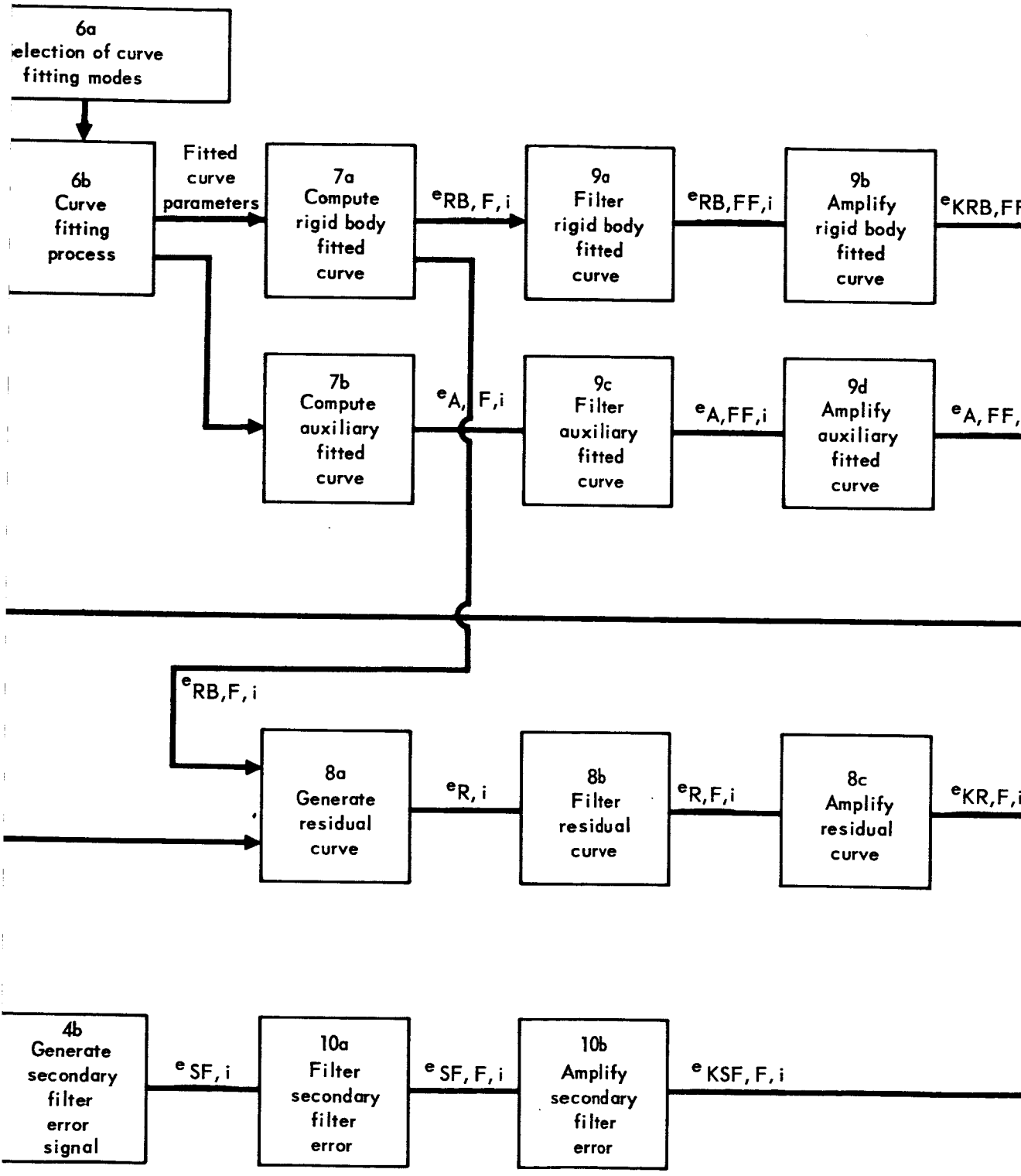
6a
election of curve fitting modes
6b
Curve fitting process
Fitted curve parameters
7a
Compute rigid body fitted curve
$e_{RB,F,i}$
9a
Filter rigid body fitted curve
$e_{RB,FF,i}$
9b
Amplify rigid body fitted curve
$e_{KRB,FF}$
7b
Compute auxiliary fitted curve
$e_{A,F,i}$
9c
Filter auxiliary fitted curve
$e_{A,FF,i}$
9d
Amplify auxiliary fitted curve
$e_{A,FF,}$
$e_{RB,F,i}$
8a
Generate residual curve
$e_{R,i}$
8b
Filter residual curve
$e_{R,F,i}$
8c
Amplify residual curve
$e_{KR,F,i}$
4b
Generate secondary filter error signal
$e_{SF,i}$
10a
Filter secondary filter error
$e_{SF,F,i}$
10b
Amplify secondary filter error
$e_{KSF,F,i}$

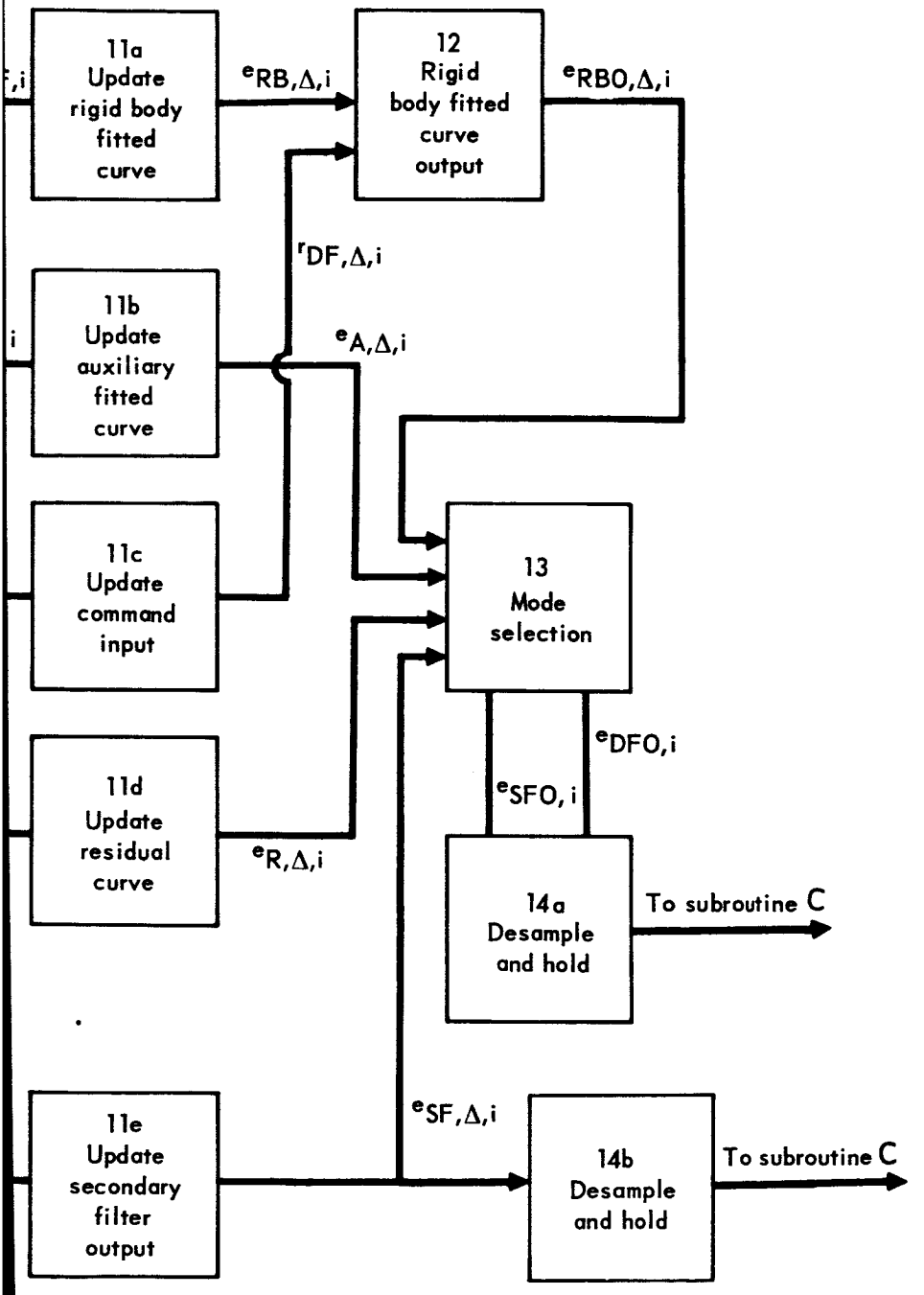
11a
Update
rigid body
fitted
curve
$e_{RB,\Delta,i}$
12
Rigid
body fitted
curve
output
$e_{RBO,\Delta,i}$
$r_{DF,\Delta,i}$
11b
Update
auxiliary
fitted
curve
$e_{A,\Delta,i}$
11c
Update
command
input
13
Mode
selection
11d
Update
residual
curve
$e_{R,\Delta,i}$
$e_{DFO,i}$
$e_{SFO,i}$
14a
Desample
and hold
To subroutine C
11e
Update
secondary
filter
output
$e_{SF,\Delta,i}$
14b
Desample
and hold
To subroutine C

4. Error Signal Generation

4a. Generate Digital Filter Error Signal

$$e_{DF,i} = r_{DF,i} - \theta_{DF,i}$$

4b. Generate Secondary Filter Error Signal

$$e_{SF,i} = r_{SFF,i} - \theta_{SF,i}$$

5. Fade-in Function

The Digital Filter curve fitting processes is restarted for any of the following conditions:

1. If the number of samples from the last fade-in exceeds "MSS" samples. This corresponds to periodic restarting (Note: MSS can be greater than M_{max}).

2. If a discontinuity occurs in the error signal so that the difference between two consecutive samples exceeds a predetermined value of L

$$|e_{DF,i-1} - e_{DF,i}| > L \qquad \text{restart fitting process}$$
$$i = M \leq M_{max}$$

3. If the rate of change of the error signal exceeds a predetermined value of L so that

$$|e_{DF,i-2} - 2\, e_{DF,i-1} + e_{DF,i}| > \dot{L}$$
$$i = M \leq M_{max}$$

then restart curve fitting process.

6. Amplitude Crive Fitting Process of the Digital Adaptive Filter

6a. The curve fitting modes are selected by the following Control function

$M \geq MO > 0$ No fitting
$M \geq MA > 1$ One parameter amplitude fitting
$M \geq MB > 2$ Two parameter amplitude fitting
$M \geq MC > 3$ Three parameter amplitude fitting

where M is the present sample counted from the start of the fade-in process.

6b. Curve Fitting Process

1. A memory of M_{max} samples is filled with the Digital Filter sampled error signal. When the memory is filled the oldest stored samples are dropped as the new samples are received.

$$e_{i,M} = e_{i+1,M-1} \qquad i = 1,2.\text{---}M_{max}$$

2. To the samples stored in the computer memory, a curve of the following form is fitted

$$e_F(t) = A\ e^{-\alpha t}\ \cos\ \beta t + B\ e^{-\alpha t}\ \sin\ \beta t + C\ e^{-\delta t}$$

The various forms of amplitude fitting are defined as,

(1) One parameter fitting - The amplitude C is computed with a selected δ value and A, B, α, β, = 0
and a fitted curve form of

$$e_F(t) = C\ e^{-\delta t}$$

(2) Two parameter fitting - The amplitudes A and B are computed with values for α and β known and C, δ, = 0,
and a fitted curve form of
$e_F(t) = A\ e^{-\alpha t}\ \cos\ \beta t + B\ e^{-\alpha t}\ \sin\ \beta t$

(3) Three parameter fitting - The amplitudes A, B, and C are computed with values for α, β, and δ known, and a fitted curve form of $e_F(t) = A\ e^{-\alpha t}\ \cos\ \beta t + B\ e^{-\alpha t}\ \sin\ \beta t + C\ e^{-\delta t}$

The fitted curve amplitudes are found by solving the following matrix equations

<u>One Parameter Fitting</u>

$$C = \left[\bar{u}_C \cdot \bar{u}_C\right]^{-1} \left[\bar{u}_C \cdot \bar{E}\right]$$

<u>Two Parameter Fitting</u>

$$\begin{bmatrix} A \\ B \end{bmatrix} = \begin{bmatrix} \bar{u}_A \cdot \bar{u}_A & \bar{u}_A \cdot \bar{u}_B \\ \bar{u}_B \cdot \bar{u}_A & \bar{u}_B \cdot \bar{u}_B \end{bmatrix}^{-1} \begin{bmatrix} \bar{u}_A \cdot \bar{E} \\ \bar{u}_B \cdot \bar{E} \end{bmatrix}$$

<u>Three Parameter Fitting</u>

$$\begin{bmatrix} A \\ B \\ C \end{bmatrix} = \begin{bmatrix} \bar{u}_A \cdot \bar{u}_A & \bar{u}_A \cdot \bar{u}_B & \bar{u}_A \cdot \bar{u}_C \\ \bar{u}_B \cdot \bar{u}_A & \bar{u}_B \cdot \bar{u}_B & \bar{u}_B \cdot \bar{u}_C \\ \bar{u}_C \cdot \bar{u}_A & \bar{u}_C \cdot \bar{u}_B & \bar{u}_C \cdot \bar{u}_C \end{bmatrix}^{-1} \begin{bmatrix} \bar{u}_A \cdot \bar{E} \\ \bar{u}_B \cdot \bar{E} \\ \bar{u}_C \cdot \bar{E} \end{bmatrix}$$

where

$$u_{Ai} = e^{-\alpha t_{i-1}} \cos \beta\, t_{i-1}$$

$$u_{Bi} = e^{-\alpha t_{i-1}} \sin \beta\, t_{i-1}$$

$$u_{Ci} = e^{-\delta t_{i-1}}$$

$$E_i = e_{DF,i} \qquad i = 1,2,\cdots M \quad M \le M_{max}; \; t_{i-1} = \frac{(i-1)}{m}$$

and as an example

$$\bar{u}_A \cdot \bar{u}_B = \sum_{i=1}^{M} u_{Ai}\, u_{Bi}$$

$$\bar{u}_A \cdot \bar{E} = \sum_{i=1}^{M} u_{Ai}\, E_i$$

7. Fitted Curve Computation

7a. Rigid body fitted curve (two parameter fitting).

$$e_{RB,F,i} = A\, e^{\frac{-\alpha(i-1)}{m}} \cos\left(\frac{\beta\,(i-1)}{m}\right) + B\, e^{\frac{-\alpha(i-1)}{m}} \sin\left(\frac{\beta\,(i-1)}{m}\right)$$

7b. Auxiliary fitted curve (one parameter fitting)

$$e_{A,F,i} = C\, e^{\frac{-\delta(i-1)}{m}}$$

$$i = M \qquad M \le M_{max}$$

8. Residual Curve Generation

8a. The residual curve is formed by the relationship

$$e_{R,i} = e_{DF,i} - e_{RB,F,i} \qquad i = 1,2,\cdots M$$

8b. The residual curve is filtered by compensation of the type

$$e_{R,F,i} = \sum_{j} R_{jR3} e_{R,\, i-j} - \sum_{s} C_{SR3}\, e_{R,\, F,\, i-s}$$

8c. The residual curve is amplified by the gain K_R

$$e_{KR,F,i} = K_R\, e_{R,F,i}$$

9. Filtered Curves

9a. Filtered fitted curve

The rigid body fitted curve is filtered by compensation of the following type

$$e_{RB,FF,i} = \sum_j R_{jR4}\, e_{RB,F,i-j} - \sum_s C_{sR4}\, e_{RB,FF,i-s}$$

9b. The filtered fitted curve is amplified by the gain K_F

$$e_{KRB,FF,i} = K_F\, e_{RB,FF,i}$$

9c. The auxiliary curve is filtered by compensation of the following type

$$e_{A,FF,i} = \sum_j R_{jR5}\, e_{A,F,i-j} - \sum_s C_{sR5}\, e_{A,FF,i-s}$$

9d. The filtered auxiliary curve is filtered by the gain K_A

$$e_{KA,FF,i} = K_A\, e_{A,FF,i}$$

10. Generate Secondary Filter Composite Error

10a. The secondary filter error signal is modified by compensation of the type

$$e_{SF,F,i} = \sum_j R_{jR6}\, e_{SF,i-j} - \sum_s C_{sR6}\, e_{SF,F,i-s}$$

10b. The filtered secondary filter error signal is amplified by the gain K_S

$$e_{KSF,F,i} = K_S\, e_{SF,F,i}$$

11. Signal Updating

The fitted curves and secondary filter signals are updated by an amount Δt to compensate for computer compensation time.

11a. Fitted curve updating

$$e_{RB,\Delta,i} = e_{KRB,FF,i} + X_{IF}(e_{KRB,FF,i} - e_{KRB,FF,i-1})\,(m\,\Delta t) + \frac{Y_{IF}}{2}\,(e_{KRB,FF,i} - 2\,e_{KRB,FF,i-1} + e_{KRB,FF,i-2})\,[m\,\Delta t(1+m\,\Delta t)]$$

11b. Auxiliary curve updating

$$e_{A,\Delta,i} = e_{KA,FF,i} + X_{1A}\,(e_{KA,FF,i} - e_{KA,FF,i-1})\,(m\Delta t) + \frac{Y_{1A}}{2}\,(e_{KA,FF,i} - 2\,e_{KA,FF,i-1} + e_{KA,FF,i-2})\left[m\Delta t(1+m\Delta t)\right]$$

11c. Command input updating

$$r_{DF,\Delta,i} = r_{DFF,i} + X_{1D}\,(r_{DFF,i} - r_{DFF,i-1})\,m\Delta t + \frac{Y_{1D}}{2}\,(r_{DFF,i} - 2\,r_{DFF,i-1} + r_{DFF,i-2})\left[m\Delta t(1+m\Delta t)\right]$$

11d. Residual curve updating

$$e_{R,\Delta,i} = e_{KR,F,i} + X_{1R}\,(e_{KR,F,i} - e_{KR,F,i-1})\,(m\Delta t) + \frac{Y_{1R}}{2}\,(e_{KR,F,i} - 2\,e_{KR,F,i-1} + e_{KR,F,i-2})\left[m\Delta t(1+m\Delta t)\right]$$

11e. Secondary filter updating

$$e_{SF,\Delta,i} = e_{KSF,F,i} + X_{1S}\,(e_{KSF,F,i} - e_{KSF,F,i-1})\,(m\Delta t) + \frac{Y_{1S}}{2}\,(e_{KSF,F,i} - 2\,e_{KSF,F,i-1} + e_{KSF,F,1-2})\left[m\Delta t(1+m\Delta t)\right]$$

The X_1 and Y_1 coefficients indicate if linear (X=1, Y=0) updating, quadratic (X=1, Y=1) updating or if no (X=0, Y=0) updating is desired.

12. Fitter Curve Channel Output

The prefiltered command signal is added to the filtered fitted curve

$$e_{RBO,\Delta,i} = e_{RB,\Delta,i} - r_{DF,\Delta,i}$$

13. Mode Selection - Subroutine B has two output channels e_{DFO} and e_{SFO} where,

$$e_{DFO,i} = K_1\,e_{RBO,\Delta,i} + K_2\,e_{A,\Delta,i} + K_3\,e_{sF,\Delta,i} + K_4\,e_{R,\Delta,i}$$

and

$$e_{SFO,i} = K_5\,e_{SF,\Delta,i}$$

14. Desample and Hold - A zero order hold is used on the output of the digital filter and secondary filter paths.

C.3 Subroutine C

Linear compensation is programmed for the digital filter and secondary filter loops. This compensation has the following transfer functions.

Digital filter loop:

$$\frac{1 + (\tau DC1)S}{1 + (\tau DC2)S + (\tau DC3)S^2} \cdot \frac{1 + (\tau DC4)S + (\tau DC5)S^2}{1 + (\tau DC6)S + (\tau DC7)S^2}$$

Secondary filter loop:

$$\frac{1 + (\tau SC1)S}{1 + (\tau SC2)S + (\tau SC3)S^2} \cdot \frac{1 + (\tau SC4)S + (\tau SC5)S^2}{1 + (\tau SC6)S + (\tau SC7)S^2}$$

C.4 Subroutine D

The engine actuator was simulated by the following transfer function

$$\frac{1}{1 + (\tau BE1)S + (\tau BE2)S^2 + (\tau BE3)S^3}$$

For vehicles 1 and II these time constants were evaluated as, $\tau BE1 = 7.2565E\text{-}2$, $\tau BE2 = 7.62E\text{-}4$ and $\tau BE3 = 3.2124E\text{-}5$
Subroutine D has position, rate and acceleration limits incorporated. These limits are denoted by

BEL - position limit

BELD - rate limit

BELDD - acceleration limit

C.5 Subroutine E

The following airframe equations of motion were simulated

I - Moment equation

$$\ddot{\phi} = \ddot{\phi}_R + \ddot{\phi}_B + \ddot{\phi}_S + \ddot{\phi}_E \qquad \text{where:}$$

$$\ddot{\phi}_R = -(C_1\alpha + C_2\beta_R) + C_3[13.2qA(\ell_{CG} - 4.15)\sin^2\alpha]/I_{xx},$$

$$C_3 = \begin{array}{l} 0 \text{ if } |\alpha| < .0873 \\ 1 \text{ if } \alpha \geq .0873 \end{array}$$

$$\ddot{\phi}_B = \frac{1}{I_{xx}} \left[(F \ell_{CG}) \sum_{i=1}^{4} Y_i'(x_\beta) \eta_i - F \sum_{i=1}^{4} Y_i(x_\beta) \eta_i \right]$$

$$\ddot{\phi}_S = \frac{1}{I_{xx}} \sum_{i=1}^{3} (\ell_{si} \ddot{Z}_{si} + (\frac{F-X}{m}) Z_{si}) m_{si}$$

$$\ddot{\phi}_E = \frac{-1}{I_{xx}} \left[(\ell_{CG} S_E + I_E) \ddot{\beta}_R + (\frac{F-X}{m}) S_E \beta_R \right]$$

II - Force equation

$$\ddot{Z} = \ddot{Z}_R + \ddot{Z}_B + \ddot{Z}_{SM} \qquad \text{where:}$$

$$\ddot{Z}_R = \frac{1}{m} \left[(F-x)\phi + R'\beta_R + N'\alpha \right]$$

$$\ddot{Z}_B = - \frac{F}{m} \sum_{i=1}^{4} Y_i'(x_\beta) \eta_i$$

$$\ddot{Z}_{SM} = - \frac{1}{m} \sum_{i=1}^{3} m_{si} \ddot{Z}_{si}$$

III - Angle equation

$$\alpha = \alpha_w + \phi - \theta \qquad \text{where } \theta = \dot{Z}/v$$

IV - Sensor equations

$$\phi_G = \phi - \sum_{i=1}^{4} Y_i'(x_\phi) \eta_i \qquad \text{and} \qquad \dot{\phi}_G = \dot{\phi} - \sum_{i=1}^{4} Y_i'(x_{\dot{\phi}}) \dot{\eta}_i$$

$$\ddot{\tau} = (R'\beta_R + N'\alpha)/m + \ell_A \ddot{\phi} + \ddot{Z}_B + \ddot{Z}_{SM} + \sum_{i=1}^{4} Y_i(x_{\ddot{\tau}}) \ddot{\eta}_i$$

$$\alpha_T = \alpha - \sum_{i=1}^{4} Y_i'(x_\alpha) \eta_i - \frac{1}{v} (\dot{\phi} \ell_\alpha + \sum_{i=1}^{4} Y_i(x_\alpha) \dot{\eta}_i)$$

(The sensor equations are written for ℓ_A and ℓ_α positive at the maximum q flight condition.)

V - Body bending and slosh equations

$$\begin{bmatrix} I_{33}+A & B \\ C & I_{44} \end{bmatrix} \begin{bmatrix} \ddot{Z}_S \\ \ddot{N} \end{bmatrix} = \begin{bmatrix} E \\ F \end{bmatrix}$$

where: A is 3x3, B is 3x4, C is 4x3, E is 3x1, F is 4x1

and

$$a_{ij} = -m_{sj}\left(\frac{\ell_{si}\ell_{sj}}{I_{xx}} + \frac{1}{m}\right), \quad i,j = 1,2,3$$

$$b_{ij} = +Y_j(x_{si}), \quad i=1,2,3; \; j=1,2,3,4$$

$$c_{ij} = -\frac{m_{sj}}{M_i} Y_i(x_{sj}), \quad i=1,2,3,4; \; j=1,2,3$$

$$e_i = -W_{si}(2\zeta_{si}\dot{Z}_{si} + W_{si} Z_{si}) + \frac{F-X}{m}\left(\phi - \sum_{j=1}^{4} Y_i'(x_{si})\eta_j\right) - (\ddot{Z}_R + \ddot{Z}_B)$$

$$+ \ell_{si}\left\{\ddot{\phi}_R + \ddot{\phi}_B - \left[(\ell_{CG} S_E + I_E)\ddot{\beta}_R + \left(\frac{F-X}{m}\right)\right.\right.$$

$$\left.\left.(S_E \beta_R + \sum_{j=1}^{3} m_{sj} Z_{sj})\right]/I_{xx}\right\} \qquad i = 1,2,3$$

$$f_i = -W_i(2\zeta_i\dot{\eta}_i + W_i\eta_i) + \left[R' Y_i(x_\beta)\beta_R + (S_E Y_i(x_\beta) + I_E Y_i'(x_\beta))\ddot{\beta}_R\right.$$

$$\left. + Q_\alpha \alpha + \left(\frac{F-X}{m}\right)\sum_{j=1}^{3} m_{sj} Y_i'(x_{sj}) Z_{sj}\right]/M_i \qquad i = 1,2,3,4$$

also,

$$\ddot{Z} = \left[\ddot{Z}_{si}\right], \quad i = 1,2,3$$

$$\ddot{N} = \left[\ddot{\eta}_i\right], \quad i = 1,2,3,4$$

$$E = \left[e_i\right], \quad i = 1,2,3$$

$$F = \left[f_i\right], \quad i = 1,2,3,4$$

C.6 Subroutines F and G

Individual feedback paths for the digital and secondary filter control loops were programmed with attitude, attitude rate, normal acceleration, and/or angle of attack feedback. These paths were modified by a feedback gain and then summed into two separate feedback signals: one (θ_{DF}) for the digital filter, the other (θ_{SF}) for the secondary filter.

C.7 Subroutine H

The wind input (α_w) for the control loop consists of a linear table look up function α_{w1} plus a time delayed sinusoidal function α_{w2}. The latter function is represented by the expression

$$\alpha_{w2} = \alpha_{w_s} \sin\left(w_x(t-t_\alpha) + \frac{\varphi_\alpha}{57.3^\circ}\right)$$

where:

α_{w_s} is the amplitude,

w_x is the frequency,

t_α is the time delay,

and φ_α is the phase angle of the sine wave.

APPENDIX D

D.1 CONTINUOUS REPRESENTATION OF THE DIGITAL POLYNOMIAL FILTER

If the input to the filter during the time interval from time zero until time $n\tau$ is $f(t)$ and the length of the filter s memory is $n\tau$ (n+1 samples taken every τ seconds), then the output of the filter at time $n\tau$ is

$$Y(n\tau) = A + Bn\tau + Cn^2\tau^2 \tag{D.1}$$

For the continuous (or infinite sampling rate) case, A, B, and C are determined by minimizing I where

$$I = \frac{1}{n\tau}\int_0^{n\tau}[f(t) - (A + Bt + Ct^2)]^2\,dt$$

$$= \frac{1}{n\tau}\int_0^{n\tau}[f(t)^2 - 2f(t)(A + Bt + Ct^2) + (A + Bt + Ct^2)^2]dt \tag{D.2}$$

Minimizing I gives

$$\frac{\partial I}{\partial A} = \frac{1}{n\tau}\int_0^{n\tau}[-2f(t) + 2(A + Bt + Ct^2)]dt = 0 \tag{D.3}$$

$$\frac{\partial I}{\partial B} = \frac{1}{n\tau}\int_0^{n\tau}[-2t\,f(t) + 2t(A + Bt + Ct^2)]dt = 0 \tag{D.4}$$

$$\frac{\partial I}{\partial C} = \frac{1}{n\tau}\int_0^{n\tau}[-2t^2\,f(t) + 2t^2(A + Bt + Ct^2)]dt = 0 \tag{D.5}$$

Rewriting equations (D.3), (D.4), and (D.5)

$$\int_0^{n\tau} f(t)dt = A\int_0^{n\tau} dt + B\int_0^{n\tau} tdt + C\int_0^{n\tau} t^2dt \tag{D.6}$$

$$\int_0^{n\tau} t\, f(t)dt = A\int_0^{n\tau} tdt + B\int_0^{n\tau} t^2dt + C\int_0^{n\tau} t^3dt \tag{D.7}$$

$$\int_0^{n\tau} t^2\, f(t)dt = A\int_0^{n\tau} t^2dt + B\int_0^{n\tau} t^3dt + C\int_0^{n\tau} t^4dt \tag{D.8}$$

So, a filter whose memory length is $n\tau$, the output of the filter at any time T is given by

$$y(T) = A + Bn\tau + Cn^2\tau^2 \tag{D.9}$$

where A, B and C are determined from the equations

$$\int_0^{n\tau} f(T-n\tau+t)dt = n\tau A + \frac{n^2\tau^2}{2}B + \frac{n^3\tau^3}{3}C \tag{D.10}$$

$$\int_0^{n\tau} t\, f(T-n\tau+t)dt = \frac{n^2\tau^2}{2}A + \frac{n^3\tau^3}{3}B + \frac{n^4\tau^4}{4}C \tag{D.11}$$

$$\int_0^{n\tau} t^2\, f(T-n\tau+t)dt = \frac{n^3\tau^3}{3}A + \frac{n^4\tau^4}{4}B + \frac{n^5\tau^5}{5}C \tag{D.12}$$

If f(t) is fitted with a first order polynomial instead of a second

$$y(T) = A + Bn\tau \tag{D.13}$$

where A and B are determined from the equations

$$\int_0^{n\tau} f(T-n\tau+t)dt = n\tau A + \frac{n^2\tau^2}{2}B \tag{D.14}$$

and

$$\int_0^{n\tau} t\, f(T-n\tau+t)dt = \frac{n^2\tau^2}{2}A + \frac{n^3\tau^3}{3}B \tag{D.15}$$

If f(t) is fitted with a zero order polynomial instead of a first or second

$$y(T) = A \tag{D.16}$$

where A is determined from the equation

$$\int_0^{n\tau} f(T-n\tau+t)dt = n\tau A \tag{D.17}$$

D.2 FREQUENCY RESPONSE OF THE POLYNOMIAL FITTING DIGITAL FILTER

It was shown that for the continuous (or infinite sampling rate) case the output of the filter at time T when a second order polynomial is used in the fitting process is

$$y(T) = A + n\tau B + n^2\tau^2 C \tag{D.18}$$

where A, B, and C are determined from the equations

$$\int_0^{n\tau} f(T-n\tau+t)dt = n\tau A + \frac{n^2\tau^2}{2} B + \frac{n^3\tau^3}{3} C \tag{D.19}$$

$$\int_0^{n\tau} t\, f(T-n\tau+t)dt = \frac{n^2\tau^2}{2} A + \frac{n^3\tau^3}{3} B + \frac{n^4\tau^4}{4} C \tag{D.20}$$

$$\int_0^{n\tau} t^2 f(T-n\tau+t)dt = \frac{n^3\tau^3}{3} A + \frac{n^4\tau^4}{4} B + \frac{n^5\tau^5}{5} C \tag{D.21}$$

When a first order polynomial is used in the fitting process

$$y(T) = A + n\tau B \tag{D.22}$$

where A, B, and C are determined from the equations

$$\int_0^{n\tau} f(T-n\tau+t)dt = n\tau A + \frac{n^2\tau^2}{2} B \tag{D.23}$$

$$\int_0^{n\tau} tf(T-n\tau+t)dt = \frac{n^2\tau^2}{2} A + \frac{n^3\tau^3}{3} B \qquad (D.24)$$

When a zero order polynomial is used in the fitting process

$$y(T) = A \qquad (D.25)$$

$$\int_0^{n\tau} f(T-n\tau+t)dt = n\tau A \qquad (D.26)$$

The frequency response of the polynomial fitting digital filter can readily be determined by letting

$$f(t) = \sin \omega T \qquad (D.27)$$

and selecting a value for the $n\tau$, the length of the filter s memory, say

$$n\tau = 2\pi \qquad (D.28)$$

The integrals on the left sides of Equations (D-19) through (D-21), (D-23), (D-24), and (D-26) are then given by the equations

$$\int_0^{n\tau} f(T-n\tau+t)dt = \frac{1}{\omega}\left\{(\sin 2\pi\omega)(\sin \omega T) + (\cos 2\pi\omega - 1)(\cos \omega T)\right\} \qquad (D.28)$$

$$\int_0^{n\tau} t\, f(T-n\tau+t)dt = \frac{1}{\omega^2}\left\{(1-\cos 2\pi\omega)(\sin \omega T) + (\sin 2\pi\omega - 2\pi\omega)(\cos \omega T)\right\} \qquad (D.29)$$

$$\int_0^{n\tau} t^2\, f(T-n\tau+t)dt = \frac{1}{\omega^3}\left\{(4\pi\omega - 2\sin 2\pi\omega)(\sin \omega T) + (2 - 4\pi^2\omega^2 - 2\cos 2\pi\omega)(\cos \omega T)\right\} \qquad (D.30)$$

The response to a sin ωT input for the second order polynomial fitting filter can then be determined from equations (D.25), (D.26), (D.27), (D.28), (D.36), (D.37), and (D.38). The result is

$$y(T) = \frac{3}{2\pi\omega}\left\{(\cos 2\pi\omega - 1)(\cos \omega T) + (\sin 2\pi\omega)(\sin \omega T)\right\}$$

$$- \frac{6}{\pi^2\omega^2}\left\{(\sin \omega T)(1 - \cos 2\pi\omega) + (\cos \omega T)(\sin 2\pi\omega - 2\pi\omega)\right\}$$

$$+ \frac{15}{4\pi^3\omega^3}\left\{(4\pi\omega - 2 \sin 2\pi\omega)(\sin \omega T) + (2 - 4\pi^2\omega^2 - 2 \cos 2\pi\omega)\cos \omega T\right\} \quad (D.31)$$

The response to a sin ωT input for the first order polynomial fitting filter can be determined from equations (D.22) through (D.24), (D.28), and (D.29). The result is

$$y(T) = \frac{-1}{\pi\omega}\left\{(\cos 2\pi\omega - 1)(\cos \omega T) + (\sin 2\pi\omega)(\sin \omega T)\right\}$$

$$+ \frac{3}{2\pi^2\omega^2}\left\{(1 - \cos 2\pi\omega)(\sin \omega T) + (\sin 2\pi\omega - 2\pi\omega)(\cos \omega T)\right\} \quad (D.32)$$

The response to a sin ωT input for the zero order polynomial fitting filter can be determined from equations (D.25), (D.26), and (D.28). The result is

$$y(T) = \frac{1}{2\pi\omega}\left\{(\sin 2\pi\omega)(\sin \omega T) + (\cos 2\pi\omega - 1)(\cos \omega T)\right\} \quad (D.33)$$

Noting that if a system's input is sin ωT and its steady state output is a sin ωt + b cos ωt, the complex form for its frequency response can be written as

$$G(j\omega) = a + bj \quad (D.34)$$

For the second order polynomial filter of memory length 2π

$$G(j\omega) = \left[\frac{3}{2\omega\pi} \sin 2\pi\omega - \frac{6}{\omega^2\pi^2}(1 - \cos 2\pi\omega)\right.$$

$$\left. + \frac{15}{4\pi^3\omega^3}(4\pi\omega - 2 \sin 2\pi\omega)\right]$$

$$+ j\left[\frac{3}{2\omega\pi}(\cos 2\pi\omega - 1) - \frac{6}{\omega^2\pi^2}(\sin 2\pi\omega - 2\pi\omega)\right.$$

$$\left. + \frac{15}{4\pi^3\omega^3}(2 - 4\pi^2\omega^2 - 2 \cos 2\pi\omega)\right] \qquad (D.35)$$

For the first order polynomial filter of memory length 2π

$$G(j\omega) = \left[\frac{3}{2\pi^2\omega^2}(1 - \cos 2\pi\omega) - \frac{1}{\pi\omega} \sin 2\pi\omega\right]$$

$$+ j\left[\frac{3}{2\pi^2\omega^2}(\sin 2\pi\omega - 2\pi\omega) - \frac{1}{\pi\omega}(\cos 2\pi\omega - 1)\right] \qquad (D.36)$$

For the zero order polynomial filter of memory length 2π

$$G(j\omega) = \left[\frac{1}{2\pi\omega} \sin 2\pi\omega\right] + j\left[\frac{1}{2\pi\omega}(\cos 2\pi\omega - 1)\right] \qquad (D.37)$$

APPENDIX E

DERIVATION OF EQUATIONS FOR THE DIGITAL ADAPTIVE FILTER

This appendix contains the derivation of the equations used in analytical studies to determine the characteristics of the digital filter. These equations give exact solutions for the A and B amplitude parameters for known input signals for: (1) the case of an infinite memory length, and (2) the case of a finite memory length. It is also shown in this appendix how the digital filter for either one or two parameter amplitude fitting can be represented in finite difference equation form.

E.1 Derivation of Equations for Determining the A and B Amplitude Coefficients of the Digital Filter as a Function of Time When the Input Signal is Known

The closed loop rigid body signal, e_f, is assumed to be of the general form

$$e_f = A\,\epsilon^{-\alpha t}\cos\beta t + B\,\epsilon^{-\alpha t}\sin\beta t \tag{E.1}$$

The expression for $f^2(t)$, the mean square deviation between the input $e(t)$ and e_f is then

$$f^2(t) = \frac{1}{T}\int_0^T (e(t) - Ae^{-\alpha t}\cos\beta t - Be^{-\alpha t}\sin\beta t)^2\,dt$$

$$= \frac{1}{T}\int_0^T \Big\{e^2(t) - 2e(t)(A\epsilon^{-\alpha t}\cos\beta t + B\epsilon^{-\alpha t}\sin\beta t)$$

$$+ (A\epsilon^{-\alpha t}\cos\beta t + B\epsilon^{-\alpha t}\sin\beta t)^2\Big\}dt \tag{E.2}$$

The values of A and B are selected so that $f^2(t)$ is a minimum. This occurs when $\frac{\partial f^2(t)}{\partial A}$ and $\frac{\partial f^2(t)}{\partial B}$ are zero. Therefore,

$$\frac{\partial}{\partial A} f^2(t) = \frac{1}{T}\int_0^T [-2e(t)\,\epsilon^{-\alpha t}\cos\beta t + 2\epsilon^{-\alpha t}\cos\beta t(A\epsilon^{-\alpha t}\cos\beta t + B\epsilon^{-\alpha t}\sin\beta t)]dt$$

$$= 0 \tag{E.3}$$

So

$$\int_0^T e(t)\ \epsilon^{-\alpha t}\cos\ \beta t\ dt = A \int_0^T \epsilon^{-2\alpha t}\ \cos^2\ \beta t\ dt + B \int_0^T \epsilon^{-2\alpha t}\ \sin\ \beta t\ \cos\ \beta t\ dt \tag{E.4}$$

Also, by setting $\frac{\partial f^2(t)}{\partial B}$ equal to zero

$$\int_0^T e(t)\ \epsilon^{-\alpha t}\ \sin\ \beta t\ dt = A \int_0^T \epsilon^{-2\alpha t}\ \sin\ \beta t\ \cos\ \beta t\ dt + B \int_0^T \epsilon^{-2\alpha t}\ \sin^2\ \beta t\ dt \tag{E.5}$$

The integrals on the right hand sides of (E.4) and (E.5) are readily evaluated by standard integration techniques. The results are

$$\int_0^T \epsilon^{-2\alpha t}\ \sin^2\ \beta t\ dt = \left\{\frac{1-\epsilon^{-2\alpha t}}{4\alpha} - \frac{\epsilon^{-2\alpha T}\ [\beta\ \sin\ 2\beta T - \alpha\ \cos\ 2\beta T] + \alpha}{4(\alpha^2 + \beta^2)}\right\} \tag{E.6}$$

$$\int_0^T \epsilon^{-2\alpha t}\ \cos^2\ \beta t\ dt = \left\{\frac{1-\epsilon^{-2\alpha T}}{4\alpha} + \frac{\epsilon^{-2\alpha T}\ [\beta\ \sin\ 2\beta T - \alpha\ \cos\ 2\beta T] + \alpha}{4(\alpha^2 + \beta^2)}\right\} \tag{E.7}$$

$$\int_0^T \epsilon^{-2\alpha t}\sin\ \beta t\ \cos\ \beta t dt = \left\{\frac{\epsilon^{-2\alpha T}[-\alpha\ \sin\ 2\beta T - \beta\ \cos\ 2\beta T] + \beta}{4(\alpha^2 + \beta^2)}\right\} \tag{E.8}$$

The integral on the left side of (E.4) can be expressed as

$$\int_0^T e(t)\ \epsilon^{-\alpha t}\ \cos\ \beta t\ dt = \int_0^\infty e(t)\ \epsilon^{-\alpha t}\ \cos\ \beta t\ dt - \int_T^\infty e(t)\ \epsilon^{-\alpha t}\ \cos\ \beta t\ dt \tag{E.9}$$

Using the definition of the Laplace transform, the first term on the right side of equation (E.9) can be written as

$$\int_0^\infty e(t)\ \epsilon^{-\alpha t}\ \cos\ \beta t\ dt = \left\{\mathcal{L}[e(t)\ \cos\ \beta t]\right\}_{s=\alpha} \tag{E.10}$$

Using the definition of the Laplace transform and the Laplace transform shifting theorem, the second term on the right side of equation (E.9) can be written as

$$\int_T^\infty e(t)\ \epsilon^{-\alpha t}\ \cos\ \beta t\ dt = \int_0^T 0\ dt + \int_T^\infty e(t)\ \epsilon^{-\alpha t}\ \cos\ \beta t\ dt$$

$$= \left\{\epsilon^{-sT}\mathcal{L}[e(t+T)\ \cos\ \beta(t+T)]\right\}_{s=\alpha} \qquad \text{(E.11)}$$

So the integral on the left side of (E.4) becomes

$$\int_0^T e(t)\ \epsilon^{-\alpha t}\ \cos\ \beta t\ dt = \left\{\mathcal{L}[e(t)\ \cos\ \beta t] - \epsilon^{-sT}\mathcal{L}[e(t+T)\ \cos\ \beta(t+T)]\right\}_{s=\alpha} \qquad \text{(E.12)}$$

Similarly, the integral on the left side of (E.5) becomes

$$\int_0^T e(t)\ \epsilon^{-\alpha t}\ \sin\ \beta t\ dt = \left\{\mathcal{L}[e(t)\ \sin\ \beta t] - \epsilon^{-sT}\mathcal{L}[e(t+T)\ \sin\ \beta(t+T)]\right\}_{s=\alpha} \qquad \text{(E.13)}$$

The working equations for determining A and B as functions of time can now be written. They are

$$\left\{\mathcal{L}[e(t)\cos\beta t] - \epsilon^{-sT}\mathcal{L}[e(t+T)\cos\beta(t+T)]\right\}_{s=\alpha} = A\left\{\frac{1-\epsilon^{-2\alpha T}}{4\alpha} + \frac{\epsilon^{-2\alpha T}[\beta\sin 2\beta T - \alpha\cos 2\beta T] + \alpha}{4(\alpha^2+\beta^2)}\right\}$$

$$+ B\left\{\frac{e^{-2\alpha T}[-\alpha\ \sin\ 2\beta T - \beta\ \cos\ 2\beta T] + \beta}{4(\alpha^2+\beta^2)}\right\} \qquad \text{(E.14)}$$

$$\left\{\mathcal{L}[e(t)\sin\beta t] - \epsilon^{-sT}\mathcal{L}[e(t+T)\sin\beta(t+T)]\right\}_{s=\alpha} = A\left\{\frac{\epsilon^{-2\alpha T}[-\alpha\sin 2\beta T - \beta\cos 2\beta T] + \beta}{4(\alpha^2+\beta^2)}\right\}$$

$$+ B\left\{\frac{1-\epsilon^{-2\alpha T}}{4\alpha} - \frac{\epsilon^{-2\alpha T}[\beta\sin 2\beta T - \alpha\cos 2\beta T] + \alpha}{4(\alpha^2+\beta^2)}\right\} \qquad \text{(E.15)}$$

When e(t), T, α and β are known, (E.14) and (E.15) become two linear algebraic equations with A and B being the unknowns, so A and B can readily be determined at any time T.

The expressions on the left hand sides of (E.14) and (E.15) have been evaluated for e(t) inputs of the form $\epsilon^{-at}\cos\gamma t$, $\epsilon^{-at}\sin\gamma t$ and t^n. The results are summarized below.

1. The term $\left\{\mathcal{L}[e(t)\cos\beta t]-\epsilon^{-sT}\mathcal{L}[e(t+T)\cos\beta(t+T)]\right\}_{s=\alpha}$ evaluated for

(a) $e(t) = \epsilon^{-at}\cos\gamma t$ is given by the expression

$$\left[\frac{1}{2}\frac{(\alpha+a)}{(\alpha+a)^2+(\gamma+\beta)^2}+\frac{1}{2}\frac{\alpha+a}{(\alpha+a)^2+(\gamma-\beta)^2}\right]-\frac{\epsilon^{-(\alpha+a)T}}{2}\left[\frac{(\alpha+a)\cos(\gamma+\beta)T}{(\alpha+a)^2+(\gamma+\beta)^2}\right.$$

$$\left.-\frac{(\gamma+\beta)\sin(\gamma+\beta)T}{(\alpha+a)^2+(\gamma+\beta)^2}+\frac{(\alpha+a)\cos(\gamma-\beta)T}{(\alpha+a)^2+(\gamma-\beta)^2}-\frac{(\gamma-\beta)\sin(\gamma-\beta)T}{(\alpha+a)^2+(\gamma-\beta)^2}\right] \qquad \text{(E.16)}$$

(b) $e(t) = \epsilon^{-at}\sin\gamma t$ is given by the expression

$$\left[\frac{1}{2}\frac{(\alpha+\beta)}{(\alpha+a)^2+(\gamma+\beta)^2}+\frac{1}{2}\frac{(\gamma-\beta)}{(\alpha+a)^2+(\beta-\gamma)^2}\right]-\frac{\epsilon^{-(\alpha+a)T}}{2}\left[\frac{(\alpha+a)\sin(\gamma+\beta)T}{(\alpha+a)^2+(\gamma+\beta)^2}\right.$$

$$\left.+\frac{(\gamma+\beta)\cos(\gamma+\beta)T}{(\alpha+a)^2+(\gamma+\beta)^2}+\frac{(\alpha+a)\sin(\gamma-\beta)T}{(\alpha+a)^2+(\gamma-\beta)^2}+\frac{(\gamma-\beta)\cos(\gamma-\beta)T}{(\alpha+a)^2+(\gamma-\beta)^2}\right] \qquad \text{(E.17)}$$

(c) $e(t) = t^n$, $n > 0$ is given by the expression

$$\left[2^{n-1}\,n!\,\alpha^{n-1}\,(\alpha^2-\beta^2)\right]\frac{1}{(\alpha^2+\beta^2)^{n+1}}-\frac{\epsilon^{-\alpha T}T^n}{\alpha^2+\beta^2}\left[\alpha\cos\beta T-\beta\sin\beta T\right]$$

$$-\epsilon^{-\alpha T}\left[\sum_{i=0}^{n-1}\frac{T^i\,n!\,2^{n-i-1}\,\alpha^{n-i-1}}{i!\,(\alpha^2+\beta^2)^{n-i-1}}\right]\left[(\alpha^2-\beta^2)\cos\beta T-2\alpha\beta\sin\beta T\right] \qquad \text{(E.18)}$$

2. The term $\left\{\mathcal{L}[e(t)\sin\beta t]-\epsilon^{-sT}\mathcal{L}[e(t+T)\cos\beta(t+T)]\right\}_{s=\alpha}$ evaluated for

(a) $e(t) = \epsilon^{-at}\cos\gamma t$ is given by the expression

$$\left[\frac{1}{2}\frac{(\beta+\gamma)}{(\alpha+a)^2+(\beta+\gamma)^2}+\frac{1}{2}\frac{(\beta-\gamma)}{(\alpha+a)^2+(\beta-\gamma)^2}\right]$$

$$-\frac{\epsilon^{-(\alpha+a)T}}{2}\left[\frac{(\alpha+a)\sin(\beta+\gamma)T}{(\alpha+a)^2+(\beta+\gamma)^2}+\frac{(\beta+\gamma)\cos(\beta+\gamma)T}{(\alpha+a)^2+(\beta+\gamma)^2}\right.$$

$$\left.+\frac{(\alpha+a)\sin(\beta-\gamma)T}{(\alpha+a)^2+(\beta-\gamma)^2}+\frac{(\beta-\gamma)\cos(\beta-\gamma)T}{(\alpha+a)^2+(\beta-\gamma)^2}\right] \qquad (E.19)$$

(b) $e(t) = \epsilon^{-at} \sin \gamma t$ is given by the expression

$$\left[\frac{1}{2}\frac{(\alpha+a)}{(\alpha+a)^2+(\gamma-\beta)^2}-\frac{1}{2}\frac{(\alpha+a)}{(\alpha+a)^2+(\gamma+\beta)^2}\right]$$

$$-\frac{\epsilon^{-(\alpha+a)T}}{2}\left[\frac{(\alpha+a)\cos(\gamma-\beta)T}{(\alpha+a)^2+(\gamma-\beta)^2}-\frac{(\gamma-\beta)\sin(\gamma-\beta)T}{(\alpha+a)^2+(\gamma-\beta)^2}\right.$$

$$\left.-\frac{(\alpha+a)\cos(\gamma+\beta)T}{(\alpha+a)^2+(\gamma+\beta)^2}+\frac{(\gamma+\beta)\sin(\gamma+\beta)T}{(\alpha+a)^2+(\gamma+\beta)^2}\right] \qquad (E.20)$$

(c) $e(t) = t^n$, $n > 0$ is given by the expression

$$\frac{2^n\,\beta n!\,\alpha^n}{(\alpha^2+\beta^2)^{n+1}}-\epsilon^{-\alpha T}\sum_{i=0}^{n-1}\frac{T^i\,n!\,2^{n-i-1}\,\alpha^{n-i-1}}{i!\,(\alpha^2+\beta^2)^{n-i-1}}\left[(\alpha^2-\beta^2)\sin\beta T+2\alpha\beta\cos\beta T\right]$$

$$-\frac{\epsilon^{-\alpha T}}{\alpha^2+\beta^2}\left[\alpha\sin\beta T+\beta\cos\beta T\right] \qquad (E.21)$$

After selecting the desired form of inputs, the A and B fitting parameters are readily computed as a function of the fitting parameters α, β and the input parameters a, γ, and n.

E.2 Equations for Determining the A and B Amplitude Coefficients of the Digital Filter When the Input Signal is Known and the Filter Memory is Filled

It was shown that before the memory of the filter is filled, the two parameter fitting coefficients, A and B, are determined by equations (E.4) and (E.5) where e(t) is the error signal input to the filter.

Equations (E.4) and (E.5) can readily be extended to include the filled memory situation. Letting τ be the time between samples and assuming n+1 samples are stored in the computer memory, the output of the filter at time T is calculated as if time T-nτ is time zero and time T is time nτ and e(t) is shifted appropriately. Therefore, the equations for determining A and B are

$$\int_0^{n\tau} e(T-n\tau+t)\epsilon^{-\alpha t}\cos\beta t\,dt = A\int_0^{n\tau}\epsilon^{-2\alpha t}\cos^2\beta t dt + B\int_0^{n\tau}\epsilon^{-2\alpha t}\sin\beta t\cos\beta t dt \qquad (E.22)$$

$$\int_0^{n\tau} e(T-n\tau+t)\epsilon^{-\alpha t}\sin\beta t dt = A\int_0^{n\tau}\epsilon^{-2\alpha t}\sin\beta t\cos\beta t dt + B\int_0^{n\tau}\epsilon^{-2\alpha t}\sin^2\beta t dt \qquad (E.23)$$

The integrals on the right hand side of equations (E.22) and (E.23) remain constant after the memory is filled. They can be evaluated by standard integration techniques and become

$$\int_0^{n\tau}\epsilon^{-2\alpha t}\sin^2\beta t dt = \left\{\frac{1-\epsilon^{-2\alpha n\tau}}{4\alpha} - \frac{\epsilon^{-2\alpha n\tau}\left[\beta\sin 2\beta n\tau - \alpha\cos 2\beta n\tau\right]+\alpha}{4(\alpha^2+\beta^2)}\right\} \qquad (E.24)$$

$$\int_0^{n\tau}\epsilon^{-2\alpha t}\cos^2\beta t dt = \left\{\frac{1-\epsilon^{-2\alpha n\tau}}{4\alpha} + \frac{\epsilon^{-2\alpha n\tau}\left[\beta\sin 2\beta n\tau - \alpha\cos 2\beta n\tau\right]+\alpha}{4(\alpha^2+\beta^2)}\right\} \qquad (E.25)$$

$$\int_0^{n\tau}\epsilon^{-2\alpha t}\sin\beta t\cos\beta t dt = \left\{\frac{\epsilon^{-2\alpha n\tau}\left[-\alpha\sin 2\beta n\tau - \beta\cos 2\beta n\tau\right]+\beta}{4(\alpha^2+\beta^2)}\right\} \qquad (E.26)$$

Now, the integrals on the left hand sides of equations (E.22) and (E.23) can be evaluated by the technique described in (E.1). The results are

$$\int_0^{n\tau} e(T-n\tau+t)\epsilon^{-\alpha t}\cos\beta t dt = \left\{\mathcal{L}[e(T-n\tau+t)\cos\beta t] - \epsilon^{-sn\tau}\mathcal{L}[e(T+t)\cos\beta(t+n\tau)]\right\}_{s=\alpha} \qquad (E.27)$$

$$\int_0^{n\tau} e(T-n\tau+t)\epsilon^{-\alpha t}\sin\beta t dt = \left\{\mathcal{L}[e(T-n\tau+t)\sin\beta t] - \epsilon^{-sn\tau}\mathcal{L}[e(T+t)\sin\beta(t+n\tau)]\right\}_{s=\alpha} \qquad (E.28)$$

The equations for determining the A and B coefficients can now be written as

$$[e(T-n\tau+t)\cos\beta t]-\epsilon^{-sn\tau}\ [e(T+t)\cos\beta(t+n\tau)]_{s=\alpha}$$

$$= A\,\frac{1-\epsilon^{-2\alpha n\tau}}{4\alpha} + \frac{\epsilon^{-2\alpha n\tau}[\beta\sin 2\beta n\tau - \alpha\cos 2\beta n\tau]+\alpha}{4(\alpha^2+\beta^2)}$$

$$+ B\,\frac{\epsilon^{-2\alpha n\tau}[-\alpha\sin 2\beta n\tau - \beta\cos 2\beta n\tau]+\beta}{4(\alpha^2+\beta^2)} \qquad (E.29)$$

$$[e(T-n\tau+t)\sin\beta t]-\epsilon^{-2n\tau}\ [e(T+t)\sin\beta(t+n\tau)]_{s=\alpha}$$

$$= A\,\frac{\epsilon^{-2\alpha n\tau}[-\alpha\sin 2\beta n\tau - \beta\cos 2\beta n\tau]+\beta}{4(\alpha^2+\beta^2)}$$

$$+ B\,\frac{1-\epsilon^{-2\alpha n\tau}}{4\alpha} - \frac{\epsilon^{-2\alpha n\tau}\,[\beta\sin 2\beta n\tau - \alpha\cos 2\beta n\tau]+\alpha}{4(\alpha^2+\beta^2)} \qquad (E.30)$$

Once the filter input e(t) is known and T selected equations (E.29) and (E.30) reduce to two linear algebraic equations in the two unknowns A and B, hence A and B can readily be evaluated at any time T.

E.3 Finite Difference Equation Representation of the Digital Adaptive Filter as the Memory Fills

In order to facilitate the study of the closed loop operation of systems containing the digital adaptive filter, it is very desirable to be able to represent the digital adaptive filter by a finite difference equation. Then standard z transform block diagram algebra manipulations will yield the finite difference equation describing the entire closed loop system. Such things as compensating networks and fitting parameters can therefore be more readily selected.

The finite difference equation for one parameter fitting will be developed here. The resulting finite difference equation for two parameter fitting will also be given. For one parameter fitting, the error signal input to the filter is e and the output of the filter is e_f where

$$e_f = C\ \epsilon^{-\alpha t} \tag{E.31}$$

and C is selected so that the quantity $f^2(t)$,

$$f^2(t) = \frac{1}{T}\int_0^T (e-e_f)^2\ dt \tag{E.32}$$

is a minimum. Taking the derivative of $f^2(t)$ with respect to C and setting the resultant expression equal to zero yields the expression for calculating C

$$C = \frac{\int_0^T e(t)\ \epsilon^{-\alpha t}\ dt}{\int_0^T \epsilon^{-2\alpha t}\ dt} = \frac{\int_0^T e(t)\ \epsilon^{-\alpha t}\ dt}{(1\ -\ \epsilon^{-2\alpha t})/2\alpha} \tag{E.33}$$

So, the output of the filter at any time T is given by the expression

$$e_f(T) = \left[\frac{2\alpha}{1\ -\ \epsilon^{-2\alpha T}}\ \int_0^T e(t)\ \epsilon^{-\alpha t}\ dt\right]\epsilon^{-\alpha T} \tag{E.34}$$

Letting τ be the time between samples and n be the number of the sample, at time $n\tau$

$$e_f(n\tau) = \left[\frac{2\alpha}{1\ -\ \epsilon^{-2\alpha n\tau}}\ \int_0^{n\tau} e(t)\ \epsilon^{-\alpha t}dt\right]\epsilon^{-\alpha n\tau} \tag{E.35}$$

At time $(n-1)\tau$

$$e_f[(n-1)\tau] = \left[\frac{2\alpha}{1\ -\ \epsilon^{-2\alpha(n-1)\tau}}\ \int_0^{(n-1)\tau} e(t)\ \epsilon^{-\alpha t}dt\right]\epsilon^{-\alpha(n-1)\tau} \tag{E.36}$$

Now, for a first (but obviously not a necessary) approximation, τ can be assumed to be small so that $e^{-\alpha n\tau} = e^{-\alpha(n-1)\tau}$ and equation (E.35) can be rewritten as

$$e_f(n\tau) = \left[\frac{2\alpha}{\epsilon^{\alpha(n-1)\tau}\ -\ \epsilon^{-\alpha(n-1)\tau}}\ \int_0^{n\tau} e(t)\ \epsilon^{-\alpha t}dt\right] \tag{E.37}$$

Subtracting (E.36) from (E.37)

$$e_f(n\tau) - e_f[(n-1)\tau] = \left[\frac{2\alpha}{\epsilon^{\alpha(n-1)\tau} - \epsilon^{-\alpha(n-1)\tau}}\right] \int_{(n-1)\tau}^{n\tau} e(t)\ \epsilon^{-\alpha t} dt \qquad (E.38)$$

Again, as first approximation

$$\int_{(n-1)\tau}^{n\tau} e(t)\ \epsilon^{-\alpha t} dt = \tau\ \epsilon^{-\alpha(n-1)\tau}\ e[(n-1)\tau] \qquad (E.39)$$

So equation (E.38) can be rewritten as

$$e_f(n\tau) - e_f[(n-1)\tau] = \frac{2\alpha\tau}{[\epsilon^{2\alpha(n-1)\tau} - 1]} e[(n-1)\tau] \qquad (E.40)$$

This is a simple time varying finite difference equation relating the filter output e_f with the filter input e. In z-transfer function form

$$\frac{E_f(z)}{E(z)} = \frac{2\alpha\tau}{[\epsilon^{2\alpha(n-1)\tau} - 1]} \frac{z^{-1}}{1-z^{-1}} \qquad (E.41)$$

For two parameter fitting, the z-transfer function is

$$\frac{E_f(z)}{E(z)} = \left[\frac{k_1 + k_2}{k_3}\right] \frac{z^{-1}}{1 - z^{-1}} \qquad (E.42)$$

where k_1, k_2, and k_3 are functions of time, n. The z transforms are used here as a means of approximation. Strictly speaking no time varying z transforms exist.

$$k_1 = \left\{\frac{1-\epsilon^{-2\alpha(n-1)\tau}}{4\alpha} - \frac{\epsilon^{-2\alpha(n-1)\tau}[\beta\sin 2\beta(n-1)\tau - \alpha\cos 2\beta(n-1)\tau] + \alpha}{4(\alpha^2+\beta^2)}\right\} \tau\epsilon^{-2\alpha(n-1)\tau} \cos^2\beta(n-1)\tau$$

$$- \left\{\frac{\epsilon^{-2\alpha(n-1)\tau}[-\alpha\sin 2\beta(n-1)\tau - \beta\cos 2\beta(n-1)\tau] + \beta}{4(\alpha^2+\beta^2)}\right\} \tau\epsilon^{-2\alpha(n-1)\tau} \sin\beta(n-1)\tau\ \cos\beta(n-1)\tau \qquad (E.43)$$

$$k_2 = \left\{\frac{1-\epsilon^{-2\alpha(n-1)\tau}}{4\alpha} + \frac{\epsilon^{-2\alpha(n-1)\tau}[\beta\sin 2\beta(n-1)\tau - \alpha\cos 2\beta(n-1)\tau] + \alpha}{4(\alpha^2+\beta^2)}\right\}\tau\epsilon^{-2\alpha(n-1)\tau}\sin^2\beta(n-1)\tau$$

$$+\left\{\frac{\epsilon^{-2\alpha(n-1)\tau}[-\alpha\sin 2\beta(n-1)\tau - \beta\cos 2\beta(n-1)\tau] + \beta}{4(\alpha^2+\beta^2)}\right\}\tau\epsilon^{-2\alpha(n-1)\tau}\sin\beta(n-1)\tau\cos\beta(n-1)\tau \qquad \text{(E.44)}$$

$$k_3 = \left\{\frac{1-\epsilon^{-2\alpha(n-1)\tau}}{4\alpha}\right\}^2 - \left\{\frac{\epsilon^{-2\alpha(n-1)\tau}[\beta\sin 2\beta(n-1)\tau - \alpha\cos 2\beta(n-1)\tau] + \alpha}{4(\alpha^2+\beta^2)}\right\}^2$$

$$-\left\{\frac{\epsilon^{-2\alpha(n-1)\tau}[-\alpha\sin 2\beta(n-1)\tau - \beta\cos 2\beta(n-1)\tau] + \beta}{4(\alpha^2+\beta^2)}\right\}^2 \qquad \text{(E.45)}$$

E.4 Finite Difference Equation Representation of the Digital Filter With Filled Memory

The equations which determine the A and B coefficients at any time T when the filter's memory is filled are given by equations (E.27) and (E.28).

$$\int_0^{n\tau} e(T-n\tau+t)\epsilon^{-\alpha t}\cos\beta t\,dt = A(T)I_1 + B(T)I_2 \qquad \text{(E.46)}$$

$$\int_0^{n\tau} e(T-n\tau+t)\epsilon^{-\alpha t}\sin\beta t\,dt = A(T)I_2 + B(T)I_3 \qquad \text{(E.47)}$$

Here I_2 and I_3 are constants given by the equations

$$I_1 = \frac{1-\epsilon^{-2\alpha n\tau}}{4\alpha} + \frac{\epsilon^{-2\alpha n\tau}[\beta\sin 2\beta n\tau - \alpha\cos 2\beta n\tau] + \alpha}{4(\alpha^2+\beta^2)} \qquad \text{(E.48)}$$

$$I_2 = \frac{\epsilon^{-2\alpha n\tau}[-\alpha\sin 2\beta n\tau - \beta\cos 2\beta n\tau] + \beta}{4(\alpha^2+\beta^2)} \qquad \text{(E.49)}$$

$$I_3 = \frac{1-\epsilon^{-2\alpha n\tau}}{4\alpha} - \frac{\epsilon^{-2\alpha n\tau}\left[\beta \sin 2\beta n\tau - \alpha \cos 2\beta n\tau\right] + \alpha}{4(\alpha^2+\beta^2)} \tag{E.50}$$

Solving equations (E.46) and (E.47) for A(T) and B(T)

$$A(T) = \frac{I_3 \int_0^{n\tau} e(T-n\tau+t)\epsilon^{-\alpha t}\cos \beta t dt - I_2 \int_0^{n\tau} e(T-n\tau+t)\epsilon^{-\alpha t}\sin \beta t dt}{I_1 I_3 - I_2^2} \tag{E.51}$$

$$B(T) = \frac{I_1 \int_0^{n\tau} e(T-n\tau+t)\epsilon^{-\alpha t}\sin \beta t dt - I_2 \int_0^{n\tau} e(T-n\tau+t)\epsilon^{-\alpha t}\cos \beta t dt}{I_1 I_3 - I_2^2} \tag{E.52}$$

Equations (E.51) and (E.52) can be rewritten as

$$A(T) = \frac{I_3 \int_{T-n\tau}^{T} e(t)\epsilon^{-\alpha(t-T+n\tau)}\cos\beta(t-T+n\tau)dt - I_2 \int_{T-n\tau}^{T} e(t)\epsilon^{-\alpha(t-T+n\tau)}\sin\beta(t-T+n\tau)dt}{I_1 I_3 - I_2^2} \tag{E.53}$$

$$B(T) = \frac{I_1 \int_{T-n\tau}^{T} e(t)\epsilon^{-\alpha(t-T+n\tau)}\sin\beta(t-T+n\tau)dt - I_2 \int_{T-n\tau}^{T} e(t)\epsilon^{-\alpha(t-T+n\tau)}\cos\beta(t-T+n\tau)dt}{I_1 I_3 - I_2^2} \tag{E.54}$$

Now let

$$y(T) = \int_{T-\tau}^{T} e(t)\epsilon^{-\alpha(t-T+n\tau)}\cos \beta(t-T+n\tau)dt \tag{E.55}$$

and

$$y(T-\tau) = \int_{T-n\tau-\tau}^{T-\tau} e(t)\epsilon^{-\alpha(t-T-\tau+n\tau)} \cos \beta(t-T-\tau+n\tau)d\tau \tag{E.56}$$

So, assuming τ is small

$$\epsilon^{-\alpha(t-T+n\tau)} \simeq \epsilon^{-\alpha(t-T-\tau+n\tau)} \tag{E.57}$$

$$\cos \beta(t-T+n+) \simeq \cos \beta(t-T-\tau+n\tau) \tag{E.58}$$

and subtracting equation (E.56) from equation (E.55)

$$y(T) - y(T-\tau) = \int_{T-\tau}^{T} e(t)\epsilon^{-\alpha(t-T+n\tau)} \cos \beta(t-\tau+n\tau)dt$$

$$- \int_{T-n\tau-\tau}^{T-n\tau} e(t)\epsilon^{-\alpha(t-T-\tau+n\tau)} \cos \beta(t-T-\tau+n\tau)dt \tag{E.59}$$

Evaluating the integrals in equation (E.59) by rectangular integration

$$y(T) - y(T-\tau) \simeq e(T-\tau)[\epsilon^{-\alpha n\tau} \cos \beta n\tau]\tau$$

$$- e[T-(n+1)\tau][\epsilon^{0} \cos 0]\tau \tag{E.60}$$

By inspection of equations (E.53) through (E.60), it is possible then to write the finite difference equation representation of the filled memory filter

$$A(T)-A(T-\tau) = \frac{I_3\{e(T-\tau)\epsilon^{-\alpha n\tau}\cos\beta n\tau - e[T-(n+1)\tau]\}\tau - I_2\{e(T-\tau)\epsilon^{-\alpha n\tau}\sin\beta n\tau\}\tau}{I_1I_3 - I_2^2} \tag{E.61}$$

$$B(T)-B(T-\tau) = \frac{I_1\{e(T-\tau)\epsilon^{-\alpha n\tau}\sin\beta n\tau\}\tau - I_2\{e(T-\tau)\epsilon^{-\alpha n\tau}\cos\beta n\tau - e[T-(n+1)\tau]\}\tau}{I_1I_3 - I_2^2} \tag{E.62}$$

Alternatively, noting the equation (E.__) gives the output of the filter, the z transform of the filter is

$$\frac{E_f(z)}{E(z)} = \frac{\{I_3 \cos^2 \beta n\tau - 2I_2 \sin \beta n\tau \cos \beta n\tau + I_1 \sin^2 \beta n\tau\}\epsilon^{-2n\tau\alpha_\tau}}{I_1I_3 - I_2^2} \frac{z^{-1}}{1 - z^{-1}}$$

$$+ \frac{\{-I_3 + I_2\}\tau}{I_1I_3 - I_2^2} \frac{z^{-1-n}}{1 - z^{-1}} \tag{E.63}$$

APPENDIX F

ROOT LOCUS ANALYSIS OF THE CONTROL SYSTEM DESIGNS

The selections of the stability compensation network parameters for the various Vehicle I and II control systems studies were determined primarily from the hybrid simulation. The trial and error synthesis technique used in these simulation studies was supplemented by the use of the root locus analysis of the systems studied. The root locus studies saved a considerable amount of time in the selection of the required compensation and at the same time gave considerable insight into control problems existing for the study vehicles. This appendix presents the root locus plots of the Vehicle II control system Deisgns II.1, II.2, and II.3 at the maximum q flight condition. These designs were used in the analysis of the digital polynomial filter. Root locus plots are also presented for the digital adaptive filter and secondary filter system designs used with Vehicle I at the lift-off, maximum q, and burnout flight conditions. The root locus plots were obtained from an existing IBM 7094 digital computer program which found the closed loop poles by solving for the roots of the determinant of the matrix(with a size of up to 16 by 16) whose elements were the Laplace transformed coefficients (up to a second order) of the vehicle's pitching moment, normal force, angle, body bending, fuel slosh, compensation, and control equations (all including cross coupling terms of the bending and slosh). Because of the size and complexity of the matrix the accuracy of the roots obtained could not readily be checked. However, the hybrid simulation did verify (in a general way) the system stability characteristics shown on the root locus plots. One note of interest is that the cross coupling between the bending and slosh modes of Vehicle II caused the first bending mode pole location (open loop) to shift into the right half plane. This of course complicated the system compensation requirements.

F.1 Vehicle II Control System Designs

The Vehicle II root locus with the control system Design II.1 compensation is shown in Figure F.1. This design has a single notch filter compensation of the form

$$[.116]\ \frac{[\,(S+5.5)^2+(9.23)^2\,]}{(S+5.65)\,(S+2.35)}$$

designed to stabilize the bending and slosh modes, and a command compensation of

$$(1/5)\ \left(\frac{S+.1}{S+.02}\right)$$

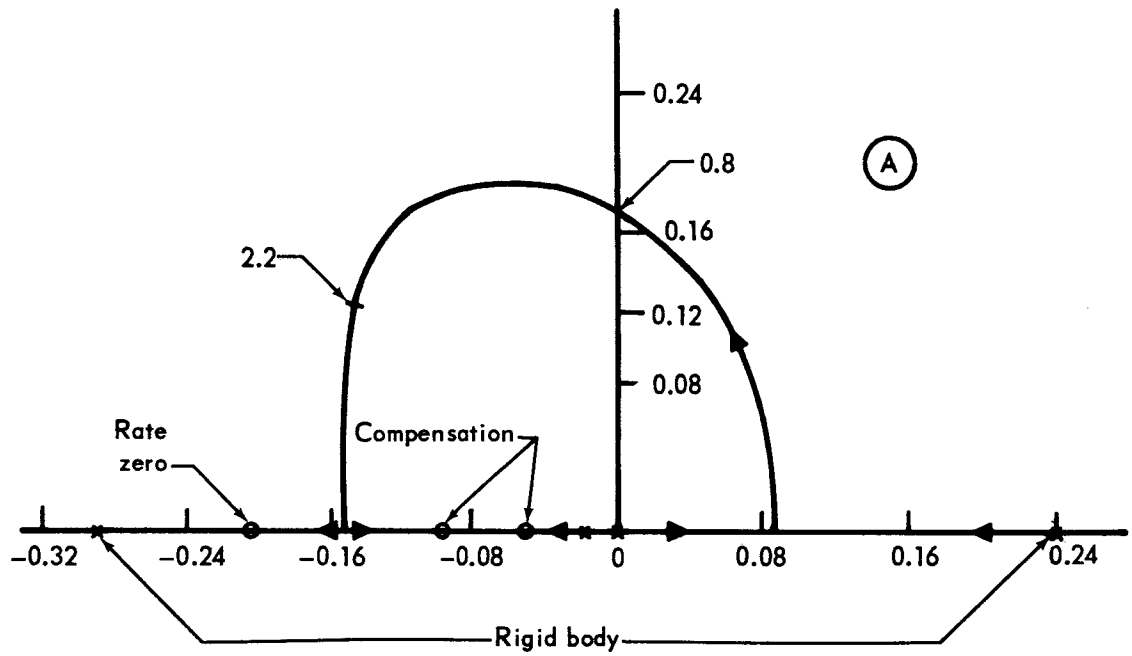

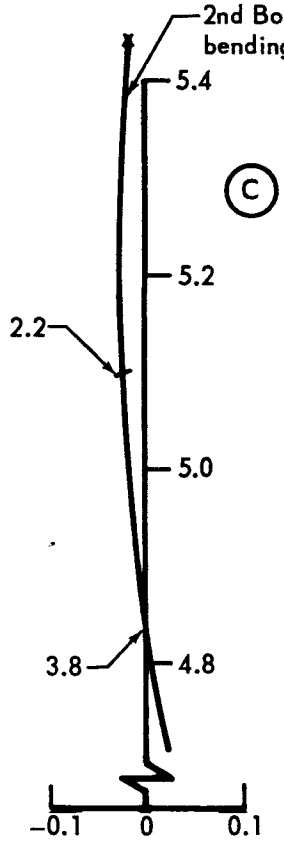

Open Loop Poles

Quantity	Location	
	Real	Imaginary
Compensation	−.02	0
	−2.35	0
	−5.65	0
Servo	−14.64	0
Rigid body	0	0
	−.29170	0
	.24050	0
Body bending	.1504	±2.498
	−.0187	±5.438
	−.0302	±8.634
	−.0580	±12.280
Propellant slosh	−.2451	±2.560
	−.0873	±2.810
	−.1010	±3.037

Open Loop Zeros

Quantity	Loc
	Real
Compensation	−.1
	−5.5
Rate Feedback	−.2049
Rigid body	−.0509
Body bending	.6190
	5.8590
	6.5450
	−.0281
	−.0094
Propellant slosh	−.0818
	−.0897
	−.4314

Figure F1 Vehicle II Root Locus of System Design II-1 Without Acceleration Feedback At the Maximum q Flight Condition

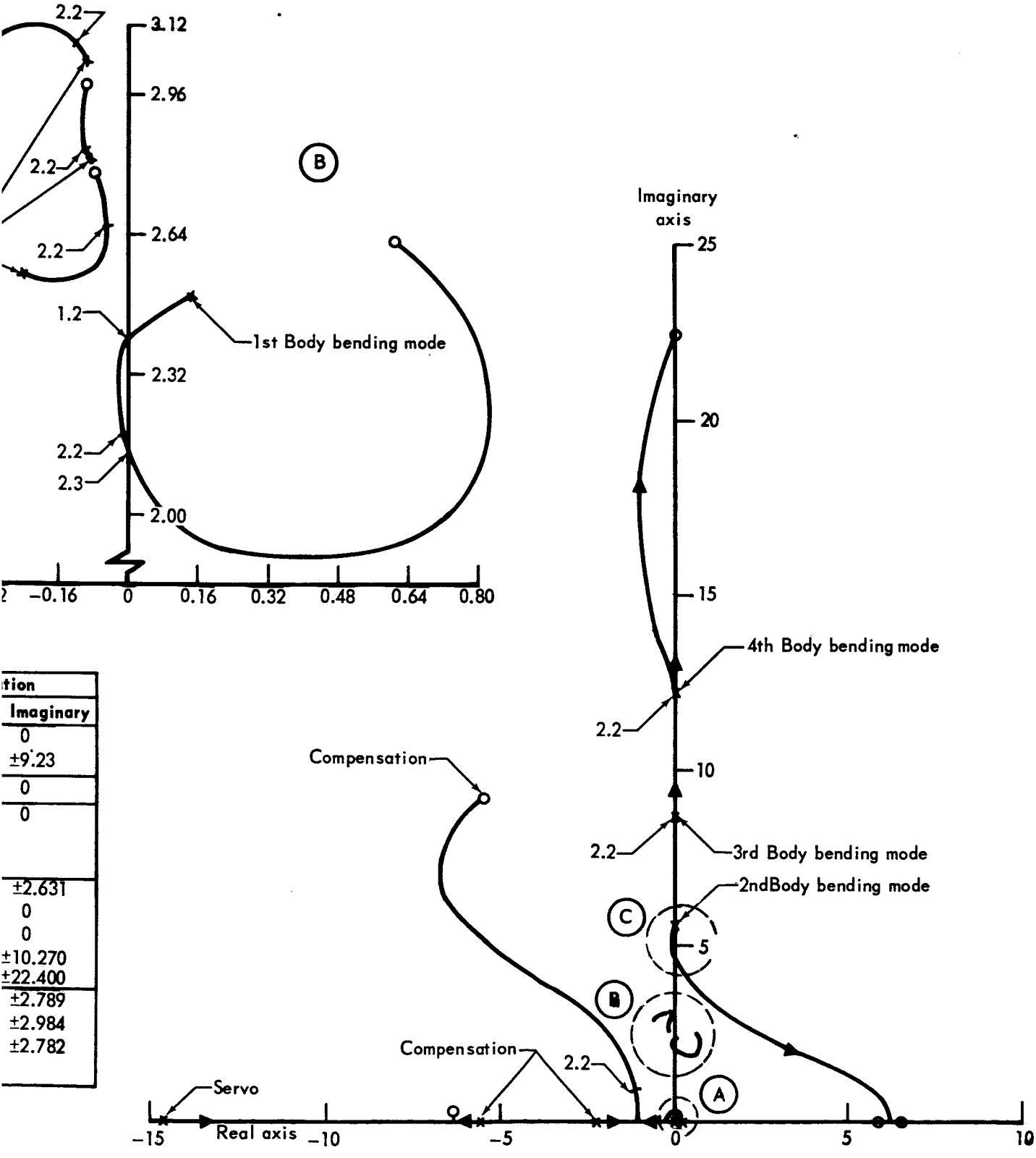

tion
Imaginary
0
±9.23
0
0
±2.631
0
0
±10.270
±22.400
±2.789
±2.984
±2.782

272-2

designed to improve the steady state response of the system. The attitude and attitude rate feedback for this configuration are $K_{\phi} = 1.0$ and $K_{\dot{\phi}} = 5.0$ respectively. The forward loop gain is $K = 2.2$ as shown on the root locus. There is no acceleration or angle of attack feedback in this root locus.

The amount of compensation used is not considered excessive considering the complexity of Vehicle II. Two important characteristics of the system are:

(1) The dominant closed loop rigid body pole, $-0.15 \pm j\ 0.125$, is closer to the origin than one might wish. It is difficult to increase the speed of response associated with this pole by linear means. Faster response to attitude commands could, however, be produced by the use of the digital adaptive filter.

(2) The damping in the area of the first bending mode and the slosh modes is less than desirable.

The latter point is an inherent difficulty of Vehicle II as is evident from the Detail B of Figure F.1 (and its inherent nature is confirmed by similar details in Figure F.2 and F.3). This detail shows two essentially vertical branches near the imaginary axis which respectively start up or down from a pole. To improve damping in this area some additional angle must be introduced by adding or moving some poles and zeros. The poles at which the two vertical branches originate are very close to each other. However, the angle change at both branches resulting from any added compensation will be almost the same unless the new compensation is located in the immediate vicinity of these poles. The consequence is that one vertical branch moves towards the imaginary axis and the other one moves away from it. This requires the compromise of setting both of these troublesome poles at the same, rather low, damping. This results in the slowly damped beat oscillation which can be observed on some of the simulation runs.

A direct remedy for this situation would be the introduction of a pole and a zero in the midst of the first bending mode and slosh poles and zeros. Such a compensation would exert little effect on the system response except in the immediate vicinity of the slosh and first bending mode poles, consequently it would effect only the slosh and first bending complex. Also, the resulting loci of the slosh and bending modes would be quite sensitive to the location of the compensation. One attempt might be to add a pole at $-0.2 \pm j\ 2.9$ and a zero at $-0.2 \pm j\ 2.66$ to the Figure F.1 compensation. This should isolate all the slosh branches in an acceptable region of the s plane except one branch which then could be independently compensated. However, such an approach would work well only as long as the first bending and slosh poles and zeros are in the exact positions assumed for the model instrumentation. Since this situation cannot always be expected, it appears more desirable to rely on some general compensation which is relatively insensitive to the inaccuracies associated with the locations of the vehicle bending and slosh modes.

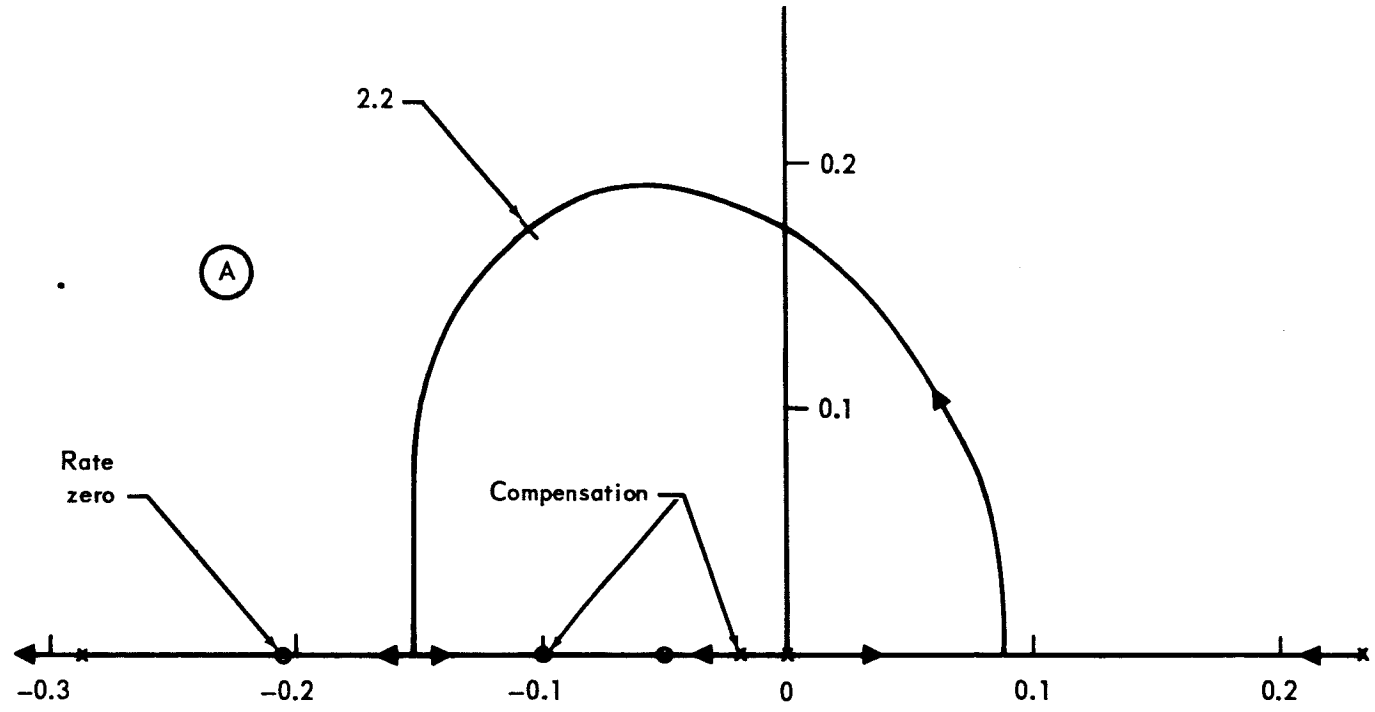

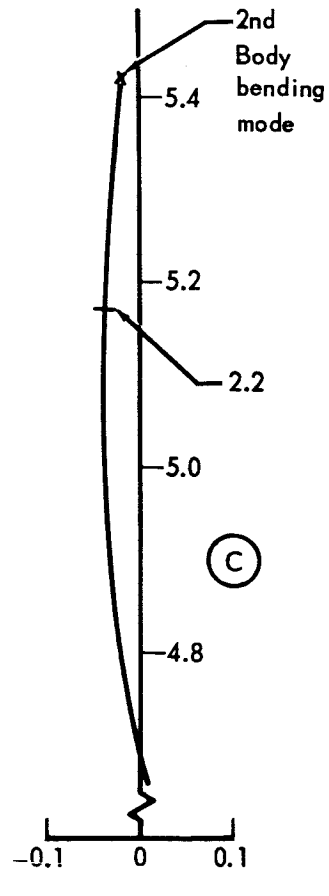

Open Loop Poles

Quantity	Location	
	Real	Imaginary
Compensation	−3.0	0
	−5.0	0
	−3.5	±8.35
Servo	−14.64	0
Rigid body	0	0
	−.2917	0
	.2405	0
Body bending	.1504	±2.498
	−.0187	±5.438
	−.0302	±8.634
	−.0580	±12.280
Propellant slosh	−.2451	±2.560
	−.0873	±2.810
	−.1010	±3.037

Open Loop Z

Quantity	Re
Compensation	−4.0
	−5.0
Rate Feedback	−.2
Rigid body	
	−.05
Body bending	.6
	5.8
	6.4
	−.0
	−.0
Propellant slosh	−.0
	−.0
	−.4

Figure F2 Vehicle II Root Locus of System Design II.2 Without Acceleration Feedback At the Maximum q Flight Condition

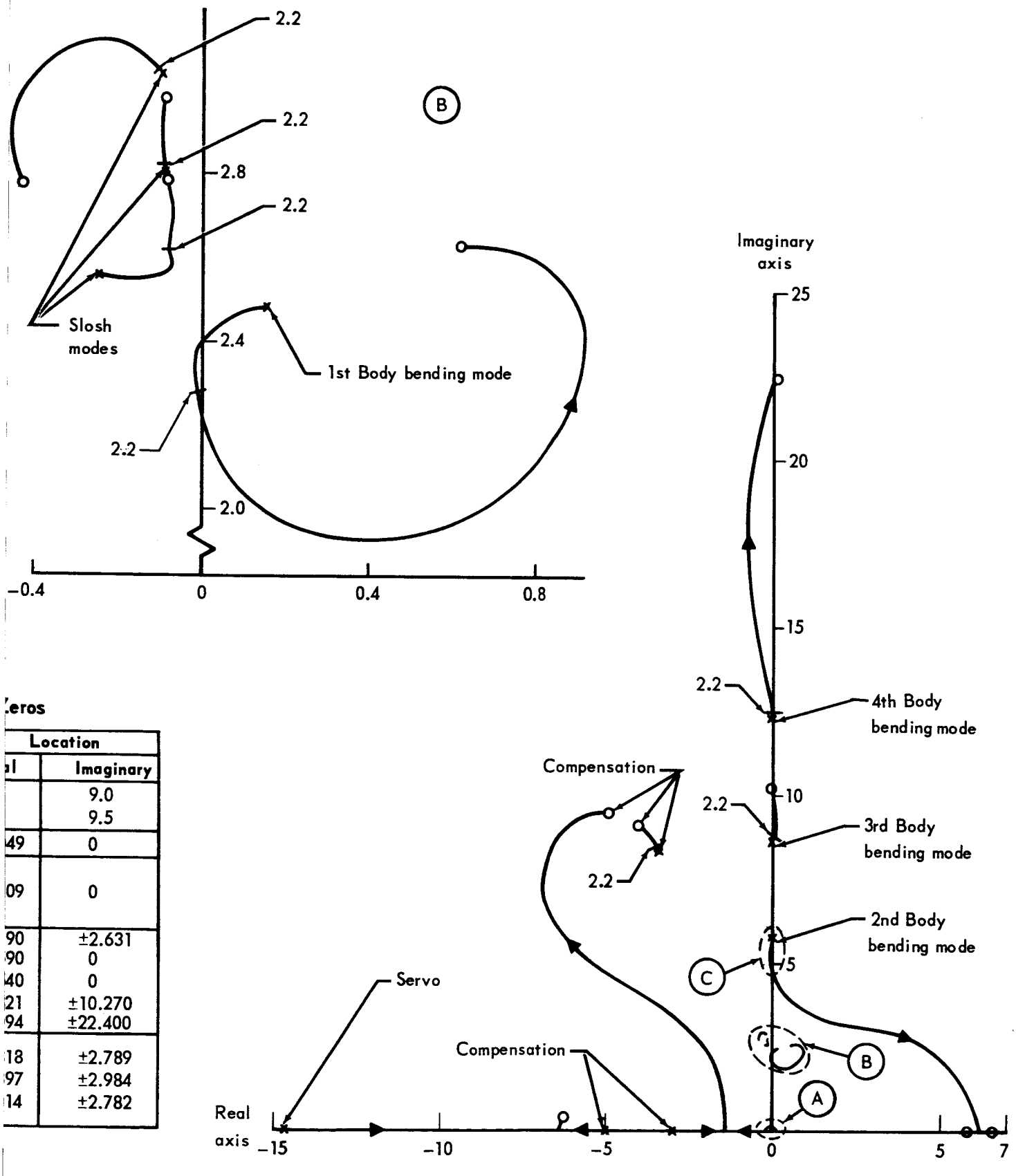

Zeros

Location	
al	Imaginary
	9.0
	9.5
49	0
09	0
90	±2.631
90	0
40	0
21	±10.270
94	±22.400
18	±2.789
97	±2.984
14	±2.782

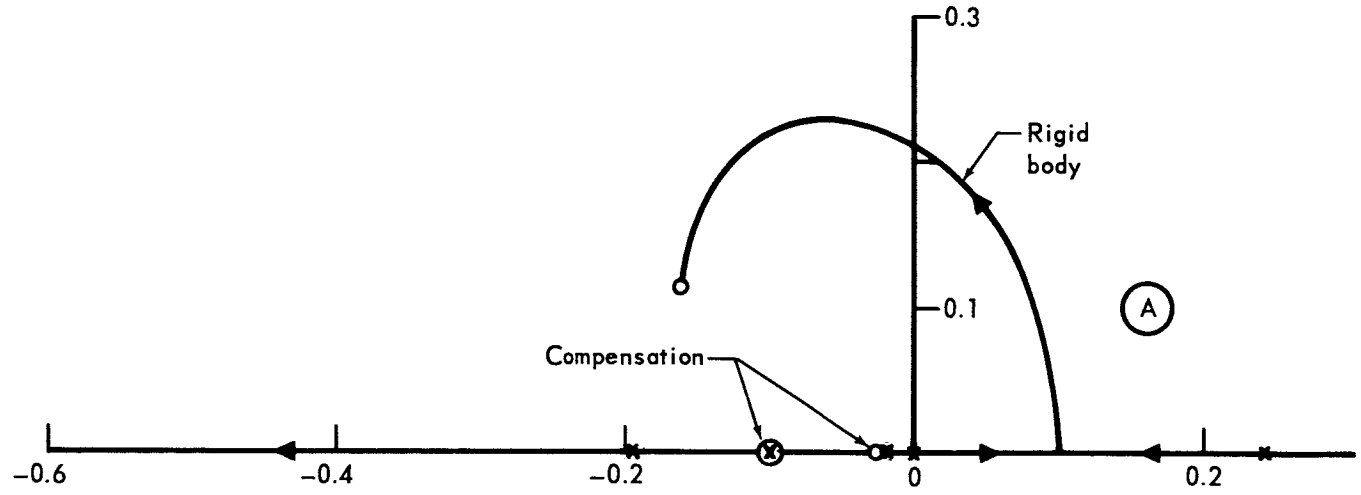

Open Loop Poles

Quantity	Location	
	Real	Imaginary
Compensation	−.02	0
	−.10	0
	−2.35	0
	−5.65	0
Servo	−14.64	0
Rigid body	0	0
	−.2918	0
	.2405	0
Body bending	.1504	±2.498
	−.0187	±5.438
	−.0302	±8.634
	−.0580	±12.280
Propellant slosh	−.2451	±2.560
	−.0874	±2.810
	−.1010	±3.037

Open Loop Zeros

Quantity	Location	
	Real	Imaginary
Compensation	−.100	0
	−9.167	±9.091
Rate & ACC feedback	−.16	±.1141
Rigid body	−.026	0
	−6.353	±1.195
Body bending	.5979	±2.588
	6.2350	±1.127
	−.0819	±10.220
	.0098	±22.190
Propellant slosh	−.0818	±2.789
	−.0907	±2.990
	−.4178	±2.762

Figure F3a Vehicle II Root Locus of System Design II.3 With Acceleration Feedback At the Maximum q Flight Condition

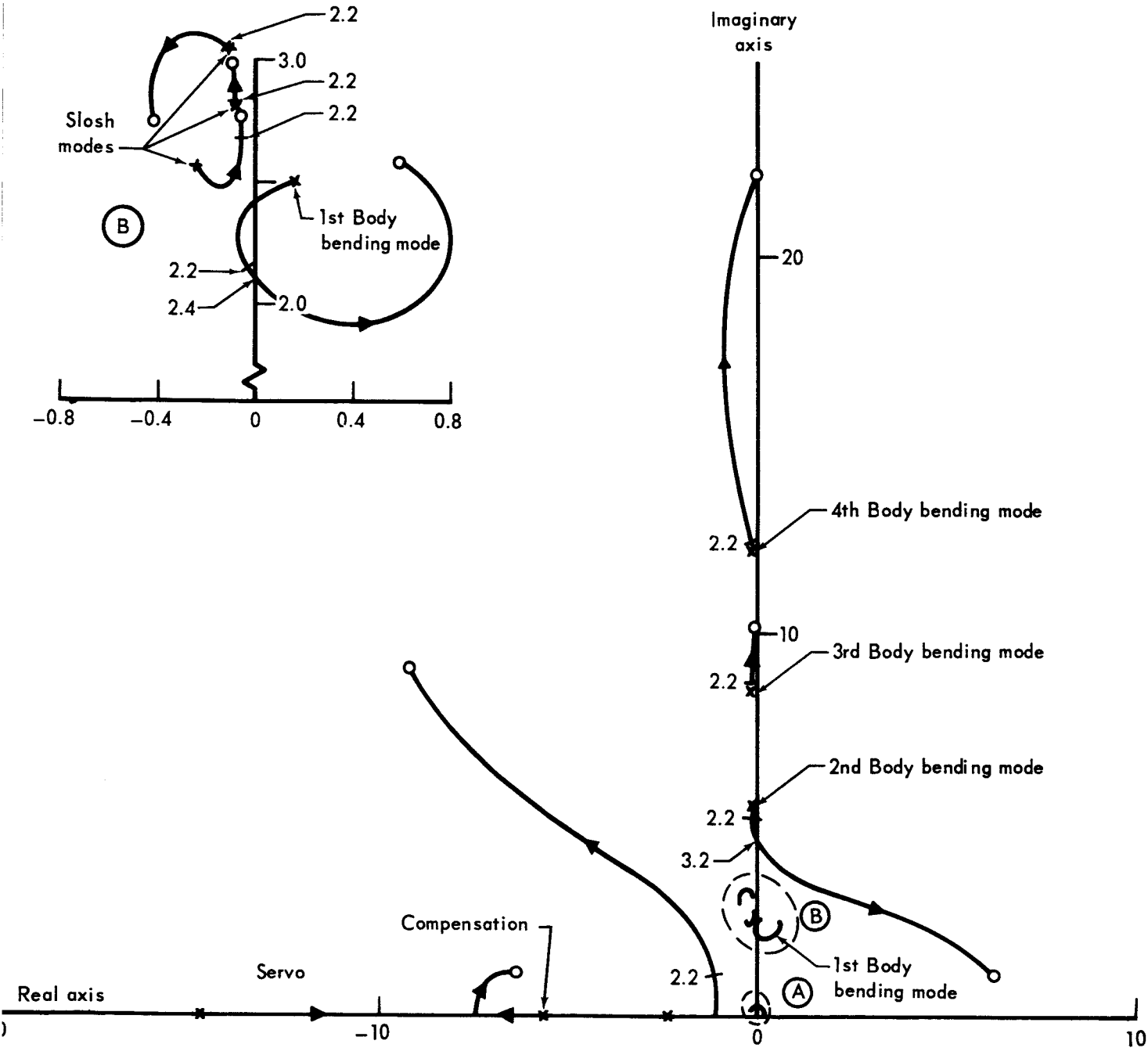
2.2
3.0
2.2
2.2
Slosh
modes
B
1st Body
bending mode
2.2
2.4
2.0
-0.8
-0.4
0
0.4
0.8
Imaginary
axis
20
4th Body bending mode
2.2
10
3rd Body bending mode
2.2
2nd Body bending mode
2.2
3.2
B
1st Body
bending mode
A
Compensation
Servo
2.2
Real axis
-10
0
10

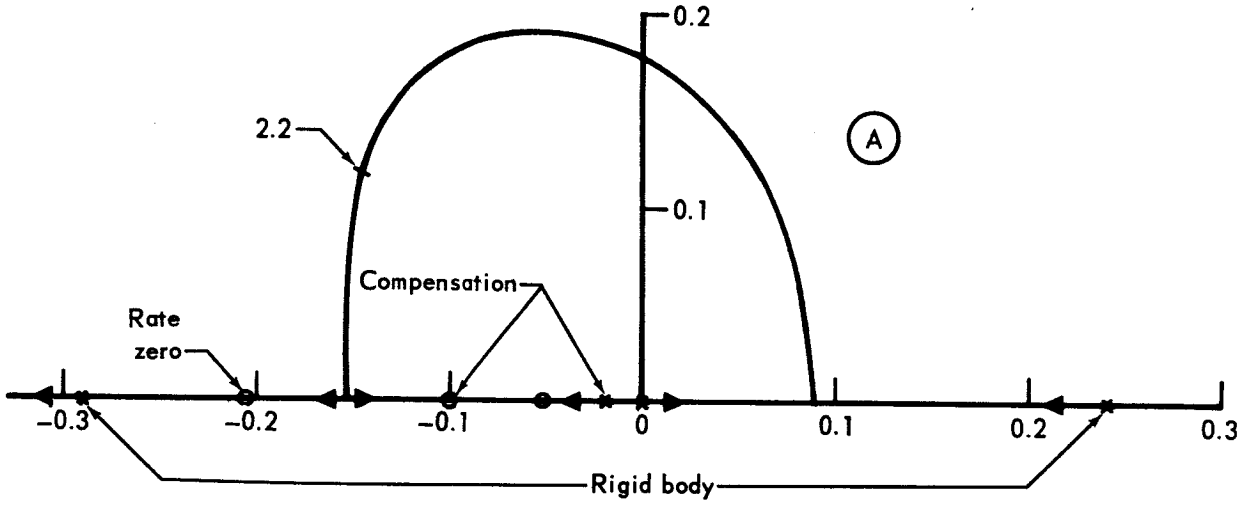

Open Loop Poles

Quantity	Location	
	Real	Imaginary
Compensation	−.02	0
	−2.35	0
	−5.65	0
Servo	−14.64	0
Rigid body	0	0
	−.2918	0
	.2405	0
Body bending	.1504	±2.498
	−.0187	±5.438
	−.0302	±8.634
	−.0580	±12.280
Propellant slosh	−.2451	±2.560
	−.0873	±2.810
	−.1010	±3.038

Open Loop Zeros

Quantity	Location	
	Real	Imaginary
Compensation	−.100	0
	−9.167	±9.091
Rate Feedback	−.2049	0
Rigid body	−.0509	0
Body bending	.6190	±2.631
	5.8590	0
	6.5450	0
	−.0821	±10.270
	−.0094	±22.400
Propellant slosh	−.0818	±2.789
	−.0897	±2.984
	−.4314	±2.782

Figure F3b Vehicle II Root Locus of System Design II.3 Without Acceleration Feedback At the Maximum g Flight Condition

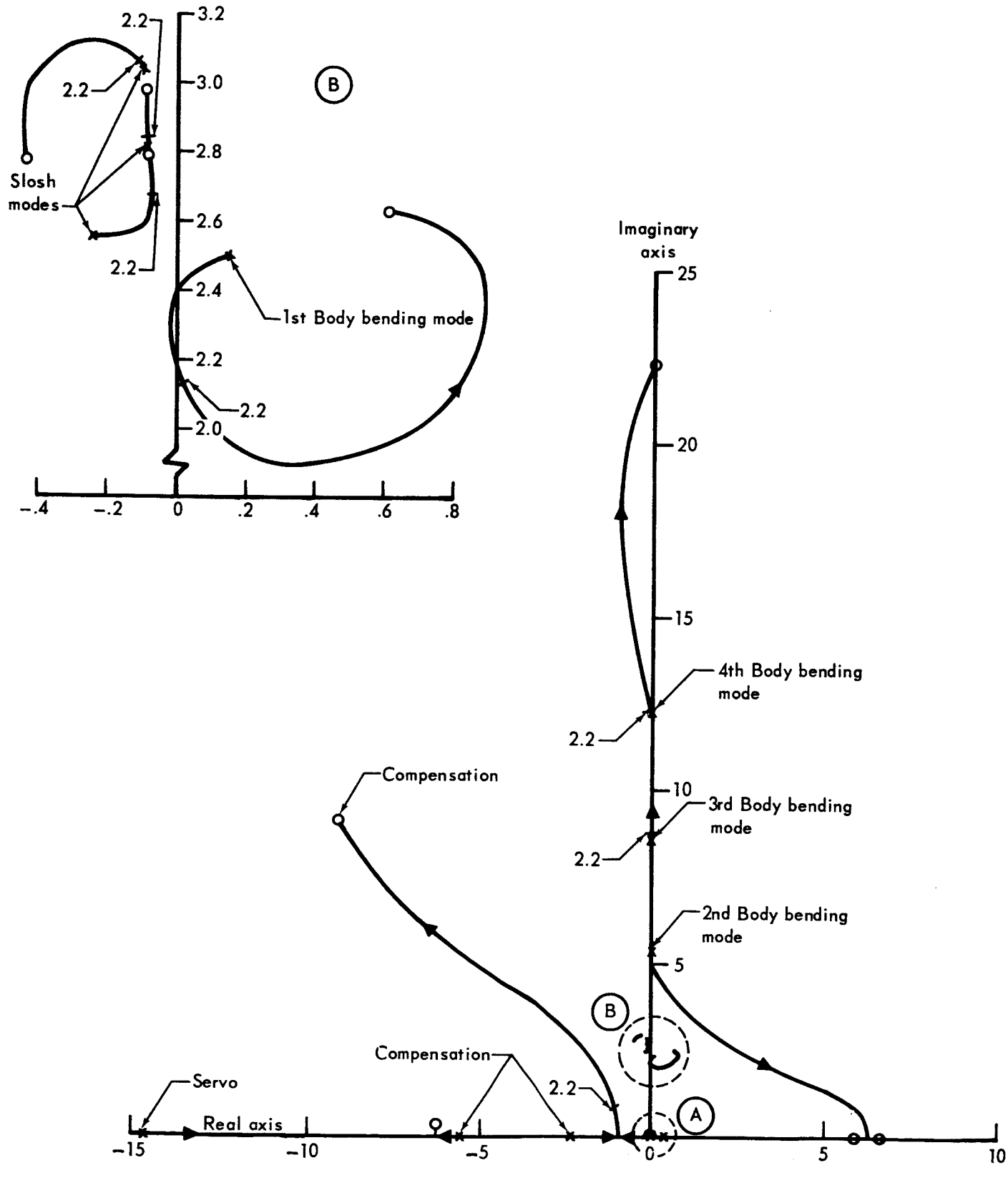
2.2
3.2
3.0
2.8
2.6
2.4
2.2
2.0
2.2
2.2
Slosh modes
B
1st Body bending mode
2.2
-.4
-.2
0
.2
.4
.6
.8
Imaginary axis
25
20
15
4th Body bending mode
2.2
10
3rd Body bending mode
2.2
2nd Body bending mode
5
Compensation
B
Compensation
Servo
2.2
A
Real axis
-15
-10
-5
0
5
10

In Figure F.2, Design II.2 is displayed in root locus form. This design uses a somewhat more complex compensation using two notch filters rather than one. It is apparent, however, that the vehicle's stability is not as satisfactory as obtained in Design II.1. Design II.1 is the preferred design.

Designs II.1 and II.2 are actually selected to operate with an acceleration feedback path incorporating the digital polynomial filter. The filter, however, cannot be readily incorporated in a root locus plot because of its sampled nature. Thus, the acceleration feedback was omitted in Figure F.1 and F.2. Omitting the acceleration feedback should cause little difference in the bending mode region, although it will lower the rigid body frequency. Evidence of this is given by Figures F.3a and F.3b, which are root locus plots for Design II.3. Since Design II.3 uses a linear low pass filter in the acceleration feedback path, the acceleration feedback loop was able to be incorporated in the root locus computation. This has been done in Figure F.3a. In Figure F.3b, the acceleration feedback was omitted as it has been in Figures F.1 and F.2. Comparing Figures F.3a and F.3b, it may be observed that the changed caused by the removal of the acceleration feedback are insignificant except for some decrease in the predominant closed loop rigid body mode frequency. It is expected that similar changes would occur if the root loci for the runs of Figures F.1 and F.2 could be obtained with acceleration feedback and the digital polynomial filter.

F.2 Vehicle I Control System Designs

Most of the studies conducted with Vehicle I concentrated on the development of the digital adaptive filter technique. This required the design of a secondary filter loop and a digital filter loop. Figures F.4, F.5, and F.6 show the root locus plots of the secondary filter configuration for the lift-off, maximum q, and burnout flight conditions respectively. The secondary filter has attitude and attitude rate feedback, with compensation consisting of a single notch filter, a lag network, and the command compensation network. It was desired that the same compensation could be used throughout the flight trajectory. It was found that the selected compensation gave adequate system performance and stability at the lift-off and maximum q flight conditions as shown in Figures F.4 and F.5.

However, this compensation is shown to be inadequate for the burnout flight condition. Figure F.6 shows the first bending mode to be unstable. The instability is caused by the cross coupling between the first body bending mode and the slosh modes. This was verified in the simulation studies which showed that the removal of the slosh mode equations would stabilize the first bending mode. The secondary filter compensation would, therefore, have to be modified as a function of time. The simulation studies indicated that relocating the compensation zeros from $[(S + 1)^2 + 14^2]$ to $[(S + 1.5)^2 + 10^2]$ and the compensation poles from $(S + 16)^2$ to $(S + 10)^2$ will help stabilize the first mode. This aspect of the secondary filter design was not pursued because of the shift of interest to the digital polynomial filter.

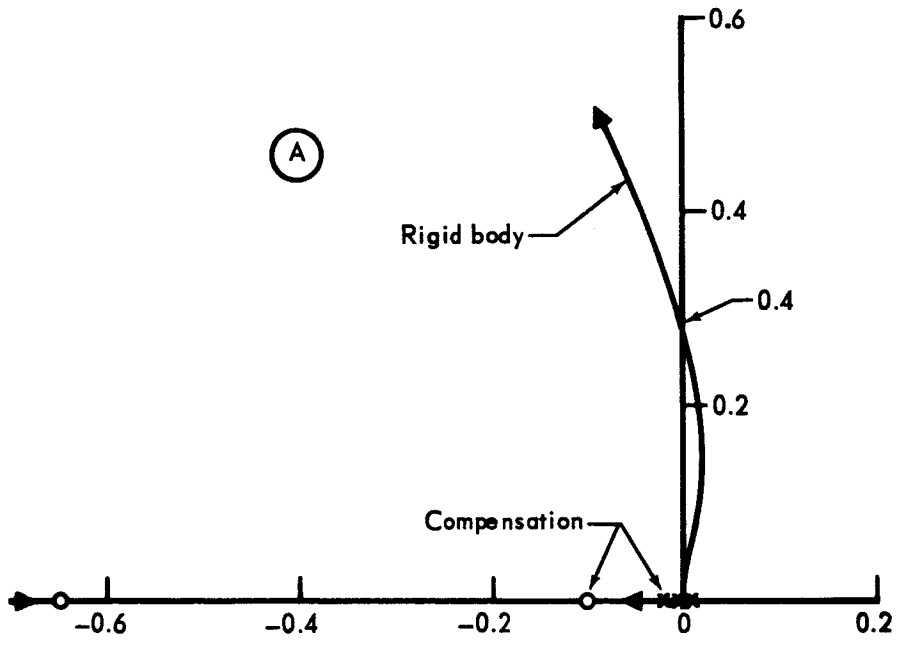

Open Loop Poles

Quantity	Location	
	Real	Imaginary
Compensation	−.02	0
	−4.00	0
	−16.00	0
	−16.00	0
Servo	−14.64	0
Rigid body	0	0
	0	0
Body bending	−.0118	±4.736
	−.0501	±11.520
	−.0778	±17.330
Propellant slosh	−.0646	±2.139
	−.0782	±2.343
	−.0713	±2.233

Open Loop Zeros

Quantity	Location	
	Real	Imaginary
Compensation	−.1	0
	−1.0	14.0
Rate Feedback	−.6495	0
Rigid body	−7.439	±4.442
Body bending	7.3560	±3.591
	.8985	±10.540
	.0092	±21.670
Propellant slosh	−.0642	±2.138
	−.0643	±2.120
	−.0808	±2.351

278-1

Figure F4 Vehicle I Root Locus of the Secondary Filter at the Lift-Off Flight Condition

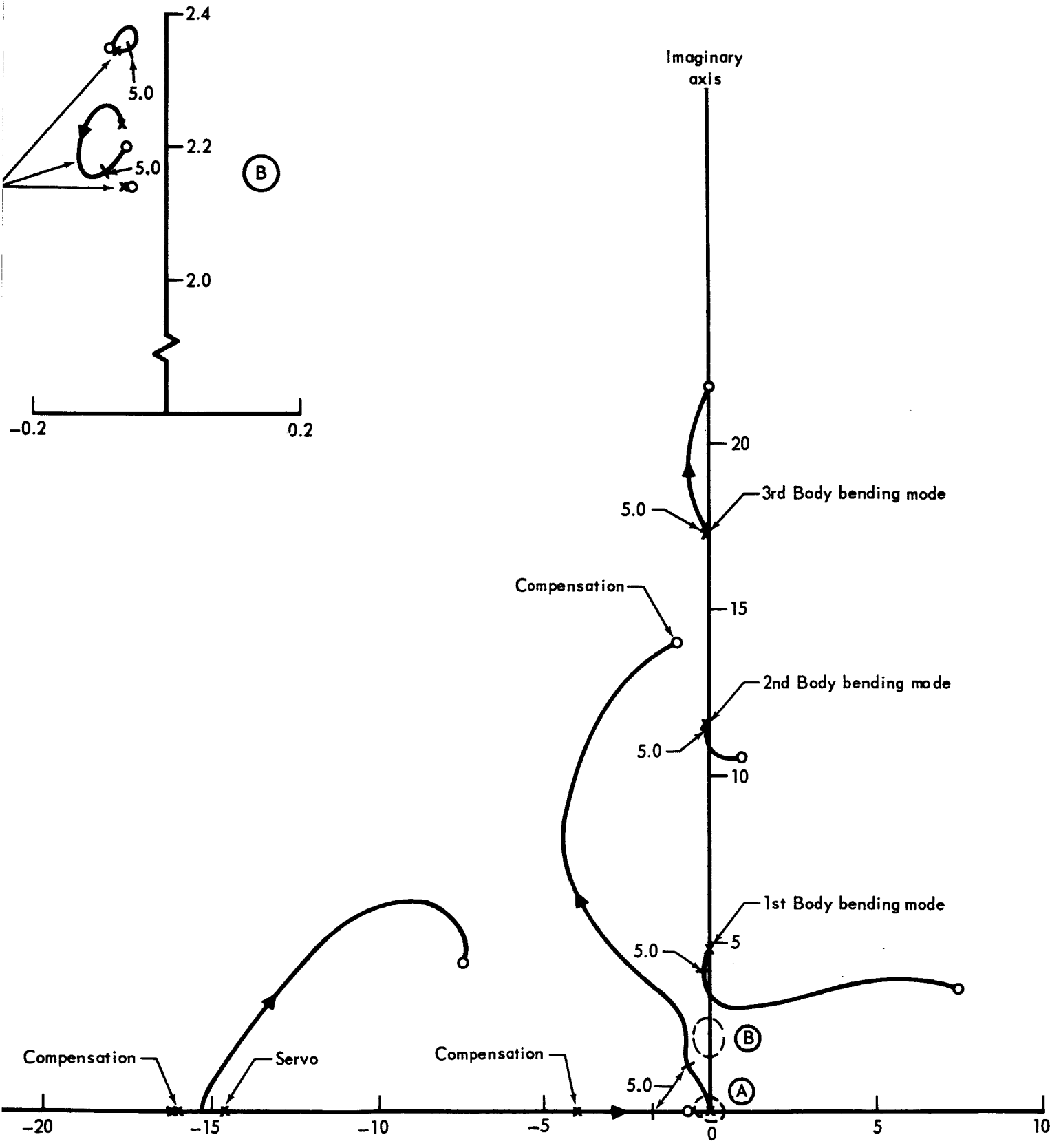
2.4
5.0
2.2
5.0
B
2.0
-0.2
0.2
Imaginary axis
20
3rd Body bending mode
5.0
Compensation
15
2nd Body bending mode
5.0
10
1st Body bending mode
5
5.0
B
Compensation
Servo
Compensation
5.0
A
-20
-15
-10
-5
0
5
10

278-2

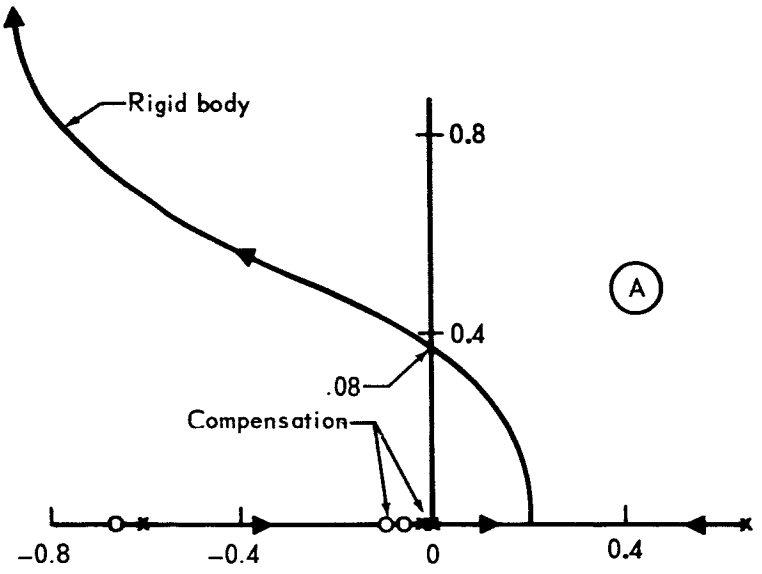

Open Loop Poles

Quantity	Location	
	Real	Imaginary
Compensation	−.02	0
	−4.00	0
	−16.00	0
	−16.00	0
Servo	−14.64	0
Rigid body	0	0
	−.6064	0
	.5516	0
Body bending	.0071	±4.945
	−.0471	±12.500
	−.0724	±17.260
Propellant slosh	−.0849	±2.785
	−.1133	±3.079
	−.1119	±3.186

Open Loop Zeros

Quantity	Location	
	Real	Imaginary
Compensation	−.1	0
	−1.0	±14.0
Rate Feedback	−.6636	0
Rigid body	−.0619	0
	−8.5640	±6.18
Body bending	7.9790	±6.011
	1.2570	±10.040
	.0786	±23.240
Propellant slosh	−.0846	±2.784
	−.1377	±3.117
	−.0756	±3.067

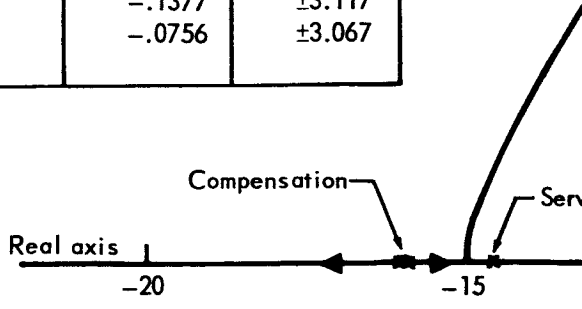

Figure F5 Vehicle I Root Locus of the Secondary Filter at the Maximum q Flight Condition

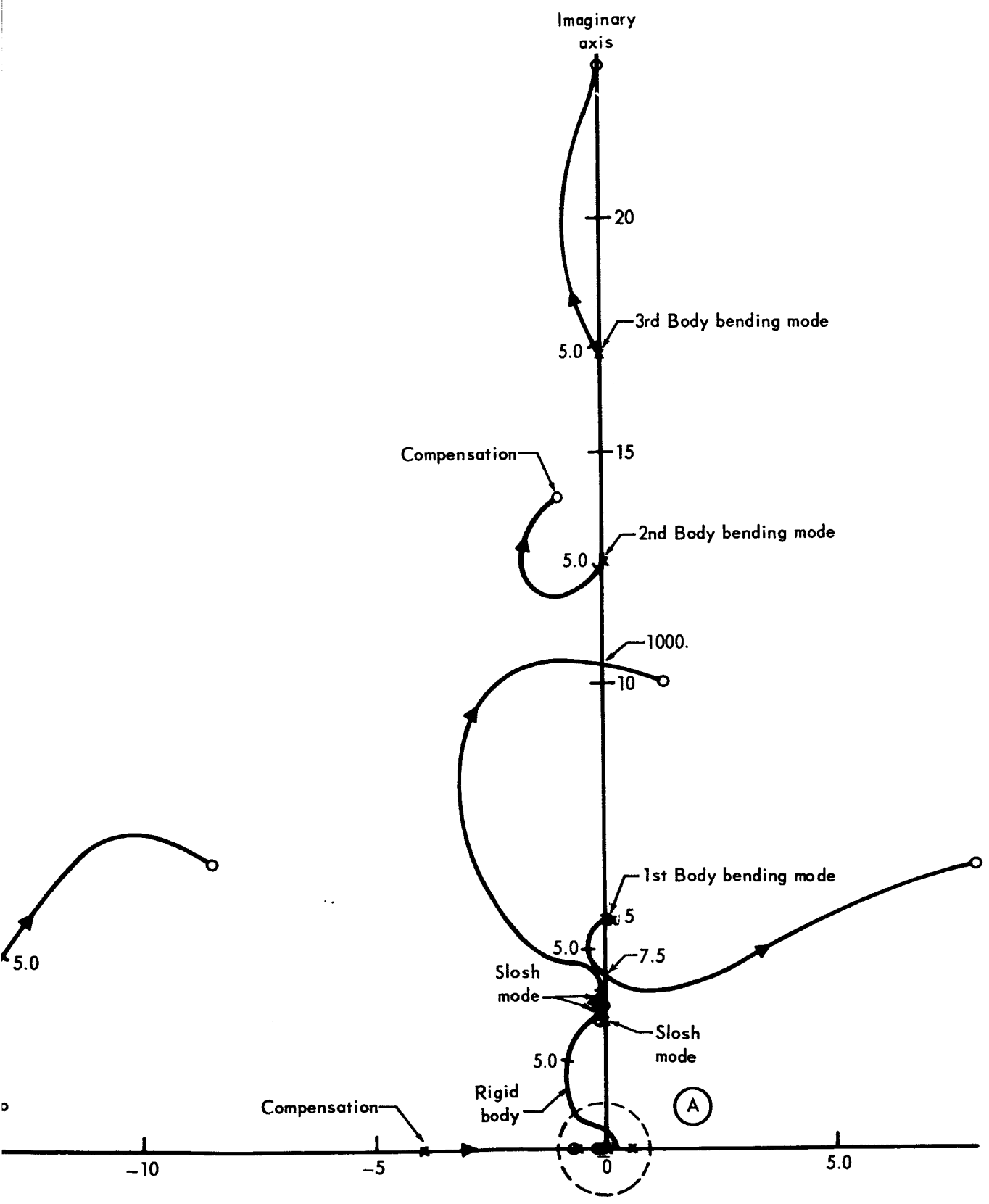
Imaginary axis
20
3rd Body bending mode
5.0
Compensation
15
2nd Body bending mode
5.0
1000.
10
1st Body bending mode
5
5.0
7.5
Slosh mode
Slosh mode
5.0
Rigid body
Compensation
A
5.0
−10
−5
0
5.0

279-2

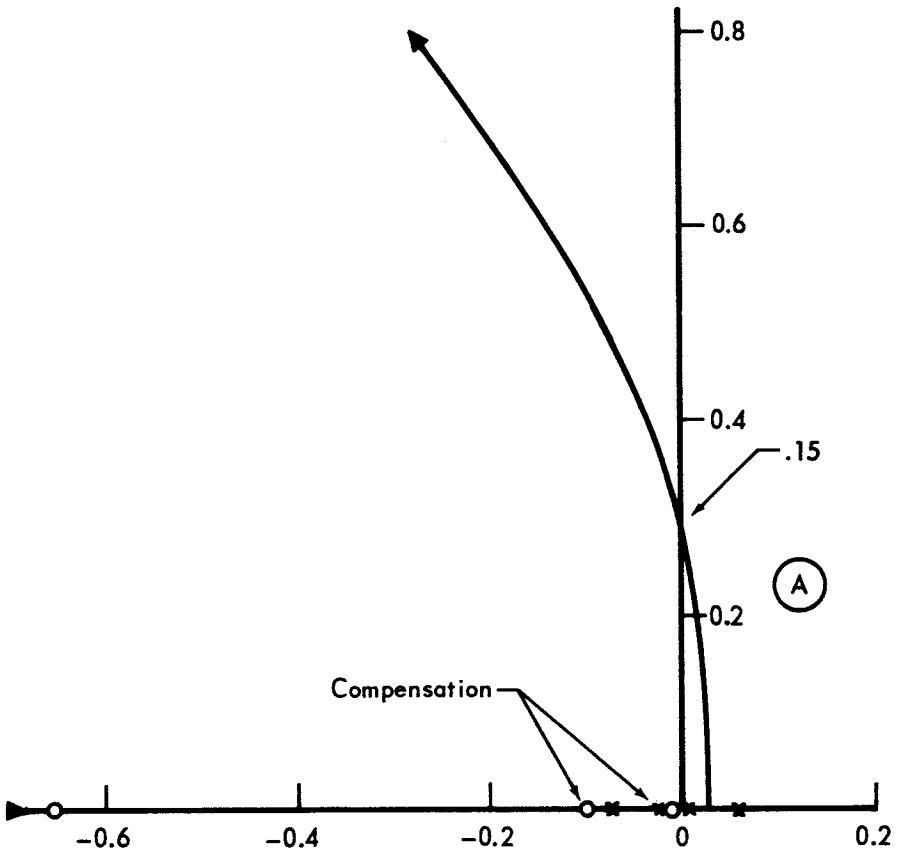

Open Loop Poles

Quantity	Location	
	Real	Imaginary
Compensation	−.02	0
	−4.00	0
	−16.00	0
	−16.00	0
Servo	−14.64	0
Rigid body	0	0
	−.0735	0
	.0571	0
Body bending	.4037	±5.68
	−.0681	±15.34
	−.1429	±29.14
Propellant slosh	−.1097	±3.609
	−.1170	±3.813
	−.5860	±5.447

Open Loop Zeros

Quantity	Location	
	Real	Imaginary
Compensation	−.1	0
	−1.0	±14.0
Rate Feedback	−.6528	0
Rigid body	−.0164	0
	7.4730	0
	−8.4050	0
Body bending	−.2012	±5.190
	.1025	±22.390
	−1.3290	±31.110
Propellant slosh	−.1088	±3.607
	−.1145	±3.806
	.9361	±9.848

Figure F6 Vehicle 1 Root Locus of the Secondary Filter at the Burn-Out Flight Condition

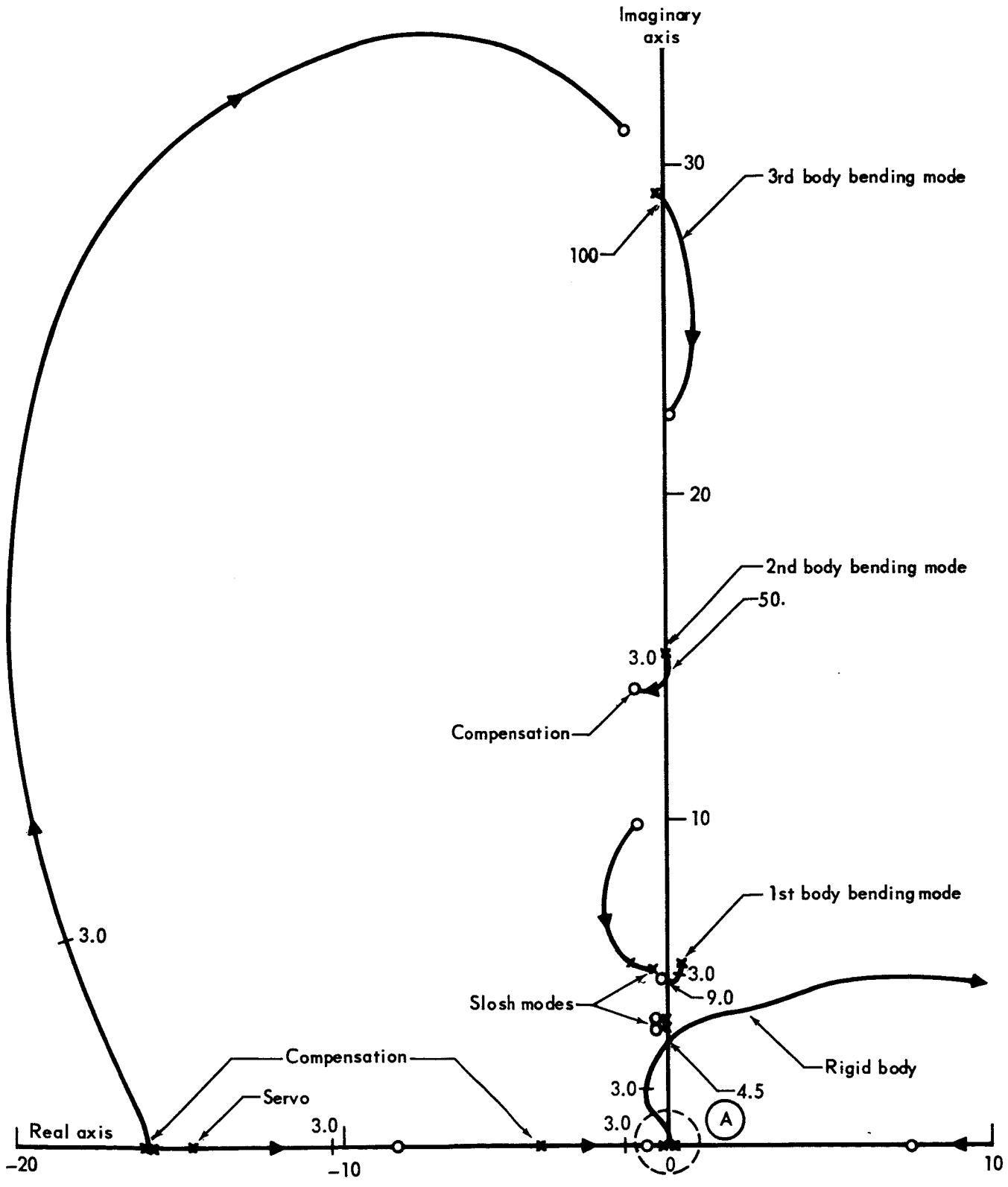
Imaginary axis
30
3rd body bending mode
100
20
2nd body bending mode
50.
3.0
Compensation
10
1st body bending mode
3.0
3.0
9.0
Slosh modes
Rigid body
Compensation
Servo
3.0
4.5
3.0
3.0
A
Real axis
-20
-10
0
10

240-2

The root locus plots of the digital adaptive filter design for Vehicle I is shown in Figures F.7, F.8, and F.9 for the lift-off, maximum q, and burnout flight conditions, respectively. To obtain these figures, the digital adaptive filter was set equal to unity (1.0). The digital adaptive filter loop uses attitude feedback only with an equivalent rate feedback compensation in the forward loop. This feature shows up in the figures primarily by the relocation of the bending mode zeros since the bending signal sensed by the rate gyro is not present. The stability compensation used in the digital adaptive filter loop is similar to that used in secondary filter loop with the compensation zeros at $[(S + 1)^2 + 12^2]$ instead of $[(S + 1)^2 + 14^2]$. Stability of the digital adaptive filter control loop as shown is not essential since the digital adaptive filter separates the rigid body response from the control system error signal. The rigid body response as computed by the digital adaptive filter is transient in nature and is driven to zero as a function of time. This essentially opens the control loop in the steady state and requires the vehicle control to be transferred to the secondary filter loop.

Figures F.7 and F.8 show the first body bending mode to be unstable for a forward loop gain of 5.0 the nominal gain of the lift-off and maximum q flight conditions. The simulation studies documented in this report show that the digital adaptive filter is capable of providing good transient control of the vehicle in the presence of these instabilities. The burnout flight condition which used a forward loop gain of 3.0 also showed that the digital adaptive filter was effective in extracting the rigid body signal.

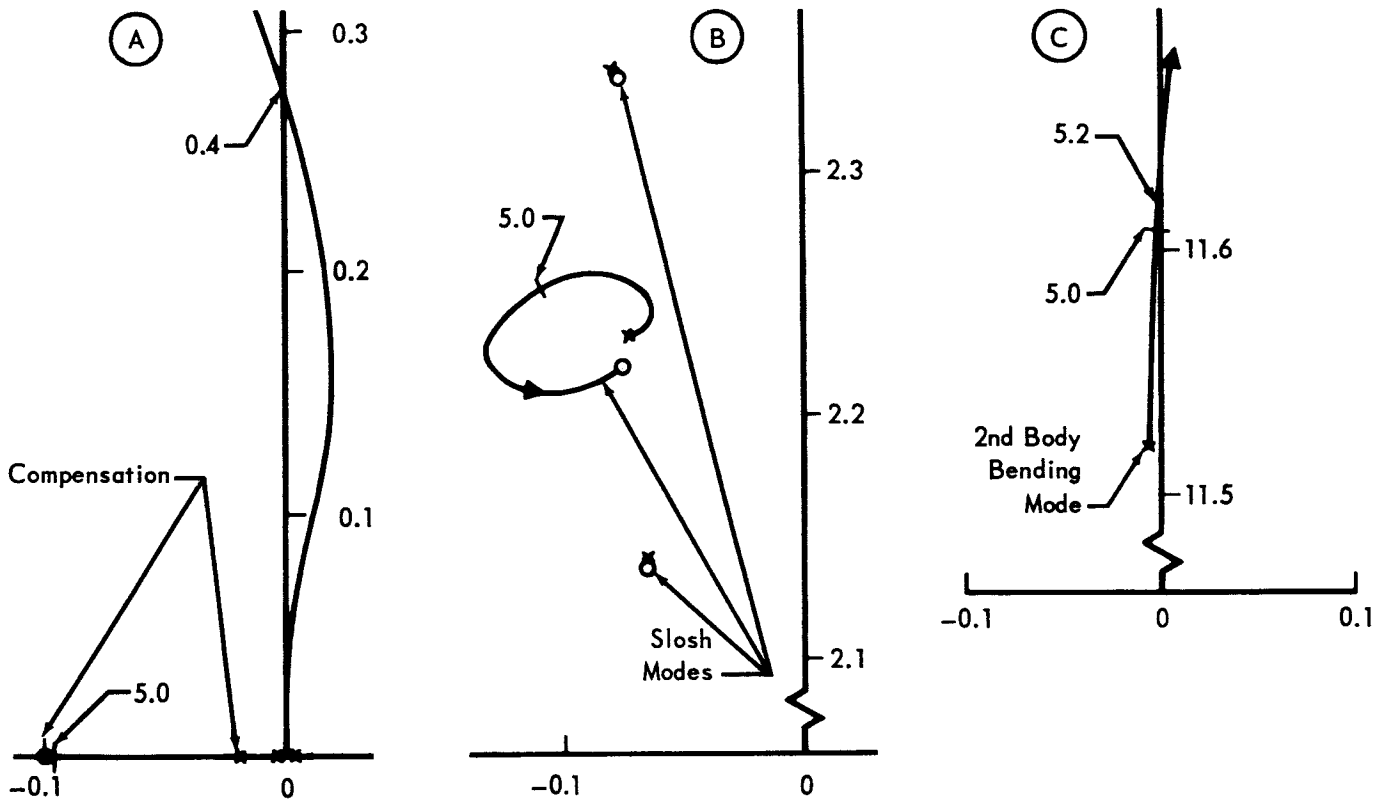

Open Loop Poles

Quantity	Location	
	Real	Imaginary
Compensation	−.02	0
	−4.00	0
	−16.00	0
	−16.00	0
Servo	−14.64	0
Rigid body	0	0
	0	0
Body bending	−.01179	4.736
	−.05010	11.520
	−.07790	17.330
Propellant slosh	−.0713	2.233
	−.0646	2.139
	−.0782	2.343

Open Loop Zeros

Quantity	Location	
	Real	Imaginary
Compensation	−.1	0
	−1.0	±12.0
Rate Feedback	−.6667	0
Rigid body	−3.957	0
	3.961	0
Body bending	−9.3820	±7.556
	9.3490	±7.648
	.0002	±21.570
Propellant slosh	−.0645	±2.139
	−.0738	±2.220
	−.0762	±2.341

F.7 Vehicle I Root Locus of the Control Loop With the Digital Adaptive Filter Compensation at the Lift-Off Flight Condition

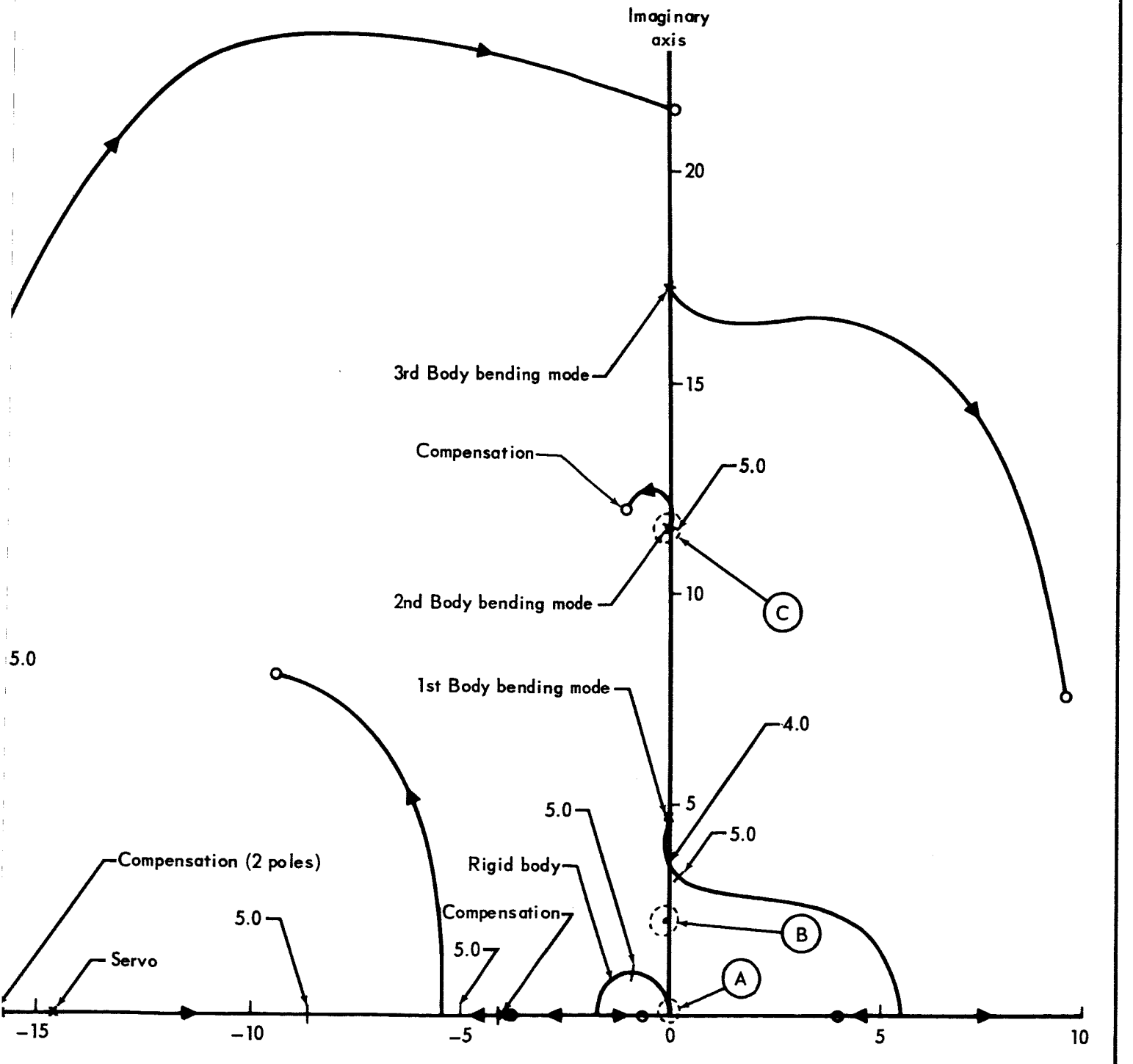
Imaginary axis
20
3rd Body bending mode
15
Compensation
5.0
2nd Body bending mode
10
C
5.0
1st Body bending mode
4.0
5
5.0
5.0
Compensation (2 poles)
Rigid body
5.0
Compensation
B
5.0
Servo
A
-15
-10
-5
0
5
10

282-2

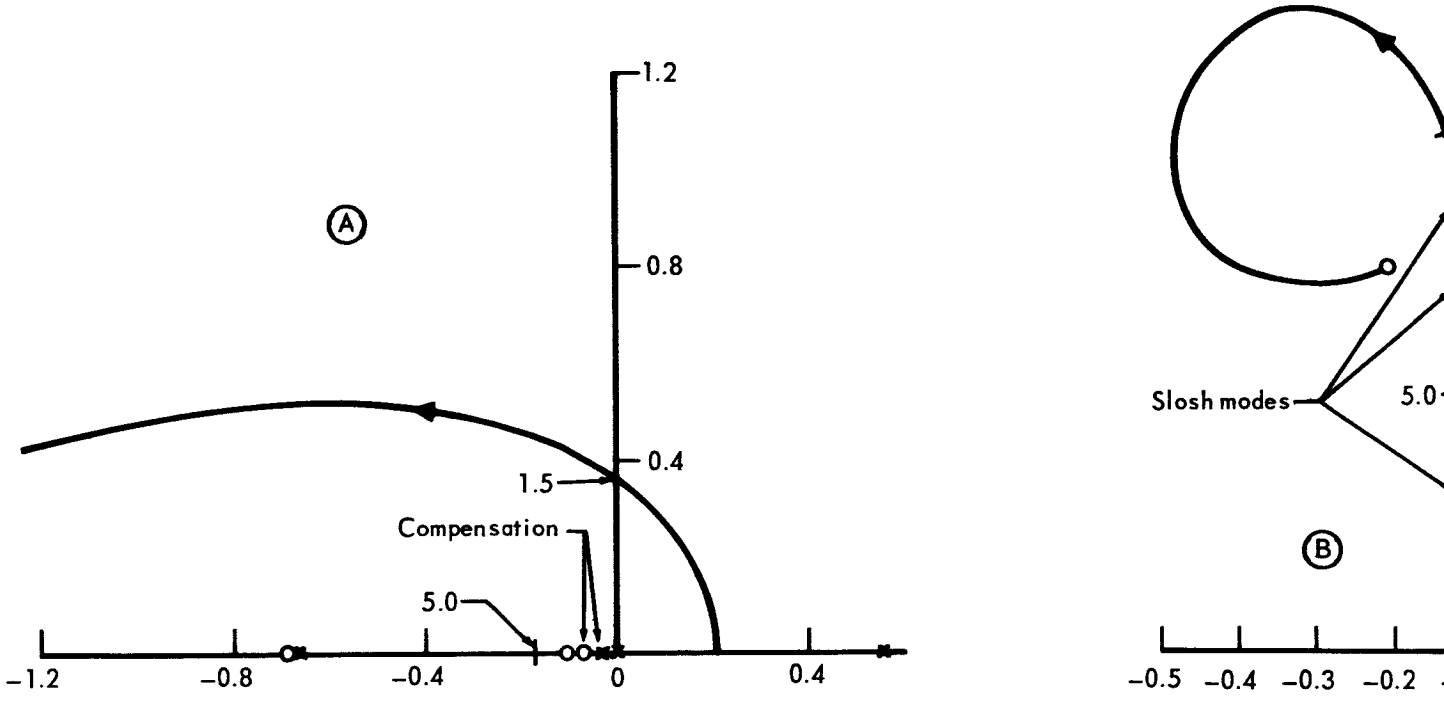

Open Loop Poles

Quantity	Location	
	Real	Imaginary
Compensation	−.02	0
	−4.00	0
	−16.00	0
	−16.00	0
Servo	−14.64	0
Rigid body	0	0
	−.6064	0
	.5516	0
Body bending	.0071	±4.945
	−.0471	±12.500
	−.0724	±17.260
Propellant slosh	−.0849	±2.785
	−.1133	±3.079
	−.1119	±3.186

Open Loop Zeros

Quantity	Location	
	Real	Imaginary
Compensation	−.1	0
	−1.0	±12.0
Rate Feedback	−.6667	0
Rigid body	−.0621	0
	5.3900	0
	−5.4500	0
Body bending	−13.0800	±3.184
	13.1100	±3.640
	−.0021	±22.250
Propellant slosh	−.0846	±2.783
	−.0106	±3.119
	−.2124	±3.094

Figure F8 Vehicle 1 Root Locus of the Control Loop With the Digital Adaptive Filter Compensation at the Maximum q Flight Condition

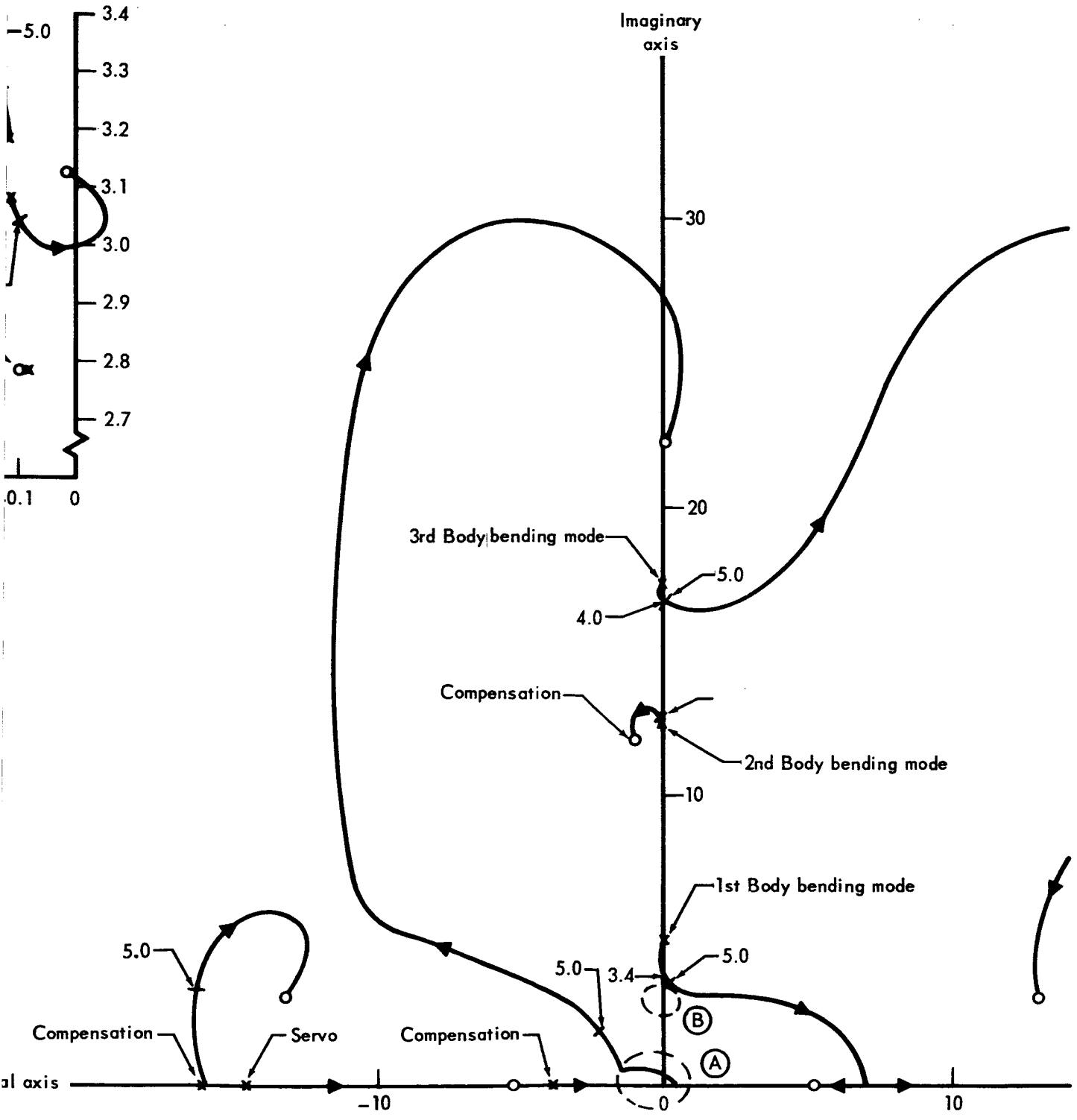
Imaginary axis
30
20
10
3rd Body bending mode
5.0
4.0
Compensation
2nd Body bending mode
1st Body bending mode
5.0
5.0
3.4
5.0
B
A
Compensation
Servo
Compensation
al axis
−10
0
10
−5.0
3.4
3.3
3.2
3.1
3.0
2.9
2.8
2.7
0.1
0

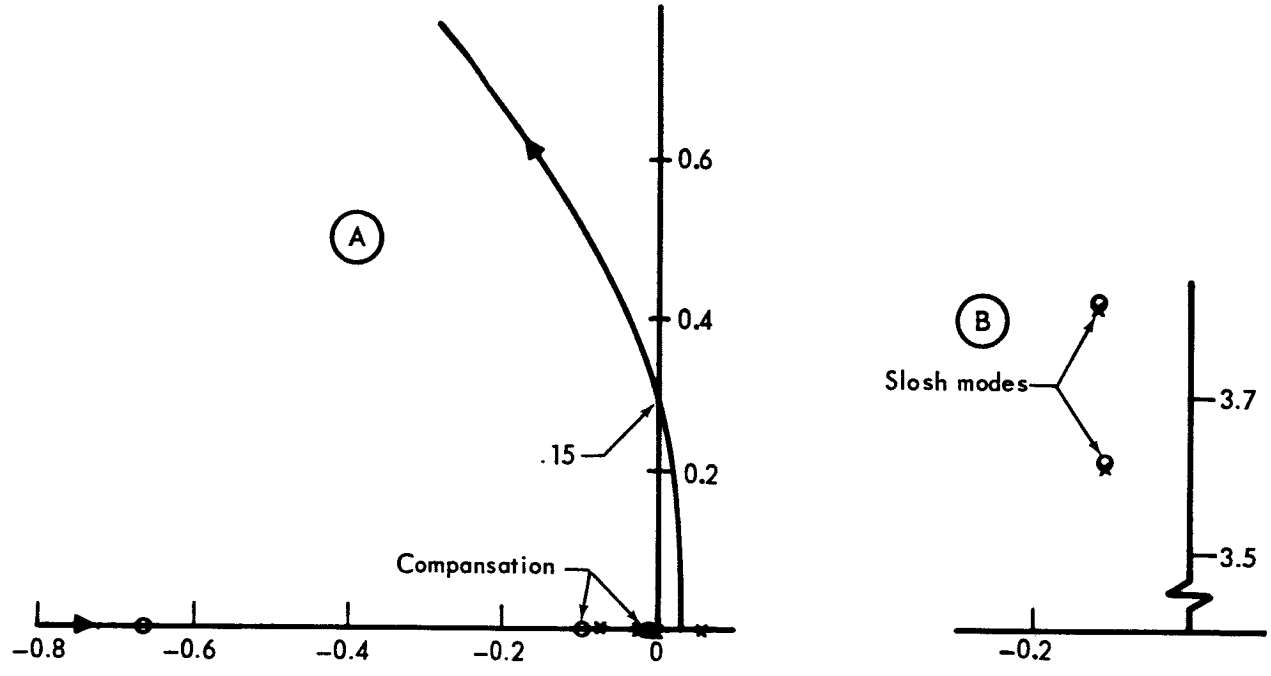

Open Loop Poles

Quantity	Location	
	Real	Imaginary
Compensation	−.02	0
	−4.00	0
	−16.00	0
	−16.00	0
Servo	−14.64	0
Rigid body	0	0
	−.0735	0
	.0571	0
Body bending	.4037	±5.68
	−.0681	±15.34
	−.1429	±29.14
Propellant slosh	−.1097	±3.609
	−.1170	±3.813
	−.5856	±5.447

Open Loop Zeros

Quantity	Location	
	Real	Imaginary
Compensation	−.1	0
	−1.0	±12.0
Equivalent Rate	−.6667	0
Rigid body	−.0164	0
	−4.2630	0
	4.2910	0
Body bending	−.0242	±21.53
	−13.3400	±13.51
	13.2800	±13.63
Propellant slosh	−.1101	±3.611
	−.1181	±3.817
	−.1636	±5.102

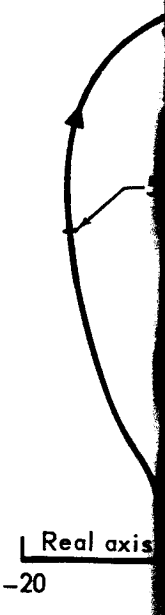

Figure F9 Vehicle 1 Root Locus of the Control Loop With the Digital Adaptive Filter Compensation at the Burn-Out Flight Condition

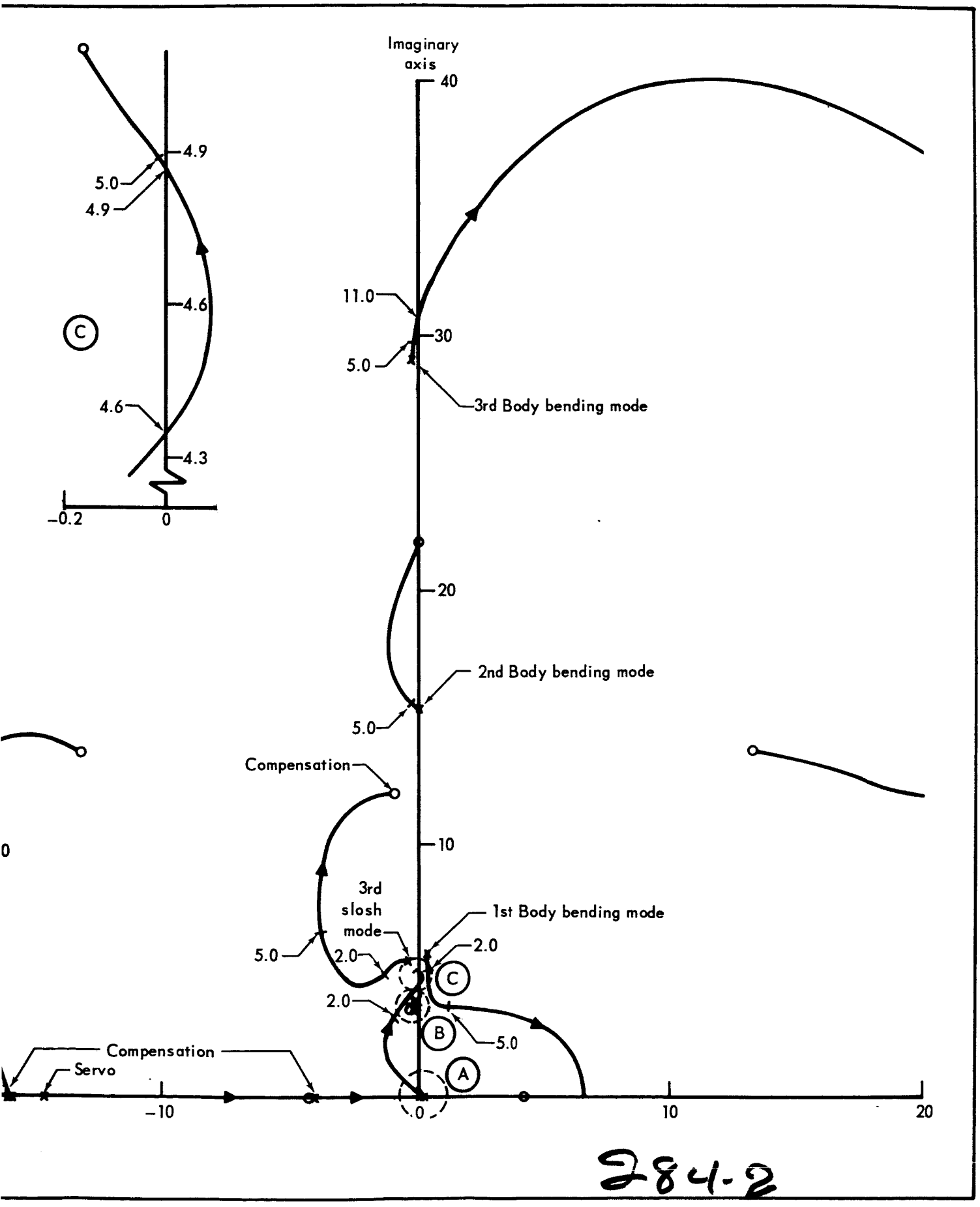
Imaginary axis
40
30
20
10
4.9
5.0
4.9
4.6
C
4.6
4.3
−0.2
0
11.0
5.0
3rd Body bending mode
2nd Body bending mode
5.0
Compensation
3rd slosh mode
5.0
2.0
2.0
1st Body bending mode
2.0
C
2.0
B
5.0
A
Compensation
Servo
−10
0
10
20

284-2

APPENDIX G

SPECIFICATION SET TYPE COMPENSATION

When an engineer synthesizes a control system, he starts with a knowledge or assumption of the transfer function and a set of performance specifications affecting the accuracy (error constants), damping (damping rates, peak overshoot, height of response peak, etc.), speed (peak time, rise time, resonant frequency), filtering ability (bandwidth), etc., required in the application of his control system. On an elastic booster, some very important components of these specifications are the extent to which the bending modes are excited in a transient, the damping of these modes, and the stresses created in the airframe.

The engineer then proceeds conventionally by cut-and-try techniques (root locus, Nyquist, etc.) to select poles and zeros in the compensating transfer function which will keep the system performance within the set of prescribed specifications. Aside from the cut-and-try approach, this technique has much to recommend it. The specifications included in the set can be tailored to the actual needs and aims of the control system so that they can be truly realistic and representative measures of the vehicle performance. These specifications can be chosen to emphasize the particular aspects of the performance that are of actual concern in the particular design. This method gives not only realism but also flexibility since none of the specifications is required to be included or excluded. Decision on the selection of the specifications to be used depends exclusively on the need. The difficulty with the practical application of much of modern, optimal, control theory is that the criteria which can be handled mathematically in the solution are too restrictive in nature to define and to incorporate the realistic aspects of good performance meaningfully.

One difficulty with the specification set type linear design is the large amount of intuition which goes into the cut-and-try type design. This fact requires a skilled human operator. Consequently, it is not applicable where the design or redesign must be done continuously as in an on-board adaptive control for a booster. To make the process applicable to this situation, it must first be mechanized. This mechanization was shown to be possible in Reference 5 . The specification must be expressed mathematically in terms of the system pole and zero locations. A set of nonlinear equations are obtained which must be solved simultaneously. A solution can be accomplished in an adaptive situation quite efficiently by the use of an iterative linearization technique such as the Newton-Raphson method. The successive parameter corrections are likely to be quite small (usually less than 10%) so search techniques based on local linearization would be efficient. For this technique to be successful, it is essential to find mathematical descriptions for the various items in the specification set which are reasonably manageable in the iteration process. The details of the proposed specification set procedure are summarized in Section G.2.

As presented here, the design is for the equality type of specification while most of the specifications used currently are of the inequality type; for instance, overshoot less than some fixed number, m. It is definitely possible to extend the specification set work to include the inequality type specifications but this will require additional development of the technique.

G.1 Advantages of the Specification Set Type of Adaptation

(1) Specification set can be made a realistic description of good performance.

(2) Specification set is a flexible description of good performance. Neither the number nor the type of specifications is inherently limited.

(3) It is well suited to airborne digital computer operation.

(4) Running time or time share requirements are moderate and reasonable.

(5) Since the identification process is not influenced by the parameter adjustment process, no stability problem arises.

(6) The parameter adjustment does not depend on high accuracy of the identification.

(7) Specification set constitutes a transfer-on-board of true and tried engineering practices, so its effects are well understood and the likelihood of undesirable side effects is at a minimum.

(8) Specific effort in the location of sensors and advance knowledge of elastic body mode shapes is not required with specification set.

(9) Used in conjunction with the identification process, described in Reference 6 , practically no advance knowledge of the vehicle characteristics would be necessary to obtain good system performance.

G.2 Specific Equations for Specification Set Type Adjustment

The basic principles of the specification set type parameter adjustment were introduced in References 5 and 7 , and detailed working equations have now been established and they are summarized here. These equations could serve as a suitable basis for establishing a computer program of maximum flexibility.

G.2.1 System Equations - It is assumed that the system can be represented by the following equations:

Plant

$$G_p(s) = \frac{A \prod_{i=1}^{k} (s-z_i)}{\prod_{i=1}^{n} (s-p_i)} = \frac{A \prod_{i=1}^{k_1} (s-z_i) \prod_{i=1}^{k_2} (s-R_e z_i \pm jI_m z_i)}{\prod_{i=1}^{n_1} (s-p_i) \prod_{i=1}^{n_2} (s-R_e p_i \pm jI_m p_i)} \quad (G.1)$$

Feed Forward Compensation

$$G_c(s) = \frac{A_c \prod_{i=1}^{I} (s-\zeta_i)}{\prod_{i=1}^{J} (s-\pi_i)} = \frac{A_c \prod_{i=1}^{I_1} (s-\zeta_i) \prod_{i=1}^{I_2} (s-R_e \zeta_i \pm jI_m \zeta_i)}{\prod_{i=1}^{J_1} (s-\pi_i) \prod_{i=1}^{J_2} (s-R_e \pi_i \pm jI_m \pi_i)} \quad (G.2)$$

Feedback Compensation

$$H(s) = \frac{A_h \prod_{i=1}^{K} (s-\xi_i)}{\prod_{i=1}^{L} (s-\eta_i)} = \frac{A_h \prod_{i=1}^{K_1} (s-\xi_i) \prod_{i=1}^{K_2} (s-R_e \xi_i \pm jI_m \xi_i)}{\prod_{i=1}^{L_1} (s-\eta_i) \prod_{i=1}^{L_2} (s-R_e \eta_i \pm jI_m \eta_i)} \quad (G.3)$$

Closed Loop

$$K(s) = \frac{G_c(s)\, G_p(s)}{1 + H(s)\, G_c(s)\, G_p(s)} = \frac{B \sum_{x=0}^{M} a_x s^x}{\sum_{y=0}^{N} b_y s^y} \quad (G.4)$$

$$K(s) = \frac{B \prod_{i=1}^{k+I+L} (s-w_i)}{\prod_{i=1}^{n+J+L} (s-q_i)} = \frac{B \prod_{i=1}^{M_1} (s-w_i) \prod_{i=1}^{M_2} (s-R_e w_i \pm jI_m w_i)}{\prod_{i=1}^{N_1} (s-q_i) \prod_{i=1}^{N_2} (s-R_e q_i \pm jI_m q_i)} \quad (G.5)$$

G.2.2 Performance Specifications for Specification Set

		Symbol	No. of Equations Required
1. Displacement error coefficient	See note*	K_d	$b_d = 1$
2. Velocity error coefficient	See note*	K_v	$b_v = 1$
3. Acceleration error coefficient	See note*	K_a	$b_a = 1$
4. Peak time specifications		$(s-R_e q_h \pm jI_m q_h)$	b_1 assumes b_1 pair of complex poles $h=1,2,\ldots b_1$
4.1 Peak time		T_{p_h}	
4.2 Number of complex pole pairs to be used		b_1	
4.3 Boundary of region of complex pole pairs**		A_1	
5. Settling time specifications. This specification reduces the number of unknowns $R_e u_j$ by specifying the real part of the complex poles selected from the specified area i.e., $R_e q_h = 8/T_{s_h}$ where $h = 1,2,\ldots b_1'$.		$(s-R_e q_h \pm jI_m q_h)$ T_{s_h}	Effectively reduces the number of Eqs by b_1' $h=1,2,\ldots b_1'$
5.1 Number of complex pole pairs to be used		b_1'	

*If K_d is specified K_v and K_a must be omitted.

If K_v and/or K_a are specified then the equation for K_d must be omitted and a pole at the origin included in $G_p(s)$

**Definition of boundary regions of complex poles are given in Section G.2.3.

	Symbol	No. of equations Required
6. Overshoot specifications		
6.1 Flexible body modes	$(s-R_{e}q_{\ell} \pm jI_{m}q_{\ell})$	c_1 Assumes c_1 pair of complex poles $\ell=1,2,\ldots c_1$
6.1.1 Overshoot	$m_{F.B.\ell}$	
6.1.2 Peak time associated with overshoot	$T_{p_{\ell}}$	
6.1.3 Number of complex pole pairs to be used	c_1	
6.1.4 Boundary of region of complex pole pairs**	A_2, A_3	
6.1.5 Specification of minimum damping of flexible body modes. This specification reduces the number of unknowns similar to section 9.3.2.5, i.e. $R_{e}q_{\ell}=h_{\ell}, \ell=1,2,\ldots c_1'$	$h_{\ell}=R_{e}q_{\ell}$	Effectively reduces no. of equations by c_1'
6.2 Principal rigid body response	$(s-R_{e}q_{m} \pm jI_{m}q_{m})$	c_2 Assumes c_2 pair of complex poles $m=1,2,\ldots c_2$
6.2.1 Overshoot (resultant from complex poles)	m_{c_m}	
6.2.2 Peak time associated with overshoot	T_{p_m}	
6.2.3 Number of complex pole pairs to be used	c_2	
6.2.4 Boundary of region of complex pole pairs**	A_4	
6.3 Effects of small real roots	$(s-q_R)$	c_3 Assumes c_3 small real roots $R=1,2,\ldots c_3$
6.3.1 Effective steady state error	m_{R_R}	
6.3.2 Effective peak time	T_{P_R}	
6.3.3 Number of real poles	c_3	
6.3.4 Boundary of region of real poles	Nearest to origin	

**Definition of boundary regions of complex poles are given in Section G.2.3.

	Symbol	No. of Equations Required
7. Bandwidth	w_{bw}	$b_w = 1$

G.2.3 Definition of Boundary Regions of Complex Pole Pairs

(1) Peak Time and Settling Time

b_1 pairs of complex closed loop poles are to be selected from the indicated region and are to be the pole pairs nearest the imaginary axis and are to be numbered consecutively from the imaginary axis

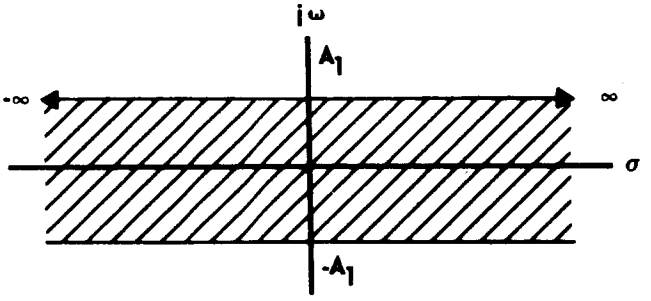

(2) Overshoot - Flexible Body Modes

c_1 pairs of complex closed loop poles are to be selected from the indicated region and are to be the pole pairs nearest the real axis and are to be numbered consecutively from the real axis.

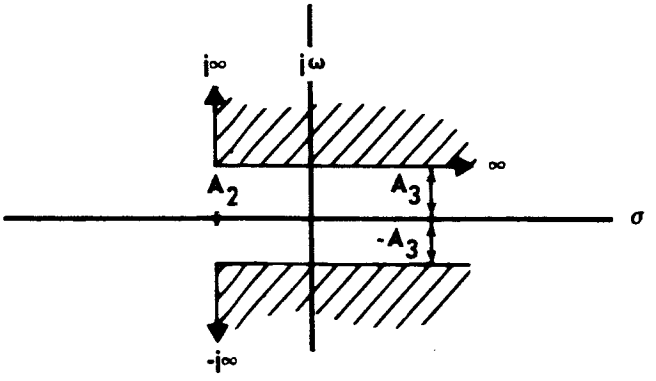

Note: $A_3 > A_1$ if settling time is specified in Section G.2.2.5.

(3) Overshoot - Principal Rigid Body Response

c_2 pairs of complex closed loop poles are to be selected from the indicated region and are to be the pole pairs nearest the imaginary axis and are to be numbered consecutively from the imaginary axis.

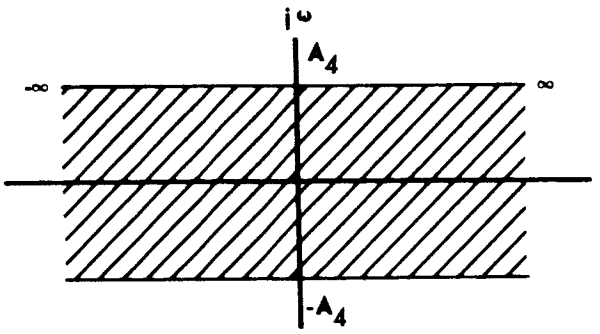

(4) Small Real Root Effects

c_3 small real closed loop poles are to be selected and are to be the poles nearest the imaginary axis and are to be numbered consecutively from the imaginary axis.

G.2.4 Specification of System Size — Total = real + complex

Plant numerator	$k = k_1 + 2\,k_2$	(G.6)
Plant denominator	$n = n_1 + 2\,n_2$	(G.7)
Forward loop compensation network numerator	$I = I_1 + 2\,I_2$	(G.8)
Forward loop compensation network denominator	$J = J_1 + 2\,J_2$	(G.9)
Feedback loop compensation network numerator	$K = K_1 + 2\,K_2$	(G.10)
Feedback loop compensation network denominator	$L = L_1 + 2\,L_2$	(G.11)

Where the total number of condition equations must equal the number of free variables.

$$b_d + b_v + b_a + b_1 + c_1 + c_2 + c_3 + b_w + n + L = n + J + L + I + K + L + 1 \qquad \text{(G.12)}$$

G.2.5 Starting Inputs; u_{j_o}

1. Open loop poles and zeros of plant as determined from the signal component identification process; z_i, p_i
2. Estimate of solutions for undefined open and closed loop poles and zeros and closed loop gain; ζ_{i_o}, $R_e\zeta_{i_o}$, $I_m\zeta_{i_o}$, ξ_{i_o}, $R_e\xi_{i_o}$, $I_m\xi_{i_o}$, η_{i_o}, $R_e\eta_{i_o}$, $I_m\eta_{i_o}$, w_{i_o}, $R_ew_{i_o}$, $I_mw_{i_o}$, q_{i_o}, $I_mq_{i_o}$, $R_eq_{i_o}$, B_o. (Note A and π_i need not be specified). For all the estimates the number of real and complex pairs must agree with the specified values of Section G.2.3.

G.2.6 Convergence Tolerance - The iteration process is to stop when:

$$|\Delta u_{ir}| \leq \mu_1 \qquad (G.13)$$

for real poles, zeros and gain

$$|R_e \Delta u_{ir}| \leq \mu_2 \qquad (G.14)$$

$$|I_m \Delta u_{ir}| \leq \mu_3 \qquad (G.15)$$

for complex poles and zeros

or after N iterations.

G.2.7 Specification Set Equations - A simplified flow diagram of the specification set method is presented below. The program consists of two basic parts: 1) iteration of the linearized condition equations to determine the closed loop gains and all of the compensation parameters except the gain and the denominator of the forward loop compensation network; 2) determination of remaining compensation parameters.

SIMPLIFIED FLOW DIAGRAM - PARAMETER ADJUSTMENT

BY SPECIFICATION SET

COMPUTED INPUTS

Determination of p_i and z_i from signal component identification method

STATIC INPUTS

Problem Definition
Size of $G_p(s)$; k,n
Size of $G_c(s)$; I,J
Size of $H(s)$; K,L
Selection of Specification Parameters
$K_d, K_v, K_a, T_x, m_{F.B.}, m_c, m_r$
$w_{bw}, b_1, c_1, c_2, c_3, A_1, A_2, A_3, A_4$
Initial estimates of system variables, U_{jo}
Iteration controls, μ_1, μ_2, μ_3 or N

Evaluation of coefficients of conditional equations and solution for $\Delta U_{j(r-1)}$

U_{jr}

$\Delta U_{j(r-1)}$

Test for Convergence

Yes

No

Re evaluation of solution estimates

$U_{jr} = U_{j(r-1)} + \Delta U_{j(r-1)}$

Stop iteration and define $U_{j(r-1)} = U_j$

U_j

Calculation of remaining system parameters
A, Π_i

Where U_{jr} is defined as the j^{th} variable as determined after the r^{th} iteration

The adjusted parameter values are obtained by iteration of the conditional equations which may be written in the following matrix form

$$\left[F_x\ (U)_r\right]_{\substack{H_3 x 1 \\ 0<x\leq H_3}} + \left[\left[\frac{\partial F_x(U)_r}{\partial u_j}\right]_{\substack{H_3 x H_3 \\ 0<j\leq H_1 \\ \text{elements} = 0 \\ \text{otherwise}}} + \left[\frac{\partial F_x(U)_r}{\partial R_e\ u_j}\right]_{\substack{H_3 x H_3 \\ H_1<j\leq H_2 \\ \text{elements} = 0 \\ \text{otherwise}}} + \left[\frac{\partial F_x(U)_r}{\partial I_m\ u_j}\right]_{\substack{H_3 x H_3 \\ H_2<j\leq H_3 \\ \text{elements} = 0 \\ \text{otherwise}}}\right]_{H_3 x H_3} x \left[\begin{bmatrix}[\Delta u_{jr}\ ] \\ 0<j\leq H_1\end{bmatrix} \begin{bmatrix}[\Delta R_e\ u_{jr}] \\ H_1<j\leq H_2\end{bmatrix} \begin{bmatrix}[\Delta I_m\ u_{jr}\ ] \\ H_2<j\leq H_3\end{bmatrix}\right]_{H_3 x 1} \tag{G.16}$$

then

$$\left[\begin{bmatrix}[\Delta u_{jr}\ ] \\ [\Delta R_e\ u_{jr}] \\ [\Delta I_m\ u_{jr}]\end{bmatrix}\right] = -\left[\left[\frac{\partial F_x(U)_r}{\partial u_j}\right] + \left[\frac{\partial F_x(U)_r}{\partial R_e\ u_j}\right] + \left[\frac{\partial F_x(U)_r}{\partial I_m\ u_j}\right]\right]^{-1} x \left[F_x\ (U)_r\right] \tag{G.17}$$

where $F_x(U)_r = F_x\ (u_o, \ldots u_{H_1 r_1}, R_e u_{(H_1+1)r}, \ldots R_e\ u_{H_2 r}, I_m\ u_{(H_2+1)r}, \ldots I_m\ u_{H_3 r})$ (G.18)

and $u_{jr} = u_{j(r-1)} + \Delta u_{j(r-1)}$ etc. (G.19)

In particular when

$$\begin{cases} j = 0 & u_j = B & D(j) = 1 \\ 0 < j \le k_1 & u_j = z_i & D(j) = 1 \\ k_1 < j \le k_1 + I_1 & u_j = \zeta_i & D(j) = 1 \\ k_1 + I_1 < j \le k_1 + I_1 + K_1 & u_j = \xi_i & D(j) = 1 \\ k_i + I_1 + K_1 < j \le H_1 & u_j = q_i & D(j) = -1 \end{cases} \quad \text{(G.20)}$$

$$\begin{cases} H_1 < j \le H_1 + k_2 & R_e\, u_j = R_e\, z_i & D(j) = 1 \\ H_1 + k_2 < j \le H_1 + k_2 + I_2 & R_e\, u_j = R_e\, \zeta_i & D(j) = 1 \\ H_1 + k_2 + I_2 < j \le H_1 + k_2 + I_2 + K_2 & R_e\, u_j = R_e\, \xi_i & D(j) = 1 \\ H_1 + k_2 + I_2 + K_2 < j \le H_2 & R_e\, u_j = R_e\, q_i & D(j) = -1 \end{cases} \quad \text{(G.21)}$$

$$\begin{cases} H_2 < j \le H_2 + k_2 & I_m\, u_j = I_m\, z_i \\ H_2 + k_2 < j \le H_2 + k_2 + I_2 & I_m\, u_j = I_m\, \zeta_i \\ H_2 + k_2 + I_2 < j \le H_2 + k_2 + I_2 + K_2 & I_m\, u_j = I_m\, \xi_i \\ H_2 + k_2 + I_2 + K_2 < j \le H_3 & I_m\, u_j = I_m\, q_i \end{cases}$$

where

$$\begin{cases} H_1 = k_1 + I_1 + K_1 + N_1 \\ H_2 = k_1 + I_1 + K_1 + N_1 + H_1 \\ H_3 = 2H_2 - H_1 \end{cases} \quad \text{(G.22)}$$

Defining the coefficients of the matrix equation

$$o < x \leq n_1 + n_2 + L_1 + L_2 + b_d + c_1 + c_2 + c_3 + b_w$$

$$F_x(U)_r = \lambda_1 \ell n\,(K_x)^2 + \lambda_2 G_1\,(0,\, u_{or},\, 0,\, 0) + \sum_{j=1}^{H_1} D(j)\,\Big[G_1\,(y_{1x},\, u_{jr},\, 0,\, 0) - (\lambda_2 - 1) G_1(0, u_{jr}, 0, 0)\Big]$$

$$+ \sum_{j=H_1}^{H_2} D(j)\,\Big[G_1(y_{1x},\, R_e u_{jr},\, y_{2x},\, I_m u_{(j+H_2)r}) + (\lambda_2 - 1) G_1(y_{1x}, R_e u_{jr}, y_{2x},\, -I_m u_{(j+H_2)r})$$

$$- (\lambda_2 - 1)\, T_{P_x}\, y_{1x}\Big] \qquad (G.23)$$

$$\frac{\partial F_x(U)_r}{\partial u_j} = -2\lambda_3\, G_3\,(y_{1x},\, u_{jr},\, y_{2x},\, 0) + 2\,\lambda_4\,\frac{1}{(y_{3x} - u_{jr})} \qquad \underline{0 < j \leq H_1} \qquad (G.24)$$

$$\frac{\partial F_x(U)_r}{\partial R_e\, u_j} = -\,2G_3\,(y_{1x},\, R_e\, u_{jr},\, y_{2x},\, I_m u_{(j-H_1+H_2)r}) - 2\,\lambda_3\, G_3\,(y_{1x},\, R_e\, u_{jr},\, y_{2x},\, -I_m\, u_{(j-H_1+H_2)r})$$

$$- 2\,(\lambda_2 - 1)\, G_3\,(0,\, R_e\, u_{jr},\, 0,\, I_m\, u_{(j-H_1+H_2)r}) \qquad \underline{H_1 < j \leq H_2} \qquad (G.25)$$

$$\frac{\partial F_x(U)_r}{\partial I_m u_j} = -2\, G_3\,(y_{2_x},\ I_m u_{jr},\ y_{1_x},\ R_e u_{(j-H_2+H_1)_r}) + 2\,\lambda_3\, G_3\,(y_{2_x},\ -I_m u_{jr},\ y_{1_x},\ R_e u_{(j-H_2+H_1)_r}) \qquad (G.26)$$

$$-2\,(\lambda_{2-1})\, G_3\,(0,\ I_m u_{jr},\ 0,\ R_e u_{(j-H_2+H_1)_r}) \qquad H_2 < j \le H_3$$

$$n_1 + n_2 + L_1 + L_2 + b_d + c_1 + c_2 + c_3 + b_w < x \le n + L + b_d + c_1 + c_2 + c_3 + b_w + b_1$$

$$F_x(U)_r = \lambda_1 \left[y_{2_x}\, T_x - \pi \right] + \sum_{j=1}^{H_1} D(j) G_2\,(y_{1_x},\ u_{jr},\ y_{2_x},\ 0) + \sum_{j=H_1}^{H_2} D(j) G_2\,(y_{1_x}, R_e u_{jr},\ y_{2_x},\ I_m u_{(j-H_1+H_2)_r}) \qquad (G.27)$$

$$\frac{F_x(U)_r}{\partial u_j} = G_3\,(y_{2_x},\ 0,\ y_{1_x},\ u_{j_r}) \qquad 0 < j \le H_1 \qquad (G.28)$$

$$\frac{F_x(U)_r}{\partial R_e u_j} = G_3(y_{2_x},\ I_m u_{(j-H_1+H_2)_r},\ y_{1_x},\ R_e u_{jr}) + G_3\,(y_{2_x},\ -I_m u_{(j-H_1+H_2)_r},\ y_{1_x},\ R_e u_{jr}) \qquad H_1 < j \le H_2 \qquad (G.29)$$

$$\frac{F_x(U)_r}{\partial I_m u_j} = G_3\,(y_{1_x},\ R_e u_{(j-H_2+H_1)_r},\ y_{2_x},\ -I_m u_{jr}) - G_3\,(y_{1_x},\ R_e u_{(j-H_2+H_1)_r},\ y_{2_x},\ I_m u_{jr}) \qquad H_2 < j \le H_3 \qquad (G.30)$$

$$n + L + b_d + c_1 + c_2 + c_3 + b_w + b_1 < x \leq n + L + b_d + c_1 + c_2 + c_3 + b_w + b_1 + b_v + b_a$$

$$F_x(U)_r = K_x + \sum_{j=1}^{H_1} D(j)\, G_3\,(y_{1_x},\ 0,\ y_{2_x},\ 0) + 2 \sum_{j=H_1}^{H_2} D(j)\, G_3\,(R_e\, u_{jr},\ 0,\ I_m\, u_{(j-H_1+H_2)r},\ 0) \qquad (G.31)$$

$$\frac{F_x(U)_r}{\partial u_j} = -\lambda_1 \frac{1}{(u_{jr})^2} - 2\lambda_2 \frac{1}{(u_{jr})^3} \qquad 0 < j \leq H_1 \qquad (G.32)$$

$$\frac{F_x(U)_r}{\partial R_e\, u_j} = 2\lambda_1 G_4(\,(R_e\, u_{jr})^2,\ -(I_m\, u_{(j-H_1+H_2)r})^2,\ 0,\ 0) + 2\lambda_2 G_4(\,(R_e\, u_{jr})^2,\ -(I_m\, u_{(j-H_1+H_2)r})^2,\ 0,\ 0) \qquad (G.33)$$

$$\times\, G_3\,(R_e u_{jr},\ 0,\ I_m u_{(j-H_1+H_2)r},\ 0) \qquad H_1 < j \leq H_2$$

$$\frac{F_x(U)_r}{\partial I_m\, u_j} = -2\, G_3\,(R_e\, u_{(j-H_2+H_1)r},\ 0,\ I_m\, u_{jr},\ 0)\, G_3\,(I_m\, u_{jr},\ 0,\ R_e\, u_{(j-H_2+H_1)r},\ 0)$$

$$\times \left[\lambda_1 + 2\lambda_2\, G_3\,(I_m\, u_{jr},\ 0,\ R_{e\ (j-H_2+H_1)},\ 0)\right] \qquad (G.34)$$

$$H_2 < j \leq H_3$$

DEF

RANGE OF x	λ_1	λ_2	λ_3
$0 < x \leq n_1$	1	1	0
$n_1 < x \leq n_1 + n_2$	1	1	1
$n_1 + n_2 < x \leq n_1 + n_2 + L_1$	1	1	1
$n_1 + n_2 + L_1 < x \leq n_1 + n_2 + L_1 + L_2$	1	1	1
$x = n_1 + n_2 + L_1 + L_2 + b_d$	1	1	0
$n_1 + n_2 + L_1 + L_2 + b_d < x \leq n_1 + n_2 + L_1 + L_2 + b_d + c_1$	-1	0	1
$n_1 + n_2 + L_1 + L_2 + b_d + c_1 < x \leq n_1 + n_2 + L_1 + L_2 + b_d + c_1 + c_2$	-1	0	1
$n_1 + n_2 + L_1 + L_2 + b_d + c_1 + c_2 < x \leq n_1 + n_2 + L_1 + L_2 + b_d + c_1 + c_2 + c_3$	-1	0	1
$x = n_1 + n_2 + L_1 + L_2 + b_d + c_1 + c_2 + c_3 + b_w$	-1	1	1
$n_1 + n_2 + L_1 + L_2 + b_d + c_1 + c_2 + c_3 + b_w < x \leq n + L_1 + L_2 + b_d + c_1 + c_2 + c_3 + b_w$	0	–	–
$n + L_1 + L_2 + b_d + c_1 + c_2 + c_3 + b_w < x \leq n + L + b_d + c_1 + c_2 + c_3 + b_w$	0	–	–
$n + L + b_d + c_1 + c_2 + c_3 + b_w < x \leq n + L + b_d + c_1 + c_2 + c_3 + b_w + b_1$	1	–	–
$x = n + L + b_d + c_1 + c_2 + c_3 + b_w + b_1 + b_v$	1	0	–
$x = n + L + b_d + c_1 + c_2 + c_3 + b_w + b_1 + b_v + b_a$	0	1	–

TABLE G.1

INING THE EQUATION PARAMETERS FOR THE VARIOUS RANGES OF x

3	λ_4	K_x	y_{1_x}	y_{2_x}
)	−1	A_h	P_x	0
1	0	A_h	$R_e\, P_{(x - n_1)}$	$I_m P_{(x - n_1)}$
1	0	A_h	$\eta_{(x - n_1 - n_2)\, r}$	0
1	0	A_h	$R_e\, \eta_{(x - n_1 - n_2 - L_1)\, r}$	$I_m\, \eta_{(x - n_1 - n_2 - L_1)\, r}$
)	1	$1 + \frac{1}{K_d}$ ·	0	0
1	1	$^{m}F.B._1$	$R_e\, q_{(l = x - n_1 - n_2 - L_1 - L_2 - b_d)\, r}$	$I_m\, q_{(l = x - n_1 - n_2 - L_1 - L_2}$
1	1	$^{m}c_m$	$R_e\, q_{(m = x - n_1 - n_2 - L_1 - L_2 - b_d - c_1)\, r}$	$I_m\, q_{(m = x - n_1 - n_2 - L_1 - L_2}$
1	1	$^{m}R_R$	$q_{(R = x - n_1 - n_2 - L_1 - L_2 - b_d - c_1 - c_2)\, r}$	0
1	0	$1/\sqrt{2}$	0	w_{bw}
–	–	–	$R_e\, P_{(x - n_1 - n_2 - L_1 - L_2 - b_d - c_1 - c_2 - c_3 - b_w)}$	$I_m\, P_{(x - n_1 - n_2 - L_1 - L_2 - }$
–	–	–	$R_e\, \eta_{(x - n - L_1 - L_2 - b_d - c_1 - c_2 - c_3 - b_w)\, r}$	$R_e\, \eta_{(x - n - L_1 - L_2 - b_d - c_1}$
–	–	–	$R_e\, q_{(h = x - n - L - b_d - c_1 - c_2 - c_3 - b_w)\, r}$	$I_m\, q_{(h = x - n - L - b_d - c_1 -}$ or $8/T_{Sh}$
–	–	$-\frac{1}{K_v}$	u_{i_r}	0
–	–	$-\left(\frac{2}{K_a} + \frac{1}{K_v{}^2}\right)$	0	u_{i_r}

	$y3_x$	T_x
	P_x	–
	–	–
	–	–
	–	–
	–	–
$-b_d)\,r$ or h_e	–	$T_p(l = x - n_1 - n_2 - L_1 - L_2 - K_o)$
$-b_d - c_1)\,r$	–	$T_p(m = x - n_1 - n_2 - L_1 - L_2 - b_d - c_1)$
	–	$T_p(R = x - n_1 - n_2 - L_1 - L_2 - b_d - c_1 - c_2)$
	–	–
$_d - c_1 - c_2 - c_3 - b_w)$	–	–
$- c_2 - c_3 - b_w)\,r$	–	–
$c_2 - c_3 - b_w)\,r$	–	$T_p(h = x - n - L - b_d - c_1 - c_2 - c_3 - b_w)$
	–	–
	–	–

where

$$G_1 (y_1, y_2, y_3, y_4) = \ln \left[(y_1 - y_3)^2 + (y_3 - y_4)^2\right] \quad (G.35)$$

$$G_2 (y_1, y_2, y_3, y_4) = \tan^{-1} \frac{(y_3 - y_4)}{(y_1 - y_2)} \quad (G.36)$$

$$G_3 (y_1, y_2, y_3, y_4) = \frac{(y_1 - y_2)}{(y_1 - y_2)^2 + (y_3 - y_4)^2} \quad (G.37)$$

$$G_4 (y_1, y_2, y_3, y_4) = \frac{-(y_1 + y_2)}{(y_1 - y_2)^2 + (y_3 - y_4)^2} \quad (G.38)$$

G.3 Experimental Results for Parameter Adjustment With "Specification Set"

A limited amount of experimental documentation of the "specification set" parameter adjustment technique has been carried out in the form of two examples. These examples incorporate simulated trajectory runs in the sense that the aerodynamic derivatives, or more directly, the poles and zeros of the airframe transfer function are varied in the manner they would vary on a typical section of the trajectory. The airframe transfer function used is typical of the rigid body of large unstable boosters. The specification set incorporates the velocity error constant, K_v, peak overshoot, m, at the predominant frequency with a step input, and the peak time, T_p, the time interval needed to reach the peak overshoot following a step input.

It must be emphasized that the purpose of these examples is solely to illustrate the mechanics and the effectiveness of the parameter adjustment techniques. The selection of the particular airframe transfer function is incidental. There is no implication that the particular selection of the set of three performance criteria is optimum in any sense or that it is even desirable. Neither is any optimality or even desirability implied about the selection of the three adjustable parameters.

The two examples shown both use the loop gain and the rate feedback constant (or rate feedback zero location) for two of the variable parameters. However, Example I uses a variable forward loop pole for compensation and Example II a variable forward loop zero for compensation.

Example I - A list of the assumptions used for Example I are:

(1) Poles and zeros of the airframe transfer function:

pole: $p_1 = 0$ This pole is fixed.

pole: p_2 and p_3 varying as shown in Figure G.1a. Note that p_2 is in the right half plane denoting an unstable airframe.

zero: z_1 varying as shown in Figure G.1a.

In addition, there is a compensating zero at $z_2 = \zeta_1 = -3.5$ which is held constant, so it is not an adjustable parameter and accordingly, it will be handled as if it were part of the airframe. So, for the example:

Number of plant poles: $n = 3$
Number of plant zeros: $k = 2$
Number of compensation poles: $J = 1(\pi 1)$
Number of compensation zeros: $I = 0$
Number of poles in feedback: $L = 0$
Number of zeros in feedback: $K = 1(\xi_1)$

(2) Specification Set:

Velocity error constant: $K_v \geq 10$

Peak overshoot at the predominant frequency: $m \leq 10$ percent

Time to reach peak overshoot: $T_p \leq 2$ seconds

Total number of specifications: $Q = 3$

(3) Variable Parameters:

Loop gain, B

Rate feedback gain, $1/\xi_1$

Forward loop compensating pole or equivalent time constant, π_1

Number of parameters, $J + I + L + K + 1 = 3$ since $L = I = 0$, $J = K = 1$.

Total number of equations, $n + 2L + J + K + I + 1 = 6$.

The results of the parameter adjustment are shown in Figure G.1b. Adjustments were made every ten seconds along the trajectory starting with the previous parameter values. The iteration was carried to very satisfactory accuracy (error at the 10^{-2} - 10^{-3} level) in not more than two steps. One step required less than 0.2 seconds with a computer program which is not optimized for running time. Optimizing the running time should cut this time to a fraction of the present value.

a) Variation with flight time of airframe parameters

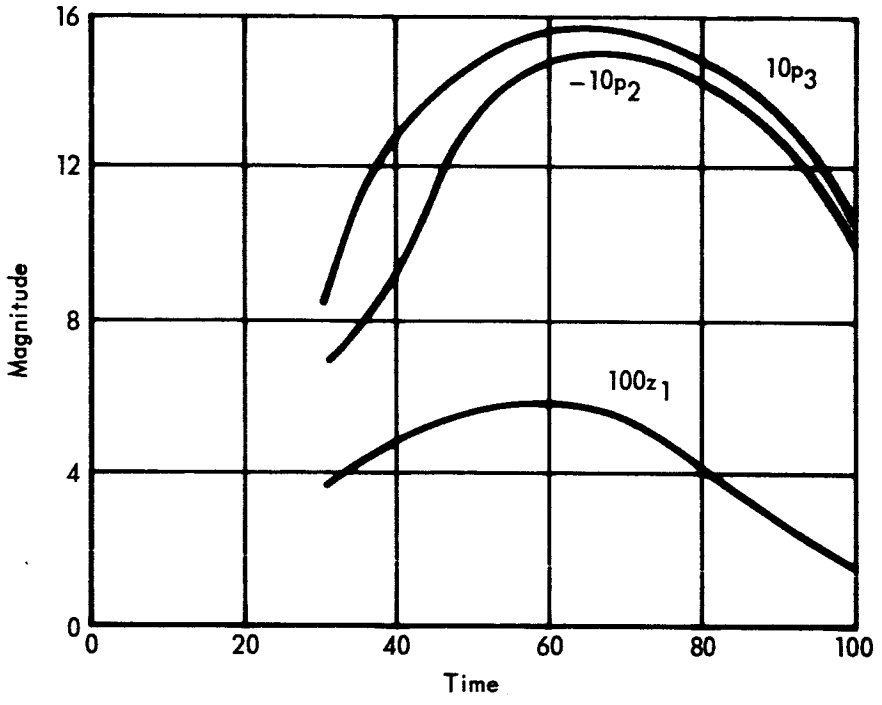

b) Variation with flight time of parameters ξ, π and B of compensating networks

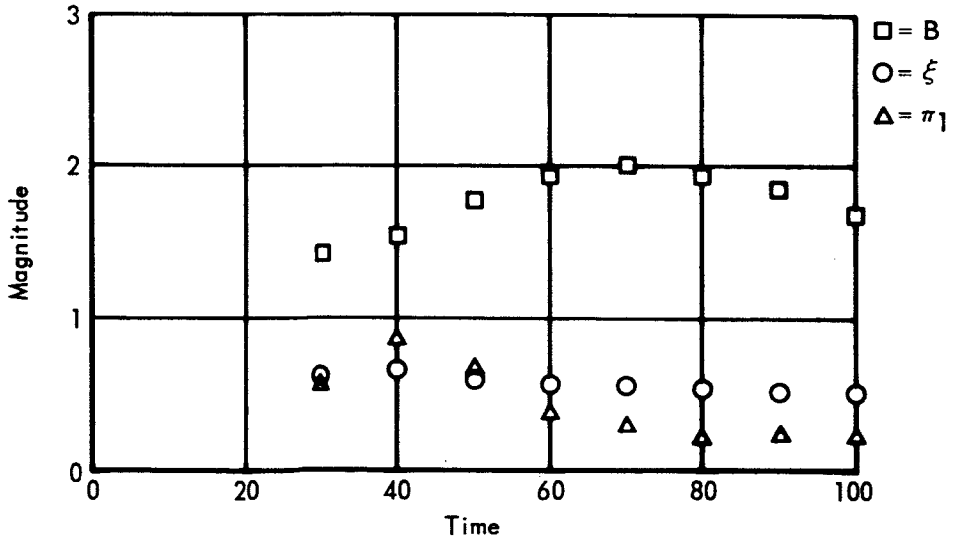

Figure G.1 Illustration of Specification Set Parameter Adjustment Process Used in Example 1

Example II - A list of the assumptions of the example follows:

(1) Poles and zeros of the airframe transfer function:

pole: $p_1 = 0$ This pole is fixed.

pole: p_2 and p_3 varying as shown in Figure G.2a.

zero: z_1 varying as shown in Figure G.2a.

In addition, there is a fixed, forward loop compensating pole at $p_4 = 0.005$ which is not an adjustable parameter so it will be handled as if it were part of the airframe. So, for the example:

Number of plant poles: $n = 4$

Number of plant zeros: $k = 1$

(2) Specification Set:

Velocity error constant: $K_v \geq 10$

Peak overshoot at the predominant frequency: $m \leq 10$ percent

Time to reach peak overshoot: $T_p \leq 2$ seconds

Total number of specifications: $Q = 3$

(3) Variable Parameters:

Loop gain, B

Rate feedback gain, $1/\xi_1$

Forward loop compensating zero or equivalent time constant, ζ_1

Number of parameters, $J + I + L + K + 1 = 3$ since $L = J = 0$, $I = K = 1$

Total number of equations, $n + 2L + J + K + I = 1 = 7$

The results of the parameter adjustment are shown in Figure G.2b. Adjustments were made every five seconds along the trajectory starting with the previous parameter values. The iteration was carried to very satisfactory accuracy (error at the 10^{-2} - 10^{-3} level) in about two steps. However, the accuracy was usually satisfactory for practical purposes after just one step. One step required less than 0.2 seconds with a process which is in no way optimized for running time. Optimizing the running time should cut it to a fraction of the present. When the updating interval was increased to ten and then fifteen seconds resulting in a larger change of the parameters per interval of

a) Variation with flight time of airframe parameters

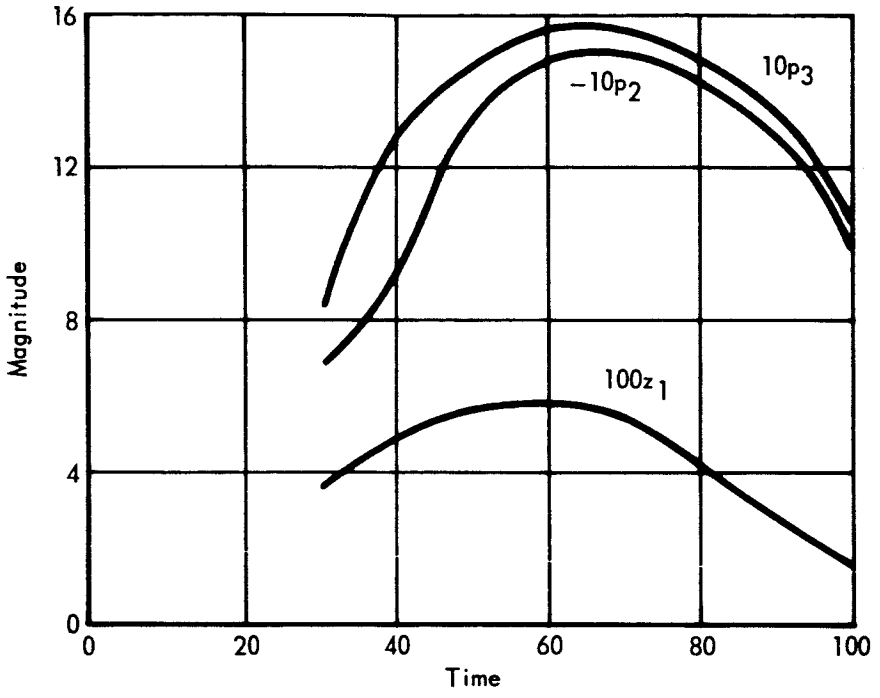

b) Variation with flight time of parameters ξ_1, ζ_1 and B of compensating networks

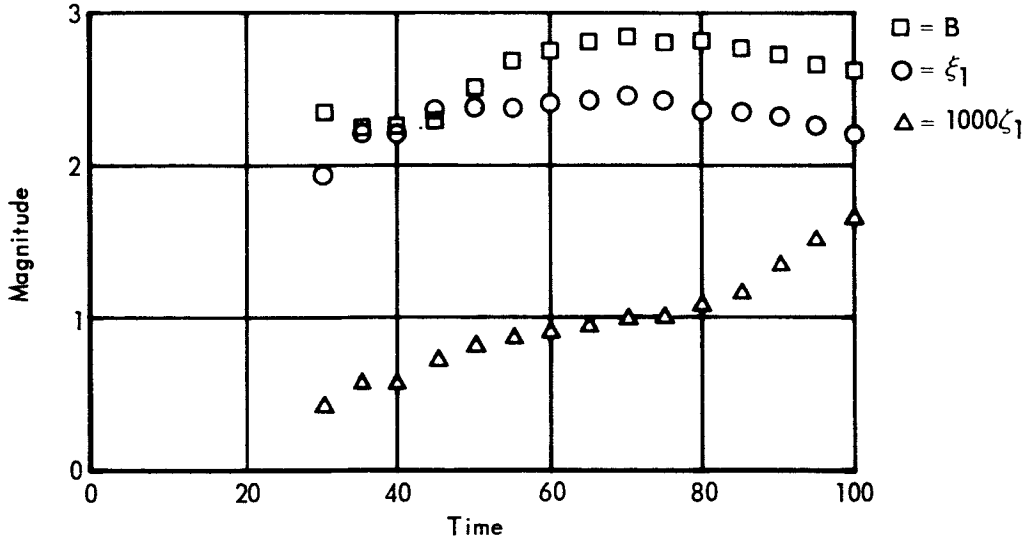

Figure G.2 Illustration of Specification Set Parameter Adjustment Process Used in Example II

parameter adjustment, the number of iterations tended to increase by one for every five second increase of the interval.

The location of the poles and zero of the airframe at t =30 seconds are shown in Figure G.3 along with the compensating pole and zero location selected by the specification set type parameter adjustment process of Example I.

These results indicate that the proposed parameter adjustment technique can handle the adaptive problem with impressive speed, efficiency and effectiveness.

$q_1, q_2 = -0.592 \pm J\,2.04$
$q_3 = -0.62$
$q_4 = -.037$
$p_1 = -0.82$
$p_2 = 0.68$

$\xi = -0.60$
$\pi_1 = -0.57$
$z_1 = -3.5$

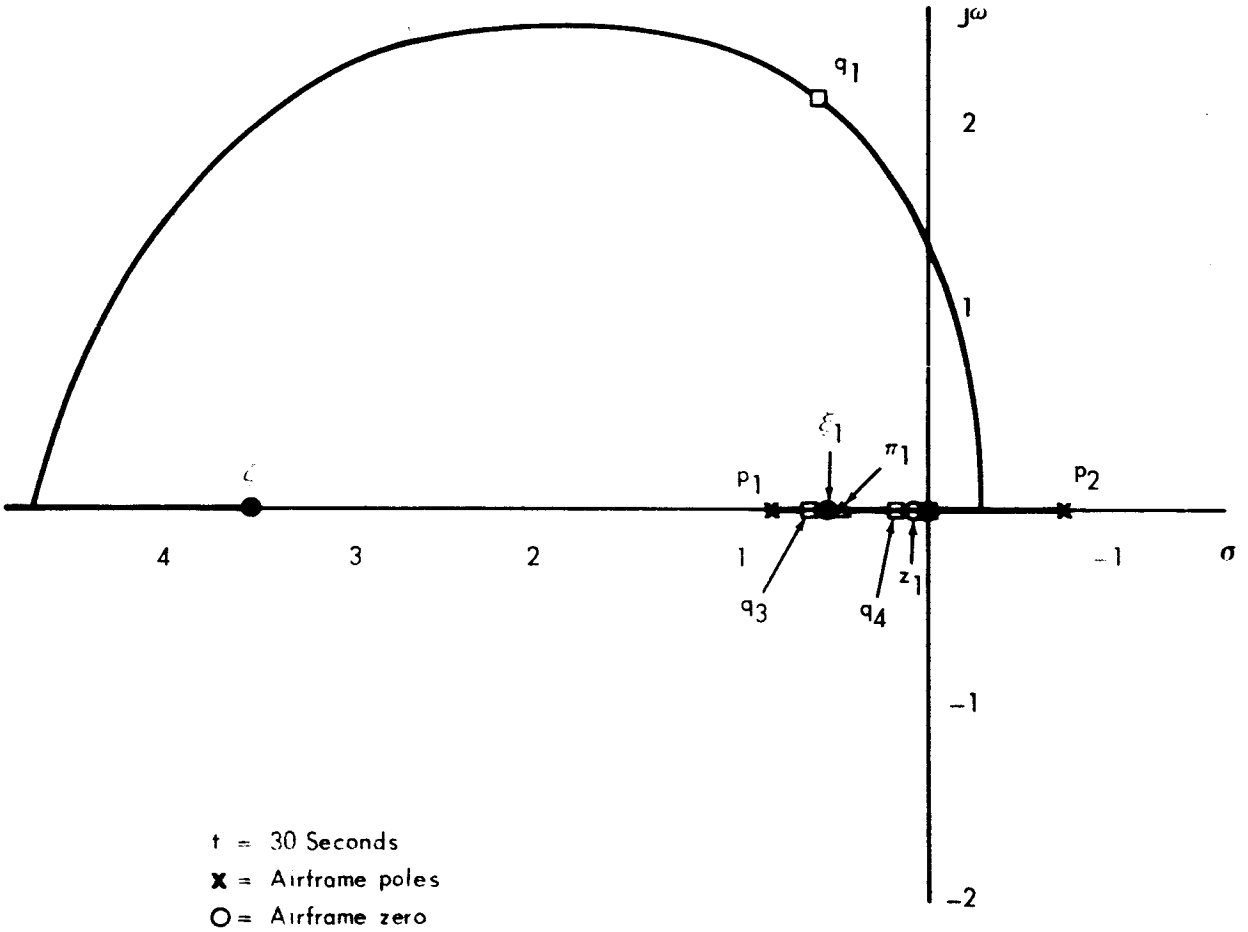

t = 30 Seconds
✖ = Airframe poles
○ = Airframe zero
△ = Forward loop compensating pole
● = Compensating zero
□ = Closed loop poles

Figure G.3 Pole and Zero Locations of the Control System as Compensated by the Method in Example I